A GEOLOGICAL AND GEOCHEMICAL STUDY OF THE SKIDDER BASALT AND SKIDDER TRONDHJEMITES: AND THE GEOLOGY, ORE PETROLOGY AND GEOCHEMISTRY OF THE SKIDDER PROSPECT AND ITS ACCOMPANYING ALTERATION ZONE: BUCHANS AREA, CENTRAL NEWFOUNDLAND

JACOB WAYNE PICKETT

NOTICE

The quality of this microform is heavily dependent upon the quality of the original thesis submitted for microfilming. Every effort has been made to ensure the highest quality of reproduction possible.

If pages are missing, contact the university which granted the degree.

Some pages may have indistinct print especially if the original pages were typed with a poor typewriter ribbon or if the university sent us an inferior photocopy.

Reproduction in full or in part of this microform is governed by the Canadian Copyright Act, R.S.C. 1970, c. C-30, and subsequent amendments.

AVIS

La qualité de cette microforme dépend grandement de la qualité de la thèse soumise au microfilmage. Nous avons tout fait pour assurer une qualité supérieure de reproduction.

S'il manque des pages, veuillez communiquer avec l'université qui a conféré le grade.

La qualité d'impression de certaines pages peut laisser à désirer, surtout si les pages originales ont été dactylographiées à l'aide d'un ruban usé ou si l'université nous a fait parvenir une photocopie de qualité inférieure.

La reproduction, même partielle, de cette microforme est soumise à la Loi canadienne sur le droit d'auteur, SRC 1970, c. C-30, et ses amendements subséquents.

A GEOLOGICAL AND GEOCHEMICAL STUDY OF THE SKIDDER BASALT AND SKIDDER TRONDHJEMITES: AND, THE GEOLOGY, ORE PETROLOGY AND GEOCHEMISTRY OF THE SKIDDER PROSPECT AND ITS ACCOMPANYING ALTERATION ZONE; BUCHANS AREA, CENTRAL NEWFOUNDLAND.

BY

©Jacob Wayne Pickett, B.Sc.

A thesis submitted to the School of Graduate Studies in partial fulfillment of the requirements for the degree of Master of Science

Department of Earth Sciences
Memorial University of Newfoundland

May, 1988

St. John's Newfoundland

ISBN 0-315-50484-6

Frontispiece

The Skidder Area: a clear day on a portion of the "vast fishing-rock, enveloped in everlasting fog, placed in an Arctic position in the Atlantic Ocean" (quote from Alexander Murray (Murray, 1877); written by him to point out the misconceived notion of Newfoundland that many people had at the time).

ABSTRACT

The Skidder Basalt, which outcrops in an area of central Newfoundland immediately to the northwest of Red Indian Lake and approximately 12 km southwest of the town of Buchans, is a spilitized, tholeiitic, sub-alkaline assemblage composed mainly of mafic variolitic and non-variolitic pillow lava, mafic pillow breccia and massive mafic flows; these extrusive rocks are interlayered with lesser amounts of mafic pyroclastic rocks and chert, and are intruded by diabase dykes. Units typically strike northeast to east-northeasterly and dip steeply; facing directions are typically northwesterly, although local reversals, particularly in the vicinity of the Skidder Prospect, are noted. Foliations trend northeasterly and dip steeply. Several northeasterly, northerly and northwesterly trending lineaments are evident on aerial photographs, and many correspond to linear magnetic features.

Rocks of the Skidder Basalt are dominated by secondary mineral assemblages. Typically, albitized plagioclase phenocrysts occur in an intergranular to intersertal groundmass of albite, chlorite, quartz, dense granular sphene, and variable amounts of subhedral to acicular opaque minerals. Primary clinopyroxene and chromite, and secondary calcite, amphibole and epidote are constituents of some samples. Clinopyroxene and albitized plagioclase in some low-Zr Skidder basalts exhibit quench-texture morphologies. Formation of varioles, present in some of the low-Zr Skidder basalts, is suggested to be a result of quenching. Spilitization of the Skidder Basalt has involved albitization of plagioclase, chloritization of basaltic glass, alteration of ferromagnesian minerals to chlorite and lesser amphibole, and alteration of opaque Fe-Ti oxides to dense intergranular sphene. Geochemically, spilitization has resulted in redistribution of SiO_2 and total iron, removal of K_2O and MgO, and extensive addition of Na_2O. The spilitization

is suggested to have resulted from interaction of the rocks with circulating seawater under conditions of low seawater/rock ratios.

The chemistry of Skidder Basalt clinopyroxenes and chromites suggests it has greater similarity to ocean-floor basalts than to basalts formed in an island arc environment. The Skidder Basalt rocks define tholeiitic trends and plot either within the ocean floor basalt field or overlap the ocean floor basalt and island arc tholeiite fields on trace element variation diagrams. It is geologically and geochemically more similar to the pillow lava sections of ophiolite complexes than to the Buchans Group basalts. The Skidder Basalt probably formed in an extensional tectonic environment at a slow-spreading oceanic or back-arc basin ridge.

Low-Al_2O_3, oceanic-type trondhjemite dykes and pods intrude, or are interlayered with, the Skidder Basalt in places. They are chemically similar to trondhjemites considered to represent late magmatic differentiates of basaltic magma.

The Skidder Prospect is an ophiolite-type volcanogenic massive sulphide deposit hosted by basaltic pillow lavas, mafic pillow breccias and aquagene tuffs of the Skidder Basalt. Brecciated, quartz-veined, unlayered and lesser bedded jasper and jasper-rich siltstone are spatially associated with the massive sulphides. Trondhjemite dykes intrude rocks in the Skidder Prospect area in several places.

The deposit contains possible and probable reserves of 200 000 tonnes grading 2% copper and 2% zinc accompanied by very minor amounts of lead. The sulphides occur mainly in two lenses composed of semimassive to massive unlayered and layered pyrite containing lesser amounts of chalcopyrite and low-iron sphalerite. Rare galena, hematite and magnetite are also noted. Quartz, chlorite and lesser calcite are the predominant gangue minerals. Abundant disseminated sulphides, mostly pyrite, occur in a quartz- and/or chlorite ± talc- rich stringer zone underlying the massive sulphides.

Distinct alteration zones characterized by secondary mineral assemblages envelop the massive sulphide lenses and flank the underlying stringer zone, typically up to 150 m away from the sulphide-bearing zones. The alteration primarily involves large increases in the amount of intersertal chlorite and quartz; replacement of mafic minerals by chlorite; and replacement of albitized plagioclase by quartz and lesser phengitic sericite. Quartz has been removed and replaced by chlorite, in places. Chlorites from the alteration zone are significantly enriched in magnesium relative to those of typical spilitized Skidder Basalt. Calcite and epidote, which occur in abundance in the Skidder Basalt, are absent in the most intensely altered rocks of the Skidder Prospect alteration zone.

Geochemically, the alteration is characterized by sporadic enrichment of K, Rb, Ba and Pb; depletion of Ca, Sr and Na; and redistribution of Si in most of the altered rocks. Magnesium and zinc are enriched in intensely chloritized zones. The Zn probably occurs in tiny sphalerite grains intimately associated with high-Mg chlorite. The sporadic enrichment of K and related elements is evident up to 400 m away from the sulphide-bearing zones; the other geochemical effects are recognizable only about 150 m away. Incompatible elements Zr, Y, P and, to a lesser extent, Ti; and compatible elements Cr and Ni have remained stable, even in intensely altered rocks. Chondrite-normalized rare earth element patterns associated with sulphide-poor samples, including some that are relatively unaltered to others that are silicified and intensely chloritized, are similar to those of spilitized Skidder Basalt. Sulphide-rich samples are depleted in REE concentrations relative to the others and some show relative depletion of Ce and the middle REE; characteristics shown by chondrite-normalized REE patterns for seawater.

Lead isotope ratios of the Skidder prospect sulphides are some of the least radiogenic of Newfoundland mineral deposits. On the $^{207}Pb/^{204}Pb$ vs. $^{206}Pb/^{204}Pb$ diagram, they plot along the mantle lead evolution curve of Zartman and Doe (1981).

The genetic model suggested for formation of the Skidder Prospect is similar to that proposed for other ophiolite-related massive sulphide deposits. Metals are suggested to have been leached from underlying rocks by heated, deep circulating, modified seawater possibly similar in composition to that being emitted at present on the East Pacific Rise. The metals were probably carried in solution as chloride complexes. Local faulting provided upward access to the seafloor for the metal-bearing hydrothermal fluids where the massive sulphides are suggested to have been deposited possibly in a manner similar to those now forming on the East Pacific Rise. Mixing between the hot, upwelling, metal-bearing hydrothermal fluid and cool, shallow-convecting seawater is suggested to have produced the associated alteration effects and the disseminated-sulphide stockwork zone. Much of the spatially associated jasper has probably been produced by oxidative leaching of sulphides exposed on the seafloor.

To my wife
Paula
and our children
Christopher, Angela and Stephanie;
without whose encouragement, patience and
understanding
this work would never have been completed

ACKNOWLEDGEMENTS

I would like to acknowledge my supervisor, D.F Strong, for his support and patience over the duration of this study. J.G. Thurlow is thanked for suggesting the thesis topic. Dr. Thurlow, E.A. Swanson, D.M Barbour and other members of the staff of Abitibi Price Mineral Resources and ASARCO gave generous assistance during my stay at Buchans in the summer of 1983. L. Boone provided able assistance in the field.

Financial support for field aspects of the study were provided by the Geological Survey of Canada through contract 19SR.23233-3-0434. Additional financial support was provided by a fellowship from Memorial University of Newfoundland; the Buchans Scholarship Fund of ASARCO Incorporated; and by D.F. Strong, who provided funds from his NSERC grant.

Useful reviews of portions of the material presented in this thesis have been provided by J.M. Duke, G.R. Dunning, R.V. Kirkham, D.F Strong and H.S. Swinden. Scott Swinden is especially thanked for sobering thoughts regarding presentation of the geochemical data. I also wish to thank Greg Dunning for allowing me to use some of his geochemical data from the Annieopsquotch Ophiolite as a comparison to that of the Skidder Basalt.

Much appreciated technical assistance was provided by G. Andrews, P. Moore and G. Veinott.

All diagrams and tables were designed and constructed by the author using an Apple Macintosh microcomputer. R.M. Hopkins is acknowledged for allowing the use of a Department of Engineering and Applied Science laser printer to produce the final manuscript.

A final acknowledgement goes to the graduate students of Decadence Alley who contributed substantially to the touch of insanity required to undertake tasks such as these.

TABLE OF CONTENTS

LIST OF TABLES

LIST OF FIGURES

Chapter 1
INTRODUCTION

1.1 Location and Access

The Skidder area is located in central Newfoundland immediately to the northwest of Red Indian Lake and approximately 12 km southwest of the town of Buchans. The study area (approximately 24 km^2) occupies the northwest part of the Lake Ambrose map sheet (12 A/10; scale 1:50 000) and extends into the southwest corner of the Buchans map sheet (12 A/15; scale 1:50 000) (Figure 1-1). The Skidder Prospect which is located near the centre of the study area occurs at latitude 48° ≈ 43.5' north and longitude 56° ≈ 56' west. The northern portion of the study area is included in Reid Lot 232 and its southern portion is covered by ground held under the Anglo Newfoundland Development Corporation Charter. Mineral rights to the area are presently (1988) held by BP-Selco Ltd. having been purchased from former owners Abitibi Price Mineral Resources and the American Smelting and Refining Company (ASARCO).

Access to the southern portion of the study area and to within 900 m of the Skidder Prospect may be gained by branching from paved highway Route 350 at approximately 5 km east of Buchans and thence travelling west via 14 km of gravel-surfaced woods-access road along the north shore of Red Indian Lake (Figure 1-1). A muskeg trail leads from the gravel road northward to the Skidder Prospect. Road access may be restricted during times of heavy rainfall due to washouts, and alternate means of access either by all-terrain vehicle, by boat on Red Indian Lake, or by helicopter must be used. The northwestern portion of the study area is readily accessed by helicopter only.

1.2 Physiography and Glaciation

Twenhofel and MacClintock (1940) show the Skidder area as part of the High Central Plateau, a portion of the Atlantic Upland stretching from Red Indian Lake westward

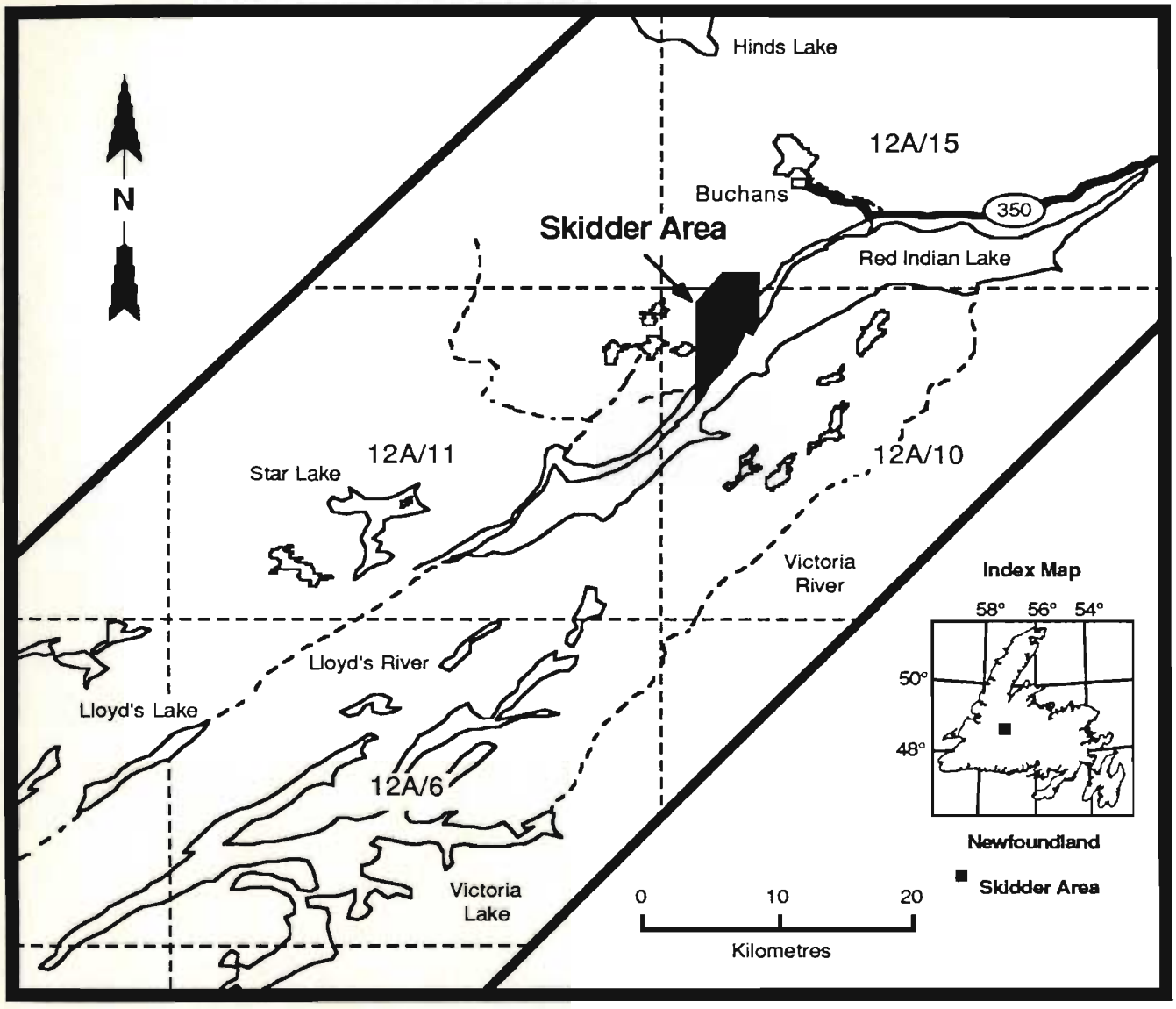

Figure 1-1: Location map for the Skidder area.

to Grand Lake. According to them, the High Central Plateau represents a glacially modified, subaerially developed peneplain of Tertiary age. Hills rising above the general level of the peneplain are considered to be glacially plucked monadnocks, their upper surface marking the level of a late Cretaceous-early Tertiary peneplain which Twenhofel and MacClintock (1940) term the Long Range Peneplain.

The study area is dominated by a glacier- and stream-dissected ridge rising approximately 150 m along a densely wooded slope from Red Indian Lake about 1.5 km to the southeast. Hills having a further relief of 30 to 40 m cap the ridge. One bare outcrop ridge immediately northwest of the arrow-shaped lake in the southwestern portion of the study area rises to about 350 m above the level of Red Indian Lake. Numerous lakes, ponds and bogs are present. Drainage, including Skidder Brook, the only large stream in the immediate area, is southeasterly into Red Indian Lake.

According to Vanderveer and Sparkes (1979), directional glacial striae in the vicinity of Red Indian Lake, within the study area, indicate an early south-southeasterly flow of ice followed by later flow to the southwest. This is substantiated by till fabric analysis carried out by these same authors about 2 km south of the study area.

1.3 Previous Work

Previous geological work in the study area has been dominated by exploration and prospecting conducted by ASARCO under agreement with the Anglo Newfoundland Development Corporation which became known as Price Newfoundland Ltd. and subsequently as Abitibi-Price Mineral Resources. Government surveys in the area have included: regional geological mapping by the Geological Survey of Canada (Riley, 1957; Williams, 1970) and by the Government of Newfoundland, Department of Mines and Energy (Kean, 1979; Kean and Jayasinghe, 1980); aeromagnetic surveys by the Geological Survey of Canada (Geological Survey of Canada, 1954a; 1954b; 1968); and a regional lake

sediment survey conducted by the Newfoundland Department of Mines and Energy (Butler and Davenport, 1978).

Murray (1881) notes "a great display of igneous and eruptive rocks of various mineral qualities which have greatly disturbed and altered the sedimentary formations for the whole length of the Exploits River and Red Indian Pond (Lake)". He correlated the rocks in the Red Indian Lake area with "Silurian" rocks to the north.

Sargent (1928) defined the Central Mineral Belt, which includes the Skidder area, as being a southwesterly narrowing wedge extending from Notre Dame Bay southwestward to the Rose Blanche-Cinq Cerf area on the south coast. He divided the "Red Indian Lake District" into two series: i) an older one of andesitic and trachytic lavas and pyroclastic rocks which strike northeast and dip northwest and; ii) a later series of granite, granite porphyry and basalt.

Newhouse (1931) shows much of the Skidder area to be underlain by fine to medium grained ophitic-textured diabase and the remainder by pillowed andesites and basalts of the "Cambro-Ordovician" Buchans Series. He also mentions well banded white and green cherts with jasper occurring along Skidder Brook that are "probably several hundred feet thick". He describes poorly consolidated shales, arkoses and conglomerates that occur immediately to the southwest of the Skidder area and reports that thin shale beds near the top of the stratigraphic section contain carbonaceous material and Carboniferous plant remains.

George (1937) shows the Skidder area geology to be dominated by diabase and Buchans Series rocks and the staff of the Buchans Mining Company (1955) show the area to be underlain by basic volcanic rocks of the Basal Formation of the Buchans Series which they suggest to be possibly of Ordovician age.

Relly (1960) recommended changing the Buchans Series of Newhouse (1931) to the Buchans Group. He shows the Skidder area to be underlain by Ordovician(?) or Precambrian(?) andesite and basalt flows and agglomerate.

Swanson and Brown (1962) correlate the Buchans Group with the Roberts Arm Group of Notre Dame Bay. They describe the Footwall Andesite (in which the Skidder area rocks had been included) as a thick (4000' (1219 m)) sequence of predominantly basaltic pillowed and massive flows containing interbedded pyroclastic rocks.

Published results of regional geological mapping by H. Williams for the Geological Survey of Canada during 1965 and 1966 (Williams, 1970) show the Skidder area as being underlain by "green to purple and red amygdaloidal lava (locally pillowed) and agglomerate" plus lesser massive green lava. Williams (1967; 1970) re-assigned these and other rocks of the Buchans Group to the Silurian on the basis of lithological similarities of the volcanic rocks and locally interbedded red sandstones to those of the Silurian Springdale Group of north-central Newfoundland.

An ASARCO (1972) unpublished compilation map of the Skidder area at a scale of 1:12 000 shows the area to be underlain predominantly by "Silurian" basaltic to andesitic flows, tuffs and agglomerates termed "cycle 1 - basement rocks". Rocks exposed along Skidder Brook referred to as well banded white and green chert with jasper by Newhouse (1931) are shown as dacitic flows and tuffs. Felsic rocks in the northern portion of the Skidder area are termed "orange to reddish rhyolite flows and intrusives".

Results of an extensive lithogeochemical study in the vicinity of the Buchans polymetallic massive sulphide deposits and a description of the Buchans geology and orebodies (Thurlow, 1973) are published in Thurlow (1974) and Thurlow et al. (1975). Thurlow (1973; 1974) and Thurlow et al. (1975) describe the Buchans Group as consisting of four mafic to felsic volcanic cycles; cycles one and two containing the main orebodies. The Footwall andesite interpreted as forming the base of the Buchans Group and including rocks in the Skidder area is described as consisting of mainly "andesitic basalts, agglomerates, tuffs and flow breccias" accompanied by "less abundant flows and only local occurrences of pillowed flows and flow breccias" (Thurlow, 1973). "Moderate chloritization and development of calcite amygdules in blocks and bombs are characteristic

of the unit" (Thurlow, 1973). Thurlow (1973) further concludes, on petrochemical grounds, that the Buchans Group is a calc-alkaline island arc rock suite (with slight island arc tholeiite tendencies). Thurlow et al. (1975) suggest "numerous" similarities of the Buchans orebodies to the Kuroko deposits of Japan.

Thurlow (1975) discusses the geology and mineral deposits of the Buchans area in a report to the Buchans Task Force. He notes the recognition of major north to south thrust faulting and suggests a more simplified Buchans stratigraphy based on repetition of units due to the thrusting. He divides the Buchans Group into a lower and upper subgroup. The Footwall Andesite is re-assigned to the Red Indian Lake Formation, a ≥ 4000 m-thick, north-dipping, north-facing sequence of basaltic pillow lavas, pillow breccias and other volumetrically less significant lithologies which forms the base of the Buchans Group. He considers the Red Indian Lake Formation to be correlative with basalts of the Roberts Arm Group to the northeast. Thurlow (1975) describes the Skidder prospect as a pyrite, chalcopyrite, sphalerite volcanogenic massive sulphide deposit occurring in basalts of the Red Indian Formation. He notes that the sulphide deposit is associated with jasper chert and underlain by pyritic and siliceous stockwork. Thurlow (1975) points out the anomalous nature of the deposit relative to others in the Buchans area.

Barbour (1977) provides a more detailed description of the geology and mineralization of the Skidder Prospect in an unpublished company report for Price Newfoundland Limited and ASARCO.

The two subgroups of the Buchans Group and southwestward-directed thrusting with later open folding about northeast-trending axes (cf. Thurlow, 1975) are emphasized on a geological map of the Buchans area (12A/15; scale 1:50 000) compiled from regional mapping by ASARCO, Price Company Limited and by B.F. Kean (Kean, 1979). The Skidder area is included in the Basal basalt unit (Kean, 1979) which has a similar lithologic description to the Red Indian Lake Formation (cf. Thurlow, 1975). Felsic units in the

northeast portion of the Skidder area are described as pink and purplish grey spheroidal rhyolite (Kean, 1979; cf. ASARCO, 1972).

Rocks of the Skidder area are shown as mafic volcanic and volcaniclastic rocks of the "Middle Ordovician and Silurian" Buchans Group by Kean and Jayasinghe (1980). They point out the ubiquitous presence of red cherts throughout the rocks in the area, a particularly well exposed section being present along Skidder Brook (cf. Newhouse, 1931). They describe conformable relationships southeast of Red Indian Lake where a siltstone unit termed the Harbour Round Formation overlies the Victoria Lake Group and underlies mafic volcanic rocks included by them in the Buchans Group. Kean and Jayasinghe (1980) consider the Buchans Group to be post-Caradocian in age and equivalent to the Roberts Arm Group of Notre Dame Bay (cf. Dean and Strong, 1975; Williams, 1967). Also included in the report is a brief description of the Skidder Prospect. They point out that the simple mineralogy, lower metal grades and lack of associated felsic rocks make the deposit different from other polymetallic deposits in the Buchans-Roberts Arm groups (cf. Thurlow, 1975) and suggest a similarity to the Gullbridge deposit (cf. Upadhyay and Smitheringale, 1972).

Two comprehensive studies of Buchans area geology were completed in 1981. Thurlow (1981a) completed a Ph.D. thesis on the geology and ore deposits of the Buchans Group and the Geological Association of Canada (GAC) published a commemorative volume on the Buchans orebodies (Swanson et al., 1981).

Thurlow (1981a) divides the Buchans Group into two subgroups, representing two major cycles of volcanism. He describes the lower Buchans subgroup as "voluminous basaltic volcanics overlain by arkosic rocks followed by intermediate and felsic volcanics which contain the major ore deposits". He describes the Upper Buchans Subgroup as a "second volcanic cycle" including "mafic volcanism and arkose deposition" followed by eruption of "voluminous, dominantly felsic volcanics". He includes the Skidder prospect host rocks and other rocks in the Skidder area in the Footwall Basalt, the lowermost unit of

the Buchans Group. Thurlow (1981a) reiterates the importance of southwestward thrusting resulting in repetition of stratigraphic units (cf. Thurlow, 1975), and the calc-alkaline geochemical affinity of the Buchans Group rocks (cf. Thurlow, 1973). He also suggests a faulted relationship between the Buchans Group and Caradocian sedimentary rocks that overlie the Victoria Lake Group (cf. Kean and Jayasinghe, 1980).

Thurlow's in depth study of the Buchans Group geology, geochemistry and contained orebodies (Thurlow, 1981a) is synthesized in two papers (Thurlow, 1981b; Thurlow and Swanson, 1981) included in the commemorative GAC Buchans volume (Swanson et al., 1981). Also included in the volume are papers on the mining history, regional geology (Kean et al., 1981), geochronology, isotope studies and ore horizon breccias of the Buchans area as well as a geological compilation map of the central volcanic belt at a scale of 1:250 000 (to accompany Kean et al., 1981) and a geological map of the Buchans area at a scale of 1:50 000 (to accompany Thurlow and Swanson, 1981); both maps include the Skidder area. Kean et al. (1981) include the Buchans Group in their post-Caradocian "late arc" sequences and mention the Skidder Prospect as an example of mineralization in mafic (vs. felsic) volcanic rocks within the "late arc" sequences. Thurlow and Swanson (1981) include the Skidder Prospect in the Footwall Basalt unit of the Buchans Group (cf. Thurlow, 1981a).

1.4 Present Study

The prime objectives of this study are: i) to describe the geology, petrology, geochemistry and petrogenesis of the Skidder Basalt and trondhjemites that intrude it; ii) to describe the geology and ore petrology of the Skidder Prospect, a volcanogenic massive sulphide deposit hosted by the Skidder Basalt; iii) to indicate the mineralogical and chemical changes that have occurred in the host rocks to the Skidder Prospect as a result of the passage of hydrothermal fluids and subsequent sulphide deposition and; iv) to assess the environment and controls of deposition of the sulphides comprising the Skidder Prospect.

1.5 Method of Investigation

During the summer of 1983, limited regional geological mapping was carried out in the Skidder area and detailed geological mapping was done in the immediate vicinity of the Skidder Prospect. This was augmented by relogging of about one half of the 7795 m of diamond drill core from a selected number of the 38 holes drilled into the prospect by Abitibi Price Mineral Resources and ASARCO Inc. Selected outcrops were sampled for mineralogical and petrographic studies. Seventy-nine of these samples were analyzed for major and trace elements and a select number analyzed for rare-earth elements. In addition, extensive sampling of drill core was carried out concentrating mainly on a cross section of holes through the central part of the Skidder Prospect. Of these samples, 169 were analyzed for major and trace elements and a select number analyzed for rare-earth elements.

Chapter 2

REGIONAL TECTONICS AND OROGENESIS

2.1 Introduction

The Skidder area occurs in the Dunnage zone (Williams, 1978; 1979) or Dunnage terrane (Williams and Hatcher, 1983), one of four tectonic lithofacies zones into which the Newfoundland Appalachians have been divided (Figure 2-1). The northern part of the Appalachian orogen in North America, including the geology of Newfoundland, was considered by Williams (1964) to be a two-sided symmetrical system composed of Precambrian continental margins to the west (western platform) and east (Avalon platform) separated by an early Paleozoic mobile belt (the Central Volcanic Belt). Subsequently, Williams et al. (1972; 1974) divided the Canadian Appalachians into a somewhat more cumbersome nine zones designated alphabetically A to I. Williams' (1978 and 1979) subdivision of the Appalachian orogen lessened the number of zones to five which he termed the Humber, Dunnage, Gander, Avalon and Meguma zones; all of these except the Meguma zone are present in Newfoundland (Figure 2-1). The zones are suggested to record the development and later destruction of a late Precambrian/early Paleozoic Iapetus Ocean (Wilson, 1966; Stevens, 1970; Dewey and Bird, 1971; Williams, 1979).

2.2 Humber Zone

Late Precambrian rifting of the Grenvillian basement of eastern North America was accompanied by: rift-related tholeiitic volcanism, e.g. the autochthonous Lighthouse Cove Formation of northern Newfoundland (Williams and Stevens, 1969; Strong and Williams, 1972); intrusion of granitic and extrusion of volcanic rocks of alkaline affinity, e.g. the Hughes Lake Complex, exposed in an allochthonous slice northwest of Deer Lake (Williams et al., 1985); and deposition of clastic sedimentary sequences. Deposition of an easterly thickening carbonate platform and clastic prism plus shelf-edge coarse limestone

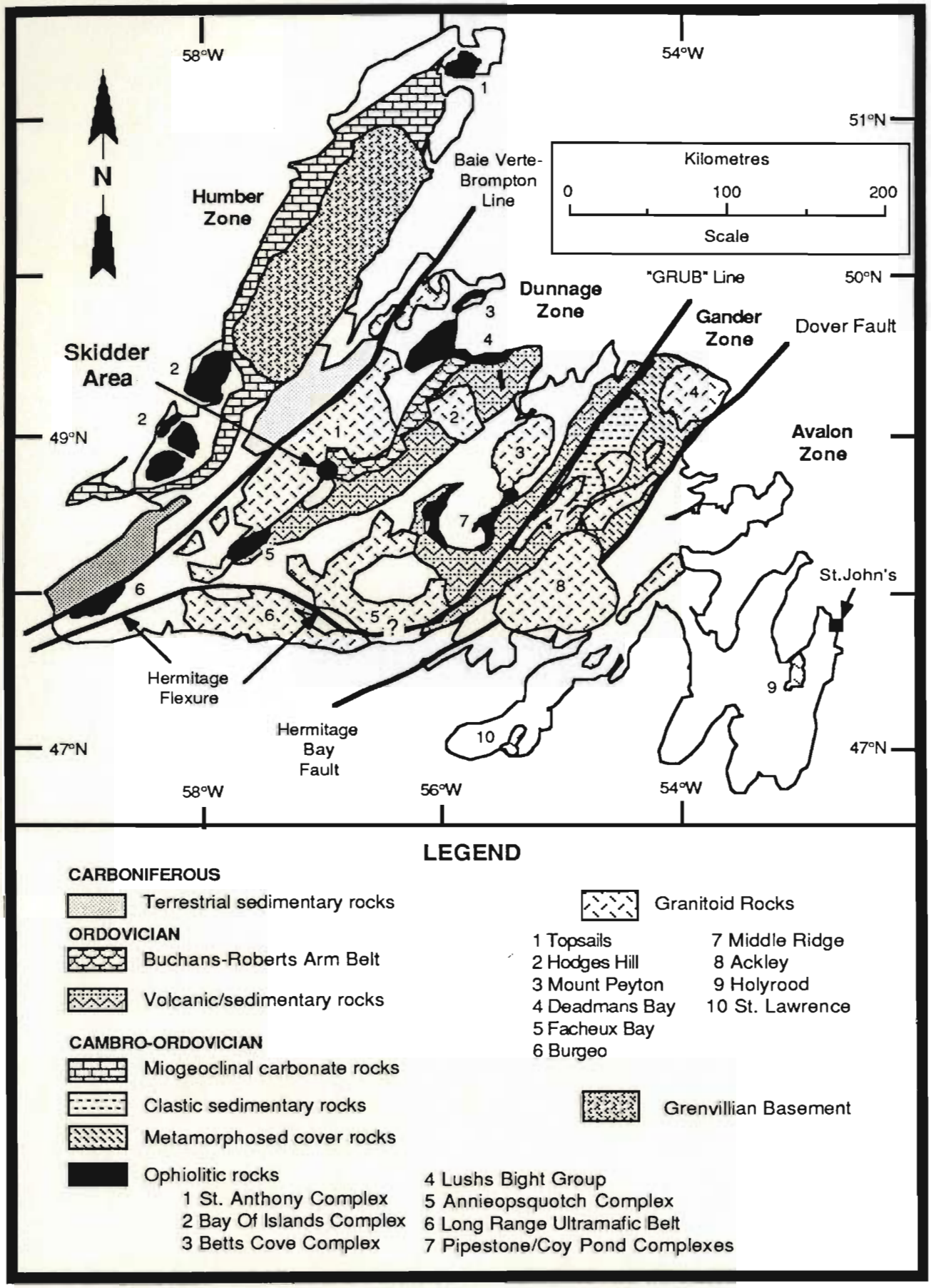

Figure 2-1: Tectonic lithofacies map of Newfoundland (modified after Williams, 1978; 1979).

breccias, turbidites and shales record the development of a Cambro-Ordovician Atlantic-type plate margin (Figure 2-1). Destruction of the margin was accompanied by uplift and development of karst topography which was followed by subsidence and deposition of deep water carbonates and later by deposition of easterly derived clastic rocks containing ophiolite debris (Stevens, 1970). Much of the Humber zone is composed of a series of westwardly emplaced allochthonous tectonic slices stacked such that successively higher slices represent rocks derived more and more distant from the continental margin (Stevens and Williams, 1973; Williams, 1979). Ophiolites, e.g. the Bay of Islands complex (Malpas, 1976), the St. Anthony Complex (Jamieson, 1979; 1980; 1982) and the Little Port Complex (e.g. Karson and Dewey, 1978) that comprise the structurally highest slices are interpreted to be remnants of oceanic crust (e.g. Malpas, 1976) (Figure 2-1). Volcanic rocks interpreted to be remnants of off-ridge volcanism are also preserved in the Humber Arm allochthon i.e. the Skinner Cove volcanic rocks (Strong, 1974), and alkalic volcanic rocks occur in the Hare Bay allochthon (Jamieson, 1977). The boundaries between the various tectonic slices are marked by thin, shaly mélange zones. Emplacement of the Taconic allochthons was essentially complete by Middle Ordovician time as indicated by the neoautochthonous Caradocian Long Point Group (Rodgers, 1965; Williams, 1979).

2.3 Dunnage Zone

The Dunnage zone is deemed to be composed of remnants of the Cambro-Ordovician Iapetus Ocean (Wilson, 1966; Stevens, 1970; Dewey and Bird, 1971; Williams, 1979) that is proposed to have reached a minimum width of 1000 km (Williams, 1980).

Dismembered to complete ophiolite sequences occur in the Dunnage, Humber and Gander zones (Figure 2-1). They represent the oldest rocks preserved in the Dunnage zone and have been interpreted as portions of oceanic crust and upper mantle. Dunning and Krogh (1985) reviewed previous dating of most Newfoundland ophiolites and presented

new U-Pb in zircon ages for several of the complexes. Their results indicate that most of the complexes are Arenigian, their ages ranging from $493.9^{+2.5}_{-1.9}$ Ma for the Pipestone Pond Complex to $477.5^{+2.6}_{-2.0}$ Ma for the Annieopsquotch Complex.

Several partially complete east-facing ophiolite sequences, e.g. the Advocate (Kidd, 1974; Hibbard, 1983) and Grand Lake (Knapp, 1980) complexes that are overlain by coarse conglomerates and olistostromal mélanges, in places mark a portion of the Baie Verte-Brompton Line (Figure 2-1). This narrow zone is suggested to be the structural boundary between the Iapetus ocean and the eastern portion of the ancient continental margin, now represented by poly-deformed and metamorphosed rocks of the Fleur de Lys Group (Piedmont Terrane) (Williams and St. Julien, 1982; Williams and Hatcher, 1983).

Dismembered ophiolites exposed southwest of Buchans to King George IV Lake, e.g. the Annieopsquotch Complex (Dunning and Herd, 1980; Dunning and Chorlton, 1985) (see Figure 2-1), are considered to represent remnants of N-type MORB Iapetus oceanic crust (Dunning and Chorlton, 1985).

Other dismembered ophiolites, e.g. the Pipestone Pond-Coy Pond Complexes and the Gander River Ultramafic Belt, occur at the Dunnage-Gander zone transition (Figure 2-1). The Pipestone Pond-Coy Pond Complexes have been thrust eastwards over continentally derived metasedimentary rocks, the Mount Cormack Terrane, (possibly correlatives of rocks exposed in the Gander Zone) which led Colman-Sadd and Swinden (1984) to suggest that they are exposed in a tectonic window and hence that much of the Dunnage zone may be allochthonous. Results of a *P*-wave travel time residual seismographic study led Stewart (1984) to also suggest an allochthonous model for much of central Newfoundland resulting in "an average crustal thickening of 10 km relative to adjacent platformal areas".

The Gander River Ultramafic Belt "GRUB Line" (Figure 2-1) has been interpreted to mark the eastern edge of the Dunnage zone (Blackwood, 1978; Williams, 1978). However, fossiliferous early Ordovician metavolcanic and terrigenous metasedimentary

rocks of the Indian Bay Formation that are similar to Dunnage zone rocks are exposed well to the east of the "GRUB Line" (Wonderley and Neuman, 1984). Wonderley and Neuman suggest that these rocks were thrust eastward over the Gander zone.

At least two of the partially preserved ophiolite sequences in Notre Dame Bay, the Lushs Bight Group (Strong, 1973; Kean, 1983; 1984) and the Betts Cove Complex (Figure 2-1) are conformably overlain by Lower Ordovician volcanic and sedimentary sequences, the Western Arm and Snooks Arm Groups respectively. The Western Arm Group is thought to be of island arc affinity (Marten, 1971a; 1971b; Kean, 1984) and the Snooks Arm Group has been variably interpreted as being deposited in an island arc (Upadhyay, 1973) or oceanic-island type of environment (Jenner and Fryer, 1980). The ophiolitic Betts Cove Complex itself is unusual in that it contains high-Mg, low-Ti flows interpreted to be boninites by Coish et al. (1982).

Development of an east-dipping subduction zone in the lower Ordovician resulted in island arc volcanism now represented as several volcanic and volcaniclastic groups of rocks throughout the Dunnage zone (e.g. Strong et al., 1974; Dean, 1978; Kean et al., 1981). Dean (1978) and Kean et al. (1981) divided the island arc volcanic and volcaniclastic rocks of the Dunnage zone into two sequences, the pre-Caradocian or "early arc" (Figure 2-1) and the post-Caradocian or "late arc" sequences separated by a laterally extensive Caradocian shale horizon.

A controversy has developed over contact relationships between the "late arc" Roberts Arm Group (Figure 2-1) and the Caradocian sedimentary rocks known to overlie the "early arc" sequences. Dean (1978) states that the volcanic olistostromal Sops Head complex of Notre Dame Bay interpreted as a "giant slump deposit" resulted from "tectonic disturbances during initiation of Roberts Arm volcanism" and conformably overlies the post-Caradocian Sansom Greywacke. Dean (1978) equates the Sops Head Complex with the late Ordovician Boones Point Complex. Nelson (1981) indicates that volcanic material in the Boones Point Complex is very similar to rocks of the Roberts Arm Group and that

this material represents chaotic debris shed from uplifted and southeasterly thrusted Roberts Arm Group rocks. Thus he states that the Roberts Arm Group was laid down prior to late Ordovician volcanism in the area.

Fossil evidence from the Buchans Group (Nowlan and Thurlow, 1984) and U-Pb in zircon ages of $475^{+3.5}_{-2}$ Ma for the Buchans Group, 474 ± 1.5 Ma for the Roberts Arm Group and 462^{+4}_{-2} Ma for the "early arc" Tulks Hill Volcanics (Dunning, 1986) as well as Pb isotope studies on massive sulphide deposits that occur in a number of the volcanic sequences (Swinden and Thorpe, 1984) suggest that the "late arc" Buchans-Roberts Arm Group rocks are, in fact, correlative with "early arc" sequences but probably deposited in areas far removed from each other.

In the Notre Dame Bay area the stratigraphic successions of the "early arc" sequences (Figure 2-1) are dominantly interbedded submarine mafic volcanic and volcaniclastic rocks with local, areally restricted, felsic domes composed mostly of pyroclastic rocks. The domes are suggested to represent the culmination of mafic to felsic volcanic cycles (Dean, 1978; Swinden and Thorpe, 1984). Turbidite sequences containing abundant volcanic detritus are associated with the volcanic and volcaniclastic rocks.

Felsic pyroclastic rocks are more abundant in the "early arc" (Figure 2-1) Victoria Lake Group of central Newfoundland. These rocks form extensive, laterally continuous sheets of lapilli tuff, crystal lithic tuff and porphyritic rhyolite (Kean and Jayasinghe, 1980). Mafic volcanic rocks in the Victoria Lake Group are primarily pyroclastic aquagene tuffs, lapilli tuffs and volcanic breccia (Kean and Jayasinghe, 1980). An extensive clastic sedimentary sequence overlies the volcanic and volcaniclastic rocks of the Victoria Lake Group. These interbedded greywackes, volcaniclastic sandstone-conglomerates and black argillites are interpreted to be derived from surrounding volcanic terranes.

Volcanic rocks of the Summerford and Davidsville groups exposed in the eastern portions of the Dunnage zone (Figure 2-1) and formerly included in the "early arc" sequence (Dean, 1978) have since been interpreted to have formed in an oceanic island

environment (Pickerill et al., 1981; Jacobi and Wasowski, 1985). Similarly, volcanic blocks in the Dunnage mélange have also been found to be geochemically similar to ocean-floor enriched tholeiites and have been equated to the Summerford Group (Wasowski and Jacobi, 1985).

Volcano-sedimentary rocks along the Hermitage flexure (Figure 2-1), e.g. the Baie d'Espoir and Bay du Nord Groups, have been considered coeval with the Victoria Lake and Notre Dame Bay "early arc" sequences (Chorlton, 1980; Colman-Sadd, 1980; Swinden, 1982). A U-Pb in zircon age for the Bay du Nord group of 468 ± 2 Ma agrees with this interpretation but two U-Pb in zircon dates for the La Poile Group (402 ± 5 Ma and 423 ± 3 Ma) are considerably younger and suggest that more than one pulse of volcanism is represented in the La Poile Group rocks (Dunning, 1986).

The Buchans-Roberts Arm Groups (Figure 2-1) are subaqueous, bimodal, basalt-rhyolite assemblages of calc-alkaline affinity (Thurlow, 1973; Dean, 1978; Thurlow, 1981a; 1981b). The Roberts Arm Group consists predominantly of pillow lavas, massive basalts, volcanic breccias, some chert, siltstone and greywacke (Bostock, 1978). Accumulations of felsic volcanic rocks, interpreted to be volcanic centres, cap the more mafic sequences (Bostock, 1978; Dean, 1978). Bostock (1978) indicates that the Roberts Arm Belt is exposed as fault-bounded blocks.

Mafic volcanic rocks of the Buchans Group are, for the most part porphyritic, amygdaloidal, pillowed basalts, pillow breccia, massive flows and lesser pyroclastic rocks exhibiting features of quiet effusion (Thurlow, 1973; 1981a; Thurlow and Swanson, 1981). Felsic volcanic rocks (host to the Buchans ore bodies) are primarily dacitic to rhyolitic tuffs and breccias that have features characteristic of explosive eruption. Clastic sedimentary rocks including mudstone, siltstone, greywacke and polymictic volcanic conglomerate are associated with the felsic pyroclastic rocks.

Caradocian shales of the Dunnage Zone are overlain by late Ordovician to early Silurian greywacke-conglomerate, flysch-turbidite sedimentary rocks (Strong, 1977; Dean,1978).

Several Silurian-Devonian mafic to felsic volcanic and felsic plutonic rocks occur in the western portion of the Dunnage Zone. These volcanic-volcaniclastic sequences, e.g. the Springdale Group, the King's Point Complex, the Cape St. John Group (and others), and plutonic rocks of the Topsails Igneous Complex, have been interpreted by Coyle and Strong (1987) to represent different structural levels of several calderas and related subjacent plutons. They suggest that magmatic activity at this time was related to large-scale melting of thickened and subducted continental crust by trapped heat and basaltic magma following closure of the Iapetus Ocean. The magmatic activity is suggested to have occurred in a transpressional tectonic regime.

2.4 Gander Zone

The eastern margin of Iapetus is generally thought to be represented by the Gander zone (Williams, 1979) (Figure 2-1) or Gander Terrane (Williams and Hatcher, 1982; 1983). Rocks of the Gander zone include a thick sequence of pre-Middle Ordovician arenaceous rocks, the Gander Group, that, in most places, is polydeformed and metamorphosed. The Gander Group is underlain to the east by migmatites and granitic gneisses. Blackwood and Kennedy (1975) interpreted the latter which they termed the "Bonavista Bay gneiss complex" to be possible Precambrian basement and that the Gander group unconformably overlay the gneisses. Jenness (1963) and Blackwood (1978), on the other hand, suggest that the Gander Group, the granitic gneisses and migmatites are a conformable sequence which underwent prograde metamorphism from east to west.

The Dunnage-Gander zone contact is generally considered to be marked by the Gander River Ultramafic Belt (the "GRUB" line), GRUB line rocks having been thrust over the Gander Group (e.g. Blackwood, 1979). The late Llanvirnian to early Llandeillian

(Stouge, 1980) Davidsville Group nonconformably overlies the GRUB line rocks (Blackwood 1979) and has been interpreted to conformably overlie the Gander Group (Blackwood, 1980). Currie et al. (1979) interpret Davidsville Group sedimentary rocks in the Carmanville area as being a resedimented assemblage deposited on the continental slope and toe of the Iapetus ocean. Pajari et al. (1979) and Pickerill et al. (1981) further suggest that associated Carmanville volcanic rocks which they interpret as being of oceanic island affinity are olistoliths and that together with ultramafic olistoliths represent allochthonous masses of lower Paleozoic oceanic crust and upper mantle and super-incumbent volcanics that were obducted eastward. Pickerill et al. (1981) consider the Gander River ultramafic belt rocks to be tectonically emplaced remnants of oceanic crust and upper mantle.

2.5 Avalon Zone

There is a general consensus that the Avalon zone (Figure 2-1) of Newfoundland has a separate lower Paleozoic geological history from that of the zones to the west and its geology has been compared to that of the Pan-African continent (e.g. Schenk, 1971; Hughes, 1972; Strong, 1979a; O'Brien et al., 1983). It may represent a true "suspect terrane" (Coney et al., 1980; Williams and Hatcher, 1982; 1983). The Avalon and Gander zones are separated by the Dover-Hermitage Fault (Blackwood and Kennedy, 1975; Blackwood and O'Driscoll, 1976) (Figure 2-1) represented by a 300-500 m-wide mylonite zone (Blackwood, 1978) and interpreted as a major sinistral wrench fault system (Blackwood, 1985). Sinistral movement along the Dover-Hermitage Fault system of eastern Newfoundland and the Long Range-Cape Ray fault systems of western Newfoundland is suggested to have resulted in clockwise rotation of structural elements of the Dunnage-Gander zones producing the main Hermitage (Figure 2-1) and other subsidiary flexures of the Central Mobile Belt (Church and Stevens, 1971; Hanmer, 1981; O'Brien et al., 1986)

The Avalon zone consists predominantly of late Precambrian volcanic and sedimentary sequences that are relatively undeformed and unmetamorphosed compared to adjacent rocks of the Gander zone (Williams, 1979).

King et al. (1974) divided the stratigraphy of the Avalon Peninsula into three assemblages. The lower assemblage consists of late Precambrian marine and terrestrial volcanic rocks i.e. the Harbour Main and Love Cove Groups, and related plutonic rocks. Hughes (1970) suggested that these rocks were of island arc affinity whereas Papezik (1970) indicated a Basin and Range rift type of environment for deposition of the Harbour Main Group. These volcanic rocks are conformably (?) overlain by fine grained submarine turbiditic siliceous siltstones and sandstones of the Conception and Connecting Point Groups (Williams and King, 1976; Strong et al., 1978). Included in the former is the Gaskiers Formation, a late Precambrian "tillite" composed of glaciogenic subaqueous debris flows (Gravenor, 1980).

The middle assemblage includes a shallowing upward sequence from basinal deltaic black shales (e.g. the St. John's Group) through green sandstones to molasse-like red sandstones and conglomerates (e.g. the Cabot Group) (King, 1986). Short-lived Proterozoic rifting of the western Avalon zone is recorded in alkalic basalts passing upward into ocean-floor related pillow lavas and a gabbroic as represented by the Burin Group (Strong et al., 1978; Strong, 1979a). Mild tectonism of Burin Group rocks was followed by subaerial bimodal volcanism as represented by the Marystown and Mortier Bay Groups (Strong et al., 1978; Strong, 1979a).

The upper sequence of the Avalon Zone in Newfoundland is recorded by deposition of uppermost Precambrian to Cambrian conglomerates, sandstones and shales in fault-bounded basins, e.g. the Rencontre and Chapel Island formations exposed in the Fortune Bay area (Smith and Hiscott, 1984), and deposition of macrotidal cross-bedded quartz arenites of the platformal lower Cambrian Random Formation (Hiscott, 1982). Volumetrically small amounts of basaltic volcanic rocks are interbedded with middle

Cambrian shales on the Avalon peninsula. These rocks have alkaline geochemical affinities and are considered to be indicative continental fracturing in an extensional tectonic environment (Greenough and Papezik, 1985). Upper Cambrian (?) to Arenigian micaceous sandstones, siltstones, shales and ironstones interpreted to have been laid down in a tidal environment (e.g., Ranger et al., 1984) occur in the Bell Island area of the Avalon zone.

2.6 Accretionary History

Williams and Hatcher (1982; 1983) describe the accretionary history of the various tectonic zones (terranes) and suggest a relationship between accretion of the various terranes and periods of deformation, metamorphism, and plutonism. Thus, the Middle Ordovician Taconic orogeny affected the eastern margin of the North American miogeocline, the margins of the Dunnage Terrane and most of the Gander Terrane. They suggest that accretion of the Dunnage Terrane to the North American miogeocline was effected by its obduction during the Taconic orogeny and that subduction of the Dunnage Terrane beneath and/or obduction across the Gander Terrane also occurred during this orogeny. The mid-Paleozoic Acadian orogeny affected all of the Newfoundland Appalachians except for areas of the eastern Avalon Terrane and has been suggested to be related to "compression and shearing across the orogen in response to the accretion of the Avalon Terrane" (Williams and Hatcher, 1983). The late Paleozoic Alleghanian orogeny resulted in large scale deformation of rocks in the southern Appalachians but affected rocks in northern portions of the Appalachians only locally (Williams and Hatcher, 1982; 1983).

2.7 Granitoid Plutonism

Granitoid plutonism in the Newfoundland Appalachians ranges in age from Precambrian to Carboniferous (e.g. Strong, 1980; Strong, 1982). Precambrian granitic rocks in Newfoundland are represented by folded Precambrian granitoid rocks in the Long Range Grenvillian outlier (Figure 2-1), and late Precambrian calc-alkaline granite,

granodioritic plutons, e.g. the Holyrood granite (Strong and Minatidis, 1975) and the Swift Current Granite (e.g. Dallmeyer et al., 1981a), which intrude late Precambrian volcanic rocks of the Avalon zone (Figure 2-1).

Ordovician granitoid plutonism is represented by late-differentiate trondhjemites associated with ophiolites (e.g. Malpas, 1979; cf. Pederson and Malpas, 1984) or other trondhjemites which intrude amphibolites and are interpreted as being formed as partial melts of metamorphosed basaltic rocks, e.g. the Twillingate trondhjemite (Payne and Strong, 1979). Small tonalitic to granitic, probably subvolcanic stocks are associated with felsic portions of several Ordovician volcanic sequences in Notre Dame Bay (Dean, 1978) and in the Buchans area (e.g. Thurlow, 1981a; 1981b; Stewart, 1987).

Dallmeyer et al. (1981b) report a U-Pb in zircon age of 460 ± 20 Ma for the Lockers Bay Granite located in the Gander zone within the immediate vicinity of the Dover Fault. The Lockers Bay Granite is interpreted by them to have been formed by anatexis related to migmatite formation during high grade regional metamorphism of the Hare Bay Gneiss. $^{40}Ar/^{39}Ar$ in biotite ages of 370 ± 6 Ma for the same pluton led them to suggest a "prolonged tectonothermal evolution for the Gander Zone".

The Ordovician or Silurian (?) tonalitic to granitic Port aux Basques granite of southwestern Newfoundland is interpreted by Dingwell (1980) and Wilton (1985) as having been formed by partial melting of surrounding rocks during intense metamorphism and tectonism possibly related to "continuation of stresses that caused ophiolite obduction" (Wilton, 1985). The tonalitic Cape Ray Granite, also of southwestern Newfoundland, is suggested by Wilton (1985) to have been produced by partial melting of ophiolitic material due to over-thickening by thrusting or obduction. However, subsidiary megacrystic S-type phases of the Cape Ray Granite suggest underplating by continental crust (Wilton, 1985).

Numerous granitic batholiths of Devonian age occur throughout eastern portions of the Humber, Dunnage and Gander zones and in western portions of the Avalon zone (e.g., Strong and Dickson, 1978; Strong, 1980). These include hornblende- ± biotite-bearing

granites, e.g. the bimodal mafic-silicic Mount Peyton batholith (Figure 2-1) interpreted by (Strong, 1979b; Strong and Dupuy, 1982) as having been generated by crustal melting due to intrusion of a mantle-derived magma. Other types include: biotite-microcline megacrystic granites, e.g. the Middle Brook Granite; muscovite-biotite "two-mica" granites, e.g. the Middle Ridge granite; and alkaline-peralkaline granites such as the Topsails Igneous Complex (Strong, 1980) (Figure 2-1).

Strong (1980) suggests that Devonian plutonism resulted from continued plate compression and rotation after closing of Iapetus. This resulted in over-thickening of the crust and "megashearing" which, in turn, caused crustal melting. He further suggests that the hydrous accessory minerals present in the different granitoids i.e. muscovite, biotite or hornblende represent increasing degrees of partial melting in a compressive-shearing environment. In contrast, he suggests that the peralkaline, alkaline granitoids probably formed in locally extensional crustal environments. Taylor et al. (1980), for example, indicate that the peralkaline, alkaline Topsails Igneous Complex probably developed from an "interaction of local crustal extension, basaltic intrusion, and volatile fluxing, with subsequent high-level intrusion and fractionation, along with metasomatism by magmatically derived fluids". More complex intrusive histories are being suggested for some of the all-inclusive batholithic suites. Tuach et al., 1986, for example, identify 10 plutonic phases in the the Ackley Granite. They note that the northwestern portion of the Ackley Granite which intrudes rocks of the Gander terrane is geochemically distinct from its southeastern portion which intrudes rocks of the Avalon terrane; reflecting differences in the composition of the source rocks. Also, although the the southeastern portion of the Ackley Granite has overall "I-type" granite (Chappell and White, 1974) affinities, more silicic, mineralized varieties have "A-type" (Collins et al., 1982) affinities.

Carboniferous plutonism in Newfoundland is not widespread. The alkaline-peralkaline alaskitic St. Lawrence granite (Figure 2-1) dated at 334 ± 5 Ma has been interpreted to have been formed in an extensional tectonic environment (Teng and Strong,

1976; Strong et al., 1978; Strong, 1982). The late Devonian-early Carboniferous Strawberry and Isle aux Morts granites exposed near the Cape Ray fault zone on the southwest coast have been interpreted by Wilton (1985) to be "A-Type" granites (Collins et al., 1982) which were formed by partial melting of depleted granulitic crust. Since the Strawberry granite intrudes the ophiolitic Long Range mafic-ultramafic complex Wilton (1985) suggests that felsic granulite basement underlies the ophiolite complex, implying that the Long Range ophiolite complex is allochthonous and that significant underplating of proto-North American crust has occurred in southwestern Newfoundland.

2.8 Carboniferous Sedimentary Rocks

Late Devonian to early Carboniferous right-lateral wrench faulting in western Newfoundland is suggested to have resulted in a graben structure into which non-marine sedimentary rocks of the Deer Lake Group were deposited (e.g. Hyde, 1984) (Figure 2-1). Non-marine Carboniferous sandstones and conglomerates also outcrop on the northwest shore of Red Indian Lake immediately south of the Skidder Area (Figure 2-1).

2.9 Mesozoic Dykes

Jurassic to Cretaceous lamprophyre dykes in Notre Dame Bay (Strong and Harris, 1974) and a Triassic northeast-trending tholeiitic diabase dyke cutting the Avalon peninsula (Papezik and Hodych, 1980) have been attributed to extensional tectonics related to the opening of the modern Atlantic Ocean.

Chapter 3
GEOLOGY OF THE SKIDDER BASALT

3.1 Introduction

The Skidder Basalt underlies an area of approximately 30 km^2 located about 10 km south of the town of Buchans in central Newfoundland (Figures 1-1 and 3-1). It comprises basaltic pillow lava, pillow breccia and massive flows plus lesser diabase dykes, gabbro, mafic pyroclastic rocks and chert. Trondhjemite pods and dykes intrude the Skidder Basalt in places.

The Skidder Basalt had previously been included in the Footwall Basalt of the Buchans Group (Thurlow, 1981a; 1981b). Thurlow (1981a) describes the Footwall Basalt as being "the lowermost unit of the Buchans Group....", consisting of "a 'thick' (≈ 3800 m), laterally continuous sequence composed mainly of basaltic pillow lava and pillow breccia interbedded with lesser pyroclastic rocks and discontinuous lenses of multicoloured, bedded chert". Thurlow and Swanson (1987) subsequently reinterpreted the stratigraphy of the Buchans Group; they include the Footwall Basalt in the Sandy Lake Formation, the uppermost unit of the Buchans Group.

Thurlow (personal communication to D.F. Strong, 1983) pointed out that, although the basaltic host rocks to the Skidder Prospect "appear to be part of the Buchans Group...", "the proximity to the Star Lake Gabbro allows the possibility that the basalts are ophiolitic". In contrast to those of the Footwall Basalt (Sandy Lake Formation), basalts in the Skidder area are spilitized (see Chapter 4) and pillows in some Skidder area basalts are variolitic. Also, pillows in basalts from the Skidder area contain fewer in number and smaller-sized amygdules than those of the Footwall Basalt. The Skidder area rocks also have a higher magnetic susceptibility than those of the Footwall Basalt (Figure 3-2). On the basis of these differences, Pickett and Barbour (1984) assigned the Skidder area rocks to a new unit

LEGEND

CARBONIFEROUS

15 Sandstone, conglomerate; and minor amounts of limestone and siltstone

SILURIAN

14 Amphibole ± pyroxene, amphibole-biotite and biotite, one or two feldspar granites

13 Amphibole, pyroxene gabbro to syenite

12 Agmatite comprising mafic to ultramafic blocks in a granitoid matrix

11 Red micaceous sandstone

Springdale Group

10 Rhyolite, rhyolite breccia, laharic breccia, minor subaerial basalt

ORDOVICIAN OR SILURIAN

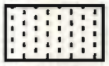

9 Feeder Granodiorite

8 Massive to moderately foliated granodiorite containing many small mafic to ultramafic fragments

7 Moderately to strongly foliated tonalite to diorite containing many mafic to ultramafic inclusions

Hungry Mountain Complex

6 Moderately to strongly foliated hornblende gabbro, diorite, tonalite, and granodiorite; many mafic inclusions

ORDOVICIAN

5a Mafic pillow lava, pillow breccia, and interpillow chert (B.F. Kean, personal communication, 1988)

5b Mafic lava (locally pillowed), agglomerate, tuff; and minor amounts of sedimentary rocks

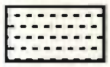

4 Siltstone, conglomerate; minor limestone and siltstone

Buchans Group

3 Mafic to intermediate volcanic rocks (locally pillowed); felsic volcanic breccia and agglomerate; rhyolite and dacite flows; tuff; chert; greywacke; conglomerate; sandstone; and siltstone

Victoria Lake Group

2a Mafic to intermediate tuff, lesser mafic flows, pillow lavas and minor felsic volcanic rocks

2b Felsic pyroclastic rocks and rhyolite flows, minor unseparated mafic volcanic rocks

Dismembered Ophiolite Suites, and Mafic to Ultramafic Rocks of Uncertain Affinity

1 Undivided

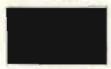

1a Skidder Basalt

1b Sheeted diabase dykes

1c Gabbro

1d Layered troctolite, gabbro, pyroxenite

Legend to accompany Figure 3-1.

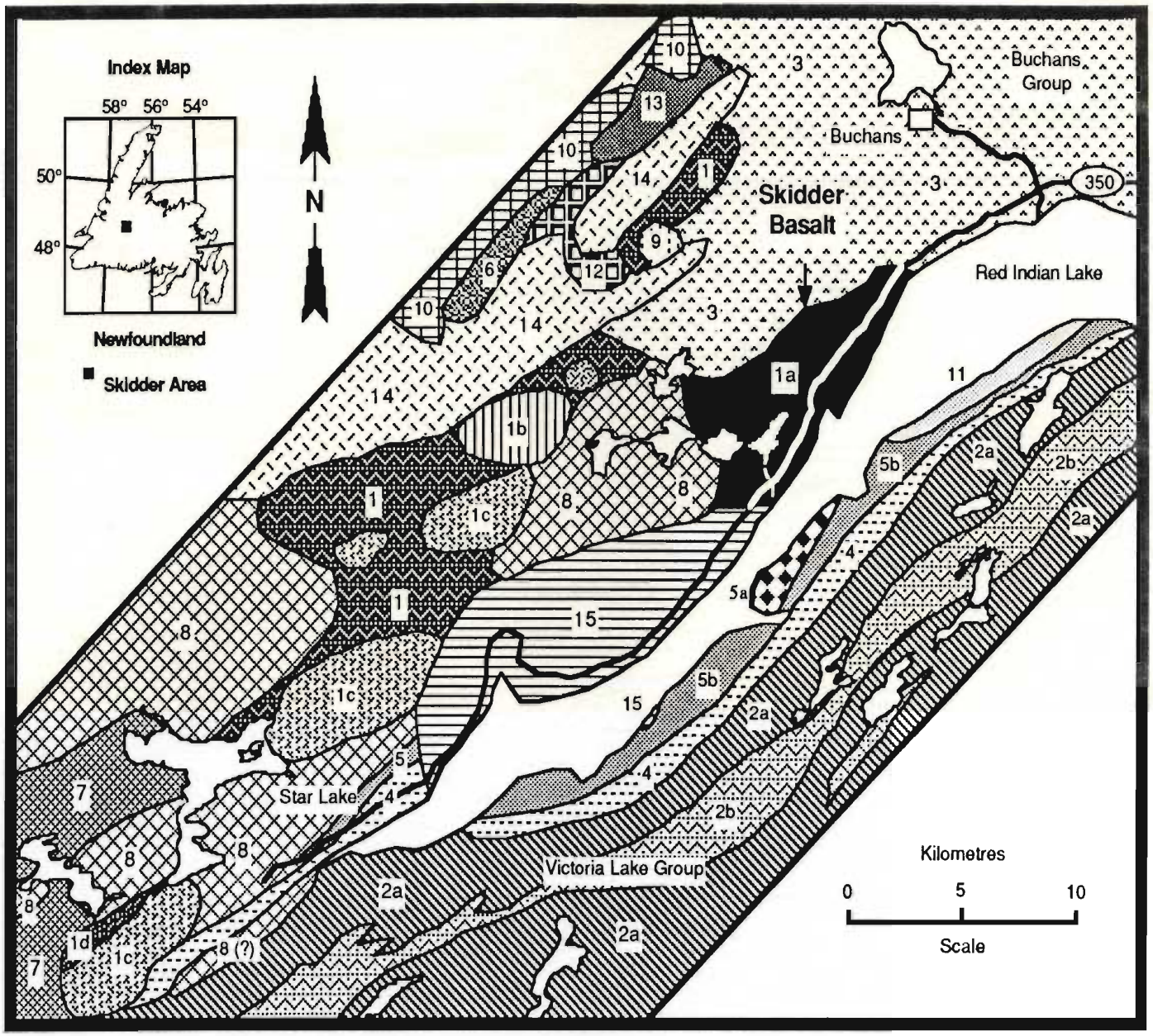

Figure 3-1: Regional geology of the Skidder area: modified after Kean (1979); Dunning (1984); Kean and Jayasinghe (1980); Thurlow and Swanson (1981); and Whalen and Currie (1987).

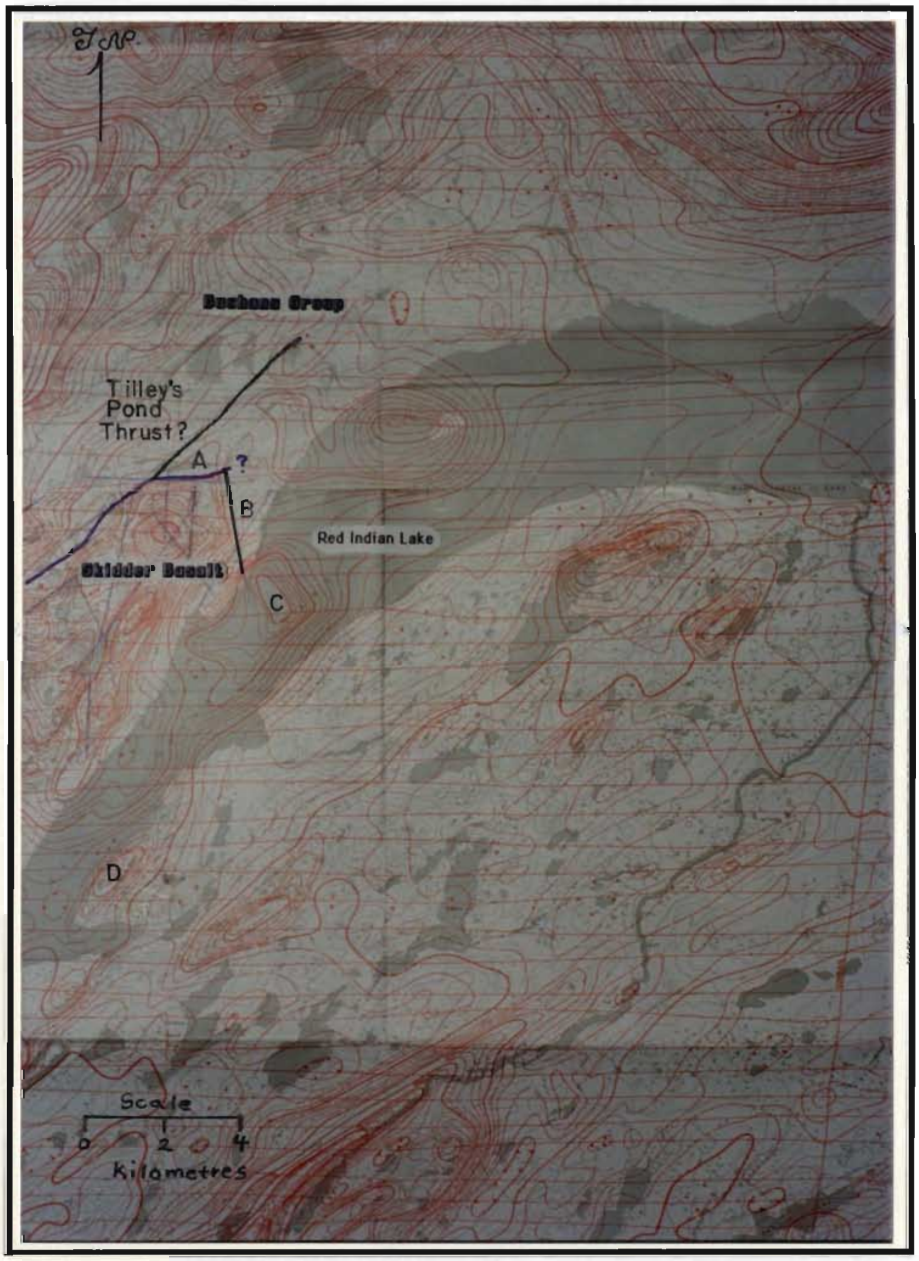

Figure 3-2: Photograph of part of the bottom portion of GSC Aeromagnetic Map 177G (Buchans, NTS 12A/15, Scale 1:63,360), and part of the top portion of GSC Aeromagnetic Map 187G (Lake Ambrose, NTS 12A/10, Scale 1:63,360). Note that rocks of the Skidder Basalt have a higher magnetic susceptibility than those of the Buchans Group to the north, and higher than most rocks of the Victoria Lake Group, which outcrops to the southeast of Red Indian Lake.

called the Skidder Basalt. As indicated below and in Chapters 4 and 5, the Skidder Basalt probably represents the upper portion of a now dismembered ophiolite.

The Skidder Basalt has not been dated either paleontologically or radiometrically. However, the Annieopsquotch Complex to the south and other ophiolite sequences in Newfoundland are Arenigian in age as indicated by U-Pb in zircon radiometric dates reported by Dunning (1984) and by Dunning and Krogh (1985). A similar age is assumed for the Skidder Basalt.

3.2 Regional Setting

The Skidder Basalt forms part of the Dunnage Zone (Williams, 1979) or Dunnage Terrane (Williams and Hatcher, 1982; 1983) of central Newfoundland. The Dunnage Zone comprises: Cambro-Ordovician ophiolitic rocks and Ordovician island arc sequences deposited during the early opening and closing of the Iapetus Ocean (Dean, 1978; Williams 1979); and post-closure Silurian caldera-related volcanic and volcaniclastic rock sequences (Coyle and Strong, 1987). The ophiolitic rocks and island arc sequences are overlain by Devonian to Carboniferous terrestrial sedimentary rocks and intruded by Ordovician to Carboniferous intrusive rocks.

3.2.1 Surrounding rock units and contact relationships

The Skidder Basalt is bounded to the north and northwest by the early-Middle Ordovician (Nowlan and Thurlow, 1984; Dunning, 1986; Dunning et al., 1987) Buchans Group (Unit 3, Figure 3-1). Thurlow (1981a) and Thurlow and Swanson (1981) report the Buchans Group to be a calc-alkaline suite of volcanic and volcaniclastic rocks of island arc affinity. However, the dominantly bimodal (basalt-rhyolite) nature of the Buchans Group led Kirkham (1987) to suggest that rocks of the Group were formed during a period of tectonic extension accompanying arc rifting and dismemberment after subduction-related calc-alkaline volcanism had ceased. Kirkham and Thurlow (1987) use the similarities of

the Buchans Group rocks and related sulphide deposits to those in the Kuroko area of Japan to further suggest that the Buchans Group was possibly formed in a submarine resurgent caldera tectonic environment. They point out that this provides an appropriate environment of formation for the debris flows which incorporate the MacLean channel transported sulphide ores (Binney, 1987).

Calon and Green (1987), McClay (1987) and Thurlow and Swanson (1987) envisage the Buchans Group as being a thrust belt composed of a complex array of thrust-related duplex structures and related antiformal stacks that have resulted from south to southeasterly directed thrusting sometime between the Middle Ordovician and the Middle Silurian (Kirkham, 1987). Having recognized the greater structural complexity of the Buchans Group, Thurlow and Swanson (1987) introduced a more simplified stratigraphy for the Buchans area removing the former division of the Buchans Group into upper and lower subgroups and consolidating the stratigraphic sequences into five formations.

Rocks of the Lundberg Hill Formation (Thurlow and Swanson, 1987), lowermost of the Buchans Group and formerly the Wiley's Prominent Quartz Sequence (Thurlow and Swanson, 1981), occur immediately to the north of the Skidder Basalt. Lithologies include: quartz-feldspar-phyric felsic pyroclastic rocks (outcrop sample location S 63, Figure 3-3; unit 5, Figure 3-4); massive and pillowed basalts (unit 6, Figure 3-4); and lithic arkose, aquagene tuff breccia, feldspathic tuffs, tuffaceous wacke, siltstone and cherty mudstone (unit 7, Figure 3-4).

The contact between the Buchans Group and Skidder Basalt was not observed in the field by the author since areas proximal to the contact that were traversed by him are covered by glacial drift. On Figure 3-4 the northwestern contact between the Skidder Basalt and the Buchans Group is shown to be a thrust fault; possibly a continuation of the Tilley's Pond thrust fault (Figure 3-2) (Thurlow and Swanson, 1987). A thrust fault contact is considered plausible on the basis of similar structures recognized elsewhere in the Buchans area (Thurlow and Swanson, 1987). The assumed thrust fault follows a

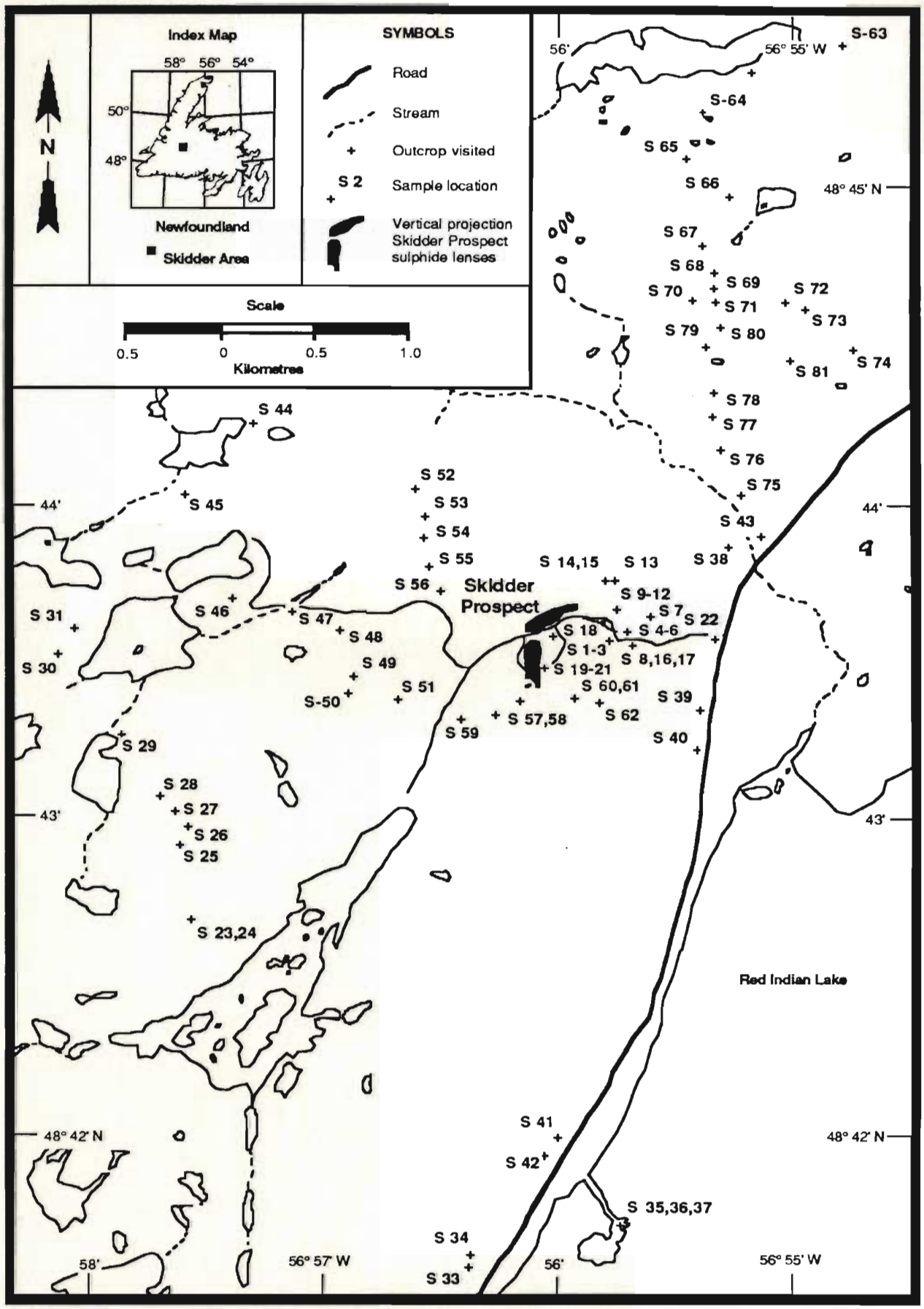

Figure 3-3: Sample location map, Skidder area.

LEGEND

ORDOVICIAN

BUCHANS GROUP

Lundberg Hill Formation (Thurlow and Swanson, 1987)

7 Lithic arkose, aquagene tuff-breccia, feldspathic tuffs; minor interbedded siltstone (Thurlow and Swanson, 1981;1987)

6 Massive and pillowed basalt (Thurlow and Swanson, 1981;1987)

5 Quartz-feldspar-phyric dacitic pyroclastic rocks (Thurlow and Swanson, 1981;1987)

SKIDDER BASALT

Pillowed and massive basalt; pillow breccia; lesser diabase dykes, gabbro, trondhjemite, mafic tuff and jasper

4 Trondhjemite

3 Pillowed and massive basalt having Zr concentrations ≥ 85 ppm

2 Pillowed and massive basalt containing Zr > 50 < 85 ppm; includes undivided Skidder Basalt

1 Pillowed and massive basalt having Zr concentrations ≤ 50 ppm

SYMBOLS

Road

Stream

Outcrop visited +

Geological unit; contacts approximate or assumed

Diabase dyke dk

Strike and dip of pillows:
(tops known, inclined; dip unknown) 70°
(tops unknown, inclined; dip unknown) 70°

Bedding:
(tops known, overturned) 70°
(tops unknown, inclined) 80°

Foliation:
(inclined, dip unknown) 80°

Anticline:
(location approximate, assumed) ?

Syncline

Thrust fault (?)
(assumed dip in direction of teeth) ?

Vertical projection of Skidder Prospect sulphide lenses

Legend and symbols to accompany Figure 3-4

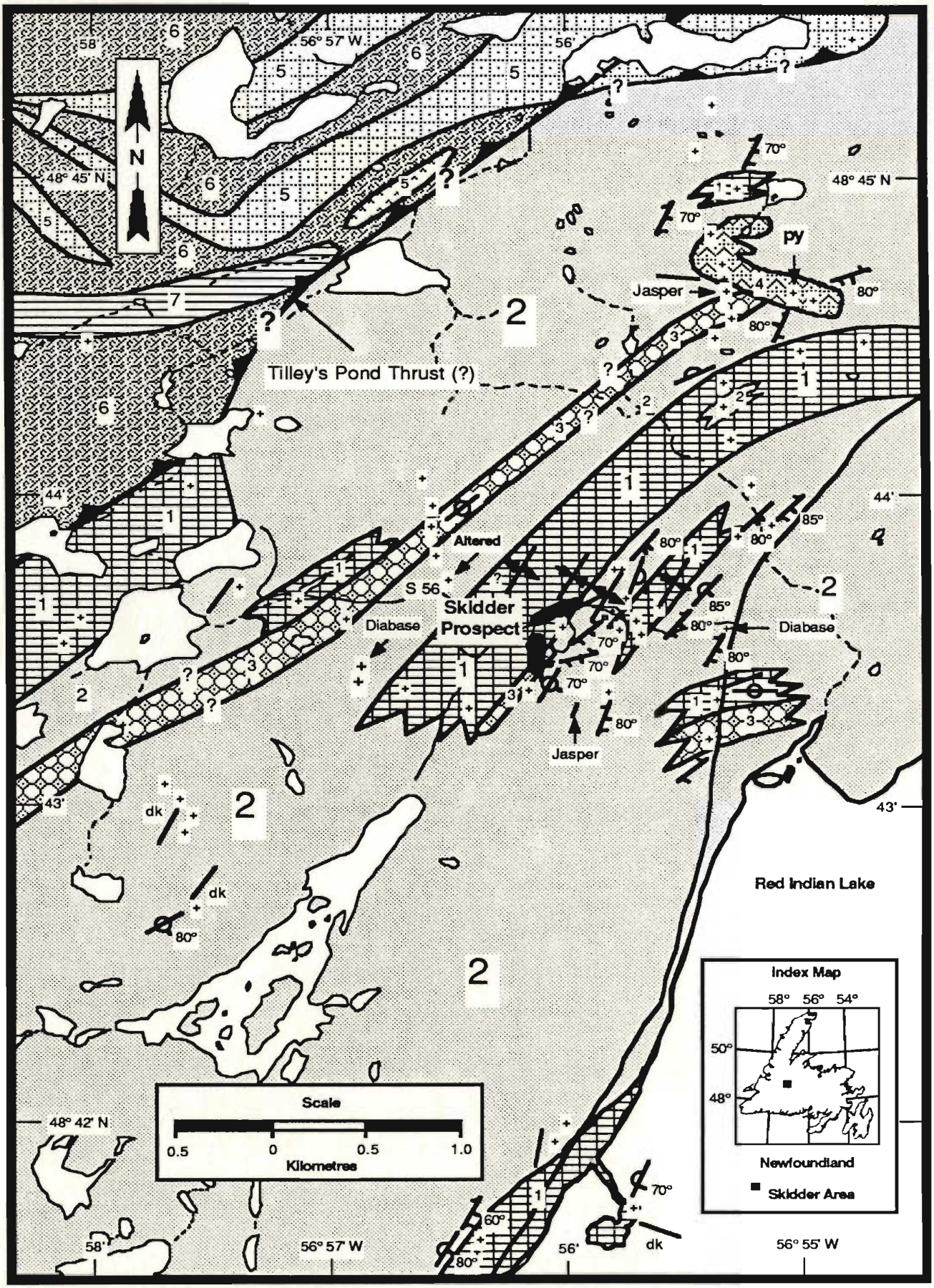

Figure 3-4: Geological compilation map, Skidder area. Legend and symbols on facing page.

northeasterly trending lineament shown both topographically and by regional magnetic susceptibility contrasts (Figure 3-2) (Geological Survey of Canada, 1954a; 1954b; 1968).

As shown on Figure 3-2 an easterly trending lineament (lineament A) and a north-northwesterly trending lineament (lineament B) mark the north and east contacts between the area of high magnetic susceptibility suggested to be underlain by Skidder Basalt rocks and the area of low magnetic susceptibility possibly indicative of Buchans Group rocks. The geometry of lineament "A" in relationship to the possible extension of the Tilley's Pond thrust fault is consistent with stacking of thrust slices in a manner similar to that suggested for the Buchans Group to the north (Thurlow and Swanson, 1987). Lineament "A" possibly represents a thrust fault related to southerly directed thrust faulting and along which a slice of Buchans Group rocks have been thrust over rocks of the Skidder Basalt. The Tilley's Pond fault possibly represents a thrust fault structurally higher than that suggested to be represented by lineament "A". It is possibly related to subsequent southeasterly directed thrusting which has thrust Buchans Group rocks over the Skidder Basalt and over other Buchans Group rocks in lower structural slices including those structurally above Lineament "A" (cf. Thurlow and Swanson, 1987). Lineament "B" may represent a high angle tear fault (cf. Thurlow and Swanson, 1987). Rocks in some areas beneath Red Indian Lake such as in area "C" on Figure 3-2 have a high magnetic susceptibility and in this way are similar to the Skidder Basalt. Assuming that the area of high magnetic susceptibility labelled "C" on Figure 3-2 is underlain by Skidder Basalt, the suggested fault represented by lineament "B" would have a right lateral displacement of 2.5 km.

Rocks in the Harbour Round area on the southeastern shore of Red Indian Lake also have a high magnetic susceptibility (area "D" on Figure 3-2). Rocks underlying area "D" (unit 5a, Figure 3-1) include pillow basalts, mafic pillow breccias and interpillow chert; geochemically they have 1-1.5% TiO_2 and 100-150 ppm Zr (B.F. Kean, personal communication 1988). These rocks are thus geologically and, on the basis of limited

information, geochemically similar to the Skidder Basalt (cf. Chapter 5). Kean and Jayasinghe (1980) included units 5a and 5b (Figure 3-4) into one unit which they considered to be part of the Buchans Group. The contact between unit 5 and bedded siltstone and chert of the Harbour Round Formation (unit 4, Figure 3-1) is suggested by Kean and Jayasinghe (1980) to be conformable in the Harbour Round area but faulted elsewhere. However, B.F. Kean (personal communication, 1988) suggests that the contact between the two units in the Harbour Round area is most probably a fault also. The Harbour Round Formation conformably overlies mafic flows, pillow lavas, mafic pyroclastic rocks (unit 2a, Figure 3-1) and felsic pyroclastic rocks (unit 2b, Figure 3-1) of the pre-Caradocian Victoria Lake Group (Kean, 1977; Kean and Jayasinghe, 1980).

To the west, the Skidder Basalt is intruded by massive to moderately foliated granodiorite which contains many small mafic to ultramafic fragments (Whalen and Currie, 1983; 1987) (unit 8, Figure 3-1). These and similar rocks in the area, e.g. the Hungry Mountain Complex (unit 6, Figure 3-1) to the northwest of the Skidder Basalt, and mafic and ultramafic inclusion-bearing tonalites (unit 7, Figure 3-1) exposed to the southwest, are suggested to be post-ophiolite intrusive suites (Dunning, 1984; Whalen and Currie, 1987). Dunning (1984) suggests that the tonalites were produced by partial melting of imbricated and partially subducted oceanic crust but with a component of Grenvillian continental crust or derived sediments; the latter is indicated by the presence in the tonalites of residual zircons having an age of 1400 Ma.

To the south, the Skidder Basalt is unconformably overlain by brown, red and minor grey conglomerates and sandstones of the Carboniferous Shanadithit Formation (Unit 15, Figure 3-1) (Kean, 1978; Kean and Jayasinghe, 1980).

3.2.2 Regional synthesis

As suggested above, the Skidder Basalt probably represents the upper portion of a now dismembered ophiolite. Dunning (1984) proposes that a number of ophiolitic

fragments (including units 1b and 1c and probably much of unit 1 on Figure 3-1) exposed from Buchans to the southwest tip of Newfoundland were once part of a continuous sheet of oceanic crust (cf. Church and Stevens, 1971). He suggests that the slab of oceanic crust was "systematically decoupled from mantle lithologies along the layered critical zone and emplaced over the partially subducted continental margin". The tonalitic rocks (unit 7 and possibly unit 8, Figure 3-1) which now completely surround small ophiolitic fragments and partially surround the larger are considered by Dunning (1984) to have been produced by partial melting of a "mixed package of subducting rocks, including oceanic crust, Fleur de Lys-type sediments and continental crust..." that "intruded and, in some cases, engulfed and disrupted the ophiolitic rocks". Stewart (1984); Colman-Sadd and Swinden (1984); and Wilton (1985) cite various types of evidence to suggest that much or even all of the Dunnage zone may be allochthonous.

3.3 Rock Types

The Skidder Basalt comprises a sequence of mafic pillow lava, pillow breccia and massive flows plus lesser diabase dykes, gabbro, mafic pyroclastic rocks and chert. The rocks are altered as indicated by the presence of secondary calcite, epidote and ubiquitous chlorite. Secondary minerals fill vesicles, irregular vugs, fractures and intergranular spaces. In places, they partially to completely replace primary minerals throughout the rock.

On Figure 3-4, rocks of the Skidder Basalt have been subdivided into three types to show the distribution, in the Skidder area, of basalts of different composition based on their Zr concentrations. The types are low-Zr basalts (≤ 50 ppm), intermediate Zr basalts (50-85 ppm), and high Zr basalts (> 85 ppm). Although there is no implication that rocks comprising these various subdivisions have different source regions or are of otherwise consistently different character, they are distributed as coherent clusters on Figure 3-4 (see Chapter 5).

3.3.1 Mafic rocks having Zr concentrations ≤ 50 ppm

Approximately one third of the analyzed mafic outcrop samples, which include massive and pillowed basalt, pillow breccia and diabase dykes, have Zr concentrations below 50 ppm (see Chapter 5). These low-Zr mafic rocks occur in the northwestern and southern portions of the area mapped and in the vicinity of the Skidder Prospect (Figure 3-4). About two thirds of the low-Zr lavas show well developed close-packed pillow structures. Pillows are typically less than 500 cm across but locally are up to 1 m in diameter. They are round but irregular in cross-section. Interpillow material, typically hyaloclastite, is generally more chloritic than that making up the pillows themselves. In some areas small irregular jasper bodies fill pillow interstices.

The low-Zr basalts, both pillowed and massive, are light green and are fine- to medium-grained. An estimated 25 per cent of them are amygdaloidal. The amygdules which are filled by calcite and to a lesser extent by epidote, quartz or chlorite are typically 2-4 mm in diameter and make up less than 10 per cent of the rock.

Some pillows contain light grey varioles, 3-6 mm in diameter, within a green, chloritic matrix (Figure 3-5). In general, these pillows have a 2-3 cm-thick, chlorite-rich, non-variolitic outer rim. The varioles are typically 3-4 mm in diameter, are individually distinct in outer portions of the pillow but coalesce to form a continuous mass in pillow cores. Smaller variolitic pillows (< 20 cm in diameter) generally do not have coalesced cores (Figure 3-6).

3.3.2 Mafic rocks having Zr concentrations of 51-85 ppm

About one half of the mafic outcrop samples analyzed have Zr concentrations between 51 and 85 ppm (Chapter 5). Close-packed pillow lava comprise about one half, massive flows approximately one quarter, pillow breccia about 10% and mafic dykes about 15% of these intermediate-Zr mafic rocks. They occur throughout the Skidder area (Figure 3-4).

Figure 3-5: Variolitic pillow lava, sample location S 35 (Figures 3-3 and 3-4).

Figure 3-6: Small variolitic pillow showing incomplete coalescence of varioles in its centre, sample location S 35 (Figures 3-3 and 3-4).

The rocks are medium green and fine- to medium-grained. Locally the massive flows have been auto-brecciated. Pillows are similar in size and outline to those of the low-Zr basalts. However, none of the intermediate-Zr pillowed flows observed in outcrop are variolitic. Pillow interstices are filled by chlorite-rich hyaloclastite and, in places, irregular jasper bodies. About one quarter of the flows are amygdaloidal; amygdules are filled by calcite and lesser epidote, chlorite or quartz.

Pillow breccias include broken pillow breccia (Carlisle, 1963) consisting of angular basaltic fragments within a chloritic and, in some places, epidote-rich matrix (Figure 3-7). Other pillow breccias are more characteristic of isolated pillow breccia (Carlisle, 1963). These consist of rounded "mini-pillows" 5-20 cm in diameter that occur within a darker green, more chloritic, hyaloclastite matrix. The matrix characteristically comprises 30 to 60 per cent of the rock.

Calcite, epidote and chlorite fill open spaces as well as intergranular areas throughout the rock. In addition, fibrous actinolite rosettes occur as fracture fillings in basalts exposed on Halfway Mountain in the vicinity of rock sample locations S 23 to S 28 (Figures 3-3 and 3-4).

3.3.3 Mafic rocks having Zr concentrations > 85 ppm

About 15% of the mafic outcrop samples analyzed have Zr concentrations > 85 ppm (Chapter 5). About 50% of these high-Zr mafic rocks consist of close-packed pillow lava, the remaining 50% being massive flows. High-Zr mafic rocks outcrop northwest and immediately south of the Skidder Prospect as well as along the road in the eastern portion of the Skidder area (Figure 3-4).

The rocks are medium to dark green-grey and fine to medium grained. Pillows are subrounded and about 0.5-0.75 m across. About one half of the flows contain calcite-filled amygdules; in a few areas the amygdules are up to 2 cm across which is larger than those

Figure 3-7: Broken pillow breccia; located about 50 m northwest of sample location S 28 (Figures 3-3 and 3-4).

found in the lower-Zr mafic rocks. Calcite, epidote, chlorite and locally quartz fill open spaces as well as intergranular areas throughout the rock.

3.4 Mafic Intrusive Rocks

Diabase dykes occur in several areas (Figure 3-4) intruding both massive and pillow lava as well as pillow breccia (Figure 3-8). Samples S 37 and S 27A, two of four of the mafic dykes analyzed, have Zr concentrations of 30 and 32 ppm respectively. One of these low-Zr dykes, S 37, intrudes low-Zr mafic rocks but the other intrudes mafic rocks having intermediate Zr concentrations. The remaining two dykes have higher Zr concentrations (61 and 73 ppm) and intrude intermediate-Zr mafic rocks. The dykes are light to medium green, (higher-Zr dykes being darker), fine to medium grained and range in width from 20 cm to 1 m. The medium green, medium grained, intermediate-Zr diabase dykes (?) occur at sample locations S 22 and S 49 (See Figures 3-3 and 3-4). At both of these locations the contact of the diabase with adjacent rocks is not exposed.

Subophitic intergrowths of 2 mm-long plagioclase and chloritized, epidotized clinopyroxene are visible in hand specimens of some of the dykes. Ubiquitous chloritization and the presence of secondary calcite, epidote and, locally, quartz suggest that the dykes have been altered like the surrounding basaltic flows. Calcite- and, in one sample, quartz-filled amygdules are present in some of the dykes.

3.5 Mafic Pyroclastic Rocks

Mafic pyroclastic rocks in the Skidder area consist of medium green-grey tuffs. These tuffs have an overall massive appearance and are poorly bedded. Bedding can be seen on the weathered surface of a 0.5 m-thick unit in a well exposed outcrop on the shores of Red Indian Lake at sample location S 36 (Figure 3-9). However, on a fresh surface the tuff is indistinguishable from a massive flow.

Figure 3-8: Diabase dyke cutting broken pillow breccia, sample location S 27 (Figures 3-3 and 3-4).

Figure 3-9: Bedded mafic ash tuff showing "loading" features, sample location S 36 (Figures 3-3 and 3-4).

3.6 Chert

Jasper and red cherty siltstone fill pillow interstices in several areas. The interpillow jasper bodies are typically irregular in outline and conform to the shape of the open spaces. In addition, two larger jasper units each having a minimum strike length of 10 m have been mapped. One of the units, about 25 cm thick, is interlayered with massive basalt immediately south of the Skidder Prospect (Figure 3-4). The second outcrops in the northeastern portion of the area shown on Figure 3-4 at sample location S 70 (Figures 3-3 and 3-4). It is about 2 m thick and occurs at the contact between basaltic rocks to the south and a body of trondhjemite to the north (Figures 3-4 and 3-10). The large jasper units are typically brecciated and quartz veined. Quartz also fills areas between breccia fragments. Some of the fragments show discontinuous, convoluted layering.

3.7 Skidder Trondhjemites

A small body of trondhjemite outcrops about 2.5 km northeast of the Skidder Prospect (Figure 3-4). Discordant contacts suggesting intrusion of the trondhjemite into adjacent mafic rocks are exposed in some areas. However, as indicated above, a 1 m-thick unit of jasper marks the contact between the trondhjemite and basaltic rocks at one locality. The trondhjemite is light grey to light green, fine grained and massive.

Light grey-green, fine grained trondhjemite dykes intrude the Skidder Basalt in the immediate vicinity of the Skidder Prospect (see Chapter 6). Trondhjemite dykes also intrude altered mafic rocks at sample location S 73 near a pyrite-rich alteration zone at sample location S 72 located about 2.5 km to the northeast of the Skidder Prospect (Figure 3-3). The dykes, which are typically less than 5 m thick, strike approximately northeast and dip steeply to the southeast. In most areas the dykes are very fine grained and massive but in some areas they contain about 5 per cent feldspar phenocrysts which are typically 1 to 3 mm across. In many areas layering is present within 30 cm of the contact between the

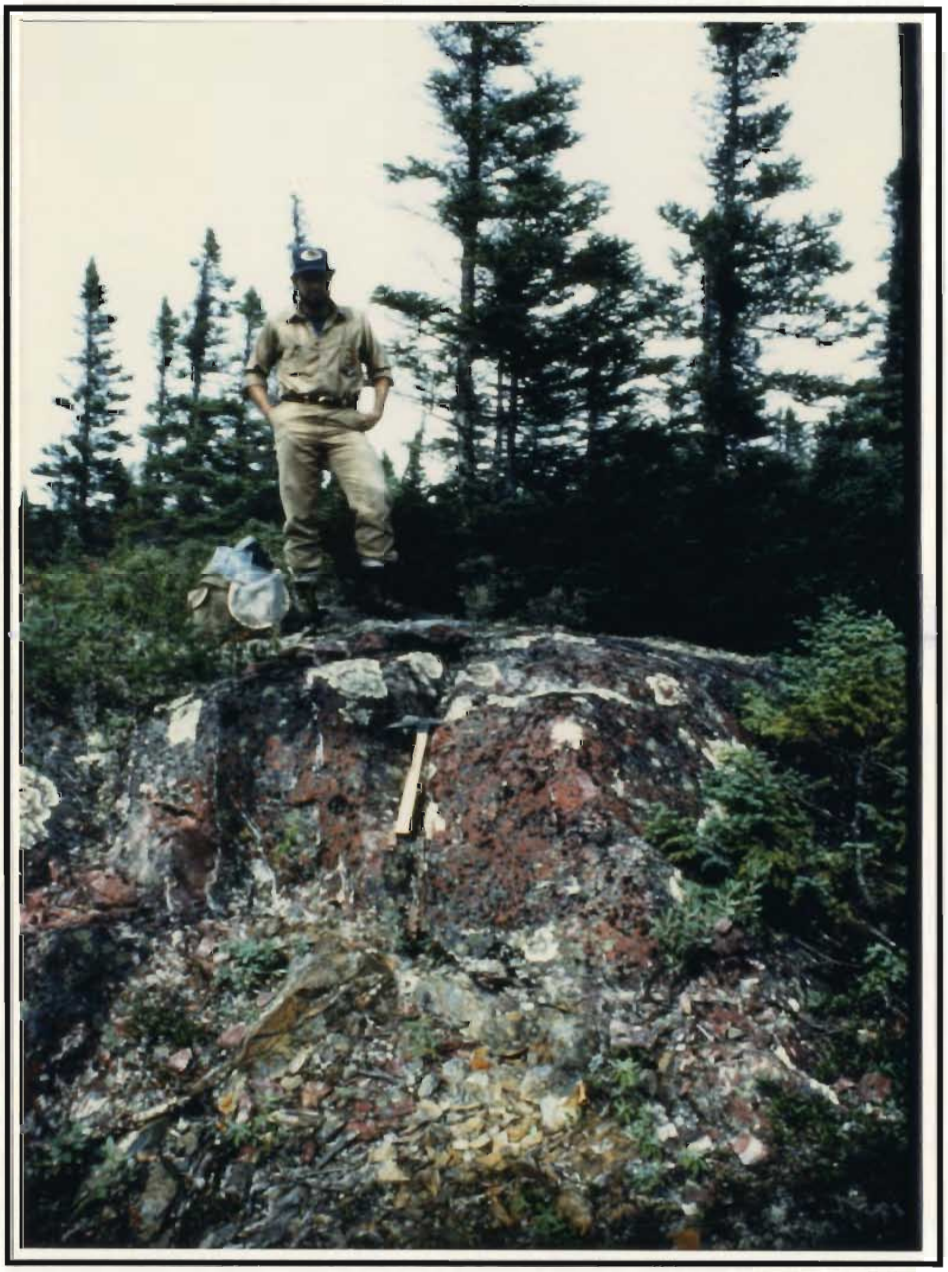

Figure 3-10: Thick jasper unit at sample location S 71 (Figures 3-3 and 3-4).

dykes and adjacent units. The layers, typically 0.5 to 1 cm wide and ranging in colour from light and dark grey-green to buff, parallel the dyke contact.

At sample location S 10 (Figures 3-3 and 3-4), angular 2-4 cm-long fragments of wall rock are incorporated into a trondhjemite dyke (Figure 3-11). The xenoliths are darker green and relatively more chloritic than the surrounding trondhjemite. Malpas (1979) reports the occurrence of similar partially resorbed xenoliths in trondhjemitic dykes of the Bay of Islands Ophiolite Complex.

3.8 Metamorphism

Rocks of the Skidder Basalt examined in outcrop typically contain mineral assemblages characteristic of spilites and greenschist facies metamorphism. Epidote, calcite and, in places, chlorite veins and amygdules are common. In addition, alteration of mafic minerals to chlorite is ubiquitous. Pervasive alteration of mafic minerals to epidote, particularly in the matrix to pillow breccia fragments, is also noted in some areas. Quartz veins and amygdules are common in the vicinity of the Skidder Prospect but are rare elsewhere.

3.9 Local Structures

Individual flow units as well as pyroclastic and sedimentary rocks in the western two thirds of the map area strike generally northeasterly and dip steeply to the southeast (Figure 3-4). However, in the easterly portion of the map area some units strike easterly and dip steeply to the south. Diabase dykes strike 025°-035° in most places. However, a dyke outcropping at sample location S 37 strikes 110°.

Foliations trend predominantly northeasterly but in a few localities a second foliation striking approximately 075° is present; the foliations dip steeply in all areas. Pillows, where suitable for determining stratigraphic tops, indicate northwest facing of units in most areas (Figure 3-12) except in the immediate vicinity of the Skidder Prospect

Figure 3-11: Trondhjemite containing several 2-3 cm-long mafic xenoliths, sample location S 10 (Figures 3-3 and 3-4).

Figure 3-12: Basaltic pillow lava at sample location S 7 looking northwest (Figures 3-3 and 3-4). The pillows indicate flow tops are to the northwest here.

where some indicate a southwest facing of units. Loading structures in a mafic tuff unit at sample location S 36 (Figures 3-3 and 3-4) indicate northwest facing of units in that area.

Reversals in facing direction of pillows in the Skidder Prospect area (Figure 3-4) and the local geology of the Skidder Prospect itself (see Chapter 6) suggest folding about possible northeast trending axes in the area. Fold axes shown on Figure 3-4 are assumed on the basis of reversals in pillow facing direction, their exact trend is unknown. Flexuring of the trend of units from northeasterly to easterly in the eastern portion of the area shown on Figure 3-4 suggests late, large scale open folding about a north to northwest, steeply south-plunging axis.

Thurlow and Swanson (1987) indicate that thrust faults in the Buchans area propagated preferentially along earlier fault planes and that an anticlinal axis present at the surface of, and parallel to, the Ski Hill-Buchans River fault system was generated during thrusting. Similarly, folding in the vicinity of the Skidder Prospect may be related to southeastward compression related to the thrusting episode.

Several topographic lineaments are evident on aerial photographs of the Skidder area and many of these correspond to linear magnetic features. The linears strike in three dominant directions: northeasterly, northerly, and approximately northwesterly (Figure 3-13).

The northeast-trending topographic lineament (Number 1, Figure 3-13) which separates rocks of relatively high magnetic susceptibility to the southeast from less magnetic rocks to the northwest is suggested to mark the northwesterly contact of the Skidder Basalt and the Buchans Group as discussed in Section 3.2.1.

A second northeast-trending lineament (Number 2, Figure 3-13) passes through the Skidder Prospect and through a pyrite-rich zone about 2.5 km to the northeast at sample location S 72 (Figure 3-13).

This lineament may represent an "old" fracture zone which provided access for the intrusion of several trondhjemite dykes that occur in the vicinity of the Skidder Prospect

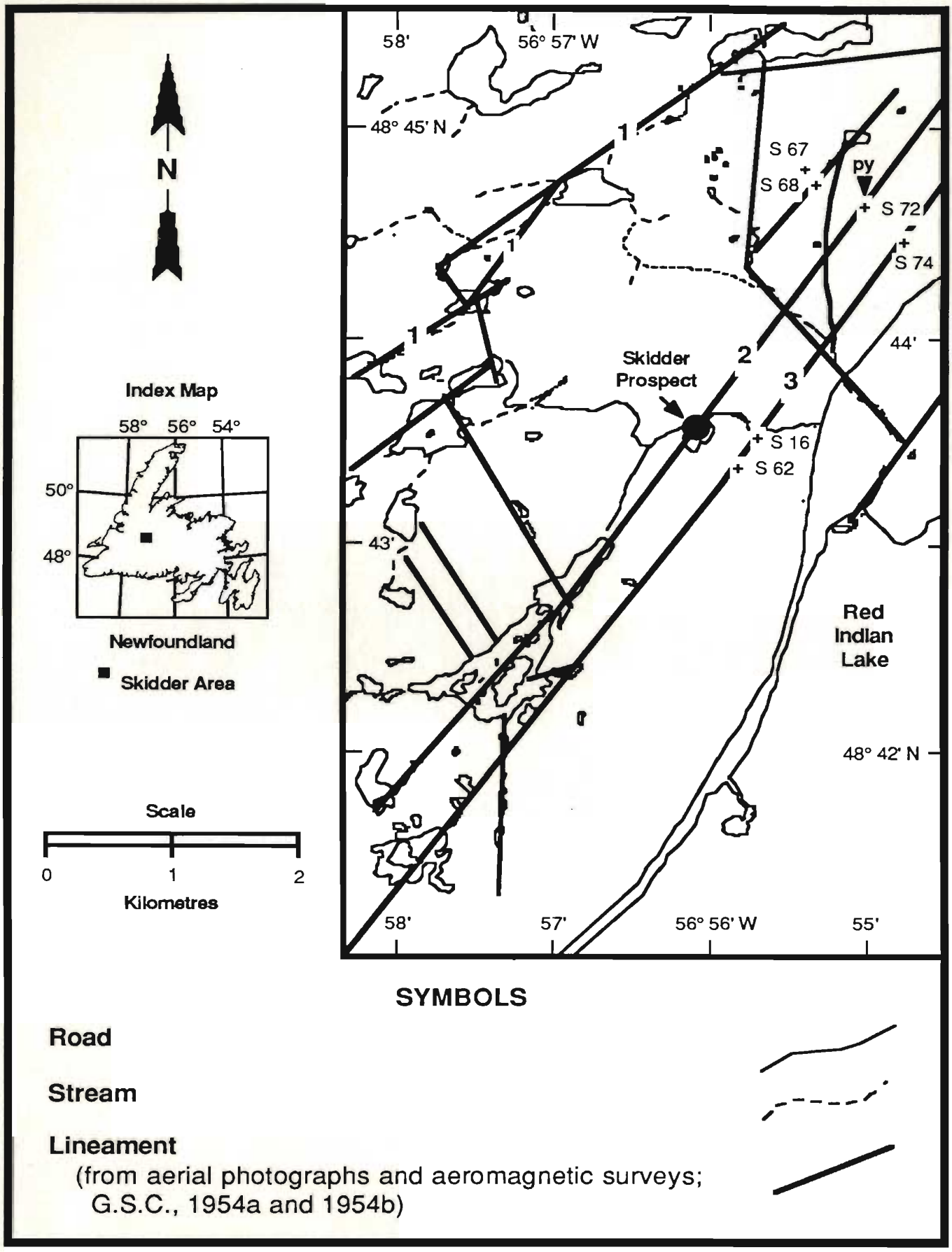

Figure 3-13: Lineaments in the Skidder area.

and near the pyrite-rich zone at S 72. It also may have provided a locus for upward migration of metal-bearing hydrothermal fluids that produced the intense alteration associated with the Skidder Prospect and the pyrite-rich zone at S 72.

The association of sulphide-rich zones and trondhjemites is not unique to the Skidder area for Malpas (1979) reports the occurrence of a small trondhjemitic stock in the vicinity of the Gregory Copper deposit in the Bay of Islands Ophiolite Complex.

The structural significance of the northeast-trending lineament present southeast of the Skidder Prospect (Number 3, Figure 3-13) is unknown but basalt samples collected along this lineament contain significantly higher concentrations of large ion lithophile elements (K, Rb and Ba) than other Skidder Basalt samples. This suggests that hydrothermal fluids may also have permeated along a possible fracture zone related to this lineament.

The structural significance of the north and north-northwesterly trending lineaments shown on Figure 3-13 is unknown. They may however be topographic expressions of high-angle tear faults like the north-northwesterly trending tear faults noted in the Buchans Group to the north (Thurlow and Swanson, 1987). Thurlow and Swanson (1987) relate these faults to south-southeasterly directed thrusting in the Buchans area.

Chapter 4

PETROGRAPHY AND MINERAL CHEMISTRY

4.1 Petrography of the Skidder Basalt

4.1.1 Introduction

In thin section, extrusive rocks of the Skidder Basalt are dominated by secondary mineral assemblages. In general, albitized plagioclase phenocrysts occur in an intergranular to intersertal groundmass of albite, chlorite, quartz, dense granular sphene, and variable amounts of subhedral to acicular opaque minerals. Primary clinopyroxene and chromite as well as secondary calcite, amphibole and epidote are constituents of some samples.

A geochemical subdivision of the Skidder basaltic rocks is used as a basis for the following petrographic descriptions, since differences in some of the basaltic compositions are reflected by differences in texture and mineral proportions. The geochemistry of the Skidder Basalt is discussed fully in Chapter 5.

4.1.2 Low-zirconium basalts (≤ 50 ppm)

Thin sections of low-Zr Skidder basalts are typically composed of secondary albite, chlorite and lesser quartz and sphene; amphibole, calcite and epidote are present in some sections. Primary magmatic minerals preserved in some samples include small amounts of subhedral chromite and relict clinopyroxene. Many of these rocks show textures characteristic of quenching, some are variolitic, and a few display intergranular or intersertal texture.

4.1.2.1 Quench-textured low-zirconium basalts

Table 4-1 shows the basalt types and gives a partial geochemical analysis and qualitative estimate of the abundances of common minerals in the low-Zr basalts.

Table 4-1: Petrographic table showing rock type, partial geochemical analysis and mineralogy of basaltic outcrop samples having Zr concentrations ≤ 50 ppm; samples not analyzed but of similar mineralogy and texture are also included

Key:	See Figures 3-3 and 6-1 for sample locations
	Mineral abbreviations: Ab-albite, Cpx-clinopyroxene, Cl-chlorite, Cc-calcite, Ep-epidote, Qz-quartz, Chr-chromite, Amph-amphibole, hm-hematite, py-pyrite
	Abundance of mineral relative to its average content in mafic rocks from the Skidder area: x-low, xx-medium, xxx-high
	See Appendix B for complete whole rock analyses and description of analytical methods

Sample Name	Rock Type	SiO_2 %	TiO_2 %	MgO %	Zr ppm	Ab	Cpx	Cl	Sphene	Cc	Ep	Qz	Chr	Opaques	Amph	Other Minerals and Comments
S 1A	Pillowed basalt					xx	xxx	xxx	xx			x				calcic plagioclase (?)
S 1B	Pillow basalt/Pillow breccia					xx		xxx	xx	xxx		x	xx			foliated
S 1C	Pillow basalt/Pillow breccia					x	?	xxx	xx	xxx		x	xx			variolitic
S 5	Pillowed basalt	42.4	0.7	4.2	33	xxx		xx	xx	xxx		x		xx		acicular opaques (xx)
S 6	Massive/Pillowed basalt					xxx		xx	xx	xx	xxx	x		xx		
S 7A	Pillowed basalt	47.8	0.7	6.2	38	xx		xx	xx	xxx	xxx	x				serpentine (?)
S 9A	Pillowed basalt	48.9	0.8	3.1	50	xxx		xx	xx	xxx		xx	xx	xx		
S 11	Pillowed basalt	48.0	1.1	5.0	47	xxx	x	xx	xx	xx	xx	x		xx		acicular opaques (xx)
S 30	Massive basalt	49.4	0.6	5.7	30	xxx	xx	xx	xx	xx	x	x	xx	x	xx	olivine pseudomorphs
S 31	Pillowed basalt	48.6	0.7	4.5	34	xx	?	xx	xx	xx		xx	xx	x	?	variolitic, spinel (?)
S 35A	Pillowed basalt	48.5	0.6	8.9	38	xx		xxx	xx	x	x	x	xxx	x	xxx	
S 35B	Pillowed basalt					x	x	xxx	xx		x	x	xx	x	xxx	variolitic
S 39	Pillowed basalt	50.6	0.8	7.4	50	xxx	xx	xx	xx		x	x		x	x	
S 45	Pillowed basalt	45.9	0.6	6.5	39	xx	xx	xx	xx	x	x	x		x	x	porphyritic
S 55A	Pillowed basalt					xx	?	xx	xx	xx		x	x	x	x	variolitic
S 55B	Pillowed basalt					xx	?	xx	xx	x		x	x	x	x	variolitic
S 59	Pillowed basalt	47.9	0.5	11.1	16	xx	xxx	xxx	xx		x	x	xx		xx	
S 66B	Massive basalt	53.6	0.9	4.4	41	xx	xx	xx	xx			x		xxx	xx	
S 80A	Feldspar porphyritic basalt					xx		xx	x	x		xx		xx		
S 81	Massive basalt	50.0	0.9	8.9	44	xx	xx	xx	xx	x		x				
	AVERAGE	48.5	0.7	6.3	38											

Albite is abundant in most sections; it occurs typically as randomly oriented laths usually less than 0.5 mm long, but in some sections (e.g. S 30), shows quench textures. Quench-textured albite occurs: as elongate 1 mm-long skeletal laths, in places grouped into fan-shaped (Figure 4-1) to radially aligned clusters (Figure 4-2); and as hollow rectangular "belt buckle"-shaped (cf. Lofgren, 1974) grains (Figure 4-3). Albite locally occurs as "open space" fillings. For example, chlorite-filled vugs in thin section S 80A contain several 1-2 mm-long albite laths that do not show quench-texture morphologies in contrast to albite elsewhere in the section.

Plagioclase other than albite has been identified in only one Skidder Basalt thin section, i.e. S 59 where it occurs as phenocrysts (?) partially altered to calcite and albite.

Clinopyroxene typically occurs as colourless to light brown, 0.5 to 1 mm-long elongate grains (Figures 4-4 and 4-5) that combine to form masses displaying "quench-texture" morphologies. Textures considered by Lofgren (1974) to be typical of quenching such as spherulitic, bow-tie, fan, plumose and axiolitic (Figure 4-6) morphologies are shown in several sections. Section S 59, for example, is dominated by elongate clinopyroxene throughout, which, in places, forms fan-shaped clusters. Thin section S 30 contains irregularly shaped areas dominated by tabular elongate axiolitic clinopyroxene accompanied by accessory sphene and intersertal chlorite. Clinopyroxene is partially to completely altered to amphibole or chlorite in some areas.

Amphibole occurs as elongated prismatic crystals or fibrous masses that partially surround or completely replace clinopyroxene grains. Textures characteristic of quenching of the now replaced clinopyroxene are preserved in places. For instance, 0.5 mm-long brown pleochroic radial plumose masses of amphibole (Figure 4-7) and intersertal chlorite are seen in quenched areas around amygdules. In other areas, amphibole comprises mat-like intergrowths preserving axiolitic or other quench-texture morphologies. Amphibole, in some places, is altered to talc or chlorite.

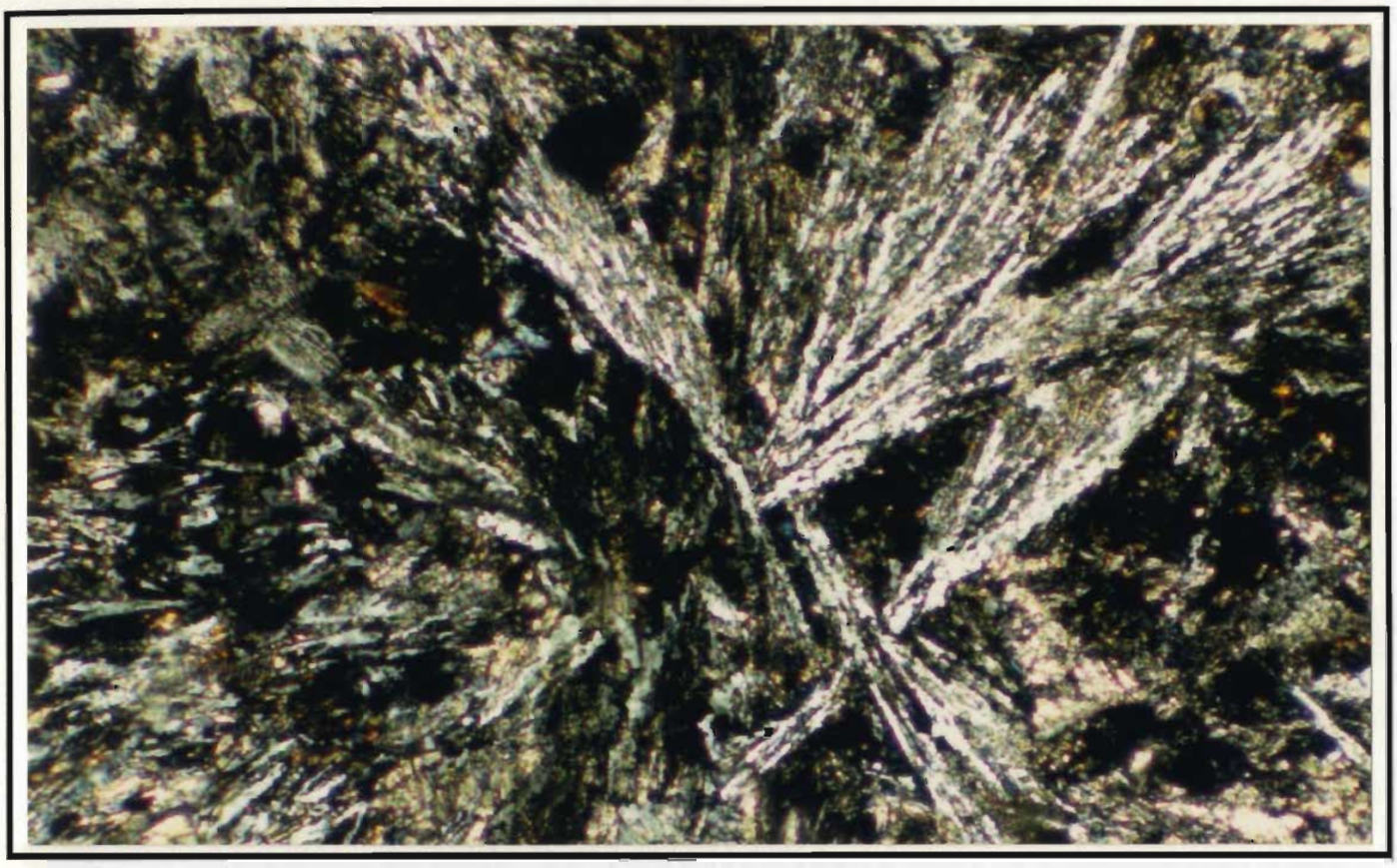

Figure 4-1: Quench-textured plagioclase showing fan-shaped to plumose morphologies (cf. Lofgren, 1974); thin section S 31, crossed nicols, 10 x. —— 0.2 mm ——

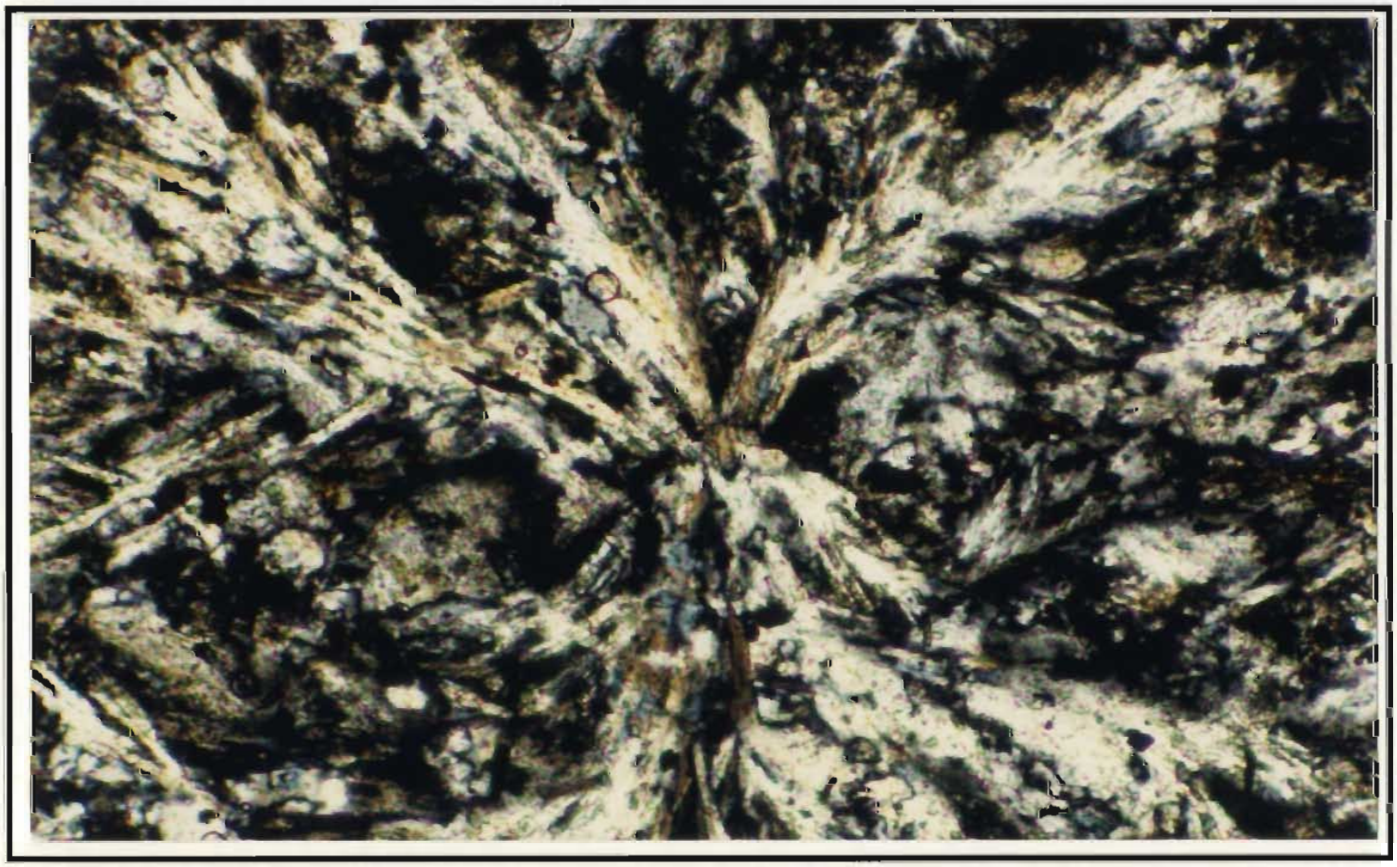

Figure 4-2: Spherulitic cluster of quench-textured plagioclase; thin section S 55B, crossed nicols, 10 x.
—— 0.2 mm ——

Figure 4-3: Quench-textured plagioclase showing "belt buckle" texture (cf. Lofgren, 1974); thin section S 30, crossed nicols, 10 x. —— 0.2 mm ——

Figure 4-4: Haphazardly distributed, elongate clinopyroxene grains; thin section S 30, plane polarized light, 10 x. —— 0.2 mm ——

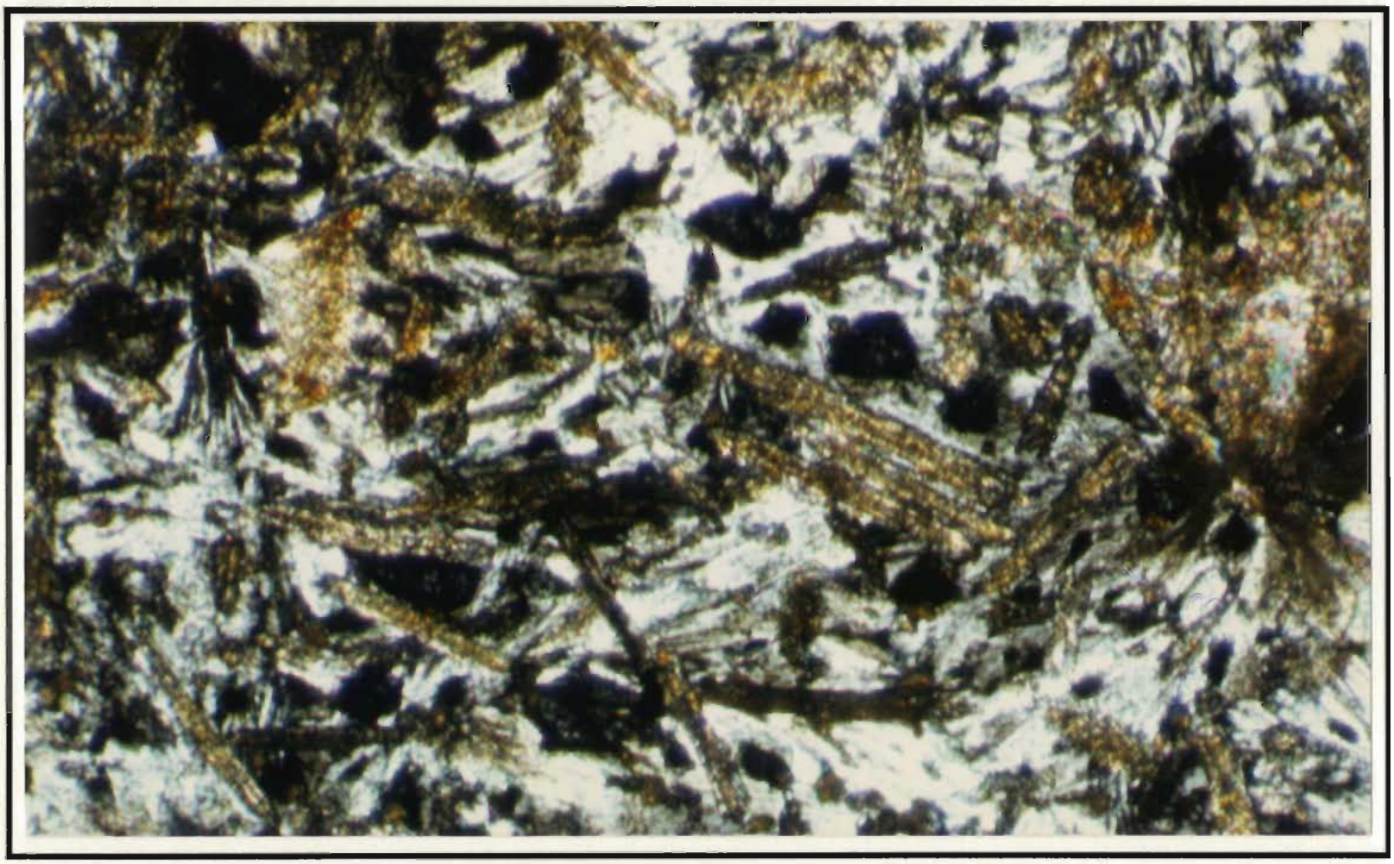

Figure 4-5: Haphazardly distributed, elongate clinopyroxene grains; thin section S 30, crossed nicols, 10 x. —— 0.2 mm ——

Figure 4-6: Quench-textured, axiolitic clinopyroxene (cf. Lofgren, 1974); thin section S 30, crossed nicols, 20 x. —— **0.1 mm** ——

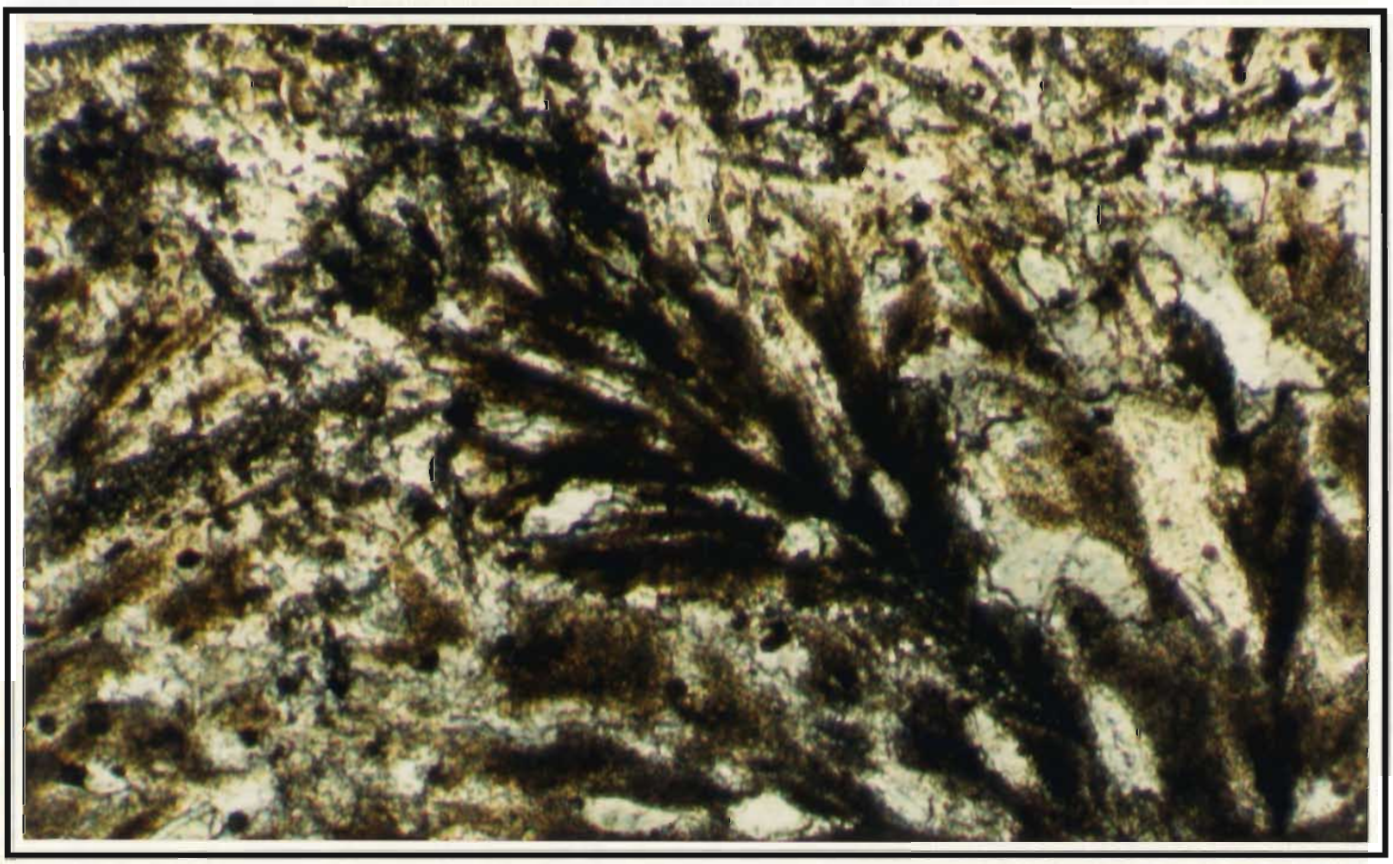

Figure 4-7: Plumose (cf. Lofgren, 1974) amphibole, probably after clinopyroxene; thin section S 30, plane polarized light, 10 x. —— **0.2 mm** ——

Sphene occurs as subhedral granules that, in places coalesce to form dense irregular masses. The grains are typically greyish brown under plane-polarized light and show internal-reflection effects under crossed nicols. Chromite occurs as opaque to brown translucent subhedral grains (Figure 4-8) typically less than 0.1 mm in diameter disseminated throughout the thin section. Chromite may also occur as inclusions in chlorite or calcite-filled areas that are pseudomorphic after olivine (Figure 4-9). Unidentified tiny subhedral opaque grains are disseminated throughout the samples.

Chlorite typically occurs as fine grained, light green pleochroic, anhedral masses intersertal to other minerals. It displays brown to anomalous blue interference colours. Secondary quartz fills fractures and vesicles; and in thin section S 35B, quartz fills spaces pseudomorphic after olivine (Figure 4-10). Quartz also occurs in the groundmass as anhedral grains intersertal to other minerals. Calcite occurs typically as irregular masses and as fracture fillings. In places it occurs with albite as a replacement product of plagioclase. Secondary epidote occurs as light olive green pleochroic, equant to prismatic grains which are 1.5 to 2 mm in length. Epidote may be distributed throughout the sample but most commonly fills vugs and fractures. In a few thin sections radially aligned needles of epidote occur.

4.1.2.2 Variolitic low-zirconium basalts

In the Skidder Basalt, varioles are defined by a greater abundance of albitized plagioclase and quartz which, in some sections, occur as radial growths around a common centre. The varioles differ considerably in detail however. Minerals that make up both variolitic and nonvariolitic portions of the sample typically display quench-texture morphologies.

Varioles in thin section S 35B are dominated by a haphazardly arranged network of elongate skeletal clinopyroxene (?) (amphibole-pseudomorphed clinopyroxene or olivine (?)) accompanied by interstitial quartz and albite (?). The intersertal material typically

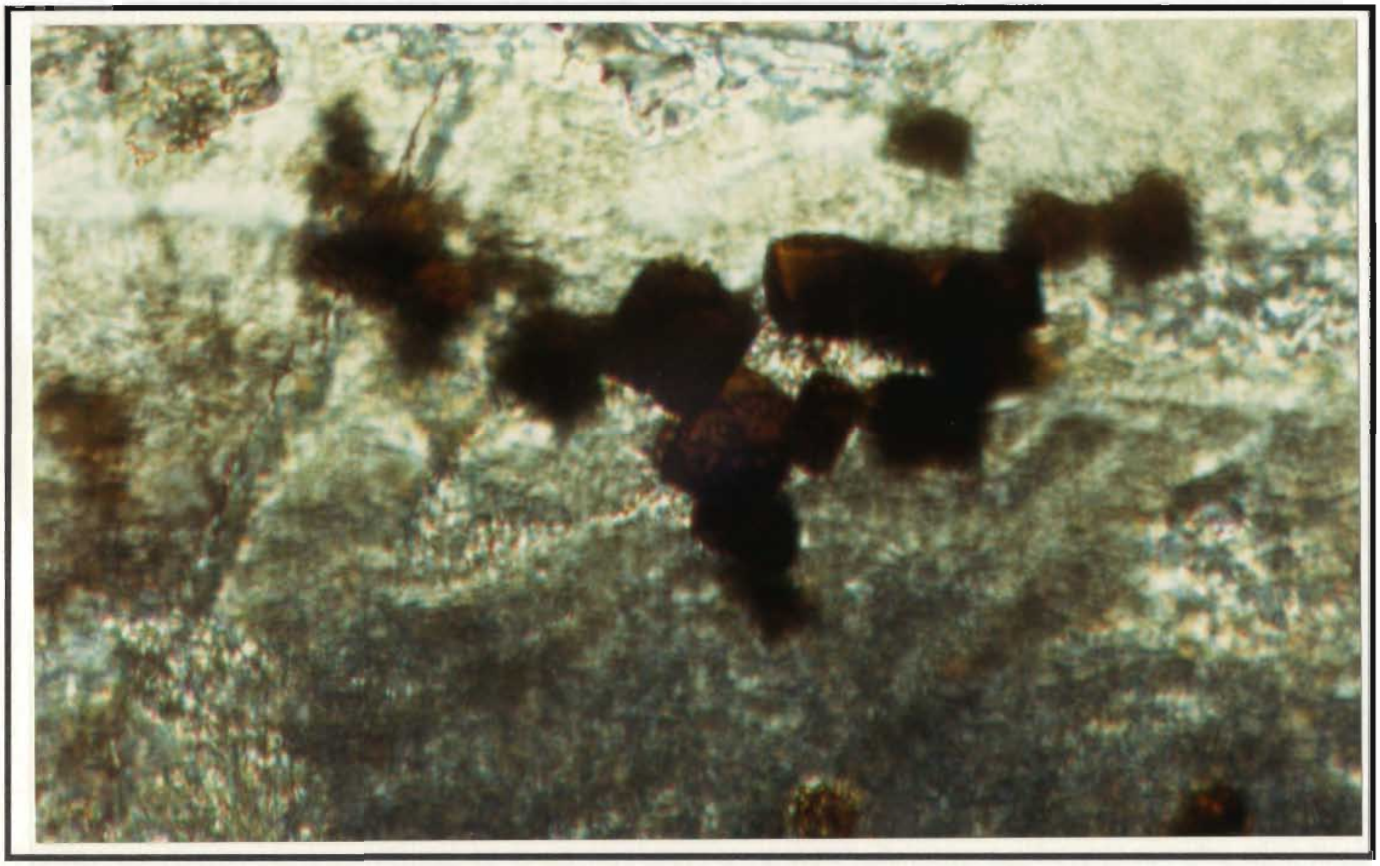

Figure 4-8: Subhedral, translucent brown grains of chromite; thin section S 30, plane polarized light, 50 x. —— 0.04 mm ——

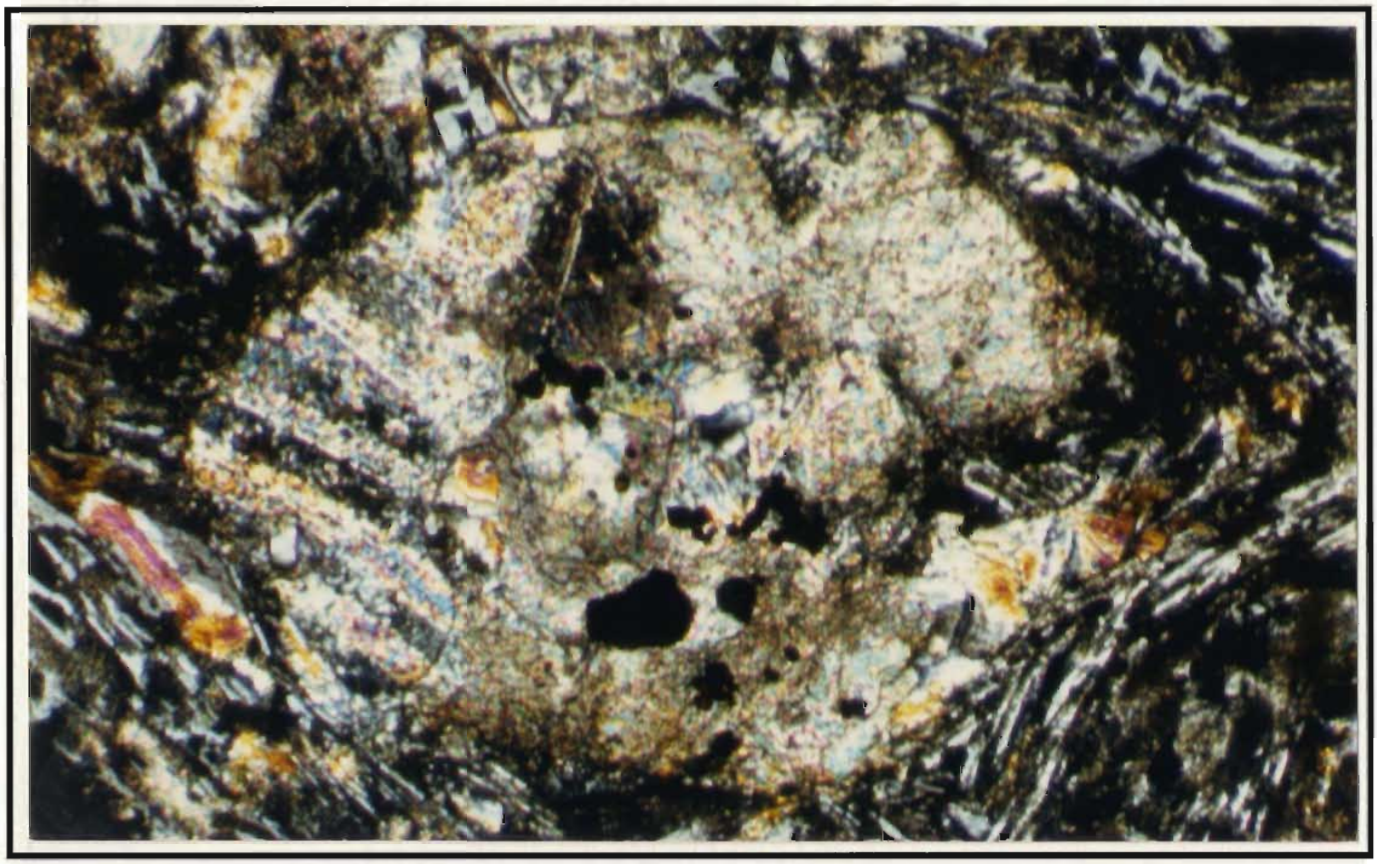

Figure 4-9: Calcite grains, pseudomorphic after olivine, note several subhedral chromite inclusions and one inclusion of magnetite (large opaque grain); thin section S 30, crossed nicols, 10 x.
—— 0.2 mm ——

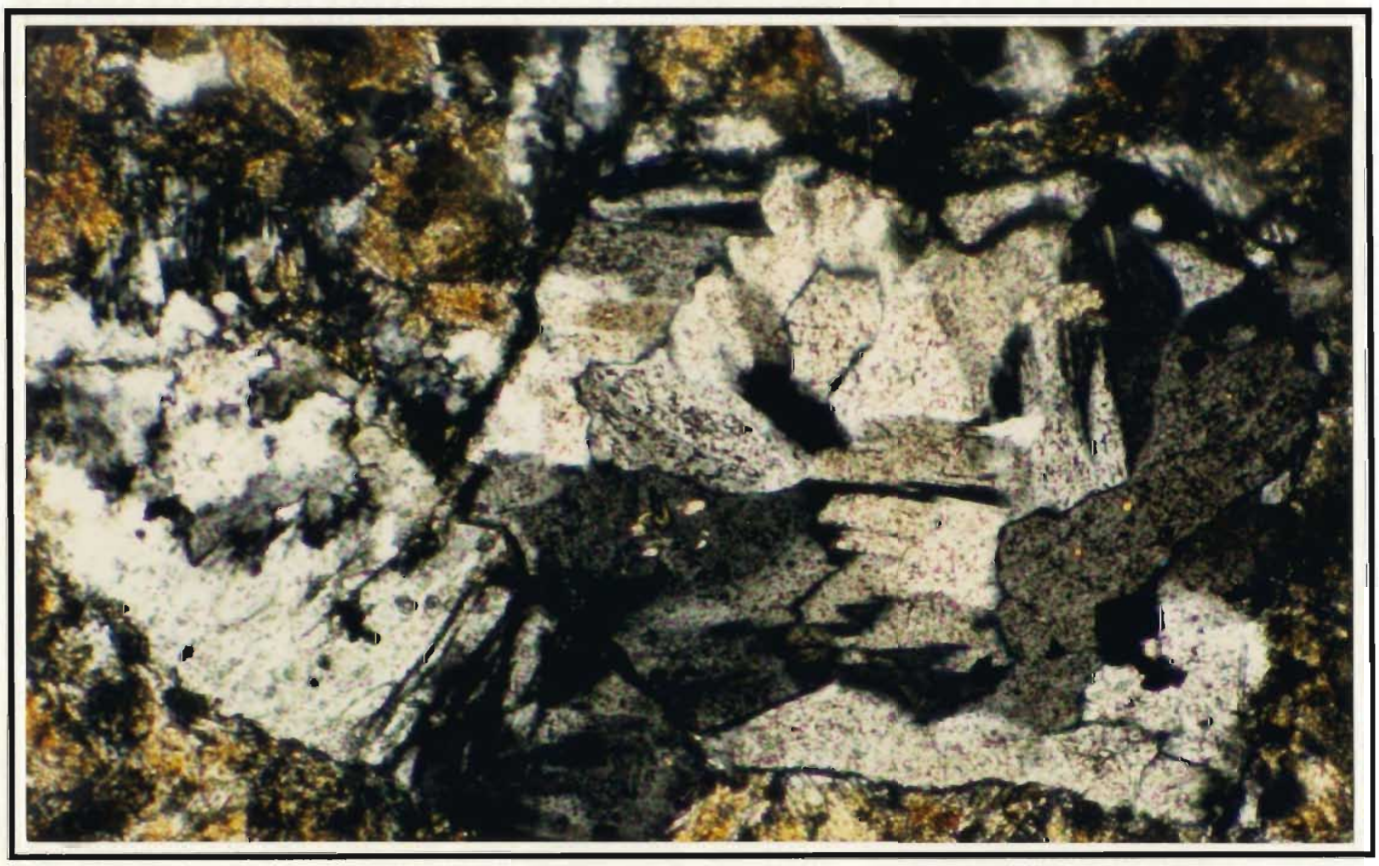

Figure 4-10: Quartz grains, pseudomorphic after olivine; thin section S 35B, crossed nicols, 10 x.
—— 0.2 mm ——

shows radial extinction and, in turn, imparts a radial extinction to the variole as a whole. Some varioles in thin section S 31 have a central area dominated by radial quartz or albite (Figures 4-11 and 4-12). Haphazardly arranged, elongate, skeletal grains similar to those in S 35B are present in S 31, however the grains in the latter sample have low birefringence and parallel extinction suggesting albite (?) may be pseudomorphing quenched olivine or clinopyroxene in this instance (Figures 4-13 and 4-14). In S 31 and to a lesser extent in S 35B, the elongate skeletal grains occur outside the varioles as well as inside and some crystals cross the boundary between variole and matrix (Figures 4-13 and 4-14). Varioles in thin section S 55A are composed of radially aligned, plumose to fan-shaped clusters of felsic material (albite (?) and quartz (?)) accompanied by ovoid chlorite-filled areas. Albitized plagioclase crystals (2 mm in length) form the core of a few of the varioles (Figure 4-15). Other varioles in this section have a central core of anhedral quartz, lesser chlorite and accessory sphene surrounded by an outer ring of radially aligned felsic material. In thin section S 66B varioles (?) 1 to 1.5 mm across are composed of clusters of elongate clinopyroxene grains haphazardly to roughly radially arranged about their centres. Lesser amounts of indeterminate felsic material fill the interstices. Thin section S 1C contains varioles having a central core of radially aligned albite and intersertal chlorite that is surrounded by an outer ring of secondary calcite (Figure 4-16).

Chlorite and lesser albite ± amphibole and/or clinopyroxene dominate the mineralogy of the matrix to the varioles. In thin section S 35B, matrix areas are composed predominantly of tiny clusters of axiolitic, fan-shaped, spherulitic or plumose 0.1 mm-long clinopyroxene (Figures 4-17 and 4-18), in places altered to amphibole. Accessory sphene and intersertal chlorite make up most of the remainder. In thin section S 31, the matrix to the varioles is dominated by skeletal albite which occurs as haphazardly oriented laths, or plumose, fan-shaped or spherulitic masses. Intricate patterns displayed by axiolitic or spherulitic albite (?) (replacing clinopyroxene (?)) are also present. Interstitial areas between grains are filled by chlorite. Matrix areas in thin section S 55B are filled

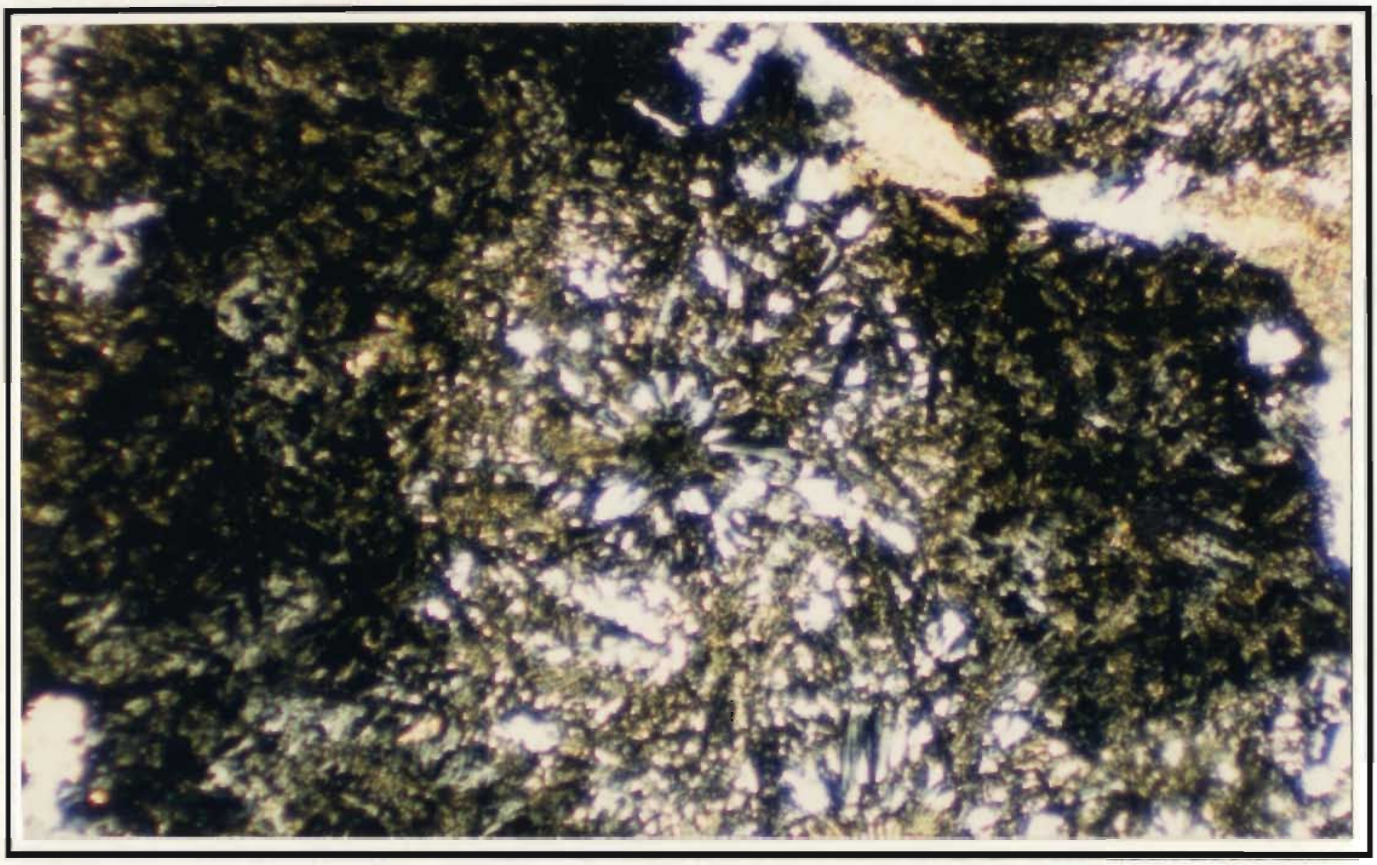

Figure 4-11: Variole having central core of radially aligned quartz or albite; thin section S 31, crossed nicols, 3.2 x. **— 0.5 mm —**

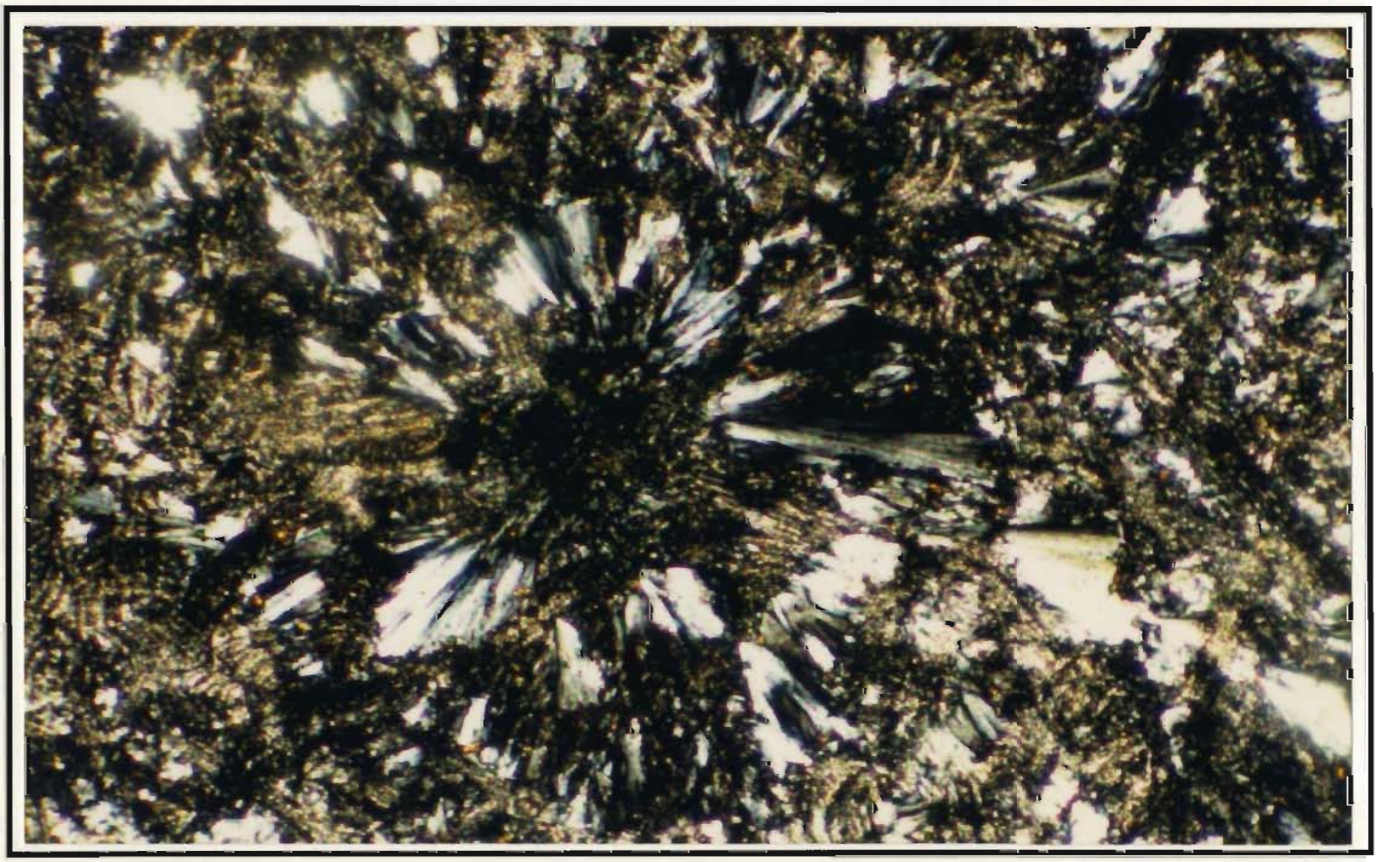

Figure 4-12: Expanded view of central portion of variole shown in Figure 4-11; thin section S 31, crossed nicols, 10 x. **—— 0.2 mm ——**

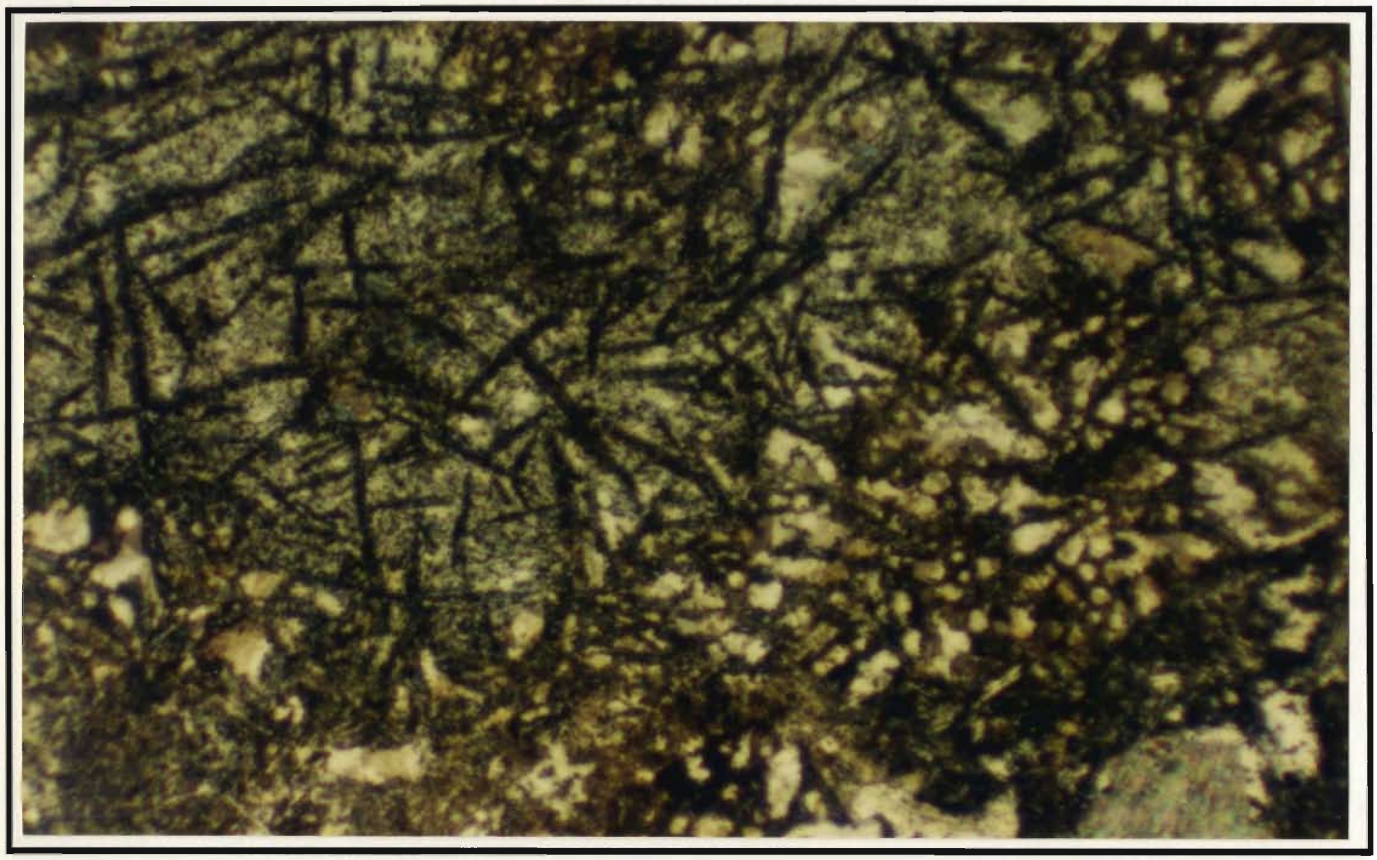

Figure 4-13: Haphazardly distributed, elongate grains of olivine or clinopyroxene pseudomorphed by albite (?); thin section S 31, plane polarized light, 3.2 x. **— 0.5 mm —**

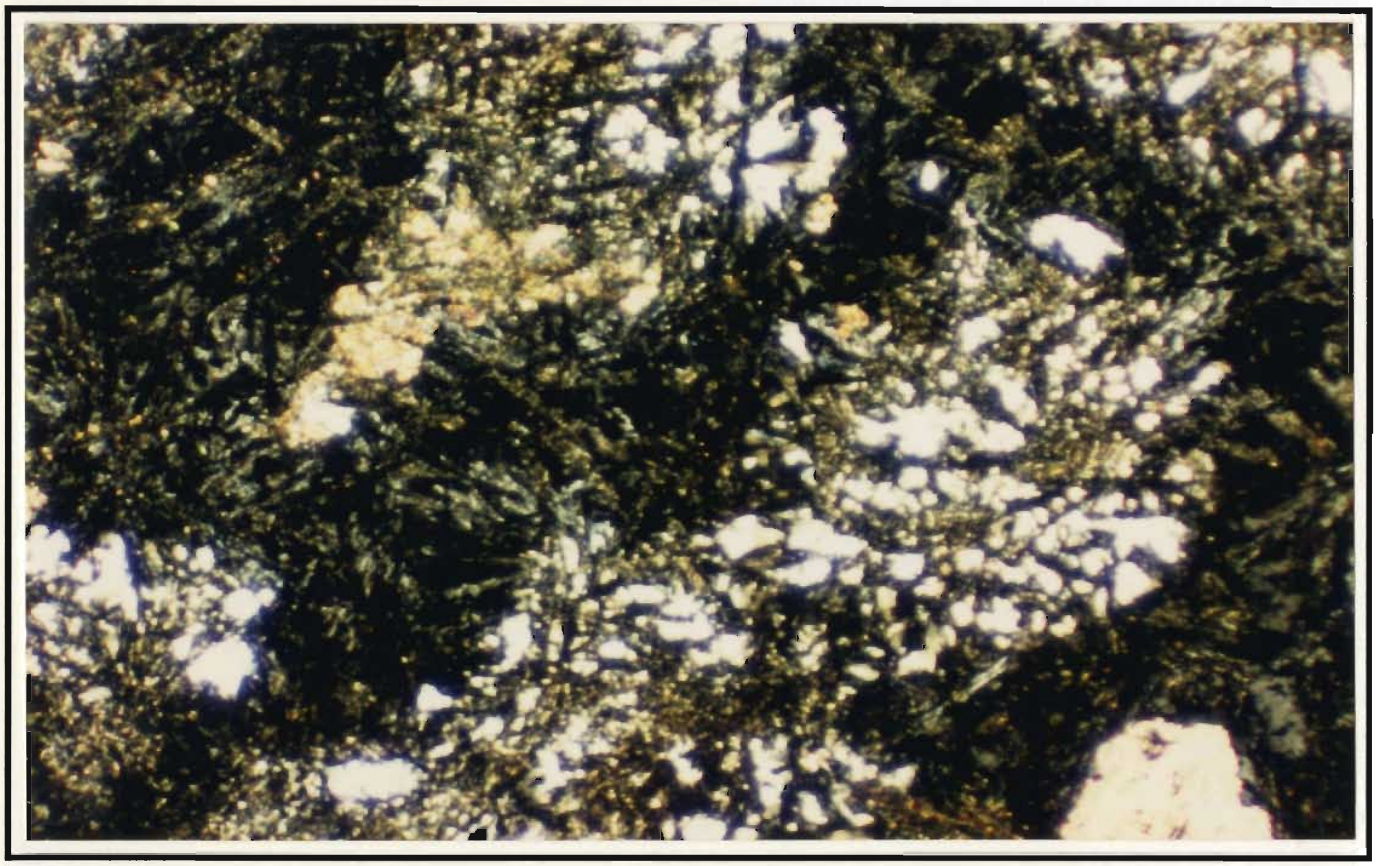

Figure 4-14: Area shown in Figure 4-13 under crossed nicols; note varioles, and occurrence of elongate grains in varioles and matrix; thin section S 31, crossed nicols, 3.2 x. **— 0.5 mm —**

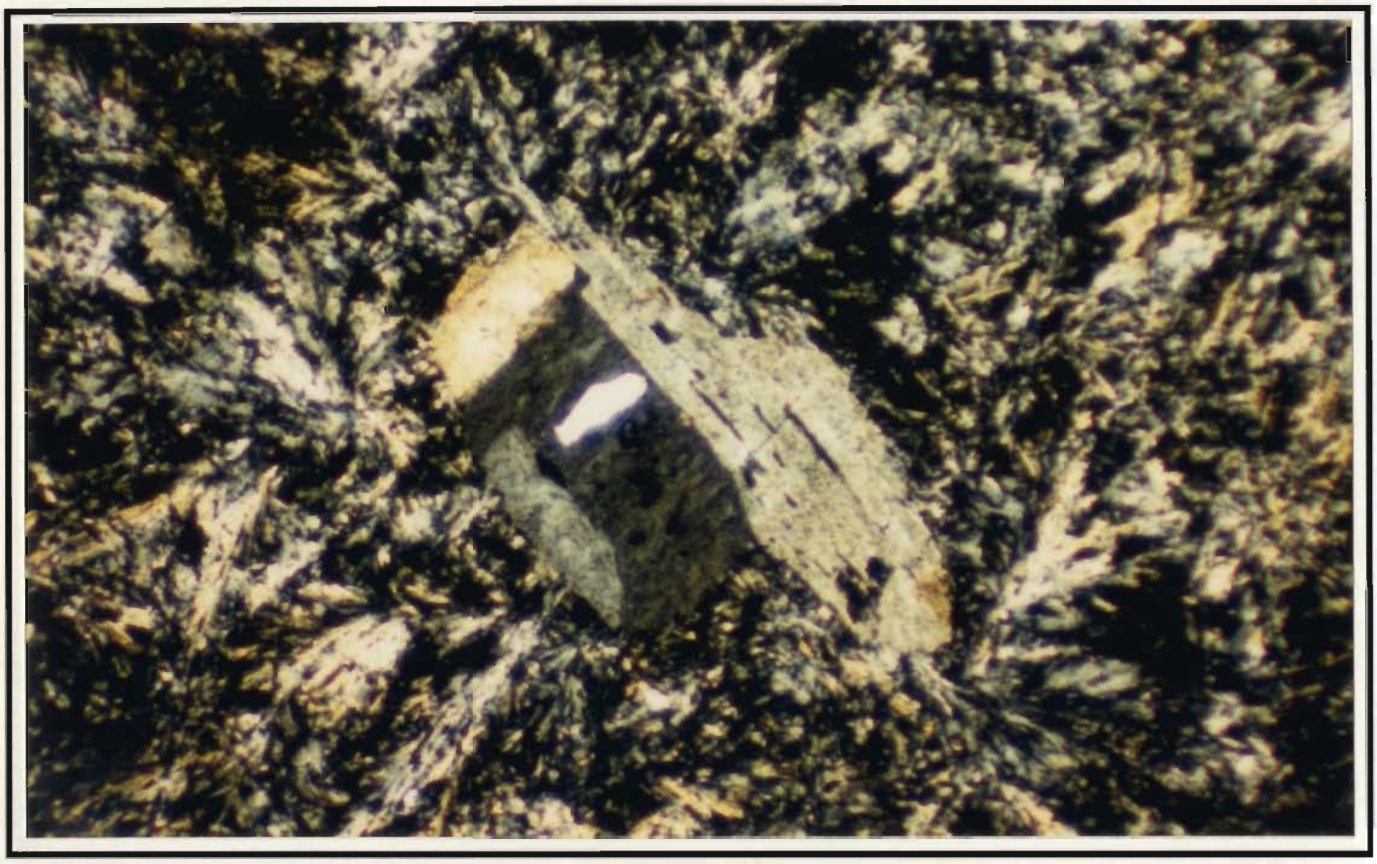

Figure 4-15: Albitized plagioclase grain in core of variole; thin section S 55, 3.2 x, crossed nicols.
— 0.5 mm —

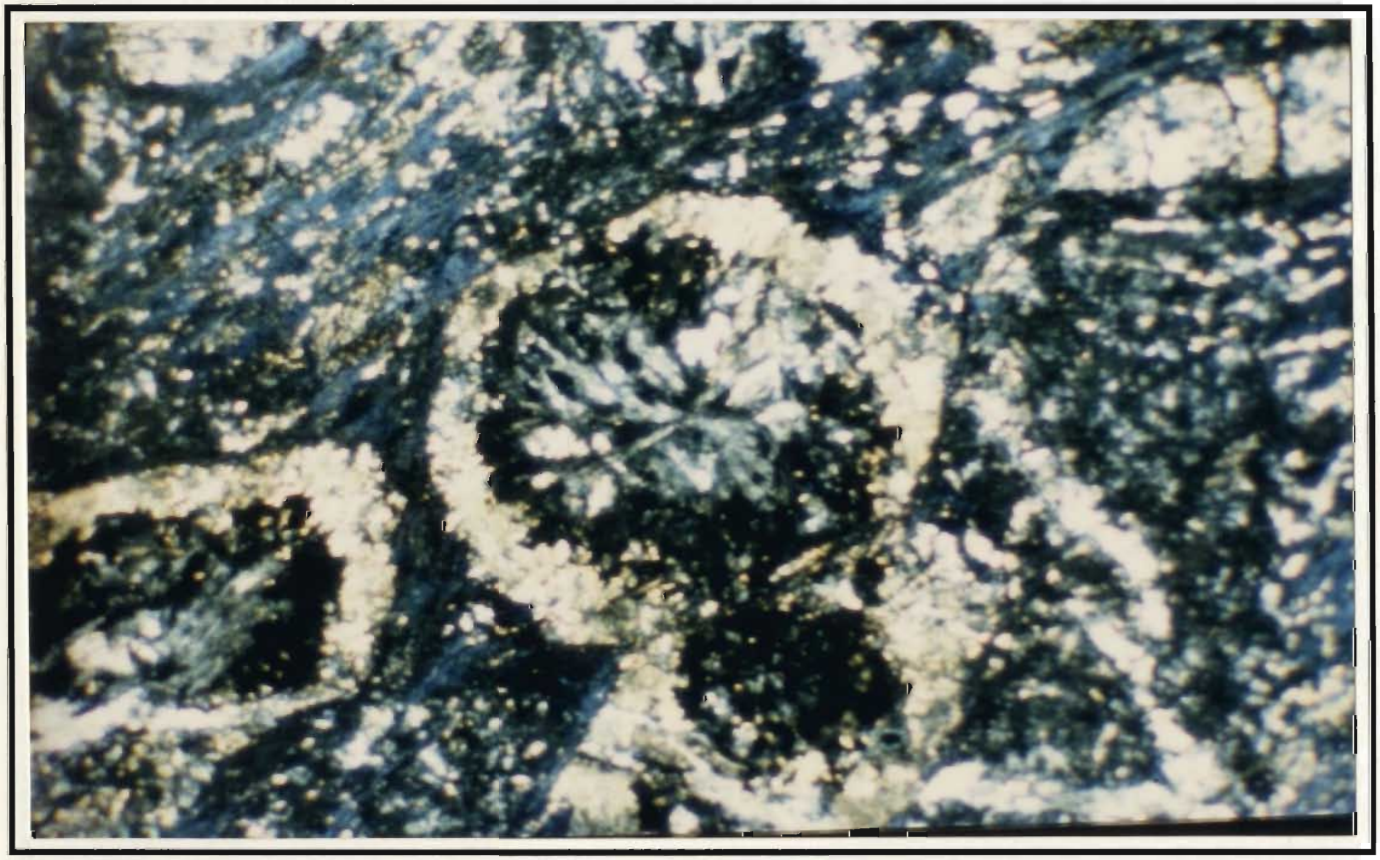

Figure 4-16: Varioles having a central core of radially aligned albite and intersertal chlorite surrounded by an outer ring of secondary calcite; thin section S 1C, crossed nicols, 3.2 x.
— 0.5 mm —

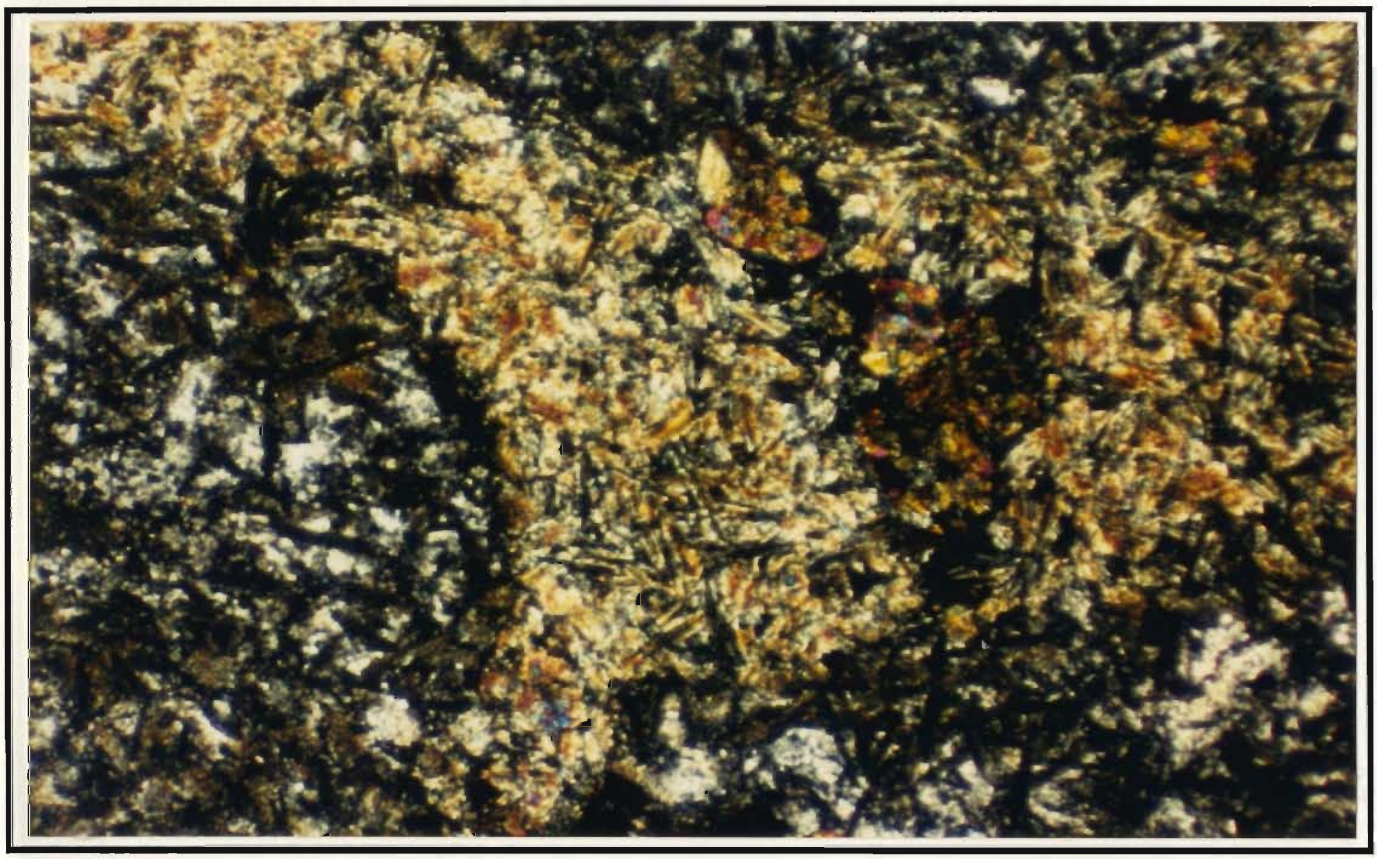

Figure 4-17: Quench-textured, axiolitic clinopyroxene (cf. Lofgren, 1974) in matrix to varioles (rounded outlines in left and bottom right portions of picture); thin section S 35B, crossed nicols, 3.2 x. **— 0.5 mm —**

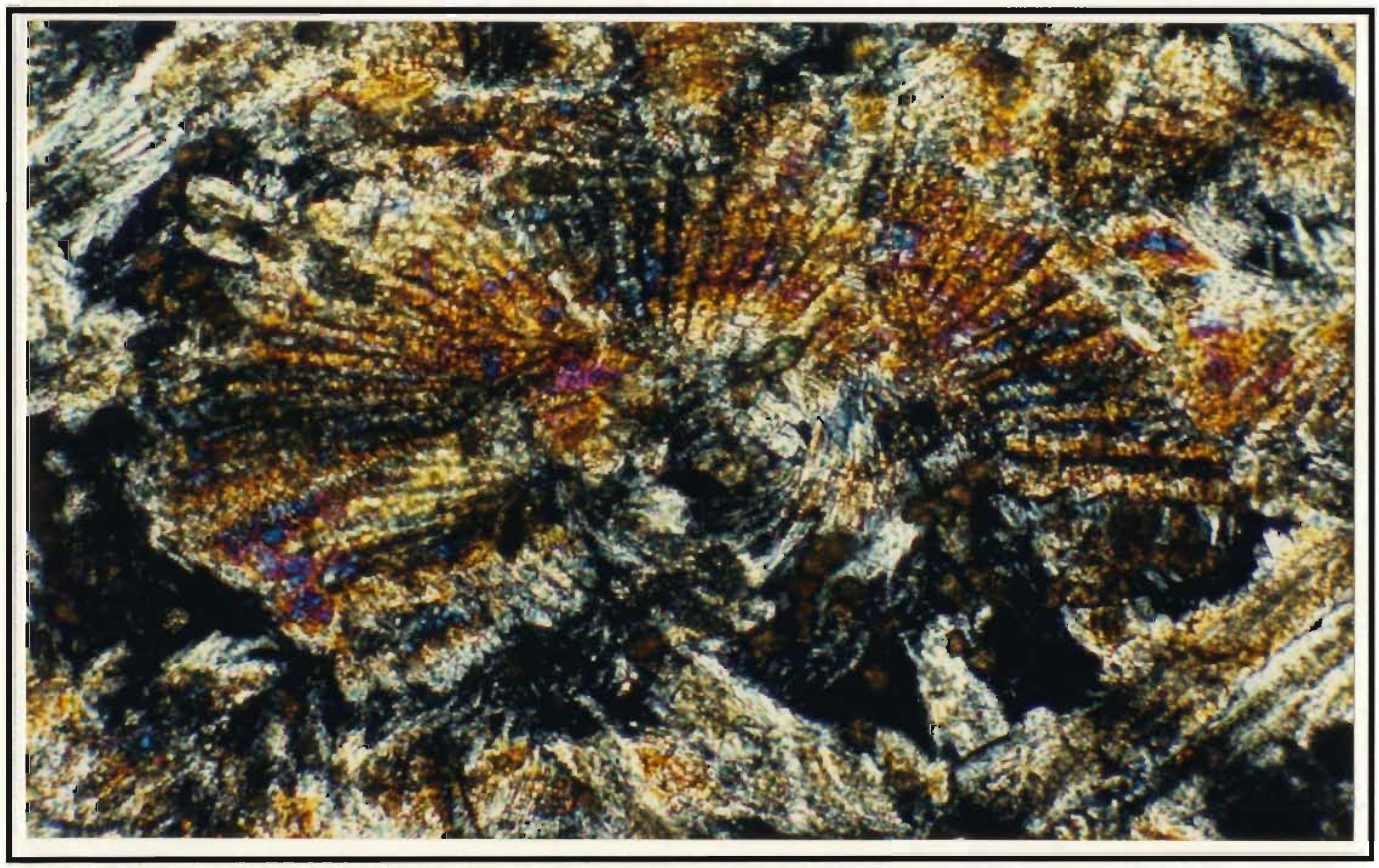

Figure 4-18: Expanded view of quench-textured, axiolitic clinopyroxene between varioles; thin section S 35B, crossed nicols, 20 x. **—— 0.1 mm ——**

predominantly by chlorite; in S 66B, elongate albite laths and intersertal chlorite dominate outside the varioles; and in thin section S 1C, chlorite, accessory sphene and lesser subhedral chromite occupy the matrix between varioles.

4.1.2.3 Intersertal- and intergranular-textured low-zirconium basalts

A few of the low-zirconium basalts do not show quench-texture morphologies. These are composed of intergranular to subophitic intergrowths of tiny (< 0.1 mm long) stubby prismatic clinopyroxene and albitized plagioclase (0.1 to 0.4 mm long) accompanied by intersertal anhedral chlorite and lesser quartz. Accessory sphene and, in some places, subhedral opaque minerals ± secondary calcite and epidote comprise the remainder. Secondary K-feldspar is present in sample S 81 (see Section 4.4.4).

The intersertal- and intergranular-textured low-Zr Skidder basalts are similar texturally to those having intermediate Zr concentrations described in the next section.

4.1.3 Basalts having Zr concentrations of 51-85 ppm

Table 4-2 shows the rock types and gives a partial geochemical analysis and qualitative estimate of the abundances of common minerals in Skidder Basalt extrusive rocks having Zr concentrations of 51-85 ppm. Albite, intersertal chlorite and quartz, plus intergranular accessory sphene and subhedral opaque minerals occur in all sections. Most sections have a few 1-1.5 mm-long albitized plagioclase phenocrysts (?) and some also contain a few 1 mm-long relict clinopyroxene phenocrysts (?). Some samples have intergranular to subophitic intergrowths of albitized plagioclase and stubby prismatic clinopyroxene (Figures 4-19 and 4-20). An overall increase in amount of sphene, subhedral opaque minerals (magnetite (?)) and intersertal anhedral quartz is noted with with an increase in Zr concentration. Some samples contain acicular opaque minerals (magnetite (?)) in addition to or in place of subhedral opaque minerals.

Table 4-2: Petrographic table showing rock type, partial geochemical analysis and mineralogy of basaltic outcrop samples having Zr concentrations of 51-85 ppm; samples not analyzed but of similar mineralogy and texture are also included

Key:	See Figures 3-3 and 6-1 for sample locations
	Mineral abbreviations: Ab-albite, Cpx-clinopyroxene, Cl-chlorite, Cc-calcite, Ep-epidote, Qz-quartz, Chr-chromite, Amph-amphibole, hm-hematite, py-pyrite
	Abundance of mineral relative to its average content in mafic rocks from the Skidder area: x-low, xx-medium, xxx-high
	See Appendix B for complete whole rock analyses and description of analytical methods

Sample Name	Rock Type	SiO_2 %	TiO_2 %	MgO %	Zr ppm	Ab	Cpx	Cl	Sphene	Cc	Ep	Qz	Chr	Opaques	Amph	Other Minerals and Comments
S 13A	Basalt					xx		xx	xxx	x		xx		xx		
S 13C	Basalt	68.2	0.9	1.2	80	xx		x	xx	xx		xxx		xx		silicified
S 14A	Pillow breccia	54.0	1.0	4.6	68	xxx	x	xx	xx	xx	x	xx		xx		
S 14B	Pillow breccia	55.2	1.1	6.2	60	xxx	x	xx	xx	x	x	xx		xx		acicular opaques (xx)
S 15A	Pillow breccia	53.8	1.0	6.2	60	xxx	x	xx	xx		xx	xx		xx		
S 16	Pillow breccia	55.5	1.0	6.1	51	xx		xx	xx	x		xx		xxx		K-feldspar (xx)
S 19	Massive basalt	48.1	1.1	7.1	62	xx	xxx	xx	xx	xx	x	x		x	xx	
S 23	Pillowed basalt	46.9	1.6	8.0	82	xx	xx	xx	xxx	xx		x		xxx		
S 27B	Pillow breccia	52.8	1.7	6.6	74	xxx		xx	xxx		xx	x		xx		
S 28	Pillowed basalt	51.8	1.1	7.1	61	xxx	xxx	xx	xx		x	x		xx		
S 41	Massive basalt	49.8	1.2	7.6	68	xxx		xx	xx	xx	xxx	xx		x		acicular opaques (xxx)
S 43	Pillowed basalt	38.4	1.0	5.1	64	xx		xx	xx	xxx		x	x	xx		acicular opaques (xx)
S 44	Pillowed basalt	47.8	1.2	8.1	72	xx	xx	xxx	xx	xx		x		x		
S 52B	Pillowed basalt	52.2	1.0	6.3	80	xxx	xx	xx	xx		xx	x		xxx		
S 52C	Pillowed basalt					xxx	xx	xx	xx	x		x		xxx		
S 53	Pillowed basalt	50.9	1.1	7.6	66	xx	xx	xx	xx	x		x	x	x	xx	
S 56	Pillow breccia (?)	44.4	1.1	13.1	74	xx		xxx	xx	x		xx		x		altered (?)
S 57	Massive basalt	49.8	0.9	7.4	58	xx	xx	xx	xx	xx	xx	x		x		
S 60	Pillowed basalt	51.8	1.3	6.7	82	xx	x	xx	xx		xx	x		x	?	acicular opaques (xx)
S 61	Massive basalt	49.1	1.6	6.4	80	xx	xxx	xx	xxx			x		xxx		medium/coarse grained
S 64	Pillowed basalt	43.8	1.1	9.0	59	xx		xx	xx	xxx		x	x	x	?	acicular opaques (x)
S 79	Pillowed basalt	49.4	1.2	5.9	78	xx	xx	xx	xx	x	x	x		x		acicular opaques (xxx)
	AVERAGE	50.7	1.2	6.8	69											

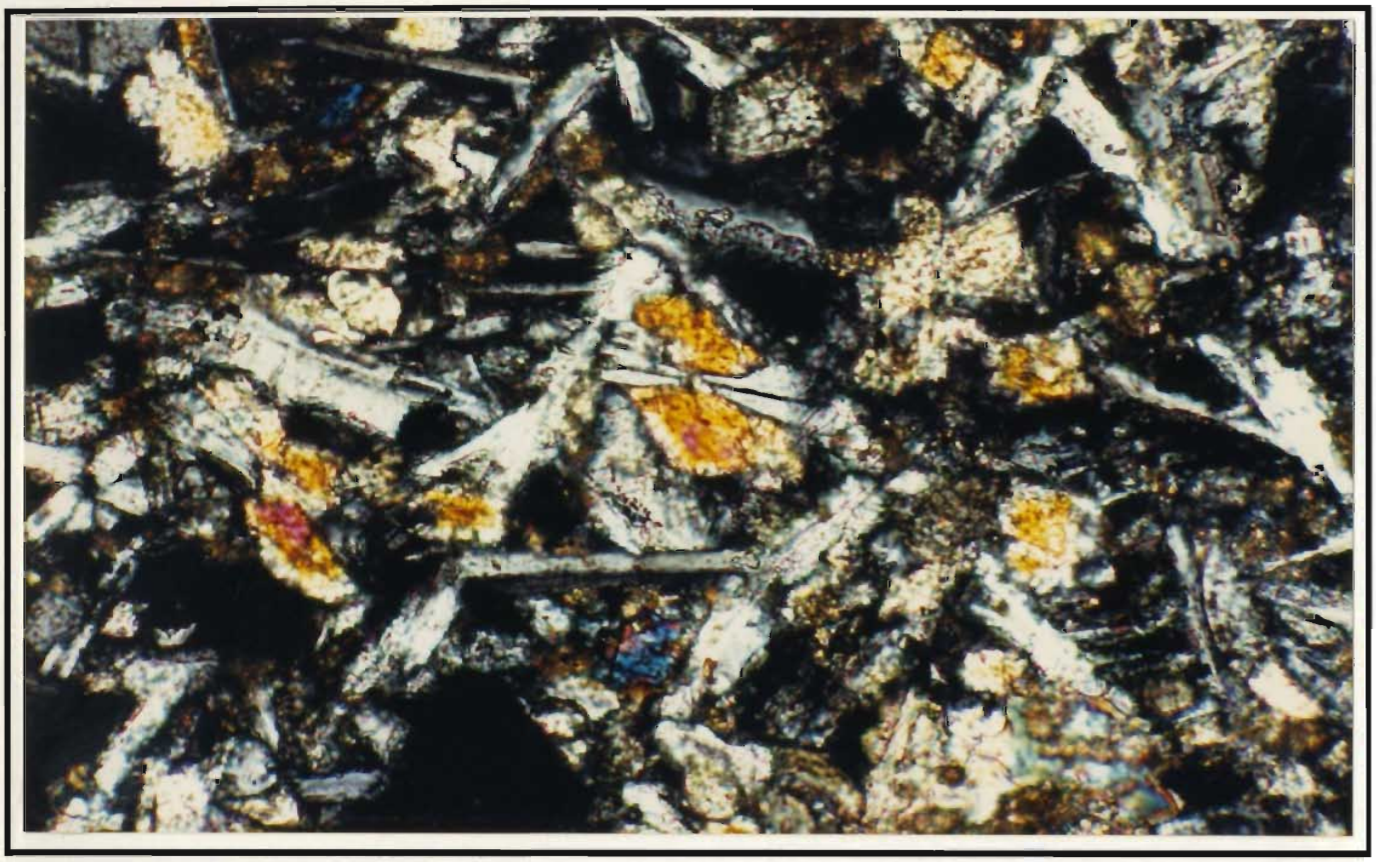

Figure 4-19: Subophitic intergrowth of plagioclase and clinopyroxene; thin section S 53, crossed nicols, 20 x. —— **0.1 mm** ——

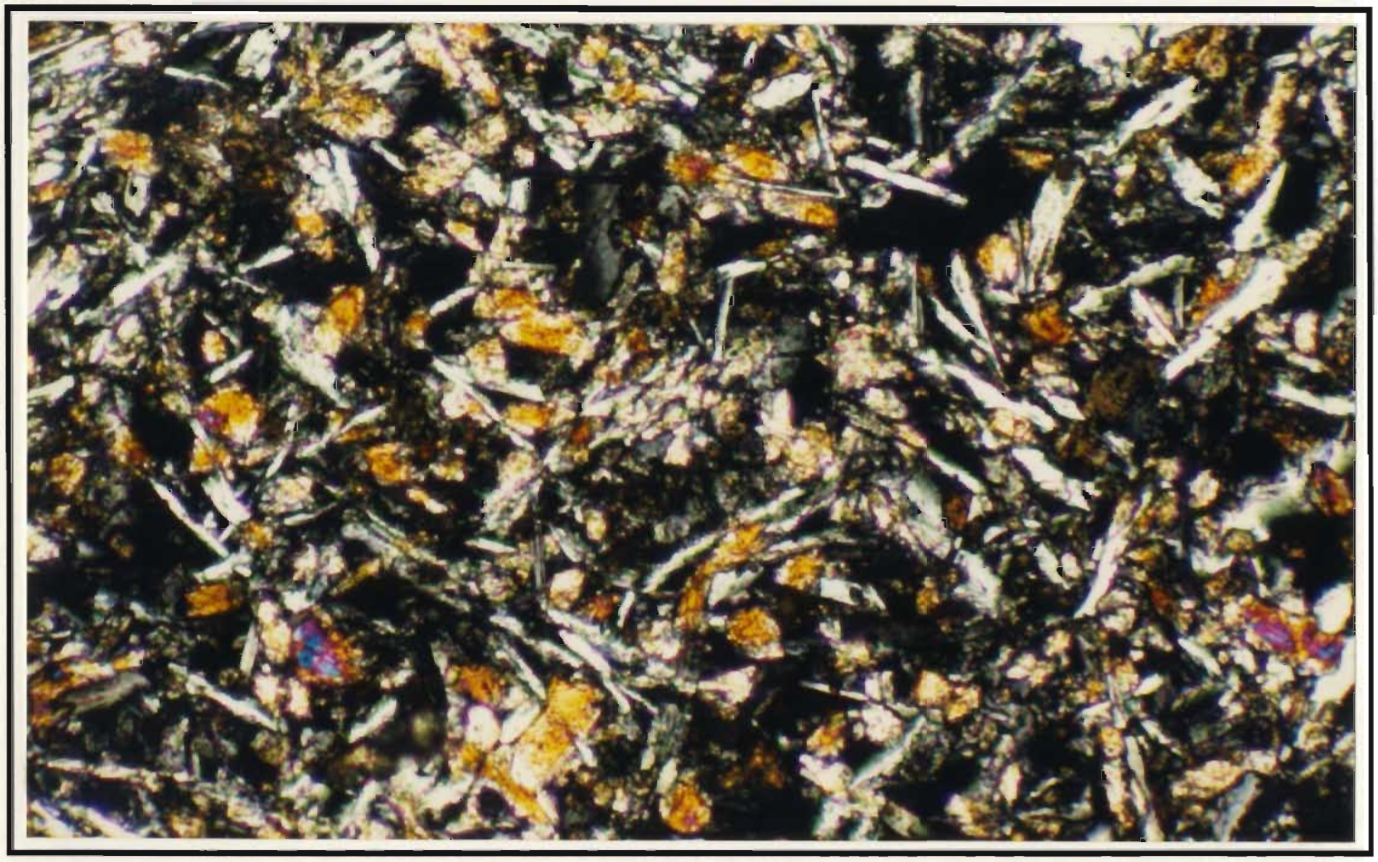

Figure 4-20: Intergranular to subophitic "stubby" clinopyroxene grains and elongate albite laths within intersertal chlorite and quartz; thin section S 53, crossed nicols, 10 x. —— **0.2 mm** ——

Quench-textured elongate clinopyroxene grains and stubby prismatic grains, both types being subophitically intergrown with albitized plagioclase in places, occur in a few of the lower-Zr samples included in this group (e.g. sample S 19). Segregation vesicles (Smith, 1967; Baragar et al., 1977) are noted in samples S 19, S 43 and S 60. They are typically filled by: quench-textured clinopyroxene, partially altered to amphibole; quench-textured albite showing radial extinction; and intersertal chlorite — many have a calcite core. In most other sections, clinopyroxene occurs as pale brown to colourless stubby prismatic grains which are typically 0.1-0.5 mm in length. A few 1 to 1.5 mm-long clinopyroxene phenocrysts (?) are present in some sections. In places these grains are subophitically intergrown with albitized plagioclase. Larger prismatic clinopyroxene grains typically show "hourglass" extinction. Edges of some of the clinopyroxene grains are altered to amphibole. In a few sections, subophitic glomeroporphyritic clusters of 0.5 mm-long albite and clinopyroxene are noted.

In the samples containing segregation vesicles, albite, which shows radial extinction, occurs with chlorite and, in some sections, clinopyroxene. However, albite most commonly occurs as elongate laths 0.1-1 mm in length haphazardly arranged throughout the thin section. Albite grains are roughly aligned in thin sections of the few rocks that are well foliated. Most thin sections contain several 1-1.5 mm-long phenocrysts (?) of albitized plagioclase. In places these occur as glomeroporphyritic clusters (Figure 4-21). Most albite grains show albite twinning and some "phenocrysts" display pericline twinning. Locally, albite ± calcite, chlorite and quartz fill vugs. Albite in vugs is generally coarser grained than that which occurs throughout the remainder of the thin section.

Chlorite, typically pale green, occurs most commonly as fine grained anhedral masses intersertal to other minerals. It also fills vugs, vesicles and fractures. In some sections it displays pale green to colourless pleochroism. In a few sections, vug-filling chlorite forms radial aggregates; in thin section S 13A, vug-filling chlorite ± talc show radial growth morphologies.

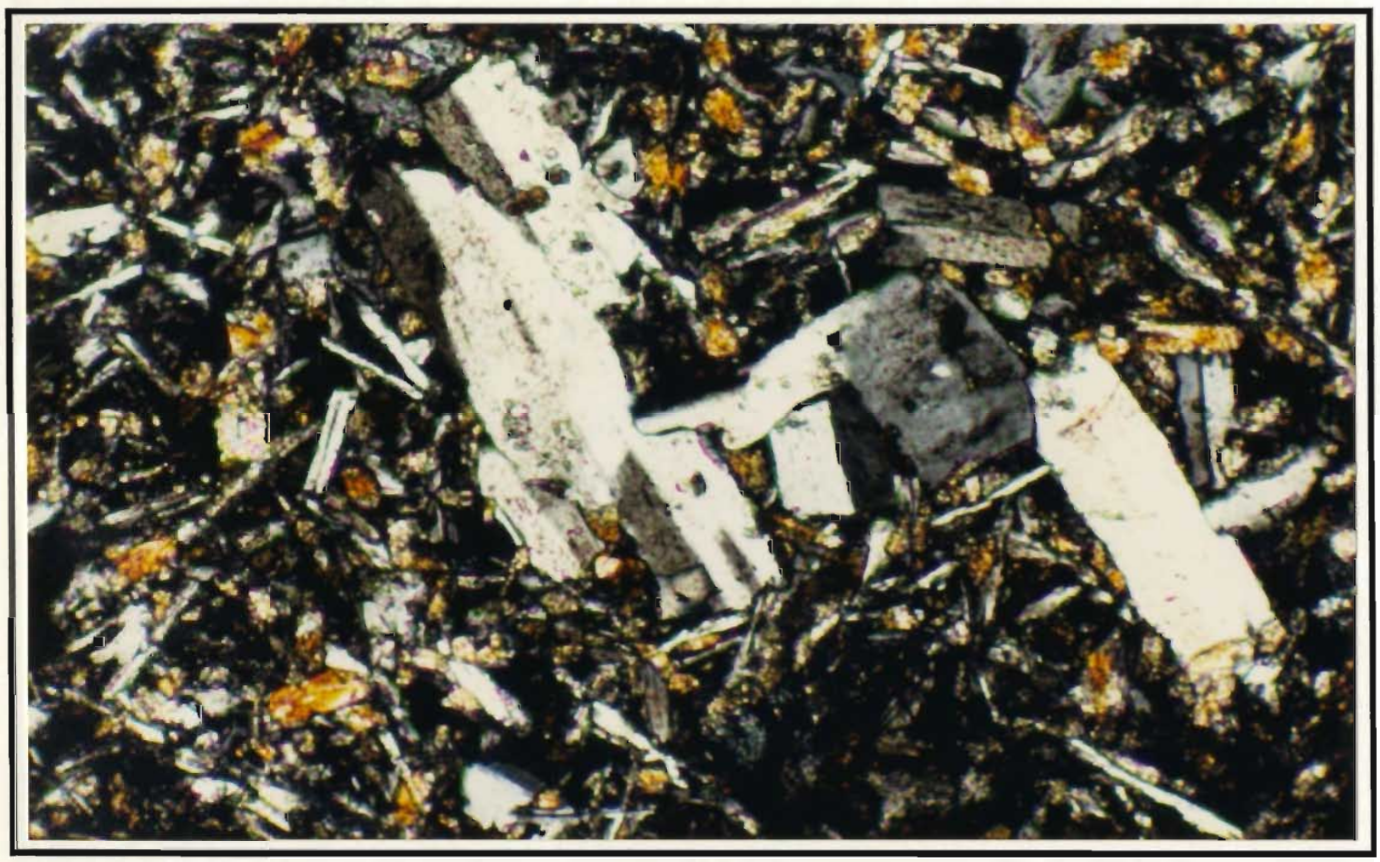

Figure 4-21: Glomeroporphyritic albitized plagioclase in intergranular clinopyroxene and albite; and intersertal chlorite and quartz; thin section S 53, crossed nicols, 10 x.

—— 0.2 mm ——

Sphene occurs throughout the samples as small brown subhedral to anhedral grains < 0.1 mm across that, in places, are joined to others to form dense irregular masses. Tiny subhedral opaque minerals occur in intergranular areas throughout the samples. Intersertal anhedral quartz, in places showing undulatory extinction, occurs with chlorite in the groundmass. It also fills vugs, vesicles and fractures. In some sections of samples close to the Skidder Prospect, quartz partially or totally replaces intersertal chlorite and albite. Amphibole occurs typically as optically continuous pale green to colourless fibrous grains that, in many areas, enclose remnant grains of clinopyroxene. Irregular masses composed of calcite grains are haphazardly distributed throughout some sections; anhedral calcite also fills vugs, vesicles and fractures. Secondary epidote occurs as pleochroic, light olive green, equant to prismatic grains that are 1.5 to 2 mm across. Epidote is randomly distributed throughout some samples but in most areas it fills vugs and fractures. In a few samples, epidote occurs as radially aligned needles.

Secondary K-feldspar occurs in thin section S 16 as "rims" surrounding albitized carbonatized feldspar phenocrysts and as stubby irregular grains in the matrix (see Section 4.4.4). The K-feldspar does not show twinning characteristic of microcline and is similar to untwinned albite; the two minerals being difficult to distinguish optically.

In rare instances, Skidder basalts included in this group show a bimodal grain-size distribution. For example in thin section S 61, glomeroporphyritic, subophitic 0.5 to 1.5 mm-long clinopyroxene and 1 to 3 mm-long albitized plagioclase make up about one half of the sample. The remainder consists of finer grained (0.1 mm long or less) stubby prismatic clinopyroxene and albite laths; intergranular sphene and subhedral opaque minerals; and intersertal chlorite and lesser quartz.

4.1.4 Mafic flows having Zr concentrations > 85 ppm

Table 4-3 shows the basalt types and gives a partial geochemical analysis and qualitative estimate of the abundances of common minerals in the high-Zr mafic flows.

Table 4-3: Petrographic table showing rock type, partial geochemical analysis and mineralogy of basaltic outcrop samples having Zr concentrations > 85 ppm; samples not analyzed but of similar mineralogy and texture are also included

Key:	See Figures 3-3 and 6-1 for sample locations
	Mineral abbreviations: Ab-albite, Cpx-clinopyroxene, Cl-chlorite, Cc-calcite, Ep-epidote, Qz-quartz, Chr-chromite, Amph-amphibole, hm-hematite, py-pyrite, mag-magnetite, ilm-ilmenite
	Abundance of mineral relative to its average content in mafic rocks from the Skidder area: x-low, xx-medium, xxx-high
	See Appendix B for complete whole rock analyses and description of analytical methods

Sample Name	Rock Type	SiO_2 %	TiO_2 %	MgO %	Zr ppm	Ab	Cpx	Cl	Sphene	Cc	Ep	Qz	Chr	Opaques	Amph	Other Minerals and Comments
S 21A	Pillowed basalt	58.7	1.6	4.1	95	xxx		xx	xxx	x		xx		xx		
S 21B	Pillowed basalt					xxx		xx	xxx	x		xx		xx		anatase (?)/brookite (?) (x)
S 29	Massive basalt or Andesite (?)	56.7	1.9	2.4	110	xxx		xx	xxx	x		xx		xxx		
S 77	Pillowed basalt	57.7	1.3	3.1	88	xx		xx	xxx	xx		xx		xxx		
	AVERAGE	57.7	1.6	3.2	98											
S 7B	Pillowed Basalt	69.8	0.4	2.3	92	xx		xx	xx	x		xxx	?	xx		silicified

Table 4-4: Petrographic table showing rock type, partial geochemical analysis and mineralogy of miscellaneous outcrop samples from the Skidder area

Key:	As per Table 4-3 above

Sample Name	Rock Type	SiO_2 %	TiO_2 %	MgO %	Zr ppm	Ab	Cpx	Cl	Sphene	Cc	Ep	Qz	Chr	Opaques	Amph	Other Minerals and Comments
S 22	Diabase dyke	48.5	1.0	7.2	68	xx		xx	xx	xx	xx	x		xxx		mag. pseudomorphs of ilm.
S 25	Diabase/Gabbro (?)	49.8	1.5	7.4	73	xx	xxx	xx	xxx		x	x		xxx		
S 49	Diabase/Gabbro (?)	58.8	0.8	4.1	64	xx	xx	xx	xx	x		xx		xx	xx	calcic plagioclase (?)
Complete whole rock analysis for S 71 presented in Table 6-34																
S 71	Jasper	86.8	0.0	0.0	8							xxx				hematite (xxx)
S 9B	Mafic tuff					xxx		xxx	xx	xx		x		xx		serpentine (?)
S 10B	Mafic tuff (?)	53.2	0.9	5.6	46	xxx	x	xx	xx	xx		x		xxx		

These samples are predominantly composed of 0.2 mm-long albite laths; intergranular sphene and subhedral opaque minerals; and intersertal chlorite and quartz. A few 0.5 to 1 mm-long albitized plagioclase phenocrysts (?) are present. Quartz and lesser chlorite and calcite fill vugs, vesicles and fractures. In thin section, greater amounts of quartz, opaque minerals, and sphene; a lesser amount of chlorite; and a lack of preserved clinopyroxene distinguish these rocks from lower-Zr basalts.

4.1.5 Mafic intrusive rocks

Mafic intrusive rocks within the Skidder Basalt sequence include some which are clearly diabase dykes and others which make up an entire outcrop and may thus be either large sills, dykes or small gabbroic bodies. The mineralogy of these rocks is similar to the basalts.

Thin section S 25 (Table 4-4) is predominantly composed of intergranular or subophitically intergrown 1 to 2 mm-long albitized plagioclase and 0.5 to 1 mm-long clinopyroxene (Figure 4-22). The clinopyroxene is typically very pale brownish green to colourless and, in places, shows hourglass extinction. In places it is partially altered to amphibole and chlorite. Skeletal opaque minerals (0.1-0.4 mm across), subhedral opaque minerals and sphene are distributed throughout the sample. Some of the skeletal grains are probably altered, pseudomorphed ilmenite as indicated by alteration to sphene around grain edges. Intersertal anhedral chlorite and quartz make up the remainder of the groundmass. The sample also contains a few segregation vesicles (Smith, 1967; Baragar et al., 1977), each comprising a chlorite- ± epidote- filled vesicle, about 2 mm across, surrounded by a 0.5 mm-wide rim composed of fine grained albite and clinopyroxene; intergranular sphene and opaque minerals; and intersertal chlorite (Figure 4-23).

Thin section S 22 (Table 4-4) is similar in texture and mineralogy to S 25 but is more extensively altered. Clinopyroxene has been completely altered to chlorite or replaced by various combinations of epidote, calcite and locally quartz. Skeletal opaque grains

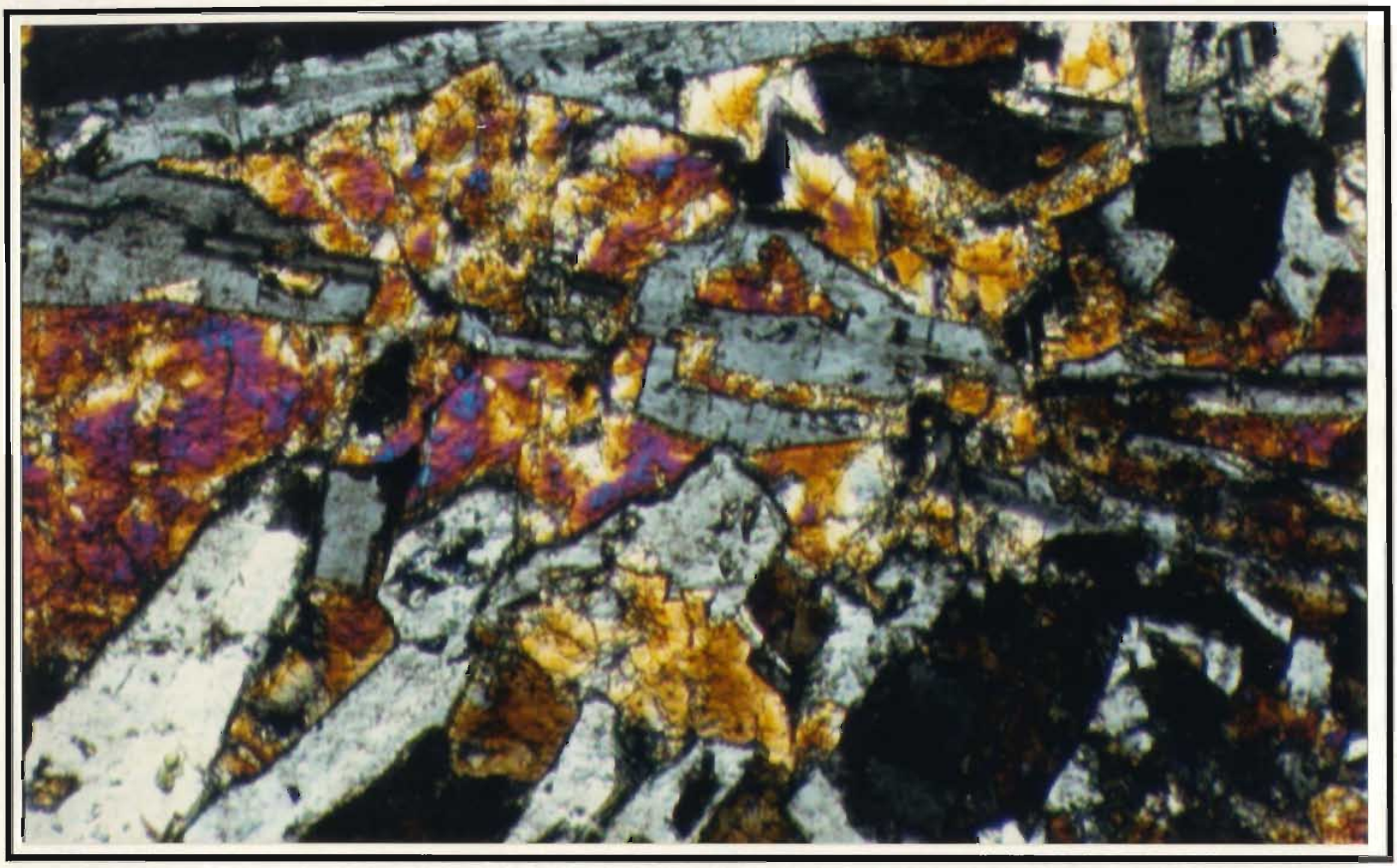

Figure 4-22: Subophitically intergrown albitized plagioclase and clinopyroxene; thin section S 25, crossed nicols, 10 x. —— **0.2 mm** ——

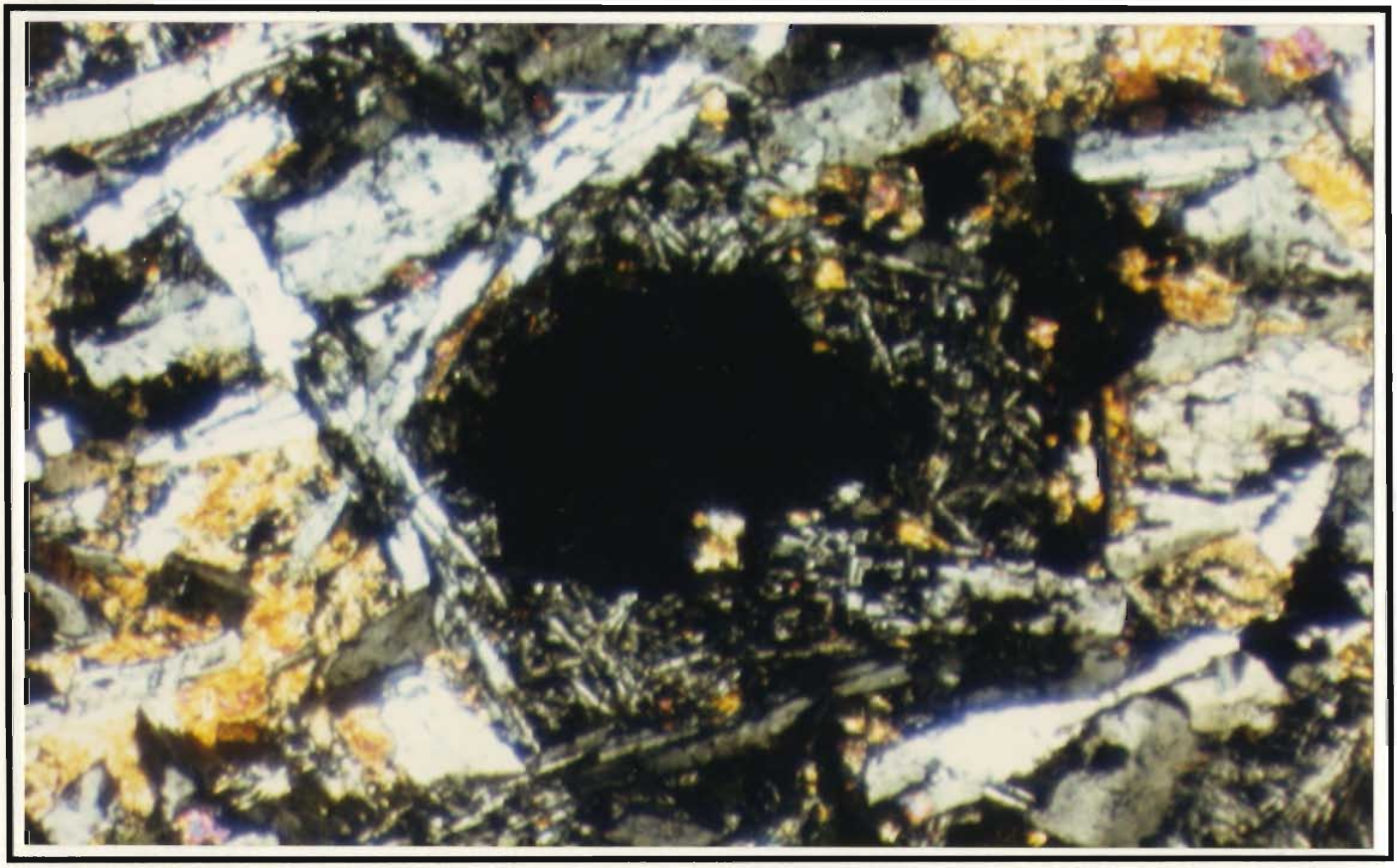

Figure 4-23: Segregation vesicle; thin section S 25, crossed nicols, 3.2 x. — **0.5 mm** —

(magnetite pseudomorphs of ilmenite) occur throughout the sample (Figure 4-24). Albite and calcite replace plagioclase; calcite also occurs as irregular masses throughout the sample. Segregation vesicles similar to those described in S 25 are also noted.

Thin section S 49 (Table 4-4) has a bimodal grain-size distribution. About one third of the section is composed of: 2 mm-long albitized, epidotized plagioclase laths which, in places, are replaced by quartz; and 1-1.5 mm-long clinopyroxene grains that are partially to completely replaced by amphibole, chlorite ± epidote. Amphibole ± quartz, epidote and lesser amounts of calcite fill vugs. The remaining two thirds of the section comprises: intergranular 0.1-0.2 mm-long albite laths; lesser amounts of clinopyroxene altered to amphibole and chlorite; sphene; and intersertal chlorite and quartz.

4.1.6 Jasper

Thin section S 71 (Table 4-4) is from a large 3.4 m-thick jasper unit exposed near the trondhjemite pod northeast of the Skidder Prospect (Figures 3-3 and 3-4). It contains ubiquitous quartz spherulites (0.1-0.2 mm in diameter) which occur in a hematite-rich matrix. Some of the spherulites have a central hematized core (Figure 4-25). The remainder of the sample consists of hematite and quartz. Variations in the amount of hematite define a streaky "layering" in nonspherulitic parts of the sample. Anhedral quartz grains, 0.2-0.5 mm across, fill fractures and one ovoid vug.

4.1.7 Mafic tuff

Thin section S 9B of interflow mafic tuff consists of 0.1-0.2 mm-long albite (some of which is altered to quartz); anhedral elongated quartz grains; intersertal chlorite; intergranular subhedral opaque minerals, 0.05 mm across, and tiny grains of sphene. One crosscutting calcite-chlorite vein is present and irregular masses of calcite occur throughout the section. Aligned albite grains along with elongated quartz and chlorite masses define a foliation in the sample.

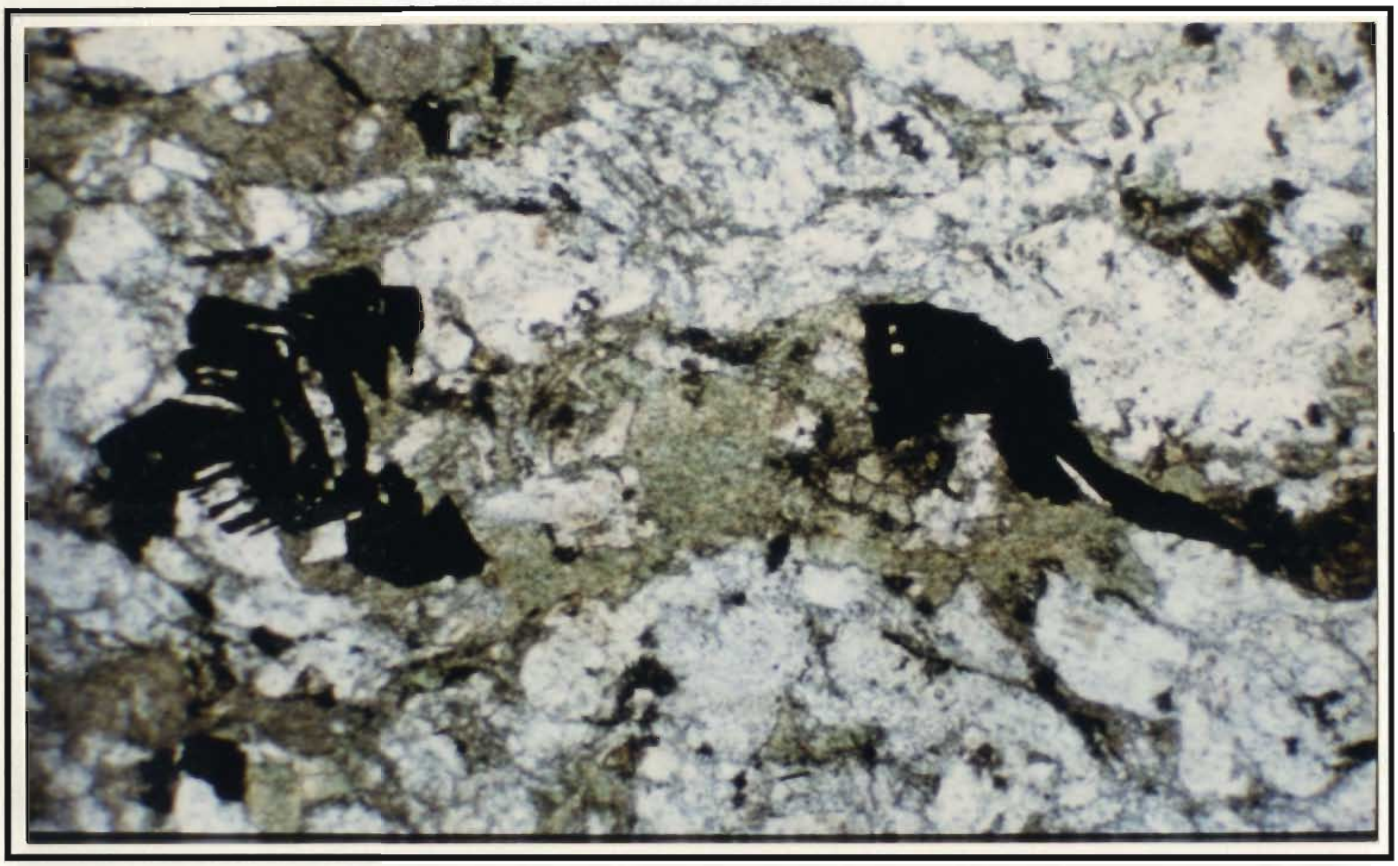

Figure 4-24: Magnetite pseudomorph of skeletal ilmenite; thin section S 22, plane polarized light, 10 x.
—— 0.2 mm ——

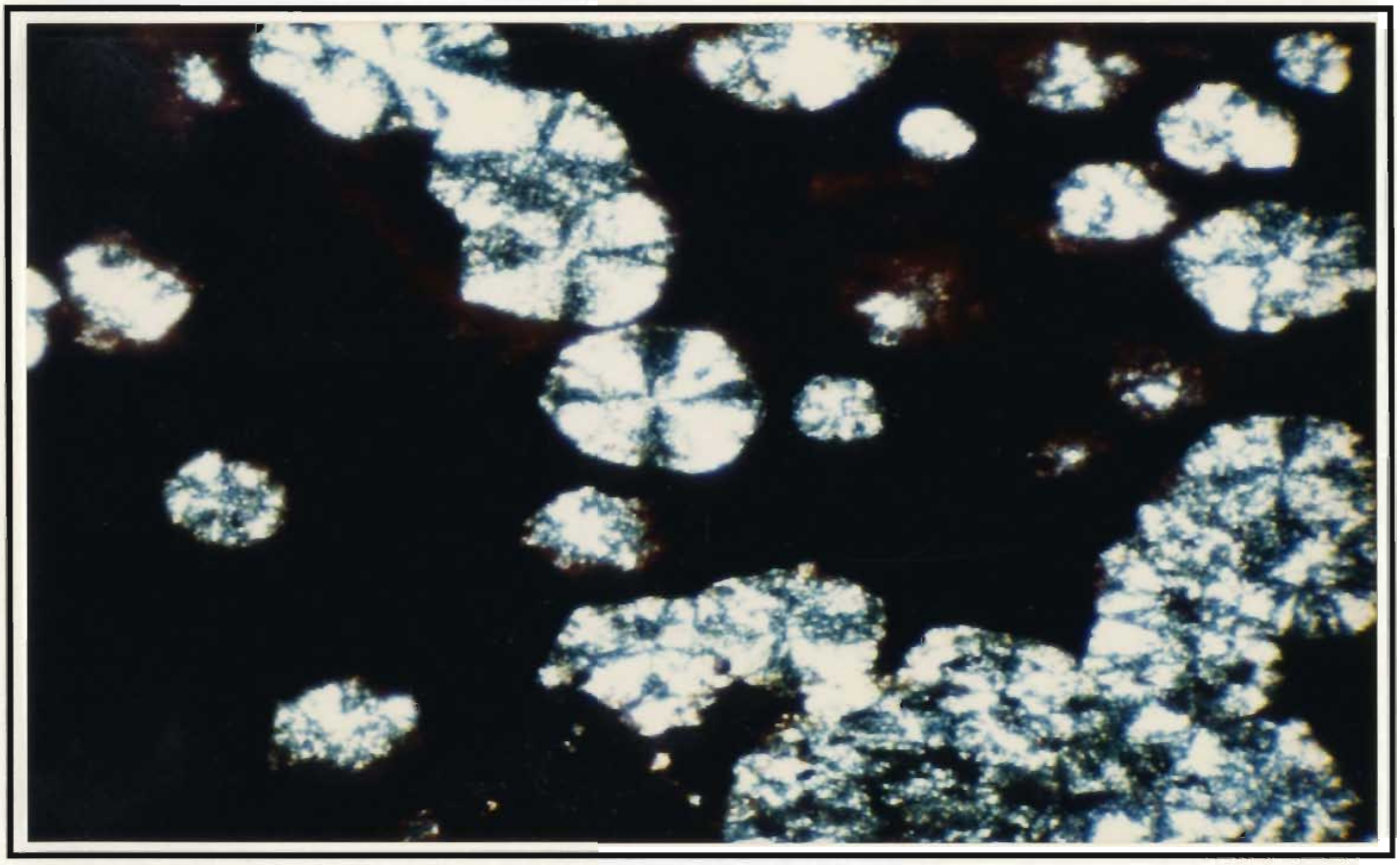

Figure 4-25: Quartz spherulites; thin section S 71, crossed nicols, 10 x. —— 0.2 mm ——

4.2 Petrography of the Skidder Trondhjemites

4.2.1 Trondhjemite dykes

Table 4-5 gives a partial geochemical analysis and qualitative estimate of the abundances of common minerals in outcrop samples of Skidder area trondhjemites. The trondhjemite dykes are composed of 1 to 3 mm-long, albitized plagioclase and quartz phenocrysts in a matrix of anhedral quartz grains (≤ 0.1 mm across) and 0.1 mm-long albite laths (Figure 4-26). In places, large grains of albitized plagioclase ± quartz occur as glomeroporphyritic clusters. Minor amounts of chlorite occur as elongate anhedral masses intersertal to quartz and albite. Quartz, chlorite, or calcite or a combination of these minerals fill fractures and vugs. Sericite veinlets are present in some samples. Pyrite and minor amounts of other opaque minerals; sphene; and tiny subhedral zircon are finely disseminated throughout the samples.

Sample S 10C contains two angular 2-4 cm-long fragments of mafic wall rock that have been incorporated into the trondhjemite. The xenoliths have been altered such that they are similar in most respects to the assimilating trondhjemite except for a greater amount of intersertal chlorite and correspondingly lesser quartz.

4.2.2 Trondhjemite pod

Samples of the trondhjemite pod exposed about 2.5 km northeast of the Skidder Prospect (Figures 3-3 and 3-4; Table 4-5) have a mineralogy similar to that of the dykes. Quartz, which occurs as anhedral grains ≤ 0.1 mm across, and 0.1 mm-long albite are the dominant minerals. In addition, abundant quartz grains 0.2-0.3 mm across and having anhedral to, in places, rounded outlines are ubiquitous in some samples. A few 1 to 3 mm-long albitized plagioclase and quartz phenocrysts are present in most samples. In thin section S 73, quartz amygdules 2-3 mm in diameter, are noted. Vugs in section S 69 are filled by quartz, or locally by quartz and 0.8 mm-long albite. Sample S 68 contains "quenched" areas filled with spherulitic felsic material displaying radial extinction

Table 4-5: Petrographic table showing partial geochemical analysis and mineralogy of outcrop samples of Skidder trondhjemites

Key:	See Figures 3-3 and 6-1 for sample locations
	Mineral abbreviations: Ab-albite, Cpx-clinopyroxene, Cl-chlorite, Cc-calcite, Ep-epidote, Qz-quartz, Chr-chromite, Amph-amphibole, hm-hematite, py-pyrite
	Abundance of mineral relative to its average content in mafic rocks from the Skidder area: x-low, xx-medium, xxx-high
	See Tables 5-12 and B-10 (S 72) for complete whole rock analyses

Sample Name	Rock Type	SiO_2 %	TiO_2 %	MgO %	Zr ppm	Ab	Cpx	Cl	Sphene	Cc	Ep	Qz	Chr	Opaques	Amph	Other Minerals and Comments
S 2	Trondhjemite dyke	77.4	0.1	0.6	142	xxx		x	x			xxx		xx		
S 4	Trondhjemite dyke	80.2	0.1	0.7	133	xxx		x	x	x		xxx		xx		hm, zircon
S 10A	Trondhjemite	75.6	0.2	1.1	169	xxx		x	x			xxx		xx		zircon
S 10C	Silicified mafic inclusions					xxx		xx	xx	x		xxx		xx		
S 13B	Trondhjemite	76.1	0.4	1.0	132	xx		x	xx			xxx		x	x	py, hm; silicified
S 68	Trondhjemite	67.9	0.4	1.4	220	xx		x	x	x		xxx		xx		sericite (xxx), zircon
S 69	Trondhjemite	76.9	0.3	0.4	182	xx			x	x		xxx		x		
S 72	Trondhjemite	74.5	0.2	1.7	182			x	x			xxx		x		sericite (xx), zircon; altered
S 73	Trondhjemite	80.0	0.3	0.6	170	xx		x	x			xxx		x		zircon
	AVERAGE	76.1	0.3	0.9	166											

Table 4-6: Petrographic table showing partial geochemical analysis and mineralogy of outcrop samples of the Buchans Group; sample S 63 is of the Lundberg Hill Formation, and samples S82A and S 82B are of the Sandy Lake Formation (cf. Thurlow and Swanson, 1987)

Key:	Mineral abbreviations: Ab-albite, Cpx-clinopyroxene, Cl-chlorite, Cc-calcite, Ep-epidote, Qz-quartz, Chr-chromite, Amph-amphibole, hm-hematite, py-pyrite
	Abundance of mineral: x-low, xx-medium, xxx high
	See Appendix B for complete whole rock analyses and description of analytical methods

Sample Name	Rock Type	SiO_2 %	TiO_2 %	MgO %	Zr ppm	Ab	Cpx	Cl	Sphene	Cc	Ep	Qz	Chr	Opaques	Amph	Other Minerals and Comments
S 63	Quartz feldspar porphyry	65.5	0.4	1.6	142	x		x	x			xx		xx		
S 82A	Pillowed basalt	44.4	0.6	6.8	53	x		xx	xx	xxx		x	x	x		K-feldspar (?), sericite (?)
S 82B	Pillowed basalt	47.9	0.6	5.5	59	xx		xx	xx	xxx		xx		x		K-feldspar (?), sericite (?)

Figure 4-26: Intergranular quartz and albite, and minor intersertal chlorite; thin section S 4, crossed nicols, 20 x. —— **0.1 mm** ——

(segregation vesicles (?)). This sample also contains quartz- ± chlorite-filled vugs; and amygdules composed of calcite and lesser amounts of fine grained anhedral quartz. Sericite veinlets are present in some sections. Like the trondhjemite dykes, disseminated pyrite, minor amounts of subhedral opaque minerals, sphene and tiny subhedral zircon occur throughout most samples.

Altered sample S 72 (Figures 3-3 and 3-4; Table 4-5) is characterized by a lack of albite. It comprises anhedral quartz grains (≤ 0.1 mm across) and an intergranular, typically interlocked network of sericite grains. Quartz veins, consisting of anhedral quartz grains 2-2.5 mm across, are also present. Disseminated pyrite and very minor amounts of chlorite, sphene and zircon make up the remainder of the section. A few quartz-chlorite veins and open-space fillings are noted.

4.3 Petrography of the Buchans Group

Thin sections S 82A and S 82B are of two samples of pillowed basalt from the Sandy Lake Formation of the Buchans Group collected along the side of Highway 350 about 25 km east of the town of Buchans, near Mary March Provincial Park (Table 4-6). The samples contain abundant calcite ± quartz amygdules, 3 mm in diameter. Irregular masses of calcite occur throughout the sections. Various combinations of calcite, quartz and chlorite form 1 mm-wide pseudomorphs of olivine (?) or clinopyroxene (?) in places. Subhedral grains of chromite are present in many of the pseudomorphs. In addition, the samples contain a few 1 mm-long calcite ± quartz pseudomorphs of plagioclase (?). The groundmass consists of 0.1-0.2 mm-long carbonatized, sericitized plagioclase laths; intersertal light green chlorite and anhedral quartz; and accessory, intergranular sphene.

Thurlow (1981a) describes the petrography of the Footwall Basalt pillow lavas of the Buchans Group as follows: "The pillow lavas are normally feldspar phyric with laths less than 2 mm long and of andesine-labradorite composition. Colourless to light brown augite phenocrysts are locally present and may attain sizes up to one centimetre, although those of 1-2 mm are most common. The groundmass consists of a fine grained intergrowth of plagioclase, clinopyroxene and much less magnetite. Matrix plagioclase is variably altered to various combinations of epidote, calcite, clay minerals and sericite and is locally replaced by pumpellyite. Clinopyroxene may be altered to epidote and chlorite."

Thin section S 63 (Figure 3-3; Table 4-6) is of quartz feldspar porphyritic dacite (felsic tuff (?)) from the Lundberg Hill Formation (formerly Wiley's Prominent Quartz sequence). The mineralogy is dominated by abundant rounded quartz grains (up to 7 mm across) and cloudy, brownish feldspar grains (2-4 mm across) that occur in a brownish aphanitic matrix. Accessory subhedral opaque minerals and sphene are also present.

4.4 Mineral Chemistry

Electron microprobe analyses of minerals from a suite of Skidder basalt samples, ranging from quench-textured, low-Zr basalts to high-Zr mafic rocks, were done to: i) indicate possible variations in the chemistry of preserved primary minerals with changes in composition of the host rock; ii) determine the composition of primary minerals such as clinopyroxene and chromite to be used as possible indicators of tectonic setting for the Skidder Basalt; iii) determine if variations in the composition of secondary minerals such as chlorite reflect variations in host rock composition and iv) examine the chemistry of secondary minerals to investigate effects of spilitization on the Skidder Basalt. Minerals in two Buchans Group samples, one of Sandy Lake Formation basalt (S 82A) and the other of quartz-feldspar-phyric dacite of the Lundberg Hill Formation (S 63), were analyzed for comparison with the Skidder Basalt. Minerals were analyzed using a JEOL JXA-50A wavelength dispersive electron microprobe; analytical techniques are given in Appendix A.

4.4.1 Clinopyroxenes

4.4.1.1 Introduction

Many of the elements that are common in basalts (except potassium) can be incorporated into the clinopyroxene structure. Although spilitized basalts such as those of the Skidder area are dominated by secondary mineral assemblages, clinopyroxenes in spilites elsewhere have been found to be in equilibrium with magmatic Ca-rich feldspars, not secondary albite, and are considered to have a primary magmatic origin (e.g. Battey, 1974; Vallance, 1974).

Kushiro (1960) and LeBas (1962) showed that the composition of clinopyroxenes varies according to the chemistry of the host lavas. Thus, clinopyroxenes from alkali basalts are Al- and Ti-rich but Si-poor relative to clinopyroxenes from tholeiitic lavas; and clinopyroxenes from island arc tholeiites have lower Cr and Ti contents than clinopyroxenes from ocean floor basalts. Using these differences, several scattergrams and

ternary diagrams of clinopyroxene components have been proposed to discriminate basalts of different tectonic settings (e.g. Kushiro, 1960; LeBas, 1962; Nisbet and Pearce, 1977; and Leterrier et al., 1982). However, as shown by Coish and Taylor (1979) and discussed by Leterrier et al. (1982), factors other than the chemistry of the host lava play a role in determining clinopyroxene compositions. Coish and Taylor (1979) and Grove and Bence (1977) show that cooling rate can profoundly affect the amounts of minor components such as Ti and Al incorporated into the clinopyroxene structure. They indicate that clinopyroxenes from basalts showing quench textures typically have higher Ti and Al contents. Coish and Taylor (1979) suggest that greater amounts of Ti and Al are present in quenched clinopyroxenes partly due to the preference of growth over diffusion from growth surfaces during rapid crystallization. "Impurities " such as Ti and Al which have lower distribution coefficients between clinopyroxene and liquid relative to the major components would normally be expelled from the clinopyroxene structure under slow-cooling equilibrium conditions but are retained during rapid crystallization (cf. Grove and Bryan, 1983). Also, rapid crystallization suppresses the ability of plagioclase to nucleate more than that of olivine and clinopyroxene, thereby increasing the availability of Al and Ca ions for incorporation into the clinopyroxene structure (Grove and Bryan, 1983). Coupled substitution, e.g. Si for Al, in the tetrahedral site also affect clinopyroxene composition, e.g. greater amounts of Al will result in lesser amounts of Si being present. Hence, availability and incorporation of components such as Al or Ti in clinopyroxene affect the contents of other elements. These other factors may result in mis-classification of the basalt types on diagrams utilizing elements such as Ti and Al (Coish and Taylor, 1979).

Clinopyroxenes that do not show quench textures but contain high Al may be indicative of deep seated or xenocrystic origin since solubility of Al in clinopyroxene increases with pressure (Stolper, 1980; Grove and Bryan, 1983). High Cr contents in clinopyroxenes may also indicate a similar origin (Bence and Bender, 1978).

4.4.1.2 Discussion of results

Electron microprobe analyses of Skidder Basalt clinopyroxenes are presented in Table 4-7; they are arranged in ascending order on the basis of Zr concentration in whole rock (Chapter 5). Clinopyroxenes in thin sections S 59 and S 19 are predominantly elongate grains showing evidence of quenching. Clinopyroxenes from thin section S 81 are typically stubby grains displaying intergranular texture. Clinopyroxene analyses presented for samples S 53, S 79 and S 60 are predominantly of large grains. These grains are probably not xenocrysts but microphenocrysts in equilibrium with the final melt from which the rocks crystallized since small, matrix clinopyroxenes analyzed in S 53 and S 79 are not of significantly different chemical composition from the larger grains. Thin section S 25 is of a medium grained diabase in which the clinopyroxenes typically display subophitic intergrowth with albitized plagioclase.

Analyses of clinopyroxenes in samples S 59 and S 19, which show quench textures, are enriched in Ti, Al and Ca, and depleted in Si and Mg relative to the others (Table 4-7; Figure 4-27). The high Ti and Al in the quench-textured clinopyroxenes is supportive of conclusions drawn by Coish and Taylor (1979), Grove and Bence (1977), Leterrier et al. (1982) and Grove and Bryan (1983) as discussed in the introduction above. Sample S 19 has a relatively high whole rock Zr concentration relative to other quench-textured Skidder basalts. Clinopyroxenes in this sample also contain higher Ti concentrations than those of lower-Zr, quench-textured basalts probably reflecting a greater concentration of Ti in the liquid from which they crystallized. The relatively high contents of Ca and Al in these clinopyroxenes may reflect suppression of plagioclase nucleation due to rapid cooling thereby making more Ca and Al available to be incorporated into the clinopyroxene structure (Grove and Bryan, 1983). Low contents of Mg and Si in the clinopyroxenes reflect coupled substitution effects since Al substitutes for Si, and Al and Ca substitute for Mg in the clinopyroxene structure.

Table 4-7: Electron microprobe analyses of Skidder Basalt clinopyroxenes; analyses that have been averaged are presented in Table A-2, Appendix A

	Zr ≤ 50 ppm				Zr>50≤85 ppm				
Weight %	S 59	S 59	S 81	S 81	S 19	S 19	S 19	S 53	S 53
SiO_2	48.65	47.90	50.53	48.59	48.90	48.19	46.11	53.43	53.59
TiO_2	0.73	1.54	0.67	1.02	1.43	2.08	3.18	0.47	0.50
Al_2O_3	6.04	4.63	4.09	6.48	6.35	6.86	6.06	3.08	2.52
Cr_2O_3	0.26	0.04	0.13	0.10	0.11	0.10	0.08	0.62	0.22
FeO*	7.40	11.17	9.48	8.06	10.30	10.12	10.12	6.45	8.26
MnO	0.15	0.14	0.27	0.18	0.29	0.16	0.25	0.16	0.25
NiO	0.03	0.00	0.05	0.07	0.02	0.03	0.00	0.03	0.07
MgO	13.27	13.14	15.46	14.64	11.89	12.00	12.25	17.19	16.60
CaO	21.66	19.74	20.14	20.10	21.24	21.58	19.44	19.40	18.86
Na_2O	0.28	0.12	0.22	0.15	0.39	0.35	0.27	0.25	0.27
K_2O	0.01	0.01	0.00	0.01	0.01	0.00	0.01	0.01	0.00
Total	98.46	98.43	101.04	99.40	100.93	101.47	97.77	101.09	101.14
Si	1.836	1.834	1.866	1.814	1.822	1.788	1.775	1.932	1.948
Ti	0.021	0.044	0.019	0.029	0.040	0.058	0.092	0.013	0.014
Al	0.269	0.209	0.178	0.285	0.279	0.300	0.275	0.131	0.108
Cr	0.008	0.001	0.004	0.003	0.003	0.003	0.002	0.018	0.006
Fe	0.234	0.358	0.293	0.252	0.321	0.314	0.326	0.195	0.251
Mn	0.005	0.005	0.008	0.006	0.009	0.005	0.008	0.005	0.008
Ni	0.001	0.000	0.002	0.002	0.001	0.001	0.000	0.001	0.002
Mg	0.746	0.750	0.851	0.814	0.660	0.663	0.703	0.926	0.899
Ca	0.876	0.810	0.797	0.804	0.848	0.858	0.802	0.751	0.735
Na	0.020	0.009	0.016	0.011	0.028	0.025	0.020	0.017	0.019
K	0.000	0.000	0.000	0.000	0.000	0.000	0.000	0.000	0.000
Total	4.015	4.021	4.033	4.019	4.012	4.015	4.004	3.990	3.990
Fe/(Fe+Mg)	0.24	0.32	0.26	0.24	0.33	0.32	0.32	0.17	0.22
Oxygens	6	6	6	6	6	6	6	6	6
Analyses	4	1	3	1	3	4	1	3	1
Whole Rock (complete analyses presented in Appendix B)									
Zr (ppm)	16	16	44	44	62	62	62	66	66
TiO_2 (%)	0.49	0.49	0.87	0.87	1.13	1.13	1.13	1.09	1.09
Fe_2O_3 (%)**	10.12	10.12	10.78	10.78	9.23	9.23	9.23	9.51	9.51
MgO (%)	11.13	11.13	8.87	8.87	7.08	7.08	7.08	7.64	7.64

* Total iron as FeO

** Total iron as Fe_2O_3

Table 4-7 (continued): Electron microprobe analyses of Skidder Basalt clinopyroxenes having Zr concentrations > 50 ≤ 85 ppm

	Large Grain									
	Rim	Core								
Weight %	S 53	S 53	S 25	S 25	S 79	S 79	S 79	S 60	S 60	S 60
SiO_2	52.82	52.46	52.01	51.82	54.71	53.44	52.26	52.25	52.91	51.34
TiO_2	0.57	0.83	0.67	0.87	0.39	0.52	0.72	0.65	0.50	0.78
Al_2O_3	2.69	3.70	3.59	3.98	2.71	3.50	3.79	3.07	2.05	3.12
Cr_2O_3	0.14	0.03	0.05	0.08	0.10	0.11	0.04	0.16	0.03	0.03
FeO*	9.15	9.74	8.64	8.33	7.41	7.98	10.67	9.08	12.00	11.61
MnO	0.27	0.14	0.23	0.17	0.18	0.16	0.25	0.20	0.25	0.28
NiO	0.01	0.05	0.02	0.02	0.00	0.02	0.01	0.04	0.02	0.01
MgO	16.31	15.38	14.92	15.52	17.25	16.82	15.20	16.28	16.65	15.11
CaO	18.54	19.19	19.60	19.89	20.99	19.51	19.44	19.98	16.55	18.29
Na_2O	0.34	0.36	0.18	0.28	0.26	0.27	0.31	0.22	0.29	0.38
K_2O	0.00	0.00	0.01	0.00	0.00	0.01	0.01	0.01	0.01	0.01
Total	100.84	101.88	99.89	100.96	104.00	102.31	102.70	101.91	101.24	100.95
Si	1.935	1.909	1.923	1.897	1.934	1.920	1.897	1.903	1.944	1.903
Ti	0.016	0.023	0.018	0.024	0.010	0.014	0.020	0.018	0.014	0.022
Al	0.116	0.159	0.157	0.172	0.113	0.148	0.162	0.131	0.089	0.136
Cr	0.004	0.001	0.001	0.002	0.003	0.003	0.001	0.005	0.001	0.001
Fe	0.280	0.296	0.267	0.255	0.219	0.240	0.324	0.276	0.369	0.360
Mn	0.008	0.004	0.007	0.005	0.005	0.005	0.008	0.006	0.008	0.009
Ni	0.000	0.001	0.000	0.001	0.000	0.000	0.000	0.001	0.001	0.000
Mg	0.890	0.834	0.822	0.847	0.909	0.900	0.823	0.884	0.912	0.835
Ca	0.728	0.748	0.776	0.780	0.795	0.751	0.756	0.780	0.652	0.726
Na	0.024	0.025	0.013	0.020	0.018	0.018	0.022	0.016	0.021	0.027
K	0.000	0.000	0.000	0.000	0.000	0.000	0.000	0.000	0.000	0.001
Total	4.002	4.001	3.986	4.002	4.007	4.000	4.013	4.019	4.008	4.020
Fe/Fe+Mg	0.239	0.262	0.245	0.232	0.194	0.210	0.282	0.238	0.288	0.301
Oxygens	6	6	6	6	6	6	6	6	6	6
Analyses	1	1	2	3	1	2	3	2	2	3
Whole Rock (complete analyses presented in Appendix B)										
Zr (ppm)	66	66	73	73	78	78	78	82	82	82
TiO_2 (%)	1.09	1.09	1.45	1.45	1.15	1.15	1.15	1.27	1.27	1.27
Fe_2O_3 (%)**	9.51	9.51	11.68	11.68	13.49	13.49	13.49	13.68	13.68	13.68
MgO (%)	7.64	7.64	7.35	7.35	5.90	5.90	5.90	6.66	6.66	6.66

* Total iron as FeO

** Total iron as Fe_2O_3

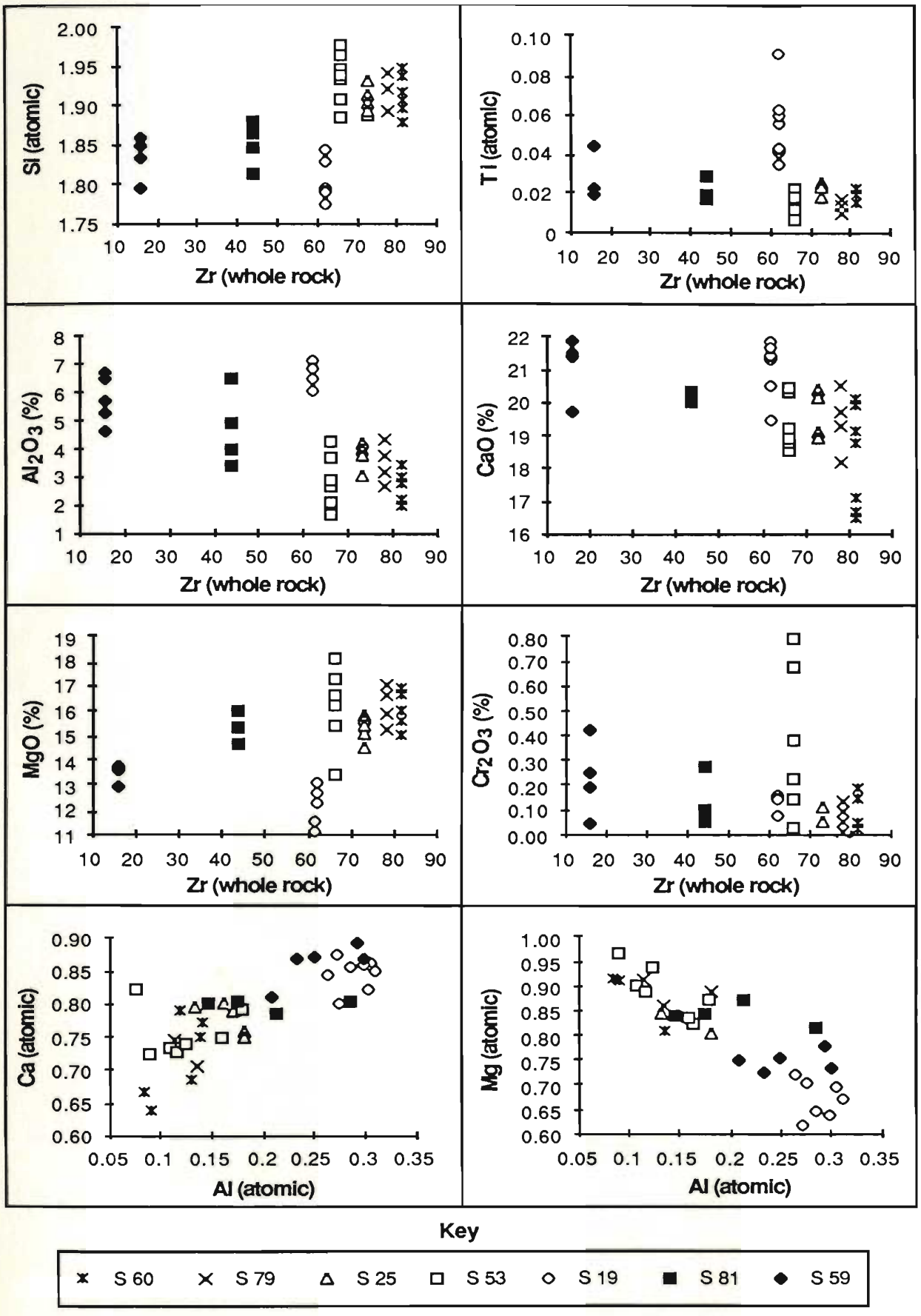

Figure 4-27: Miscellaneous X-Y plots for Skidder Basalt clinopyroxenes. See text for discussion.

Some clinopyroxenes in sample S 53 have high Cr contents despite the relatively high whole rock Zr concentration of the host rock (Table 4-7; Figure 4-27). The highest Cr contents of the clinopyroxenes analyzed in this sample are in small stubby grains; and the rim of a large clinopyroxene grain in the sample has higher Cr and lower Al and Ti contents than its core (Table 4-7; Figure 4-27). This would suggest that the melt from which the high-Cr clinopyroxenes in S 53 crystallized was enriched in Cr.

A chromite grain analyzed in thin section S 53 contains a higher Ti content than other Skidder Basalt chromites (Section 4.4.2) and as indicated above several of the clinopyroxenes in the sample have high Cr contents. Irvine (1967; 1976) reports a peritectic relationship between chromite and clinopyroxene. Thus, the compositions of clinopyroxene and chromite in S 53 may reflect a point in magmatic evolution at which clinopyroxene joined the liquidus and was forming at the expense of chromite. Alternatively, the high-Ti chromite composition may have resulted from Cr-spinel crystallization triggered by an influx of fresh magma since Dick and Bullen (1984) indicate that magma mixing may trigger Cr-spinel crystallization even at low Cr concentrations (Irvine, 1967).

4.4.1.3 Quadrilateral plots and discrimination diagrams

The Skidder Basalt clinopyroxenes plot mainly in the augite field on the pyroxene quadrilateral, with the exception of the quench-textured, Ti-enriched samples which plot as salites (Figure 4-28). They plot within the Al^{iv}-rich portion of the "others" diagram of Papike et al. (1974) (Figure 4-28). Proportions of the pyroxene quadrilateral components in the Skidder Basalt clinopyroxenes are similar to those in clinopyroxenes from both ocean floor basalts and island arc lavas, which essentially overlap on the pyroxene quadrilateral although some ocean floor basalt clinopyroxenes crystallizing from late-stage melts may reach more iron-rich compositions (Basaltic Volcanism Study Project (BVSP), 1981a;

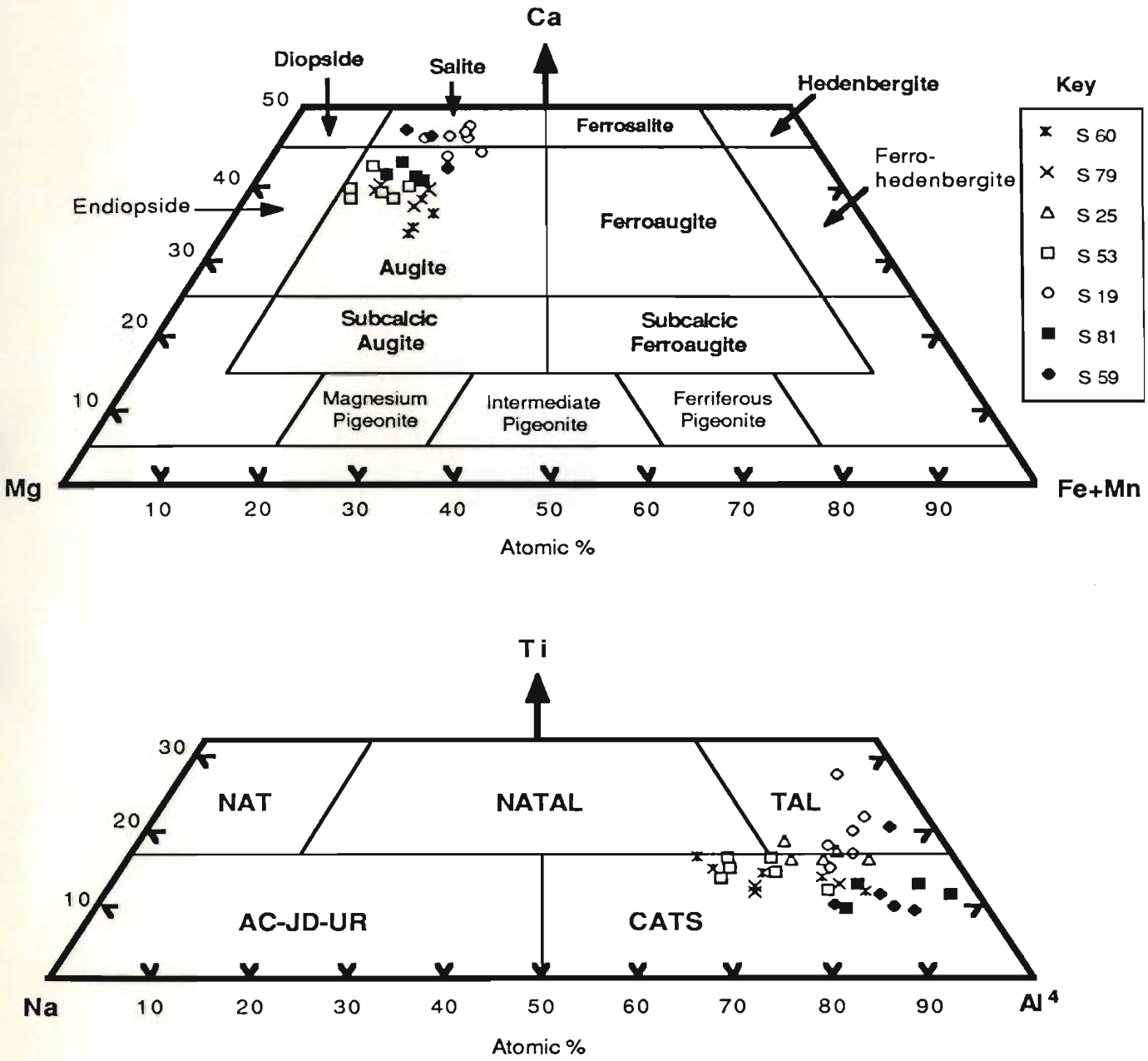

Figure 4-28: Skidder Basalt clinopyroxenes plotted on the pyroxene quadrilateral (Poldervaart and Hess, 1951; Deer et al., 1966) and the "Others" diagram of Papike et al, (1974).

1981c). Clinopyroxenes of endiopside composition, which are often reported to occur in orogenic basalts (Ewart, 1976) but are rare in ocean floor basalts (e.g. BVSP, 1981a), are not noted in the Skidder Basalt.

On Figures 4-29, 4-30 and 4-31, the Skidder Basalt clinopyroxenes are plotted on diagrams after LeBas (1962), Nisbet and Pearce (1977) and Leterrier et al. (1982) used by them to discriminate between different basalt types. On the SiO_2 vs. Al_2O_3 diagram (Figure 4-29), most of the non-quench-textured clinopyroxenes plot in the field of clinopyroxenes from non-alkaline basalts, but the quench-textured clinopyroxenes plot in the fields of clinopyroxenes from alkaline or peralkaline basalts (see discussion regarding quench-textured clinopyroxenes in Section 4.4.1.2 above) (cf. Coish and Taylor, 1979).

On the TiO_2-MnO-Na_2O diagram (Figure 4-30) some of the Skidder Basalt clinopyroxenes plot within the ocean floor basalt field; quench-textured clinopyroxenes from S 19 plot in the within plate, alkali basalt field; but most plot in overlapping fields, predominantly that of all basalts.

On the Ti vs. (Ca + Na) diagram used by Leterrier et al. (1982) to distinguish tholeiitic and calc-alkaline basalts from alkali basalts, the Skidder Basalt clinopyroxenes plot on the tholeiitic and calc-alkaline basalt side of the dividing line, within the tholeiitic and calc-alkaline basalt field (Figure 4-31a). Clinopyroxenes that show quench-textured morphologies (those in samples S 19 and S 59) have not been plotted on Figures 4-31a and 4-31b. Leterrier et al. (1982) cautioned that only pyroxene phenocrysts should be used on the diagrams to avoid compositional variations due to quenching and other factors. Clinopyroxene compositions plotting within the tholeiitic and calc-alkaline basalt field on Figure 4-31a are plotted on the second discrimination diagram of Leterrier et al. (1982) (Figure 4-31b). Seventy per cent of the Skidder Basalt clinopyroxenes plot on the non-orogenic basalt side of the dividing line on this diagram and most plot within the non-orogenic basalt field.

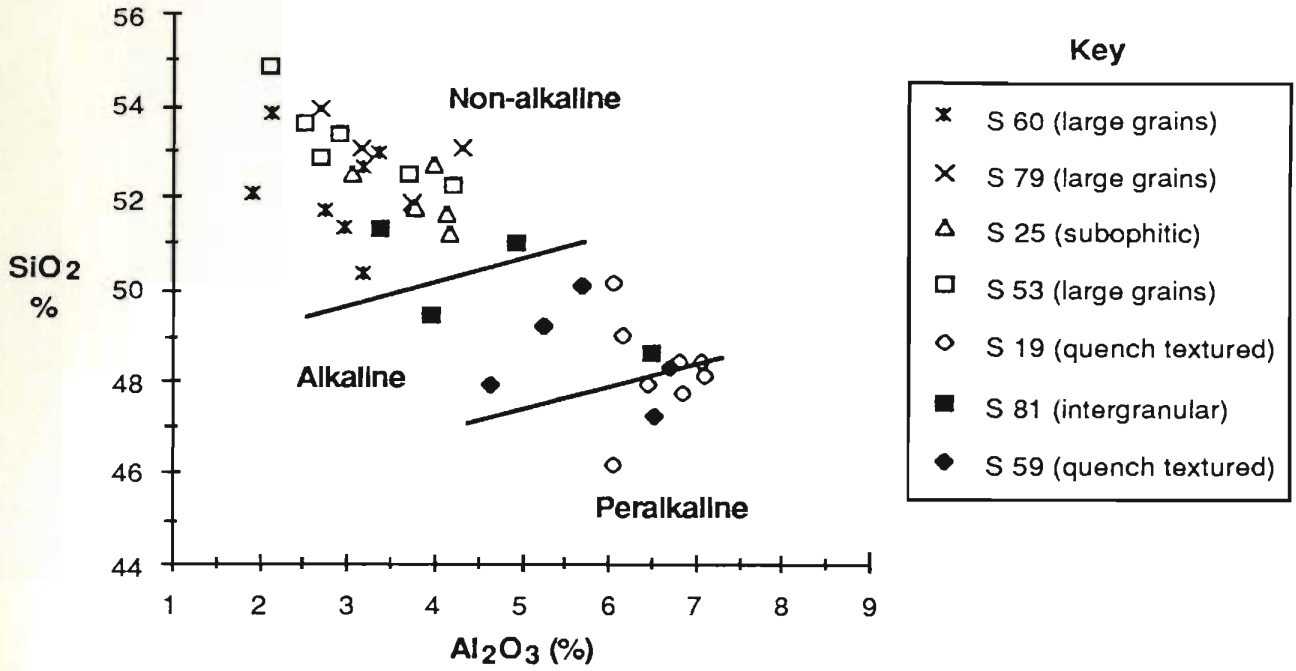

Figure 4-29: Skidder Basalt clinopyroxenes plotted on SiO_2-Al_2O_3 diagram. Fields for different basalt types after Le Bas (1962).

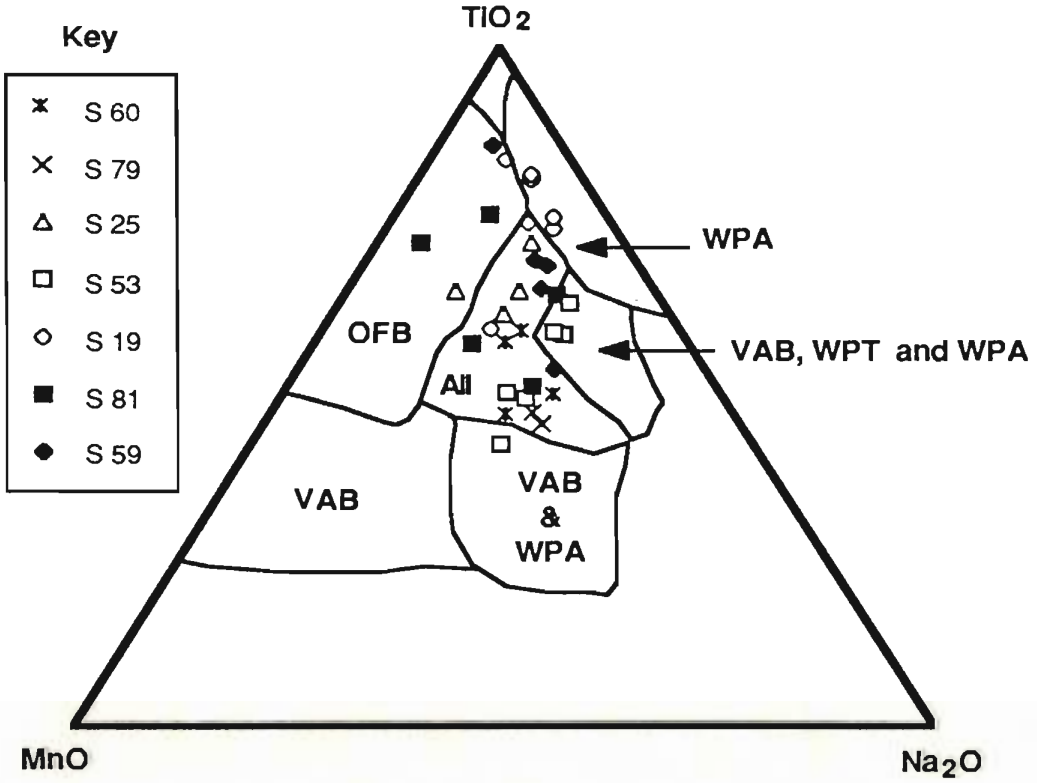

Figure 4-30: Clinopyroxenes from Skidder Basalt plotted on triangular diagram of weight per cent TiO_2 -MnO-Na_2O, used by Nisbet and Pearce (1977) to discriminate between basalts from different tectonic settings.
Key: VAB-volcanic arc basalts; OFB-ocean floor basalts; WPA-within plate alkalic basalts; and WPT-within plate tholeiitic basalts.

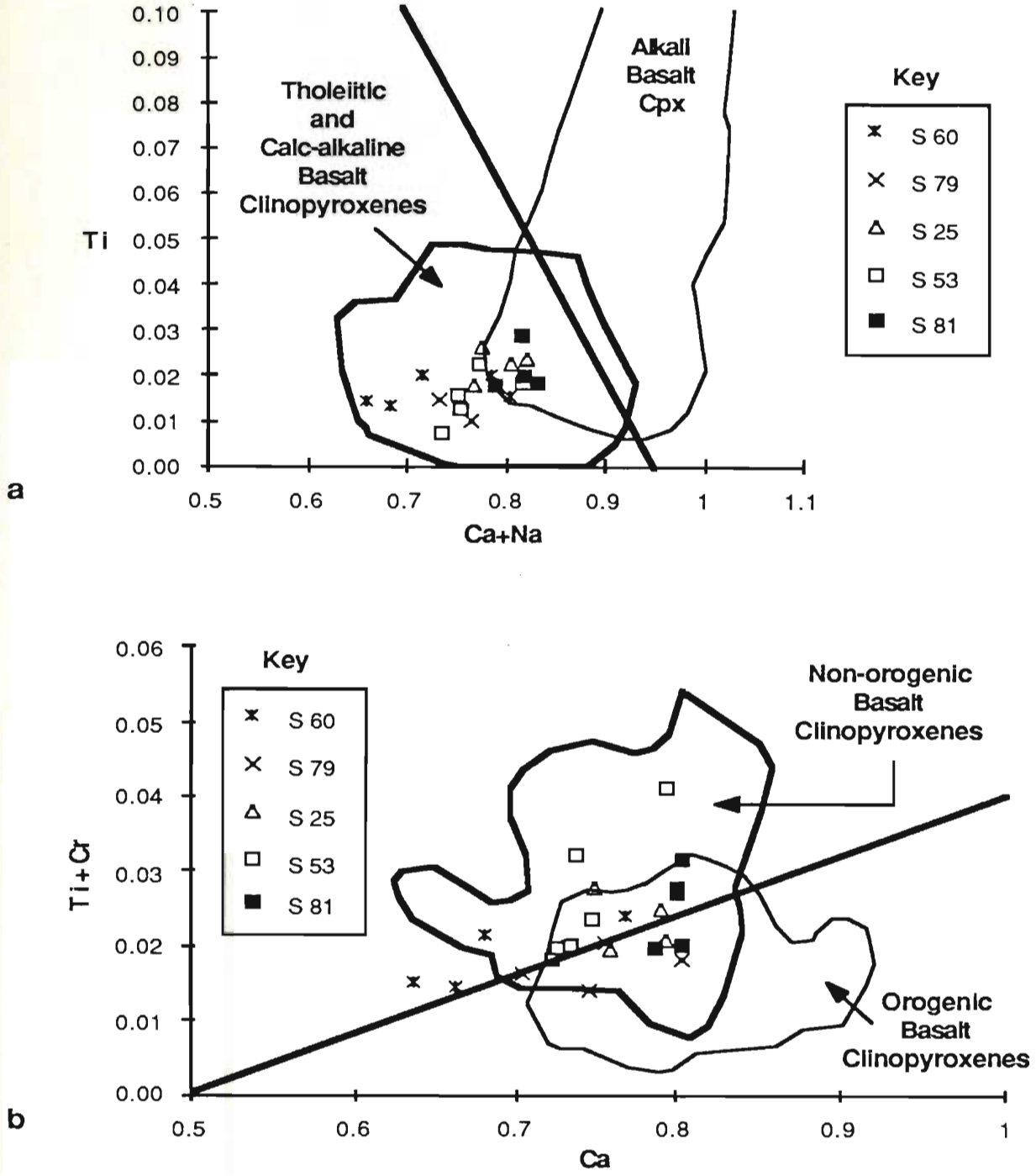

Figure 4-31: Clinopyroxenes from the Skidder Basalt plotted on discrimination diagrams after Leterrier et al. (1982). Values shown are in atomic proportions based on 6 oxygens. Samples in the key are arranged from highest Zr concentration at the top (S 60) to lowest Zr concentration at the bottom (S 81). Ninety-two per cent of clinopyroxenes from non-alkali basalts plot to the left of the line in the top figure, and 86% of clinopyroxenes from alkali basalts plot to the right of the line. Eighty-one per cent of clinopyroxenes from non-orogenic basalts plot above the line in the bottom figure, and 80% of clinopyroxenes from orogenic basalts plot below the line.
Abbreviation: cpx-clinopyroxene.

4.4.2 Chromites

4.4.2.1 Introduction and presentation of results

Chromite in the Skidder Basalt occurs as disseminated, opaque to translucent brown, subhedral grains, typically less than 0.1 mm in diameter. In places, the chromite grains are included in chlorite- or calcite-filled areas that are pseudomorphic after olivine (Figure 4-9). Although chromite is most common in the low-Zr Skidder basalts its occurrence is sporadic; Dick and Bullen (1984) report a similar irregular distribution of chromite in abyssal basalts, noting only a limited correlation between the occurrence of Cr-spinel and chromium in whole rock.

In Buchans Group basalt sample S 82A, subhedral grains of chromite occur in calcite-quartz-chlorite-bearing areas pseudomorphic after olivine (?) or clinopyroxene (?).

Electron microprobe analyses of Skidder Basalt chromites are presented in Table 4-8. Sample S 30 is of quench-textured, low-Zr basalt and sample S 53 is of non-quench-textured, intermediate-Zr basalt. Samples SK 28 75 and SK 28 78 are of chrome-rich basalts from the Skidder Prospect alteration zone (Chapter 6). Comparison of the chromite compositions of samples SK 28 75 and SK 28 78 to those of other Skidder Basalt samples suggests that the chromite compositions have been little affected by the alteration resulting from the Skidder Prospect mineralizing event. The Skidder Basalt chromites show little variation in major components Cr, Al, Fe and Mg (Table 4-8). Minor components Ti and Ni show greater variation such that chromites from sample S 53, which contains the highest whole rock Zr concentration, have the highest Ti and lowest Ni contents (Table 4-8).

Compared to the Skidder Basalt chromites, those of the Buchans Group are much more refractory, being significantly enriched in Cr and depleted in Al, Ti and Ni (Table 4-8). This is evident on Figure 4-32 and on Figure 4-33, the latter being the Cr/(Cr + Al) "Cr#" vs. Mg/(Mg + Fe^{2+}) "Mg#" plane of the spinel prism (cf. Stevens, 1944; Irvine, 1965). Fe^{2+} and Fe^{3+} in the Skidder Basalt and Buchans Group basalt chromites plotted on

Table 4-8: Analyses of Skidder Basalt and Buchans Group basalt chromites

							Skidder Prospect chlorite, quartz, pyrite alteration zone				Buchans Group Basalt Sandy Lake Formation		
Weight %	S 30	S 30	S 30	S 30	S 30	S 53	SK 28 75	SK 28 75	SK 28 78	SK 28 78	S 82A	S 82A	S 82A
SiO_2	0.11	0.07	1.18	1.00	0.13	0.10	0.13	0.09	0.10	0.18	0.12	0.08	0.09
TiO_2	0.74	0.48	0.52	0.53	0.49	1.02	0.52	0.45	0.63	0.56	0.36	0.40	0.34
Al_2O_3	21.29	23.78	20.44	21.18	21.16	22.36	24.55	22.76	24.41	23.50	14.41	13.93	12.60
Cr_2O_3	33.93	36.64	37.55	38.48	39.12	35.95	37.92	39.75	40.05	40.66	48.75	50.67	51.45
FeO*	23.80	23.25	23.57	26.38	23.89	26.49	25.00	24.98	21.42	22.17	24.55	25.12	24.94
MnO	0.28	0.21	0.06	0.70	0.14	0.23	0.25	0.30	0.21	0.23	0.31	0.33	0.24
NiO	0.23	0.22	0.16	0.22	0.16	0.14	0.13	0.16	0.18	0.16	0.18	0.05	0.11
MgO	13.01	14.04	12.28	12.11	13.11	12.49	12.03	11.75	14.07	13.76	12.38	11.24	10.82
CaO	1.12	0.21	0.80	0.61	0.37	0.06	0.01	0.03	0.01	0.02	0.71	0.02	0.09
Na_2O	0.09	0.10	0.06	0.05	0.02	0.08	0.04	0.11	0.00	0.01	0.00	0.00	0.00
Total	94.61	99.00	96.63	101.28	98.59	98.93	100.58	100.38	101.09	101.27	101.78	101.86	100.68
Atomic proportions (based on 4 oxygens)													
Ti	0.019	0.011	0.013	0.013	0.012	0.025	0.012	0.011	0.014	0.013	0.009	0.010	0.008
Al	0.835	0.880	0.784	0.784	0.798	0.843	0.900	0.844	0.879	0.850	0.547	0.531	0.490
Cr	0.892	0.909	0.966	0.955	0.990	0.909	0.932	0.988	0.967	0.986	1.241	1.296	1.341
Fe	0.662	0.610	0.641	0.692	0.639	0.708	0.650	0.657	0.547	0.569	0.661	0.680	0.687
Mg	0.645	0.657	0.595	0.566	0.625	0.595	0.558	0.551	0.640	0.629	0.594	0.542	0.532
Si+Mn+Ni+Na+Ca	0.063	0.026	0.076	0.079	0.026	0.020	0.017	0.023	0.013	0.017	0.041	0.014	0.016
Total	3.117	3.095	3.076	3.089	3.091	3.099	3.069	3.074	3.060	3.064	3.094	3.074	3.073
Fe^{2+}	0.334	0.350	0.392	0.415	0.383	0.421	0.453	0.454	0.369	0.380	0.399	0.471	0.480
Fe^{3+}	0.328	0.260	0.250	0.277	0.256	0.287	0.197	0.203	0.178	0.188	0.262	0.209	0.207
$Fe^{3+}/Fe^{3+}+Cr+Al)$	0.160	0.127	0.125	0.138	0.125	0.141	0.097	0.100	0.088	0.093	0.128	0.103	0.102
Cr/(Cr+Al)	0.517	0.508	0.552	0.549	0.554	0.519	0.509	0.539	0.524	0.537	0.694	0.709	0.732
Mg/(Mg+Fe^{2+})	0.659	0.652	0.603	0.577	0.620	0.586	0.552	0.548	0.634	0.623	0.598	0.535	0.525
Whole Rock (complete analyses presented in Appendix B)													
Zr (ppm)	30	30	30	30	30	66	50	50	51	51	53	53	53
TiO_2 (%)	0.61	0.61	0.61	0.61	0.61	1.09	0.55	0.55	0.88	0.88	0.58	0.58	0.58
Cr (ppm)	349	349	349	349	349	182	483	483	773	773	455	455	455
Fe_2O_3 (%)**	7.60	7.60	7.60	7.60	7.60	9.51	10.36	10.36	7.24	7.24	7.98	7.98	7.98
MnO (%)	0.13	0.13	0.13	0.13	0.13	0.16	0.17	0.17	0.10	0.10	0.32	0.32	0.32
MgO (%)	5.70	5.70	5.70	5.70	5.70	7.64	16.68	16.68	9.08	9.08	6.79	6.79	6.79

* Total iron as FeO
** Total iron as Fe_2O_3
Fe^{2+} and Fe^{3+} calculated assuming stoichiometric spinel formula

Figure 4-33 were assigned assuming stoichiometric proportions of components according to the ideal spinel formula $R^{2+}R^{3+}{}_2O_4$. The Skidder Basalt chromites form a tight cluster near the Cr-rich portion of the field for abyssal basalts (Dick and Bullen, 1984) on Figure 4-33 whereas the Buchans Group samples plot at higher Cr#'s outside the abyssal basalt field and within the field of Aleutian basalts (Dick and Bullen, 1984).

Figure 4-34a compares the chromite compositions of the Skidder and Buchans Group basalts to those of basalts from different tectonic settings using the Cr# vs. Mg# plane of the spinel prism. On these diagrams, the Skidder Basalt chromite compositions overlap the Cr-rich portions of the fields for chromites from abyssal and back arc basin basalts but are less Cr-rich than chromites of Aleutian basalts, boninites and basalts from the Troodos Ophiolite. The Buchans Group basalt chromites, which plot in the field of chromites from the Aleutian basalts, have similar Cr#'s but slightly lower Mg#'s than the Troodos Ophiolite basalt chromites and have lower Cr#'s than chromites from boninites.

The Skidder basalt chromites overlap the Cr-rich region of the abyssal peridotite chromite field (Dick and Bullen, 1984) and the lower portion of the field for chromites from harzburgites of the Bay of Islands Ophiolite (Malpas, 1976) (Figure 4-34b). Both the Skidder Basalt and Buchans group basalt chromites have Cr#'s less than those of the Betts Cove Ophiolite (Coish and Church, 1979) which overlap the field for boninite chromites (Cameron et al., 1980) (Figure 4-34b).

Data presented by Malpas and Strong (1975) indicate that most chromites from the Great Bend and Pipestone Pond ultramafic bodies of central Newfoundland and those of the Burlington Peninsula have higher Cr#'s than the Skidder Basalt chromites and many are more refractory than chromites of the Buchans Group basalt.

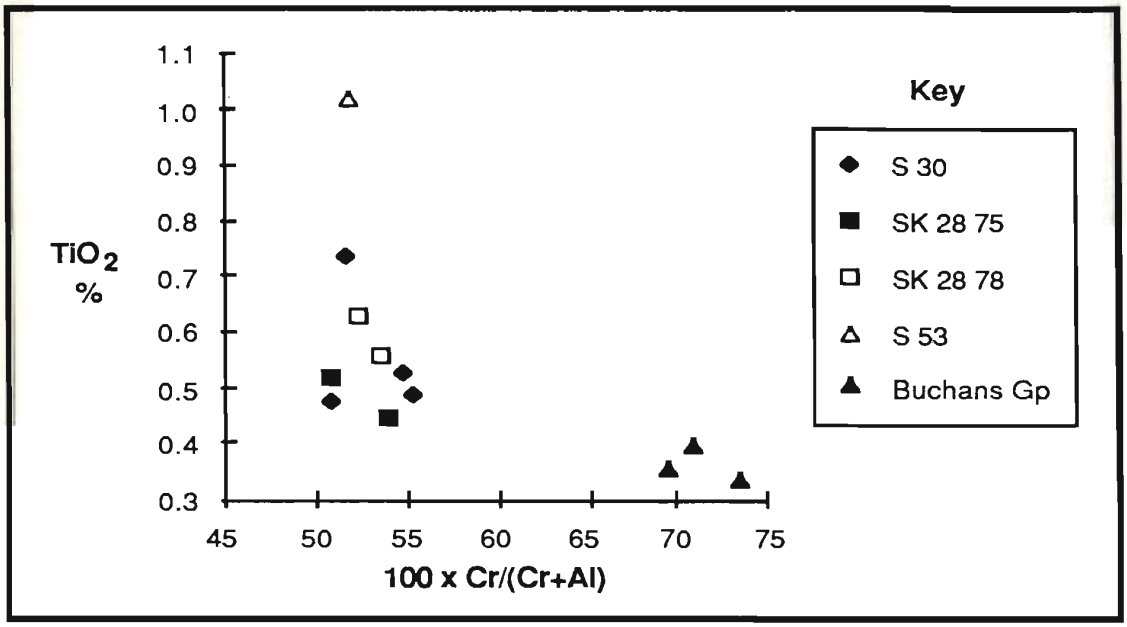

Figure 4-32: Weight per cent TiO_2 vs. 100 x Cr/(Cr+Al) for Skidder Basalt and Buchans Group chromites.

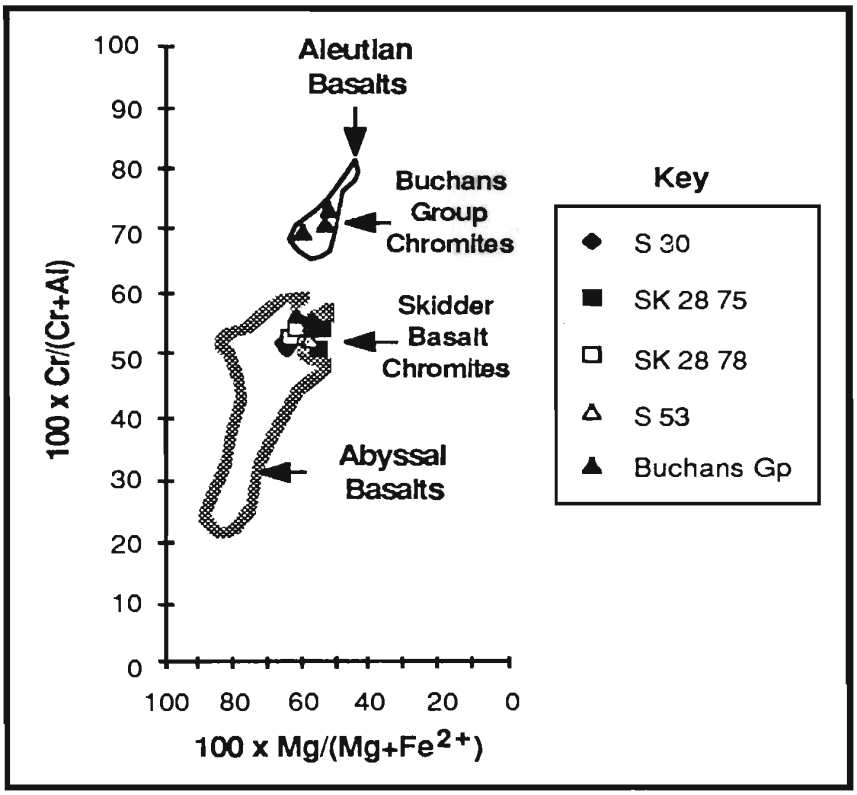

Figure 4-33: Skidder Basalt and Buchans Group chromite compositions plotted on 100 x Cr/(Cr+Al) vs. 100 x Mg/(Mg+Fe^{2+}) diagram (after Stevens, 1944; Irvine, 1965). Fe^{2+} assigned assuming stoichiometric proportions of components according to the ideal spinel formula. Fields for abyssal and Aleutian basalts after Dick and Bullen (1984).

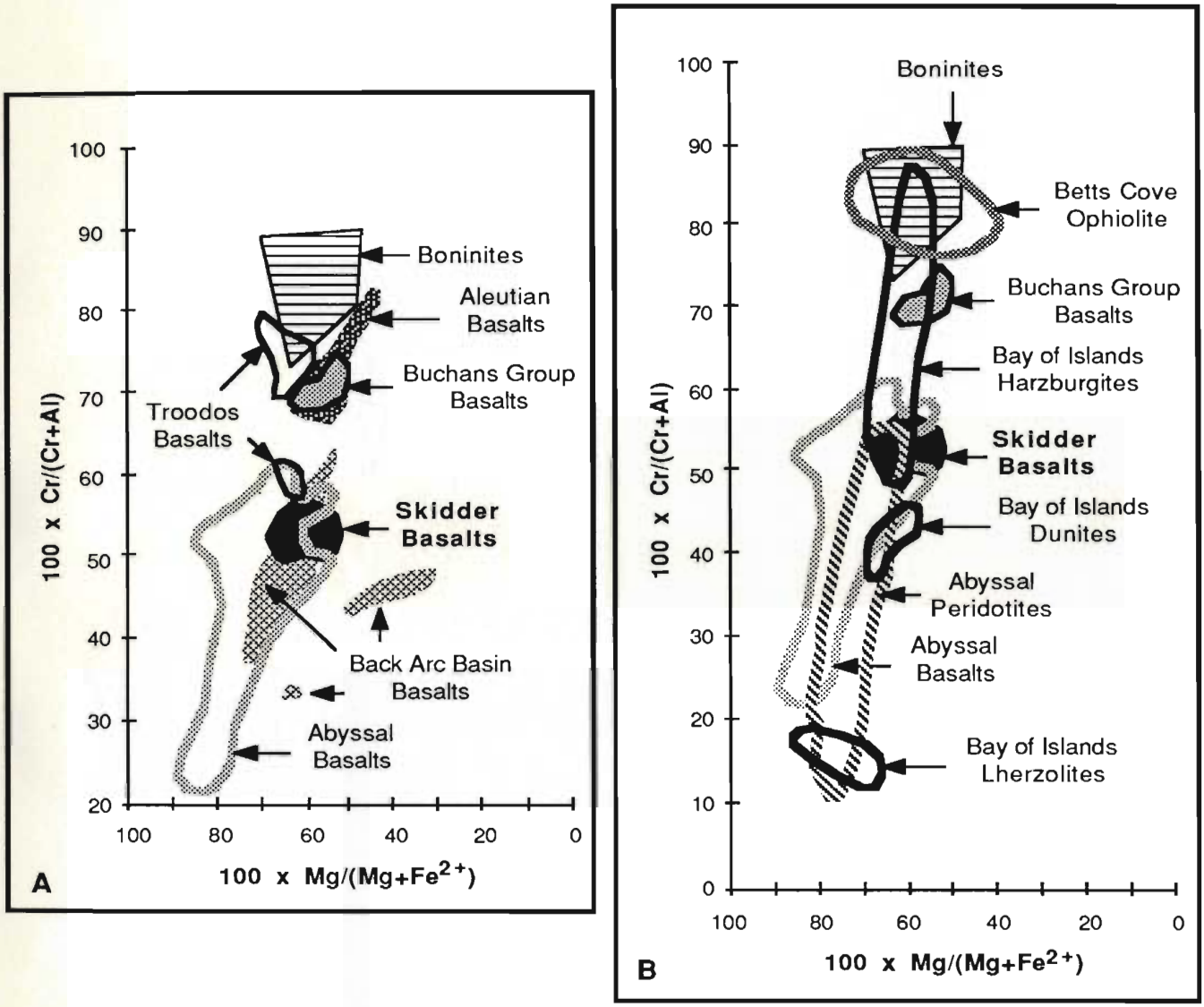

Figure 4-34: Skidder Basalt and Buchans Group chromite compositions compared to those of basalts and ultramafic rocks from various tectonic settings, and to those of Newfoundland ophiolites. Abyssal basalts chromites are from Sigurdsson and Schilling (1976), Dick and Bryan (1978), and Dick and Bullen (1984); the boninite chromites are from Cameron et al. (1980); the Aleutian basalts chromites are from Dick and Bullen (1984) (personal communication to them from C. Nye); the back arc basin basalts chromites are from Ridley et al. (1974), Saunders and Tarney (1979), Mattey et al. (1980), and Dick and Bullen (1984); and the Troodos basalts chromites are from Dick and Bullen (1984). Chromites from abyssal peridotites are from Dick and Bullen (1984); those from the Bay of Islands ophiolite are from Malpas (1976); and those from the Betts Cove ophiolite are from Coish and Church (1979).

4.4.2.2 Chromian spinel and basalt petrogenesis

Chromian spinel is sensitive to bulk rock composition and the petrogenesis of the host rock (e.g. Irvine, 1965; 1967; Thayer, 1970; and Dick and Bullen, 1984). Major factors that affect its composition include: a) preferential partitioning of two of its major components Mg and Fe^{2+} into the solid while Al partitions into the melt; b) partitioning of Mg and Fe^{2+} between spinel and silicate melt being temperature dependent, re-equilibration of olivine and spinel at lower temperatures causes a shift to lower Mg#'s; c) higher pressures (8-9 kb) favouring aluminum-rich spinel compositions and d) the ratio of Fe^{2+} to Fe^{3+} in spinel being dependent upon fO_2.

The most significant chemical variation noted in chromites from alpine peridotites, abyssal and island arc basalts, boninites and layered intrusions is the reciprocal variation of Cr and Al and the relatively small but persistent decrease in Mg# with increasing Cr# (e.g. Irvine, 1965; 1967; Dick and Bullen, 1984). An increase in Cr# from aluminous chromites of lherzolites, thought to represent primary or only slightly depleted mantle, to those of harzburgites, which are considered to be the residuum from partial melts that produce overlying "oceanic" crustal rocks, has been demonstrated for the Bay of Islands ophiolite (Malpas and Strong, 1975) and to a lesser extent for alpine-type peridotites (Dick and Bullen, 1984). Chromites from abyssal basalts (Dick and Bullen, 1984), back-arc-basin basalts (Dick and Bullen, 1984) and early formed oceanic crustal material, e.g. dunites from the Bay of Islands ophiolite (Malpas, 1976), occupy intermediate positions between lherzolite and harzburgite (Figure 4-34). Chromite compositions from oceanic fracture zones, e.g. the Islas Orcadas Fracture Zone (Le Roex et al., 1983), have lower Cr#'s and would plot at the lower part of the abyssal basalt field on Figure 4-34.

Chromian spinel accompanied by olivine crystallizes early in most basic igneous melts; it stops crystallizing shortly after the appearance of plagioclase (Dick and Bullen, 1984). In the ternary system SiO_2 - Mg_2SiO_4 - $MgCr_2O_4$, chromite co-precipitates with forsterite or a magnesium-rich pyroxene along liquidus boundaries very close to the SiO_2 -

forsterite join (Dick and Bullen, 1984); thus, only small amounts of Cr_2O_3 are required to precipitate chromite even at potentially olivine- or pyroxene-rich compositions (Irvine, 1965).

Chromian spinel is a common accessory mineral of "primitive" abyssal basalts but rare in more differentiated basalts of this type. High-Al spinels in abyssal basalts are restricted to subhedral and resorbed grains in basalts representative of the most primitive melt compositions. Dick and Bullen (1984) conclude that, since most abyssal and alpine peridotites have compositions restricted to a narrow range of Mg#'s on the Cr# vs. Mg# diagram, they probably crystallized at a relatively uniform temperature of about 1100-1200°C.

The upper limit of spinel Cr#'s can give an indication of the degree of depletion of the underlying mantle (Dick and Bullen, 1984). Dick and Bullen (1984) suggest that during the production of abyssal basalts mantle melting has not proceeded beyond the diopside-in/diopside-out phase boundary for abyssal peridotites, suggesting a thermal divide exists at this degree of melting and, under the pressure conditions for production of these melts, a steep rise in temperature is required for further melting to occur.

Volcanic arc lavas and Alaskan intrusives, which are thought to have formed in magma reservoirs beneath island arcs, have chromites with Cr#'s higher than those of abyssal basalts. According to Irvine (1976) Cr#'s increase with the amount of silica in the melt. Chrome-rich spinels from island arc lavas may thus reflect high silica content of the parental melt (Dick and Bullen, 1984) and/or greater degrees of partial melting (beyond the diopside-in/diopside-out thermal divide). Interaction with hydrous fluids may provide the catalyst required to produce the greater amounts of melting. The refractory, high Cr#'s of boninite chromites clearly supports the conclusions of several workers (e.g. Crawford et al., 1981; Cameron et al., 1983) that these fore-arc rocks have been derived from melting of multiply depleted sub-arc mantle facilitated by interaction with slab-derived hydrous fluids.

Irvine (1976) showed that, in high-alumina melts, spinel Cr#'s and Mg#'s decrease with co-precipitating olivine until plagioclase joins olivine on the liquidus (Figure 4-35). Spinel Cr#'s increase slightly after plagioclase becomes a liquidus phase (Dick and Bullen, 1984). It is evident on Figure 4-35 that spinels coexisting with melts richer in SiO_2 have higher Cr#'s. Suggested schematic crystallization paths for abyssal basalts, island arc lavas, and boninites are presented on Figure 4-35 based on their respective chromite compositions. The suggested crystallization path for MORB on Figure 4-35 supports the mineral crystallization order suggested for abyssal basalts (e.g. Perfit et al., 1980; BVSP, 1981a), i.e. Cr-spinel + olivine; Cr-spinel + olivine + plagioclase; and plagioclase + clinopyroxene ± olivine. Note that the suggested crystallization path for island arc basalts on Figure 4-35 supports the late appearance of plagioclase on the liquidus of melts from which these rocks crystallized (cf. Perfit et al., 1980). For island arc basalts, Perfit et al., (1980) suggest a mineral crystallization order of: Cr-spinel + olivine; Cr-spinel + olivine + clinopyroxene; and clinopyroxene + plagioclase ± olivine. The Skidder Basalt Cr-spinel compositions would suggest a mineral crystallization order similar to abyssal basalts.

On ~~the basis of~~ chromite compositions the Skidder Basalt is suggested to have a similar petrogenesis to that of either abyssal or back arc basin basalts. In contrast, the more refractory chromite compositions of the Buchans Group basalt sample suggests a petrogenesis similar to island arc lavas for the Buchans Group basalts and thereby supports the conclusion reached by several workers in the Buchans area, i.e. that the Buchans Group was formed in an island arc setting (cf. Thurlow 1973; Thurlow et al., 1975; Thurlow, 1981a; Thurlow and Swanson, 1981).

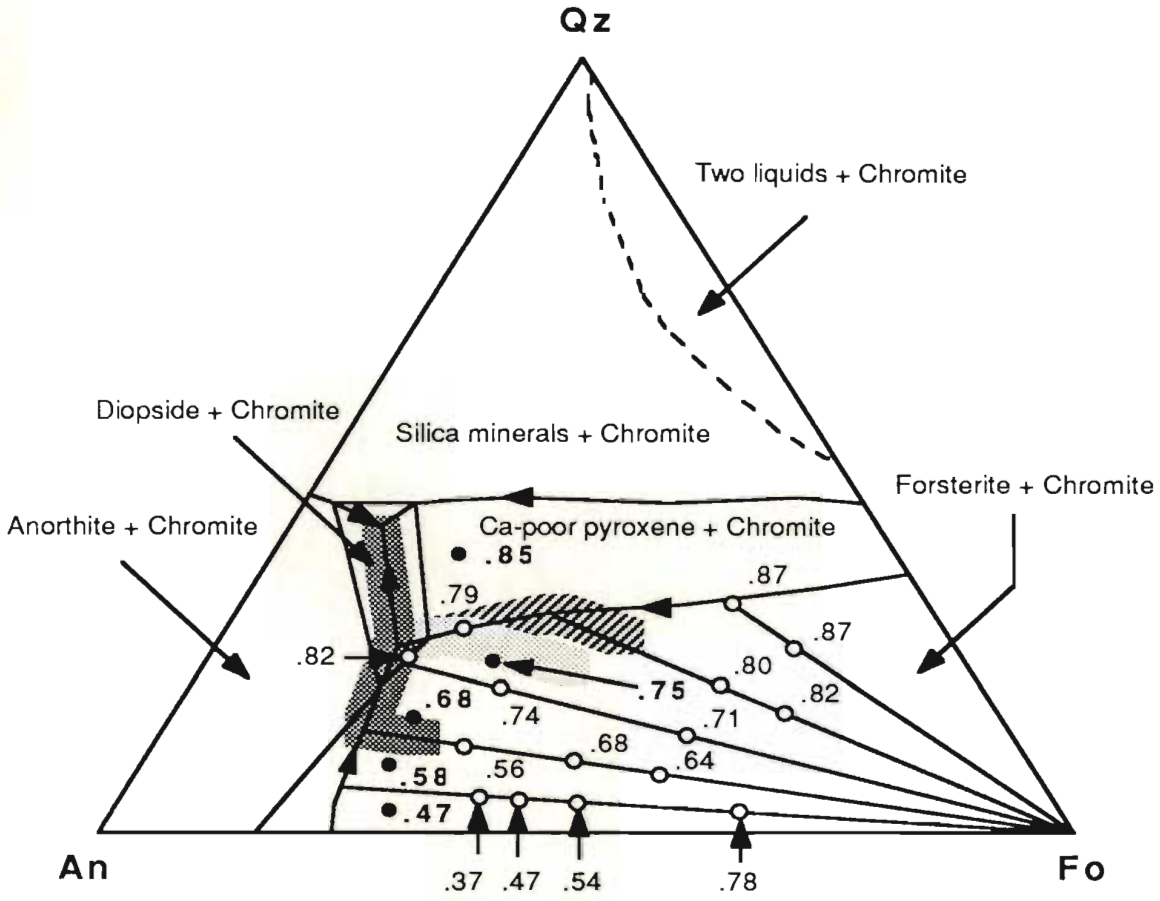

Figure 4-3 Silicate relations in the plane Fo-An-Qz (after Dick and Bullen, 1984). Cr/(Cr+Al) ratio of spinel in experimentally crystallized basalts of various compositions are shown (after Dick and Bullen, 1984; from Irvine, 1976). Open circles are experimentally crystallized synthetic glass compositions from Irvine (1976). Solid circles are natural glass and rock compositions (Dick and Bullen, 1984). Numbers next to symbols are the Cr/(Cr+Al) ratio of spinels co-existing with the particular melt composition (Irvine, 1976). Patterned lines are schematic illustrations of crystallization paths for MORB, Island arc lavas, and boninites based on the Cr/(Cr+Al) ratios of their chromites. Skidder Basalt chromite compositions have Cr/(Cr+Al) ratios of less than 0.55, suggesting a crystallization path similar to MORB.
Abbreviations: Qz-quartz, An-anorthite, Fo-forsterite.

4.4.3 Plagioclase

Analyses of plagioclase from a suite of Skidder Basalt samples are presented in Table 4-9, where they have been grouped according to whole rock Zr content of the host. Analyses of the same grain or grains which show a minimal variance in composition have been averaged. All analyses that have been averaged are presented in Appendix A (Table A-3).

Feldspars analyzed include: phenocrysts in thin sections S 59, S 60 and S 21A, which were analyzed in an effort to find primary magmatic calcium-rich plagioclase; feldspars displaying quench textures, including "belt-buckle"-textured feldspar in thin section S-30 and fan-spherulitic feldspar in thin section S 35A; and groundmass feldspar laths in several of the thin sections. The central portion of an altered feldspar phenocryst in sample S 59, of bytownite composition, represents the only non-albite plagioclase composition analyzed. All others are albite with molecular percentages ranging from 97 to 99% Ab, 0.6-2.2% An and 0.1-0.4% Or. There is no significant variation in albite compositions between albitized phenocrysts and groundmass laths or between albite displaying quench versus intergranular textures.

Table 4-10 lists analyses of feldspar phenocrysts and groundmass feldspars from Buchans Group basalt S 82A and Lundberg Hill Formation dacite S 63. Analyses that have been averaged are presented in Appendix A (Table A-3). Feldspars analyzed in basalt S 82A are of albite composition, having only 1.1 to 1.4 molecular per cent anorthite but up to 5.3 molecular per cent orthoclase. Plagioclase phenocrysts and groundmass feldspar analyzed in dacite S 63 are also albites. They have a similar range of orthoclase components as the basalt but their anorthite components are slightly greater.

Average albite compositions for the Skidder Basalt groupings and for the Buchans Group basalt and dacite are presented in Table 4-11. Plagioclase grains in Skidder basalts having higher Zr concentrations have a slightly higher average molecular percentage of albite and correspondingly lower molecular percentage of anorthite than plagioclase grains

Table 4-9: Electron microprobe analyses of plagioclase from the Skidder Basalt; analyses that have been averaged are presented in Table A-3, Appendix A

		Zr≤50 ppm			Zr>50≤85 ppm		Zr≥85 ppm
Rock Type	**Basalt**	**Basalt**			**Diabase**	**Basalt**	**Basalt**
Mineral	Bytownite	Albite	Albite	Albite	Albite	Albite	Albite
Weight %	**S 59**	**S 59**	**S 30**	**S 35A**	**S 25**	**S 60**	**S 21A**
SiO_2	52.40	68.17	68.80	67.48	69.36	67.86	69.31
TiO_2	0.01	0.03	0.02	0.01	0.01	0.03	0.00
Al_2O_3	20.39	19.45	19.83	19.19	19.98	19.85	19.00
Cr_2O_3	0.02	0.02	0.00	0.01	0.02	0.01	0.00
FeO*	1.89	0.25	0.07	0.29	0.14	0.56	0.02
MnO	0.00	0.02	0.03	0.04	0.00	0.03	0.01
NiO	0.03	0.01	0.00	0.00	0.00	0.04	0.02
MgO	0.02	0.02	0.00	0.00	0.01	0.03	0.01
CaO	18.74	0.35	0.34	0.48	0.21	0.25	0.14
Na_2O	2.18	11.66	11.96	11.59	12.59	11.82	11.92
K_2O	0.00	0.05	0.07	0.04	0.02	0.06	0.04
Total	95.68	100.02	101.12	99.13	102.34	100.54	100.46
Atomic Proportions (based on 8 oxygens)							
Si	2.545	2.984	2.979	2.983	2.973	2.96	3.013
Ti	0.000	0.001	0.001	0.000	0.000	0.00	0.000
Al	1.167	1.004	1.012	1.000	1.009	1.02	0.974
Cr	0.001	0.001	0.000	0.000	0.001	0.00	0.000
Fe	0.077	0.009	0.003	0.011	0.005	0.02	0.001
Mn	0.000	0.001	0.001	0.001	0.000	0.00	0.000
Ni	0.001	0.000	0.000	0.000	0.000	0.00	0.001
Mg	0.001	0.001	0.000	0.000	0.001	0.00	0.000
Ca	0.975	0.017	0.016	0.023	0.010	0.01	0.007
Na	0.205	0.989	1.004	0.993	1.046	1.00	1.005
K	0.000	0.003	0.004	0.002	0.001	0.00	0.002
Total	4.973	5.009	5.019	5.014	5.046	5.027	5.003
Analyses	1	4	1	1	1	4	3
Molecular %							
Ab	17.4	98.1	98.1	97.5	99.0	98.5	99.2
An	82.6	1.6	1.5	2.2	0.9	1.1	0.6
Or	0.0	0.3	0.4	0.2	0.1	0.3	0.2
Whole Rock (complete analyses given in Appendix B)							
Zr (ppm)	16	16	30	38	73	82	95

* Total iron as FeO

Table 4-10: Electron microprobe analyses of feldspars from the Buchans Group; sample S 82A is a basalt from the Sandy Lake Formation, and sample S 63 is a quartz-feldspar-phyric dacite of the Lundberg Hill Formation (cf. Thurlow and Swanson, 1987); analyses that have been averaged are presented in Table A-3, Appendix A

	Buchans Group Basalt				Lundberg Hill Formation Dacite			
	Albite			Sodic K-Feldspar	Albite			K-Feldspar
Weight %	S 82A	S 82A	S 82A	S 82A	S 63	S 63	S 63	S 63
SiO_2	68.04	67.37	66.77	62.42	67.65	68.62	66.00	63.55
TiO_2	0.00	0.00	0.03	0.05	0.00	0.00	0.01	0.00
Al_2O_3	19.44	18.91	20.02	21.91	19.58	19.64	20.17	23.32
Cr_2O_3	0.03	0.00	0.00	0.01	0.01	0.02	0.00	0.00
FeO*	0.21	0.33	0.52	1.49	0.05	0.03	0.45	0.78
MnO	0.00	0.01	0.00	0.00	0.01	0.00	0.00	0.04
NiO	0.00	0.05	0.05	0.00	0.03	0.01	0.00	0.01
MgO	0.02	0.07	0.25	1.00	0.00	0.00	0.06	0.21
CaO	0.29	0.31	0.24	0.15	0.29	0.79	0.87	0.00
Na_2O	12.05	11.89	11.34	6.68	11.57	11.10	10.86	0.98
K_2O	0.07	0.28	0.98	3.80	0.07	0.19	1.04	8.80
Total	100.15	99.22	100.20	97.51	99.24	100.40	99.46	97.69
Atomic Proportions (based on 8 oxygens)								
Si	2.979	2.983	2.940	2.846	2.981	2.987	2.929	2.890
Ti	0.000	0.000	0.001	0.002	0.000	0.000	0.000	0.000
Al	1.003	0.987	1.039	1.178	1.017	1.008	1.055	1.250
Cr	0.001	0.000	0.000	0.000	0.000	0.001	0.000	0.000
Fe	0.008	0.012	0.019	0.057	0.002	0.001	0.017	0.030
Mn	0.000	0.000	0.000	0.000	0.000	0.000	0.000	0.002
Ni	0.000	0.002	0.002	0.000	0.001	0.000	0.000	0.000
Mg	0.001	0.005	0.016	0.068	0.000	0.000	0.004	0.014
Ca	0.014	0.015	0.011	0.007	0.013	0.037	0.041	0.000
Na	1.023	1.021	0.968	0.591	0.988	0.937	0.934	0.086
K	0.004	0.016	0.055	0.221	0.004	0.011	0.059	0.511
Total	5.032	5.041	5.051	4.969	5.006	4.982	5.040	4.783
Analyses	1	1	1	1	4	1	1	1
Molecular %								
Ab	98.3	97.1	93.6	72.1	98.3	95.2	90.3	14.5
An	1.3	1.4	1.1	0.9	1.3	3.7	4.0	0.0
Or	0.4	1.5	5.3	27.0	0.4	1.1	5.7	85.5
Whole Rock (complete analyses given in Appendix B)								
Zr (ppm)	53	53	53	53	142	142	142	142

* Total iron as FeO

Table 4-11: Averages of albite analyses from the Skidder Basalt compared to those of the Buchans Group

	Skidder Basalt Average Albite			Buchans Group Average Albite	
Weight %	Zr≤50 ppm	Zr>50≤85 ppm	Zr>85 ppm	Basalt S 82A *	Dacite S 63
SiO_2	68.35	68.16	69.31	67.39	67.54
TiO_2	0.02	0.03	0.00	0.01	0.00
Al_2O_3	19.59	19.87	19.00	19.46	19.69
Cr_2O_3	0.01	0.01	0.00	0.01	0.01
FeO*	0.22	0.47	0.02	0.35	0.11
MnO	0.03	0.02	0.01	0.00	0.01
NiO	0.00	0.03	0.02	0.03	0.02
MgO	0.01	0.03	0.01	0.11	0.01
CaO	0.40	0.24	0.14	0.28	0.47
Na_2O	11.75	11.98	11.92	11.76	11.37
K_2O	0.05	0.05	0.04	0.44	0.25
Total	100.43	100.90	100.46	99.86	99.47
Atomic Proportions (based on 8 oxygens)					
Si	2.980	2.965	3.013	2.967	2.973
Ti	0.001	0.001	0.000	0.000	0.000
Al	1.007	1.019	0.974	1.010	1.022
Cr	0.000	0.000	0.000	0.000	0.000
Fe	0.008	0.017	0.001	0.013	0.004
Mn	0.001	0.001	0.000	0.000	0.000
Ni	0.000	0.001	0.001	0.001	0.001
Mg	0.001	0.002	0.000	0.007	0.001
Ca	0.019	0.011	0.007	0.013	0.022
Na	0.993	1.010	1.005	1.004	0.971
K	0.003	0.003	0.002	0.025	0.014
Total	5.013	5.031	5.003	5.042	5.008
Analyses	6	5	3	3	6
Molecular %					
Ab	97.9	98.6	99.2	96.3	96.5
An	1.8	1.1	0.6	1.3	2.2
Or	0.3	0.3	0.2	2.4	1.4

* Total iron as FeO

in basalts having lower Zr concentrations. Plagioclase grains from the Buchans Group rocks contain a higher average molecular percentage of orthoclase than those from the Skidder Basalt.

4.4.4 Potassium feldspars

Samples S 81 and S 16 are enriched in potassium relative to other Skidder Basalt samples (Chapter 5). These are two of several potassium-enriched samples collected from outcrops that occur along a prominent lineament (Figure 3-10). Electron microprobe analyses of mineral phases in thin sections of these rocks indicate that the potassium-bearing phase is K-feldspar (Table 4-12).

Two analyses from S 81 are presented in Table 4-12; one of albite containing a minor anorthite component and the second of K-feldspar with a significant molecular percentage of albite.

Analyses of feldspar phenocrysts and groundmass feldspar laths in thin section S 16 show feldspar compositions having a low anorthite component but a range of Ab/Or ratios. Orthoclase components range from 0.4 to 10.9 molecular per cent in albites, 17.1 to 19.1 in sodic K-feldspar and 82.9 to 98.5 molecular per cent in K-feldspar. K-feldspar having a high orthoclase component occurs as stubby grains in the groundmass and as rims around albitized feldspar phenocrysts. In each case the K-feldspar is untwinned and optically indistinguishable from albite. Analyses of one large feldspar grain show the central portion of the grain to be essentially pure albite and the rim to be almost pure K-feldspar.

Results of experiments conducted to investigate the interaction of basalt and heated seawater suggest that spilitization of basalts may occur as a result of the interaction of basalt with heated circulating seawater (e.g. Mottl, 1983a and 1983b). Potassium is leached from basalt by seawater at temperatures in excess of 150°C (e.g. Mottl, 1983b), a process which possibly played a role in the very low average content of potassium in the Skidder Basalt

Table 4-12: Electron microprobe analyses of feldspars from potassium-rich Skidder Basalt samples

							Large Grain					
							Centre	Rim	Sodic	Sodic		
Mineral	Albite	K-feldspar	Albite	Albite	Albite	Albite	Albite.	K-feldspar	K-feldspar	K-feldspar	K-feldspar	K-feldspar
Weight %	S 81	S 81	S 16	S 16	S 16	S 16	S 16	S 16	S 16	S 16	S 16	S 16
SiO_2	69.46	66.49	68.39	68.90	67.68	67.71	68.55	63.48	68.39	68.20	67.18	67.38
TiO_2	0.00	0.00	0.00	0.00	0.00	0.00	0.00	0.00	0.01	0.00	0.00	0.02
Al_2O_3	20.32	19.52	18.70	19.20	19.13	19.42	18.64	17.50	19.07	19.08	17.81	17.52
Cr_2O_3	0.01	0.00	0.01	0.00	0.00	0.00	0.01	0.00	0.00	0.00	0.00	0.02
FeO*	0.18	0.09	0.02	0.21	0.10	0.76	0.16	0.11	0.29	0.47	0.02	0.47
MnO	0.03	0.03	0.01	0.01	0.01	0.00	0.00	0.00	0.03	0.01	0.03	0.01
NiO	0.01	0.03	0.01	0.00	0.05	0.05	0.02	0.01	0.05	0.00	0.00	0.01
MgO	0.01	0.02	0.01	0.05	0.00	0.33	0.00	0.00	0.01	0.25	0.00	0.07
CaO	0.56	0.54	0.03	0.11	0.10	0.00	0.11	0.00	0.09	0.00	0.00	0.00
Na_2O	12.05	3.93	12.16	11.55	11.90	10.12	12.25	0.16	9.94	9.55	1.93	0.51
K_2O	0.06	11.97	0.07	0.27	0.65	1.88	0.04	15.93	3.11	3.43	14.21	15.28
Total	102.69	102.62	99.39	100.30	99.62	100.27	99.78	97.19	100.99	100.99	101.18	101.29
Atomic Proportions (based on 8 oxygens)												
Si	2.965	2.960	3.010	3.004	2.985	2.977	3.009	3.017	2.997	2.992	3.039	3.053
Al	1.023	1.025	0.970	0.987	0.995	1.007	0.965	0.981	0.985	0.987	0.950	0.936
Ca	0.026	0.026	0.001	0.005	0.005	0.000	0.005	0.000	0.004	0.000	0.000	0.000
Na	0.997	0.339	1.038	0.976	1.018	0.863	1.043	0.015	0.845	0.812	0.169	0.045
K	0.003	0.680	0.004	0.015	0.037	0.105	0.002	0.966	0.174	0.192	0.820	0.883
Others	0.009	0.007	0.002	0.011	0.006	0.051	0.007	0.005	0.014	0.034	0.002	0.025
Total	5.023	5.037	5.025	4.998	5.045	5.004	5.031	4.983	5.019	5.017	4.981	4.942
Analyses	1	1	2	1	1	1	1	1	1	1	1	1
Molecular %												
Ab	97.2	32.5	99.5	98.0	96.1	89.1	99.3	1.5	82.6	80.9	17.1	4.8
An	2.5	2.5	0.1	0.5	0.4	0.0	0.5	0.0	0.4	0.0	0.0	0.0
Or	0.3	65.1	0.4	1.5	3.5	10.9	0.2	98.5	17.0	19.1	82.9	95.2
Whole Rock (complete analyses given in Appendix B)												
Zr (ppm)	44	44	51	51	51	51	51	51	51	51	51	51
K_2O (%)	0.71	0.71	1.45	1.45	1.45	1.45	1.45	1.45	1.45	1.45	1.45	1.45

* Total iron as FeO

(Chapter 5). The presence of K-feldspar as rims around albitized feldspar in sample S 16 suggests that the potassium has been introduced by way of a fluid which passed through the rock after spilitization. The presence of a foliation defined by feldspar grains in thin section S 16 supports the possibility that the lineament along which the potassium-rich samples occur marks a fault zone which provided a passageway for the ascending fluid.

4.4.5 Amphiboles

All amphiboles observed in the Skidder Basalt are secondary, having formed by alteration of clinopyroxene or, in some places, possibly olivine. Greater amounts of amphibole are noted in the low-Zr basalts where it occurs as elongated prismatic crystals or fibrous masses. In places, pleochroic, brown, plumose masses of amphibole and intersertal chlorite are present in quench-textured areas around amygdules. In other areas, amphibole comprises mat-like intergrowths pseudomorphing primary axiolitic or other quench textures. In a few areas, amphibole forms an alteration rim around clinopyroxene grains.

Three electron microprobe analyses of Skidder Basalt amphiboles are presented in Table 4-13. The amphiboles have negligible Fe^{3+} contents according to the methods of Stout (1972) and Papike et al., (1974) used to estimate minimum and maximum Fe^{3+}. They are Na rich, and, according to the classification scheme of Leake (1978) and Hawthorne (1983) are silicic edenite (S 30), ferroan pargasitic hornblende (S 19 (1)) and edenitic hornblende (S 19 (2)).

The amphiboles have Al_2O_3 contents below 10% which, according to Liou and Ernst (1979), is characteristic of metamorphic amphiboles in ophiolites and may be indicative of low pressure origin. Low Na in the M_4 site, also typical of these amphiboles, has similarly been attributed to a low pressure origin (Brown, 1977). The high Na content

Table 4-13: Electron microprobe analyses of Skidder Basalt amphiboles

Weight %	S 30	S 19(1)	S 19(2)	
SiO_2	56.52	40.48	43.23	
TiO_2	0.03	0.57	1.31	
Al_2O_3	6.16	9.59	9.98	
Cr_2O_3	0.05	0.09	0.06	
FeO*	6.77	10.98	10.57	
MnO	0.16	0.08	0.10	
NiO	0.05	0.03	0.00	
MgO	6.79	9.64	10.34	
CaO	13.28	13.63	15.63	
Na_2O	6.88	8.67	2.64	
K_2O	0.04	0.03	0.04	
Total	96.73	93.79	93.90	
Atomic Proportions (based on 23 oxygens)				
Si	8.078	6.397	6.637	T site
Al^4	0.000	1.603	1.363	
Al^6	1.038	0.183	0.443	M(1-3)sites
Ti	0.003	0.068	0.151	
Fe^{3+}	0.000	0.000	0.000	
Cr	0.006	0.011	0.007	
Mg	1.446	2.270	2.366	
Fe^{2+}	0.809	1.451	1.357	
Mn	0.019	0.011	0.013	
Ni	0.006	0.004	0.000	
Ca	2.034	2.308	2.571	M4 site
Na	0.000	0.000	0.000	
Na	1.907	2.656	0.786	A site
K	0.007	0.006	0.008	
Total	15.354	16.968	15.702	
$Mg/(Mg+Fe^{2+})$	0.641	0.610	0.635	

Minimum and maximum Fe^{3+} calculated according to the methods of Stout, 1972; Papike et al., 1974; and Hawthorne, 1983

Whole Rock (complete analyses presented in Appendix B)

SiO_2 (%)	49.40	48.10	48.10
TiO_2 (%)	0.61	1.13	1.13
Al_2O_3 (%)	13.50	14.50	14.50
Cr (ppm)	349	144	144
Fe_2O_3 (%)**	7.60	9.23	9.23
MnO (%)	0.13	0.16	0.16
Ni (ppm)	156	67	67
MgO (%)	5.70	7.08	7.08
CaO (%)	10.80	9.43	9.43
Na_2O (%)	5.20	5.02	5.02
K_2O (%)	0.02	0.12	0.12
Zr (ppm)	30	62	62

* Total iron as FeO
** Total iron as Fe_2O_3

of the amphiboles is probably a result of interaction of the rocks with seawater during spilitization.

4.4.6 Chlorites

4.4.6.1 Introduction and presentation of results

In the Skidder Basalt away from the Skidder Prospect alteration zone, chlorite occurs typically as fine grained, light green, pleochroic, anhedral masses intersertal to other minerals. It also fills vugs, vesicles, fractures and fills areas pseudomorphic after olivine. In a few sections, vug-filling chlorite occurs as radial aggregates. It typically displays brown to anomalous blue interference colours.

In Buchans Group basalt sample S 82A, chlorite occurs in the groundmass as light green anhedral grains intersertal to other minerals, and, along with calcite and quartz, forms olivine (?) or clinopyroxene (?) pseudomorphs.

Electron microprobe analyses of chlorites from Skidder Basalt samples unaffected by the Skidder Prospect mineralizing event are presented in Appendix A (Table A-4). Within a given sample, there is little variance in the composition of chlorites overall, and intersertal chlorite compositions do not vary significantly from those of chlorites filling open spaces or in areas pseudomorphic after other minerals. Therefore, analyses of chlorites which have similar compositions and occur in the same thin section have been averaged. The averaged chlorite analyzes are presented in Table 4-14. The samples, arranged by increasing whole rock Zr content, cover the range of Skidder Basalt compositions. Chlorites analyzed from Buchans Group sample S 82A are also listed in Appendix A (Table A-4), and an average of the analyses is presented in Table 4-14.

All but one of the unmineralized Skidder basalt chlorites are classified as pycnochlorites according to the classification scheme of Hey (1954) (Figure 4-36); the remaining chlorite is classified as ripidolite. Chlorites from most of the Skidder basalts having Zr concentrations less than 85 ppm plot in the ocean floor metabasalt field (Melson

Table 4-14: Electron microprobe analyses of Skidder Basalt and Buchans Group basalt chlorites; analyses that have been averaged are presented in Table A-4, Appendix A

	Zr ≤ 50 ppm					Zr > 50 ≤ 85 ppm							Zr > 85 ppm			Buchans
Rock Type	Basalt					Basalt			Diabase		Basalt		Basalt			Group
Weight %	S 59	S 59	S 30	S 35A	S 81	S 16	S 19	S 53	S 22	S 25	S 79	S 60	S 21A	S 21A	S 29	S 82A
SiO_2	29.07	28.08	27.85	28.54	28.86	28.58	28.96	28.31	29.94	28.32	27.90	28.30	29.82	26.98	27.56	27.83
TiO_2	0.00	0.02	0.00	0.00	0.01	0.01	0.01	0.01	0.02	0.02	0.01	0.02	0.01	0.02	0.03	0.01
Al_2O_3	19.53	19.50	18.09	18.41	17.57	18.79	19.46	18.67	18.25	19.52	17.87	18.34	17.55	18.34	19.77	18.78
Cr_2O_3	0.05	0.06	0.12	0.06	0.00	0.02	0.03	0.03	0.01	0.01	0.02	0.02	0.00	0.03	0.02	0.02
FeO*	18.38	19.05	22.24	19.43	24.21	21.72	23.00	23.64	19.03	24.34	27.29	24.34	24.81	24.43	28.97	19.50
MnO	0.30	0.31	0.21	0.35	0.49	0.41	0.31	0.23	0.41	0.23	0.38	0.27	0.59	0.59	0.54	0.40
NiO	0.05	0.08	0.09	0.08	0.05	0.01	0.03	0.04	0.02	0.05	0.04	0.03	0.01	0.03	0.01	0.08
MgO	20.07	19.72	18.03	20.17	17.26	18.16	17.87	16.75	21.50	16.58	15.17	16.97	17.66	15.42	13.42	19.25
CaO	0.10	0.12	0.09	0.03	0.13	0.06	0.11	0.15	0.06	0.08	0.10	0.09	0.05	0.23	0.05	0.12
Na_2O	0.04	0.02	0.02	0.04	0.06	0.04	0.05	0.05	0.02	0.03	0.03	0.05	0.11	0.03	0.01	0.04
K_2O	0.04	0.06	0.02	0.03	0.03	0.06	0.02	0.01	0.01	0.02	0.03	0.02	0.03	0.03	0.02	0.03
Total	87.64	87.02	86.76	87.12	88.64	87.87	89.86	87.88	89.28	89.18	88.81	88.44	90.64	86.13	90.41	86.06
Atomic Proportions (based on 28 oxygens)																
Si	5.875	5.756	5.833	5.856	5.968	5.876	5.845	5.878	5.961	5.805	5.858	5.860	6.031	5.781	5.719	5.794
Al	4.659	4.714	4.468	4.454	4.281	4.559	4.631	4.570	4.284	4.715	4.423	4.484	4.184	4.632	4.837	4.609
Fe	3.109	3.268	3.896	3.335	4.187	3.736	3.882	4.105	3.169	4.173	4.792	4.219	4.196	4.377	5.029	3.397
Mn	0.052	0.054	0.036	0.061	0.086	0.072	0.054	0.041	0.070	0.039	0.067	0.047	0.101	0.107	0.094	0.070
Mg	6.046	6.021	5.628	6.167	5.317	5.563	5.377	5.183	6.382	5.065	4.746	5.240	5.323	4.924	4.151	5.971
Other	0.065	0.077	0.070	0.051	0.068	0.052	0.059	0.068	0.031	0.046	0.051	0.057	0.065	0.086	0.030	0.070
Total	19.80	19.89	19.93	19.92	19.91	19.86	19.85	19.84	19.90	19.84	19.94	19.91	19.90	19.91	19.86	19.91
Fe/Fe+Mg	0.34	0.35	0.41	0.35	0.44	0.40	0.42	0.44	0.33	0.45	0.50	0.45	0.44	0.47	0.55	0.36
Analyses	3	3	6	2	2	3	5	3	4	4	2	4	1	3	4	3
Whole Rock (complete analyses presented in Appendix B)																
Zr (ppm)	16	16	30	38	44	51	62	66	68	73	78	82	95	95	110	53
Fe_2O_3 (%)**	10.12	10.12	7.60	8.86	10.78	12.18	9.23	9.51	11.19	11.68	13.49	13.68	9.45	9.45	10.2	7.98
MgO (%)	11.13	11.13	5.70	8.94	8.87	6.07	7.08	7.64	7.15	7.35	5.9	6.66	4.09	4.09	2.37	6.79

* Total iron as FeO

** Total iron as Fe_2O_3

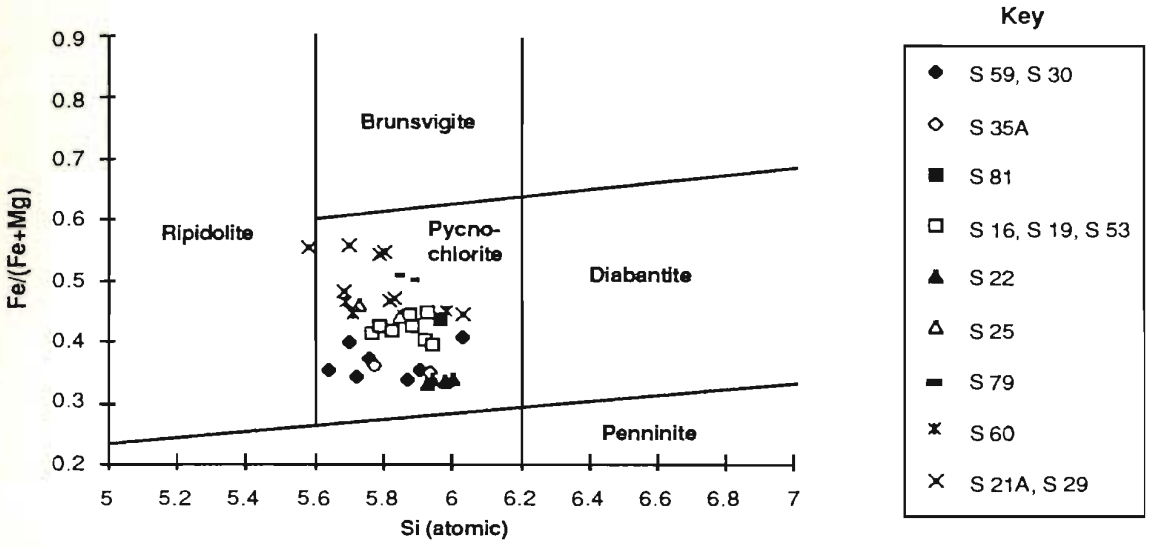

Figure 4-36: Skidder chlorite compositions plotted on classification diagram after Hey (1954).

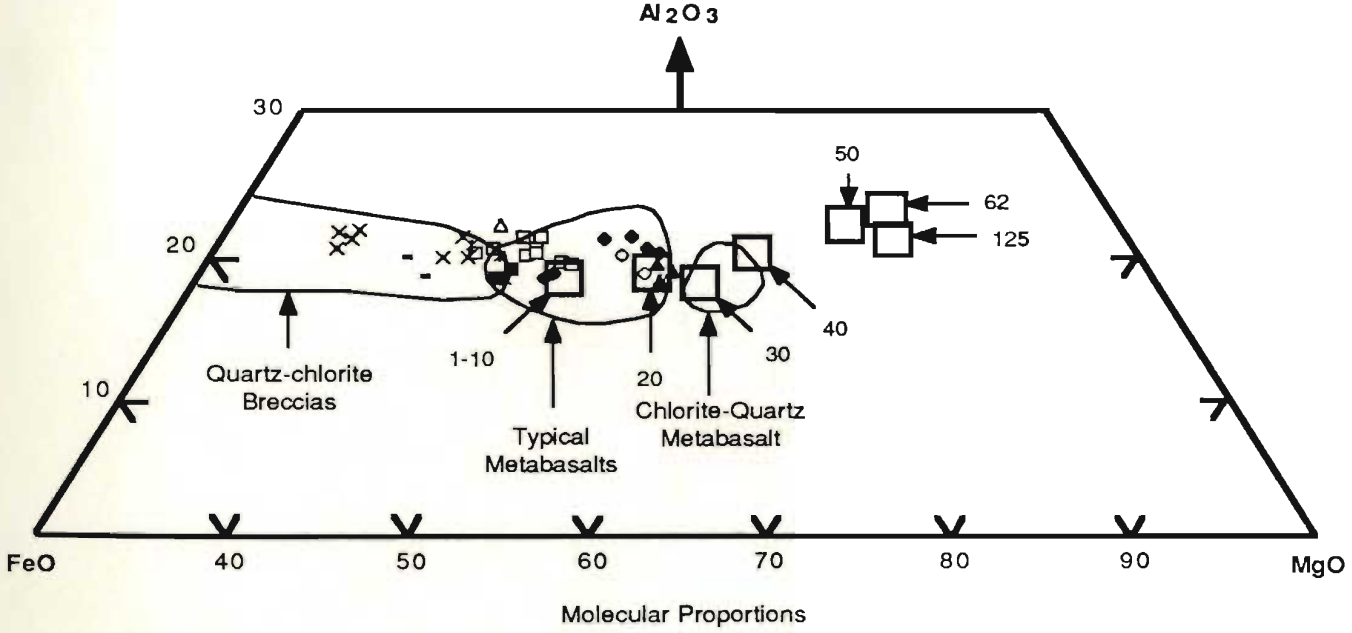

Figure 4-37: Skidder Basalt chlorite compositions compared to those of typical metabasalts, quartz-chlorite breccias and a chlorite-quartz metabasalt from sea-floor greenstones (after Melson and van Andel, 1966; Humphris and Thompson, 1978; Mottl 1983a). Large open squares represent chlorite compositions for different sea water/rock ratios from model predictions of Mottl (1983a). Key as per Figure 4-36.

and van Andel, 1966; Humphris and Thompson, 1978; Mottl, 1983a) on the Al_2O_3-FeO-MgO diagram (Figure 4-37) but chlorites from Skidder basalts having higher Zr concentrations extend to higher FeO compositions and plot within the quartz-chlorite breccia field.

A Pearson correlation coefficient matrix showing correlations between components of Skidder Basalt chlorites as well as correlations between the chlorite components and those of the whole rock is presented in Table 4-15. Substitution of FeO for MgO in Skidder Basalt chlorites is indicated by their strong negative correlation with each other (Table 4-15 and Figure 4-38). FeO* (total iron in chlorite) increases and MgO decreases significantly with increasing Zr in whole rock (Tables 4-14; 4-15; and Figure 4-38). This is reflected by positive correlations of FeO* and concomitant negative correlations of MgO (in chlorite) with whole rock TiO_2, Na_2O and SiO_2 (Table 4-15). It is also reflected by negative correlations of FeO* and by positive correlations of MgO in chlorite with Cr, Ni and MgO in whole rock (Table 4-15). Thus, in most Skidder basalts the FeO/(FeO + MgO) ratio in chlorites reflects whole rock composition increasing with increasing Zr concentration (Table 4-15 and Figure 4-38).

SiO_2 in chlorite shows a slight to moderate negative correlation with FeO* and moderate positive correlation with MgO in chlorite (Table 4-15). It also shows a very weak negative correlation with TiO_2 and Zr and a weak positive correlation with MgO in whole rock (Table 4-15). SiO_2 correlates negatively with the hydrous component of the chlorites as indicated by its positive correlation with analytical totals (Figure 4-38). MnO in chlorite shows a weak positive correlation with FeO*, and, like FeO, correlates positively with TiO_2, SiO_2 and Zr in whole rock. Note that MnO in chlorite does not correlate positively with MnO in whole rock (Table 4-15). Cr_2O_3 and NiO present in the chlorites correlate positively with each other and negatively with Zr in whole rock. Al_2O_3 shows no clear variation with basalt composition (Table 4-14). This is reflected in the general lack of

Table 4-15: Pearson correlation coefficient matrix for Skidder Basalt chlorites

Number of samples = 49

Chlorite	SiO_2	Al_2O_3	Cr_2O_3	FeO*	MnO	NiO	MgO	FeO/(FeO+MgO)	Total
SiO_2	***1.00***								
Al_2O_3	.00	***1.00***							
Cr_2O_3	-.19	.00	***1.00***						
FeO*	*-.34*	.00	-.21	***1.00***					
MnO	.00	.00	*-.36*	.28	***1.00***				
NiO	.00	.00	**.56**	*-.33*	**-.49**	***1.00***			
MgO	**.58**	-.05	.07	***-.91***	-.26	.20	***1.00***		
FeO/(FeO+MgO)	**-.47**	.00	-.16	***.98***	.27	-.27	***-.97***	***1.00***	
Total	**.59**	.26	*-.34*	*.34*	.13	*-.36*	.00	.17	***1.00***

Chlorite

* Total Iron as FeO
weight % of mineral components rather than atomic proportions were used in the calculation of the correlation matrix

Whole Rock	SiO_2	Al_2O_3	Cr_2O_3	FeO*	MnO	NiO	MgO	FeO/(FeO+MgO)	Total
SiO_2 (%)	*-.31*	.00	-.22	**.57**	***.68***	**-.45**	***-.62***	***.61***	.00
TiO_2 (%)	-.16	.10	**-.52**	***.80***	**.50**	**-.59**	***-.75***	***.79***	*.37*
Al_2O_3 (%)	.24	.00	*-.35*	-.13	.22	-.15	.22	-.20	.12
Cr (ppm)	.00	.00	**.58**	**-.58**	*-.36*	***.63***	**.52**	**-.57**	-.26
Fe_2O_3 (%)**	.00	.00	**-.59**	.15	.00	**-.41**	.00	.08	.18
MnO (%)	*.32*	-.18	-.27	*-.31*	.10	.00	*.36*	*-.35*	.00
Ni (ppm)	.00	.00	***.65***	***-.68***	**-.51**	***.70***	***.62***	***-.67***	*-.31*
MgO (%)	.29	.00	.00	***-.74***	**-.42**	*.35*	***.67***	***-.73***	-.14
CaO (%)	.00	.00	**.50**	*-.33*	***-.72***	***.60***	*.31*	*-.33*	.00
Na_2O (%)	*-.32*	.00	.00	***.72***	*.30*	-.21	***-.65***	***.71***	.07
K_2O (%)	.13	.00	-.20	-.09	.25	*-.30*	.11	-.10	.00
Zr (ppm)	-.06	.00	**-.53**	***.76***	**.51**	***-.61***	***-.67***	***.74***	*.37*

Chlorite

** Total iron as Fe_2O_3

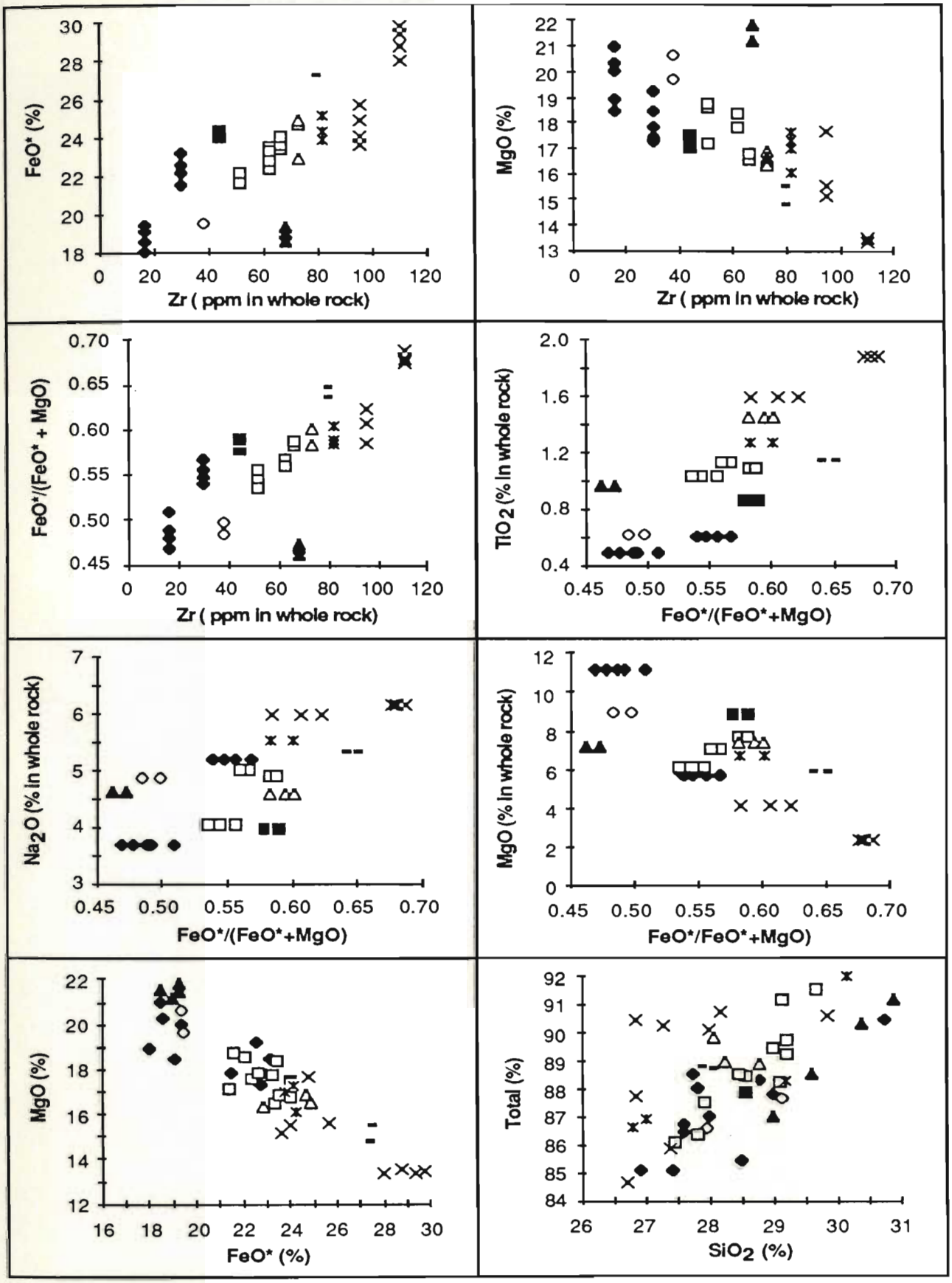

Figure 4-38: Miscellaneous X-Y plots for Skidder Basalt chlorites. FeO* - Total iron as FeO. Key as per Figure 4-36. See text for discussion.

correlation between Al_2O_3 and most of the other chlorite and whole rock components (Table 4-15).

4.4.6.2 Discussion

Mottl (1983a) predicts that in metabasalts that have interacted with seawater, chlorite compositions are governed by seawater/basalt ratios. Chlorites display an increase in Mg, Al and H_2O and a decrease in Si and Mn with increasing seawater/rock ratios (Seyfried and Mottl, 1982; Mottl, 1983a). Figure 4-37 shows that Skidder Basalt chlorites in rocks unaffected by the Skidder Prospect mineralizing event have compositions typical of low seawater/basalt ratios (about 1-20). However, the higher-Zr Skidder samples define a trend toward FeO enrichment and MgO depletion on this diagram, indicating some measure of host rock compositional control on the composition of the chlorites. In the Skidder Basalt much of the chlorite (accompanied by quartz) occurs in the groundmass intersertal to other minerals and probably formed by alteration of basaltic glass, the composition of which is sensitive to magmatic differentiation. Chlorites formed in this manner would be expected to reflect, in part, the composition of the basaltic glass and thus the host rock composition.

Chlorites from diabase dyke sample S 22 contain higher MgO and lower FeO contents than would be predicted from the FeO*/(FeO* + MgO) vs. Zr trend defined by chlorites from the other Skidder Basalt samples (Figure 4-38). According to Mottl (1983a) increased alteration of the rock as a result of its interaction with greater amounts of seawater would result in the formation of more magnesian chlorites. Petrographic examination of thin section S 22 has shown the rock to be extensively altered, e.g. clinopyroxene microphenocrysts (?) are replaced completely by epidote and calcite in S 22 whereas in several other Skidder Basalt thin sections clinopyroxene grains are well preserved.

4.4.7 Epidote

4.4.7.1 Introduction and presentation of results

Epidote is present in many Skidder Basalt samples covering the range of compositions from low- to high-Zr basalts. It occurs typically as pleochroic, light olive green, equant to prismatic grains that are 1.5 to 2 mm in diameter. It is randomly distributed throughout some samples but most commonly fills vesicles, vugs and fractures. In a few thin sections, radially aligned needles of epidote are noted. Epidote, calcite and locally quartz partially or completely replace clinopyroxene in some Skidder area mafic intrusive rocks, e.g. S 22 and S 25. Also, epidote, accompanied by albite, replaces plagioclase laths in a few samples, e.g. thin section S 49.

Electron microprobe analyses of Skidder Basalt epidotes are presented in Table 4-16, where they are arranged in ascending order according to host-rock Zr concentration. Note that total iron is shown as FeO on Table 4-16, although most Fe in epidote is present as Fe^{3+} (e.g. Deer et al., 1966). The epidotes are relatively iron rich, having a pistacite (Ps) component, as indicated by the Fe/(Fe + Al) ratio, between 23 and 33 molecular per cent.

Correlations between epidote and host rock compositions (Table 4-17) indicate some measure of bulk rock compositional control on the Fe and Ca content of the Skidder Basalt epidotes. FeO* (total iron in epidote) correlates positively with Zr and Fe_2O_3** (total iron) in whole rock; and negatively with CaO, Ni and Cr in whole rock. Although it does not show a large variation, CaO in epidote correlates negatively with FeO in epidote and negatively with Zr, Na_2O and Fe_2O_3** in whole rock. CaO in epidote shows a strong positive correlation with CaO in whole rock. Analysis totals of the epidotes show a positive correlation with Zr, Fe_2O_3**, TiO_2; and a negative correlation with Ni and Cr in whole rock. SiO_2 in epidote correlates positively with Na_2O in whole rock, and negatively with MgO and Al_2O_3 in whole rock.

Table 4-16: Electron microprobe analyses of Skidder Basalt epidotes

															Skidder Prospect	
Weight %	S 59	S 30	S 35A	S 22	S 22	S 22	S 25	S 25	S 25	S 79	S 60	S 60	S 60	S 60	SK 27 8	SK 27 8
SiO_2	37.41	42.03	38.18	42.14	38.89	38.93	38.73	39.04	39.42	38.54	39.60	39.73	39.07	39.30	38.05	37.39
TiO_2	0.02	0.03	0.23	0.01	0.17	0.17	0.06	0.13	0.11	0.03	0.06	0.08	0.05	0.06	0.02	0.00
Al_2O_3	23.66	17.51	24.13	19.95	23.78	22.98	24.05	25.52	23.08	22.17	22.03	22.05	22.99	21.23	22.41	20.89
Cr_2O_3	0.05	0.08	0.05	0.00	0.00	0.00	0.00	0.01	0.04	0.00	0.04	0.02	0.00	0.04	0.01	0.03
FeO*	11.73	7.51	10.25	13.75	11.26	12.10	10.20	8.92	12.59	13.75	14.01	13.76	13.01	14.44	12.39	14.77
MnO	0.11	0.00	0.06	0.11	0.11	0.19	0.09	0.17	0.17	0.07	0.11	0.01	0.11	0.08	0.18	0.12
NiO	0.03	0.02	0.05	0.04	0.02	0.05	0.03	0.00	0.01	0.03	0.00	0.10	0.01	0.03	0.05	0.05
MgO	0.04	0.17	0.45	0.12	0.04	0.16	0.08	0.00	0.34	0.01	0.00	0.02	0.84	0.05	0.02	0.00
CaO	23.51	26.95	21.97	21.93	23.49	23.14	23.71	23.47	22.84	23.75	22.13	21.95	21.93	23.18	24.47	24.54
Na_2O	0.03	0.03	0.04	0.09	0.04	0.01	0.00	0.00	0.09	0.03	0.00	0.00	0.01	0.00	0.00	0.00
K_2O	0.01	0.01	0.01	0.00	0.01	0.02	0.02	0.00	0.01	0.01	0.00	0.00	0.00	0.01	0.03	0.00
Total	96.60	94.34	95.42	98.14	97.81	97.75	96.97	97.26	98.70	98.39	97.98	97.72	98.02	98.42	97.63	97.79
Atomic Proportions (based on 12.5 oxygens)																
Si	3.077	3.488	3.132	3.399	3.139	3.157	3.139	3.125	3.166	3.140	3.218	3.230	3.159	3.203	3.117	3.105
Al	2.294	1.713	2.334	1.897	2.263	2.197	2.298	2.408	2.186	2.130	2.111	2.114	2.191	2.040	2.164	2.045
Fe	0.807	0.521	0.703	0.928	0.760	0.821	0.691	0.597	0.846	0.937	0.952	0.936	0.880	0.984	0.849	1.026
Mg	0.005	0.021	0.055	0.014	0.005	0.019	0.010	0.000	0.041	0.001	0.000	0.002	0.101	0.006	0.002	0.000
Ca	2.072	2.396	1.931	1.895	2.031	2.011	2.059	2.013	1.966	2.074	1.927	1.912	1.900	2.024	2.148	2.183
Others	0.020	0.014	0.032	0.025	0.026	0.030	0.014	0.020	0.036	0.014	0.014	0.013	0.013	0.015	0.021	0.014
Total	8.276	8.154	8.188	8.159	8.224	8.236	8.210	8.163	8.241	8.296	8.222	8.207	8.243	8.272	8.301	8.372
Fe/(Fe+Al)	0.26	0.23	0.23	0.33	0.25	0.27	0.23	0.20	0.28	0.31	0.31	0.31	0.29	0.33	0.28	0.33
Whole rock (complete analyses presented in Appendix B)																
SiO_2 (%)	47.90	49.40	48.50	48.50	48.50	48.50	49.80	49.80	49.80	49.40	51.80	51.80	51.80	51.80	47.10	47.10
Al_2O_3 (%)	15.10	13.50	14.50	15.10	15.10	15.10	14.00	14.00	14.00	15.30	14.80	14.80	14.80	14.80	16.00	16.00
Fe_2O_3 (%)**	10.12	7.60	8.86	11.19	11.19	11.19	11.68	11.68	11.68	13.49	13.68	13.68	13.68	13.68	10.54	10.54
CaO (%)	8.03	10.80	7.07	5.74	5.74	5.74	8.27	8.27	8.27	4.04	4.02	4.02	4.02	4.02	9.52	9.52
Na_2O (%)	3.68	5.20	4.89	4.64	4.64	4.64	4.58	4.58	4.58	5.35	5.51	5.51	5.51	5.51	1.49	1.49
K_2O (%)	0.09	0.02	0.03	0.38	0.38	0.38	0.02	0.02	0.02	0.06	0.09	0.09	0.09	0.09	2.36	2.36
Zr (ppm)	16	30	38	68	68	68	73	73	73	78	82	82	82	82	45	45

* Total iron as FeO

** Total iron as Fe_2O_3

Table 4-17: Pearson correlation coefficient matrix for Skidder Basalt epidotes

Number of samples = 16

Epidote	SiO_2	TiO_2	Al_2O_3	FeO*	MnO	MgO	CaO	Total	Fe/(Fe+Al)
SiO_2	*1.00*								
TiO_2	.00	*1.00*							
Al_2O_3	*-.61*	*.51*	*1.00*						
FeO*	.00	-.26	.00	*1.00*					
MnO	-.26	.00	*.42*	.00	*1.00*				
MgO	.00	.00	.00	.00	.00	*1.00*			
CaO	.00	-.21	*-.40*	*-.43*	.00	-.21	*1.00*		
Total	.00	.00	.00	*.77*	*.43*	.00	*-.45*	*1.00*	
Fe/(Fe+Al)	.00	*-.47*	*-.40*	*.93*	.00	.00	-.11	.59	*1.00*

Epidote

* Total Iron as FeO

Except for Fe/(Fe+Al), which are atomic proportions, weight % of mineral components rather than atomic proportions were used in the calculation of the correlation matrix

Whole Rock	SiO_2	TiO_2	Al_2O_3	FeO*	MnO	MgO	CaO	Total	Fe/(Fe+Al)
SiO_2 (%)	.19	.00	.00	.00	-.25	.00	*-.33*	.00	.00
TiO_2 (%)	.00	.00	.21	.00	.00	.00	-.28	*.58*	.00
Al_2O_3 (%)	*-.43*	-.15	.00	*.65*	.18	.00	.00	*.39*	*.58*
Cr (ppm)	.00	.07	.00	*-.38*	.00	.00	.00	*-.75*	-.26
Fe_2O_3 (%)**	.00	.00	.00	*.63*	.00	.00	*-.54*	*.78*	*.44*
MnO (%)	-.11	.00	.00	.00	.04	.00	.00	.00	.00
Ni (ppm)	.00	.00	.00	*-.51*	.00	.00	*.38*	*-.77*	*-.34*
MgO (%)	*-.61*	.00	.28	.00	.20	.00	.00	.00	.00
CaO (%)	.00	.00	.00	*-.54*	.00	.00	*.69*	*-.51*	*-.41*
Na_2O (%)	*.43*	.18	.00	.00	*-.39*	.13	-.27	.00	.00
K_2O (%)	-.29	-.26	.00	.17	.26	.00	.19	.00	.23
Zr (ppm)	.00	.00	.00	*.34*	.00	.00	*-.47*	*.68*	.17

Epidote

** Total iron as Fe_2O_3

Correlations among epidote components include positive correlations between FeO*, MnO and analysis total; and negative correlations between Al_2O_3 and analysis total and between Al_2O_3-SiO_2, CaO-Al_2O_3, and FeO-CaO (Table 4-17).

4.4.7.2 Discussion

The presence of abundant epidote in many of the Skidder Basalt rocks enables some constraints to be placed on the temperature and fO_2 conditions under which the rocks were altered. Above 250°C, epidote appears as an abundant phase in metasomatized rocks in the Reykjanes (Tómassón and Kristmannsdóttir, 1972) and Cerro Prieto (Gulf of California) (Elders et al., 1979) geothermal fields. Liou and Ernst (1979) show that the upper limit for the greenschist assemblage albite + epidote + chlorite + actinolite is 475°C under fluid pressures of 2 kb and fO_2 values defined by the fayalite-magnetite-quartz (FMQ) buffer. Liou (1973) indicates that bulk rock composition to some extent determines epidote composition but maximum Fe^{3+} content of epidote is determined by fO_2. The pistacite component range for the Skidder Basalt epidotes (23-33%) overlaps but extends to higher values than epidotes of mid-Atlantic ridge basalts which have Ps components of 22 to 25% (Humphris and Thompson, 1978). Sivell and Waterhouse (1984b) suggest that Ps component ranges of 23 to 33%, like those of Skidder Basalt epidotes, indicate formation of the epidote under oxygen fugacities higher than the FMQ buffer and as high as the hematite-magnetite (HM) buffer.

4.4.8 Ti-bearing minerals

Titanium-bearing minerals in the Skidder Basalt include: Ti-bearing Fe-oxides; Fe-Ti oxide - sphene intergrowths; sphene; and much lesser amounts of leucoxene (anatase (?) or brookite (?)) (Tables 4-18 and 4-19). Most Fe-oxide grains analyzed are magnetite, which contain up to 3% TiO_2 (Table 4-18). Several analyses of opaque grains indicate compositions intermediate between magnetite and sphene; this suggests fine intergrowth of

Table 4-18: Electron microprobe analyses of Skidder Basalt iron-titanium oxides

							Skeletal Ilmenite (?) Alteration Products		Sphene/ Fe-Ti oxide	
Weight %	S 16	S 16	S 29	S 21A	S 21A	S 21A	S 22	S 22	S 22	S 25
SiO_2	1.19	1.17	0.50	2.55	3.38	11.14	7.62	17.43	20.59	21.17
TiO_2	0.03	3.09	0.77	0.82	2.72	11.77	13.73	17.83	45.45	22.77
Al_2O_3	0.54	0.21	0.25	1.41	0.41	2.84	1.21	1.97	1.61	0.88
Cr_2O_3	0.03	0.09	0.02	0.02	0.04	0.02	0.04	0.05	0.04	0.03
FeO*	89.84	85.29	88.95	85.36	80.39	57.72	67.10	42.00	10.56	29.21
MnO	0.01	0.03	0.06	0.10	0.04	0.00	0.01	0.04	0.25	0.01
NiO	0.01	0.02	0.10	0.09	0.03	0.05	0.04	0.01	0.00	0.06
MgO	0.05	0.06	0.16	3.77	0.02	0.05	0.52	0.48	1.62	0.08
CaO	0.04	0.21	0.20	0.31	3.48	9.58	5.33	16.23	17.01	19.86
Na_2O	0.12	0.07	0.67	0.02	0.12	0.07	0.09	0.57	0.05	0.01
K_2O	0.04	0.01	0.01	0.01	0.02	0.01	0.01	0.02	0.02	0.01
Total	91.90	90.25	91.69	94.46	90.65	93.25	95.70	96.63	97.20	94.09
Atomic Proportions										
Si	0.045	0.044	0.019	0.089	0.122	0.429	0.340	0.659	0.652	0.768
Ti	0.001	0.088	0.022	0.021	0.074	0.341	0.461	0.507	1.082	0.621
Al	0.024	0.009	0.011	0.058	0.018	0.129	0.064	0.088	0.060	0.038
Cr	0.001	0.003	0.001	0.001	0.001	0.001	0.001	0.001	0.001	0.001
Fe	2.860	2.701	2.852	2.480	2.436	1.861	2.505	1.328	0.280	0.886
Mn	0.000	0.001	0.002	0.003	0.001	0.000	0.000	0.001	0.007	0.000
Ni	0.000	0.001	0.003	0.003	0.001	0.002	0.001	0.000	0.000	0.002
Mg	0.003	0.003	0.009	0.195	0.001	0.003	0.035	0.027	0.076	0.004
Ca	0.002	0.009	0.008	0.012	0.135	0.396	0.255	0.657	0.577	0.772
Na	0.009	0.005	0.050	0.001	0.008	0.005	0.008	0.042	0.003	0.001
K	0.002	0.000	0.000	0.000	0.001	0.000	0.001	0.001	0.001	0.000
Total	2.947	2.864	2.978	2.862	2.799	3.167	3.671	3.311	2.738	3.093
Oxygens	3	3	3	3	3	4	4.5	4.5	4.5	4.5
Whole Rock (complete analyses are presented in Appendix B)										
TiO_2 (%)	1.04	1.04	1.88	1.60	1.60	1.60	0.96	0.96	0.96	1.45
Fe_2O_3 (%)**	12.18	12.18	10.20	9.45	9.45	9.45	11.19	11.19	11.19	11.68
Zr (ppm)	51	51	110	95	95	95	68	68	68	73

* Total Iron as FeO

** Total iron as Fe_2O_3

Table 4-19: Electron microprobe analyses of Skidder Basalt sphenes and leucoxene

	Sphene											Leucoxene	
Weight %	S 59	S 59	S 30	S 30	S 16	S 19	S 53	S 79	S 60	S 21A	S 29	S 21A	SK 28 75
SiO_2	32.12	33.81	29.93	32.19	39.30	32.35	28.66	31.91	32.99	30.36	30.89	0.67	0.15
TiO_2	30.75	24.44	31.06	32.57	28.27	30.75	27.37	26.60	31.90	30.30	35.16	93.41	94.23
Al_2O_3	4.10	4.02	3.46	3.08	4.57	3.31	2.96	5.78	3.01	4.11	1.94	0.18	0.13
Cr_2O_3	0.07	0.02	0.07	0.09	0.03	0.03	0.00	0.03	0.07	0.03	0.02	0.01	0.04
FeO*	3.07	5.74	2.70	2.87	1.33	1.73	3.79	4.41	2.56	2.68	0.94	0.15	0.33
MnO	0.20	0.20	0.01	0.02	0.04	0.06	0.00	0.10	0.04	0.00	0.02	0.01	0.01
NiO	0.02	0.04	0.03	0.08	0.00	0.03	0.05	0.00	0.04	0.03	0.05	0.04	0.00
MgO	1.93	5.34	0.65	0.01	0.00	0.06	0.04	1.09	0.27	0.06	0.03	0.03	0.00
CaO	26.16	25.36	26.78	28.93	27.43	27.34	27.45	25.94	28.28	27.69	28.84	0.71	0.13
Na_2O	0.03	0.16	0.04	0.00	0.03	0.05	0.36	0.05	0.03	0.00	0.02	0.01	0.00
K_2O	0.04	0.02	0.03	0.03	0.06	0.01	0.01	0.02	0.12	0.02	0.03	0.01	0.00
Total	98.49	99.15	94.76	99.87	101.06	95.72	90.69	95.93	99.31	95.28	97.94	95.23	95.02
Atomic Proportions (sphenes based on 4.5 oxygens; leucoxene based on 2 oxygens)													
Si	0.954	1.002	0.930	0.950	1.106	0.985	0.943	0.975	0.974	0.938	0.927	0.009	0.002
Ti	0.687	0.545	0.726	0.723	0.599	0.704	0.677	0.611	0.708	0.704	0.794	0.981	0.993
Al	0.144	0.140	0.127	0.107	0.152	0.119	0.115	0.208	0.105	0.150	0.069	0.003	0.002
Fe	0.076	0.142	0.070	0.071	0.031	0.044	0.104	0.113	0.063	0.069	0.024	0.002	0.004
Mg	0.085	0.236	0.030	0.000	0.000	0.003	0.002	0.050	0.012	0.003	0.001	0.001	0.000
Ca	0.832	0.805	0.892	0.915	0.827	0.892	0.968	0.849	0.895	0.917	0.927	0.011	0.002
Others	0.010	0.016	0.006	0.006	0.005	0.006	0.025	0.007	0.010	0.002	0.005	0.001	0.001
Total	2.788	2.888	2.781	2.773	2.721	2.753	2.834	2.812	2.767	2.783	2.746	1.008	1.004
Whole Rock													
TiO_2 (%)	0.49	0.49	0.61	0.61	1.04	1.13	1.09	1.15	1.27	1.60	1.88	1.60	0.55
Fe_2O_3 (%)**	10.12	10.12	7.60	7.60	12.18	9.23	9.51	13.49	13.68	9.45	10.20	9.45	10.36
CaO (%)	8.03	8.03	10.80	10.80	1.68	9.43	8.46	4.04	4.02	2.09	3.39	2.09	0.23
Zr (ppm)	16	16	30	30	51	62	66	78	82	95	110	95	50

* Total Iron as FeO
** Total iron as Fe_2O_3

Sample SK 28 75 is from the Skidder Prospect chlorite-quartz-pyrite alteration zone

the two minerals (Table 4-18). Sphene occurs as subhedral grains that, in places coalesce to form dense irregular masses. Greater amounts of sphene are present in the higher-Zr basalts. Thin sections S 22 and S 25 contain skeletal magnetite (?) grains rimmed by sphene that are probably pseudomorphic after ilmenite. Sphene, in the Skidder Basalt, shows some substitution of Fe, Al and Mg for Ti (Table 4-19) and covers a greater compositional range than sphenes from plutonic rocks of the East Taiwan Ophiolite (Liou and Ernst, 1979), or spilites from northern France (Moore-Biot, 1970) (Figure 4-39). Leucoxene analyzed in the Skidder Basalt samples is almost pure TiO_2. Limited amounts of SiO_2, CaO, Al_2O_3 and FeO in the leucoxene are probably due to the presence of a small amount of sphene.

Titanium-bearing minerals in the Skidder Basalt are probably alteration products of primary Fe-Ti oxides. Liou and Ernst (1979) suggest that primary Fe-Ti oxides unmix to ilmenite and magnetite during cooling, and that ilmenite is replaced by sphene during postmagmatic greenschist facies metamorphism. For example, Liou and Ernst (1979) and Evarts and Schiffman (1983) report intergrowth of magnetite and sphene formed by alteration of ilmenite in gabbros of the East Taiwan and Del Prieto Ophiolite respectively. Leucoxene (anatase or brookite) in the Skidder Basalt probably formed by alteration of sphene.

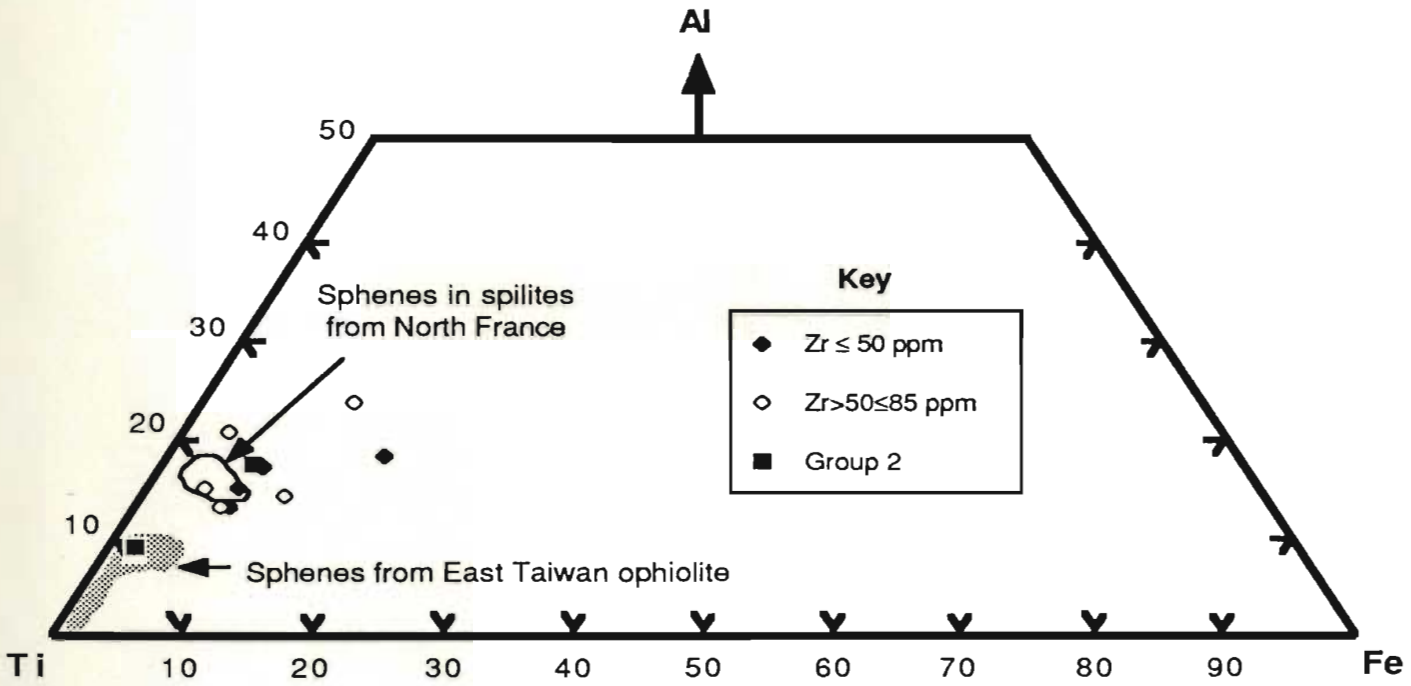

Figure 4-39: Molecular proportions of Al, Ti and Fe in analyzed Skidder Basalt sphenes. The compositional fields for 5 sphenes in Permo-Carboniferous spilites from North France (Moore-Biot, 1970), and 8 sphenes from plutonic rocks of the East Taiwan Ophiolite (Liou and Ernst, 1979) are shown for comparison.

4.4.9 Calcite

In the Skidder Basalt, anhedral calcite grains form irregular masses that occur throughout some samples, and fill vugs, vesicles and fractures in others. In places, it occurs with albite as a replacement product of plagioclase, and in some low-Zr basalts it accompanies epidote in areas probably pseudomorphic after olivine. In thin section S 22, clinopyroxene has been completely altered or replaced by various combinations of epidote, calcite and quartz.

Skidder Basalt calcite analyses, presented in Table 4-20, include: calcite from an altered plagioclase phenocryst; calcite pseudomorphing olivine; and anhedral masses of calcite distributed throughout the thin sections. Calcite grains analyzed in sample S 29, including that from an altered plagioclase phenocryst, and calcite grains in S 30, other than that forming an olivine pseudomorph, contain greater than 99% $CaCO_3$. Calcite, which occurs in an area pseudomorphic after olivine in sample S 30, contains minor amounts of Fe, Mn and Mg carbonate.

Evarts and Schiffman (1983) conclude, on the basis of textural evidence, that calcite formation postdates the main period of hydrothermal alteration in the Del Puerto ophiolite, California, and thus that the presence of calcite does not necessarily indicate high p_{CO_2} conditions during submarine hydrothermal alteration of the ophiolite. At least some of the calcite in the Skidder Basalt is also probably late as indicated by the presence, in some samples, of carbonatized albite, and calcite veins that crosscut other secondary minerals.

Table 4-20: Electron microprobe analyses of Skidder Basalt calcites

				Altered Plagioclase Phenocryst				Olivine Pseudomorph	
Weight %	S 16	S 16	S 29	S 29	S 29	S 29	S 30	S 30	S 30
SiO_2	0.02	0.32	0.35	0.14	0.16	0.15	0.17	0.00	1.37
TiO_2	0.02	0.00	0.02	0.02	0.00	0.00	0.02	0.00	0.00
Al_2O_3	0.00	0.07	0.45	0.03	0.05	0.02	0.11	0.50	0.58
Cr_2O_3	0.04	0.00	0.03	0.02	0.02	0.00	0.03	0.02	0.05
FeO*	0.32	1.70	0.11	0.03	0.00	0.01	0.15	0.68	0.99
MnO	0.50	0.43	0.38	0.26	0.34	0.13	0.06	0.59	1.02
NiO	0.00	0.00	0.00	0.00	0.07	0.03	0.00	0.01	0.00
MgO	0.11	1.69	0.03	0.03	0.05	0.00	0.02	0.27	0.74
CaO	60.84	54.75	61.79	61.58	61.11	57.91	58.19	55.07	59.50
Na_2O	0.02	0.04	0.06	0.08	0.01	0.10	0.46	0.07	0.02
K_2O	0.01	0.07	0.00	0.00	0.01	0.00	0.01	0.00	0.01
Total	61.88	59.07	63.22	62.19	61.82	58.35	59.22	57.21	64.28
Atomic Proportions (based on 1 cation)									
Si	0.000	0.005	0.005	0.002	0.002	0.002	0.003	0.000	0.019
Ti	0.000	0.000	0.000	0.000	0.000	0.000	0.000	0.000	0.000
Al	0.000	0.001	0.008	0.001	0.001	0.000	0.002	0.010	0.010
Cr	0.000	0.000	0.000	0.000	0.000	0.000	0.000	0.000	0.001
Fe	0.004	0.022	0.001	0.000	0.000	0.000	0.002	0.009	0.012
Mn	0.006	0.006	0.005	0.003	0.004	0.002	0.001	0.008	0.012
Ni	0.000	0.000	0.000	0.000	0.001	0.000	0.000	0.000	0.000
Mg	0.002	0.039	0.001	0.001	0.001	0.000	0.000	0.007	0.016
Ca	0.985	0.919	0.970	0.989	0.987	0.991	0.980	0.960	0.906
Na	0.001	0.001	0.002	0.002	0.000	0.003	0.014	0.002	0.001
K	0.000	0.001	0.000	0.000	0.000	0.000	0.000	0.000	0.000
Total	1.000	0.996	0.991	0.998	0.997	0.999	1.003	0.996	0.976
Molecular %									
$FeCO_3$	0.47	2.62	0.16	0.04	0.00	0.02	0.23	1.09	1.44
$MnCO_3$	0.74	0.67	0.55	0.38	0.50	0.20	0.09	0.95	1.49
$MgCO_3$	0.21	3.38	0.06	0.06	0.10	0.00	0.04	0.56	1.39
$CaCO_3$	98.59	93.34	99.23	99.52	99.40	99.78	99.63	97.41	95.68

* Total Iron as FeO

4.5 Discussion

4.5.1 Preserved textures

The ubiquitous presence of albite, chlorite and quartz and the presence, in many areas, of calcite and lesser amphibole indicate that rocks of the Skidder Basalt have a mineralogy similar to that of spilites (cf. Amstutz, 1974). Although these rocks are now dominated by a secondary mineral assemblage, most workers agree that spilitization is generally an ion exchange process and original textures are preserved (cf. Williams et al., 1982, p. 112-115). This is supported by the presence, in some Skidder Basalt samples, of remnant primary clinopyroxene subophitically intergrown with plagioclase that has been completely albitized; and also by the occurrence of microporphyritic, intergranular and intersertal textures; these textures being characteristic of un-spilitized basalt.

4.5.2 Quench textures

Quench-textured morphologies are common in many of the Skidder basalts having low zirconium concentrations. Some generalizations regarding these rocks that are pertinent to the following discussion are: a) it is presumed that the rocks crystallized from a low-viscosity magma; b) the presence of olivine pseudomorphs with chromite inclusions in one of the basalt samples suggests that olivine and chromite were on the liquidus of the magma before eruption; c) the lack of clinopyroxene phenocrysts suggests that it was probably not on the liquidus of the magma before eruption; d) both plagioclase and clinopyroxene show quench-type textures in the rocks; and e) abundant intersertal chlorite and lesser quartz suggest that much of the groundmass was probably composed of basaltic glass.

Williams et al. (1982) suggest several kinetic controls of igneous texture, i.e. temperature, magma viscosity and crystallization rates (cf. Carmichael et al., 1974). They point out that crystallization of a mineral occurs in two stages: 1) nucleation of a crystallite and 2) growth of the nucleus. Nucleation rate is determined by degree of undercooling,

increases with surface energy contribution to the free energy of the crystalline nucleus and decreases with activation energy requirements (viscosity). Growth increases with amount of free energy released during crystallization of an undercooled melt and is opposed by an increase in viscosity as the temperature falls. Williams et al. (1982) also indicate that both nucleation rate and growth reach a peak and then taper off with falling temperature and degree of undercooling of the magma, but the growth peak occurs at a higher temperature than the peak nucleation rate; the two peaks being offset from each other by about 30-50°C (cf. Carmichael et al., 1974) (Figure 4-40). Thus, slowly cooling magmas would pass through a temperature and viscosity range in which nucleation rate had not peaked but growth rate had, resulting in growth of large crystals around few nuclei. Rapid nucleation but slow growth would result from undercooling of the magma beyond the growth peak to the peak of nucleation. Further undercooling of the magma to temperature and viscosity conditions under which both growth and nucleation rates fall to zero would result in a glass.

Quench textures in the Skidder Basalt rocks can thus be explained by undercooling of a magma beyond the growth peak for plagioclase and clinopyroxene to temperature and viscosity conditions favouring nucleation. Further undercooling to conditions where both growth and nucleation are inhibited would explain the formation of groundmass basaltic glass.

4.5.3 Variolitic textures

Observations regarding Skidder Basalt variolitic pillow basalts that are pertinent to the following discussion are:

1) The varioles occur typically as distinct light-coloured spherical bodies inside pillow rims and coalesce into massive forms at pillow centres. Coalescence of varioles is not complete in some small pillows.

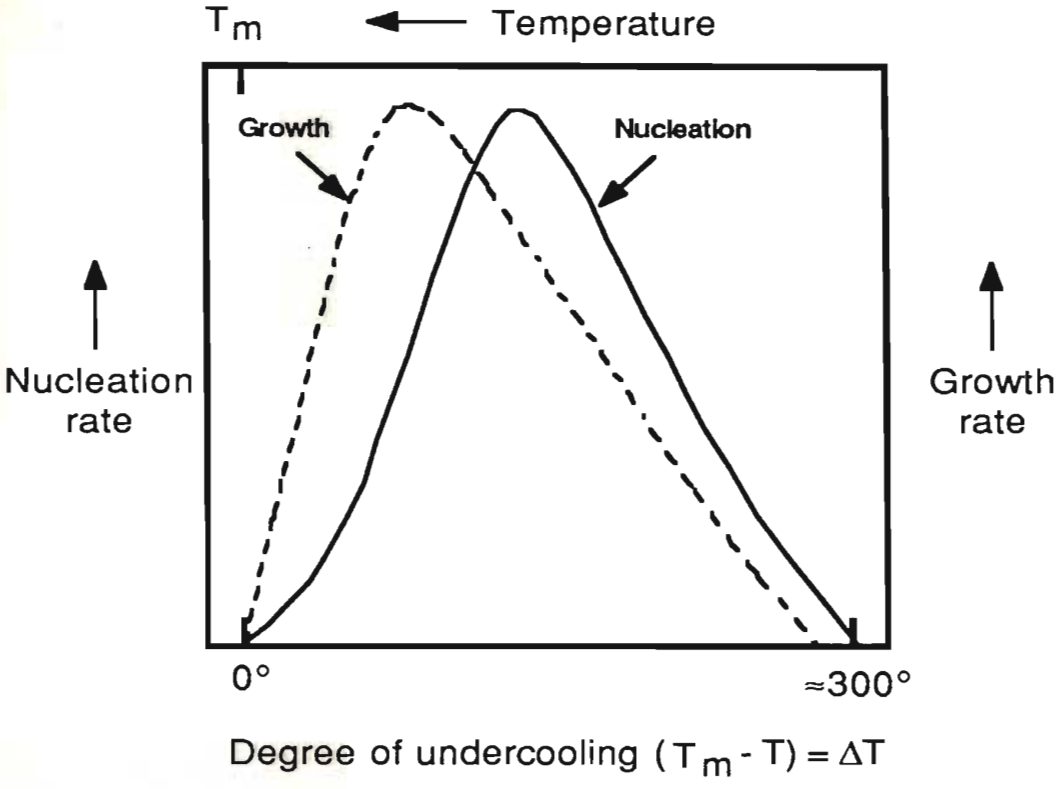

Figure 4-40: Diagrammatic representation of respective rates of nucleation and crystal growth in one-component systems with respect to melting temperature (T_m) and degree of undercooling (ΔT) of the liquid phase (after Williams et al., 1982, p.49; cf. data for $Na_2Si_2O_5$ shown by Carmichael et al., 1974, p. 165).

2) Whole rock analyses of the variolitic rocks suggest that they are of relatively "primitive" basaltic composition (Chapter 5).

3) Although separate analyses of variole and matrix were not done, the mineralogy of the varioles, predominantly albite and quartz, is indicative of a more felsic composition for the varioles than the matrix, which contains mostly ferromagnesian minerals.

4) Textures typical of quenching are predominant in both varioles and matrix.

5) Elongate grains pseudomorphing mafic minerals occur haphazardly throughout both variole and matrix in some sections.

The origin of varioles has been attributed to at least three possible mechanisms, i.e. devitrification; derivation from two distinct liquids either by magma mixing or liquid immiscibility; and quenching. Devitrification is an unlikely mechanism for the formation of varioles since they are typically of markedly different composition from their matrix, and, in many areas, varioles are noted to have coalesced to form a single mass. Also, there is very little physical or chemical evidence to support magma mixing in the Skidder basalts. Quench textures however are exhibited by variolitic lavas of the Skidder Basalt and elsewhere, e.g. in variolitic pillow lavas and diabase dykes of the Betts Cove Ophiolite (Saunders, 1985), of the St. Anthony Complex (Jamieson, 1979) and in variolitic pillowed and massive metavolcanic rocks of the Archean Abitibi greenstone belt (Gélinas, et al., 1976).

Gélinas et al., (1976) report that many of the varioles in the Abitibi Greenstone Belt comprise a central core of spherulitic albite surrounded by an intermediate quartz-albite mosaic and sometimes an outer rim of mostly sphene. They state that in several areas pseudomorphs of skeletal mafic crystals occur both inside and outside the variole and in places cross the border between variole and matrix. These features also characterize many of the Skidder Basalt varioles. Gélinas et al., (1976) separate variolitic lavas of the Abitibi greenstone belt into two types: spherulites which do not have marked differences in composition between variole and matrix, and those that do. The former they attribute to

quenching and the latter to quenching of immiscible liquids. Liquid immiscibility provides a ready explanation for differences in composition between varioles and matrix, however one difficulty with this hypothesis when considering varioles in the Skidder Basalt is that experimental work on immiscible liquids with regard to tholeiitic basaltic magmas (e.g. Dixon and Rutherford, 1979; Philpotts, 1982) have shown that liquid immiscibility may occur in iron-enriched evolved basaltic magma but not in primitive, high magnesium lavas.

Of the two plausible processes that may have produced the Skidder variolitic basalts (i.e. magma quenching or liquid immiscibility), quenching is a better known and accepted phenomenon. Bender et al. (1978) and Basaltic Volcanism Study Project (1981a) state that clinopyroxene becomes a liquidus phase after plagioclase in mid-ocean ridge basalts (MORBS) and according to Beccaluva et al. (1980) cumulus minerals in the gabbroic complexes and phenocryst phases in the lavas of the Northern Apennine Ophiolites, which have MORB type chemistry, indicate a crystallization order of Cr-spinel plus olivine, plagioclase and then clinopyroxene. Assuming a similar crystallization order for the Skidder Basalt, as supported by the presence of pseudomorphed olivine and albitized plagioclase phenocrysts and the chemistry of its chromites (Section 4.4.2), kinetic controls of crystallization described by Williams et al. (1982), can explain many of the features of the Skidder basalt varioles.

Two properties of plagioclase which would probably promote variole formation under rapid cooling conditions are: 1) plagioclase forms a continuous solid solution series such that peaks for growth and nucleation rates for different plagioclase compositions cover a considerable range of temperature and 2) although rapid crystallization suppresses the ability of plagioclase to nucleate (Grove and Bryan, 1983), the thermodynamic properties of plagioclase favour nucleation over growth, (the reverse is true for clinopyroxene) (Williams et al., 1982). Note that property "1" suggests that primary plagioclase in the central core of varioles should be more calcic than that occurring toward the variole rim;

this cannot be confirmed in the Skidder Basalt samples however since plagioclase, both in the core and rim of the varioles, has been completely albitized.

Undercooling of a magma with olivine and chromite on the liquidus through the growth peak for olivine toward its nucleation peak (Figure 4-40) would result in skeletal growth of olivine crystals throughout the lava. Gélinas et al. (1976) indicate that in the Abitibi greenstone lavas the haphazardly arranged pseudomorphs of skeletal mafic crystals in both varioles and matrix as well as across their boundary were originally quenched olivine crystals. It is thus reasonable to suggest that similar crystallites in the variolitic Skidder basalts (Figures 4-4 and 4-5) may also have been olivine. The widespread distribution of the crystallites (including within the varioles) suggests homogeneity of the lava during their formation. The presence of an albitized plagioclase crystal in the core of a variole in thin section S 55 (Figure 4-15) indicates that plagioclase in addition to olivine was on the liquidus prior to eruption of at least some of the lavas from which the Skidder Basalt rocks crystallized.

Further undercooling of the magma would have eventually reached a point where growth and nucleation of olivine ceased. As indicated above, plagioclase solid solution results in growth and nucleation peaks for various plagioclase compositions occurring over a range of temperatures. Thus, plagioclase crystals are able to nucleate and grow even under rapid cooling conditions and rapid crystallization of the plagioclase could produce the spherical forms characteristic of varioles (e.g. Lofgren, 1974). Note that phenocrysts in the lava may facilitate nucleation, providing a locus for later rapidly crystallizing mineral phases and as shown in thin section S 55B in some instances, form the core of a variole.

Still further undercooling of the magma would probably result in quench crystallization of clinopyroxene in addition to plagioclase, and finally formation of basaltic glass in the matrix and, to a lesser extent, intersertal to plagioclase in the varioles.

Coalescence of varioles in the central portion of some Skidder Basalt pillows and nonvariolitic rocks showing quench textures are suggested to be due to less rapid quenching of plagioclase and clinopyroxene.

4.5.4 Segregation vesicles

Segregation vesicles which occur in several of the samples having Zr concentrations between 50 and 85 ppm (e.g. Figure 4-22) are interpreted to be late-stage magmatic residues that infill vesicles (Smith, 1967). Smith (1967) indicates that the magmatic residue may be "drawn" into the vesicle as a result of pressure reduction from contraction during cooling of water vapor that originally filled the vesicle. Baragar et al. (1977) postulate that complete filling of the vesicles may result from magmatic dissolution of the water vapour and subsequent crystallization of hydrous minerals. Late-stage magmatic melts filling segregation vesicles may reach highly evolved compositions as evidenced by the occurrence of rhyodacite segregation vesicles in basalts from Réunion Island (Upton and Wadsworth, 1971).

Some varioles in the Skidder Basalt have small amygdules distributed throughout them and locally forming their cores. These varioles may have originally been segregation vesicles as described by Smith (1967). Baragar et al. (1977) suggest that some varioles in other ancient basalts may have formed in this manner. Note that the highly evolved nature of some late-stage melts that fill segregation vesicles provides a mechanism for formation of varioles that are of more felsic composition than their matrix.

4.5.5 Spilitization

The spilitization process predominantly involves albitization of plagioclase, chloritization of basaltic glass, alteration of anhydrous ferromagnesian minerals to hydrous counterparts and alteration of opaque Fe-Ti oxides to dense intergranular sphene (leucoxene). Chemically, spilitization of the Skidder basalts has resulted in redistribution

of SiO_2 and total iron, removal of K_2O and MgO, and extensive addition of Na_2O (Chapter 5). In some areas, clinopyroxene has been altered to amphibole or chlorite or a combination of amphibole, calcite, epidote and chlorite. Calcium and possibly iron released during chloritization of clinopyroxene probably recrystallizes in epidote, sphene and/or other secondary Ca-bearing minerals; excess silica is probably taken up by epidote or quartz. Calcium required for the formation of sphene by alteration of Fe-Ti oxides may be derived from albitization of plagioclase and/or, as indicated above, by chloritization of calcium-bearing clinopyroxene and amphibole; released iron probably recrystallizes in magnetite or epidote. Abundant intersertal chlorite has probably formed by alteration of basaltic glass or palagonite. Crystallization of quartz from excess silica released during chloritization would suggest that the ubiquitous intersertal quartz in these rocks may be mostly secondary.

4.5.6 Submarine hydrothermal alteration

Many of the mineralogical changes resulting from spilitization of the Skidder Basalt have, in other areas, been attributed to interaction with circulating heated seawater shortly after deposition of the basalts (cf. Mottl, 1983a). Evarts and Schiffman (1983), for example, conclude that zeolite to greenschist facies assemblages in the Del Puerto Ophiolite are primarily a result of submarine hydrothermal alteration and that the effects of burial metamorphism are restricted to the formation of late calcite and zeolite veins.

Figure 4-41 compares the concentrations of various solutes in seawater to that of solute species in a solution having a chloride concentration equivalent to that of seawater in full equilibrium with an assemblage comprising albite, microcline, muscovite, phlogopite and laumontite/wairakite, plotted as a function of temperature (interpolated from data presented by Giggenbach (1984)). According to Figure 4-41, solubilities of Na, K and SiO_2 in the equilibrium chloride solution increase, the solubility of Mg decreases, and that of Ca remains approximately the same with increasing temperature. The diagram also

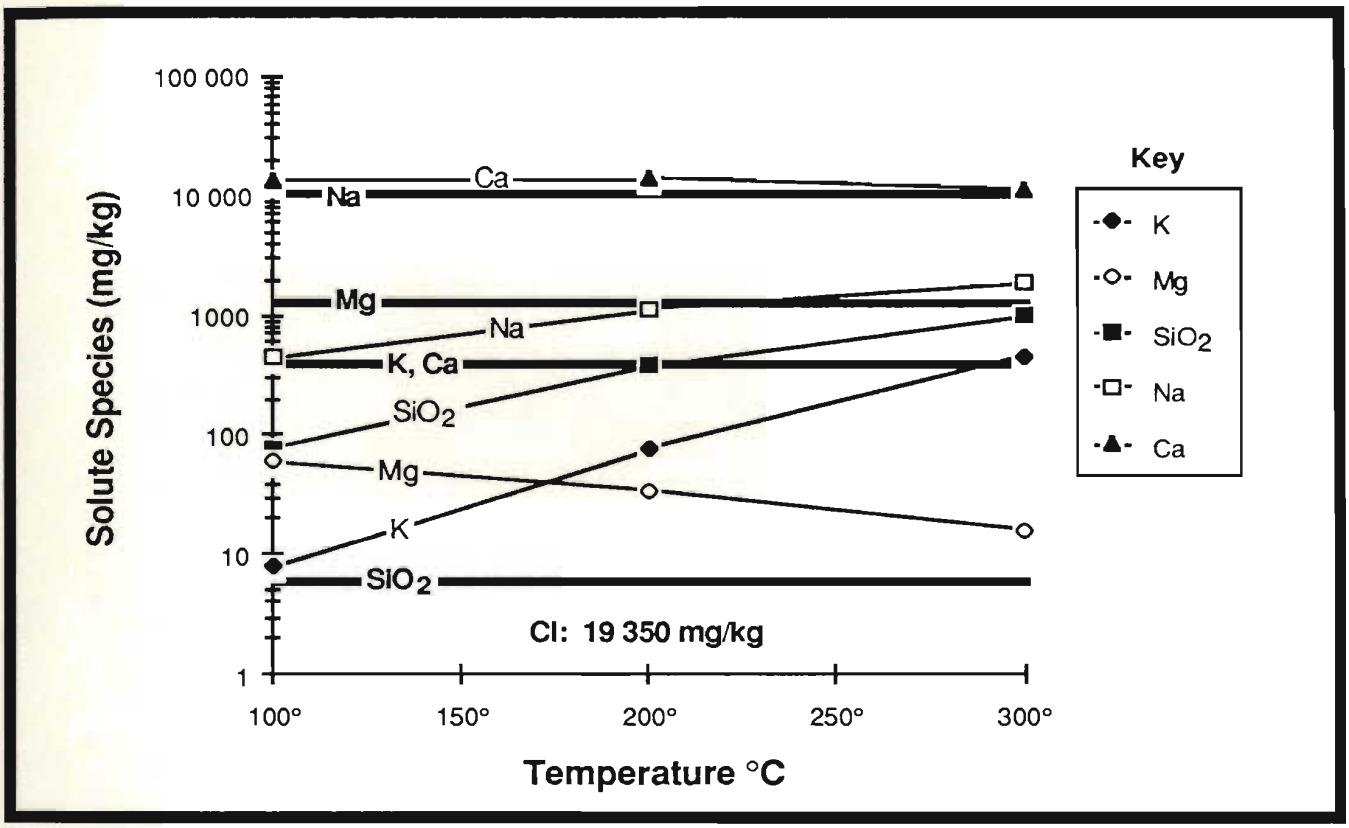

Figure 4-41: Distribution of solute species in full equilibrium between a chloride-bearing solution and an assemblage made up of albite, microcline, muscovite, phlogopite and laumontite/wairakite; as a function of temperature (interpolated from data presented in Giggenbach, 1984; Fig. 7). Chloride concentration of 19 350 mg/kg is that of seawater (Thompson, 1983). Heavy horizontal lines are concentrations of solute species in seawater (Thompson, 1983).

shows that seawater is supersaturated with respect to Na and Mg at elevated temperatures. Potassium is supersaturated in seawater with respect to the solution and assemblage presented up to at least 200°C but is slightly undersaturated at 300°C. Calcium and SiO_2 are undersaturated in seawater with respect to the equilibrium assemblage presented.

The chloride-bearing solution used by Giggenbach (1984) only approximates that of seawater, in which, for instance, the presence of SO_4^{2-} will stabilize anhydrite as a calcium-bearing phase at approximately 150°C (e.g. Rosenbauer and Bischoff, 1983). Nevertheless, Figure 4-41 illustrates several points which are in agreement with results of basalt-seawater interaction experiments and with the observed differences between the chemical composition of seawater and that of 350°C vent water from 21° N on the East Pacific Rise (Edmond, 1981). The vent water sampled at this location is an acidic (pH 3.6), metal-rich solution, that is depleted in Mg, and enriched in Ca, K and SiO_2 relative to normal seawater.

Summaries of experimental results involving basalt-seawater interaction at elevated temperatures and various water/rock ratios are presented by Rosenbauer and Bischoff (1983) and Mottl (1983a; 1983b). As reported by these authors, Mg^{2+} is removed from seawater by formation of a $Mg(OH)_2$ component which is incorporated into secondary silicates. This occurs over a range of temperatures from 70-700°C. Removal of the Mg hydroxide component results in a drop in pH of the solution to about 3 and it remains this way until Mg stops precipitating, at which time hydrolysis of silicate minerals raises the pH to near neutrality. At water/rock ratios less than 50, Mg is completely removed from the seawater. Leaching of Ca^{2+} from the rock counterbalances removal of Mg^{2+} from the seawater. According to Mottl (1983b) about half of the Ca is redeposited as anhydrite above 150°C but at higher temperatures may be redissolved by reduction of sulphate to sulphide. Removal of Na^+ from the seawater occurs at water/rock ratios ≤ 5. At a water/rock ratio of 10, Na^+ is leached from the rock below 300°C, but is precipitated from seawater at 350°C. At higher water/rock ratios, Na^+ is leached from the rock. K^+ is

leached from the rock at 150°C and above. At 300°C and higher it is leached almost completely, even at low water/rock ratios. Dissolved SiO_2 is saturated with respect to quartz at 150-200°C and is saturated or supersaturated with respect to quartz at higher temperatures.

Albite has been produced as a mineral phase in only a few basalt-seawater experiments (e.g. Seyfried and Bischoff, 1981), and, although removal of Na from seawater is predicted from the experimental results at low water/rock ratios, the actual amount of Na precipitated is not as great as is indicated to have occurred in naturally altered basalts. For example, as shown in Chapter 5, the average Na_2O content of the Skidder Basalt (4.94%) is 2-2.5% greater than average unaltered ocean floor basalts (2.3-2.8%) and 2.5-3% greater than average unaltered island arc basalts (1.9-2.4%), indicating substantial addition of Na to the Skidder Basalt as a result of spilitization. Mottl (1983b) suggests that while basalt-seawater experiments duplicate infusion of solution into the rocks, diffusion of elements away from the reaction front is not duplicated. For example, as discussed by Seyfried et al. (1978), Na may diffuse away from circulating pore fluids at pillow rims and into pillow interiors where water/rock ratios would be low enough for Na to be removed from the water and albite could form.

Formation of the abundant albite in the Skidder Basalt is most readily explained by the breakdown of calcium-bearing plagioclase through ion exchange, possibly by the following simplified reaction:

$$CaAl_2Si_2O_8 + 4SiO_2 + 2Na^+ = 2NaAlSi_3O_8 + Ca^{2+}$$ (Helgeson, 1974).

Na^+ may be provided by circulating seawater (at low water/rock ratios) and additional SiO_2 probably provided by release during chloritization of olivine and basaltic glass (much of the chlorite in the Skidder Basalt is interserial). Some of the Ca^{2+} produced by albitization of calcic-plagioclase may have been redeposited in calcium-bearing secondary minerals such as epidote and sphene. (Note that abundant calcite, which occurs as open-space fillings and, in some places, replaces other secondary minerals in the Skidder Basalt, probably

represents later redistribution of calcium as a result of burial metamorphism). As indicated in Chapter 5, the average CaO content of the Skidder Basalt (5.43%) is significantly less than the average for unaltered Ocean Floor Basalts (11.3-11.8%) and unaltered island arc basalts (11.1-11.8%). Allowing for sampling bias whereby calcite and epidote-rich areas of the samples were excluded from analysis, it is still probable that at least some Ca was removed from the Skidder Basalt during spilitization.

Albite may also be produced from the sodic portion of plagioclase by epidotization as indicated by the following reaction, which is used by Rosenbauer and Bischoff (1983) as a possible explanation for the drop in pH observed in evolved seawater-basalt experiments:

$$\underset{\text{plagioclase}}{NaAlSi_3O_8 \cdot 3CaAlSi_2O_8} + Ca^{2+} + 2H_2O = \underset{\text{clinozoisite}}{2Ca_2Al_3Si_3O_{12}(OH)} + \underset{\text{albite}}{NaAlSi_3O_8} + 2H^+.$$

An additional Fe component would have to be added to this reaction to match the Ps component of Skidder Basalt epidotes. This Fe could be provided by breakdown of Fe-Ti oxides to produce sphene.

Figure 4-42 shows the mineral stability fields of K-feldspar vs. Na-feldspar as a function of a_{Na^+}/a_{K^+} and temperature (after Giggenbach, 1984). The heavy solid line represents the a_{Na^+}/a_{K^+} of seawater assuming activity coefficients for Na^+ and K^+ are equal (Giggenbach, 1984). The stippled area represents a possible range of activity ratios for a seawater solution after reaction with basalt. The upper limit of the stippled area was chosen assuming a change from K addition to the rock below 100°C to leaching of K from the rock above 100°C (cf. Seyfried and Bischoff, 1979).

Points A, B, C and D represent a possible sequence of activity ratios that a seawater solution could have with increasing temperature and only partial equilibration with K-feldspar and Na-feldspar. The solid and dashed lines on the diagram represent the relative proportions of alkali ions which would have to be produced or consumed to reach equilibrium with the two feldspars (Giggenbach, 1984). The proportions indicate that the

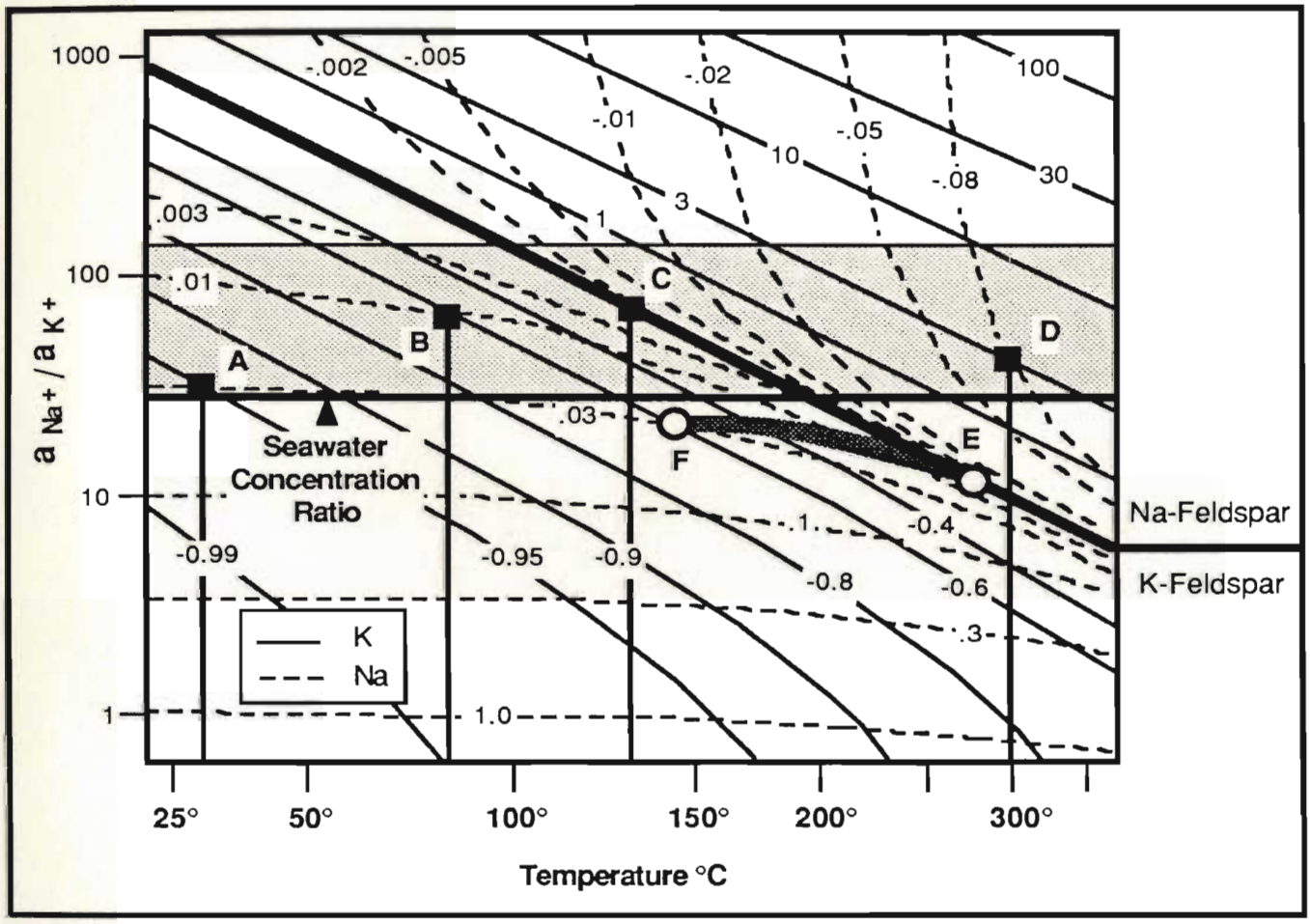

Figure 4-42: Stability fields for Na- and K-feldspars as a function of Na^+/K^+ activity ratio versus temperature (after Giggenbach, 1984). Numbered lines indicate relative proportions of alkali ions produced or consumed (-) during isothermal equilibration of a solution having a given Na^+/K^+ activity ratio, with an equilibrium assemblage containing Na- and K-feldspars (after Giggenbach, 1984). Seawater concentration ratio for Na^+/K^+ based on an assumption of equivalent activities for Na^+ and K^+. Concentrations for Na^+ and K^+ in seawater taken from Thompson (1983). See text for discussion of stippled area and points A, B, C, D, E and F.

degree of undersaturation or supersaturation with respect to K is always greater than Na and that re-equilibration of the system in response to temperature changes will dominantly involve readjustment of K contents (Giggenbach, 1984). For example, a solution at point A must deposit 95% of its potassium content but gain only 3% Na to reach equilibrium with the two feldspars. Upon heating a seawater solution would probably deposit some of its potassium such that it reaches a temperature and alkali activity ratio represented by point B. At point B, the solution is still supersaturated with respect to K such that 60% of its K content would have to be removed and 1% Na would have to be gained to attain equilibrium with the two feldspars. Upon further heating, the solution would eventually attain "accidental" equilibrium with the two feldspars, for example at point C. Upon further heating, e.g. to point D, the solution becomes oversaturated with respect to Na such that 8% would have to be removed in order to attain equilibrium. Consider, however that the solution would have to gain 300% K to obtain equilibrium.

Mottl (1983a) concludes on the basis of the mineralogy of Mid-Ocean Ridge greenstones, that seawater during downward circulation must have been heated quickly to about 250-450°C within the upper 1-2 km of the earth's crust. Figure 4-42 illustrates that seawater rapidly heated to 200-300°C should leach K from basalt and add Na to it (by the formation of albite). This is in general agreement with results of seawater-basalt interaction experiments which indicate that at temperatures greater than 150°C, K is leached from the rock and, at low water/rock ratios, Na is added to it (e.g. Rosenbauer and Bischoff, 1983).

Interaction with a heated seawater solution at temperatures above 150°C provides an explanation for the ubiquitous presence of albite in the Skidder Basalt rocks and their high Na_2O and very low K_2O contents relative to unaltered basalts (Chapter 5).

Figure 4-42 also predicts that K-bearing mineral phases will be deposited and Na-bearing phases dissolved by cooling, ascending hydrothermal solutions (Giggenbach, 1984). On Figure 4-42, consider a cooling hydrothermal fluid in equilibrium with both feldspars (Point E). In order to maintain equilibrium during cooling some ion exchange

reaction must occur, e.g. an increase in the K-feldspar component of albite. Further cooling of the solution would probably result in the solution moving away from the two-feldspar equilibrium line and becoming oversaturated with respect to K-feldspar (Point F).

Potassium enriched samples as represented by S-16 are suggested to have formed by deposition of K-feldspar from an upwelling solution along a fault zone. Several albites in sample S-16 contain higher K-feldspar components than most other Skidder basalts and other larger grains in this rock have rims comprising almost pure K-feldspar surrounding almost pure albite cores. Ion exchange reactions involving exchange of K for Na within a cooling, upwelling solution (Points E or F, Figure 4-42) could explain the relatively high K-feldspar components of some albites in S 16 and the K-feldspar rims around some larger albite grains in the sample.

Chapter 5

GEOCHEMISTRY

5.1 Introduction

Samples representing a suite of mafic rocks from the Skidder area were analyzed for major element contents and trace element concentrations. The rocks analyzed comprise mostly pillowed and massive basalts plus a few samples of mafic pillow breccias and diabase dykes. Of the 114 samples analyzed, 58 are from outcrop and the remaining 56 samples are from the Skidder Prospect drill core. Only analyses of Skidder Prospect drill core samples relatively unaffected by the Skidder Prospect mineralizing event are presented in this chapter (cf. Chapter 6). Sample preparation and analytical methods used are discussed in Appendix B; analyses are listed in Tables B-3 to B-9, Appendix B. Outcrop sample locations are shown on Figures 3-3 and 6-1; the locations of the Skidder Prospect drill holes are shown on Figure 6-1; and drill-core-sample locations are shown on Figures 6-3 to 6-10.

Portions of Sections 5.2.5, 5.2.6, 5.2.7, 5.2.10, 5.2.11, 5.2.12, 5.3.1 and 5.3.2 of this chapter are published in Pickett (1987).

5.2 Geochemistry of the Skidder Basalt

5.2.1 Major oxide and minor element statistics

Histograms showing the distribution of the Skidder Basalt geochemical data are presented as Figures B-1 to B-7, Appendix B, and probability plots are presented as Figures B-8 to B-14, Appendix B. Table 5-1 shows the mean, standard deviation and skewness of all the samples as well as a breakdown of the data into samples from outcrop vs. those from drill core, and samples of pillowed vs. massive flows. Table 5-2 summarizes the data distributions for the various major oxide and trace elements analyzed; as interpreted from the histograms and probability plots shown in Figures B-1 to B-14, and

Table 5-1: Mean, standard deviation and skewness of Skidder Basalt outcrop samples, and Skidder Prospect drill core samples that are relatively unaffected by the mineralizing event(s)

1 - Pillowed flows, pillow breccia, massive flows and diabase in outcrop and drill core
2 - Pillowed flows, pillow breccia, massive flows and diabase in outcrop
3 - Pillowed flows, pillow breccia, massive flows and diabase in drill core
4 - Pillowed flows and pillow breccia in outcrop and drill core
5 - Massive flows and diabase in outcrop and drill core

1 - Number of samples = 114
2 - Number of samples = 58
3 - Number of samples = 56
4 - Number of samples = 76
5 - Number of samples = 38

Mean

Weight %	1	2	3	4	5
SiO_2	50.39	50.02	50.77	50.21	50.74
TiO_2	1.09	1.02	1.16	1.08	1.10
Al_2O_3	15.11	14.67	15.57	15.18	14.98
Fe_2O_3	10.76	10.43	11.11	10.64	11.01
MnO	0.15	0.16	0.15	0.15	0.16
MgO	6.93	6.50	7.38	6.92	6.96
CaO	5.43	7.08	3.72	5.43	5.42
Na_2O	4.94	4.81	5.08	5.02	4.77
K_2O	0.17	0.11	0.23	0.15	0.20
P_2O_5	0.17	0.15	0.19	0.17	0.18
LOI	4.43	4.66	4.18	4.53	4.21
Total	99.57	99.61	99.54	99.49	99.74

ppm	1	2	3	4	5
Pb*	3	3	4	3	3
Rb*	2	2	3	2	2
Sr	82	86	78	83	80
Y	31	29	34	31	32
Zr	68	62	74	69	66
Nb**	5	4	5	5	5
Zn	83	75	93	78	93
Cu	40	47	32	39	42
Ni	47	52	42	47	47
Ba	29	24	34	24	38
V	327	309	347	326	331
Ce	65	57	74	63	69
Cr	146	141	151	155	128
Ga	16	15	17	16	17

Standard Deviation

	1	2	3	4	5
SiO_2	4.56	5.00	4.06	4.65	4.40
TiO_2	0.33	0.33	0.32	0.31	0.37
Al_2O_3	1.16	1.06	1.09	1.26	0.93
Fe_2O_3	1.87	1.93	1.75	2.03	1.48
MnO	0.04	0.04	0.05	0.05	0.04
MgO	2.35	2.08	2.54	2.42	2.24
CaO	3.26	3.49	1.82	3.24	3.32
Na_2O	0.96	1.01	0.90	0.92	1.03
K_2O	0.17	0.14	0.19	0.16	0.20
P_2O_5	0.13	0.14	0.12	0.12	0.16
LOI	2.34	2.75	1.82	2.50	1.99

	1	2	3	4	5
Pb*	3	3	3	3	3
Rb*	3	2	3	3	2
Sr	51	61	38	54	45
Y	12	11	13	12	13
Zr	25	23	27	25	25
Nb**	2	2	2	2	2
Zn	33	29	34	27	41
Cu	30	34	23	30	28
Ni	49	55	41	41	62
Ba	43	50	35	30	61
V	98	94	100	89	117
Ce	31	26	33	31	29
Cr	137	133	143	144	123
Ga	3	3	3	3	4

Skewness

	1	2	3	4	5
SiO_2	0.39	0.25	0.24	0.40	0.57
TiO_2	0.09	-0.01	0.41	0.03	0.55
Al_2O_3	0.16	0.20	0.46	0.07	0.25
Fe_2O_3	-0.01	0.07	-0.04	0.08	-0.01
MnO	-0.44	-0.24	-0.63	-0.59	-0.07
MgO	0.48	0.08	0.36	0.38	0.57
CaO	0.63	0.08	0.77	0.76	0.26
Na_2O	-0.19	-0.04	-0.40	-0.23	-0.16
K_2O	0.88	1.07	1.45	0.84	1.20
P_2O_5	0.91	0.61	0.70	0.69	0.88
LOI	0.86	1.25	0.64	0.90	1.06

	1	2	3	4	5
Pb*	0.36	-0.08	0.28	0.33	0.42
Rb*	0.30	1.07	0.81	1.36	0.40
Sr	0.79	0.79	0.85	0.83	0.71
Y	0.85	0.38	0.94	0.70	0.87
Zr	-0.01	0.05	0.36	-0.02	0.02
Nb**	-0.16	0.76	-1.03	-0.02	-0.42
Zn	0.21	0.31	0.26	-0.12	0.35
Cu	0.53	0.30	0.31	0.51	0.61
Ni	0.71	0.70	0.85	0.36	1.01
Ba	1.15	1.01	0.98	1.30	1.10
V	0.07	0.00	-0.12	0.34	-0.21
Ce	-0.09	-0.20	0.06	-0.05	0.16
Cr	0.98	0.90	0.95	0.76	1.08
Ga	0.03	-0.20	0.28	-0.36	0.29

* Pb and Rb concentrations in the Skidder Basalt are very low, close to the detection limit of X-ray fluorescence spectrometry, the analytical method used (Appendix B)

** Close to detection limit of the X-ray fluorescence spectrometry method

Key to Table 5-2

Percentage or ppm values at which there are slope changes on Element or Log_{10} Element vs. Probits plots shown in Figures B-8 to B-14, Appendix B

Key: **L** - lower limit of main population(s)
O/C-D/C - change in slope reflecting offset of main outcrop and drill core populations
U - upper limit of main population(s)

Qualitative description of skewness shown in Table 5-2

Key: **All** - outcrop and drill core samples
O/C - outcrop samples
D/C - drill core samples
P - pillowed flows and pillow breccia samples in outcrop and drill core
M - massive flows and diabase in outcrop and drill core
+ve - slight positive skewness
++ve - moderate positive skewness
+++ve - strong positive skewness
N - normal distribution
-ve - slight negative skewness
--ve - moderate negative skewness
---ve - strong negative skewness

Qualitative comparison of means shown in Table 5-2

Key: **O/C vs. D/C** - outcrop samples vs. drill core samples
P vs. M - pillowed flows and pillow breccia samples vs. massive flows and diabase, cf. histograms shown in Figures B-1 to B-7, Appendix A; sample group with the higher mean value shown
Plain text - slightly higher mean
Bold text - much higher mean

Table 5-2: Summary table of probability plots, histograms and statistical parameters presented in Figures B-1 to B-14, Appendix B; and Table 5-1; key on facing page

	Changes in Slope on Element or Log Element vs. Probits Plots						Skewness					Greater Mean Value	
	L	O/C-D/C	U	Others			All	O/C	D/C	P	M	O/C vs. D/C	P vs M
SiO_2	47%		62%	55%			++ve	+ve	+ve	++ve	++ve	D/C	M
TiO_2		1%		1.4%	1.85%		N	N	++ve	N	++ve	**D/C**	M
Al_2O_3	13.5%	14.5%		16%			+ve	+ve	++ve	N	+ve	**D/C**	P
Fe_2O_3			14.5%	9%			N	N	N	N	N	D/C	M
MnO			0.21%	0.17%			--ve	-ve	---ve	--ve	-ve	O/C	M
MgO			12%	8.5%	10%		++ve	N	++ve	++ve	++ve	**D/C**	M
CaO		3.5%	8% (D/C)	14%			+++ve	N	+++ve	+++ve	+ve	**O/C**	P
			12% (O/C)										
Na_2O	3%			4.5%			-ve	N	--ve	-ve	-ve	D/C	P
K_2O			0.2%	0.6%			+++ve	+++ve	+++ve	+++ve	+++ve	**D/C**	**M**
P_2O_5	0.04%		0.29% (O/C)	0.4%	0.6%		+++ve	+++ve	+++ve	+++ve	+++ve	D/C	M
LOI		4%	6%	9.5%			+++ve	+++ve	+++ve	+++ve	+++ve	**O/C**	P
Pb			8 ppm	12 ppm			++ve	N	+ve	++ve	++ve	D/C	-
Rb			7 ppm	4 ppm	9 ppm		++ve	+++ve	+++ve	+++ve	++ve	D/C	-
Sr	30 ppm		100 ppm	200 ppm	250 ppm		+++ve	+++ve	+++ve	+++ve	+++ve	O/C	P
Y		30 ppm	52 ppm	18 ppm	60 ppm		+++ve	++ve	+++ve	+++ve	+++ve	**D/C**	M
Zr			102 ppm	50 ppm	75 ppm	85 ppm	N	N	++ve	N	N	**D/C**	P
				130 ppm									
Nb			7 ppm	5 ppm	9 ppm		-ve	+++ve	---ve	N	--ve	D/C	-
Zn	35 ppm		125 ppm	175 ppm			+ve	++ve	+ve	-ve	++ve	D/C	**M**
Cu			68 ppm	4 ppm	22 ppm	120 ppm	++ve	++ve	++ve	++ve	+++ve	O/C	M
Ni	6 ppm	70 ppm		175 ppm			+++ve	+++ve	+++ve	++ve	+++ve	O/C	-
Ba	10 ppm		80 ppm	160 ppm			+++ve	+++ve	+++ve	+++ve	+++ve	D/C	M
V		310 ppm	480 ppm	170 ppm			N	N	-ve	++ve	-ve	**D/C**	M
Ce		75 ppm	120 ppm	20 ppm	40 ppm		N	-ve	N	N	+ve	**D/C**	M
Cr	25 ppm			150 ppm	330 ppm	480 ppm	+++ve	+++ve	+++ve	+++ve	+++ve	D/C	**P**
Ga		16 ppm	25 ppm	12 ppm	21 ppm		N	-ve	+ve	--ve	+ve	D/C	P

statistical parameters presented in Table 5-1.

As indicated on Table 5-2, K_2O, P_2O_5, LOI, Rb, Sr, Y, Ni, Ba and Cr show the strong positive skewness characteristic of lognormal distributions. SiO_2, Al_2O_3, MgO, Pb, Zn and Cu show slight to moderate positive skewness; Fe_2O_3, Zr, V, Ce and Ga are normally distributed; Na_2O shows slight, and MnO moderate negatively skewed distributions. CaO and TiO_2 show distributions varying from normal to moderately positively skewed. Niobium shows a variable distribution.

Table 5-1 indicates that, relative to the outcrop samples, those from the Skidder Prospect drill core have a higher average content of most of the major elements, and they have higher average concentrations of trace elements Y, Zr, Zn, V, Ce, Cr and Ga. They have lower contents of CaO, MnO, Sr, Cu, and Ni. These differences are also reflected by offset peak distributions on histograms presented in Figures B-1 to B-7, Appendix B. There is little geochemical variation between pillowed and massive flows (Table 5-1). The pillowed flows do, however, contain a greater average concentration of Cr and lesser overall Zn than the massive flows.

The presence of more than one data population is indicated for most of the major oxides and trace elements (Table 5-2). Two data populations result from the offset of the outcrop and drill core data distributions, and outliers of anomalously high and low values define separate populations in several of the major oxides and trace element data distributions (Table 5-2).

5.2.2 Principal component analysis

Table 5-3 shows a Pearson correlation coefficient matrix for the Skidder Basalt samples, and Table 5-4 lists varimax-rotated factors extracted from the major and trace element data (see Appendix C for description of method used). The various factors presented in Table 5-4 indicate groupings of interelement correlations. Eight factors were

Table 5-3: Pearson correlation matrix for Skidder Basalt outcrop samples, and Skidder Prospect drill core samples that are relatively unaffected by the mineralizing event(s) .

Number of Samples = 114

	SiO_2	TiO_2	Al_2O_3	Fe_2O_3	MnO	MgO	CaO	Na_2O	K_2O	P_2O_5	LOI	Pb	Rb	Sr	Y	Zr	Nb
SiO_2	*1.00*																
TiO_2	.10	*1.00*															
Al_2O_3	-.26	.00	*1.00*														
Fe_2O_3	.00	.46	.16	*1.00*													
MnO	-.33	.00	.00	.28	*1.00*												
MgO	-.45	-.11	.24	.15	.30	*1.00*											
CaO	-.58	-.28	-.28	-.34	.12	-.09	*1.00*										
Na_2O	.41	.18	.10	.00	-.27	-.63	-.28	*1.00*									
K_2O	-.04	.00	.36	.00	.00	.00	-.03	.00	*1.00*								
P_2O_5	.43	.45	.00	.00	-.22	-.38	-.37	.26	.00	*1.00*							
LOI	-.71	-.31	.00	-.35	.00	.16	.50	-.34	.04	-.19	*1.00*						
Pb	.00	.00	.00	.00	.15	.00	-.09	.00	.09	.00	.14	*1.00*					
Rb	-.13	.00	.27	-.14	.00	.00	.00	.14	.73	.00	.19	.27	*1.00*				
Sr	-.26	-.11	.30	-.03	.14	.05	.24	-.16	.21	-.15	.00	.00	.24	*1.00*			
Y	.48	.71	-.02	.31	-.13	-.40	-.45	.39	.00	.63	-.42	.04	-.08	-.26	*1.00*		
Zr	.35	.70	.00	.26	-.10	-.30	-.39	.29	.00	.49	-.27	.00	-.13	-.23	.86	*1.00*	
Nb	.00	.48	.00	.25	.00	.00	-.15	.00	.00	.36	.00	.00	.00	-.10	.45	.61	*1.00*
Zn	.00	.15	.28	.40	.36	.21	-.39	.00	.00	.00	-.09	.14	.00	.00	.20	.10	.00
Cu	-.26	-.28	.00	-.23	.00	.24	.33	-.27	.00	-.37	.17	.00	.00	.00	-.38	-.37	-.17
Ni	-.54	-.36	.00	-.27	.16	.48	.39	-.44	.00	-.34	.50	.00	.00	.21	-.54	-.43	-.18
Ba	-.07	.00	.14	.00	.05	.00	.00	.00	.53	.06	.00	.00	.34	.22	.00	.00	.00
V	-.26	.23	.28	.52	.00	.27	-.15	.00	.00	-.31	.00	.13	.00	.00	.00	.00	.00
Ce	.18	.43	.00	.24	.00	.00	-.33	.00	.00	.29	-.18	.00	-.24	-.17	.35	.47	.49
Cr	-.43	-.27	.08	-.32	.00	.47	.24	-.36	.00	-.22	-.41	.00	.00	.17	-.50	-.36	-.08
Ga	.12	.39	.15	.40	.00	.00	-.35	.00	.01	.26	-.31	.00	-.09	-.24	.46	.45	.41

	Zn	Cu	Ni	Ba	V	Ce	Cr
Zn	*1.00*						
Cu	-.09	*1.00*					
Ni	-.19	.29	*1.00*				
Ba	.14	.00	.00	*1.00*			
V	.28	.00	-.11	.00	*1.00*		
Ce	.00	.00	-.17	-.27	.00	*1.00*	
Cr	-.26	.21	.88	.00	-.06	.00	*1.00*
Ga	.32	-.16	-.34	.07	.08	.42	-.29

Table 5-4: Varimax-rotated factors extracted from Skidder Basalt major and trace element geochemical data

	Factor 1	Factor 2	Factor 3	Factor 4	Factor 5	Factor 6	Factor 7	Factor 8
Variance	21.7%	10.5%	13.9%	17.1%	11.9%	10.7%	6.9%	7.3%
SiO_2				-.347	**-.597**	-.351		
TiO_2	**.678**							
Al_2O_3			.432	.267	-.266	**.533**		.260
Fe_2O_3*	.296	.462				**.491**		
MnO		**.738**						
MgO		.366		**.647**	-.261	.237		
CaO					**.797**			
Na_2O		-.428		-.460				.382
K_2O			**.902**					
P_2O_5	**.432**					-.440		.239
LOI				.331	**.539**		.358	
Pb							**.807**	
Rb			**.802**				.273	
Sr			.359		.210		**-.485**	.320
Y	**.532**			-.256				.202
Zr	**.685**							
Nb	**.807**							
Zn		**.644**			-.318			
Cu								**-.680**
Ni				**.744**				
Ba		.350	**.710**			-.248		
V						**.846**		
Ce	**.683**			.238				-.234
Cr				**.825**				
Ga	**.542**				-.250			-.292

* Total iron as Fe_2O_3

extracted from the data.

Factor 1 accounting for 21.7% of the variance has large positive loadings for TiO_2, P_2O_5, Y, Zr, Nb, Ce and Ga and a moderate positive loading for Fe_2O_3* (total iron) (Table 5-4). Intercorrelations between the principal components of this factor are probably effected by magmatic processes since the elements having large positive loadings in the factor are all incompatible with early crystallizing minerals in a basaltic magma.

Factor 2 accounting for 10.5% of the variance has large positive loadings for Fe_2O_3*, MnO and Zn; moderate positive loadings for MgO and Ba; and a large negative loading for Na_2O (Table 5-4). Most elements that have positive loadings for this factor are components of chlorite, a ubiquitous phase in most of the Skidder Basalt. Magnesium and iron are major components of chlorite and the Skidder Basalt chlorites contain minor amounts of Mn (Chapters 4 and 6). Also, as discussed in Chapter 6, Zn concentrations are high in chlorite-rich rocks from the Skidder Prospect alteration zone. The negative loading for Na_2O is probably a result of volumetric effects regarding mineral components of the rock, that is, higher contents of chlorite in a sample necessitate lesser contents of albite. The positive loading for Ba in this factor is probably fortuitous.

Large positive loadings for K_2O, Rb and Ba, and moderate positive loadings for Al_2O_3 and Sr characterize Factor 3 which accounts for 13.9% of the data variance (Table 5-4). Positive correlations between the principal components of this "potassium" factor i.e. K_2O, Rb, Ba and Sr are readily explained by substitution of Rb, Ba and Sr for potassium in potassium-bearing minerals. Although aluminum is a component of most potassium silicates, it is also a component of most other silicates in the Skidder basalts; therefore, its moderate positive loading in this factor is probably fortuitous.

Factor 4 which accounts for 17.1% of the data variance is characterized by large positive loadings for MgO, Ni and Cr; slight positive loadings for Al_2O_3, LOI, and Ce; and moderate to strong negative loadings for SiO_2, Na_2O, and Y (Table 5-4). Positive intercorrelations between the principal components Cr, Ni and MgO are produced by the

compatibility of Cr, Ni and MgO with early formed minerals from a basaltic magma. The negative loading of Na_2O in this "compatible element" factor, although partly attributable to the incompatibility of Na in early forming minerals from a basaltic magma, is probably related more to the reciprocal nature of chlorite and albite contents in the rocks, that is, Mg-enriched rocks having greater chlorite and therefore lesser albite contents. Chlorite-rich rocks have higher LOI and lower SiO_2 contents than chlorite-poor rocks thereby explaining the positive loading for LOI, and the negative loading for SiO_2 in this factor. Al_2O_3 and Ce are probably fortuitous components.

Factor 5 which accounts for 11.9% of the data variance has large positive loadings for CaO and LOI; a slight positive loading for Sr; a large negative loading for SiO_2; and slight to moderate negative loadings for Al_2O_3, MgO, Zn and Ga (Table 5-4). This factor is interpreted as a "calcite factor". The positive loading for Sr in this factor can be attributed to its substitution for Ca in calcite. Larger amounts of calcite in the rock necessitate lesser amounts of silicate minerals; hence the negative loading for SiO_2, Al_2O_3, and MgO; and the positive loading for LOI in this factor. The negative loadings for Zn and Ga in the factor are not readily explained.

Large positive loadings for Al_2O_3, Fe_2O_3* and V; a moderate positive loading for MgO; and moderate negative loadings for SiO_2, P_2O_5, and Ba characterize Factor 6 which accounts for 10.7% of the data variance (Table 5-4). This factor is not readily interpreted except that a positive correlation between Fe_2O_3 and V can be explained by the incorporation of V into Fe-oxides.

Factor 7, accounting for 6.9% of the data variance, is characterized by a large positive loading for Pb; moderate positive loadings for LOI and Rb; and a large negative loading for Sr (Table 5-4). This factor is interpreted as a "Pb factor". Pb concentrations in the Skidder Basalt are near the detection limit for this element using the XRF analytical method (see Appendix B) and Pb does not correlate strongly, either positively or

negatively, with any of the other elements in the Skidder Basalt analyses. Other components of the factor are probably fortuitous.

A large negative loading for Cu; moderate negative loadings for Ce and Ga; and moderate positive loadings for Al_2O_3, Na_2O, P_2O_5, Sr and Y characterize Factor 8, which accounts for 7.3% of the data variance (Table 5-4). The large negative loading for Cu dominates this factor. Copper is a chalcophile element and does not readily enter silicate minerals but tends to occur in tiny sulphide grains (cf. Krauskopf, 1967); in contrast, aluminum and sodium, which have positive loadings in this factor, are components of silicate minerals. Other components are probably fortuitous.

In summary, two factors are interpreted to be related to magmatic processes; Factor 1, the "incompatible elements factor", and Factor 4, the "compatible elements factor". Two factors are interpreted to be related to specific minerals; Factor 2 the "chlorite factor", and Factor 5 the "calcite factor". Spilitization has masked the positive correlations of the alkalis to other incompatible elements such that potassium and elements that substitute for it form an independent "potassium factor" (Factor 3). Na_2O contributes to the variance of the data mainly through negative loadings in the "chlorite factor" and "compatible elements factor". The remaining factors comprise a possible chalcophile-element vs. lithophile-elements factor, ie. the "negative copper factor" (Factor 8); a possible combined factor comprising Al_2O_3 and Fe-oxide "subfactors" (Factor 6); and an independent factor for lead (Factor 7). None of the factors has a positive loading for SiO_2, its contribution to the variance of the data shown by negative loadings in the "compatible elements", "calcite" and "alumina-Fe-oxide" factors.

5.2.3 Geochemical subdivision

In the discussion below, mafic rocks comprising the Skidder Basalt have been subdivided into low-Zr basalts (≤ 50 ppm), intermediate-Zr basalts (51-85 ppm) and high-Zr basalts (> 85 ppm). The division at 50 ppm is arbitrary, but as shown on Figure 5-1,

the division at 85 ppm is geochemically distinct. The high-Zr samples encircled by the heavy solid line are termed Group 2 throughout the remainder of this chapter. Figure 5-2 shows that with the exception of one sample the Group 2 samples (shown as X's) are offset to higher Y values and like the Zr vs. V plot are separated from the remaining data.

Analyses of Skidder Basalt samples having Zr concentrations ≤ 50 ppm are listed in Tables B-3 and B-4, Appendix B, those having Zr values > 50 ppm but ≤ 85 ppm are shown in Tables B-5 and B-6, Appendix B. Skidder Basalt samples having Zr concentrations greater than 85 ppm but not included in Group 2 are listed in Table B-7, Appendix B; Group 2 samples are listed in Tables B-8 and B-9, Appendix B. Samples from outcrop or drill core are listed separately and they are further broken down into pillowed flows, massive flows or diabase.

The low-Zr basalts occur throughout the Skidder area (Tables B-3 and B-4, Appendix B; Figures 3-3 and 3-4; Figures 6-1 to 6-6), and include variolitic and nonvariolitic pillowed flows, massive flows and diabase dykes. Many of the low-Zr basalts display quench-textured morphologies (Chapter 4). The high-Zr basalts (Tables B-5 to B-7, Appendix B; Figures 3-3 and 3-4; 6-1 to 6-5; and 6-7 to 6-10) comprise intergranular- to intersertal-textured pillowed flows, massive flows and diabase dykes. Group 2 samples include pillowed and massive flows from outcrop and the Skidder area drill core (Tables B-5 to B-7, Appendix B; Figures 3-3; 5-1; 6-1 to 6-3; and 6-6 to 6-9). Group 2 samples from outcrops are included in Unit 3 on Figure 3-4.

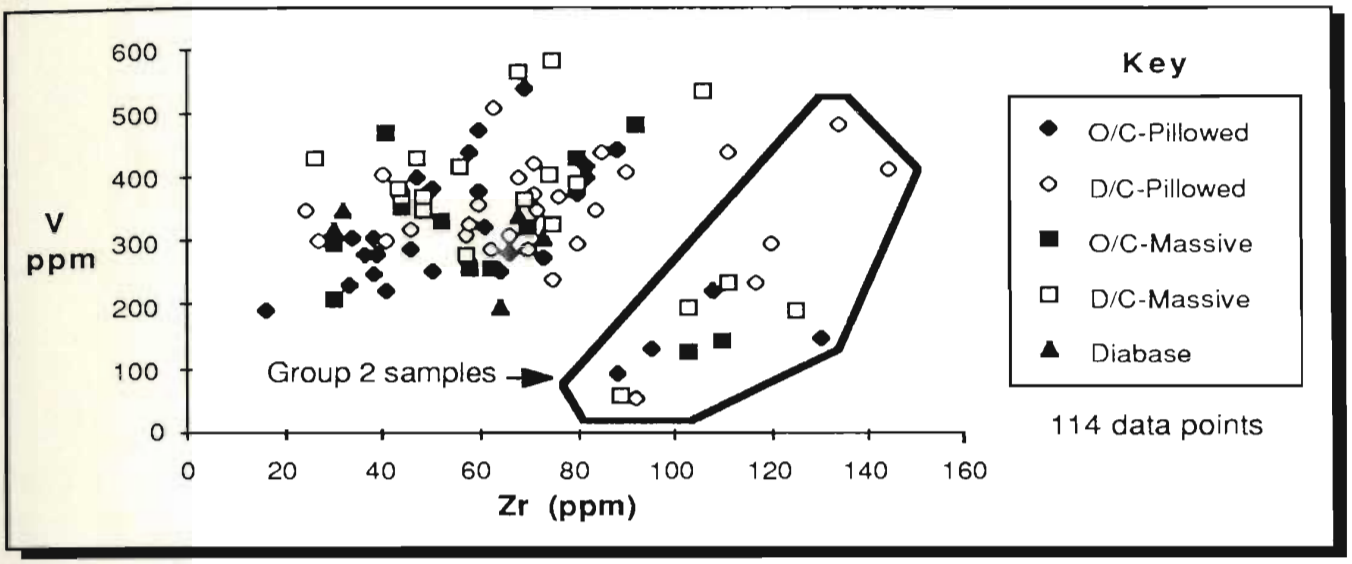

Figure 5-1: Zr vs. V plot showing three possible data groupings. See text for discussion.

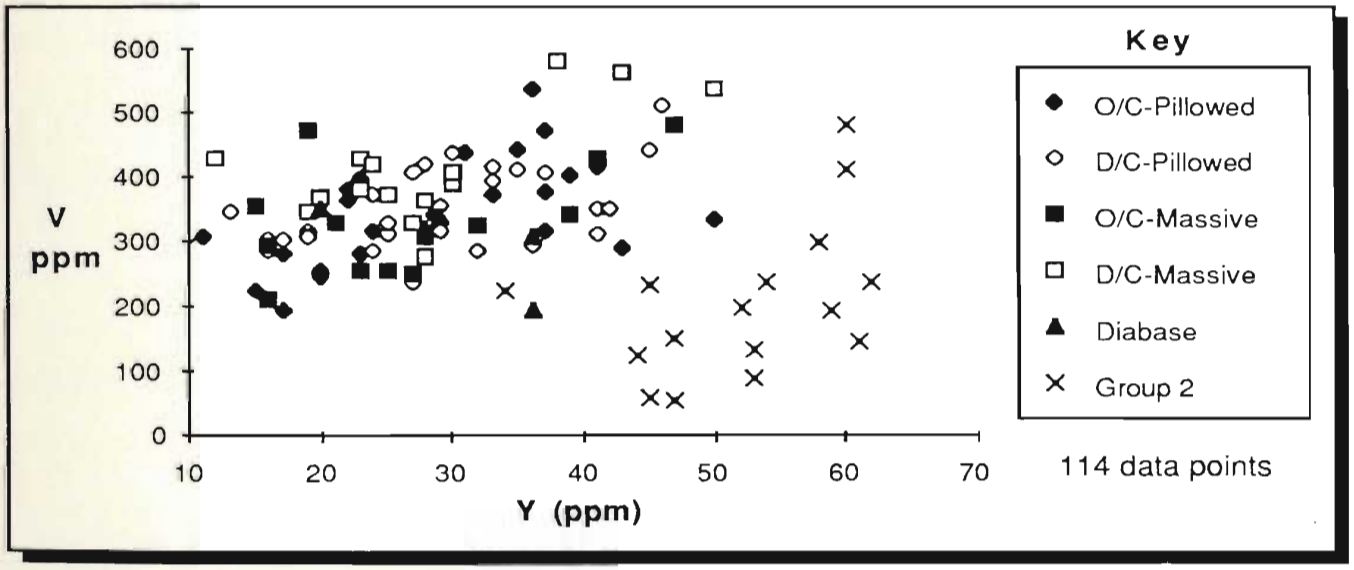

Figure 5-2: Y vs. V plot showing offset of Group 2 samples as per Figure 5-1. See text for discussion.

The mean, standard deviation, and range for the low-Zr, high-Zr and Group 2 samples are listed in Table 5-5. The means for pillowed and massive flows of the low- and high-Zr Skidder Basalts are also shown.

5.2.4 Major oxide and trace element vs. Zr plots

Major oxide or trace element vs. Zr plots and a plot of SiO_2 vs. Y are presented in Figures 5-3 to 5-9. Zr and Y are resistant to hydrothermal alteration, and, as a result of their incompatibility with early formed mafic phases in basaltic magmas, they can be used as differentiation indices (Winchester and Floyd, 1976; Pearce and Norry, 1979; Perfit et al., 1980; Basaltic Volcanism Study Project (BVSP), 1981a). Table 5-6 presents a summary of the characteristics of the various major oxides and trace elements vs. Zr plots shown as Figures 5-1 to 5-9.

SiO_2 remains approximately constant with increasing Zr and Y (Figure 5-3). Moderate scatter above and below the main trend suggests remobilization. Group 2 samples show a reversal in trend on both diagrams whereby SiO_2 decreases with increasing Zr and Y. This may be explained by fractionation of a mineral phase such as zircon with which both Zr and Y are compatible.

TiO_2 increases with increasing Zr as would be expected since both are incompatible with early fractionating mineral phases from basaltic magmas (Figure 5-3). Group 2 samples show more scatter than the others but generally show a decrease in TiO_2 with decreasing Zr. The trend of Group 2 samples on SiO_2 vs. Zr and SiO_2 vs. Y plots (Figure 5-3) suggests that the more "differentiated" of the Group 2 rocks contain lesser Zr and Y. If this is the case the TiO_2 vs. Zr diagram indicates a reduction in TiO_2 with magmatic evolution of the Group 2 samples suggesting fractionation of a phase such as magnetite, which can incorporate Ti into its structure.

Table 5-5: Mean, standard deviation and range for Skidder Basalt outcrop samples, and Skidder Prospect drill core samples that are relatively unaffected by the mineralizing event(s) Key: ∂ - standard deviation, Min - minimum, Max - maximum

	Zr ≤ 50						Zr > 50 ≤ 85						Group 2			
	31 samples				Pillowed	Massive	62 samples				Pillowed	Massive	16 samples			
weight %	Mean	∂	Min	Max	Mean	Mean	Mean	∂	Min	Max	Mean	Mean	Mean	∂	Min	Max
SiO_2	49.52	3.8	42.30	60.90	48.89	50.50	49.31	3.7	38.40	58.80	49.49	48.88	56.03	5.0	46.80	66.30
TiO_2	0.76	0.2	0.48	1.11	0.75	0.78	1.15	0.2	0.48	1.75	1.15	1.15	1.36	0.4	0.49	2.00
Al_2O_3	15.12	1.2	12.20	18.00	15.17	15.05	15.23	1.1	12.90	17.80	15.25	15.18	14.84	1.2	12.60	16.90
Fe_2O_3*	10.05	1.6	6.07	12.75	9.52	10.90	11.04	1.8	7.01	16.16	11.06	10.98	10.58	2.1	6.52	14.80
MnO	0.16	0.0	0.06	0.28	0.16	0.17	0.15	0.0	0.05	0.24	0.15	0.15	0.14	0.0	0.07	0.20
MgO	7.31	2.4	3.14	12.18	7.19	7.51	7.31	2.2	2.78	13.05	7.17	7.65	4.81	1.8	1.55	8.21
CaO	6.70	3.6	0.18	14.17	7.55	5.34	5.63	3.0	1.03	16.20	5.33	6.36	2.52	0.7	1.56	4.35
Na_2O	4.73	1.0	3.06	6.54	4.79	4.63	4.90	0.9	2.26	6.95	5.05	4.52	5.70	0.5	4.99	6.78
K_2O	0.19	0.2	0.02	0.71	0.14	0.27	0.17	0.2	0.00	0.63	0.17	0.17	0.15	0.1	0.02	0.40
P_2O_5	0.10	0.1	0.01	0.56	0.10	0.10	0.15	0.1	0.04	0.36	0.16	0.14	0.35	0.2	0.07	0.86
LOI	4.90	2.4	1.84	11.80	5.15	4.50	4.59	2.5	1.48	13.34	4.58	4.62	2.82	1.0	0.62	4.61
Total	99.55		98.36	100.84	99.43	99.76	99.63		97.75	100.85	99.56	99.80	99.30		98.26	100.53
ppm	* Total iron as Fe_2O_3															
Pb*	3	3.1	0	12	3	3	3	2.7	0	11	3	4	4	3.2	0	10
Rb*	3	2.7	0	7	2	3	2	2.8	0	15	2	2	1	1.3	0	4
Sr	93	68.5	20	347	105	72	87	42.7	12	248	81	102	50	24.8	30	118
Y	20	6.2	11	43	20	20	31	6.9	19	50	31	31	52	7.9	34	62
Zr	39	8.6	16	50	39	39	69	7.8	52	85	70	67	112	16.5	88	144
Nb**	3	1.4	1	6	3	4	5	1.5	2	9	6	5	6	1.6	3	9
Zn	84	45.7	23	258	71	104	79	24.5	36	150	79	81	97	31.9	29	148
Cu	51	34.6	0	131	47	56	41	26.6	1	121	40	45	14	15.4	0	61
Ni	67	66.0	0	331	68	65	50	38.3	0	151	48	55	7	13.4	0	49
Ba	35	46.6	0	159	31	43	26	44.9	0	316	21	39	30	34.2	0	109
V	319	67.9	190	468	295	358	353	77.0	193	579	354	351	203	116.9	54	479
Ce	46	20.7	6	84	41	54	67	31.6	17	153	66	70	83	25.0	33	116
Cr	183	153.5	15	549	201	154	162	131.9	0	497	164	156	34	50.1	0	172
Ga	14	2.6	8	18	14	15	16	3.3	10	28	16	17	19	2.8	13	23

* Pb and Rb concentrations in the Skidder Basalt are very low, close to the detection limit of X-ray fluorescence spectrometry, the analytical method used (Appendix B).

** Close to detection limit of the X-ray fluorescence spectrometry method

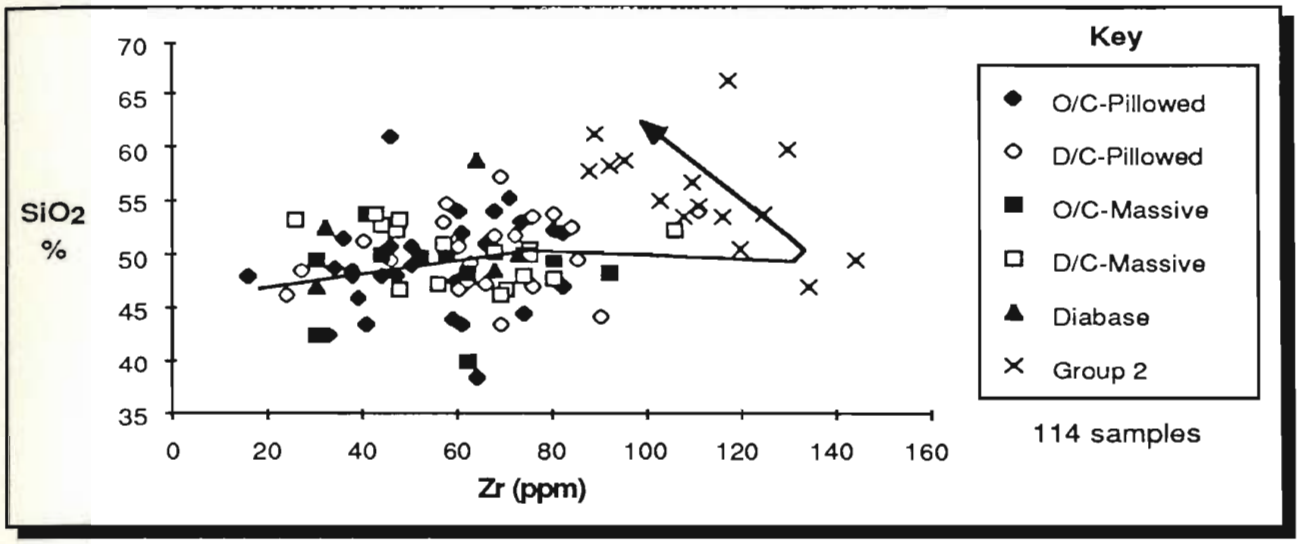

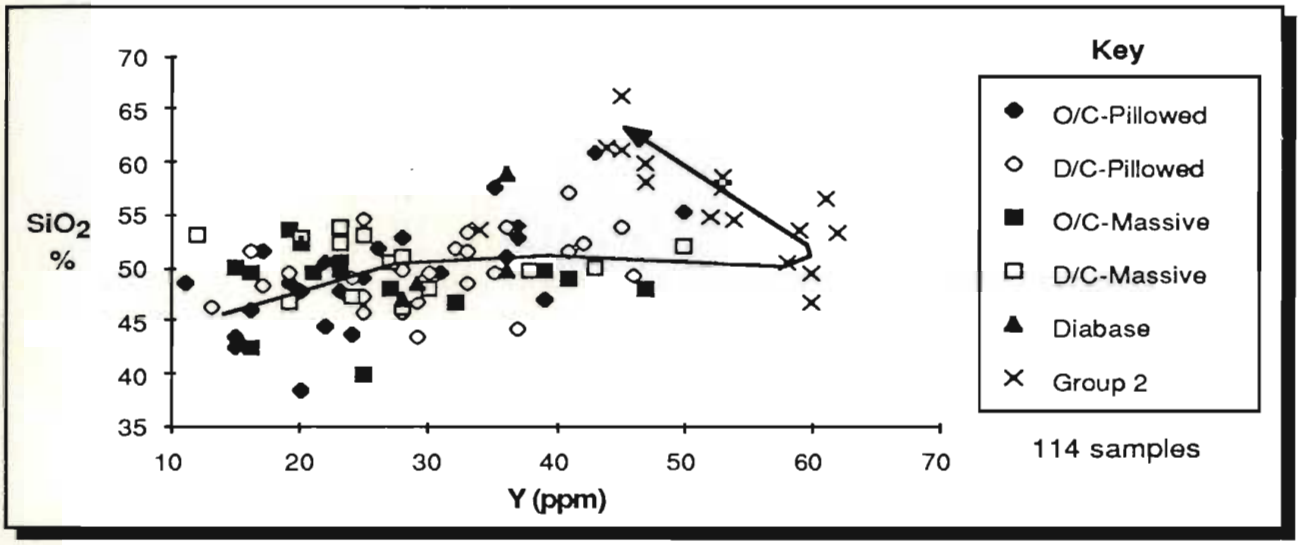

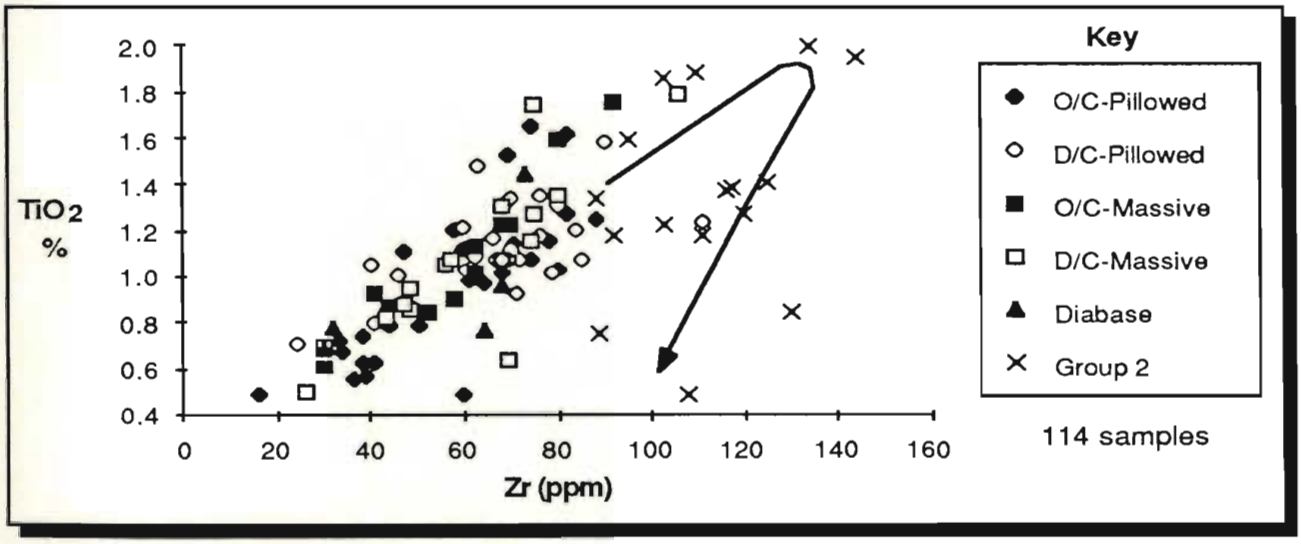

Figure 5-3: Scattergrams of SiO_2 vs. Zr and Y, and TiO_2 vs. Zr for the Skidder Basalt. Arrows indicate suggested "differentiation" trends, note reversal in trend for the Group 2 samples; see text for discussion.

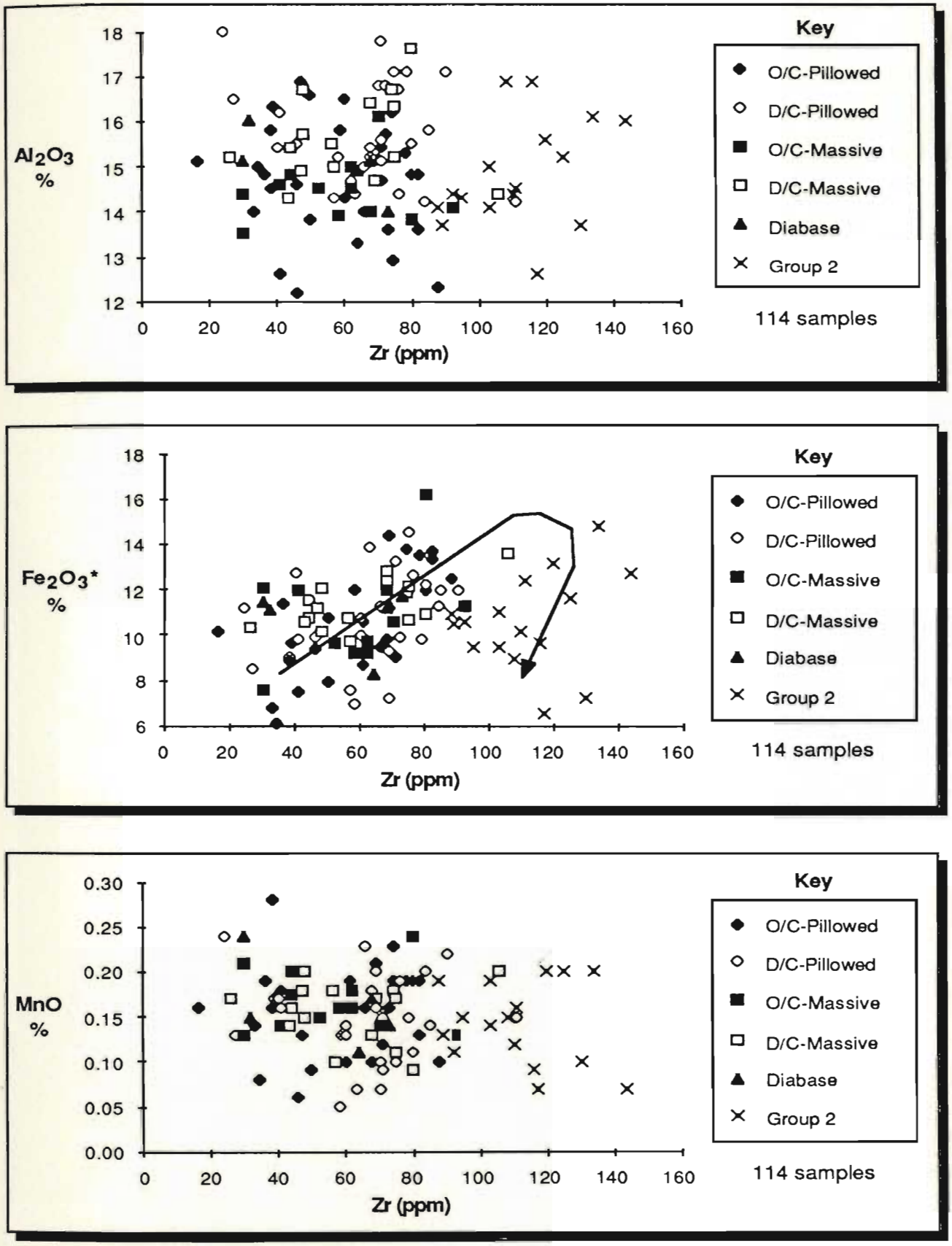

Figure 5-4: Scattergrams of Al_2O_3, Fe_2O_3 and MnO vs. Zr for the Skidder Basalt. Arrow indicates suggested "differentiation" trend. Fe_2O_3* - total iron as Fe_2O_3.

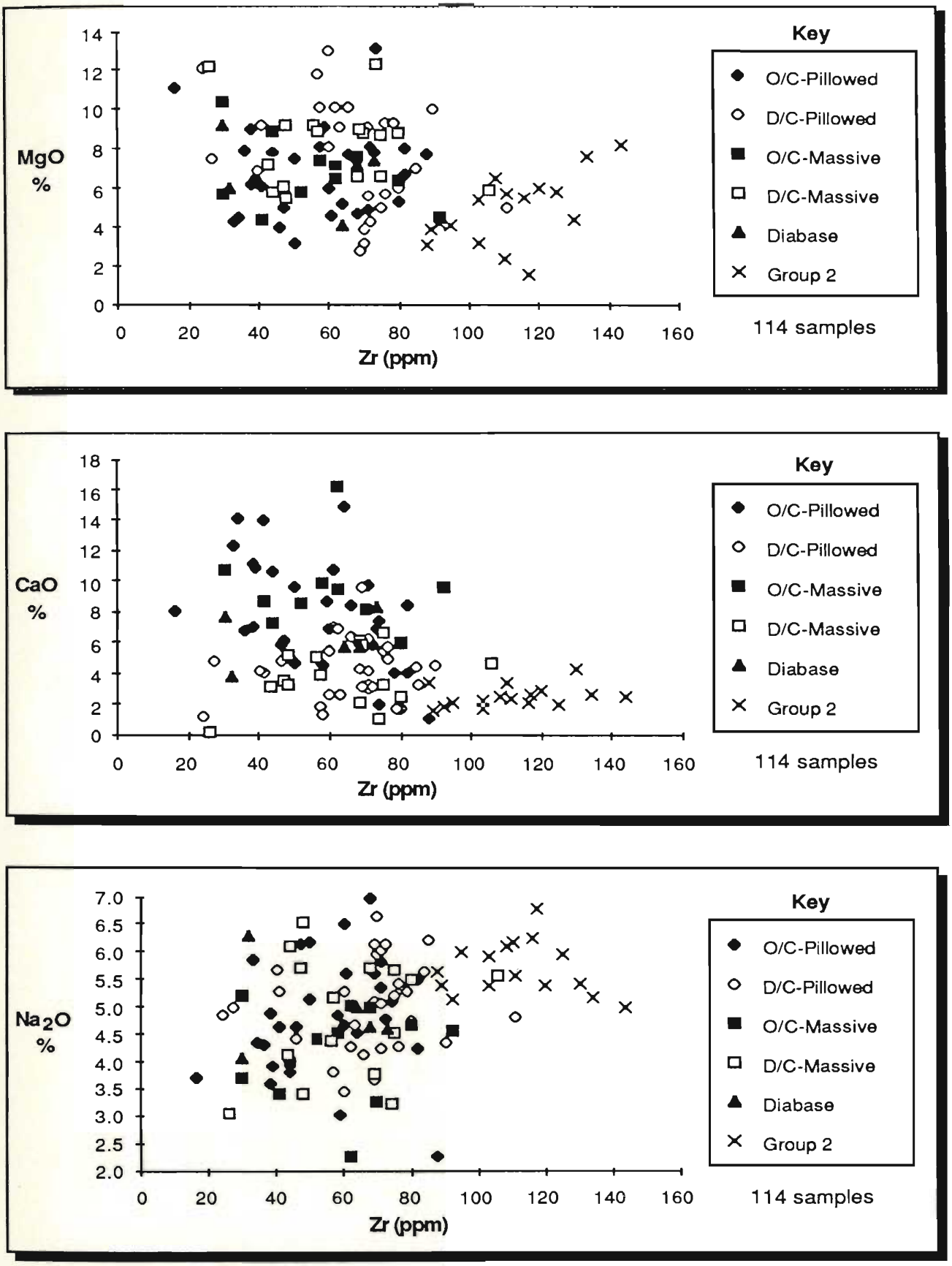

Figure 5-5: Scattergrams of MgO, CaO and Na_2O vs. Zr for the Skidder Basalt.

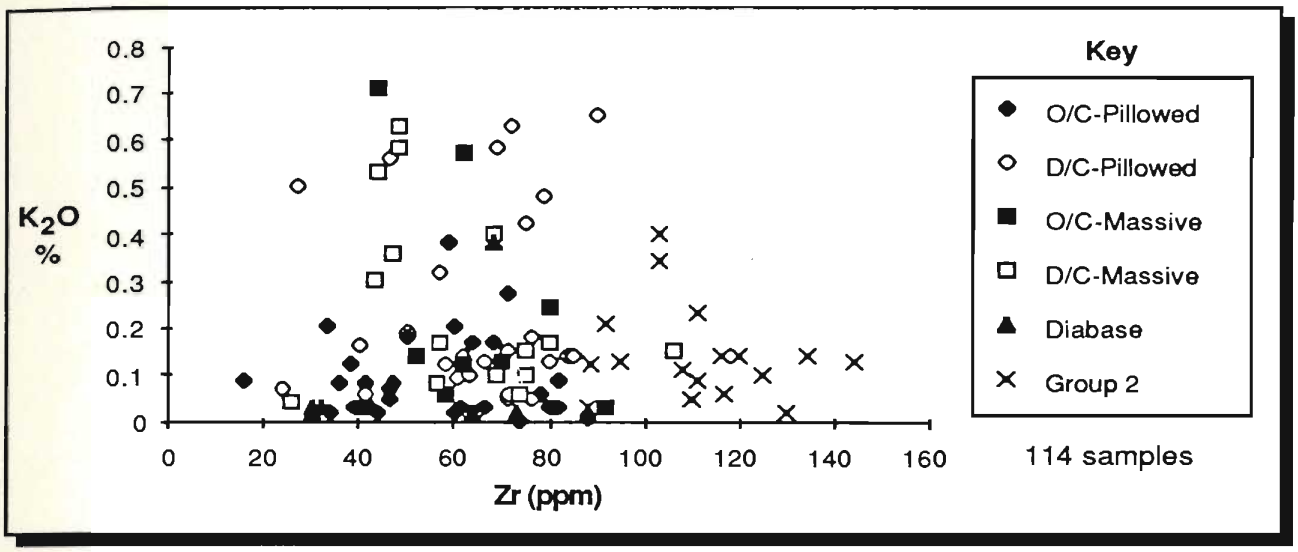

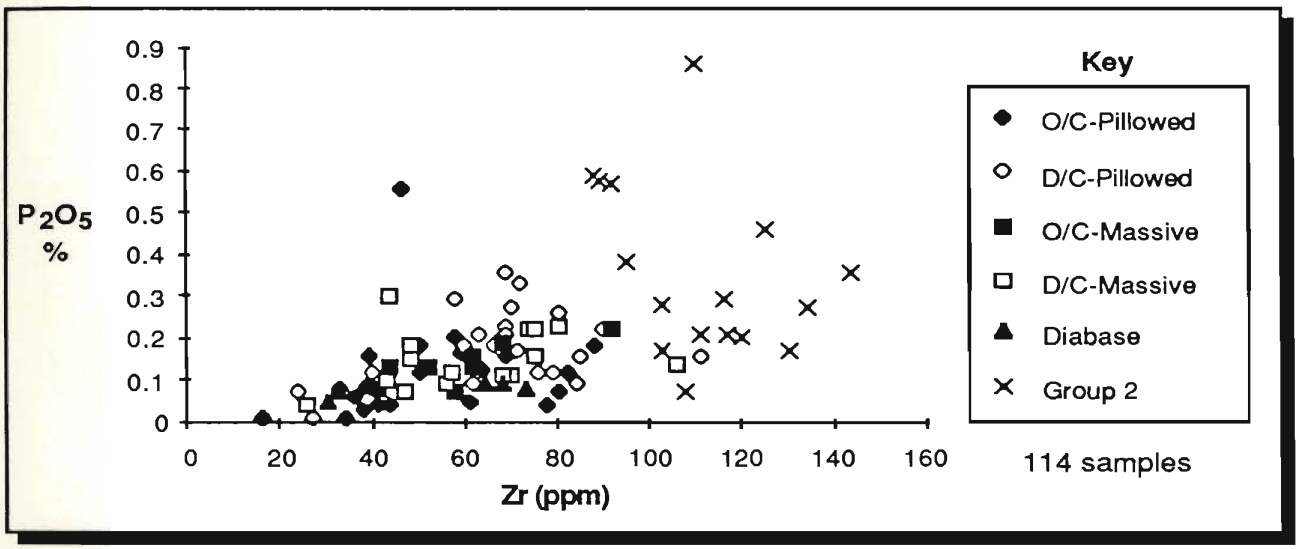

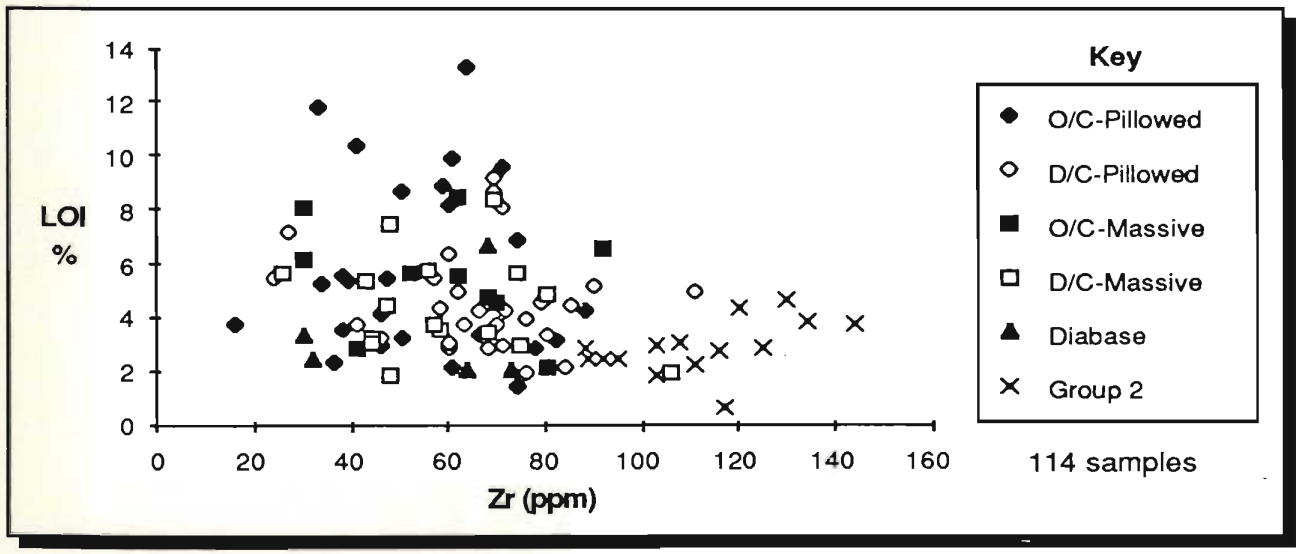

Figure 5-6: Scattergrams of K_2O, P_2O_5 and LOI vs. Zr for the Skidder Basalt.

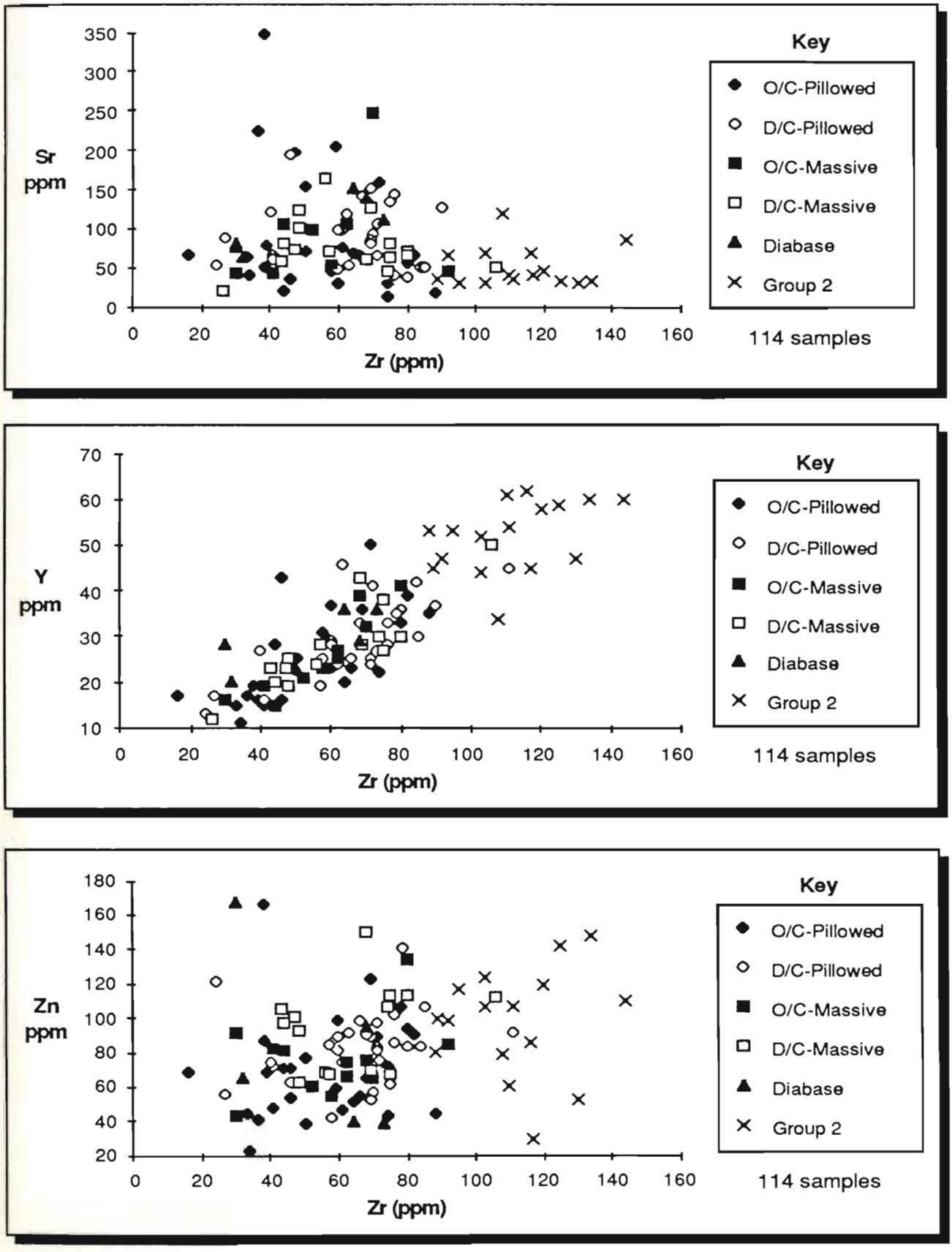

Figure 5-7: Scattergrams of Sr, Y and Zn vs. Zr for the Skidder Basalt.

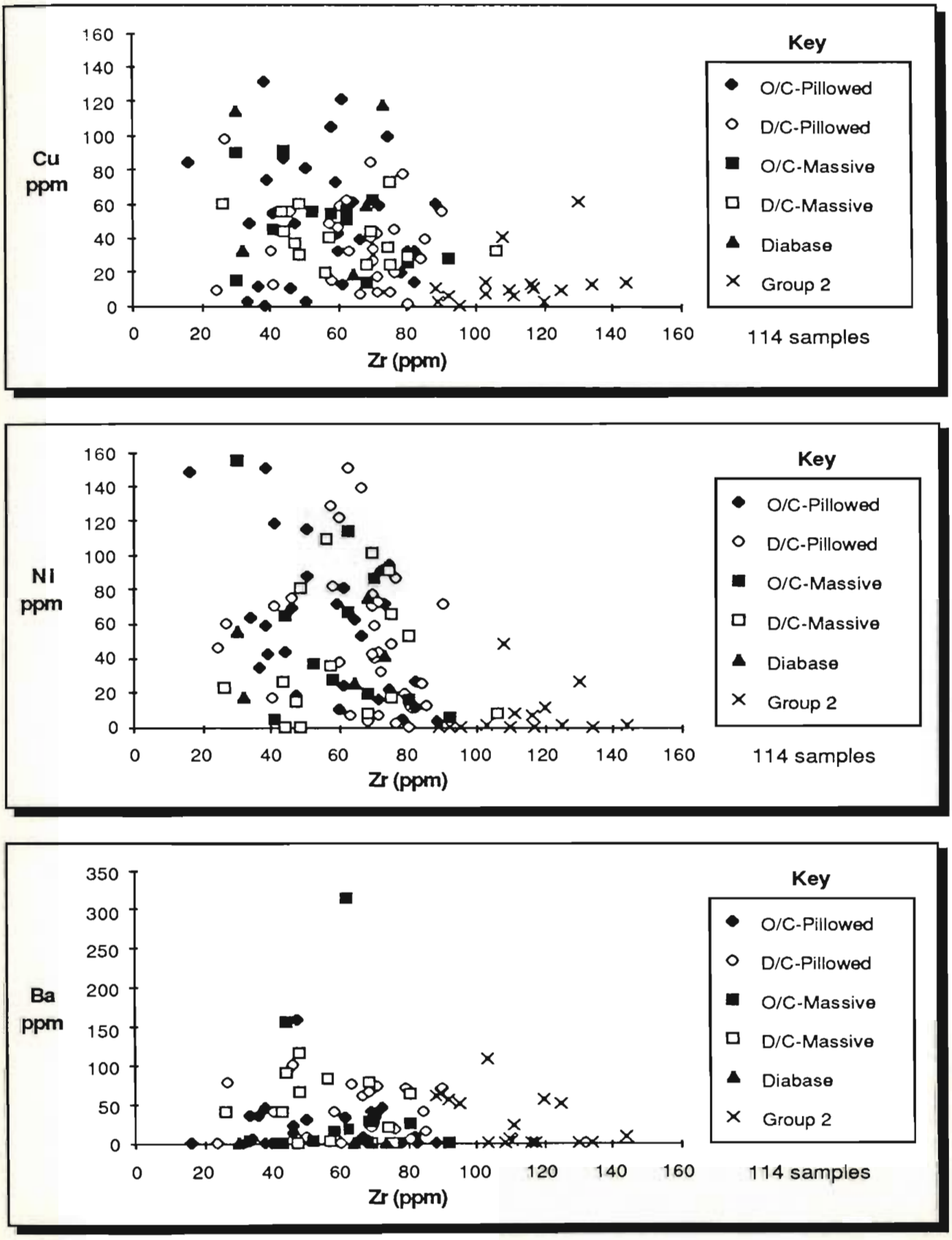

Figure 5-8: Scattergrams of Cu, Ni and Ba vs. Zr for the Skidder Basalt.

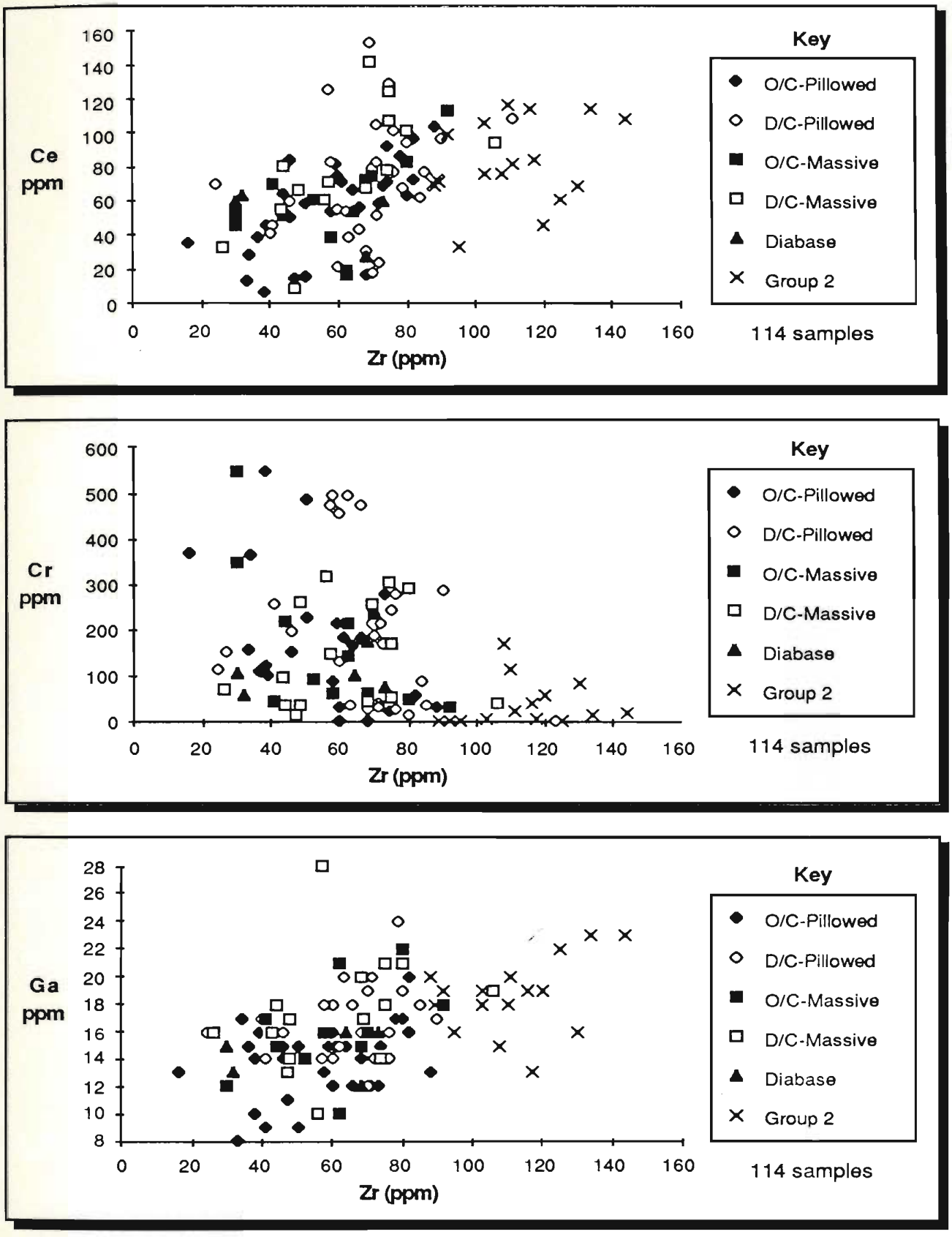

Figure 5-9: Scattergrams of Ce, Cr and Ga vs. Zr for the Skidder Basalt.

Table 5-6: Characteristics of major and trace element versus Zr plots

		Behaviour with increasing Zr		
	Degree of scatter	Mafic rocks other than Group 2	Group 2	Comments
SiO_2	moderate	constant	decreases	
TiO_2	slight/moderate	increases	increases	
Al_2O_3	extreme	?	?	
$Fe_2O_3^*$	moderate	increases	increases	Group 2 shows parallel but offset trend
MnO	moderate/extreme	decreases to Zr=50 ppm then increases to Zr=85 ppm	decreases	
MgO	extreme	decreases	increases	Scatter above and below "main" trend probably alteration related
CaO	moderate/extreme	decreases	constant	Note separation between outcrop and drill core samples
Na_2O	extreme	increases	increases to Zr=115 ppm then decreases	
K_2O	extreme	?	decreases	
P_2O_5	moderate	increases	?	
LOI	moderate/extreme	decreases	slight increase	
Pb	extreme	?	?	
Rb	extreme	?	?	
Sr	extreme	?	constant	
Y	slight	increases	increases	
Nb	moderate	increases	increases	
Zn	moderate/extreme	increases	?	
Cu	extreme	decreases	constant	
Ni	moderate/extreme	decreases	constant	
Ba	extreme			
V	moderate	increases	increases	Note possible two groupings with parallel but offset trends
Ce	moderate	increases	?	
Cr	moderate/extreme	decreases	?	
Ga	moderate	increases	increases	

Fractionation of magnetite from the magma that produced the Group 2 samples is supported by V vs. Zr and V vs. Y plots shown on Figures 5-1 and 5-2. The low- and high-Zr basalts display considerable point scatter but V shows an overall increase with increasing Zr and Y. Group 2 samples show a parallel but offset trend of decreasing V with decreasing Zr suggestive of a fractionating mineral phase such as magnetite and/or clinopyroxene from the magma(s) which produced the rocks (Shervais, 1982).

Fe_2O_3* shows moderate scatter but an overall increase with increasing Zr (Figure 5-4). The parallel but offset trend of decreasing Fe_2O_3*with decreasing Zr shown by the Group 2 samples supports fractionation of magnetite as suggested above.

A sigmoidal distribution is shown by the data on the plot of MnO vs. Zr (Figure 5-4). MnO decreases with increasing Zr at Zr values below approximately 50 ppm, increases with Zr from Zr concentrations of 50-85 ppm, and shows a decrease with increasing Zr for Group 2 samples.

Moderate to extreme scattering of points above and below the "main trend" of decreasing MgO with increasing Zr (Figure 5-5) suggests that alteration has resulted in addition of MgO to some of the rocks but removal from others. The trend of decreasing MgO with decreasing Zr shown by the Group 2 samples supports the reversal in trends suggested above for these samples.

CaO shows moderate to extreme scatter on Figure 5-5 but does show an overall decrease with increasing Zr. The greater amount of CaO in outcrop samples relative to drill core samples is evident on this diagram. Group 2 samples have consistently lower CaO values.

Na_2O shows extreme scatter on Figure 5-5 suggesting some redistribution in addition to the overall addition of Na expected as a result of spilitization. Despite modifications as a result of alteration, an overall increase with increasing Zr is indicated.

P_2O_5 shows slight to moderate scatter and overall increase with increasing Zr (Figure 5-6). The high P_2O_5 content of some Group 2 samples suggests apatite was a

fractionating phase and that some of the samples may be sampling cumulative apatite from within the magma. The very low P_2O_5 content of other Group 2 samples suggests that these samples are sampling a magma from which a phosphorus-bearing phase such as apatite has fractionated.

Y shows slight to moderate scatter on Figure 5-7 and increases in concentration with increasing Zr in the low- and high-Zr basalts, and the Group 2 samples.

Zn, Ce and Ga show moderate to extreme point scatter but show an overall increase in concentration with increasing Zr, suggestive of their being incompatible with early fractionating phases (Figures 5-7 and 5-9). Zn and Ce in Group 2 samples show a large variation and no clearly defined trend with increasing Zr concentration but Ga shows a parallel but offset trend of decreasing Ga with decreasing Zr.

Cu, Ni and Cr show moderate to extreme scatter on Figures 5-8 and 5-9 but show an overall trend of lower concentrations with increasing Zr concentration.

Other major oxides and trace elements, and loss on ignition (LOI) show extreme scatter and no consistent trends with increasing Zr.

5.2.5 Spilitization

As indicated in Chapter 4, the Skidder Basalt rocks have a mineralogy characteristic of spilites (cf. Amstutz, 1974). Secondary minerals present in the Skidder Basalt (outside the Skidder prospect alteration zone) are calcite, epidote, actinolite, albite, chlorite, and minor quartz and hematite. Mottl (1983a) suggested this mineral assemblage to be characteristic of hydrothermal alteration under relatively low water to rock ratios (less than 30) (Figure 5-10). According to experimental results summarized by Rosenbauer and Bischoff (1983) the effects of seawater interaction with rocks under low water to rock ratios should be an overall increase in Mg and probably Na, an overall decrease in Ca and K and redistribution of Si, Fe, Mn, and Zn.

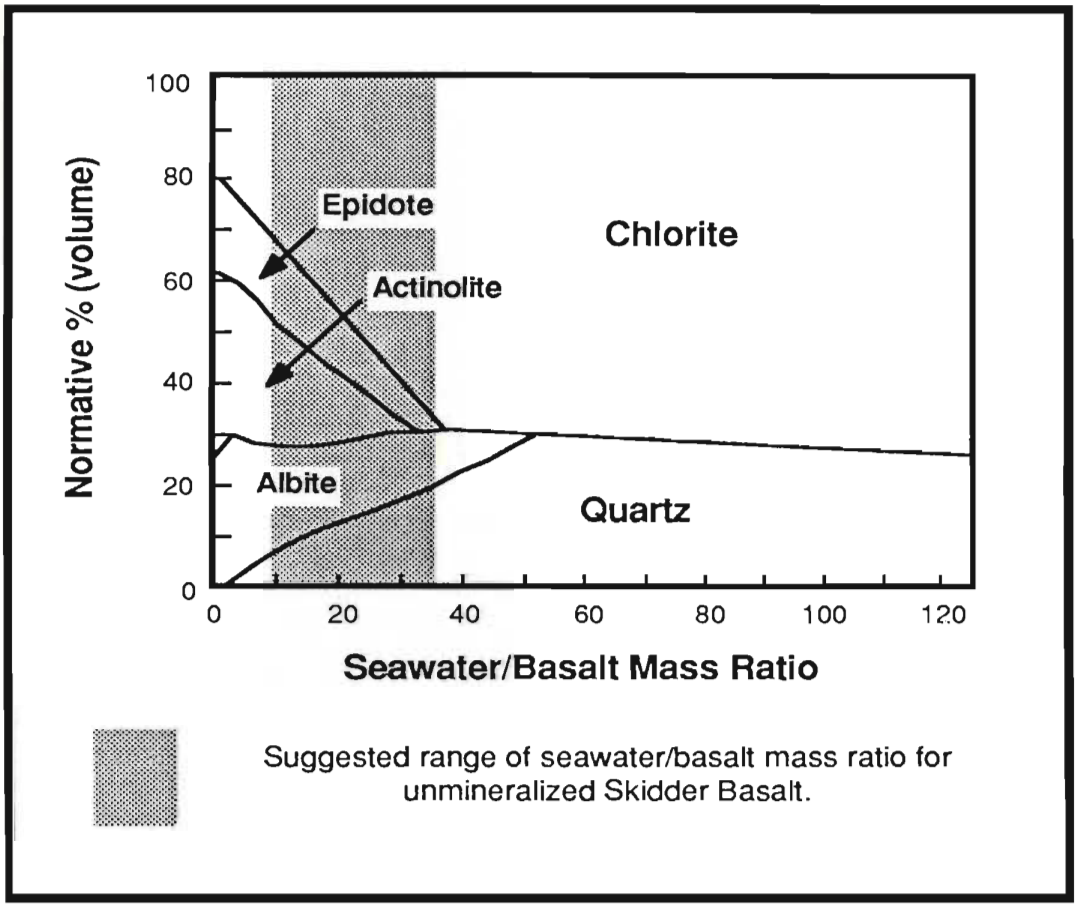

Figure 5-10: Diagram after Mottl (1983a) showing secondary mineral assemblages characteristic of various seawater/basalt ratios.

Redistribution of Si and Fe in the Skidder Basalt from spilitization is supported by the range of SiO_2 and total iron as Fe_2O_3 values at a given Zr concentration shown on the element vs. Zr plots (Figures 5-3 and 5-4; Table 5-5). Moderate scatter of points above and below the "main trend" on the diagrams suggests addition of silica and/or iron to some samples but removal from others.

Table 5-7 compares the mean composition of the Skidder Basalt with that of average ocean floor basalts, the Annieopsquotch Complex, average island arc basalts and basalts of the Buchans Group. Redistribution rather than an overall addition or removal of Si and Fe is further supported by the similarity of the average contents of SiO_2 and total iron as Fe_2O_3 in the Skidder Basalt when compared to relatively unaltered ocean floor and island arc basalts (Table 5-7). The average content of MgO is lower in the Skidder Basalt than in average ocean floor and some island arc basalts but the average Na_2O content of the Skidder Basalt is considerably higher than the others (Table 5-7). This indicates that alteration has resulted in an overall addition of Na_2O to and probably some removal of MgO from the Skidder basalts. The extreme scatter shown by MgO and Na_2O on Figure 5-5 suggests that the amount of removal/addition of these elements was independent of the original, unaltered composition of the rocks. The average content of K_2O in the Skidder Basalt is less than average unaltered ocean floor and island arc basalts (Table 5-7) indicating probable depletion in the Skidder Basalt as a result of alteration. Average CaO content of the Skidder Basalt is also less than the others. Calcium removed from feldspars as a result of albitization may have been redeposited as calcite in veins. Thus, although the low Ca contents of the Skidder Basalt may be due to alteration it may also be partially a result of sampling bias since samples rich in calcite were not analyzed and calcite veins were removed from the samples that were analyzed.

Table 5-7: Comparison of averages of major element components of the Skidder Basalt to those of ocean floor basalts, island arc basalts, the Annieopsquotch Ophiolite and the Sandy Lake Formation basalts of the Buchans Group

	Ocean Floor Basalts			Annieopsquotch Ophiolite		Skidder Basalt	Island Arc Basalts				Buchans Group Basalts	
weight %	1a	1b	2	3a	3b		4	5a	5b	6	7a	7b
SiO_2	50.53	50.93	49.56	49.28	50.69	50.39	51.90	50.73	50.63	52.00	48.80	46.60
TiO_2	1.56	1.19	1.42	1.24	1.35	1.09	0.80	0.83	0.86	0.83	0.83	0.87
Al_2O_3	15.27	15.15	16.09	14.92	14.94	15.11	16.00	17.38	18.16	17.30	15.47	16.81
FeO	10.46*	10.32*	10.17*	8.20	8.09	-	9.56*	6.96	7.79	7.53	-	-
Fe_2O_3	-	-	-	2.70	2.56	10.76**	-	3.01	3.29	-	8.63**	11.54**
MnO	-	-	-	0.20	0.26	0.15	0.17	0.19	0.19	0.19	0.14	0.13
MgO	7.47	7.69	7.69	7.56	7.14	6.93	6.77	6.97	5.61	7.39	5.80	6.72
CaO	11.49	11.84	11.34	11.05	7.14	5.43	11.80	11.51	11.15	11.70	9.90	6.27
Na_2O	2.62	2.32	2.80	2.36	3.99	4.94	2.42	2.06	1.96	2.26	3.00	1.82
K_2O	0.16	0.14	0.24	0.09	0.06	0.17	0.44	0.26	0.27	0.42	0.97	1.40
P_2O_5	0.13	0.10	-	0.10	0.12	0.17	0.11	0.09	0.10	0.13	-	-
				N = 42	N = 7	N =114		N = 43	N = 89	N =12	N = 5	N = 8

* Total iron as FeO

** Total iron as Fe_2O_3

N - Number of samples

1. Melson et al. (1976): Average basaltic glass; a) Atlantic, Pacific and Indian Ocean spreading centers, b) Indian Ocean spreading center
2. Pearce (1976): Average ocean floor basalt
3. Dunning (1984): Annieopsquotch Ophiolite a) average of sheeted dykes b) average of lavas
4. Jakes and White (1972): Average island arc tholeiite
5. Ewart (1982): Average basalts of low-K orogenic volcanic rocks a) southwestern Pacific b) northwestern Pacific
6. Basaltic Volcanism study Project (1981b): Average New Britain island arc basalts
7. Thurlow (1981a): Buchans Group, Sandy Lake Formation (Thurlow and Swanson, 1987): a) mafic flows b) mafic pyroclastic rocks

The chemical effects of spilitization on the alkalies are illustrated on Figure 5-11. Hughes (1973) showed that, on this diagram, unaltered igneous rocks plot in a field which he termed the "igneous spectrum". The Skidder basalt rocks plot outside the igneous spectrum, close to the spilite field, indicative of enrichment of Na_2O relative to K_2O in the rocks (Figure 5-11).

Goff (1984) used a ternary plot of MgO, SiO_2 and CaO/Al_2O_3 in an effort to define the mobility of Mg, Si and Ca during alteration. He outlined fields for unaltered basalts, and unaltered intermediate and felsic volcanic rocks. The Skidder Basalt samples show extreme scatter on this diagram suggesting an overall decrease in Ca and a redistribution of the other elements (Figure 5-12). For comparison, samples of Annieopsquotch Complex dykes (geochemical data presented in Dunning, 1984) occupy a restricted area in the fresh basalts field (Figure 5-12).

The redistribution of SiO_2 and total iron as well as the decrease in potassium as a result of alteration of the Skidder Basalt is supportive of alteration by seawater interaction with the rocks under low water/rock ratios. However, the substantial increase in sodium that has probably occurred as a result of spilitization of the Skidder Basalt is not predicted by experimental results (e.g. Rosenbauer and Bischoff, 1983). Mottl (1983b) uses metamorphic differentiation to explain the discrepancy in the amount of sodium increase predicted by experiments on basalt/seawater interaction and the greater increase noted in altered basalts. He suggests that sodium diffuses away from the "reaction front" under natural conditions, a process not duplicated in the experiments.

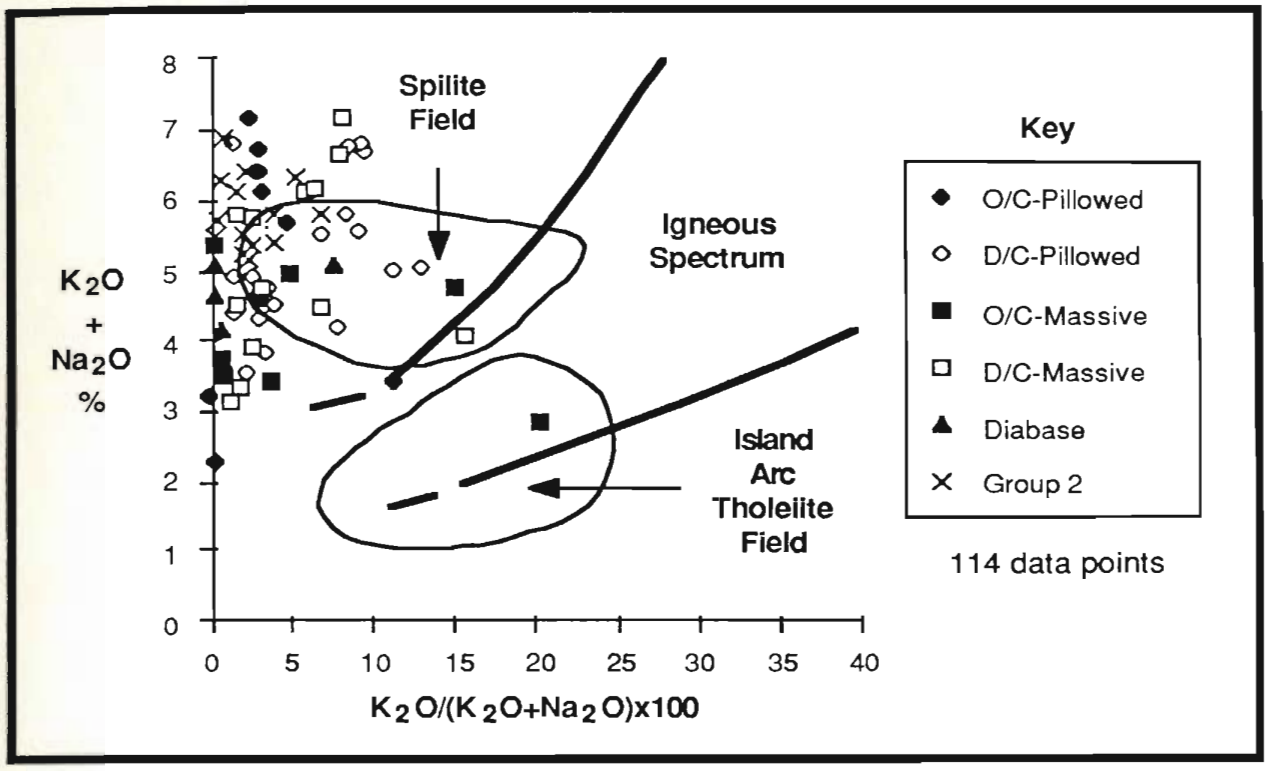

Figure 5-11: Skidder Basalt samples plotted on the "igneous spectrum" diagram of Hughes (1973). Island arc tholeiite field after Stauffer et al. (1975).

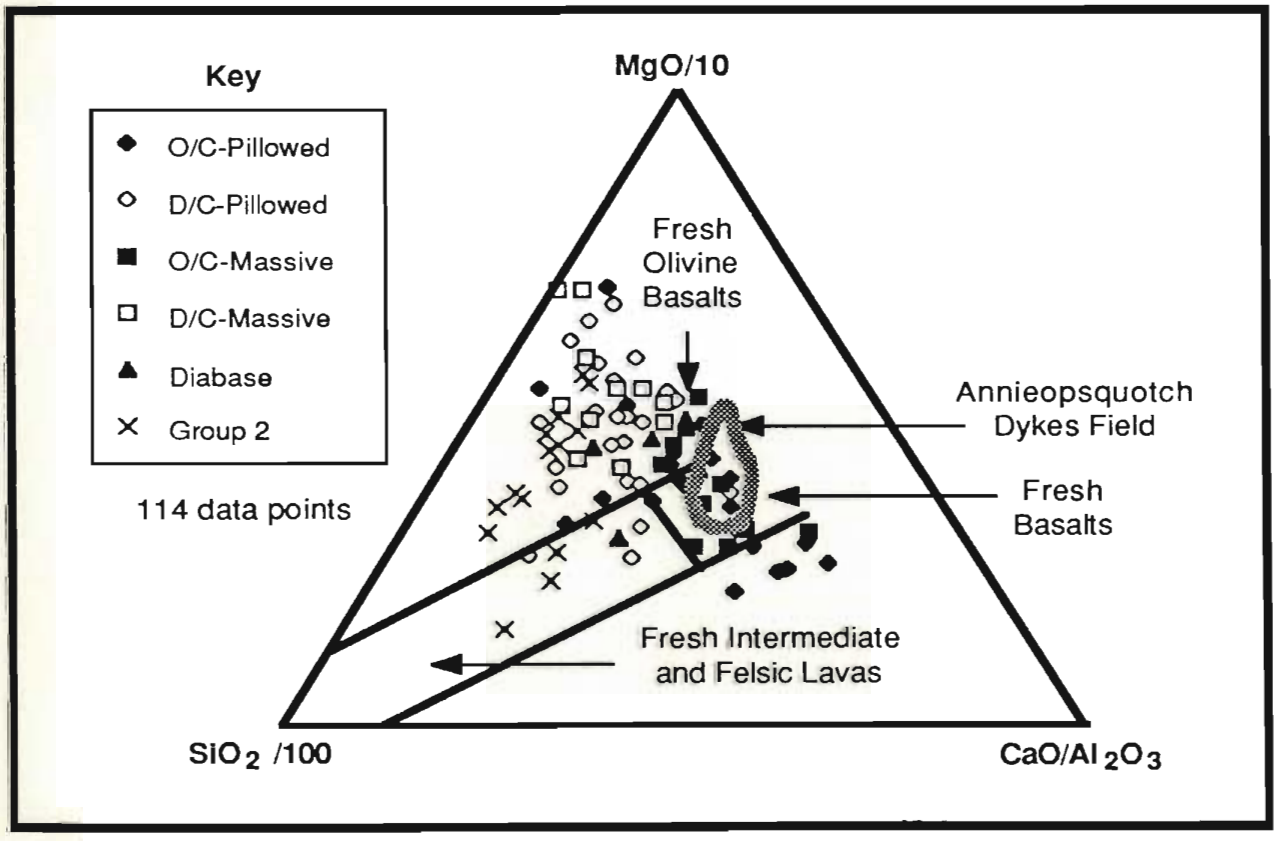

Figure 5-12: Skidder Basalt samples plotted on a ternary diagram after Goff (1984). See text for discussion.

5.2.6 Classification

Winchester and Floyd (1977) defined fields for the common volcanic rocks on a binary plot of Zr/TiO_2 (used as a differentiation index) versus Nb/Y (used as an index of alkalinity) (cf. Pearce and Cann, 1973). The Skidder Basalt rocks are classified as sub-alkaline on this diagram (Figure 5-13) and fall dominantly in the sub-alkaline basalt and basalt/andesite fields. Two of the Group 2 rocks are classified as andesites.

Garcia (1978) slightly modified fields on a Ti versus Zr diagram of Pearce and Cann (1973) used to distinguish rocks of tholeiitic versus calc-alkaline affinity. Tholeiitic magma types show an increase in Ti with differentiation whereas calc-alkaline magmas do not. The Skidder Basalt rocks define a tholeiitic trend on this diagram (Figure 5-14). Skidder Basalt samples containing lesser amounts of Ti and Zr plot dominantly in the overlapping island arc tholeiite/ocean floor basalt field and those with greater amounts of Ti and Zr plot mostly in the ocean floor basalt field.

5.2.7 Tectonic setting

Many authors (e.g. Perfit, et al., 1980; Basaltic Volcanism Study Project (BVSP), 1981a; 1981b; Pearce, 1982) have noted that mid-ocean ridge basalt suites have higher concentrations of the high field strength (HFS) cations Ti, Zr, and Y, and the compatible element Cr, and have much lower contents of the large ion lithophile (LIL) elements such as K, Rb, Ba, and Sr, than do island arc tholeiites. The high relative abundance of the LIL elements and yet low relative abundance of the HFS cations in island arc tholeiites is difficult to explain by magmatic processes since members of both element groups behave as incompatible components and would partition preferentially into early formed melts. The selective removal of the LIL elements from hydrous subducted oceanic crustal rocks by hydrothermal solutions has been suggested as one possible explanation (e.g. Best, 1975; Saunders and Tarney, 1979). Several explanations for the overall lower concentrations of the HFS cations in island arc tholeiites have been put forth; e.g. by dilution of these

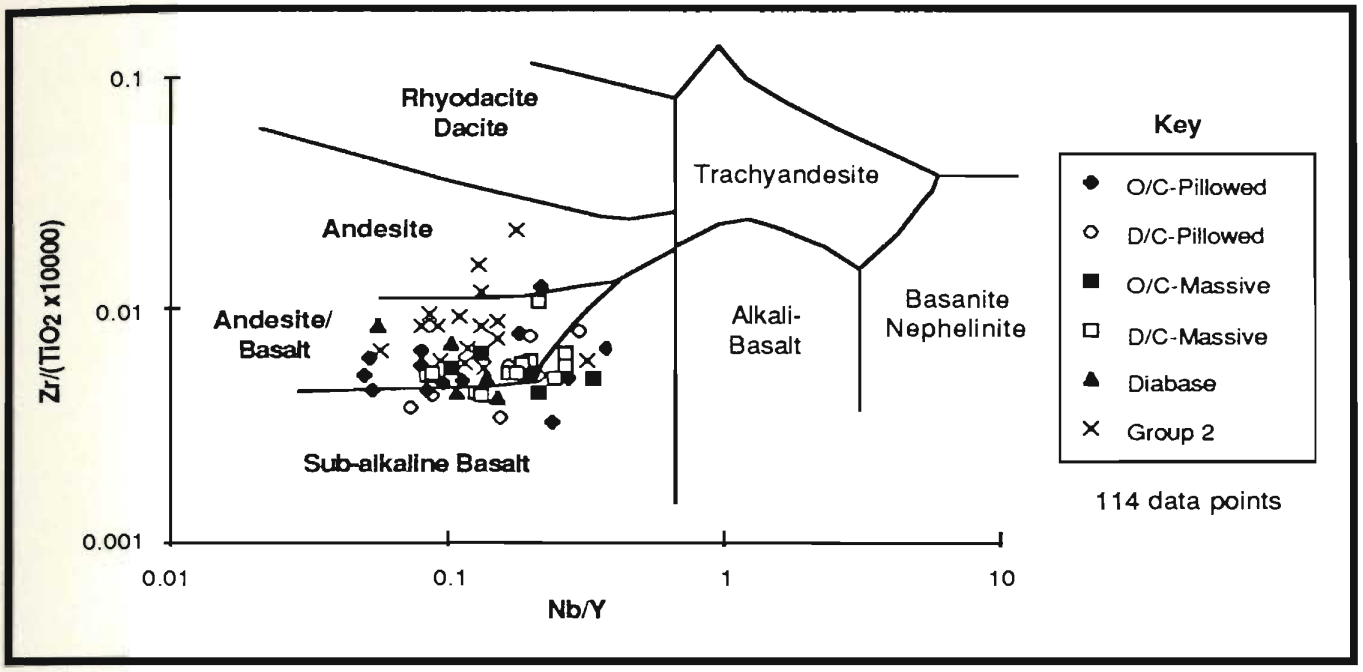

Figure 5-13: Skidder Basalt samples plotted on classification diagram after Winchester and Floyd (1977).

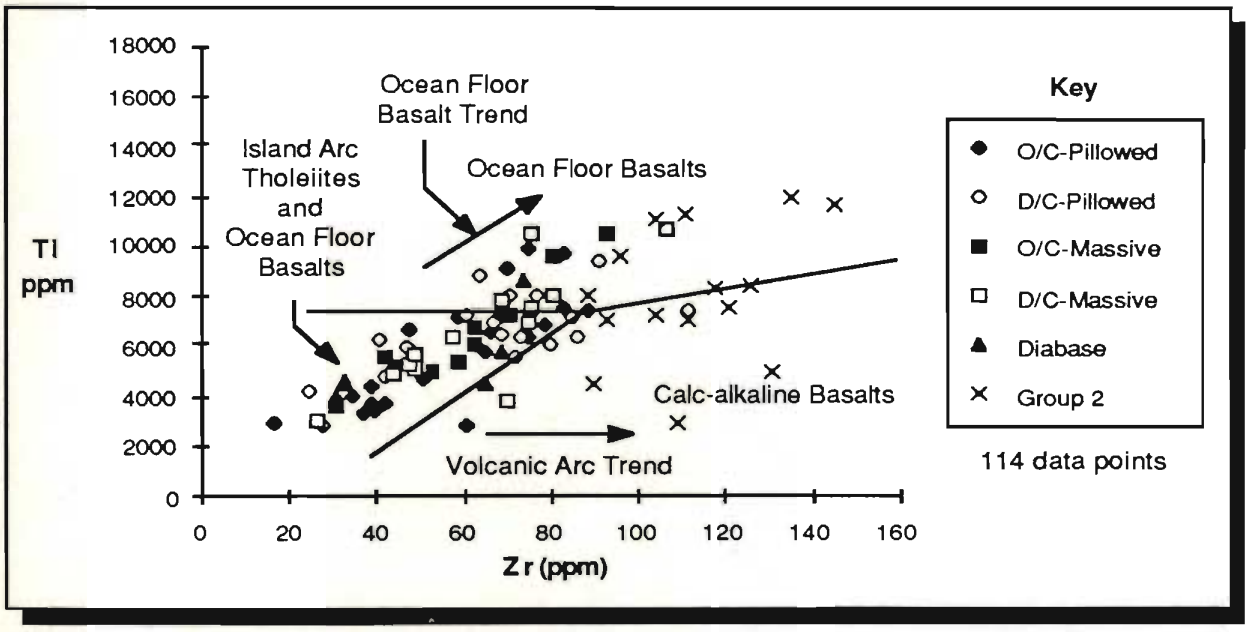

Figure 5-14: Skidder Basalt samples plotted on variation diagram used by Garcia (1978) to discriminate basalts from different tectonic settings.

elements as a result of greater degrees of partial melting (Pearce and Norry, 1979), or by stabilization of mineral phases with which the HFS cations are compatible, for example, stabilization of minor oxide phases as a result of melt generation under higher oxygen fugacity (Dixon and Batiza, 1979). An alternate explanation advanced is that ocean floor tholeiites have been enriched with respect to the HFS elements due to repeated influxes of primitive magma and subsequent magma mixing (O'Hara, 1977).

The average contents of large ion lithophile elements are lower in the Skidder Basalt rocks relative to island arc tholeiites and Buchans Group basalts and are comparable to those of average ocean floor basalts and the Annieopsquotch Ophiolite (Table 5-8). The LIL elements are used as indicators of tectonic setting here with caution since hydrothermal alteration has affected the contents of these elements in the Skidder Basalt. Basaltic Volcanism Study Project authors (BVSP, 1981a) suggest that Sr abundances of less than 200 ppm separate ocean floor tholeiitic rocks from tholeiites of other tectonic regimes. The average concentration of Sr (82 ppm) for the Skidder Basalt is approximately equal to that of the dykes and lavas of the Annieopsquotch Ophiolite and both have significantly lower average concentrations than island arc tholeiites and Buchans Group basalts and are somewhat less than average values for ocean floor basalts. Other elements used to discriminate between ocean floor and island arc tholeiites, e.g. Ti, Zr, Y, Cr, and Ni, have concentrations, in the Skidder Basalt, intermediate between the two types (Table 5-8). However, the average concentration of Y in the Skidder Basalt is only slightly less than the average for ocean floor basalts and the Annieopsquotch Ophiolite but is somewhat higher than average concentrations for island arc tholeiites.

Trace element variation diagrams commonly used to distinguish basalts from different tectonic setting are shown in Figures 5-15 to 5-19. The Skidder Basalt rocks plot dominantly within the ocean floor basalt field and a few in the low potassium tholeiite field on Figures 5-15 and 5-16 after Pearce and Cann (1973). Some samples, including several of the Group 2 samples, plot outside all fields toward the Y apex on Figure 5-15. Several

Table 5-8: Comparison of averages of minor element components of the Skidder Basalt to those of ocean floor basalts, island arc basalts, the Annieopsquotch Ophiolite and the Sandy Lake Formation basalts of the Buchans Group

	Ocean Floor Basalts		Annieopsquotch Ophiolite		Skidder Basalt	Island Arc Basalts				Buchans Group Basalts	
LARGE LOW-VALENCY CATIONS											
ppm	8	9a	3a	3b		9b	5a	5b	6	7a	7b
K	1064	1660	747	498	1411	3570	2159	2241	3487	8052	11622
Rb	1	2	1	1	2	4.7	4.1 (22)*	2.4 (2)	5.7	22	34
Ba	12.2	20	62	50	29	60	90.2 (21)	195 (8)	63.3	410	721
Pb	-	-	2	3	3		4 (18)	5.3 (1)	2.4	25	30
Sr	127	121	95	83	82	231	224 (22)	247 (3)	337.6	256	245
LARGE HIGH-VALENCY CATIONS											
ppm											
Zr	-	90	57	70	68	40	31 (21)	313 (3)	41	72	80
Ti	-	8393	7434	8093	6534	5035	4975	5156	4976	4975	5216
Nb	-	4.6	1	2	5	1.7	1.7 (5)	-	1.6	-	-
Y	-	33	36	42	31	17	16 (21)	17 (1)	17	-	-
FERRO-MAGNESIAN ELEMENTS											
ppm											
Cr	270	251	170	123	146	111	82 (20)	31 (1)	176	243	134
V	250	-	326	352	327	-	286 (20)	240 (1)	254	177	326
Ni	135	90	74	44	47	18	36 (20)	38 (1)	69	48	40
Cu	86	-	30	38	40	-	98 (20)	40 (1)	94	52	66
Zn	85	-	86	143	83	-	78 (21)	-	71	64	90
Ga	17	-	14	14	16	-	-	-	15.2	-	-

* Values in parentheses indicate number of analyses

3. Dunning (1984): Annieopsquotch Ophiolite a) average of sheeted dykes b) average of lavas
5. Ewart (1982): Average basalts of low-K orogenic volcanic rocks a) southwestern Pacific b) northwestern Pacific
6. Basaltic Volcanism study Project (1981 b): Average New Britain island arc basalts
7. Thurlow (1981a): Buchans Group, Sandy Lake Formation (Thurlow and Swanson, 1987): a) mafic flows b) mafic pyroclastic rocks
8. Basaltic Volcanism study Project (1981a): Type 1 oceanic tholeiites
9. Pearce (1982): a) Mid-ocean ridge tholeiites b) tholeiitic volcanic arc basalts

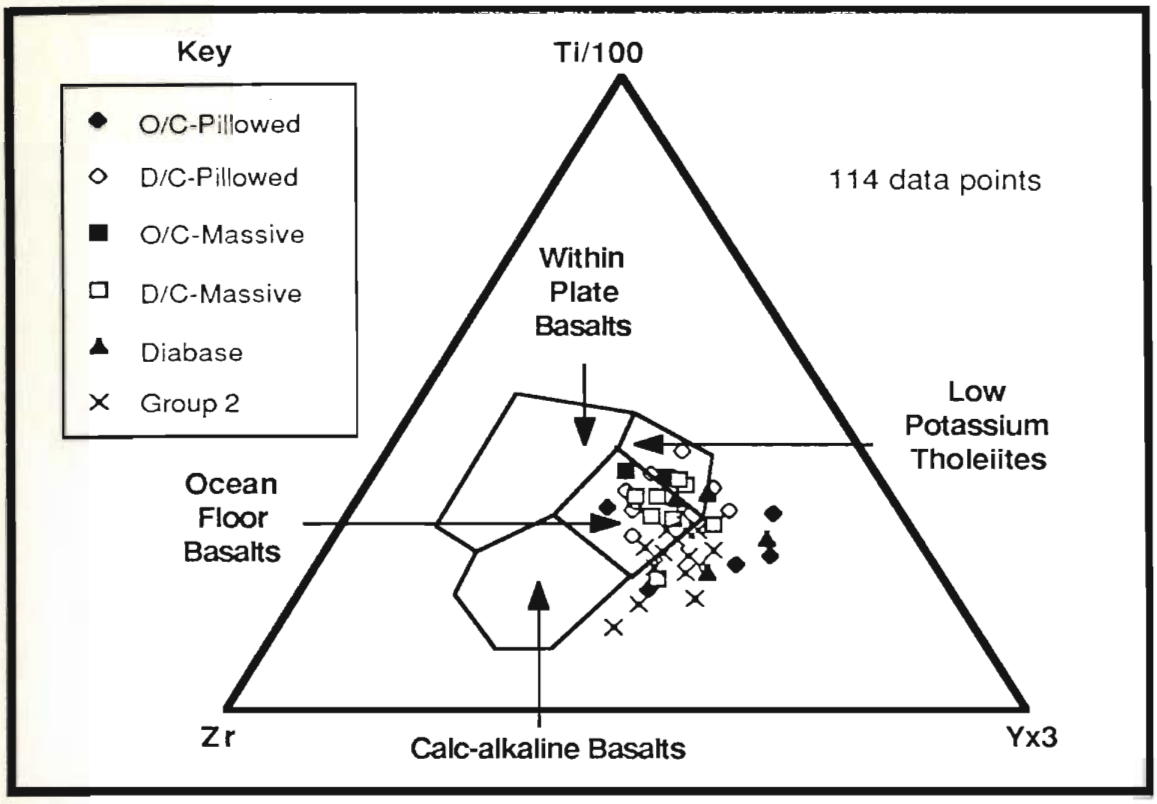

Figure 5-15: Skidder Basalt samples plotted on the Ti-Zr-Y diagram of Pearce and Cann (1973), used by them to discriminate basalts from different tectonic settings.

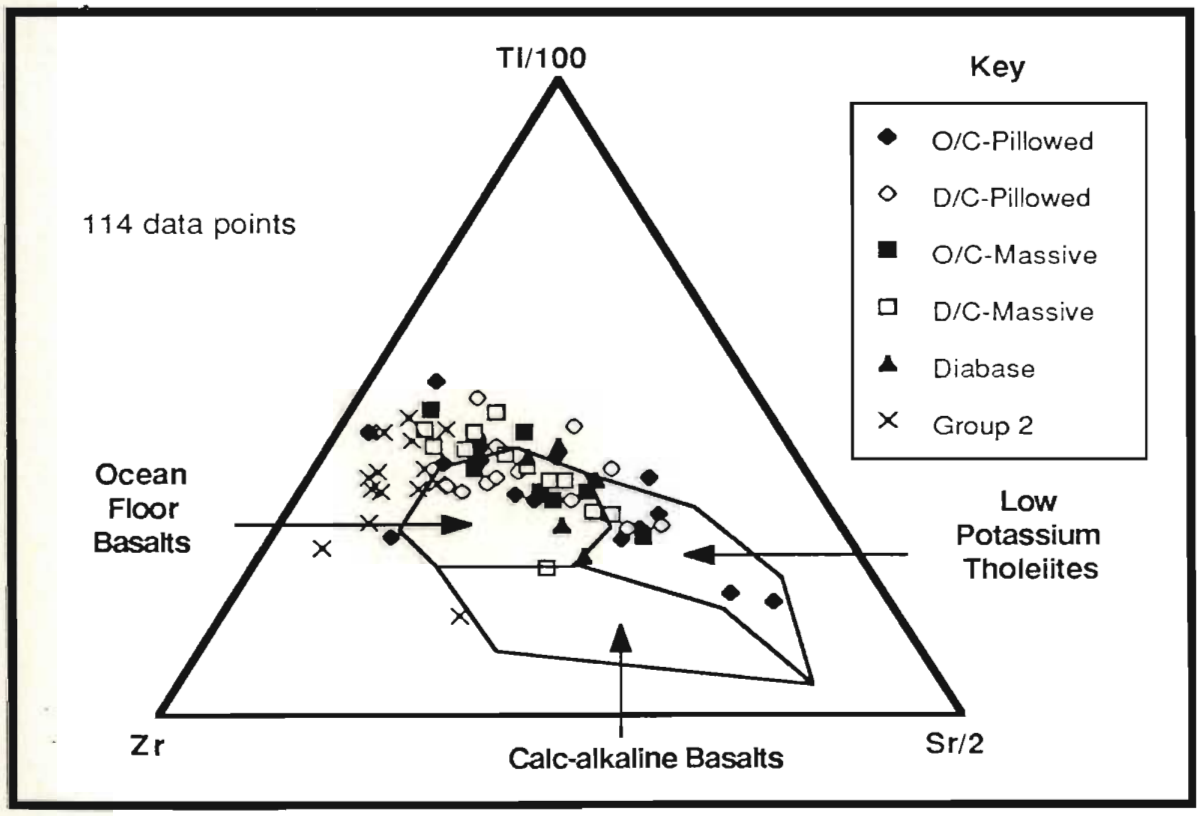

Figure 5-16: Skidder Basalt samples plotted on the Ti-Zr-Sr diagram of Pearce and Cann (1973), used by them to discriminate basalts from different tectonic settings.

samples plot outside all fields and away from the Sr apex on Figure 5-16 suggesting relative depletion in Sr for some of the Skidder Basalt rocks. In contrast to the Skidder Basalt samples, the Sandy Lake Formation basalts of the Buchans Group plot predominantly in the calc-alkaline basalts field on the Ti, Zr, Sr diagram (Thurlow, 1981a).

The Skidder Basalt rocks plot in the MORB/arc lavas and MORB/within-plate lavas fields with some scatter into the field of island arc lavas on Figure 5-17 (after Pearce, 1980). On Figure 5-18, the Skidder Basalt rocks overlap the MORB, within-plate basalts and island arc tholeiite fields at higher Cr concentrations, and plot in the within-plate basalts and island arc tholeiites fields at lower Cr concentrations (after Pearce, 1980). They plot close to the boundary of island arc and ocean floor tholeiites at higher Ni concentrations and predominantly within the island arc tholeiite field at lower Ni concentrations on Figure 5-19 (after Beccaluva et al., 1979).

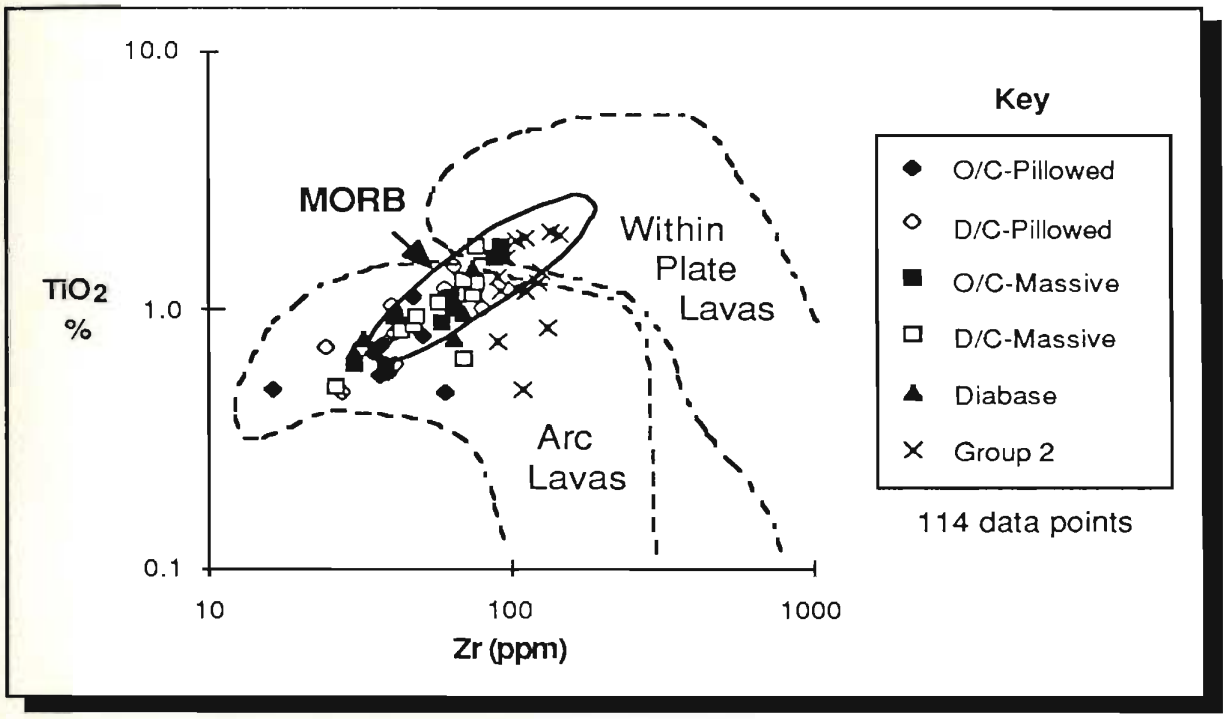

Figure 5-17: Skidder Basalt samples plotted on the TiO_2-Zr trace element variation diagram of Pearce (1980), used by him to discriminate basalts from different tectonic settings.

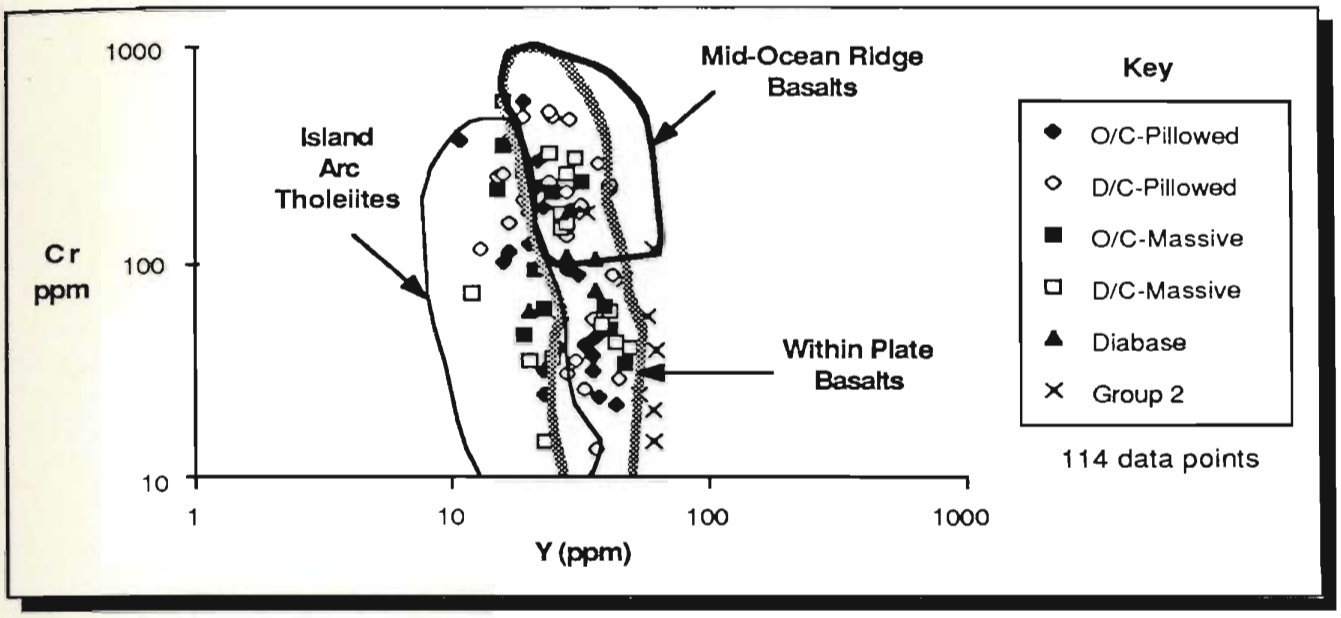

Figure 5-18: Skidder Basalt samples plotted on the Cr vs. Y diagram of Pearce (1980), used by him to discriminate basalts from different tectonic settings.

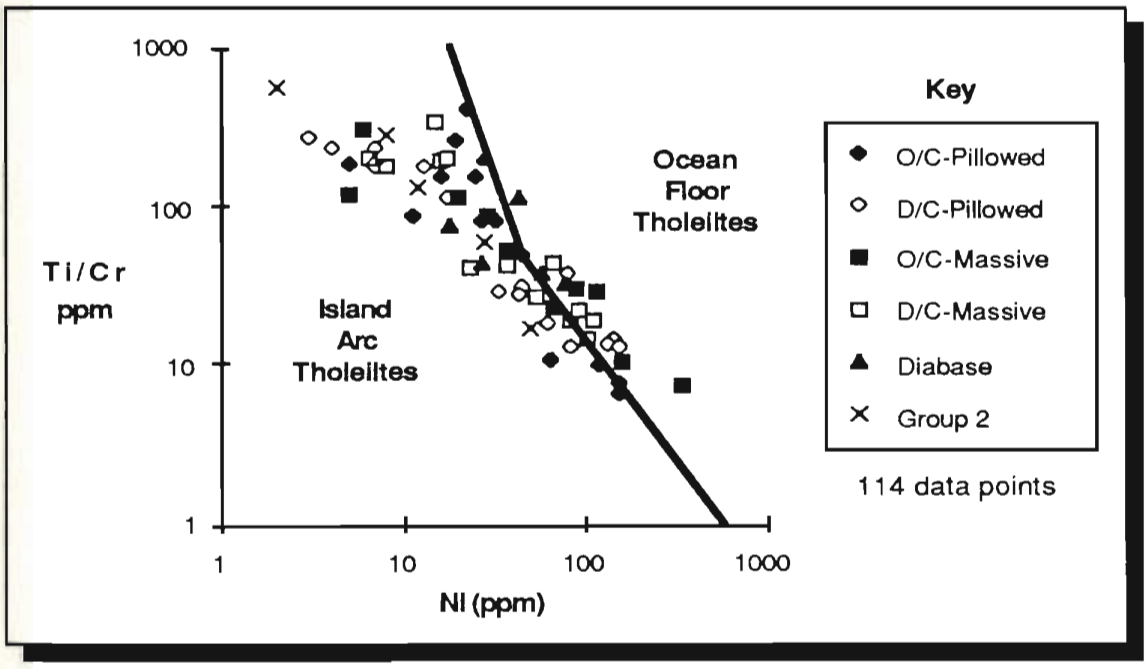

Figure 5-19: Log-log plot of Ti/Cr ratios vs. Ni in Skidder Basalt samples. Fields after Beccaluva et al. (1979).

5.2.8 Rare-Earth Element Geochemistry

5.2.8.1 Introduction

Eight relatively unaltered Skidder Basalt samples were analyzed for rare-earth element (REE) concentrations using the method of Fryer (1977). Further details of the analytical method are given in Appendix D. The samples chosen cover the range of Skidder Basalt compositions from low-Zr quench-textured basalts to high-Zr Group 2 basalts and andesites (?). Analyses are presented in Tables 5-9 and 5-10, arranged in order of increasing Zr concentrations.

Rare-earth element concentrations obtained from an analysis of internal Memorial University of Newfoundland (MUN) granite standard MUN-1 are listed in Appendix D. A comparison of the chondrite-normalized (Taylor and Gorton, 1977) REE pattern for MUN-1 from the analysis performed during this study to the range of previous analyses suggests some loss of Sm, Nd, Gd and Er and severe loss of Eu, presumably during the ion exchange process (Figure 5-20). However, the overall LREE-enriched, HREE-depleted pattern is consistent with the previous analyses.

5.2.8.2 Results

Table 5-11 shows a Pearson correlation matrix for the rare-earth elements and other selected elements in the representative suite of Skidder Basalt samples. SiO_2 shows no correlation to very weak positive correlation with the light rare-earth elements (LREE), (La, Ce, Nd and Sm) and Eu, and a weak positive correlation with the heavy rare-earth elements (HREE) Gd, Dy and Er. The "incompatible" elements Ti (TiO_2) and Zr and the alteration-modified incompatible element, Na (Na_2O), show a strong positive correlation with the LREE plus Gd and show a moderate positive correlation with Eu, Dy and Er. P_2O_5 shows a strong positive correlation with the middle rare-earth elements (MREE) Nd, Sm and Gd and moderate positive correlation with the remainder of the REE, probably reflecting the high mineral to melt distribution coefficients for all the REE in apatite but also its relatively

Table 5-9: Major element contents, and trace and rare-earth element concentrations for a representative suite of Skidder Basalt outcrop samples, and Skidder Prospect drill core samples that are relatively unaffected by the mineralizing event(s)

Weight %	S 59	SK 27 17	S 34B	SK 30 88
SiO_2	47.90	53.70	49.60	50.90
TiO_2	0.49	0.82	0.84	1.07
Al_2O_3	15.10	14.30	14.50	15.00
Fe_2O_3*	10.12	10.61	9.65	9.77
MnO	0.16	0.14	0.15	0.10
MgO	11.13	7.13	5.77	8.92
CaO	8.03	3.16	8.60	3.96
Na_2O	3.68	4.12	4.41	5.18
K_2O	0.09	0.30	0.14	0.17
P_2O_5	0.01	0.10	0.13	0.12
LOI	3.75	5.34	5.70	3.76
Total	100.46	99.72	99.49	98.95
ppm				
Pb	n.d.	4	5	3
Rb	n.d.	5	2	7
Sr	67	58	98	72
Y	17	23	21	28
Zr	16	43	52	57
Nb	4	4	4	5
Zn	68	105	60	67
Cu	84	55	56	41
Ni	148	27	37	36
Ba	n.d.	42	2	4
V	190	379	327	275
Cr	371	96	93	151
Ga	13	16	14	28

* Total iron as Fe_2O_3

n.d. - not detected

RARE EARTH ELEMENT CONCENTRATIONS

	S 59		SK 27 17		S 34B		SK 30 88	
	ppm	chondrite normalized	ppm	chondrite normalized	ppm	chondrite normalized	ppm	chondrite normalized
La	2.7	8.6	4.3	13.7	8.9	28.3	8.0	25.4
Ce	7.0	8.6	12.0	14.8	23.1	28.4	20.9	25.7
Nd	8.1	13.6	9.1	15.2	17.4	29.1	15.8	26.5
Sm	4.0	20.8	2.7	14.1	4.6	24.0	4.5	23.4
Eu	1.9	26.3	1.0	13.9	1.4	19.4	1.1	15.2
Gd	4.9	18.9	3.3	12.7	6.0	23.2	6.2	23.9
Dy	8.7	26.8	4.1	12.6	6.1	18.8	6.8	20.9
Er	4.4	20.7	2.7	12.7	2.5	11.7	3.4	16.0
Total	41.7		39.2		70.0		66.7	

Chondrite-normalizing values used are those of Taylor and Gorton (1977)

Ratios (Chondrite Normalized)				
La/Ce	1.0	0.9	1.0	1.0
La/Sm	0.4	1.0	1.2	1.1
Eu/Eu*	1.3	1.0	0.8	0.6

Eu* = (Sm+Gd)/2

Table 5-9 (continued):

Weight %	SK 27 1	S 80B
SiO_2	48.30	48.10
TiO_2	1.27	1.76
Al_2O_3	17.10	14.10
Fe_2O_3*	14.58	11.24
MnO	0.10	0.13
MgO	4.95	4.48
CaO	5.40	9.55
Na_2O	5.21	4.56
K_2O	0.42	0.03
P_2O_5	0.13	0.22
LOI	2.77	6.53
Total	100.23	100.70
ppm		
Pb	n.d.	5
Rb	3	n.d.
Sr	134	45
Y	27	47
Zr	75	92
Nb	6	9
Zn	62	85
Cu	8	28
Ni	49	6
Ba	n.d.	n.d.
V	237	480
Cr	243	34
Ga	16	18

* Total iron as Fe_2O_3
n.d. - not detected

RARE-EARTH ELEMENT CONCENTRATIONS*

	SK 27 1		S 80B	
	ppm	chondrite normalized	ppm	chondrite normalized
La	10.9	34.6	9.7	30.8
Ce	31.7	39.0	26.3	32.3
Nd	24.8	41.5	21.2	35.5
Sm	7.0	36.5	6.1	31.8
Eu	2.0	27.7	2.0	27.7
Gd	8.0	30.9	8.2	31.7
Dy	8.4	25.8	8.8	27.1
Er	3.6	16.9	4.4	20.7
Total	96.4		86.7	

Ratios (Chondrite Normalized)		
La/Ce	0.9	1.0
La/Sm	0.9	1.0
Eu/Eu*	0.8	0.9

Eu* = (Sm+Gd)/2

Table 5-10: Major element contents, and trace element concentrations of two Group 2 samples

Weight %	S 21A	S 58
SiO_2	58.70	61.30
TiO_2	1.60	1.22
Al_2O_3	14.30	14.10
Fe_2O_3*	9.45	9.45
MnO	0.15	0.14
MgO	4.09	3.17
CaO	2.09	1.65
Na_2O	5.98	5.93
K_2O	0.13	0.34
P_2O_5	0.38	0.17
LOI	2.39	1.84
Total	99.26	99.31
ppm		
Pb	6	n.d.
Rb	4	n.d.
Sr	31	32
Y	53	44
Zr	95	103
Nb	5	4
Zn	117	107
Cu	n.d.	14
Ni	n.d.	n.d.
Ba	52	1
V	131	124
Cr	n.d.	3
Ga	16	19

* Total iron as Fe_2O_3
n.d. - not detected

RARE-EARTH ELEMENT CONCENTRATIONS

	S 21A		S 58	
	ppm	chondrite normalized	ppm	chondrite normalized
La	8.8	27.9	12.4	39.4
Ce	27.9	34.3	32.1	39.5
Nd	25.6	42.9	24.2	40.5
Sm	9.0	46.9	6.9	35.9
Eu	2.2	30.5	1.9	26.3
Gd	10.3	39.8	9.3	35.9
Dy	10.9	33.5	10.3	31.7
Er	5.0	23.5	5.2	24.4
Total	99.7		102.3	

Ratios (Chondrite Normalized)		
La/Ce	0.8	1.0
La/Sm	0.6	1.1
Eu/Eu*	0.7	0.7

Eu* = (Sm+Gd)/2

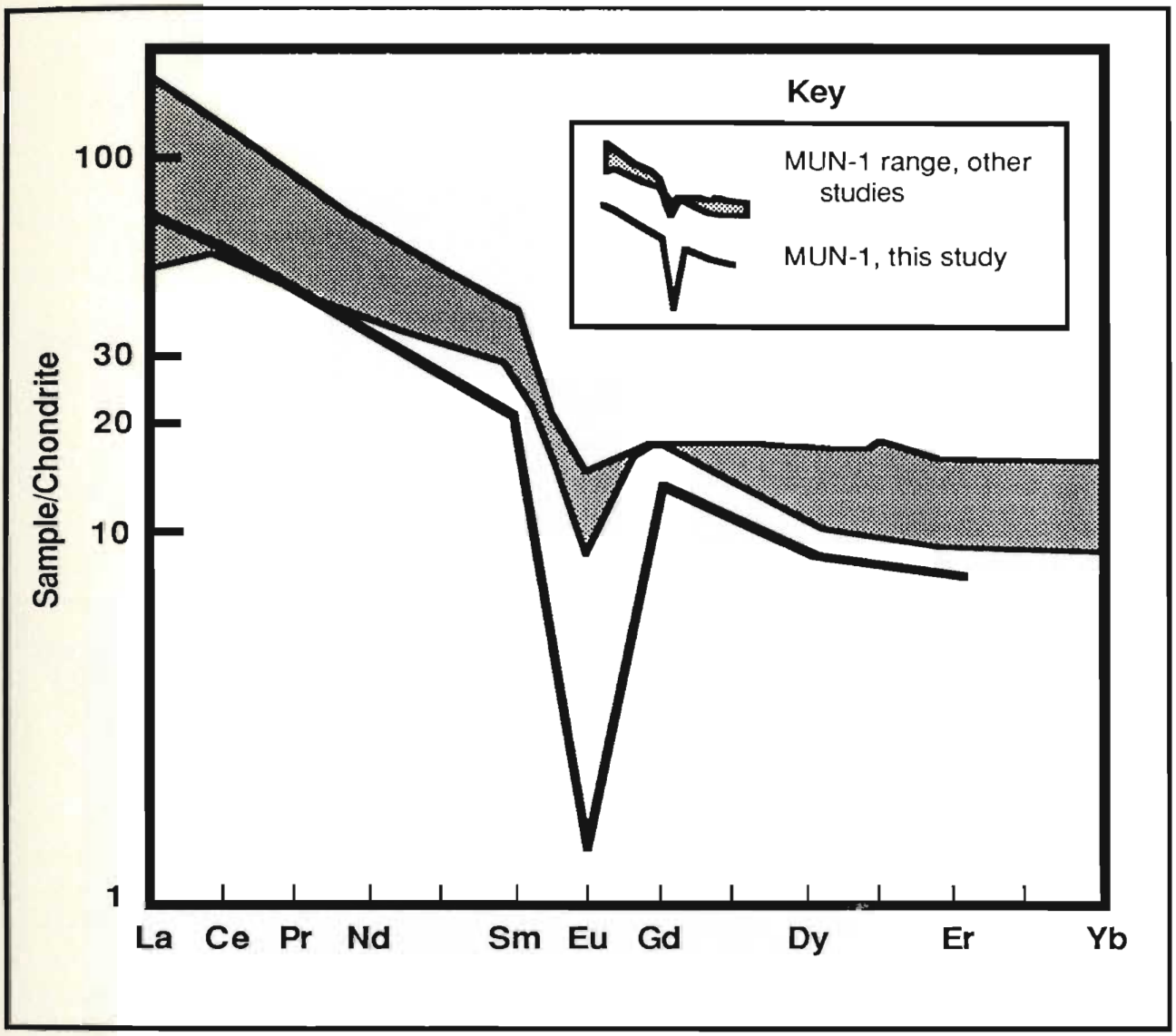

Figure 5-20: Chondrite-normalized (Taylor and Gorton, 1977) rare-earth element pattern for internal Memorial University of Newfoundland granite standard MUN-1 (analytical results presented in Table D-1, Appendix D). Results from this study are compared to the range of chondrite-normalized rare-earth element abundances for MUN-1 from other studies (D.F Strong, personal communication, 1986).

Table 5-11: Pearson correlation matrix for rare-earth element and other selected element concentrations in representative suite of Skidder Basalt samples

Number of samples = 8

	SiO_2	TiO_2	MgO	Na_2O	P_2O_5	LOI	Rb	Y	Zr	Cu	Ni	V	Cr
La	.00	.61	-.81	.73	.36	.00	.00	.50	.85	.78	-.63	.00	-.47
Ce	.00	.71	-.85	.80	.53	.00	.00	.59	.89	-.88	-.65	.00	-.47
Nd	.14	.77	-.83	.83	.68	-.24	.00	.70	.90	-.92	-.58	.00	-.43
Sm	.27	.71	-.64	.79	.77	-.46	.00	.76	.77	-.85	-.30	-.33	-.20
Eu	.00	.39	-.23	.07	.32	-.17	-.53	.48	.36	-.36	.00	-.15	.00
Gd	.32	.76	-.69	.82	.74	-.39	.00	.83	.86	-.83	-.42	-.22	-.38
Dy	.15	.40	-.19	.53	.43	-.53	-.30	.64	.51	-.46	.00	-.51	.00
Er	.36	.30	.00	.41	.29	-.48	-.31	.66	.44	-.28	.00	-.43	.00
Total REE	.22	.75	-.81	.83	.64	-.31	.00	.72	.91	-.90	-.55	.00	-.41

	La	Ce	Nd	Sm	Eu	Gd	Dy	Er
La	1.00							
Ce	.98	1.00						
Nd	.90	.97	1.00					
Sm	.62	.76	.90	1.00				
Eu	.06	.30	.54	.77	1.00			
Gd	.74	.82	.92	.97	.72	1.00		
Dy	.30	.40	.60	.83	.88	.85	1.00	
Er	.00	.00	.33	.63	.75	.68	.92	1.00
Total REE	.91	.96	.99	.90	.58	.95	.67	.45

higher distribution coefficients for the middle REE (Henderson, 1984). Y shows a strong positive correlation with Nd, Sm and the HREE and a moderate positive correlation with La, Ce and Eu, probably reflecting similarity in the chemical behaviour of Y to that of the HREE (Henderson, 1984). TiO_2, Na_2O, P_2O_5, Y and Zr all display strong positive correlations with total REE.

The "compatible" elements Mg (MgO) and Cu show a strong negative correlation with the LREE and Gd, and a weak to moderate negative correlation with Eu, Dy and Er (Table 5-11). Elements Ni and Cr, compatible with early fractionating phases in basaltic magmas, have moderate to strong negative correlations with the LREE and weak negative correlations with the remaining REE. MgO and Cu show a strong negative correlation and LOI, Ni and Cr show a weak to moderate negative correlation with total REE.

La, Ce and Nd display a strong positive correlation with Gd and with each other, and show a weak to moderate positive correlation with Eu, Dy and Er. Samarium and Gd are strongly positively correlated with all the REE and with each other. Europium, Dy and Er show a strong positive correlation with each other and moderate positive correlation with Nd and Sm.

Figures 5-21 to 5-24 present chondrite-normalized (Taylor and Gorton, 1977) patterns for the Skidder Basalt samples arranged in order of increasing Zr concentrations. REE concentrations range from 8 to 47 x chondrite as shown by a composite of all the Skidder Basalt REE patterns presented in Figure 5-25. Sample S 59, a low-Zr quench-textured basalt, gives a LREE depleted- (La/Sm = 0.4) and relatively HREE-enriched pattern with a slight positive Eu anomaly (Eu/Eu* = 1.3). The other samples have relatively flat REE to slightly LREE depleted patterns (La/Ce = 0.8-1.0 and La/Sm = 0.6-1.2) and show a general increase in total REE with increasing Zr concentration (Figures 5-21 to 5-25). Sample SK 27 17 has no Eu anomaly but samples with higher Zr concentrations have slight negative Eu anomalies (Eu/Eu* = 0.6-0.9). All samples except S 59 and SK 27 17 show depletion of the HREE relative to the others.

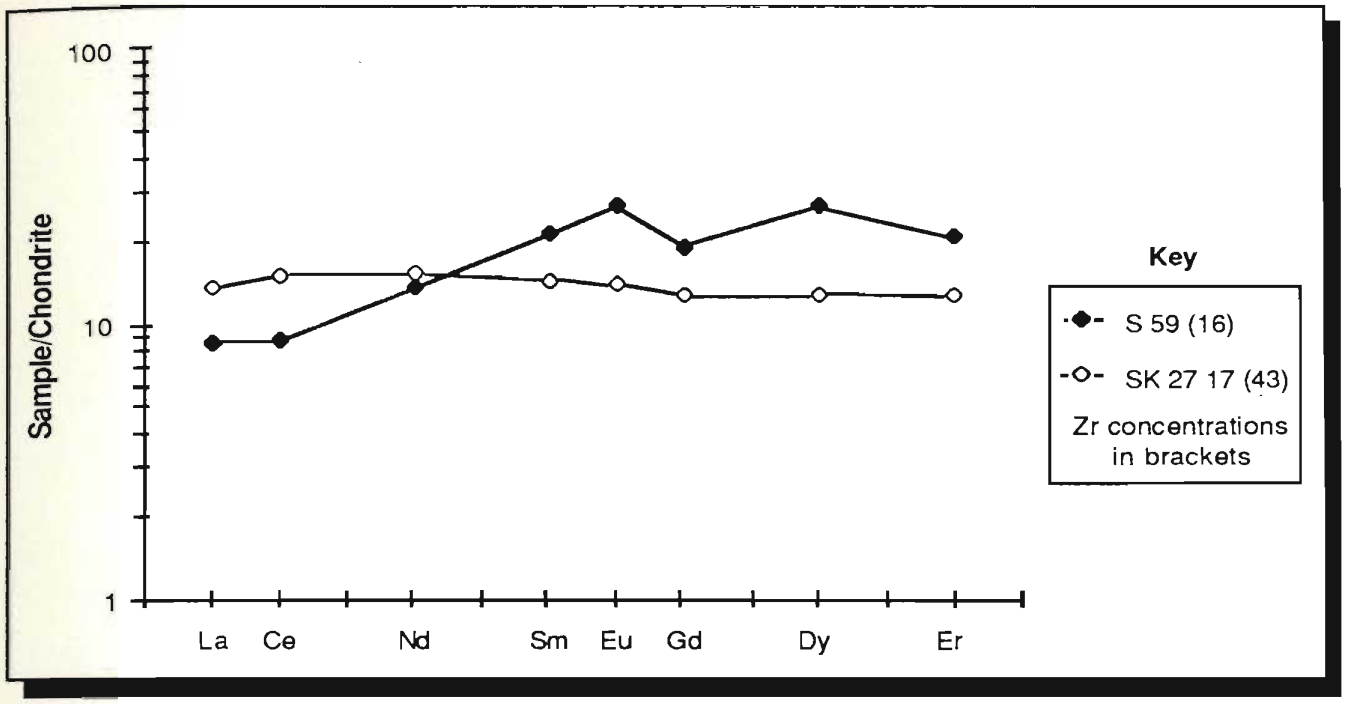

Figure 5-21: Chondrite-normalized rare-earth element patterns for Skidder Basalt samples having Zr concentrations < 50 ppm.

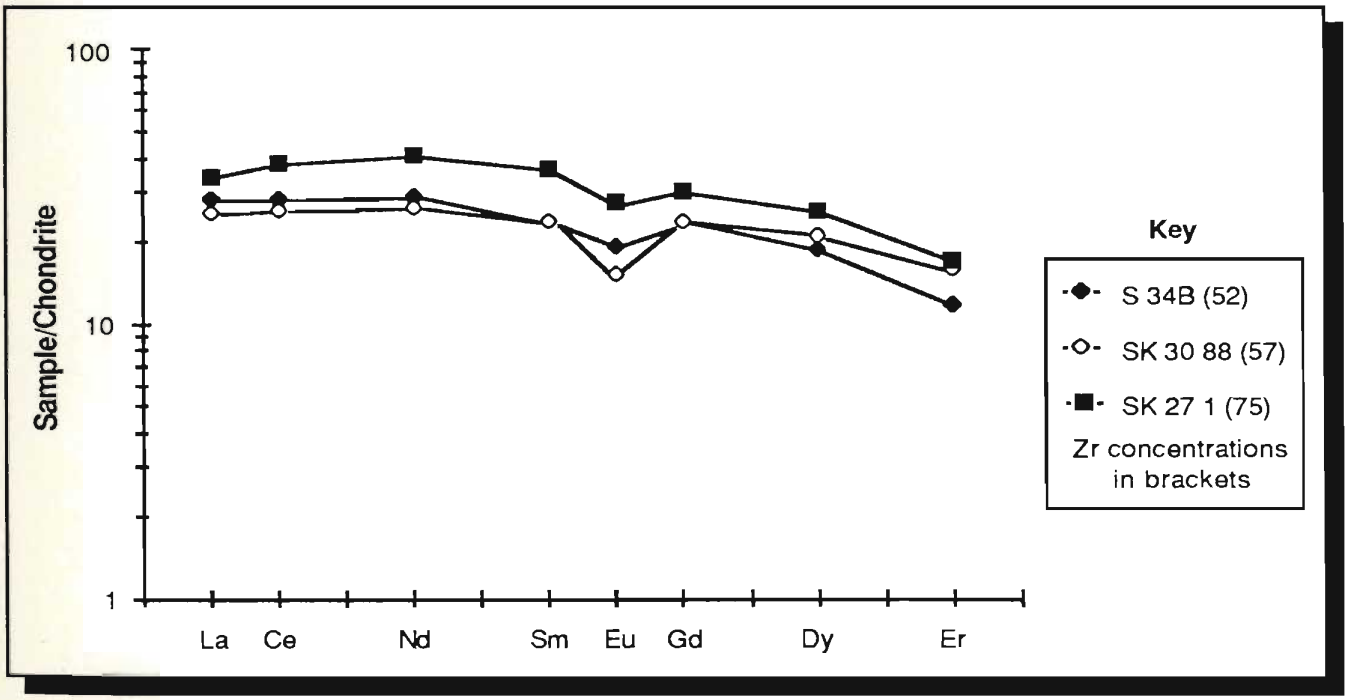

Figure 5-22: Chondrite-normalized rare-earth element patterns for Skidder Basalt samples having Zr concentrations > 50 < 85 ppm.

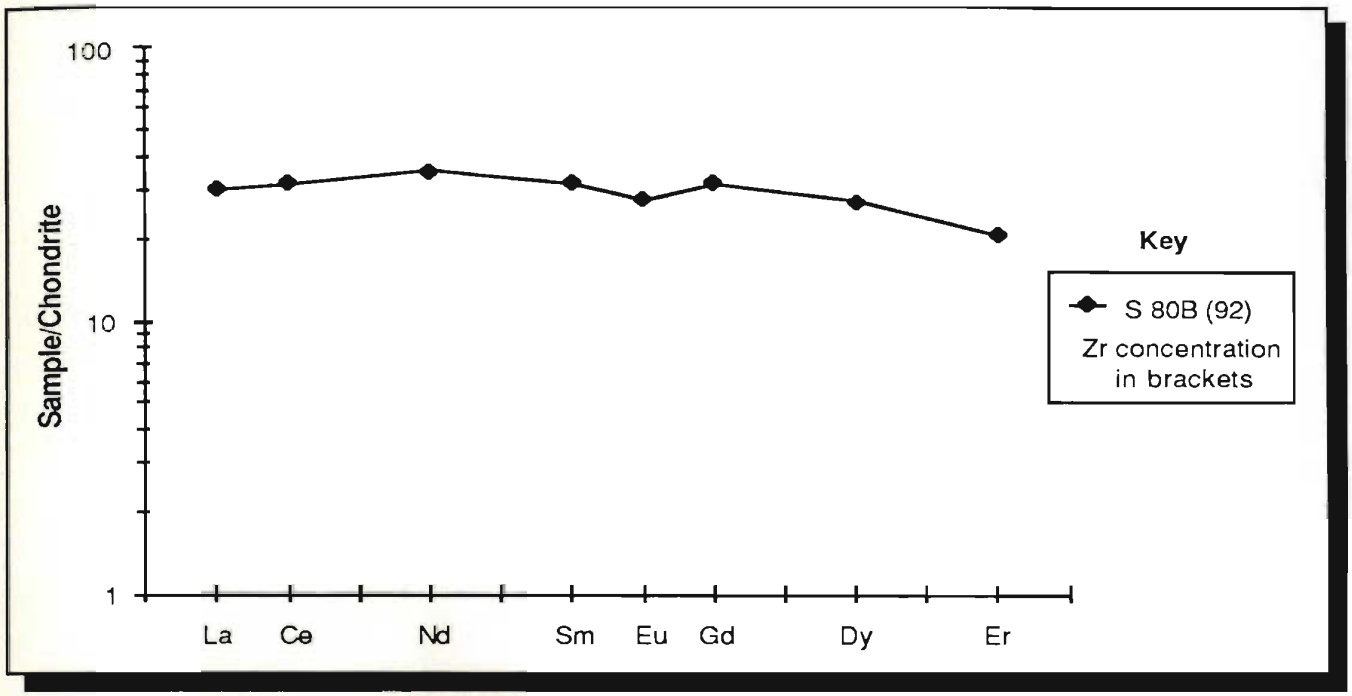

Figure 5-23: Chondrite-normalized rare-earth element pattern for Skidder Basalt sample S 80B, a high-Zr basalt not included in Group 2.

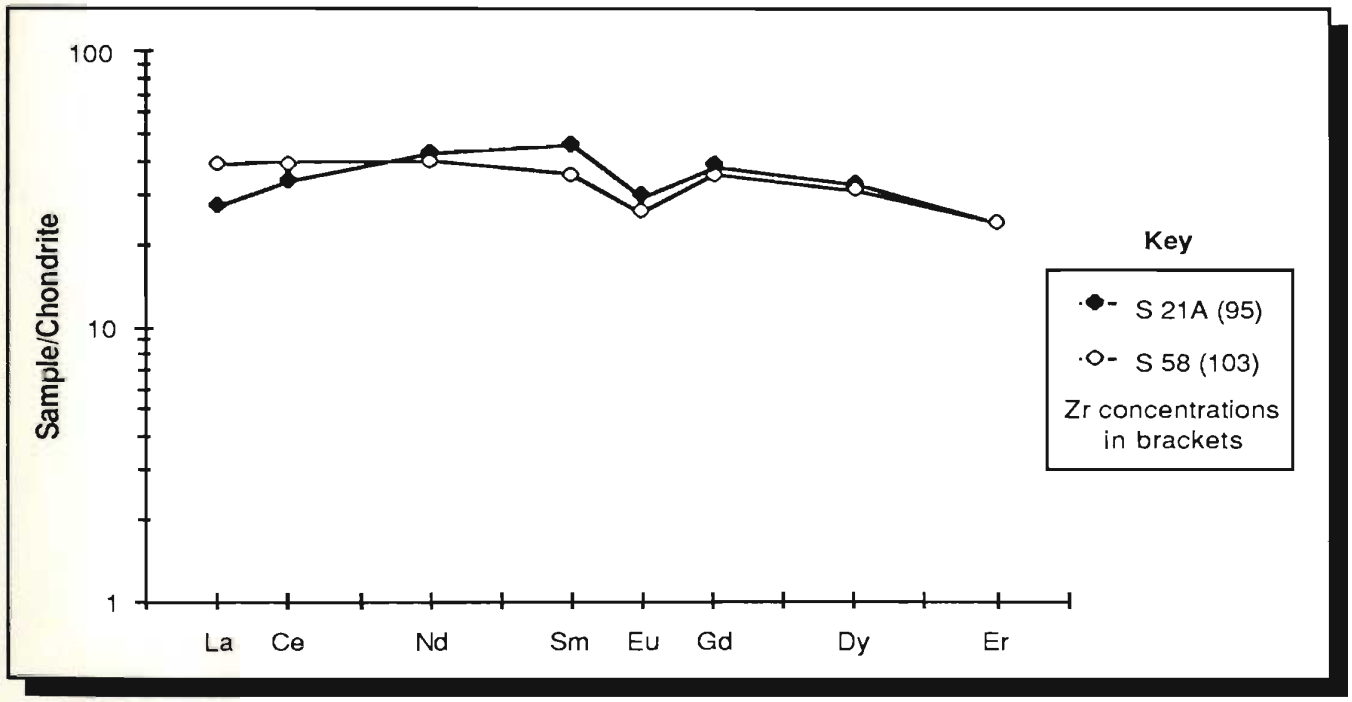

Figure 5-24: Chondrite-normalized rare-earth element patterns for Skidder Basalt Group 2 samples.

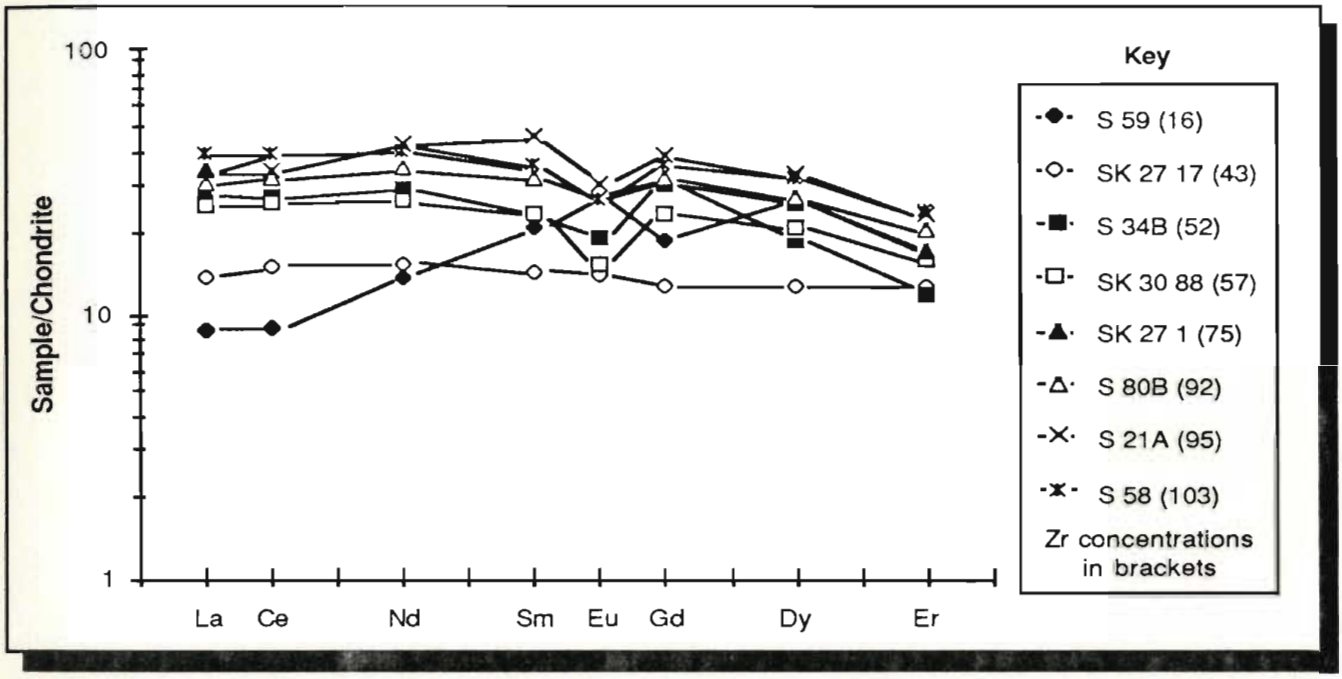

Figure 5-25: Composite of chondrite-normalized rare-earth element patterns for the Skidder Basalt.

5.2.8.3 Discussion

Studies of the effects of alteration on the REE have given conflicting results (cf. Humphris, 1984). Ludden and Thompson, (1978; 1979) report that low-temperature alteration, e.g. palagonization of submarine basalt glasses, can result in LREE enrichment, and a uniform increase in the HREE in the rims of pillows relative to the interiors. Studies of spilites have shown either enrichment of the REE (Hellman and Henderson, 1977) or no effect at all on REE concentrations (Herrmann et al., 1974) as a result of spilitization. Experimental studies on the effects of hydrothermal alteration of basalts suggest slight enrichment or depletion of the LREE, but very little modification of the HREE under hydrothermal conditions ranging from 150°C to 350°C (Menzies et al., 1979). Similar results were reported after experimental reaction of oceanic tholeiite with seawater at 500-600°C, 800-1000 bars and water/rock ratios of 1-3 (Hajash, 1984).

Under magmatic conditions, the rare-earth elements tend to concentrate in the melt (e.g. Humphris, 1984). Of the common rock forming minerals, clinopyroxene is one of the most important major phases in terms of removing REE from the liquid and also selectively enriching the liquid in the LREE (Henderson, 1984; Humphris, 1984). Distribution coefficients are low for REE partitioning in other common rock forming minerals such as olivine, magnetite and plagioclase (Eu being an exception in the latter case). However, common accessory minerals in basalt such as apatite and sphene, and possibly zircon in more differentiated compositions, play a major role in REE distribution. Mineral/melt distribution coefficients presented by Henderson (1984) for apatite and sphene in felsic rocks range from 17-50 for apatite and 27-102 for sphene. Both these minerals concentrate the MREE relative to the LREE and HREE. Zircon tends to concentrate the

HREE. Henderson (1984) reports mineral/melt distribution coefficients for Zr in felsic rocks of about 4 for the LREE, in contrast to about 48 for Dy and 345 for Lu.

With the exception of S 59, the Skidder Basalt samples show a similarity of REE patterns which supports a cogenetic origin for the basalts including the Group 2 samples. Extensive clinopyroxene fractionation which would expect to be reflected by LREE enrichment in the high-Zr basalts is not indicated. The relative depletion of the HREE in the Skidder samples, is probably a result of loss during the ion exchange process (Dunning, 1984; G. Jenner, personal communication, 1987). However, it is possible that the convex downward REE patterns shown by several of the samples may be partially controlled by the host minerals to the REE within the spilitized Skidder Basalt. Sphene is a common accessory mineral in the Skidder samples (Chapter 4) and presumably much of the phosphorus content of the samples is hosted by apatite. Both these minerals have high mineral/melt distribution coefficients for the REE and preferentially incorporate the MREE (Henderson, 1984).

Europium anomalies are often attributed to substitution of Eu^{2+} for Ca^{2+} and Na^{+} in plagioclase (e.g. Henderson, 1984). Thus, positive Eu anomalies are suggested to indicate plagioclase accumulation and negative Eu anomalies indicative of substantial plagioclase fractionation (at least 25% plagioclase removal, Basaltic Volcanism Study Project (BVSP), 1981a). Coish et al. (1982) suggest removal of Ca and Eu during albitization of plagioclase although mobilization may only be local since reprecipitation of these elements may occur by formation of epidote and/or calcite near plagioclase grains. Sun and Nesbitt (1978) also attribute Eu anomalies to alteration.

The Skidder Basalt samples do not show the severe depletion of Eu that would be expected by comparing the analysis of the MUN-1 standard conducted during this study to previous analyses of the standard (Figure 5-20) but loss of Eu and hence production of the negative Eu anomalies in the Skidder Basalt samples as a result of the analytical method cannot be ruled out. Loss of Eu as a result of albitization in some of the Skidder Basalt

samples is supported by the most pronounced negative Eu anomaly being in sample SK 30 88 which has the lowest CaO content and the highest positive Eu anomaly being in sample S 59 which has a high CaO content. However, contrary to this argument and supportive of at least some magmatic control, i.e. plagioclase fractionation, on the negative Eu anomalies in the Skidder Basalt is that sample S 80B which has the highest CaO content has a negative Eu anomaly and sample SK 27 17, which has a low CaO content has no negative Eu anomaly.

5.2.8.4 Tectonic environment

The range of chondrite-normalized REE concentrations in the Skidder Basalt is compared to that of ocean floor basalt lavas in Figure 5-26. High-Zr and Group 2 Skidder Basalt samples contain higher LREE and MREE concentrations than "normal" or N-type MORBS (Figure 5-26). A highly evolved ocean floor basalt from the Galapagos Ridge (BVSP, 1981a) contains about the same LREE and MREE concentrations as the most REE-enriched Skidder Basalt samples but it has a significantly higher HREE concentration. Some, but not all of the Skidder samples show LREE depletion a typical characteristic of N-type MORB (e.g. BVSP, 1981a; Saunders, 1984). The Skidder Basalts do not show the characteristic LREE enrichment of enriched MORBS (Erlank and Kable, 1976; Le Roex et al., 1983; Saunders, 1984,) or the extreme LREE enrichment typical of within-plate alkalic lavas from oceanic islands, represented on Figure 5-26 by Azores Islands lavas. The Skidder Basalt samples do fall within the range of "transitional" or T-type MORBS (Figure 5-26) which have intermediate REE characteristics between N-type and enriched MORBS showing either LREE depletion or enrichment.

Figure 5-27 compares REE concentrations in the Skidder Basalt to those of island arc basalts. Some of the Skidder samples show flat REE patterns characteristic of island arc tholeiites (e.g. BVSP, 1981b) but the overall abundances of REE in the Skidder Basalt are greater such that the most evolved of the New Britain island arc reference suite

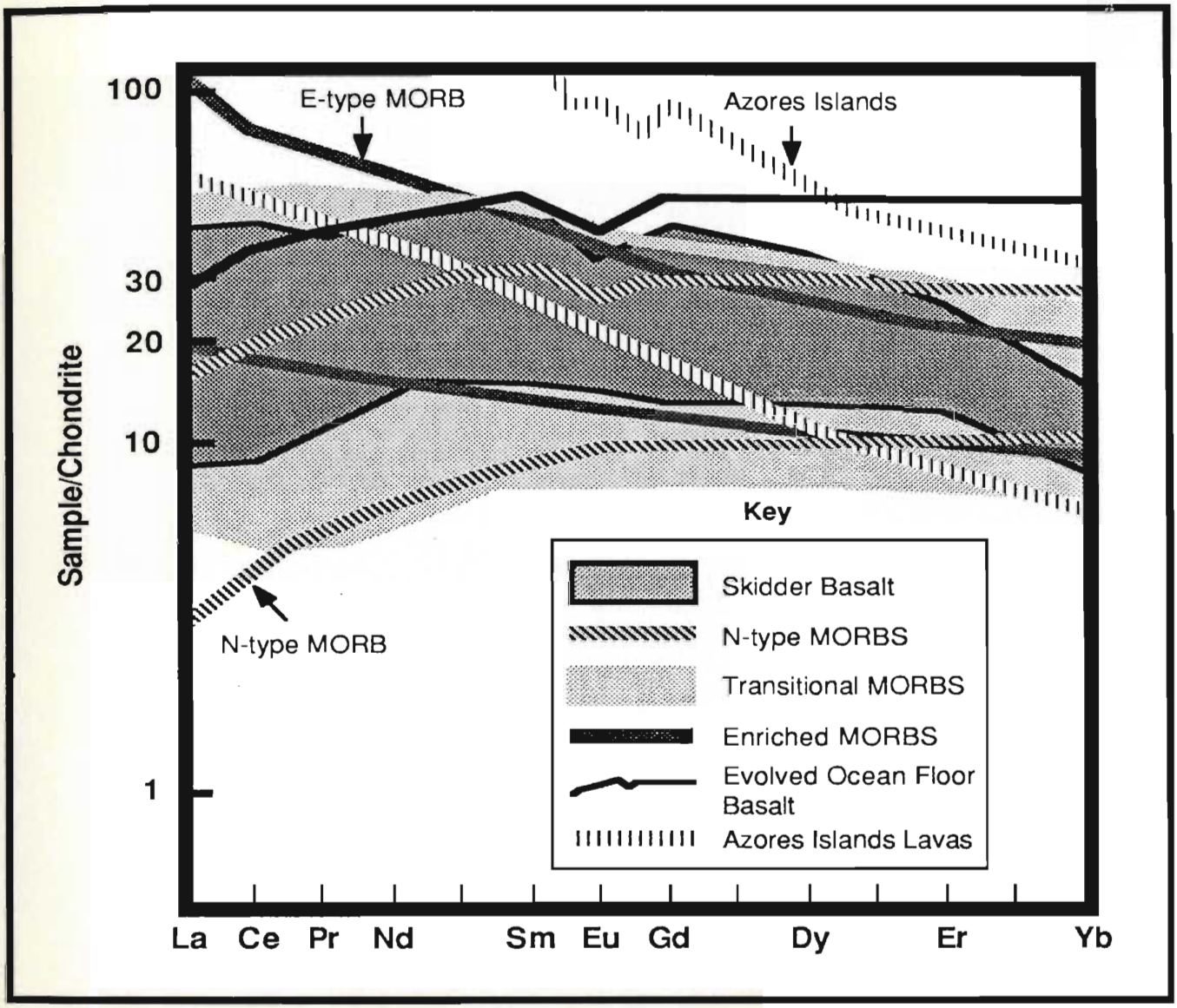

Figure 5-26: Range of chondrite-normalized rare-earth element abundances in the Skidder Basalt compared to: N-type MORBS (Saunders, 1984; data from: Frey et al., 1980; Kay et al., 1970; Saunders, 1983; Schilling, 1975a; Srivastava et al., 1980; Sun et al., 1979; Thompson et al., 1976); transitional MORBS (Saunders, 1984; data from: Langmuir et al., 1977; Wood et al., 1979; O'Nions et al., 1976); enriched MORBS (Saunders, 1984; data from: O'Nions et al., 1976; Schilling, 1975b; Wood et al., 1979); and alkalic Azores Islands Lavas (White et al., 1979). The rare earth element pattern for a highly evolved ocean floor basalt from the Galapagos Ridge is also shown (Basaltic Volcanism Study Project, 1981a).

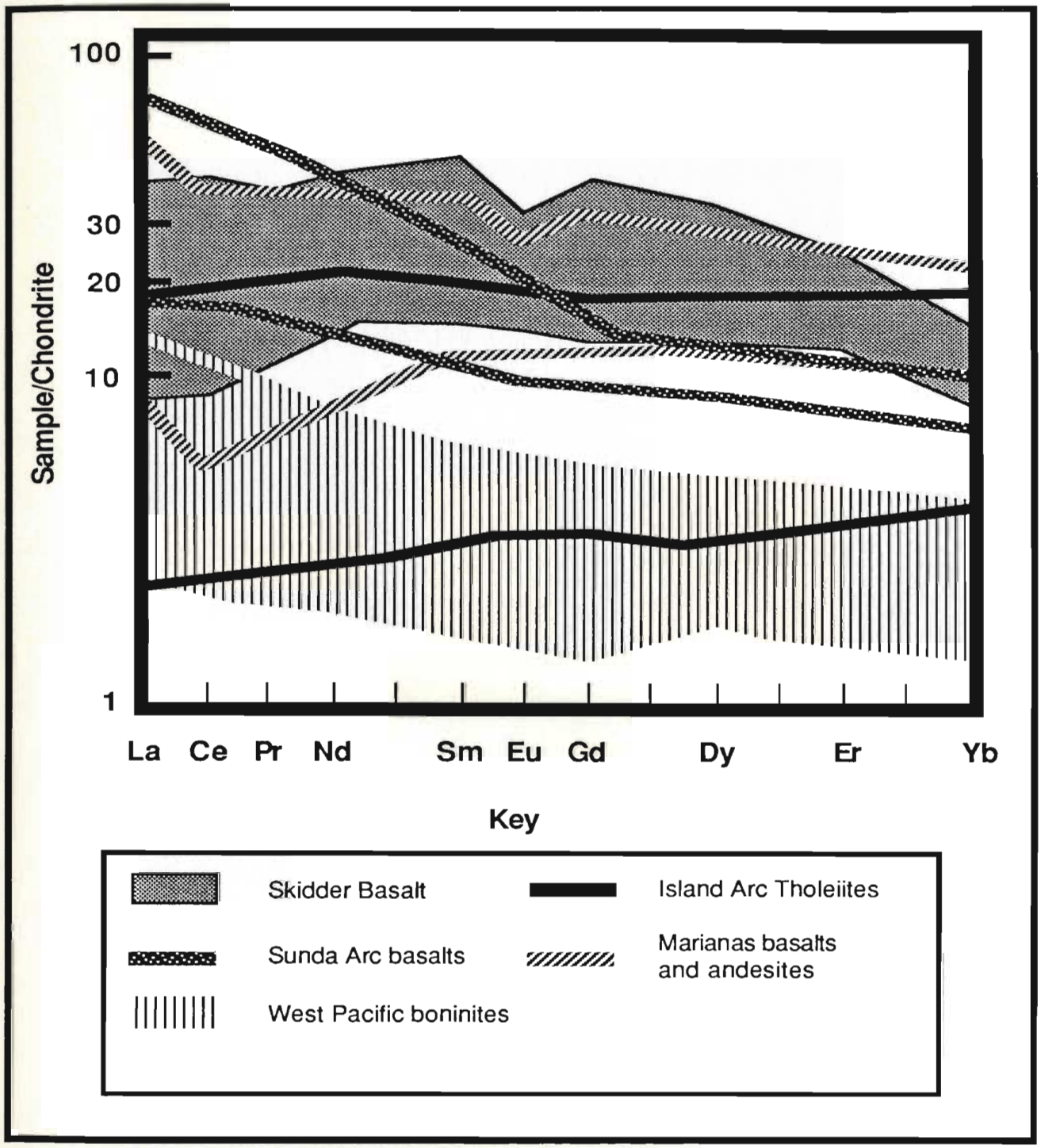

Figure 5-27: Range of chondrite-normalized rare-earth element abundances in the Skidder Basalt compared to that of: the New Britain Island Arc Tholeiite reference suite (Basaltic Volcanism Study Project, 1981b); tholeiitic and calc-alkaline basalts from the Sunda Arc (Whitford et al., 1979); basalts, basaltic andesites and andesites from the Marianas Islands (Dixon and Batiza, 1979); and modern boninites from the west Pacific (Crawford and Cameron, 1985; data taken from: Cameron et al., 1983; Jenner, 1981; Sun and Nesbitt, 1978).

(BVSP, 1981b) overlaps only the lower-Zr Skidder samples. Some of the Skidder samples have negative Eu anomalies, a characteristic usually lacking in island arc basalts (BVSP, 1981b). The Skidder Basalt samples do not show the LREE enrichment characteristic of calc-alkaline basalts represented on Figure 5-27 by the Sunda Arc (Whitford et al., 1979) and they do not show the overall REE depletion characteristic of modern boninites (Cameron et al., 1983; Jenner, 1981; Sun and Nesbitt, 1978).

Rare-earth element analyses of basalts and andesites from the Marianas Islands show considerable overlap with the Skidder Basalt but the former have a characteristic negative Ce anomaly not shown by the Skidder samples (Dixon and Batiza, 1979).

Negative Ce anomalies have been noted in several island arc suites (e.g. Jakes and Gill, 1970; Ewart et al., 1973; Taylor et al., 1969; White and Patchett, 1984); and in the Point Sal ophiolite in California (Menzies et al., 1977), interpreted by Pearce et al. (1984) as having been formed in a supra-subduction zone setting. Dixon and Batiza (1979) relate the negative Ce anomalies in the Marianas lavas to the ability of Ce to attain a quadrivalent ionic state with correspondingly smaller ionic radius; they suggest that depletion of Ce is related to depletions in other small, highly charged ions such as Ti, Zr and Hf. White and Patchett (1984) suggest that negative Ce anomalies are a "common, but not ubiquitous, feature" of island arc volcanic rare-earth element patterns. They indicate that the anomalies may be inherited from subducted altered oceanic crust or sediments or alternatively be a result of fluid-solid partitioning during dehydration of the subducting slab. Cullers and Graf (1984) also suggest that the negative Ce anomalies are source related. Menzies et al. (1977) attribute the negative Ce anomalies in the Point Sal ophiolite as being related to prolonged interaction of the lavas with sea water, the latter having a pronounced negative Ce anomaly (e.g. Humphris, 1984). Stabilization of minor oxide phases as a result of melting under hydrous conditions in the source for island arc basalts has been invoked as one possible explanation for depletion in these basalts of high field strength cations such as Ti, Zr and Nb, and the REE (e.g. Saunders et al., 1980). Presumably, conditions of

higher oxygen fugacity would tend to stabilize the quadrivalent Ce ion (cf. White and Patchett, 1984) and destabilize the Eu^{2+} ion and could provide an explanation for Ce depletion in some and a general lack of Eu anomalies in most island arc basalts. Certainly, however, lack of extensive plagioclase fractionation in island arc basalts (e.g. Perfit et al., 1980) can also provide an explanation for their lack of negative Eu anomalies.

5.2.9 Extended rare-earth element diagram

Pearce (1982) attempted to incorporate several of the geochemical features that characterize basalts from various tectonic settings onto one extended rare-earth style diagram on which average compositions are normalized to N-type MORB (Figure 5-28). On Figure 5-28 the average composition for the Skidder Basalt normalized to N-type MORB is compared to the average normalized composition for E-type MORB (Wood et al., 1979; Pearce, 1982); for alkalic oceanic island basalts from the Azores (Pearce, 1982); for the New Hebrides calc-alkaline basalts (Gorton, 1977); and for island arc tholeiites from the South Sandwich Islands (Pearce, 1982). Also presented for comparison is the average composition of the Annieopsquotch Complex dykes and lavas (calculated from geochemical data presented in Dunning, 1984).

Alkalic oceanic island basalts show a characteristic enrichment (relative to N-Type MORB) of the large ion lithophile elements (LIL) Sr, K, Rb and Ba; high field strength cations (HFS) Nb, P, Zr, Ti and Y; and rare-earth elements (REE) Ce and Sm (Pearce, 1982). E-type MORB are enriched in the LIL elements and HFS elements Nb, P and Zr plus the light REE (Pearce, 1982) relative to N-type MORB. Calc-alkaline basalts are highly enriched in the LIL elements; are depleted in HFS elements Nb, Zr, Ti and Y; but are enriched in the light rare-earth elements and P relative to N-type MORB (Pearce, 1982). Island arc tholeiites are slightly enriched in Rb and Ba but are significantly depleted in the HFS elements and Cr relative to N-type MORB (Pearce, 1982).

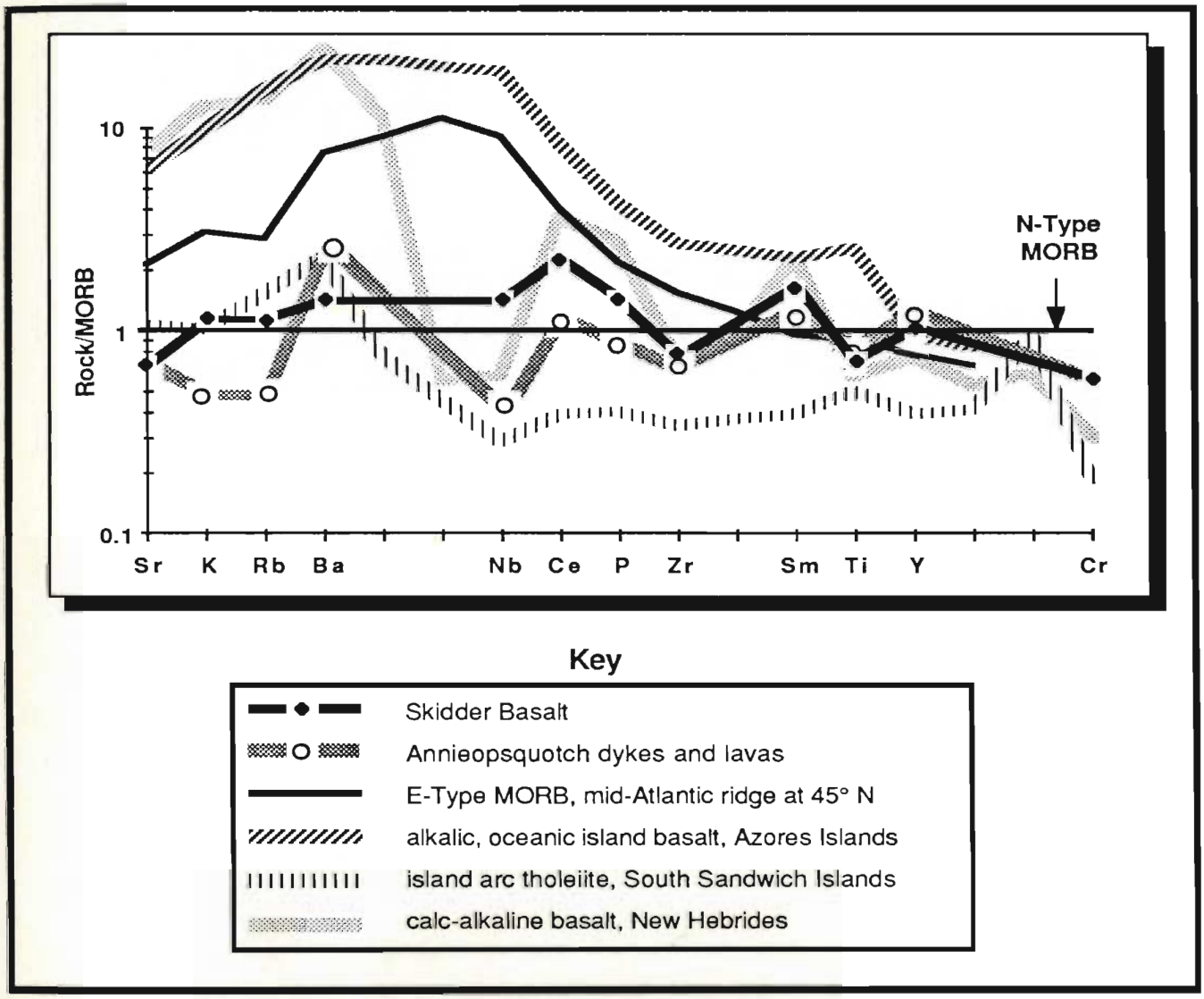

Figure 5-28: N-Type-MORB-normalized trace element patterns for: average Skidder Basalt; average Annieopsquotch dykes and lavas (data from Dunning, 1984); E-type MORB (Pearce, 1982; Wood et al., 1979); alkalic, oceanic island basalt (Pearce, 1982); island arc tholeiite (Pearce, 1982); and calc-alkaline basalt (Gorton, 1977).

The Skidder Basalt is slightly enriched in Ba, Nb, P and the LREE, is slightly depleted in Sr, and, like the Annieopsquotch Complex is slightly depleted in Zr, Ti and Cr relative to N-type MORB. Overall, both the Skidder Basalt and Annieopsquotch Complex have a pattern more similar to N-Type MORB than to the other basalt types. The Skidder Basalt does not show depletion of the HFS elements nor as much depletion of Cr as is characteristic of island arc tholeiites.

5.2.10 Petrogenetic model

Mid-ocean ridge basalt geochemistry is dominated by low pressure fractional crystallization of olivine + Cr-spinel followed by olivine + plagioclase; only late in the crystallization history does clinopyroxene become a liquidus phase (e.g. Bender et al., 1978; BVSP, 1981a). This contrasts with the liquid line of descent proposed for island arc tholeiites (cf. Perfit et al.,1980) in which clinopyroxene instead of plagioclase is the early mineral phase. Clinopyroxene replaces olivine as the liquidus phase at pressures greater than 12 kb (BVSP, 1981c). Also, Holloway and Burnham (1972) showed that plagioclase is not a stable phase under hydrous magmatic conditions and that the important crystallizing phases under these conditions are clinopyroxene, olivine and magnetite. This prompted Perfit et al. (1980) to suggest that the substitution of clinopyroxene for plagioclase as an early mineral phase in island arc tholeiites may be due to crystallization at greater depths or at higher p_{H_2O} conditions.

Skidder Basalt chromite compositions suggest a liquid line of descent for the Skidder Basalt similar to that for MORB, i.e. early crystallization of Cr-spinel and olivine, followed by olivine and plagioclase ± Cr-spinel and late fractionation of clinopyroxene (see Figure 4-34). Early crystallization of plagioclase is supported by the presence in the Skidder basalts of ubiquitous large albitized plagioclase phenocrysts. Pearce and Norry (1979) modeled the effects of fractionation of several minerals with regard to Zr and Y. These effects are shown as vectors on Figure 5-29. The trend outlined by the Skidder Basalt samples is consistent with fractionation of olivine and plagioclase. Extensive fractionation of clinopyroxene which would tend to lower the Y/Zr ratio is not observed.

Holloway and Burnham (1972) suggest that early fractionation of plagioclase from a magma is indicative of fractionation under low f_{O_2} conditions. Vanadium, which is compatible with Cr-spinel, is also compatible with clinopyroxene and magnetite under low oxygen fugacity conditions (less than or equal to log f_{O_2} of -10) (Shervais, 1982). Hence, vanadium concentrations in the Skidder Basalt should show the effects of fractionation of

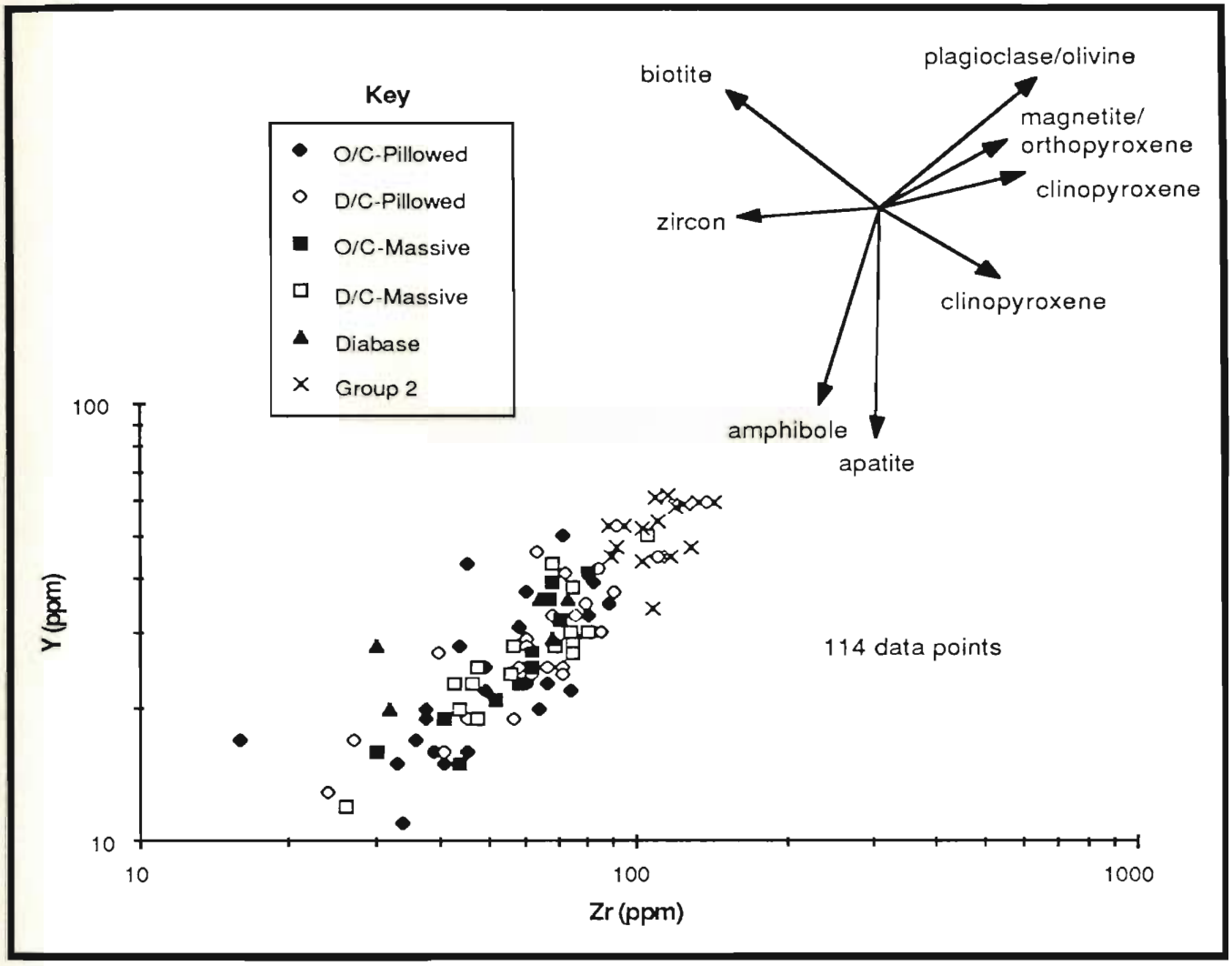

Figure 5-29: Zr vs. Y plot of the Skidder Basalt samples. Vectors show the effects of fractionation of various minerals on the Zr/Y ratio (after Pearce and Norry, 1979).

Cr-spinel, clinopyroxene and magnetite. The behaviour of Ni and Cr in basaltic magmas is dominated by the three phases olivine, Cr-spinel and clinopyroxene. Nickel partitions into olivine and Cr into Cr-spinel, which crystallize early from basaltic magmas, and both Ni and Cr partition into clinopyroxene, having distribution coefficients of 2 and 10 respectively (Sun et al., 1979).

Figure 5-30 illustrates the behaviour of V with respect to Cr and Ni in the Skidder Basalt and Figure 5-31 is a plot of log Ni versus log Cr for the Skidder Basalt samples. Although considerable point scatter is evident, the data presented on each of the three diagrams define a trend with several changes in slope as shown by the visually estimated "best fit" lines through the data. Slope changes between line segments labelled A to D on Figure 5-30 and A to E on Figure 5-31 are thought to reflect changes in the number and amount of mineral phases that were fractionating from the the magma(s) which produced the rocks. Note that the range of Ni or Cr values included in each line segment labelled A to D on Figure 5-30 is equivalent to the range of values included in each of the similarly labelled line segments on Figure 5-31. Stippled areas on Figure 5-31 outline the two fields in which data from the Annieopsquotch Dykes plot (geochemical analyses in Dunning, 1984).

Segment A on Figures 5-30 and 5-31 is thought to reflect coprecipitation of olivine and Cr-spinel ± plagioclase. Peaking of the amount of Cr-spinel and olivine fractionation is suggested by segment B which shows an overall decrease in V with decreasing Cr and Ni. The general increase in V concentration with decreasing Cr and Ni as shown by segment C is probably indicative of the coprecipitation of olivine and plagioclase and presumably marks the reduction and then cessation of Cr-spinel precipitation. The continued reduction in Cr concentrations shown by segment C suggests that clinopyroxene is probably a fractionating phase at this point in the evolution of the magma (or magmas) that produced the Skidder Basalt rocks. However, the increase in overall V concentration shown by segment C suggests that fractionation of clinopyroxene was not extensive

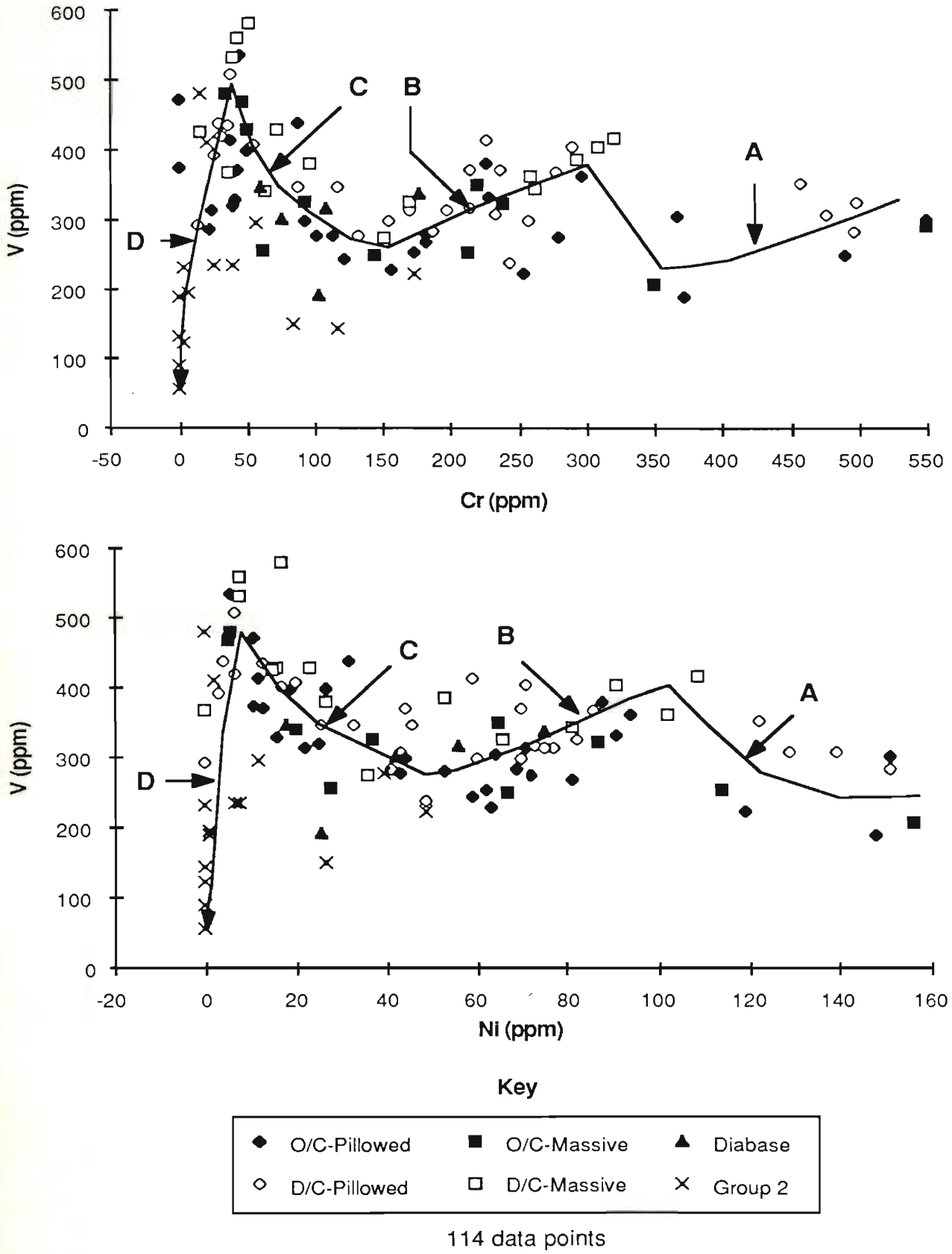

Figure 5-30: Vanadium plotted against Cr and Ni for the Skidder Basalt. Heavy lines are suggested "differentiation" trends. Line segments A, B, C and D are discussed in text.

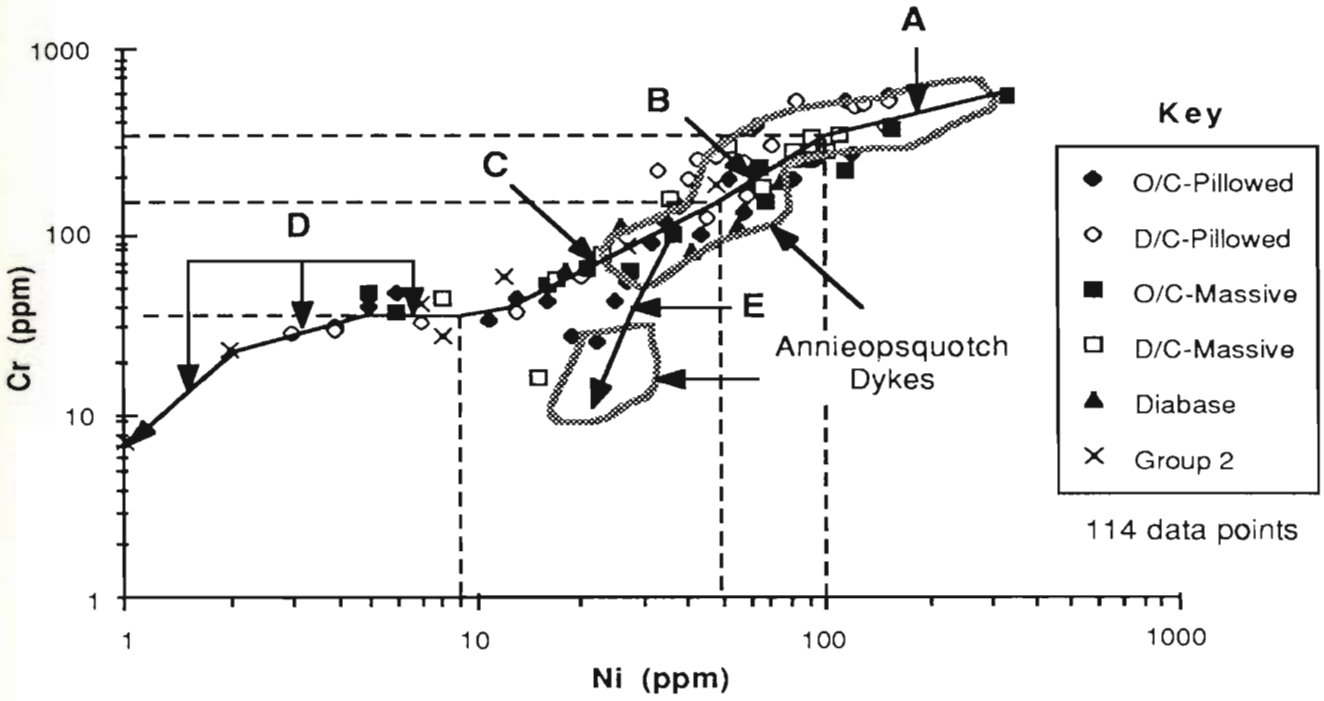

Figure 5-31: Cr vs. Ni plot for the Skidder Basalt. Heavy lines mark suggested "differentiation" trend. Line segments A, B, C and D, and the dashed lines mark the same ranges of Cr and Ni concentrations as on Figure 5-30. Stippled lines outline fields in which the Annieopsquotch diabase dykes plot (data from Dunning, 1984). Line segment E is discussed in text.

enough to prevent a buildup of V in the remaining magma or alternatively that an increase in f_{O_2} occurred thereby reducing the compatibility of V in clinopyroxene (Shervais, 1982). The marked reduction in V shown by Trend D defined mainly by Group 2 samples probably indicates more extensive fractionation of clinopyroxene and the onset of magnetite as a fractionating phase.

Trend E on Figure 5-31 defined by the Annieopsquotch Ophiolite dykes is a deviation from the Skidder Basalt trends and probably marks more extensive fractionation of clinopyroxene and a cessation of olivine precipitation in the magma that produced these rocks. Note that Skidder Basalt trends C and D on this diagram are subparallel to the Ni axis which further supports the suggestion made above, that fractionation of large amounts of clinopyroxene did not occur until late in the fractionation of the magma or magmas that produced the Skidder Basalt rocks.

5.2.11 Group 2 petrogenesis

Group 2 samples are characterized by: large variations in SiO_2, TiO_2, Fe_2O_3, P_2O_5 and V contents; high Na_2O, Zr and Y concentrations and; low MgO, CaO, Sr, Ni and Cr contents (Figures 5-3 to 5-9). The high total REE, Zr and Y concentrations and low Ni and Cr concentrations of the Group 2 samples suggest that they crystallized from a somewhat differentiated basaltic magma. Comparison of the rare-earth element patterns for the Group 2 samples and those of the other Skidder Basalt rocks (section 5.2.8) suggests that the Group 2 rocks are cogenetic with the others. Their variable TiO_2, Fe_2O_3, P_2O_5 and V contents suggest that accessory minerals such as magnetite and apatite were probably on the liquidus of the magma(s) from which they crystallized.

5.2.12 Comparison to ophiolite complexes

Spilitization, the presence of variolitic pillow lavas, the sparseness and smaller size of amygdules, the high magnetic susceptibility and tholeiitic chemistry distinguish the

Skidder Basalt from the Buchans Group basalts and illustrate its similarity to ophiolite pillow lava sequences, e.g. those of the Annieopsquotch (Dunning, 1984) and Bay of Islands Complexes (Malpas, 1976), and to pillow lavas of the ophiolitic Lushs Bight Group (Smitheringale, 1972; Strong, 1973; Kean, 1984). The ore metal content of the Skidder prospect, that is, copper and zinc and only a very minor amount of lead; and the occurrence of the prospect in basalts rather than felsic rocks further support an ophiolitic environment of formation. The presence of trondhjemite dykes and pods in the Skidder Basalt is also consistent with an ophiolitic environment.

Beccaluva et al. (1980) state that ophiolites such as the Troodos and Vourinos complexes, which plot in the island arc tholeiite field on trace element variation diagrams, have several characteristics in common. These complexes often contain lavas similar to boninites in that they have very low contents of Ti and the incompatible elements, and very high Cr and Ni concentrations. Coish and Church (1979) describe flows with similar characteristics in the Betts Cove ophiolite. Other effusive rocks present in these ophiolites are more depleted in the incompatible elements and compatible elements such as Cr and Ni than typical ocean floor tholeiites. Beccaluva et al. (1980) further state that the variation in the modal mineralogy of the Troodos and Vourinos ophiolitic rocks define a fractional crystallization order of Cr-spinel plus olivine, clinopyroxene, orthopyroxene, and then plagioclase, similar to that described for island arc tholeiites (Perfit et al., 1980). Miyashiro (1973) suggests that the Troodos ophiolite formed in an island arc environment and (Beccaluva et al., 1980) conclude that the Troodos and Vourinos ophiolites probably originated by "spreading processes above a subduction zone close to an intraoceanic converging plate margin".

According to Beccaluva et al. (1980) cumulus minerals in the gabbroic complexes and phenocryst phases in the lavas of the Northern Apennine Ophiolites, which have MORB-type chemistry, indicate a crystallization order of Cr-spinel plus olivine,

plagioclase, clinopyroxene, Ca-poor pyroxene, Fe-Ti oxides and finally apatite, similar to that suggested for MORB (cf. Bender et al., 1978; BVSP, 1981a).

The Skidder Basalt rocks have low concentrations of the large ion lithophile elements like Mid Ocean Ridge Basalts (MORB) and typically plot in the field of MORBS or overlap the MORB and island arc tholeiite fields on many trace element variation diagrams (section 5.2.7). The lack of lavas similar to boninites in the Skidder Basalt, and its indicated liquid line of descent, that is, Cr-spinel plus olivine ± plagioclase, olivine plus plagioclase, and late in the fractionating history, clinopyroxene plus magnetite and apatite suggest a greater similarity of the Skidder Basalt to MORB-type ophiolites. Pearce et al. (1984) conclude that ophiolites with MORB chemistry, which include the Macquarie Island (Griffin and Varne, 1980) and Bay of Islands ophiolites (Suen et al., 1979), may have formed in "incipient oceans, major oceans, leaky transforms" or in "back-arc basins".

Figure 5-32 compares the range of chondrite-normalized REE concentrations in the Skidder Basalt to that of several Newfoundland ophiolites. As shown, the range of Skidder Basalt REE, although extending to higher REE concentrations, overlaps that of the Annieopsquotch pillow lavas (Dunning, 1984), the Bay of Islands dykes and lavas (Suen et al., 1979) and the upper lavas of the Betts Cove ophiolite, but none of the Skidder Basalt samples show the extreme REE depletion characteristic of the Betts Cove lower lavas (Coish et al., 1982). The Annieopsquotch and Bay of Islands ophiolites are geochemically similar to N-type MORB (Dunning, 1984; Suen et al., 1979). The upper lavas of the Betts Cove ophiolite also have geochemical similarities to MORB, but the lower lavas are more similar geochemically to boninitic lavas (Coish et al., 1982).

Figure 5-33 compares the range of chondrite-normalized REE abundances in the Skidder Basalt to dykes and lavas of the Sarmiento ophiolite and metabasalts of the eastern Liguria ophiolite. With the exception of HREE depletion and slightly greater enrichment of the light REE, the range of REE abundances is similar in the Skidder Basalt to that of the eastern Liguria ophiolite, which is geochemically similar to MORB (Venturelli et al., 1981;

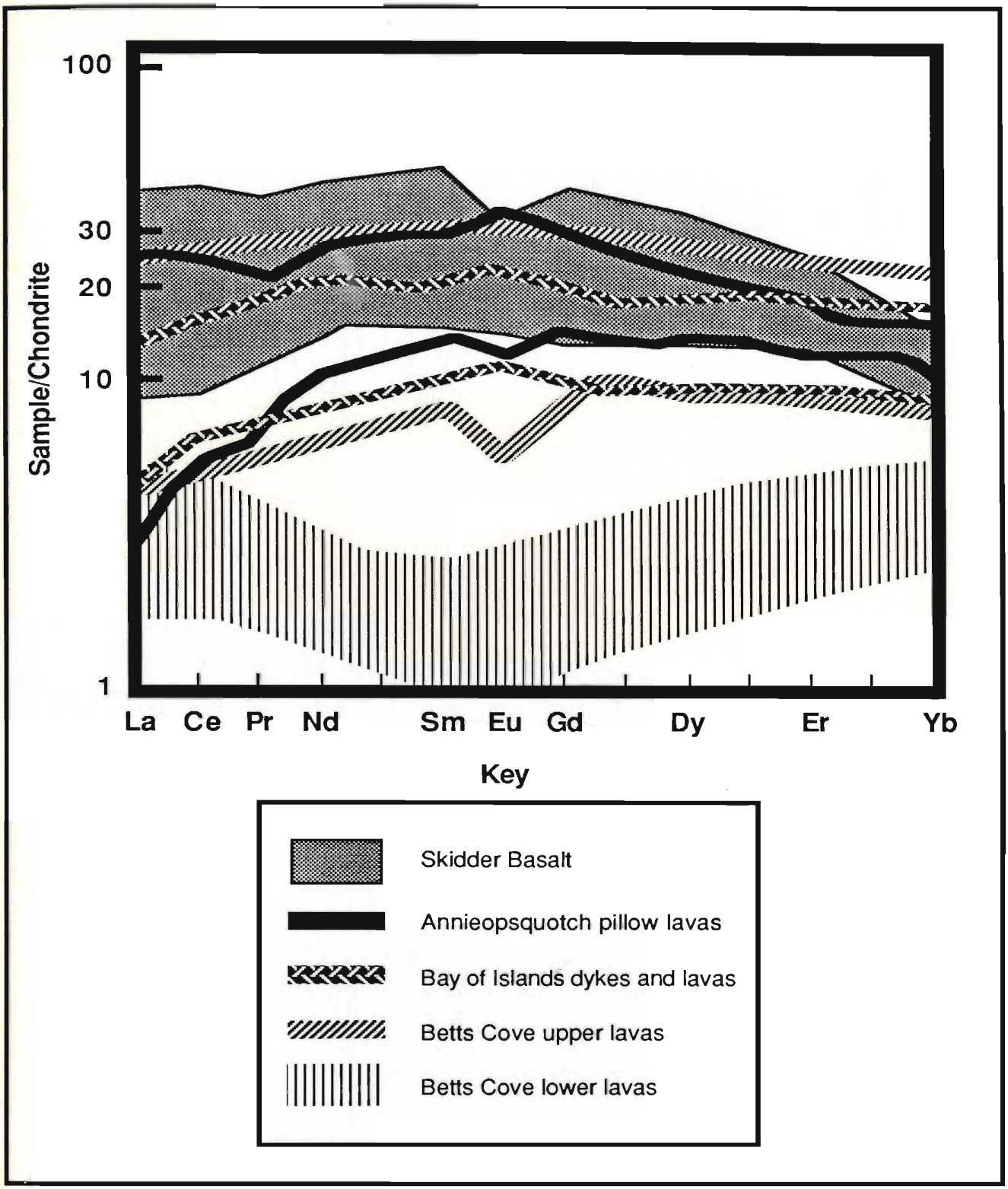

Figure 5-32: Range of chondrite-normalized rare-earth element abundances in the Skidder Basalt compared to that of the Annieopsquotch pillow lavas (Dunning, 1984); the Bay of Islands dykes and lavas (Suen et al., 1979); and the Betts Cove upper and lower lavas (Coish et al., 1982).

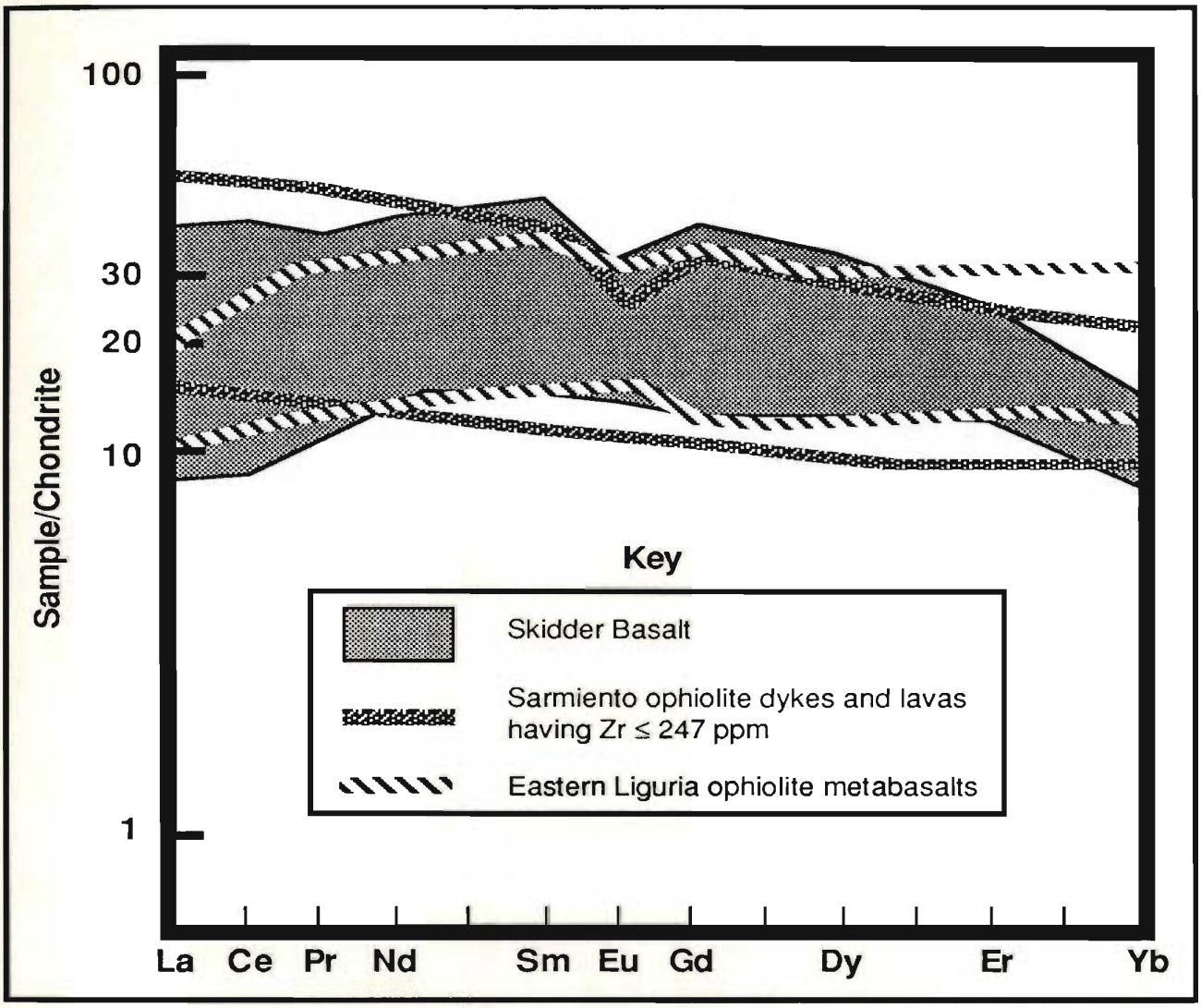

Figure 5-33: Range of chondrite-normalized rare-earth element abundances in the Skidder Basalt compared to that of dykes and lavas of the Sarmiento ophiolite (Stern, 1979), and that of metabasalts from the eastern Liguria ophiolite (Venturelli et al., 1981).

Pearce et al., 1984). The range of REE abundances in the Skidder Basalt is also similar to that of the dykes and lavas from the Sarmiento ophiolite (Figure 5-33), which formed in an Early Cretaceous extensional back arc basin (Stern, 1979). The Skidder samples, however, do not show as much LREE enrichment as those of the Sarmiento ophiolite. Intermediate icelandites and silicic dykes are present in the Sarmiento ophiolite. These rocks have higher Zr, Y and REE concentrations than the associated basalts, but have similar Ce/Yb ratios prompting Stern (1979) to suggest a cogenetic origin for the basalts, the icelandites and the silicic dykes (Stern, 1979). Ferro-gabbros in the Sarmiento ophiolite closely approximate in composition the calculated crystal extracts required to evolve ferro-basalts into icelandites and the more silicic differentiates (Stern, 1979). Stern (1979) indicates that the Sarmiento ophiolite is best modeled by a "magma chamber replenished only a limited number of times with a continuously decreasing volume of undifferentiated magma followed, subsequent to the last input of new parental magma, by closed system fractionation which results in the formation of ferro-basalts, icelandites and silicic differentiates".

The Skidder Basalt contains more rocks characteristic of differentiated basalt compositions and has lower average concentrations of incompatible elements than typical ocean floor basalts. Stern and de Wit (1980) state that these characteristics are typical of ophiolites formed at slow spreading ridges. They explain this by indicating that slow spreading ridges would probably have magma chambers that act as closed systems for longer periods of time than those at fast spreading centres where magma chambers would be constantly replenished with batches of primitive magma.

5.3 Geochemistry of the Skidder Trondhjemites

5.3.1 Introduction

Trondhjemite dykes intrude the Skidder Basalt in the vicinity of the Skidder Prospect and near the pyrite-rich zone at S 72 (Figures 3-3 and 3-4) about 2 km to the northeast. Also, a small body of trondhjemite (keratophyre (?)) intrudes or is interlayered with the Skidder Basalt in the northeastern portion of the map area (Figures 3-3 and 3-4). The trondhjemites are typically light grey-green, fine grained and massive to feldspar phyric. Rare, partially resorbed mafic xenoliths are incorporated into the trondhjemite dyke at S 10.

5.3.2 Major and trace element chemistry

Twelve analyses of trondhjemite dykes from the immediate area of the Skidder prospect are listed in Table 5-12. They comprise four outcrop samples and eight samples from the Skidder prospect drill core. Like the mafic rocks in the vicinity of the Skidder prospect massive sulphide deposit, several of these trondhjemites have been hydrothermally altered by the mineralizing event(s) (see Chapter 6). Several of the dykes contain fractures, vugs and grain interstices filled by quartz, chlorite or pyrite, or some combination of these minerals, and abundant disseminated pyrite occurs in samples SK 27 29, SK 30 51, SK 30 757 and SK 32 17. Also included in Table 5-12 are three analyses of the trondhjemitic pod exposed approximately two km northeast of the Skidder prospect and one sample of a trondhjemite dyke (?) (S 73) which occurs near the pyritized area at S 72 (Figure 3-3). The sample preparation and methods used for the trondhjemite analyses are described in Appendix B.

The rocks fit the geochemical definition of low Al_2O_3 (oceanic) type trondhjemites (Barker, 1979) for they contain: $\geq$ 68% SiO_2; $\approx$ 4-5% FeO + MgO; < 2% K_2O and; < 15% Al_2O_3. A Pearson correlation coefficient matrix for the Skidder trondhjemites is presented in Table 5-13 and selected X-Y plots are shown on Figures 5-34 and 5-35.

Table 5-12: Analyses of Skidder trondhjemite outcrop samples

	Trondhjemite Dykes					Trondhjemite Pod		
	Skidder Prospect Area							
weight %	S 2	S 4	S 10A	S 13B	S 73	S 67	S 68	S 69
SiO_2	77.40	80.20	75.60	76.10	80.00	80.00	67.90	76.90
TiO_2	0.09	0.11	0.22	0.44	0.28	0.21	0.43	0.28
Al_2O_3	11.40	10.10	11.40	10.80	10.00	10.20	14.60	11.50
Fe_2O_3*	3.06	3.01	3.21	2.76	2.61	1.86	5.32	2.04
MnO	0.03	0.06	0.05	0.03	0.02	0.02	0.06	0.02
MgO	0.60	0.69	1.12	1.00	0.59	0.36	1.35	0.39
CaO	0.04	0.25	0.46	0.73	0.10	0.13	0.89	0.14
Na_2O	5.83	5.08	5.78	5.50	4.76	4.03	4.66	5.89
K_2O	0.11	0.16	0.15	0.11	0.20	1.08	2.00	0.03
P_2O_5	0.06	0.03	0.06	0.09	0.11	0.02	0.05	0.05
LOI	0.85	1.01	1.20	1.14	0.87	0.89	2.38	0.62
Total	99.47	100.70	99.25	98.70	99.54	98.80	99.64	97.86
ppm								
Pb	1	6	1	2	3	0	7	7
Rb	2	4	2	4	1	20	35	2
Sr	22	26	31	54	21	19	48	23
Y	46	40	56	50	48	58	74	69
Zr	142	133	169	132	170	186	220	182
Nb	2	5	5	6	6	6	6	6
Zn	51	73	40	30	53	21	90	61
Cu	11	6	0	14	17	14	29	17
Ni	0	0	0	3	0	0	0	0
La	4	4	0	7	3	14	19	9
Ba	15	16	13	30	4	21	88	0
V	17	10	19	73	10	13	15	13
Ce	14	19	13	15	64	81	90	98
Cr	0	0	0	0	5	6	1	3
Ga	12	12	10	9	13	12	20	13

* Total iron as Fe_2O_3

Chondrite-normalizing values used are those of Taylor and Gorton (1977)

RARE-EARTH ELEMENT CONCENTRATIONS

	S 68	
	ppm	chondrite normalized
La	14.4	45.7
Ce	34.7	42.7
Nd	27.6	46.2
Sm	7.9	41.1
Eu	1.3	18.0
Gd	7.9	30.5
Dy	9.6	29.5
Er	5.4	25.4
Total	108.8	

Ratios (Chondrite Normalized)	
La/Ce	1.1
La/Sm	1.1
Eu/Eu*	0.5

Eu* = (Sm+Gd)/2

Table 5-12 (continued): Analyses of trondhjemite dykes from the Skidder Prospect drill core

weight %	SK 6 8	SK 27 25	SK 27 29	SK 29 45	SK 30 1	SK 30 757	SK 32 17
SiO_2	78.00	76.90	78.80	70.30	75.00	81.10	78.40
TiO_2	0.07	0.16	0.13	0.31	0.18	0.13	0.00
Al_2O_3	10.70	11.20	10.30	12.80	12.10	10.30	9.30
Fe_2O_3*	1.23	2.20	0.99	2.63	2.45	0.60	3.00
MnO	0.03	0.04	0.03	0.05	0.03	0.01	0.02
MgO	2.39	2.42	2.67	4.90	0.91	0.50	1.19
CaO	0.18	0.07	0.08	0.14	0.18	0.20	0.24
Na_2O	4.34	4.95	4.52	3.23	5.90	2.80	4.82
K_2O	0.54	0.10	0.09	1.73	0.97	1.81	0.06
P_2O_5	0.01	0.04	0.02	0.02	0.15	0.02	0.00
LOI	1.50	1.17	1.34	2.74	0.52	1.58	1.76
Total	98.99	99.25	98.97	98.85	98.39	99.05	98.79
ppm							
Pb	9	0	5	6	7	6	4
Rb	6	2	0	26	7	23	3
Sr	39	43	34	29	35	32	30
Y	53	46	50	54	49	47	49
Zr	162	163	167	211	199	170	145
Nb	5	7	4	8	6	7	6
Zn	36	67	34	72	31	54	38
Cu	14	18	17	12	19	24	13
Ni	0	0	0	0	0	0	0
La	28	5	15	18	14	11	8
Ba	104	19	25	144	86	156	5
V	15	23	14	20	17	19	12
Ce	125	77	73	84	110	84	77
Cr	5	10	4	0	8	12	4
Ga	13	12	9	17	14	12	12
Depth (feet)	143.0	379.5	444.0	691.0	11.0	757.0	523.0
Depth (metres)	43.6	115.7	135.3	210.6	3.4	230.7	159.4
Distance**	63.2	24.3	4.7	37.4	238.6	11.3	25.6

* Total iron as Fe_2O_3

** Distance from most intensely altered rocks in the drill hole

Chondrite-normalizing values used are those of Taylor and Gorton (1977)

RARE-EARTH ELEMENT CONCENTRATIONS

	SK 30 1	
	ppm	chondrite normalized
La	32.5	103.2
Ce	81.5	100.2
Nd	48.5	81.2
Sm	13.8	71.9
Eu	2.2	30.5
Gd	13.0	50.2
Dy	12.4	38.2
Er	5.5	25.8
Total	209.4	

Ratios (Chondrite Normalized)	
La/Ce	1.0
La/Sm	1.4
Eu/Eu*	0.5

Eu* = (Sm+Gd)/2

Table 5-13: Pearson correlation matrix for Skidder trondhjemites

Number of samples = 16

	SiO_2	TiO_2	Al_2O_3	Fe_2O_3*	MnO	MgO	CaO	Na_2O	K_2O	P_2O_5	LOI	Total	Pb	Rb	Sr	Y	Zr	Nb	Zn	Cu	Ni	Ba	V	Ce	Cr	Ga
SiO_2	1.00																									
TiO_2	-.59	1.00																								
Al_2O_3	-.93	.59	1.00																							
Fe_2O_3*	-.72	.44	.65	1.00																						
MnO	-.65	.23	.61	.68	1.00																					
MgO	-.48	.00	.28	.00	.36	1.00																				
CaO	-.49	.63	.42	.58	-.37	.00	1.00																			
Na_2O	.00	.00	.00	.39	.00	-.19	.00	1.00																		
K_2O	-.34	.18	.45	.00	.00	.00	.11	-.62	1.00																	
P_2O_5	.00	.35	.12	.16	.00	-.08	.00	.54	.00	1.00																
LOI	-.56	.00	.38	.17	.34	.66	.26	-.52	.56	-.41	1.00															
Total	.00	.00	.00	.34	.57	.00	.00	.00	.00	.00	.00	1.00														
Pb	.00	.00	.15	.00	.00	.00	.00	.00	.26	.00	.16	.00	1.00													
Rb	-.43	.32	.50	.00	.00	.00	.32	-.58	.96	.00	.64	.00	.07	1.00												
Sr	-.26	.28	.15	.00	.00	.00	.64	.00	.00	.00	.17	.00	.00	.00	1.00											
Y	-.52	.52	.56	.27	.00	.00	.42	.00	.28	.00	.10	-.26	.01	.43	.00	1.00										
Zr	-.60	.37	.68	.00	.00	.23	.00	.00	.70	.00	.34	-.04	.24	.66	.00	.64	1.00									
Nb	.00	.23	.00	.00	.00	.15	.00	-.45	.44	.00	.32	-.10	.00	.41	.00	.00	.39	1.00								
Zn	-.44	.17	.52	.44	.55	.00	.00	.00	.22	.00	.42	.40	.13	.33	.00	.05	.20	.00	1.00							
Cu	.00	.00	.00	.00	-.15	.00	.00	-.27	.50	.00	.00	.00	.21	.46	.26	.26	.39	.21	.00	1.00						
Ni	.00	.47	.00	.00	.00	.00	.48	.00	.00	.13	.00	.00	.00	.00	.53	.00	-.30	.00	.00	.00	1.00					
La	-.32	.00	.31	.00	.00	.44	.00	-.26	.46	.00	.41	.00	.63	.42	.00	.27	.45	.00	.00	.00	.00	1.00				
Ba	-.20	.00	.29	.00	.00	.36	.00	-.62	.82	.00	.55	.00	.51	.67	.06	.00	.44	.00	.00	.00	.00	.00	1.00			
V	.00	.49	.00	.00	.00	.00	.46	.00	.00	.15	.00	.00	.00	.00	.58	.00	-.15	.00	.00	.00	.00	.00	.00	1.00		
Ce	.00	.00	.00	-.19	-.18	.00	.00	-.29	.36	.00	.00	-.44	.54	.22	.00	.27	.55	.00	.00	.00	.00	.00	.00	.00	1.00	
Cr	.46	-.30	-.30	-.63	-.60	.00	-.32	-.36	.00	.00	.00	-.19	.00	.00	.00	.00	.00	.00	.00	.00	.00	.00	.00	.00	.00	1.00
Ga	-.69	.29	.73	.50	.35	.15	.12	.00	.67	.00	.54	.00	.41	.71	.00	.50	.74	.00	.00	.00	.00	.00	.00	.00	.00	.00

* Total iron as Fe_2O_3

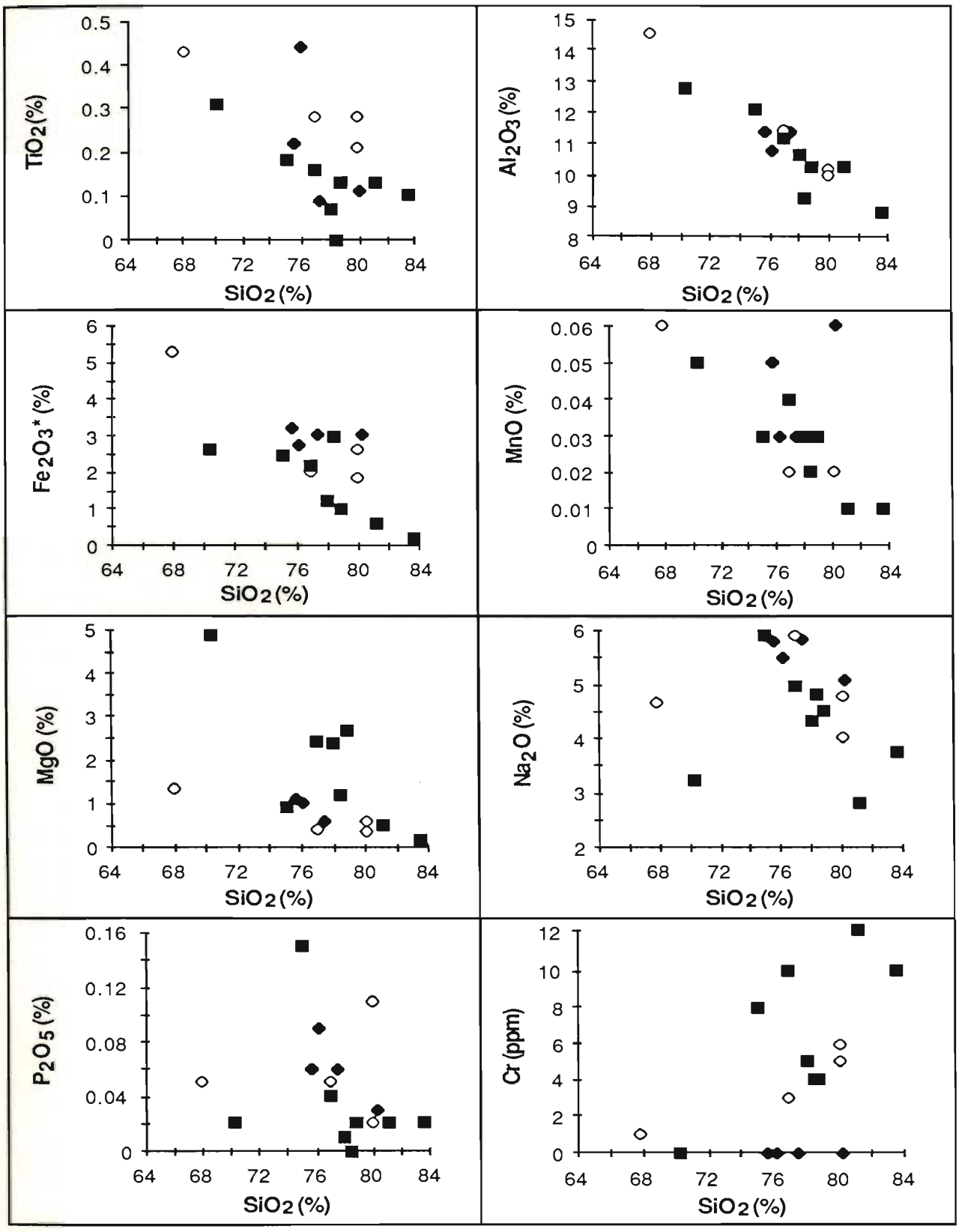

Figure 5-34: Element versus SiO_2 plots for Skidder trondhjemites.

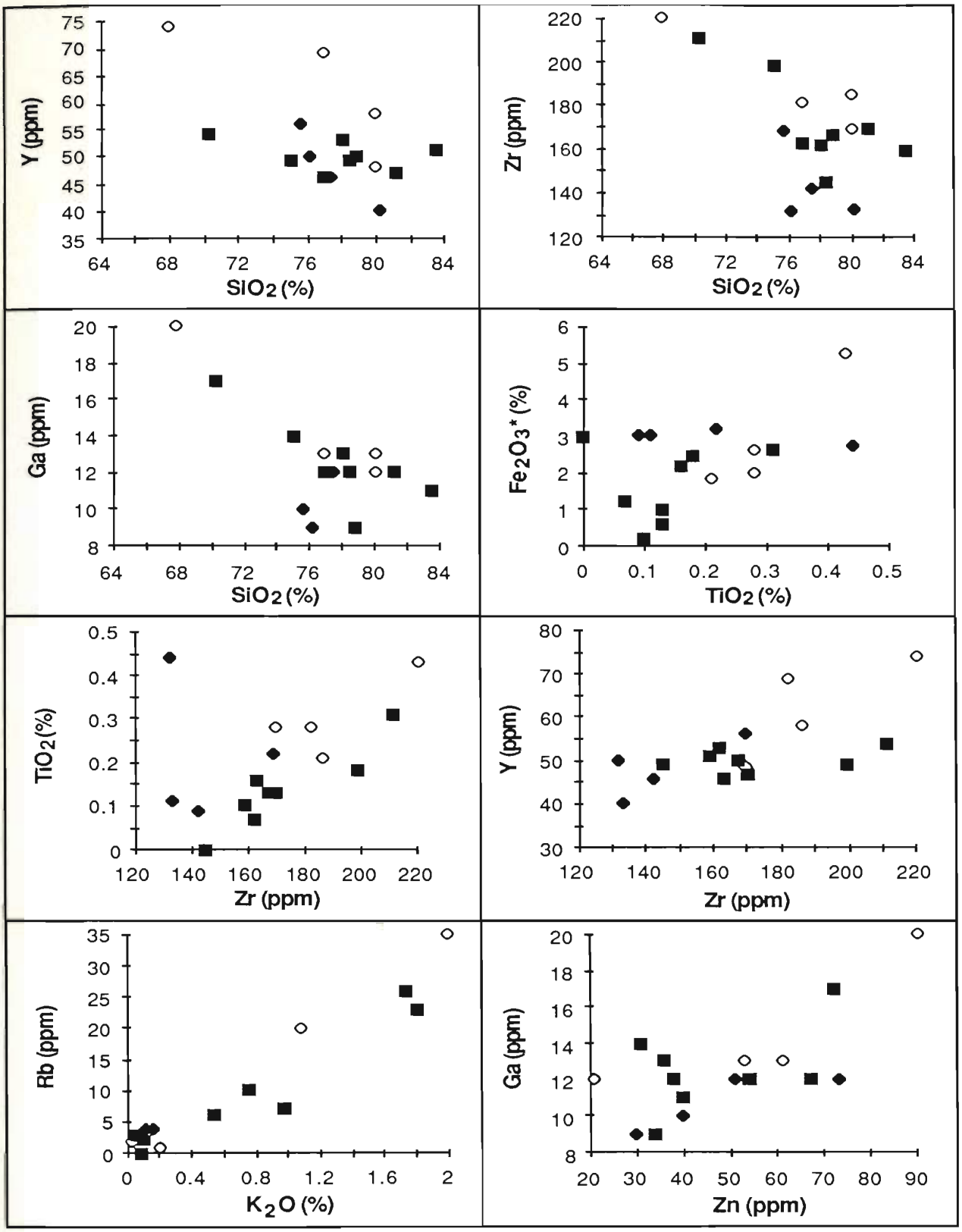

Figure 5-35: Miscellaneous X-Y plots for Skidder trondhjemites.

SiO_2 has a significant negative correlation with the other major oxides which, in turn, have positive correlations with each other (Table 5-13; Figures 5-34 and 5-35). These correlations are, in part, a result of the large amounts of SiO_2 present and the fixed total of 100%. However, the negative correlations of SiO_2 with major oxides such as TiO_2 and MnO, which are present in relatively small amounts, and with trace elements such as Zr and Y suggest that minor mineral phases, e.g. Fe-Ti oxides and zircon, fractionated from the trondhjemitic melt(s) (Table 5-13; Figures 5-34 and 5-35). Substitution of Rb and Ba for K and of Sr for Ca in minerals containing these elements is indicated by positive correlations between Rb, Ba and K_2O and between CaO and Sr.

The relatively high MgO contents of some trondhjemite dykes from the Skidder prospect drill core (Figure 5-34) are probably a result of hydrothermal alteration associated with formation of the massive sulphide deposit (see Chapter 6). Some of the trondhjemites from the Skidder prospect area also have slightly elevated Cr concentrations (Figure 5-34), which may also be due to hydrothermal alteration (??) or possibly wall rock contamination.

All but one of the Skidder trondhjemites plot in the trondhjemite field on the normative Ab-An-Or diagram according to the classification scheme of O'Connor (1965), the remaining sample plots as a granite (Figure 5-36). Most Skidder trondhjemites contain higher SiO_2 and lower Sr than the trondhjemites and granophyres from various tectonic settings presented on variation diagrams after Coleman and Peterman (1975) (Figure 5-37) and Coleman and Donato (1979) (Figure 5-38). The high SiO_2 content is probably partly due to greater differentiation of the magma which produced the Skidder trondhjemites relative to the others (see below) and possibly partly due to local introduction of silica as a result of hydrothermal alteration related to spilitization of the surrounding basalts and/or the Skidder prospect mineralizing event. The relatively low Sr concentrations of the Skidder trondhjemites is probably mainly due to hydrothermal alteration.

Many workers suggest that the low K_2O contents of oceanic plagiogranites cannot be fully explained by igneous processes and are probably a result of K removal due to

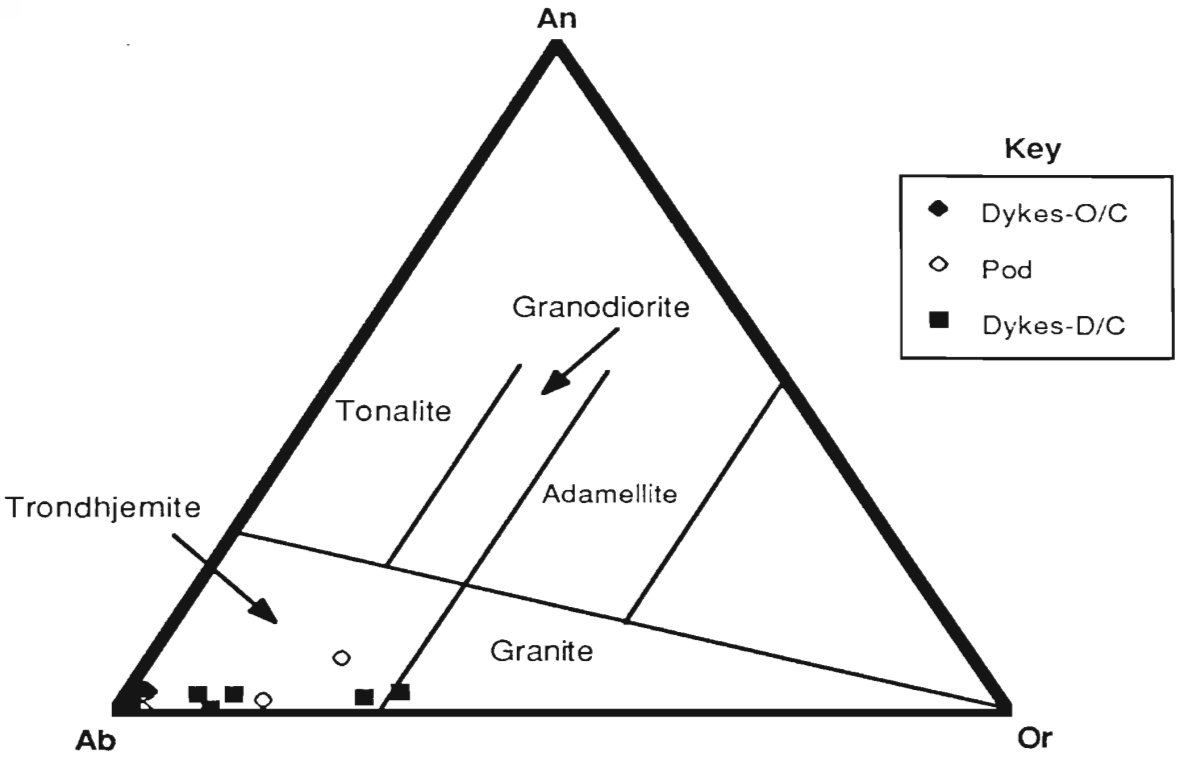

Figure 5-36: CIPW normative proportions of weight per cent albite, anorthite and orthoclase for the Skidder trondhjemites. The classification scheme is after O'Conner (1965).

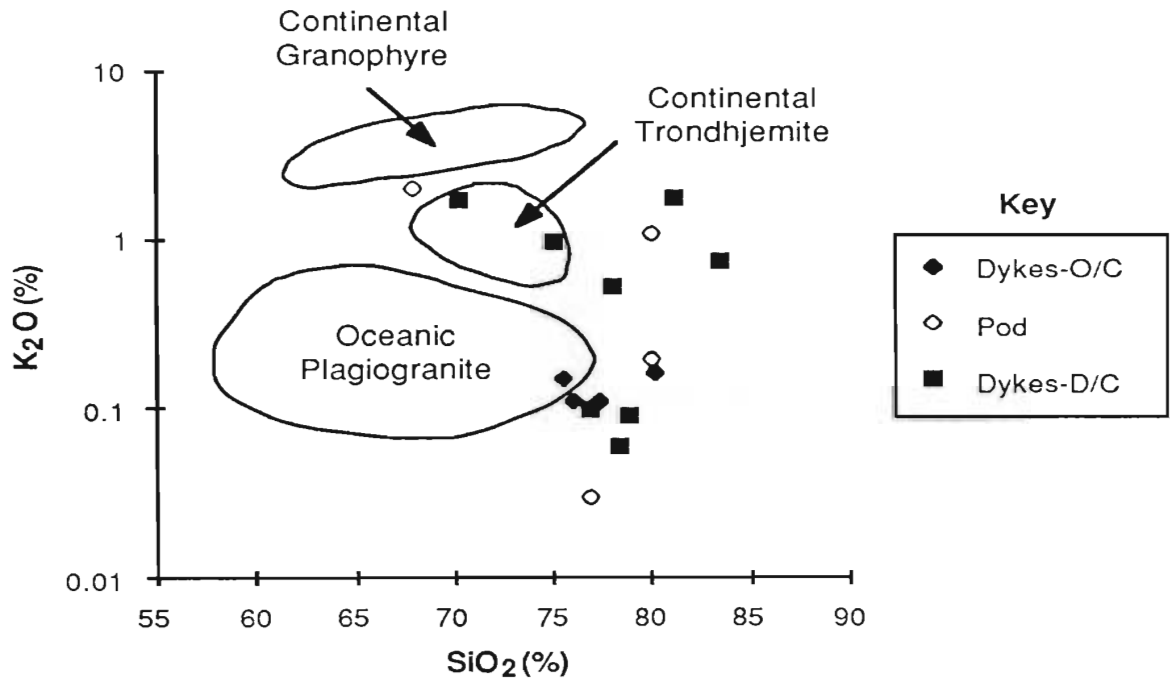

Figure 5-37: SiO_2-K_2O contents of Skidder trondhjemites compared to those of other rock suites (after Coleman and Peterman, 1975).

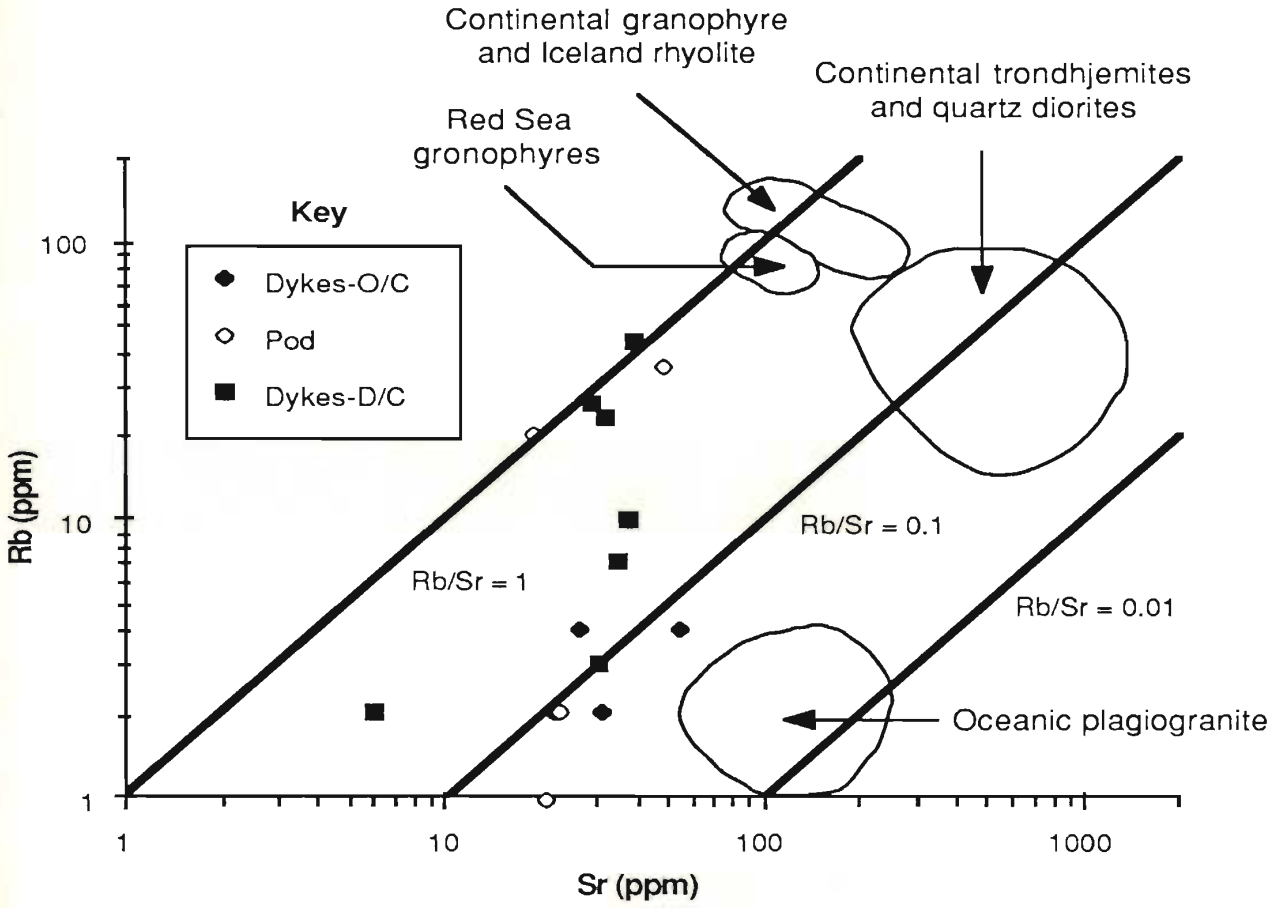

Figure 5-38: Rb/Sr variation diagram on which the Skidder trondhjemites are compared to silicic rocks from various tectonic settings (after Coleman and Donato, 1979).

interaction with hydrothermal fluids, specifically heated seawater (e.g. Coleman and Donato, 1979). The presence of hydrous phases in many ophiolite trondhjemites and late-stage gabbros, and the association of epidotite with some ophiolite trondhjemites has led some workers to postulate introduction of heated seawater into the magma from which the trondhjemites crystallized (e.g. Malpas, 1979; Sivell and Waterhouse, 1984a; Pederson and Malpas, 1984). They suggest that water saturation of the magma would result in development of a metasomatic fluid into which K, Rb and Ba would partition and be removed from the crystallizing magma. Coleman and Donato (1979) indicate that the higher K_2O and Rb contents of Iceland rhyolites and Red Sea granophyres probably better reflect the original contents of these elements from igneous processes since these rocks have not been exposed to heated seawater but have interacted with hydrothermal meteoric water, which is ineffective in removing K_2O and Rb from the rocks.

Rb and to a lesser extent K_2O contents in the Skidder trondhjemites roughly define mixing lines between the low contents characteristic of oceanic plagiogranites and the high contents typical of Iceland rhyolites and Red Sea granophyres (note however that the data is offset to higher SiO_2 and lower Sr contents) (Figure 5-37 and 5-38). While lack of interaction with seawater may explain the higher K_2O and Rb contents of some of the trondhjemite pod samples, the higher contents of these elements in some of the trondhjemite dykes from the Skidder prospect drill core suggest that addition of K_2O and Rb to the trondhjemites by interaction with upwelling hydrothermal fluids may provide a more appropriate explanation (see section 4.5.6).

Two contrasting origins have been proposed for low-Al_2O_3-type trondhjemites. For example, the Visnes plagiogranites, and trondhjemites in the Bay of Islands complex are thought to have formed by magmatic differentiation of basaltic magma (Malpas, 1979; Pederson and Malpas, 1984). In contrast, the East Karmoy trondhjemites are considered to have formed by partial melting of amphibolite (Pederson and Malpas, 1984), and the Little Port and Twillingate trondhjemites by partial melting of mafic tholeiites (amphibolites),

which are basement to, or occur at the base of, island arc sequences (Malpas, 1979; Payne and Strong, 1979). Pederson and Malpas (1984) noted that the Visnes and Karmoy trondhjemites can be distinguished by the higher concentrations of Y and Zr of the former. As shown in Table 5-14, the trondhjemites suggested to have formed by magmatic differentiation have higher average concentrations of Y and Zr than the trondhjemites considered to have formed by partial fusion. Skidder trondhjemites have significantly higher average Y concentration than the Little Port and Karmoy trondhjemites and have higher average Zr concentration than the Little Port and Twillingate trondhjemites. These features suggest that Skidder trondhjemites are more akin to those presumed to have formed by magmatic differentiation than those considered to have formed by partial fusion.

Figure 5-39 illustrates the relationship between the Skidder trondhjemites and the Skidder basalts on the basis of SiO_2 and Zr contents. Silica enrichment in basaltic magmas is typically ascribed to fractionation of Fe-Ti oxides (e.g. Dixon and Rutherford, 1979; Stern, 1979; Pederson and Malpas, 1984) but crystal fractionation alone cannot readily explain the gap in SiO_2 concentrations that is evident between the highest-SiO_2 Skidder Basalt compositions and the Skidder trondhjemites (Figure 5-39).

Dixon and Rutherford (1979) suggest that the gap in silica compositions between oceanic and ophiolite plagiogranites and associated basalts could be a result of liquid immiscibility processes. They demonstrated experimentally that extreme fractionation of basaltic liquid under low f_{O_2} conditions resulted in an Fe-enriched basaltic liquid that separated into immiscible silica-rich and Fe-rich liquids at 1010°C. They suggest that plagiogranites may be the solid equivalent of the silica-rich liquid but the crystalline equivalent of the Fe-enriched basic liquid has not been identified in mid-ocean ridge rocks or in ophiolites. Philpotts (1979) and others, however, have described occurrences of immiscible glasses in tholeiitic basalts. Philpotts (1982) showed that if immiscibility of an Fe-enriched basalt occurs at SiO_2 concentrations below 52 per cent, the felsic melt will be enriched in Na and that K will enter the mafic melt. This situation is reversed if

Table 5-14: Comparison of average Skidder trondhjemite to averages of other trondhjemites

	Trondhjemites suggested to have formed by magmatic differentiation			Trondhjemites suggested to have formed by partial fusion of amphibolites		
Name	Visnes Plagiogranites	Bay of Islands	Skidder Trondhjemites	Little Port Complex	East Karmoy	Twillingate
Reference	1	2		2	1	3
weight %	≥ 63% SiO_2	≥ 65% SiO_2				
SiO_2	73.50	75.06	77.26	71.42	76.40	74.45
TiO_2	0.32	0.20	0.20	0.23	0.17	0.22
Al_2O_3	12.64	13.10	10.97	13.56	13.19	13.02
FeO	0.48	1.33	-	2.09	0.47	-
Fe_2O_3	3.76	1.30	2.32*	0.81	0.49	2.62*
MnO	0.06	0.06	0.03	0.11	0.03	0.07
MgO	0.24	0.19	1.33	0.94	0.36	0.28
CaO	4.28	1.02	0.25	2.25	2.97	1.85
Na_2O	4.73	6.07	4.74	7.96	5.69	5.03
K_2O	0.13	0.72	0.62	0.70	0.27	0.47
P_2O_5	0.07	-	0.05	0.05	0.20	0.01
ppm						
Pb	-	1	4	3	-	3
Rb	-	8	9	12	-	10
Sr	233	80	33	129	77	97
Y	116	76	53	21	13	-
Zr	590	225	169	69	206	88
Nb	11	8	6	6	4	5
Zn	7	61	49	46	22	39
Cu	128	9	15	11	95	17
Ni	4	3	9	1	9	-
Ba	-	188	48	68	-	74
V	18	7	19	43	10	-
Cr	18	7	4	8	15	-
Ga	-	21	13	13	-	14
	N = 12	N = 3	N = 16	N = 10	N = 9	

1 Pederson and Malpas (1984)
2 Malpas (1979)
3 Payne and Strong (1979)

* Total iron as Fe_2O_3

N - number of samples

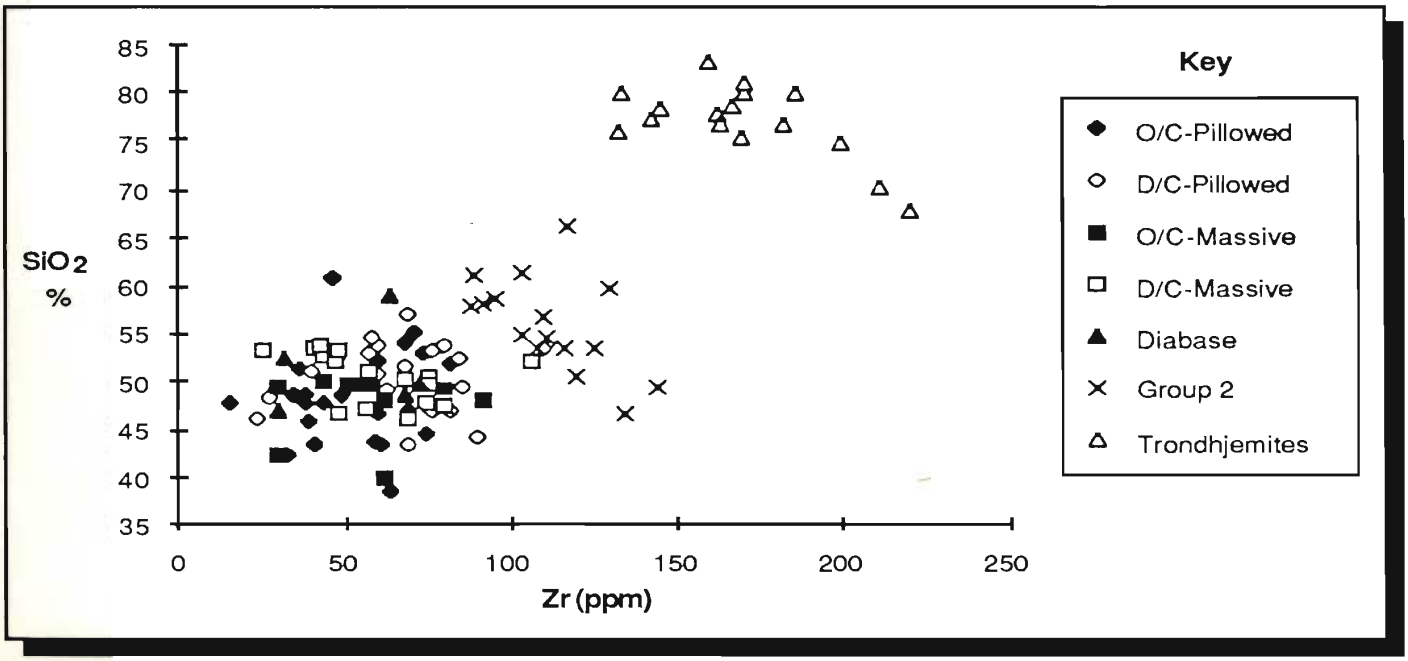

Figure 5-39: SiO_2 vs. Zr plot for Skidder area rocks.

immiscibility occurs at higher SiO_2 contents. Watson (1976) experimentally determined partition coefficients for several elements between immiscible mafic and felsic liquids in the system K_2O-Al_2O_3-FeO-SiO_2 at 1180°C and 1 atm. He found that P, Ca, Zr, Ti, Sr, Ba, Cr, Mn, Mg and the rare-earth elements all partition into the mafic melt. Thus, while major element contents of plagiogranites compare relatively well with those of the felsic portions of acid/basic immiscible liquid pairs (cf. Philpotts, 1982), experimentally determined partition coefficients for minor and trace elements between liquid immiscibility pairs (Watson, 1976) suggest that the felsic portion of an immiscible liquid would probably have lower minor and trace element concentrations than do plagiogranites (cf. Pederson and Malpas, 1984).

Pederson and Malpas (1984) suggest that magmatic differentiation involving filter pressing of differentiated interstitial liquids in gabbro provides an alternative to liquid immiscibility as an explanation for the gap in silica compositions between the Visnes plagiogranites and more mafic rocks of the Karmoy Ophiolite. The process involves crystallization under static magmatic conditions and lack of complete equilibrium between solid phases and the encompassing melt (Allègre and Minster, 1978; Pederson and Malpas, 1984)

Figure 5-40 shows that although Zr and Y reach higher concentrations in the trondhjemites, and have slightly higher Zr at a given Y concentration, no large gap exists between the highest-Zr and highest-Y Skidder basalts and the Skidder trondhjemites. Watson (1979) concluded that melts with molar ratios of $(Na_2O + K_2O) / Al_2O_3$ below 1.0 could become saturated with respect to zircon with less than 100 ppm Zr in the melt. Thus, zircon is probably a liquidus phase in a trondhjemitic melt and, if differentiation of the melt occurs, trondhjemites formed from early differentiates will probably contain more Zr than rocks formed from later differentiates of the melt. Zirconium and Y correlate negatively with SiO_2 in the Skidder trondhjemites (Table 5-13; Figure 5-39) suggesting that both were being removed from the melt which produced the trondhjemites. Vectors on Figure 5-40

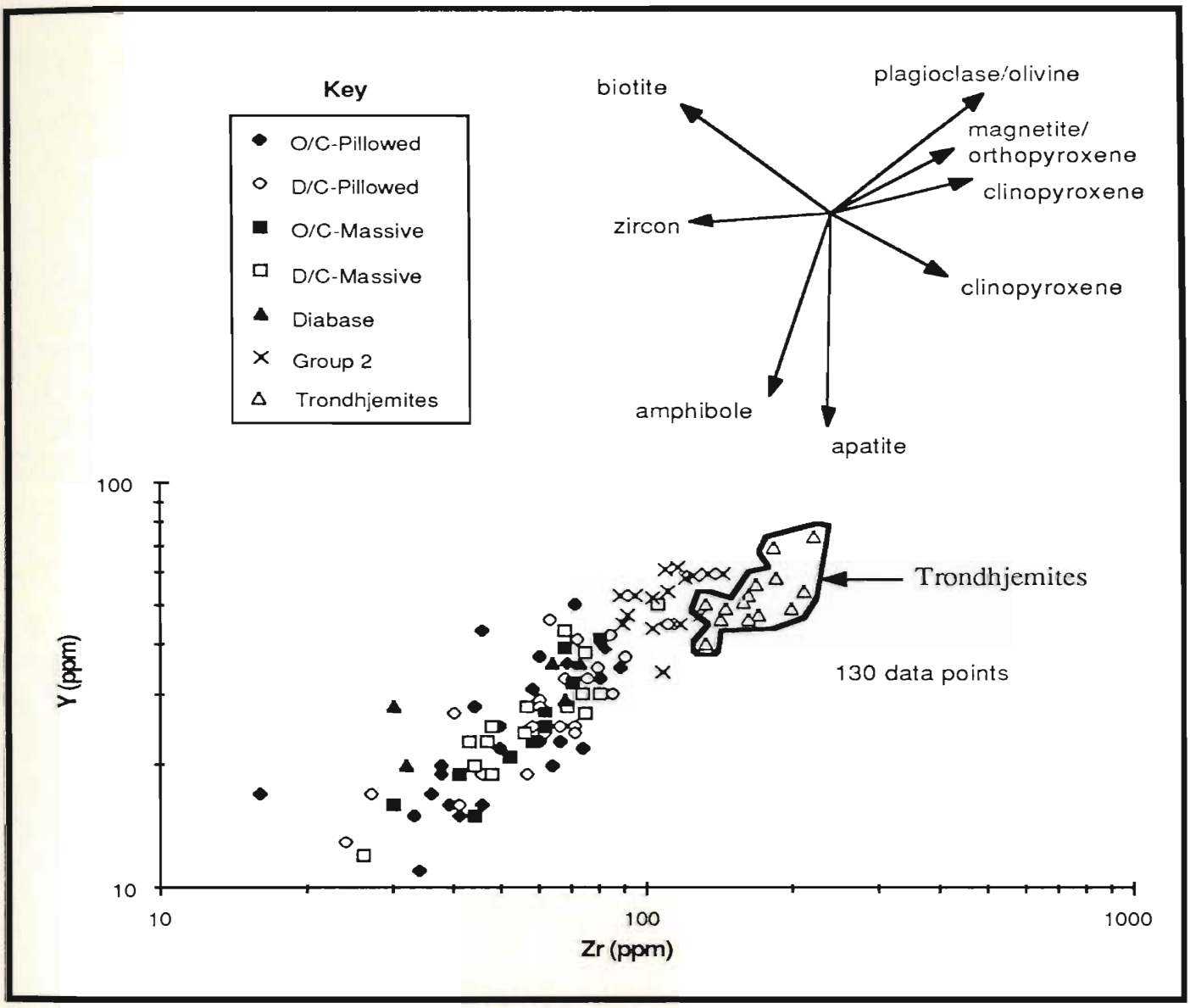

Figure 5-40: Zr vs. Y plot for the Skidder Basalt and Skidder trondhjemites. Vectors show the effects of fractionation of various minerals on the Zr/Y ratio (after Pearce and Norry, 1979).

show that fractionation of amphibole and/or apatite followed by zircon plus amphibole and/or apatite would produce the suggested trend to lower Zr and Y concentrations with increasing differentiation. With the exception of two samples, P_2O_5 shows a rough negative correlation with SiO_2 (Figure 5-34) supporting the suggested fractionation of apatite. Greater differentiation of the trondhjemitic melt accompanied by zircon and apatite ± amphibole fractionation provides one explanation for the slightly lower average Zr and Y concentrations of the Skidder trondhjemites compared to those of the Bay of Islands ophiolite and the significantly lower contents of these elements in the Skidder and Bay of Islands trondhjemites when compared to the Visnes plagiogranites.

Pederson and Malpas (1984) note that, on the basis of Zr-Y concentration, the Visnes plagiogranites, considered by them to be magmatic differentiates, lie on a Raleigh fractionation trend from more mafic members of the ophiolite; but that the anatectic East Karmoy plagiogranites are relatively depleted in Y and lie away from this trend (Figure 5-41). The Skidder trondhjemites have lower Zr and Y concentrations than the Visnes plagiogranites but do plot on the suggested Raleigh fractionation trend, occupying an intermediate position between the gabbros and the biotite diorites, which are intimately associated with the Visnes plagiogranites in some areas (Pederson and Malpas, 1984). In fact, fractionation of minor phases with which Zr and Y are compatible from a magma of similar composition to that which produced the biotite diorites could produce the trend shown by the Skidder trondhjemites.

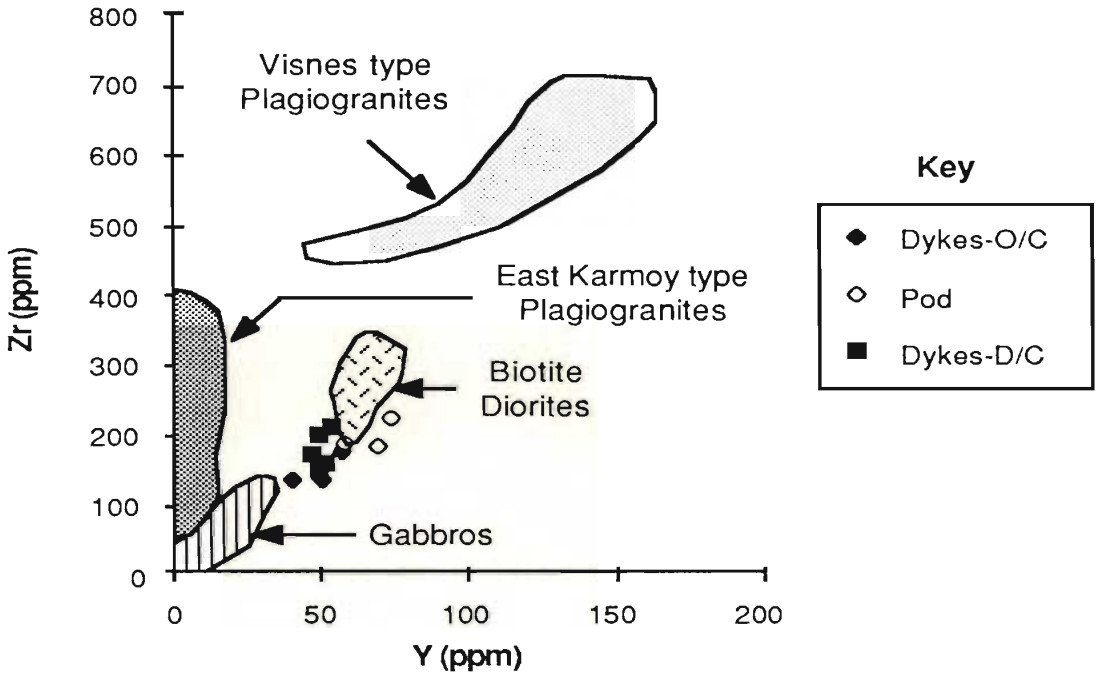

Figure 5-41: Zr and Y concentrations of the Skidder trondhjemites compared to rock suites from the Karmoy ophiolite (after Pederson and Malpas, 1984).

5.3.3 Rare-earth element chemistry

Rare-earth element (REE) patterns for two Skidder trondhjemites are presented on Figure 5-42. The rare-earth element concentrations (listed in Table 5-12) were determined using the thin film method of Fryer (1977) (see Appendix D). Sample S 68 is from the trondhjemite pod, and sample SK 30 1 is of a relatively unaltered trondhjemite dyke from the Skidder prospect drill core. The patterns are flat to slightly light rare-earth element enriched and have negative Eu anomalies. Rare-earth element concentrations for sample S 68 and the heavy REE concentrations of sample SK 30 1 generally overlap the range of REE concentrations for the high-Zr Skidder Basalt samples; but SK 30 1 has significantly higher light REE concentrations than the high-Zr Skidder Basalt samples and trondhjemite sample S 68.

On Figure 5-43, REE patterns for the Skidder trondhjemites are compared to silica-rich rocks from the Mid Atlantic Ridge and East Pacific Rise, and to ophiolite plagiogranites. The Skidder trondhjemites have total REE concentrations approximately equivalent to those of the quartz diorite from the Mid Atlantic Ridge, and their pattern of light REE enrichment is similar to, but less pronounced than that of the quartz diorite. The Skidder trondhjemites have overall REE abundances less than the high-silica glass from the East Pacific Rise and do not show the light REE depletion which characterizes this sample. The REE patterns for the Skidder trondhjemites overlap those of the Semail and Visnes plagiogranites, but the Semail and Visnes plagiogranites do not show slight light REE enrichment, which is characteristic of Skidder trondhjemite sample SK 30 1. The Skidder trondhjemites are significantly more REE enriched than the anatectic East Karmoy plagiogranites, and the negative Eu anomalies shown by the Skidder trondhjemites contrast with the positive Eu anomalies shown by the East Karmoy trondhjemites.

Zircon preferentially incorporates the heavy REE, having a mineral/melt distribution coefficient of 400 for Lu, but having mineral/melt distribution coefficients of only 10 to 20 for the light REE (Henderson, 1984). Hornblende also preferentially incorporates the

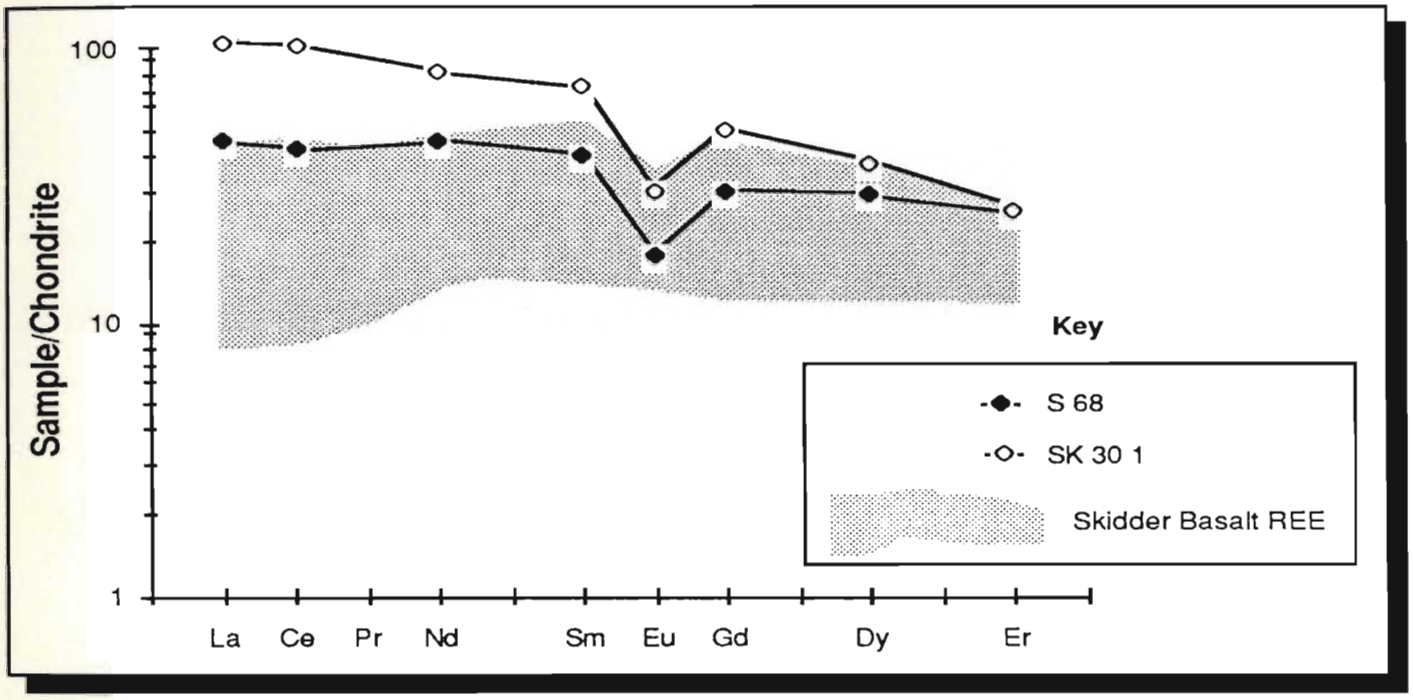

Figure 5-42: Chondrite-normalized (Taylor and Gorton, 1977) rare-earth element patterns for the Skidder trondhjemites. Range of Skidder Basalt REE concentrations shown for comparison.

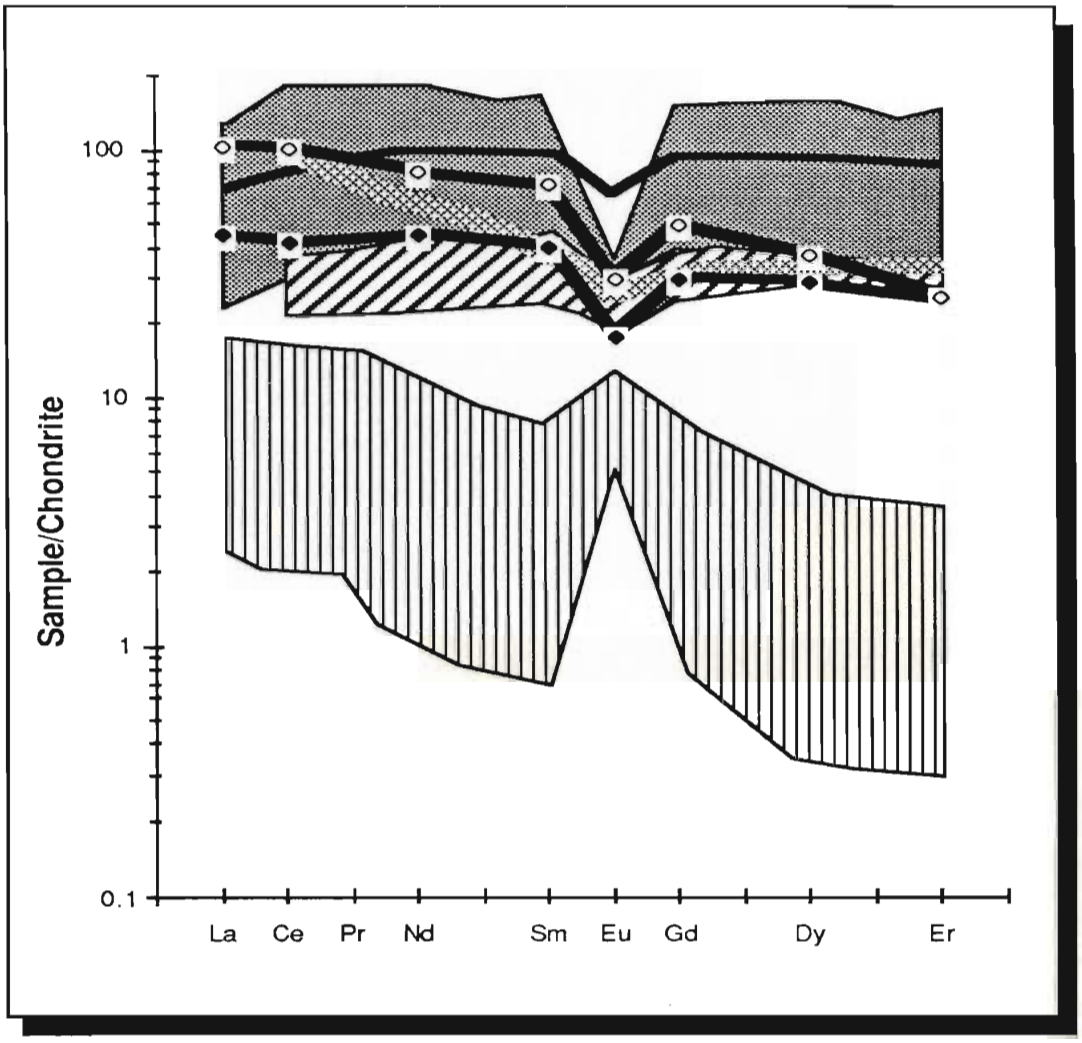

Key

Skidder trondhjemites
S 68
SK 30 1

High-silica glass
EPR 5° N (Kay et al. 1970)

Quartz diorite MAR 45' N
(Pederson and Malpas, 1984)

Semail plagiogranites
(Pederson and Malpas, 1984)

Visnes type plagiogranite
(Pederson and Malpas, 1984)

East Karmoy type
plagiogranite (Pederson
and Malpas, 1984)

Figure 5-43: Chondrite-normalized rare-earth element patterns for the Skidder trondhjemites compared to those of mid-ocean ridge silicic rocks and ophiolite plagiogranites.

heavy REE, but has much lower mineral/melt distribution coefficients, ranging from about 4-7 for the middle and heavy REE to about 1 for the light REE (Arth and Barker, 1976). Pederson and Malpas (1984) showed that, by using a two-stage process, the flat REE patterns of the Visnes plagiogranites could be produced from a light-REE-depleted, highly evolved basalt. The first stage involves removal of plagioclase and clinopyroxene from the melt, and the second involves fractionation of appropriate amounts of plagioclase, hornblende, Fe-Ti oxides, apatite and zircon. Similarly, it is suggested that the REE pattern shown by Skidder trondhjemite S 68 could be produced from evolved basalt by fractionation of appropriate amounts of these minerals. Sample SK 30 1 has higher overall REE concentrations, a lower Zr concentration, and shows relative light REE depletion relative to S 68. Fractionation of an appropriate amount of zircon from a magma of similar composition to that which produced S 68 could result in the lower Zr concentration and the relatively light-REE-enriched pattern of the magma from which SK 30 1 crystallized. The higher P_2O_5 content of SK 30 1 relative to S 68 suggests that although apatite may have been a fractionating phase in the trondhjemitic magma, not enough was removed to deplete the magma in either P or the REE.

5.4 Conclusions

The Skidder Basalt comprises a spilitized, tholeiitic, sub-alkaline, assemblage of basaltic pillow lava, pillow breccia and massive flows; accompanied by lesser amounts of mafic pyroclastic rocks and chert. Spilitization of the rocks has resulted in redistribution of SiO_2 and total iron, removal of K_2O and MgO, and extensive addition of Na_2O. The Skidder Basalt rocks define tholeiitic trends and typically plot within the ocean floor basalt field or overlap the ocean floor basalt and island arc tholeiite fields on trace element variation diagrams. (Chemistry of Skidder Basalt clinopyroxenes and chromites suggest it has greater similarity to MORB than to island arc tholeiites (Chapter 4)). The suggested paragenesis of the Skidder Basalt is olivine + Cr-spinel ± plagioclase, olivine + plagioclase and, late in the crystallization history, clinopyroxene + plagioclase + magnetite + apatite. The Skidder Basalt is geologically and geochemically more similar to the pillow lava sections of ophiolite complexes than to the Buchans Group basalts. It probably formed in an extensional tectonic environment at a slow spreading oceanic or back arc basin ridge[1].

Low-Al_2O_3 oceanic-type trondhjemite dykes and pods intrude or are interlayered with the Skidder Basalt in places. They are chemically similar to trondhjemites considered to represent late magmatic differentiates of basaltic magma.

---

[1] Re-analysis of a selected number of the Skidder Basalt samples by G. Jenner using the ICP-MS analytical technique, which provides more accurate Nb results than the X-ray fluorescence spectrometry method used in this study, showed that some of the Skidder Basalt samples are depleted in Nb, a characteristic of island arc tholeiites, others, however, are not depleted in Nb and are similar to MORB (G. Jenner, personal communication, 1988).

Chapter 6

GEOLOGY, ORE PETROLOGY AND LITHOGEOCHEMISTRY OF THE SKIDDER PROSPECT

6.1 Introduction

The Skidder Prospect, located approximately 12 km south-southwest of the town of Buchans, is a volcanogenic massive sulphide deposit hosted within mafic volcanic rocks of the Skidder Basalt (Figures 1-1, 3-1, 3-3 and 3-4). The prospect was discovered in 1971 by ASARCO Incorporated, and later outlined by information from 7795 m of drill core from 38 diamond drill holes drilled in the immediate area. The drilling was done by ASARCO Incorporated between 1971 and 1975, and by Abitibi Price Incorporated, in a joint venture with ASARCO Incorporated, during 1976 and 1977. The total probable and possible reserves for the prospect are approximately 900 000 tonnes, grading about 2% Cu and 2% Zn (Barbour, 1977). The reserves also include minor amounts of Pb and Ag (Barbour, 1977).

During the summer of 1983, the author carried out detailed geological mapping in the vicinity of the prospect, and relogged approximately 50 per cent of the drill core.

6.2 Local Geology

6.2.1 Introduction

The massive and disseminated sulphides comprising the Skidder Prospect are hosted within basaltic pillow lavas, mafic pillow breccias and aquagene tuffs of the Skidder Basalt (Figures 3-3 and 3-4). Outcrop sample locations, vertical projections of the diamond drill holes, and vertical projections of the Skidder Prospect two main semimassive to massive sulphide-bearing lenses (Lenses 1 and 2) are shown on Figure 6-1. A detailed geological compilation map of the Skidder Prospect area is presented as Figure 6-2. The distribution of units on Figure 6-2 has been determined on the basis of outcrop

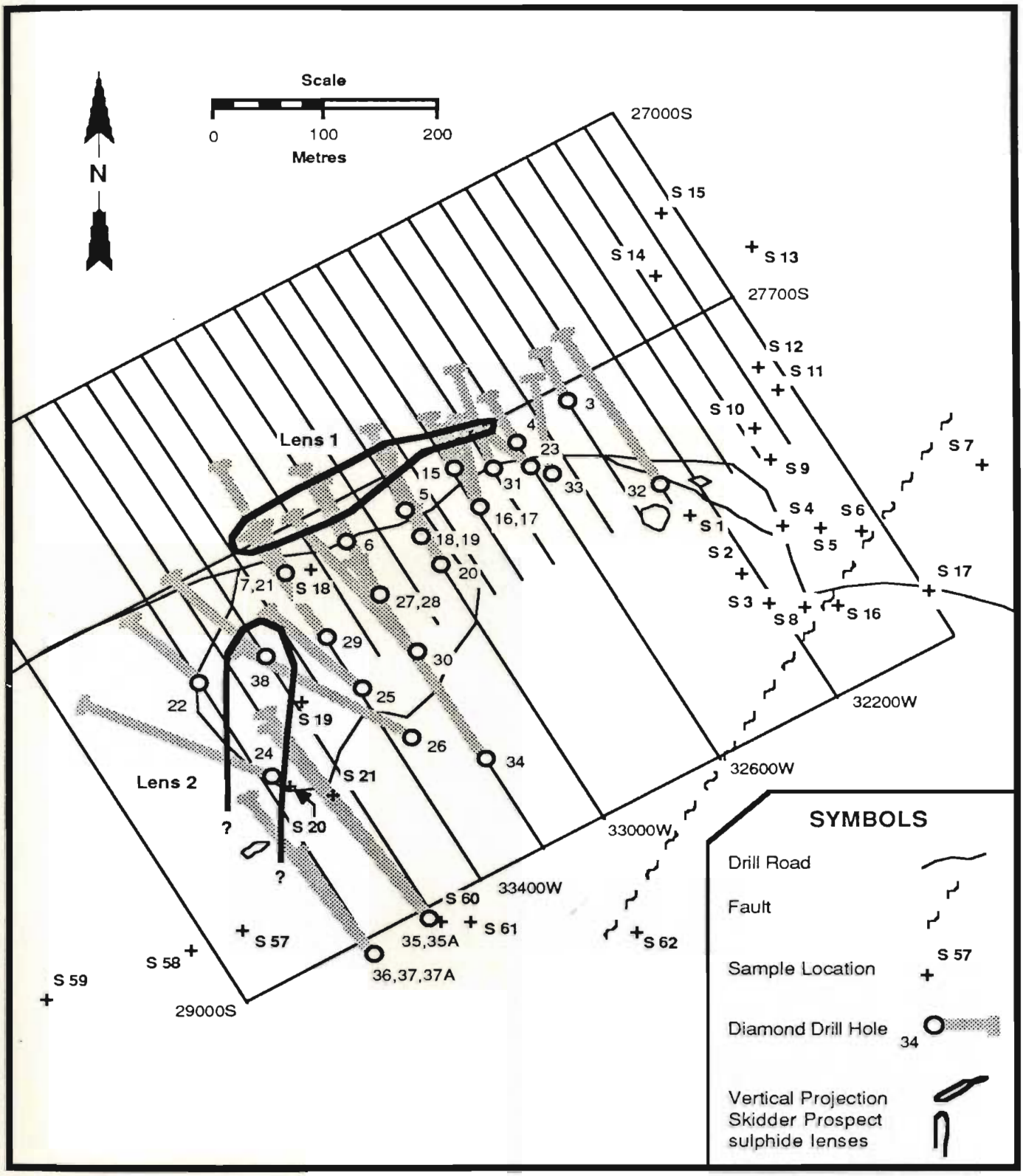

Figure 6-1: Detailed sample location map of the Skidder Prospect area. Location of drill holes and vertical projection of massive sulphide lenses after ASARCO-Price (1977).

LEGEND

ORDOVICIAN

SKIDDER BASALT

Pillowed and massive basalt; pillow breccia; lesser diabase dykes, gabbro, trondhjemite, mafic tuff and jasper

3 Pillowed and massive basalt having Zr concentrations ≥ 85 ppm

2 Pillowed and massive basalt having Zr concentrations > 50 < 85 ppm

1v Variolitic pillowed basalt

1 Pillowed and massive basalt having Zr concentrations ≤ 50 ppm

---

SYMBOLS

Drill Road

Outcrop visited

Geological unit; contacts approximate or assumed

Trondhjemite dyke

Strike and dip of pillows: (tops known, inclined; dip unknown) (tops unknown)

Bedding: (tops known, overturned) (tops unknown, inclined)

Foliation: (inclined, dip unknown)

Quartz Vein:

Fault

Diamond Drill Hole:

Vertical projection to surface of Skidder Prospect massive sulphide lenses

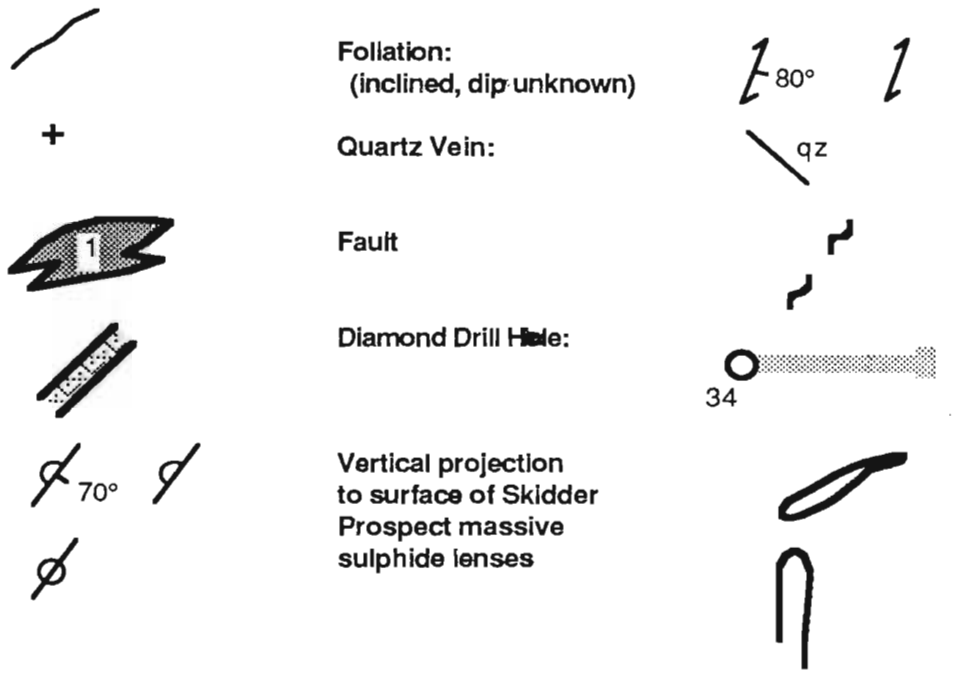

Legend and symbols to accompany Figure 6-2.

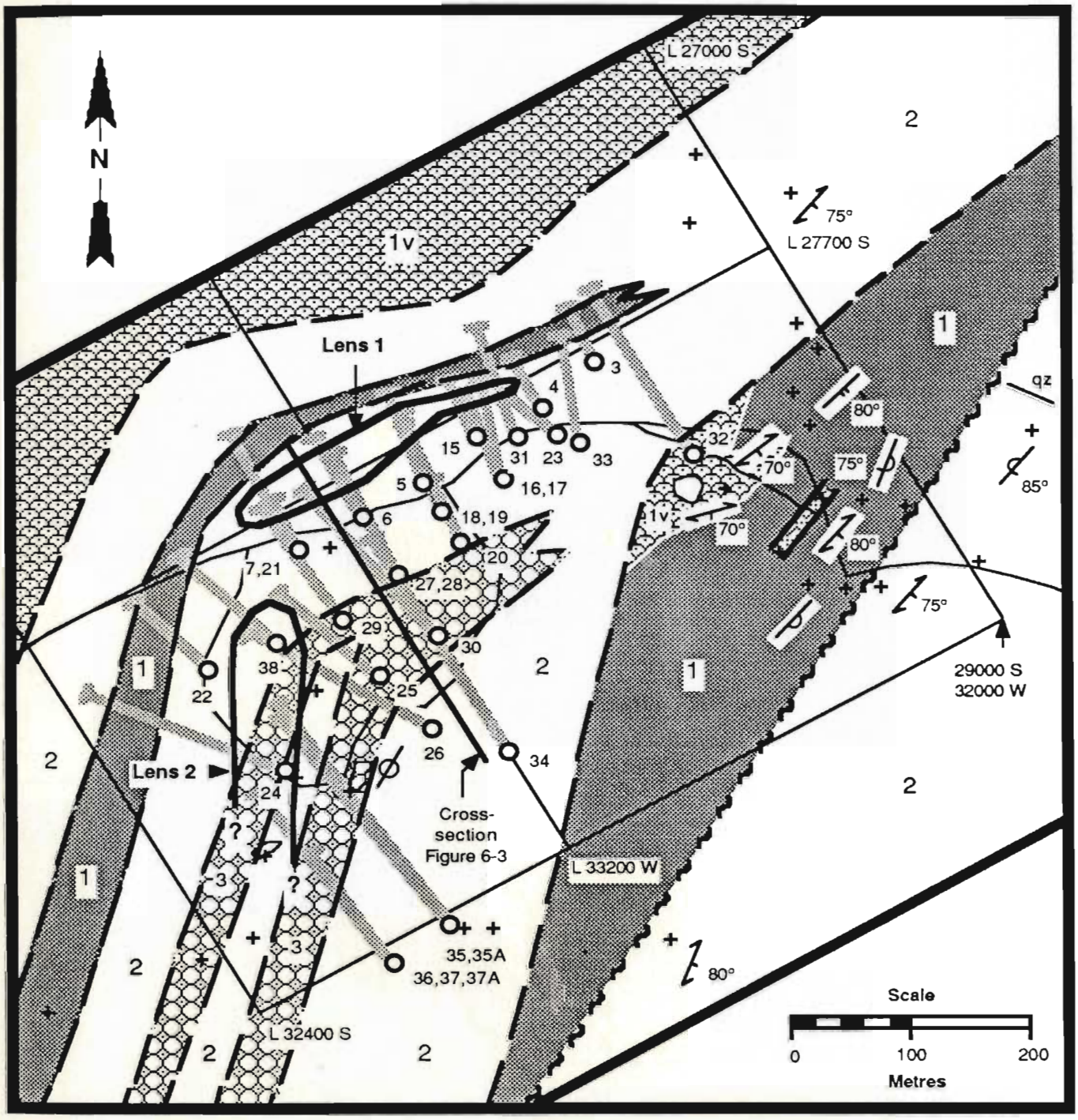

Figure 6-2: Detailed geological compilation map of the Skidder Prospect area. Location of drill holes and vertical projection of massive sulphide lenses after ASARCO-Price (1977). Legend on facing page.

observations and the projection of geological units to surface from those observed in drill core. In the vicinity of the Skidder Prospect, subdividing the Skidder Basalt into geological units is difficult since the various rock units, i.e. pillowed basalt and lesser amounts of mafic pillow breccias and aquagene tuffs, are interlayered. Thus, with the exception of distinctive variolitic pillowed basalt units, subdivisions of the mafic rock units on Figure 6-2 are based on their Zr concentrations (geochemical analyses are presented in Appendix B).

As shown below, variolitic pillowed basalts are spatially associated with sulphide-rich units of the Skidder Prospect. These basalts, projected to surface, comprise the variolitic pillow basalt unit shown in the northwestern portion of Figure 6-2. The variolitic pillowed basalts typically have Zr concentrations less than 60 ppm (see Section 6.10.1). Outcrops of variolitic pillow basalt also make up a portion of the low-Zr (< 50 ppm) basalt unit in the central-eastern portion of Figure 6-2. Most of the nonvariolitic basalts in the area have intermediate Zr concentrations. Exceptions are: a low-Zr basalt unit and a high-Zr (> 85 ppm) basalt/andesite unit in the central portion of Figure 6-2; and a low-Zr basalt unit located in its central portion.

Drill log sections for the diamond drill holes relogged by the author are presented in Figures 6-3 to 6-10, including a cross-section through the prospect along Line 33200 west (Figure 6-3) (see Figure 6-2 for location of cross-section). Patterns shown along the right side of the drill holes represent the different rock units, while those along the left side of the holes indicate the alteration secondary mineral assemblages; Zr concentrations of analyzed core samples are also indicated.

An attempt has been made to texturally subdivide the Skidder Basalt into three units on Figure 6-3. Underlying the semimassive and massive sulphide units of Lens 1 are at least 200 m of variolitic pillowed basalts. A 160 m-thick package of nonvariolitic pillowed basalt interlayered with massive basalt overlies the semimassive and massive sulphide-bearing units (see drill holes SK 27 and 28, Figure 6-3b). This package is, in turn,

overlain by mafic isolated pillow breccia (Carlisle, 1963), lesser massive basalt and/or diabase dykes, and minor pillowed basalt. The drill section for SK 29 (Figure 6-4) shows a similar sequence of units. In drill hole SK 31 (Figure 6-5) semimassive layered pyrite is interlayered with fine grained black chlorite-talc tuff.

Drill holes SK 35 and SK 37 (Figures 6-8 and 6-9) intersected semimassive and massive sulphides of Lens 2 (Barbour, 1977). Pillowed to massive basalt and very fine grained chlorite-talc tuff immediately underlie the sulphide-bearing zones in these two drill holes. Variolitic pillowed basalt and lesser massive basalt overlie the sulphide-bearing zones. Variolitic pillows are noted up to 100 m above the sulphides in SK 37A and up to 200 m above in SK 35. The variolitic pillowed basalt is overlain by interlayered nonvariolitic pillowed and massive basalt.

Trondhjemite dykes cut all units.

LEGEND

Geology

- Pillowed basalt, lesser mafic pillow breccia
- Mafic pillow breccia
- Massive basalt, diabase dykes (?)
- Diabase dyke
- Mafic tuff
- Semimassive sulphides
- M — Semimassive to massive sulphides
- T — Trondhjemite dyke
- Jasper

Alteration Mineral Assemblages

- chlorite, calcite, epidote ± hematite
- chlorite, calcite, epidote, quartz
- chlorite, quartz, calcite
- chlorite, quartz, pyrite
- quartz, chlorite, pyrite
- quartz, pyrite ± chlorite

SYMBOLS

Geological contact (Figure 6-3)

Alteration mineral assemblage boundary (Figure 6-3)

Note:

Some sample locations for drill holes SK 27, 28 and 30 not preceded by drill hole number due to lack of space.
Zr concentrations on a portion of Figure 6-8 are included in bold type in brackets following sample number.

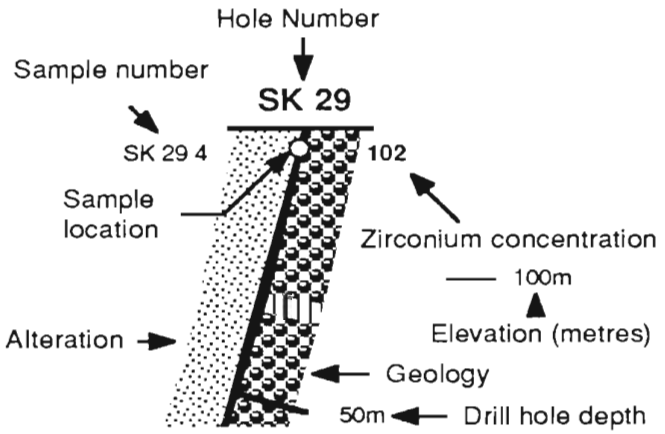

Abbreviations

py - pyrite	ep - epidote	cc - calcite
qz - quartz	hm - hematite	cl - chlorite

M semimassive and massive sulphides

T trondhjemite dyke

E.O.H - end of drill hole

Legend, symbols and abbreviations to accompany Figures 6-3 to 6-10.

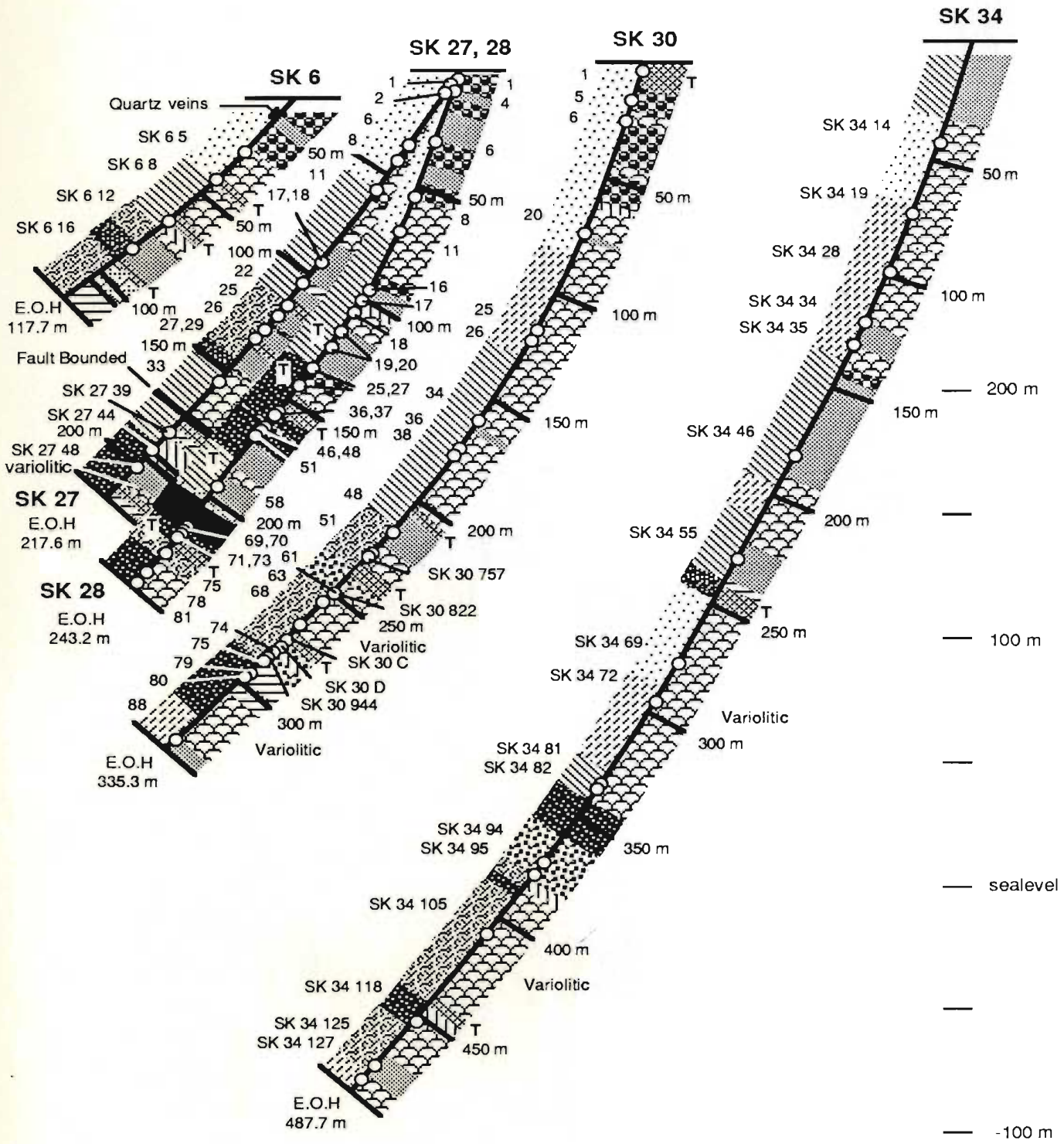

Figure 6-3a: Cross-section (looking 060°) through the Skidder Prospect at line 33200 west (see Figures 6-1 and 6-2) showing geology (right of drill hole), alteration (left of drill hole), and whole rock sample locations for drill holes SK 6, 27, 28, 30 and 34. Legend and symbols on page 234.

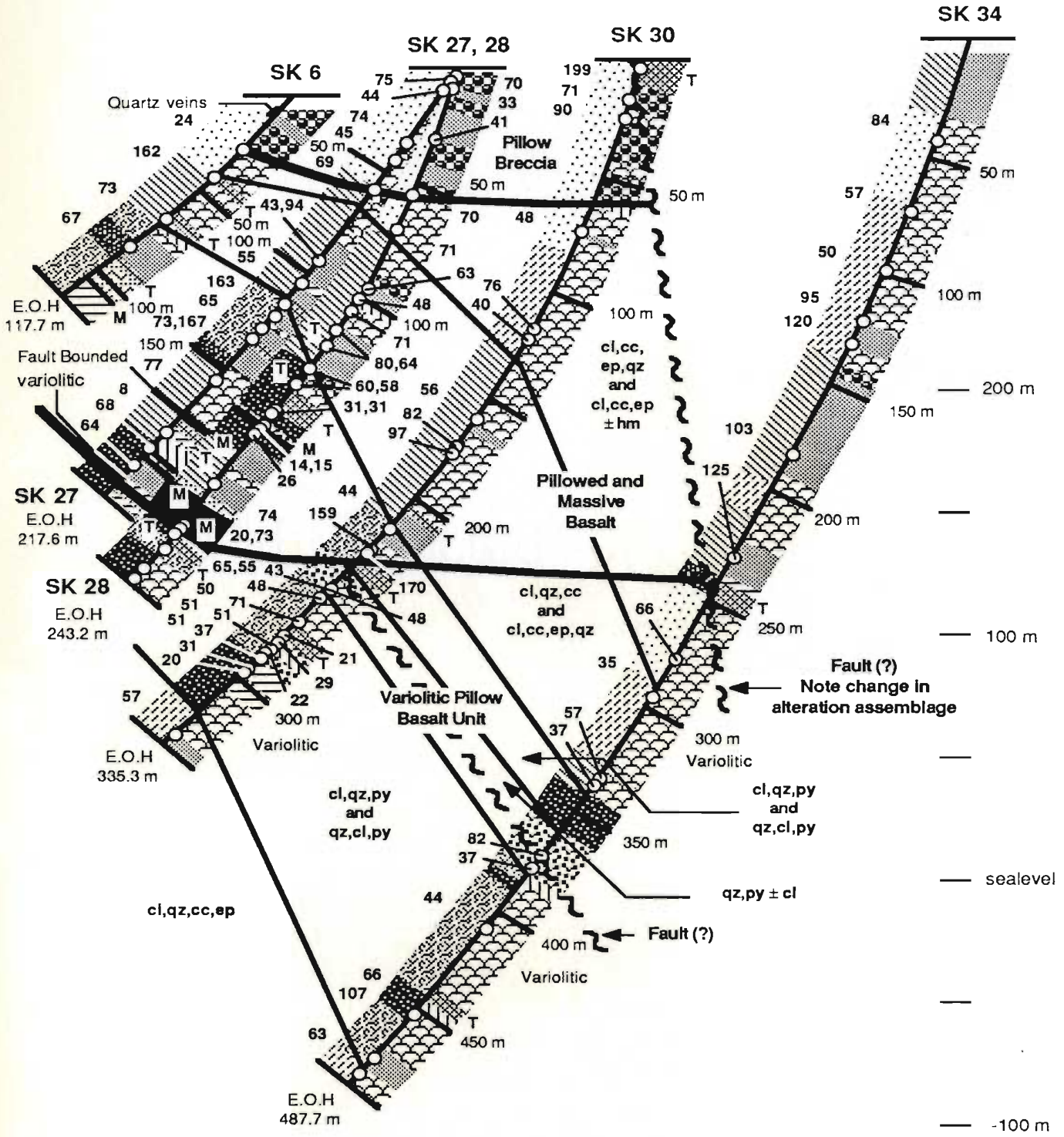

Figure 6-3b: Cross-section (looking 060°) through the Skidder Prospect at line 33200 west (see Figures 6-1 and 6-2) showing geological units and alteration zones as logged in drill holes SK 6, 27, 28, 30 and 34. Zirconium concentrations in bold type. Legend and symbols on page 234.

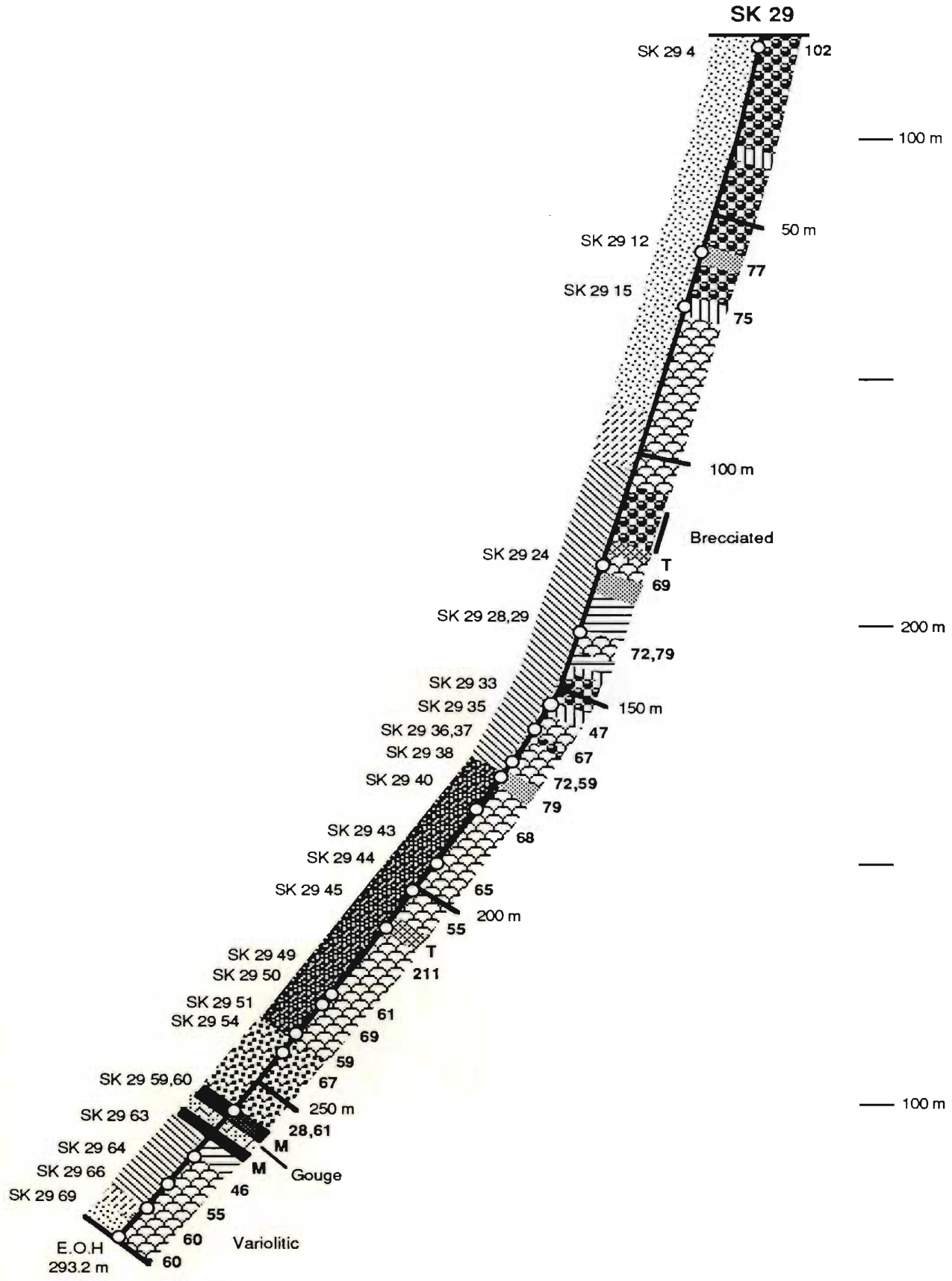

Figure 6-4: Drill section (looking ≈ 060°) showing geology (right) and alteration (left) as logged in drill hole SK 29 (see Figures 6-1 and 6-2). Whole rock sample locations in plain text to left and Zr concentrations in bold type to right of drill hole. Legend and symbols on page 234.

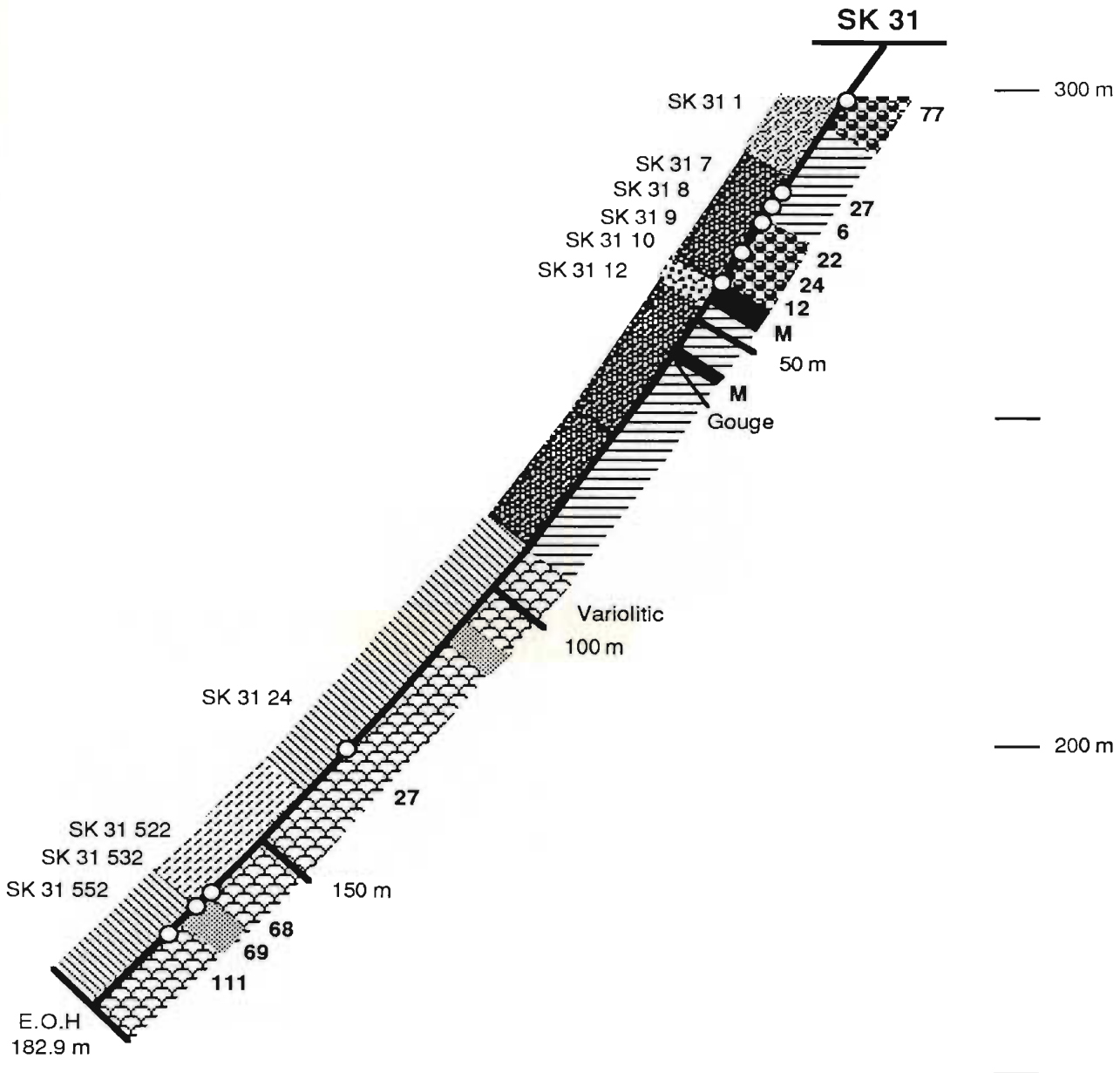

Figure 6-5: Drill section (looking ≈ 070°) showing geology (right) and alteration (left) as logged in drill hole SK 31 (see Figures 6-1 and 6-2). Whole rock sample locations in plain text to left and Zr concentrations in bold type to right of drill hole. Legend and symbols on page 234.

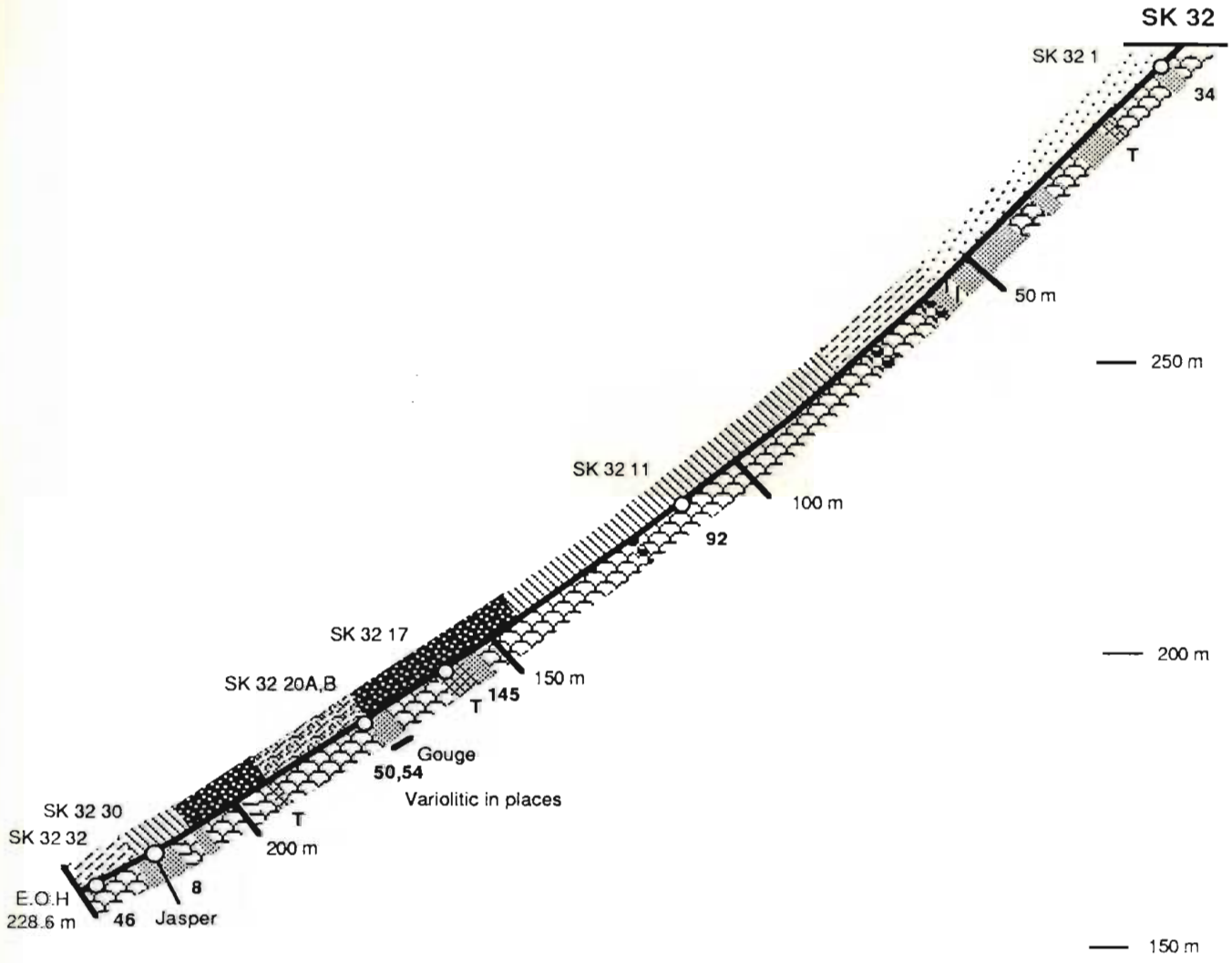

Figure 6-6: Drill section (looking 060°) showing geology (right) and alteration (left) as logged in drill hole SK 32 (see Figures 6-1 and 6-2). Whole rock sample locations in plain text to left and Zr concentrations in bold type to right of drill hole. Legend and symbols on page 234.

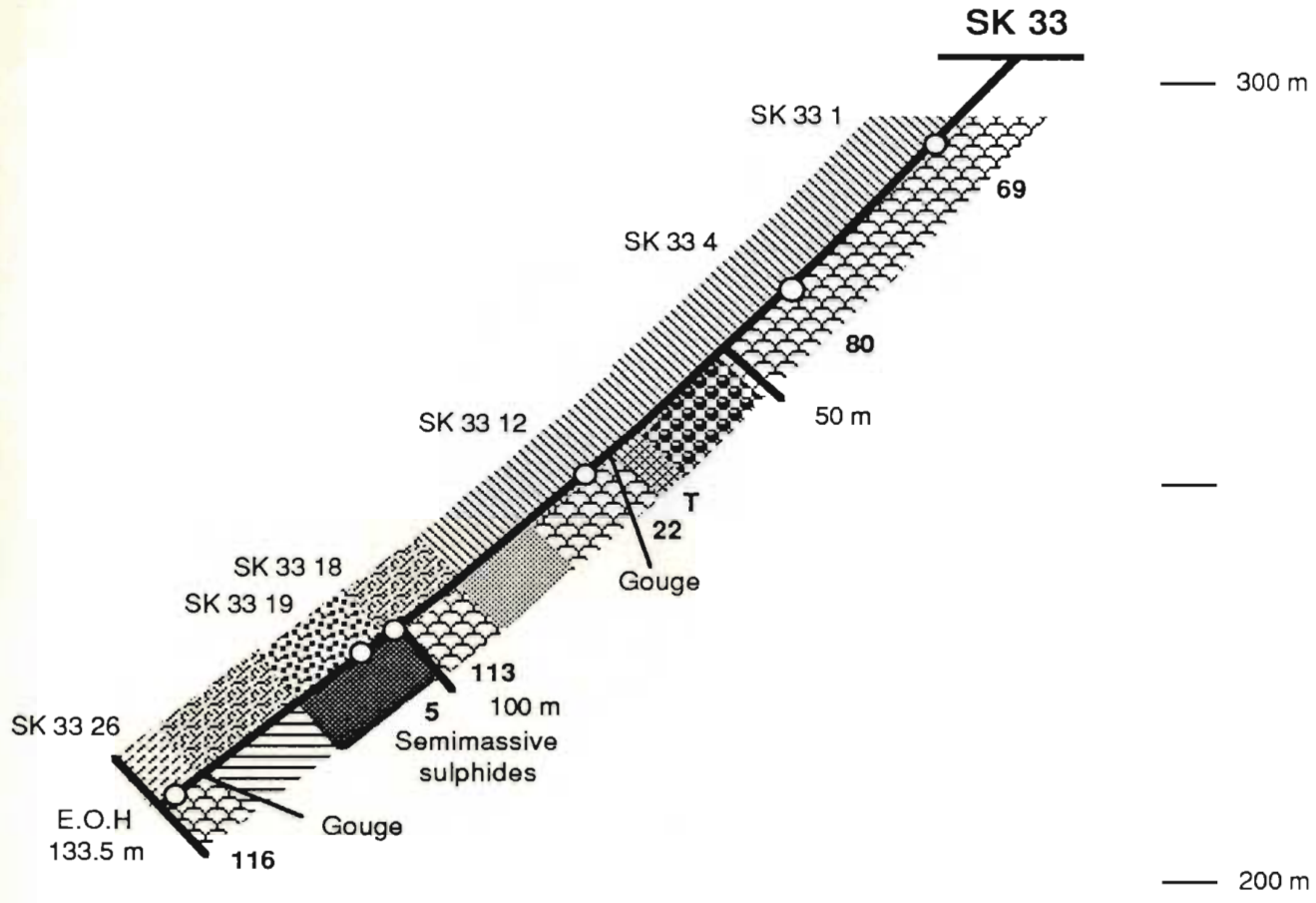

Figure 6-7: Drill section (looking 080°) showing geology (right) and alteration (left) as logged in drill hole SK 33 (see Figures 6-1 and 6-2). Whole rock sample locations in plain text to left and Zr concentrations in bold type to right of drill hole. Legend and symbols on page 234.

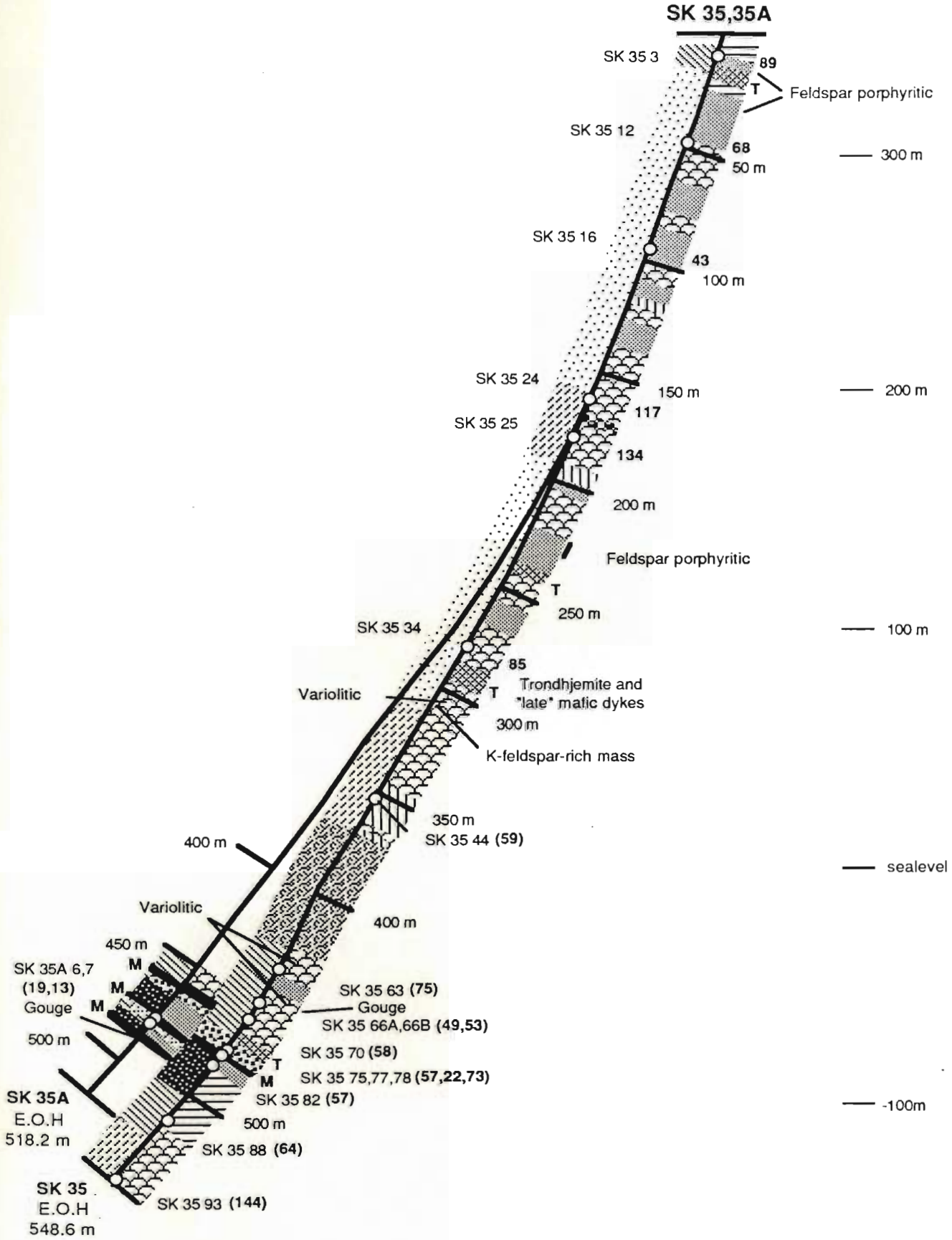

Figure 6-8: Drill section (looking 055°) showing geology (right) and alteration (left) as logged in drill holes SK 35 and 35A (see Figures 6-1 and 6-2). Whole rock sample locations in plain text and Zr concentrations in bold type. Legend and symbols on page 234.

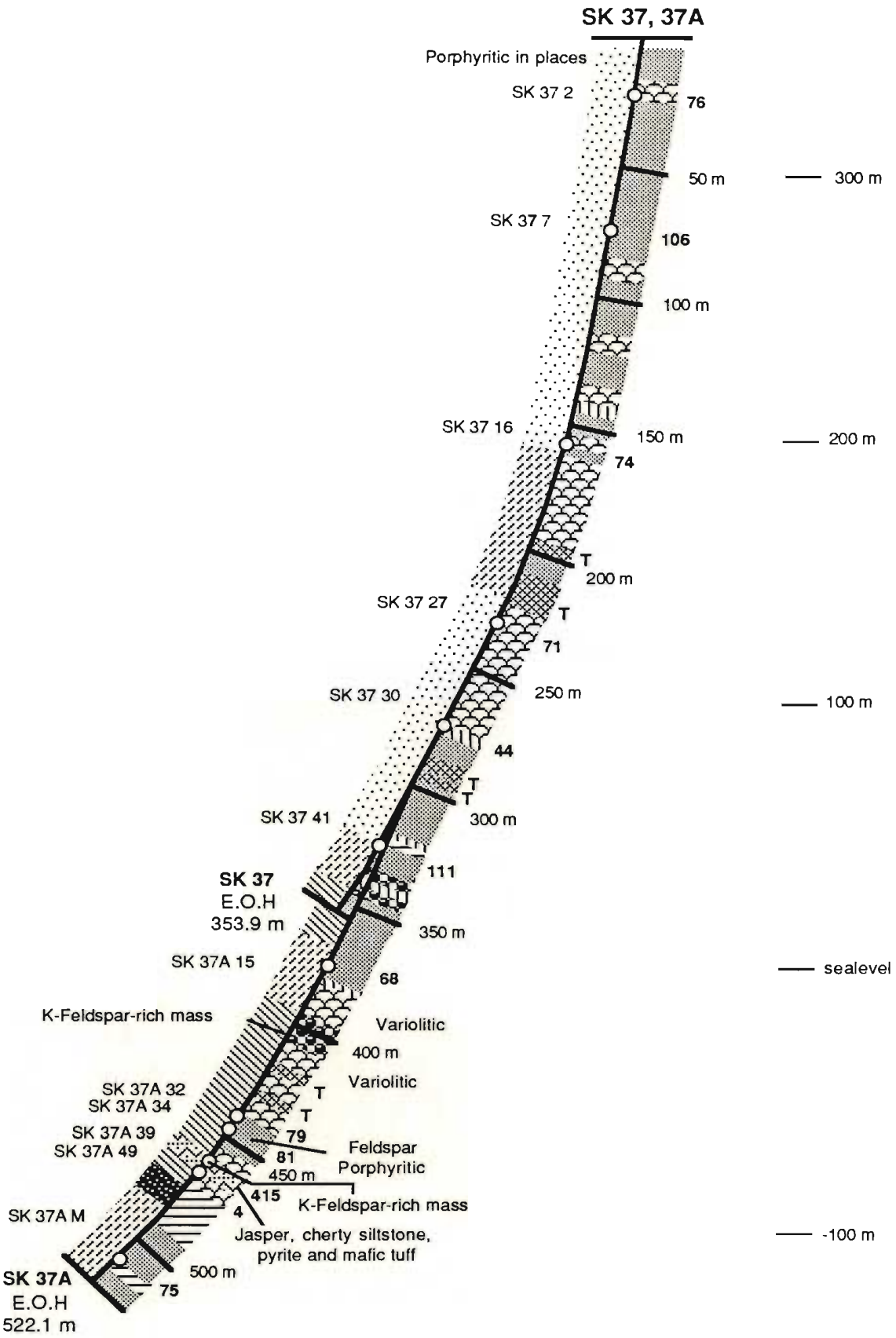

Figure 6-9: Drill section (looking 055°) showing geology (right) and alteration (left) as logged in drill holes SK 37 and 37A (see Figures 6-1 and 6-2). Whole rock sample locations in plain text (left of drill hole) and Zr concentrations in bold type (right of drill hole). Legend and symbols on page 234.

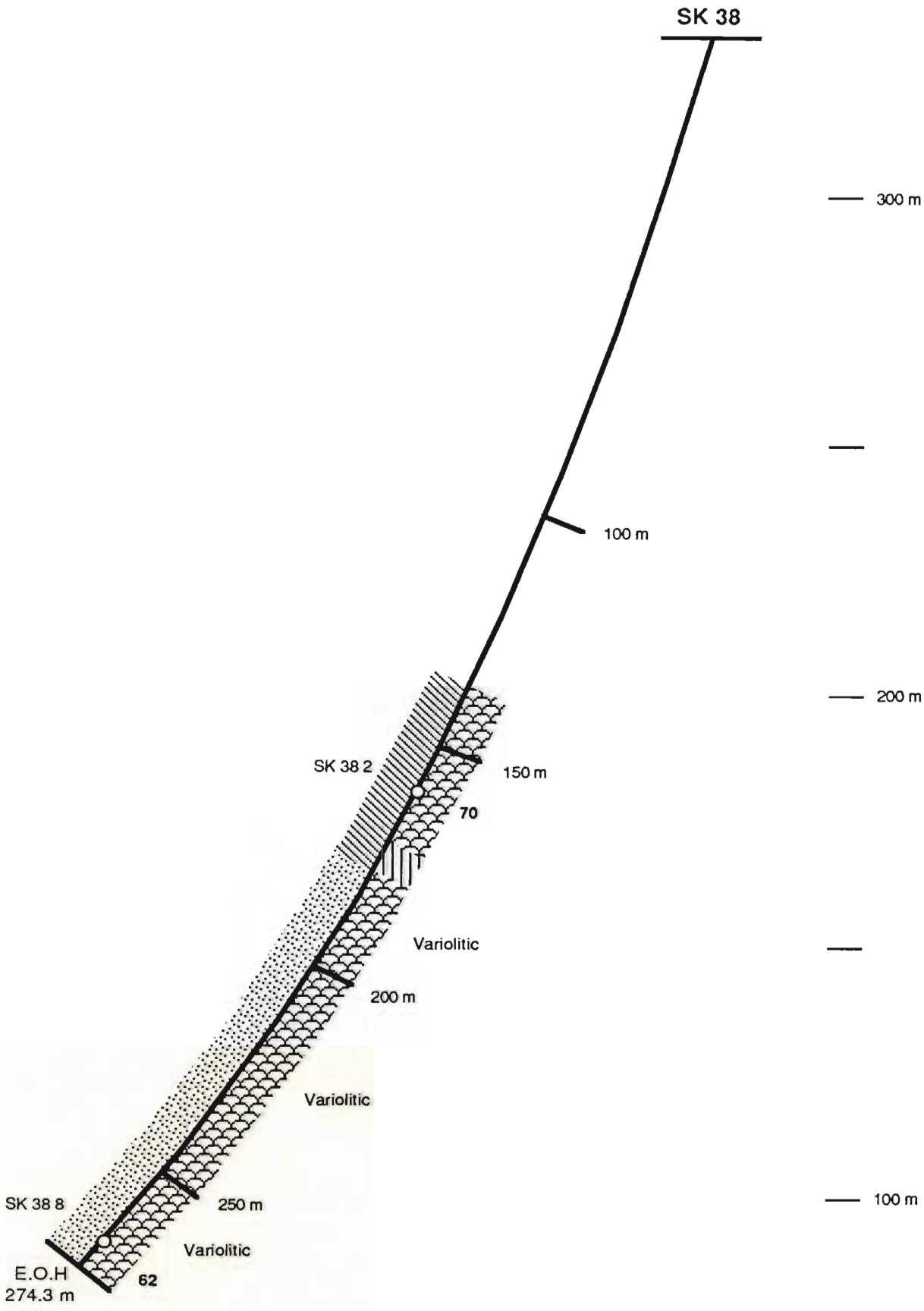

Figure 6-10: Drill section (looking ≈ 045°) showing geology (right) and alteration (left) as logged in drill hole SK 38 (see Figures 6-1 and 6-2). Whole rock sample locations in plain text to left and Zr concentrations in bold type to right of drill hole. Legend and symbols on page 234.

6.2.2 Rock unit descriptions

6.2.2.1 Pillowed basalt and pillow breccia

Pillowed basalt that is relatively unaffected by alteration associated with formation of the Skidder Prospect sulphides is generally medium green to medium grey and fine grained. Pillows are typically between 0.5 and 1 m in cross-section, but locally are up to 1.5 m across (as estimated by the spacing of chlorite-rich selvages). An estimated 25 per cent of the pillows are amygdaloidal. The amygdules are filled by calcite and/or lesser amounts of epidote, quartz or chlorite. They are typically 2-4 mm in diameter, and make up less than 10 per cent of the rock. Interpillow material, typically hyaloclastite, is generally more chloritic than that making up the pillows themselves.

Most pillow breccia units in the vicinity of the Skidder Prospect are similar to isolated pillow breccia, as described by Carlisle (1963). They consist of rounded "mini-pillows", 5-20 cm in diameter, within a darker green, more chloritic, hyaloclastite matrix. The matrix characteristically comprises 30 to 60 per cent of the rock. Lesser amounts of "broken-pillow" (Carlisle, 1963) and flow-top breccias, consisting of angular basaltic fragments within a chlorite-rich matrix, are also present.

A photograph of drill core samples representative of isolated pillow breccia units in the Skidder Prospect area is presented as Figure 6-11. Rounded miniature pillows in the sample at the top of the photograph are epidotized, as is a portion of the matrix. Hematite forms a ring just inside the pillow selvage. Note that the pervasively epidotized pillows are cut by epidote/calcite veins. Light grey-green, round, brecciated, miniature pillows occur in a darker green chlorite-rich matrix in the sample at the centre of the photograph. Chlorite-bearing veins cut the pillow at right and buff calcite fills interstices between breccia fragments at left-centre. A sample of highly silicified pillow breccia is shown at the bottom of the photograph. In this sample, interpillow areas are completely replaced by quartz and pyrite, while the pillows themselves are relatively less altered.

Figure 6-11: Photograph of drill core samples showing features of mafic, "isolated" (Carlisle, 1963) pillow breccia as noted in the Skidder Prospect drill core. Sample at top of photograph is from DDH SK 30 at 96' (29.3 m); sample at centre of photograph is from DDH SK 33 at 74.5' (22.7 m); and sample at bottom of photograph is from DDH SK 32 at 388' (118.3 m). See text for discussion.

Variolitic pillowed basalts that occur in the vicinity of the Skidder Prospect have undergone various degrees of alteration, but otherwise are similar to those exposed elsewhere in the Skidder area (see Section 3.3). The varioles are typically light grey, 3-6 mm in diameter, and, in most places, occur within a relatively more chloritic matrix. In general, the variolitic pillows have a 2-3 cm- thick, chlorite-rich, nonvariolitic outer rim. The varioles are typically individually distinct in outer portions of the pillow but coalesce to form a continuous mass in pillow cores. Smaller variolitic pillows (< 20 cm in diameter) generally do not have coalesced cores.

A photograph of drill core samples showing varioles is presented as Figure 6-12. Note that the rocks sampled have been extensively altered. Varioles are coalesced to form a continuous mass in the centre sample, but are incompletely coalesced in the sample at the top. Larger, more silicified varioles are present in the sample at the bottom. Note that pyrite occupies the interpillow area in the top sample.

6.2.2.2 Massive basalt and diabase dykes

Medium green-grey, fine- to medium-grained massive basalt flows, sills or dykes are interlayered with the pillow basalt and mafic pillow breccia. Massive flows and diabase dykes are difficult to distinguish from each other in drill core. On Figures 6-3 to 6-10 massive units that have well developed chilled margins and show intrusive relationships with adjacent rocks are shown as diabase dykes. In places, the massive units are autoclastically brecciated.

Relatively unaltered, fine- to medium-grained mafic diabase dykes intrude sulphide-rich units in places; e.g. a diabase dyke intrudes massive layered sulphides between 635' and 644.5' in drill hole SK 27 (Figure 6-17), and one intrudes intensely silicified, pyrite-bearing rocks between 1258' and 1267.5' in drill hole SK 34 (Figure 6-20).

Figure 6-12: Photograph of drill core samples showing features of variolitic pillow lavas. Sample at top of photograph is from DDH SK 37A at 1282.5' (390.9 m); sample at centre of photograph is from DDH SK 34 at 1028' (313.3 m); and sample at bottom of photograph is from DDH SK 27 at 709' (216.1 m). See text for discussion.

6.2.2.3 Mafic pyroclastic rocks

Minor amounts of mafic pyroclastic rocks are interlayered with the mafic flows in the Skidder Prospect area. The pyroclastic rocks are typically poorly bedded and range in grain size from fine grained tuffs to lapilli tuffs composed of angular medium green-grey lapilli in a chloritic matrix. A photograph showing typical features of the mafic pyroclastic rocks is presented as Figure 6-13. The sample in the top of the photograph shows light green-grey, elongate angular fragments in a darker green, more chlorite-rich matrix. The sample at the centre of the photograph is of bedded, medium green mafic tuff. Note that this rock has been significantly altered by the sulphide mineralizing event(s). Deposition of quartz and pyrite has occurred parallel to the layering. The sample at the bottom of the photograph shows rounded to subangular light green-grey mafic fragments in a dark green chlorite-rich matrix.

6.2.2.4 Trondhjemite dykes

Light grey-green, fine grained trondhjemite dykes intrude mafic rocks in the area of the Skidder Prospect. The dykes are massive to feldspar ± quartz porphyritic. The porphyritic dykes contain 5 per cent of 1 to 3 mm feldspar and lesser amounts of quartz phenocrysts in a dense matrix. In many areas, layering is present within 30 cm of the contact of the dykes with adjacent units. The layering is defined by alternating light and dark grey-green to buff, 0.5 to 1 cm wide zones that parallel the dyke contact.

Trondhjemite dykes that intrude the rocks in the vicinity of the Skidder Prospect in places separate rocks that have been affected by different intensities of alteration (e.g. the dyke at 250 m in drill hole SK 34, Figure 6-3). In other areas, particularly in the most intensely altered zones, the trondhjemite dykes have highly altered rocks on either side and are typically altered themselves (Figure 6-19). This implies that intrusion of trondhjemite dykes occurred in the Skidder Prospect area both before and after formation of sulphides.

Figure 6-13: Photograph of Skidder Prospect drill core samples showing features of mafic pyroclastic rocks. Sample at top of photograph is from DDH SK 28 at 295' (89.9 m); sample in centre of photograph is from DDH SK 31 at 193' (58.8 m); and sample at bottom of photograph is from DDH SK 29 at 467' (142.3 m). See text for discussion.

6.2.2.5 K-feldspar-rich masses

K-feldspar-rich areas, typically less than 10 cm wide (as estimated from length of cored sections), were intersected by drill holes SK 35 and SK 37. The mode of occurrence of these K-feldspar-rich masses ranges from distinct K-feldspar crystals in a black chlorite matrix (Figure 6-14) to foliated gouge zones in which rounded K-feldspar + quartz masses are incorporated in a chlorite matrix (Figure 6-15).

6.3 Sulphide-bearing Zones

6.3.1 Introduction

Detailed stratigraphic columns for the sulphide-rich zones in diamond drill holes relogged by the author are presented as Figures 6-16 to 6-24.

Drill holes SK 6, 27, 28, 30 and 34 provide a cross-section through sulphide-rich zones related to Lens 1. Semimassive to massive layered and unlayered sulphides plus spatially related jasper were intersected by drill holes SK 6, 27 and 28; disseminations and veins of sulphides in intensely altered rocks were intersected in SK 30 and 34. Brecciated jasper is underlain by 0.3 m of massive pyrite in DDH SK 6 (Figure 6-16). Thin massive sulphide zones interlayered with brecciated jasper, massive basalt and mafic lapilli tuff occur over a 75' (22.8 m) section in SK 27 (Figure 6-17). In places, the massive sulphides in SK 27 are cut by post-ore diabase dykes. Several gouge zones are noted. Two sulphide-rich zones were intersected by drill hole SK 28 (Figure 6-18). Massive and layered sulphides; pyrite, chlorite-rich tuff; intensely silicified, quartz-pyrite-bearing rock; and brecciated jasper comprise the upper zone which has a cored thickness of 28.5' (8.7 m). The lower sulphide-rich zone, which occurs 100' (30.5 m) below the upper, represents one of the thickest cored sections of massive sulphides in the Skidder Prospect. In the lower zone, 16.5' (5.0 m) of brecciated jasper and lesser massive pyrite overlie 39.5' (12.0 m) of layered and unlayered massive sulphides (Figure 6-18).

Figure 6-14: Photograph of drill core sample showing K-feldspar crystals in black chlorite. Sample is from DDH SK 37 at 392.5' (119.6 m).

Figure 6-15: Photograph of drill core sample showing rounded K-feldspar/quartz masses in a foliated chlorite-bearing gouge zone. Sample is from DDH SK 37A at 1510.5' (460.4 m).

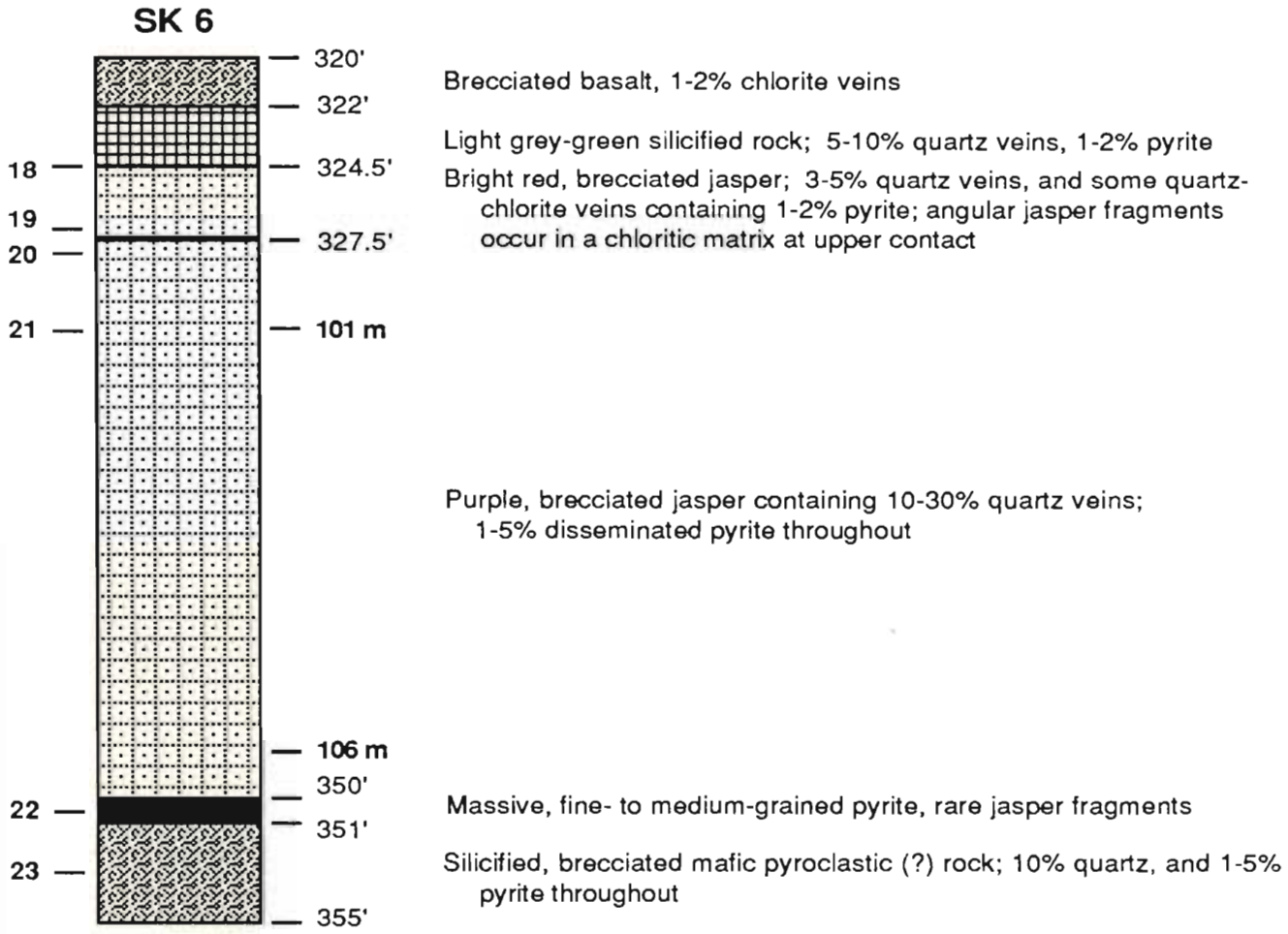

Figure 6-16: Stratigraphic column showing sulphide-bearing units noted in core from diamond drill hole SK 6. Sample locations and numbers indicated on left side of stratigraphic column; hole-depths, in feet and metres, on right.

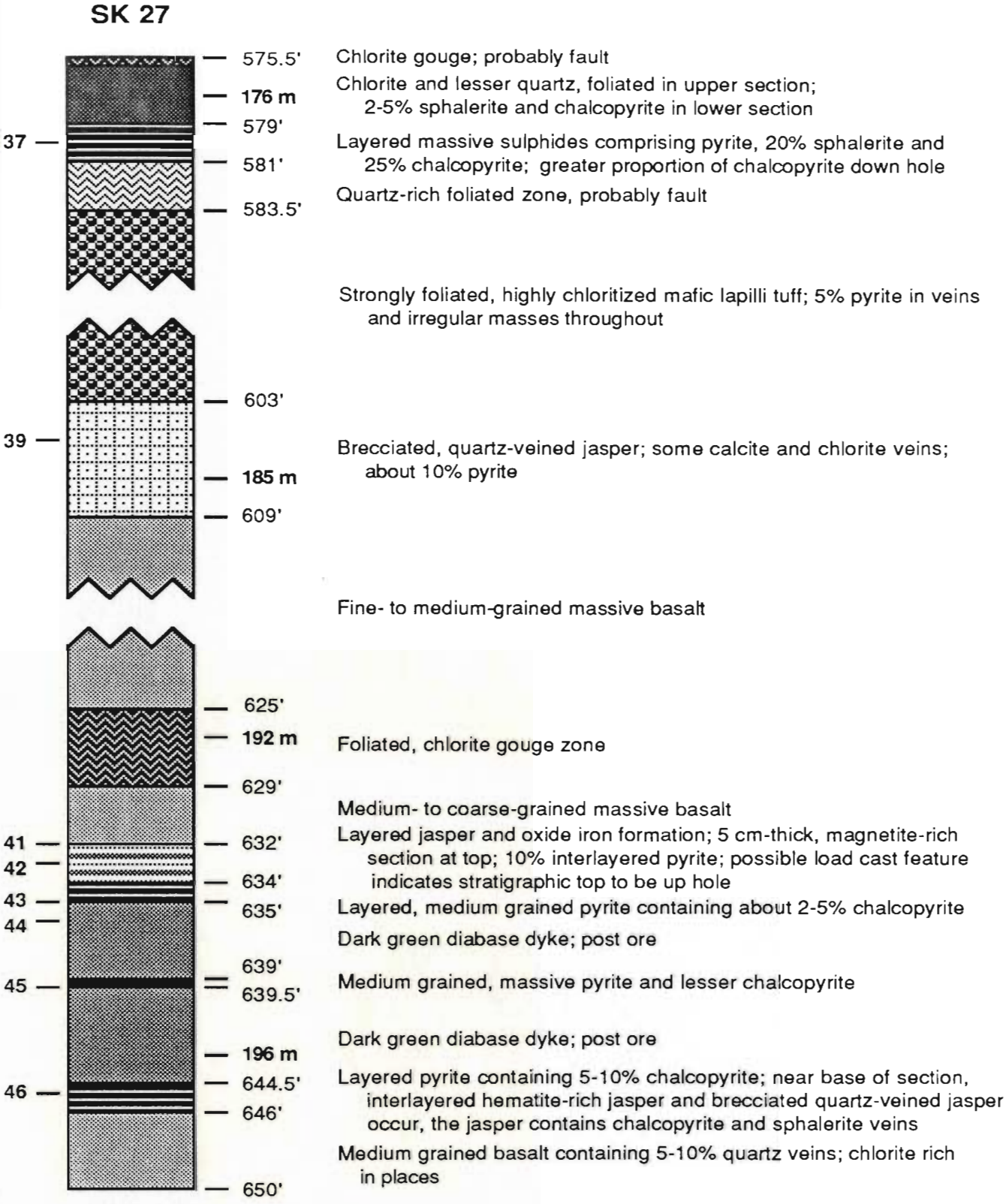

Figure 6-17: Stratigraphic column showing sulphide-bearing units noted in core from diamond drill hole SK 27. Sample locations and numbers indicated on left side of stratigraphic column; hole-depths, in feet and metres, on right.

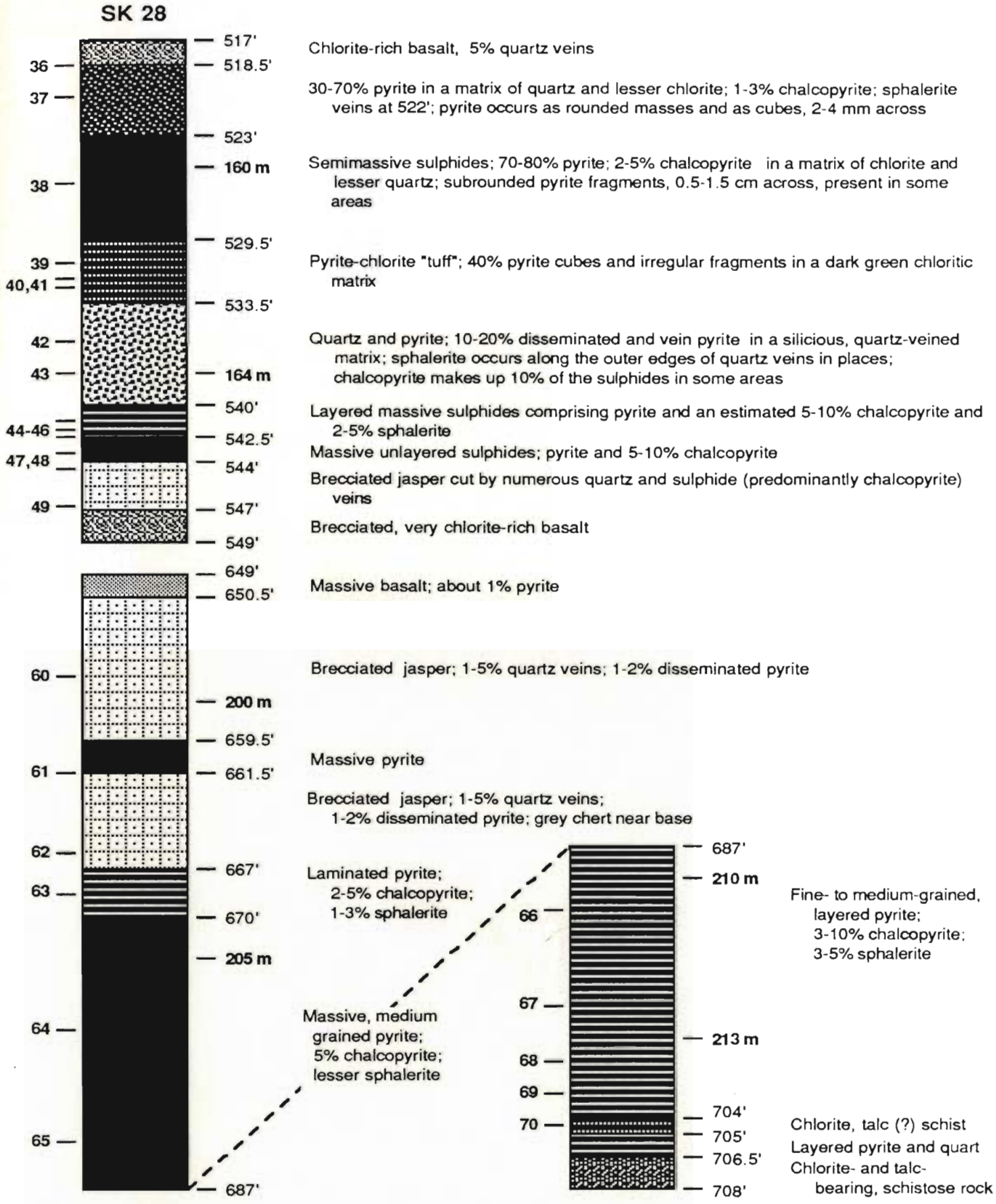

Figure 6-18: Stratigraphic column showing sulphide-bearing units noted in core from diamond drill hole SK 28. Sample locations and numbers indicated on left side of stratigraphic column; hole-depths, in feet and metres, on right.

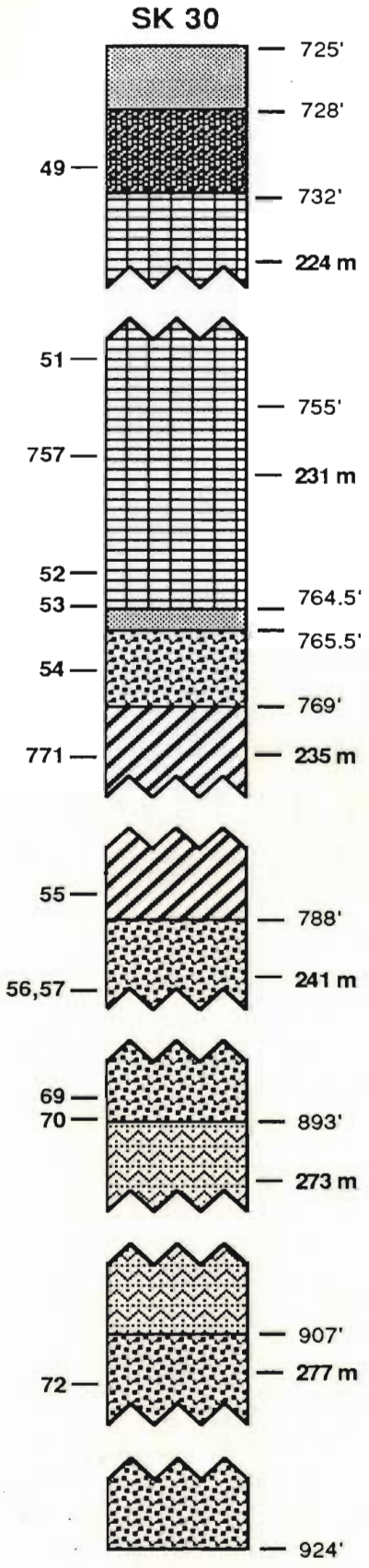

Fine grained basalt; 1-2% pyrite; silicified in sections

Very dark green, intensely chloritized, talcose rock; 10% quartz; pyrite veins

Highly silicified, brecciated rock; several 5-10 cm-wide, cross-cutting quartz veins; minor pyrite in thin chlorite veinlets

Highly silicified, buff, brecciated rock; 10-15% thin, chlorite, pyrite, quartz veins

Basalt; quartz-filled amygdules

Quartz, much of which occurs in veins, and 10 to 80% medium grained pyrite; few preserved fragments of original host rock

Variably silicified, mafic rock; quartz veinlets throughout

10-80% typically medium- to coarse-grained pyrite in intensely silicified rock; about 50% of this section contains highly altered fragments of brecciated mafic host rock, recognizable varioles in places; about 20-50% quartz veins; 1-5% chalcopyrite and sphalerite in 0.5-0.75 cm-wide quartz veins between 800 and 825 feet, sphalerite typically occurs along vein walls

Light grey-green, brecciated, quartz-veined trondhjemite dyke; contains finely disseminated pyrite throughout; rock consists almost totally of quartz within 30 cm of contact

10-80% typically medium- to coarse-grained pyrite in intensely silicified rock; about 30% of this section contains highly altered fragments of brecciated mafic host rock, recognizable varioles in places; about 20-50% quartz veins.

Figure 6-19: Stratigraphic column showing sulphide-bearing units noted in core from diamond drill hole SK 30. Sample locations and numbers indicated on left side of stratigraphic column; hole-depths, in feet and metres, on right.

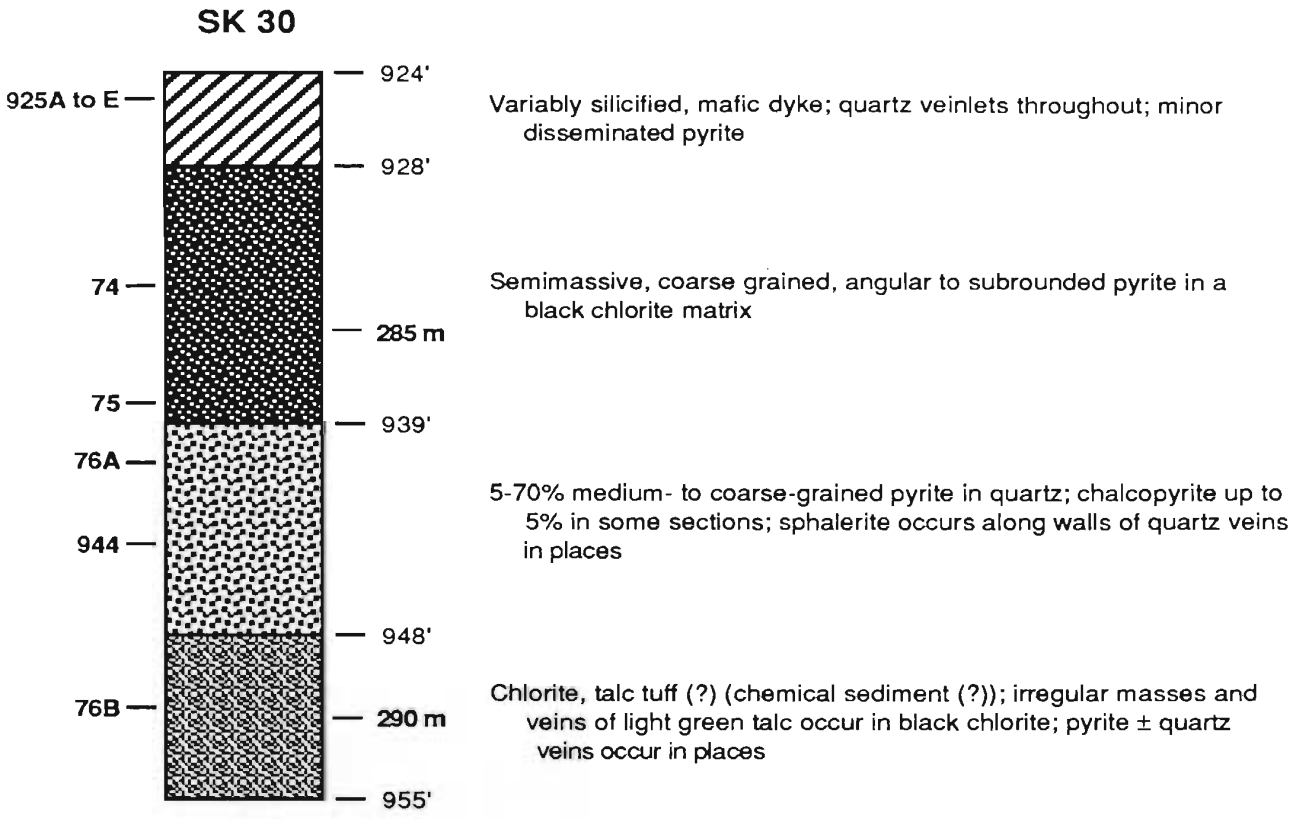

Figure 6-19 (continued): Stratigraphic column showing sulphide-bearing units noted in core from diamond drill hole SK 30. Sample locations and numbers indicated on left side of stratigraphic column; hole-depths, in feet and metres, on right.

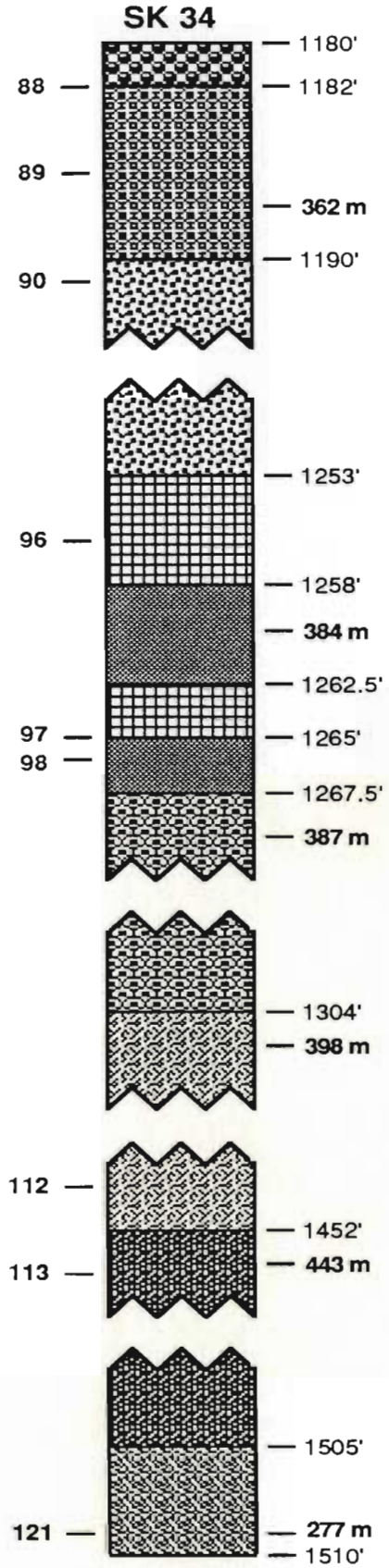

Highly chloritic pillow breccia; 15% quartz veins; 3-5% pyrite, much of which is in quartz veins

25-75% pyrite in massive and vein quartz; minor chalcopyrite and rare sphalerite, the latter occurring on the outside edges of quartz veins

5-25% pyrite in massive and vein quartz; rare sphalerite, typically occurring on the outside edges of quartz veins; few fragments of intensely altered host rock, including varioles in some places

White-grey quartz containing very finely disseminated pyrite; few chlorite veinlets

Medium grey-green, amygdaloidal, "late" mafic dyke

White-grey quartz containing very finely disseminated pyrite; few chlorite veinlets

Medium grey-green, amygdaloidal, "late" mafic dyke

Variably silicified, chloritic, variolitic pillow basalt; selvages very chloritic; about 1% quartz veins and 2-5% disseminated pyrite and pyrite veinlets more silicified and chloritic from 1275'-1297'; pyrite typically less than 25% but up to 80% in places

Variably silicified, variably chloritic, intensely altered mafic rock; 5-10% quartz veins; 5-10% black chlorite masses; 5-30% medium grained pyrite; some irregular masses of intensely altered host rock, including varioles in places

Highly chloritic, intensely altered mafic rock; some sections indicate part of unit may be a very fine grained chlorite-talc tuff (?) (chemical sedimentary rock (?)); other sections suggest unit is very intensely altered mafic volcanic rock, eg. the presence of altered varioles; unit typically contains 5% pyrite; also 5% pyrite-bearing quartz veins in places

Chloritized, variably silicified basalt; about 1% pyrite

Figure 6-20: Stratigraphic column showing sulphide-bearing units noted in core from diamond drill hole SK 34. Sample locations and numbers indicated on left side of stratigraphic column; hole-depths, in feet and metres, on right.

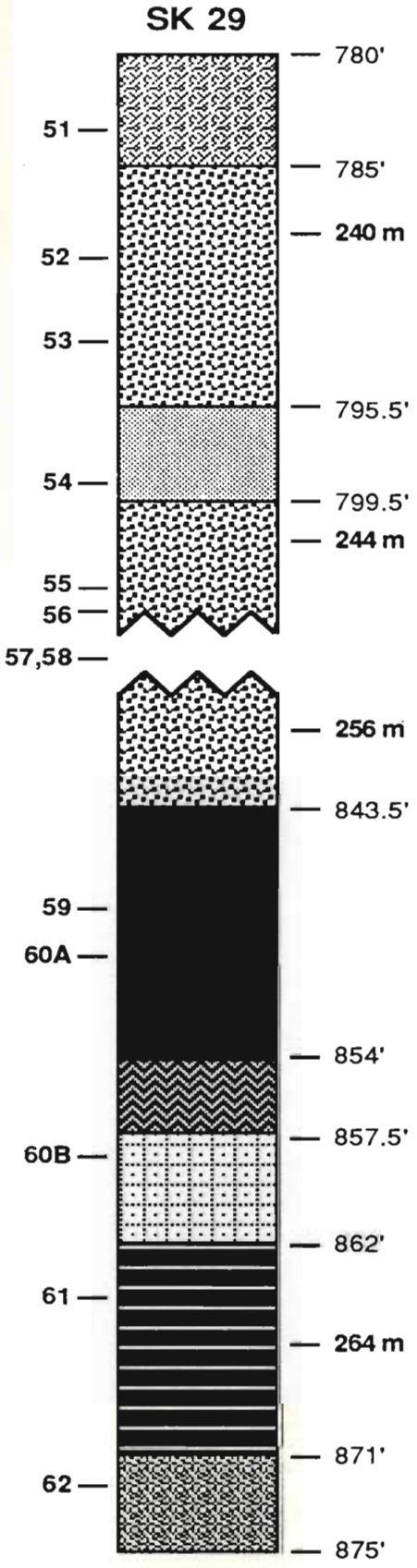

Highly chloritized, pillowed basalt; 5% quartz veins, several of which are pyrite bearing

Massive quartz and pyrite; about 10% quartz veins cut more massive, silicified sections; about 10-15% pyrite occurs as veins and irregular masses; rare chalcopyrite and sphalerite in quartz veins

Dark green, medium-grained, very carbonate-rich basalt (?)

Predominantly massive quartz containing about 15% quartz veins, and 30-50% pyrite, in veins and irregular masses; rare chalcopyrite and sphalerite in quartz veins; rare preserved host rock consisting of grey, amygdaloidal, intensely altered basalt

Massive, medium- to coarse-grained pyrite (70-90%) in predominantly quartz gangue; minor chalcopyrite and sphalerite in quartz veins from 850 to 854 feet

Chlorite- and talc (?)-rich gouge zone; quartz-carbonate veins present; slickenslides noted

Brecciated, brick-red jasper; about 5-10% quartz veins; 2% pyrite and chalcopyrite veinlets from 857.5-858.5 feet; 1-2% pyrite veins below 858.5 feet; jasper is layered, and less brecciated from 861.5-862 feet

Massive and layered fine grained pyrite containing minor amounts of sphalerite and chalcopyrite; calcite and quartz are predominant gangue minerals

Moderately to strongly foliated, very chlorite-rich, talcose (?) rock; about 1% pyrite and 1% quartz and calcite veinlets

Figure 6-21: Stratigraphic column showing sulphide-bearing units noted in core from diamond drill hole SK 29. Sample locations and numbers indicated on left side of stratigraphic column; hole-depths, in feet and metres, on right.

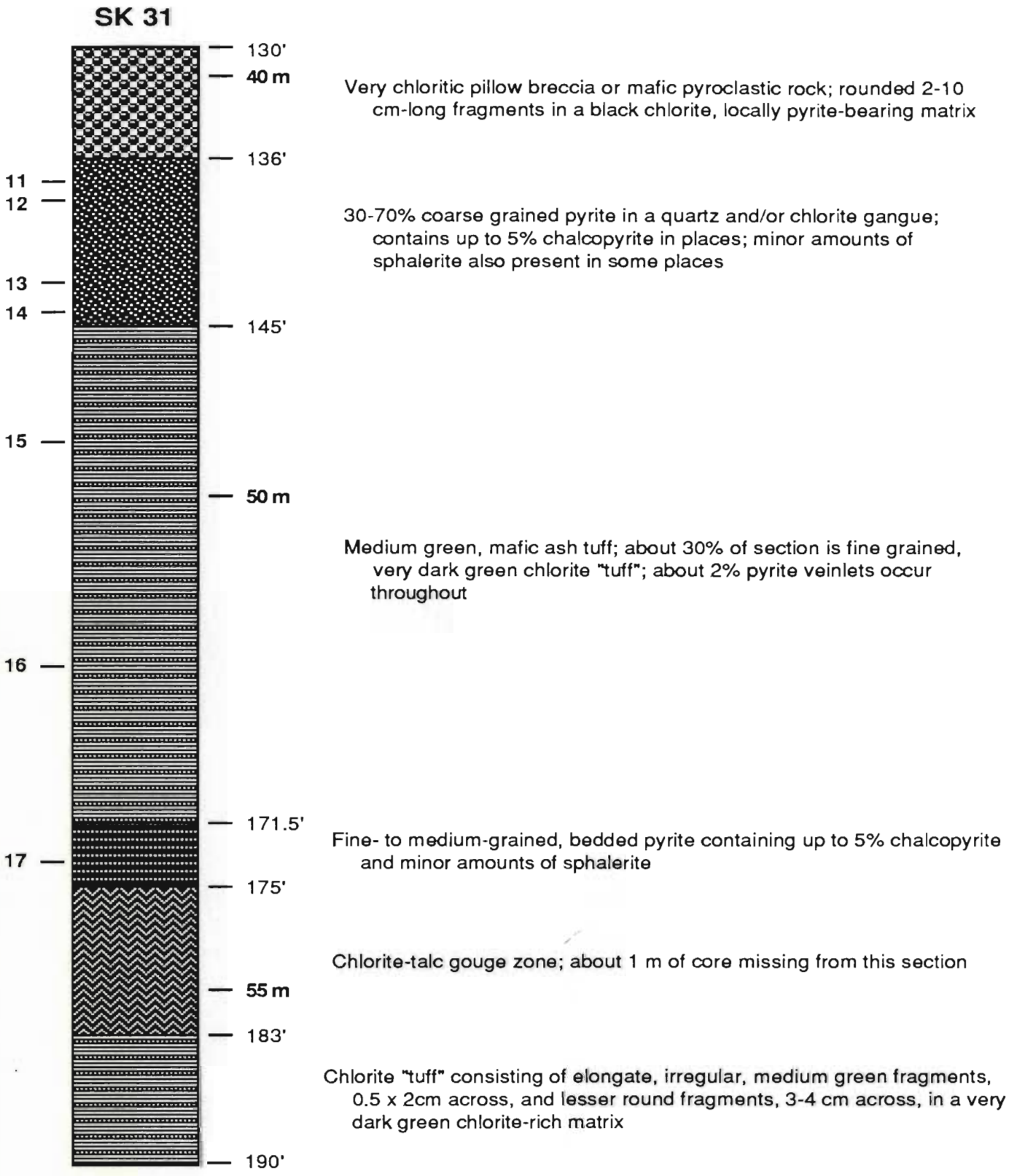

Figure 6-22: Stratigraphic column showing sulphide-bearing units noted in core from diamond drill hole SK 31. Sample locations and numbers indicated on left side of stratigraphic column; hole-depths, in feet and metres, on right.

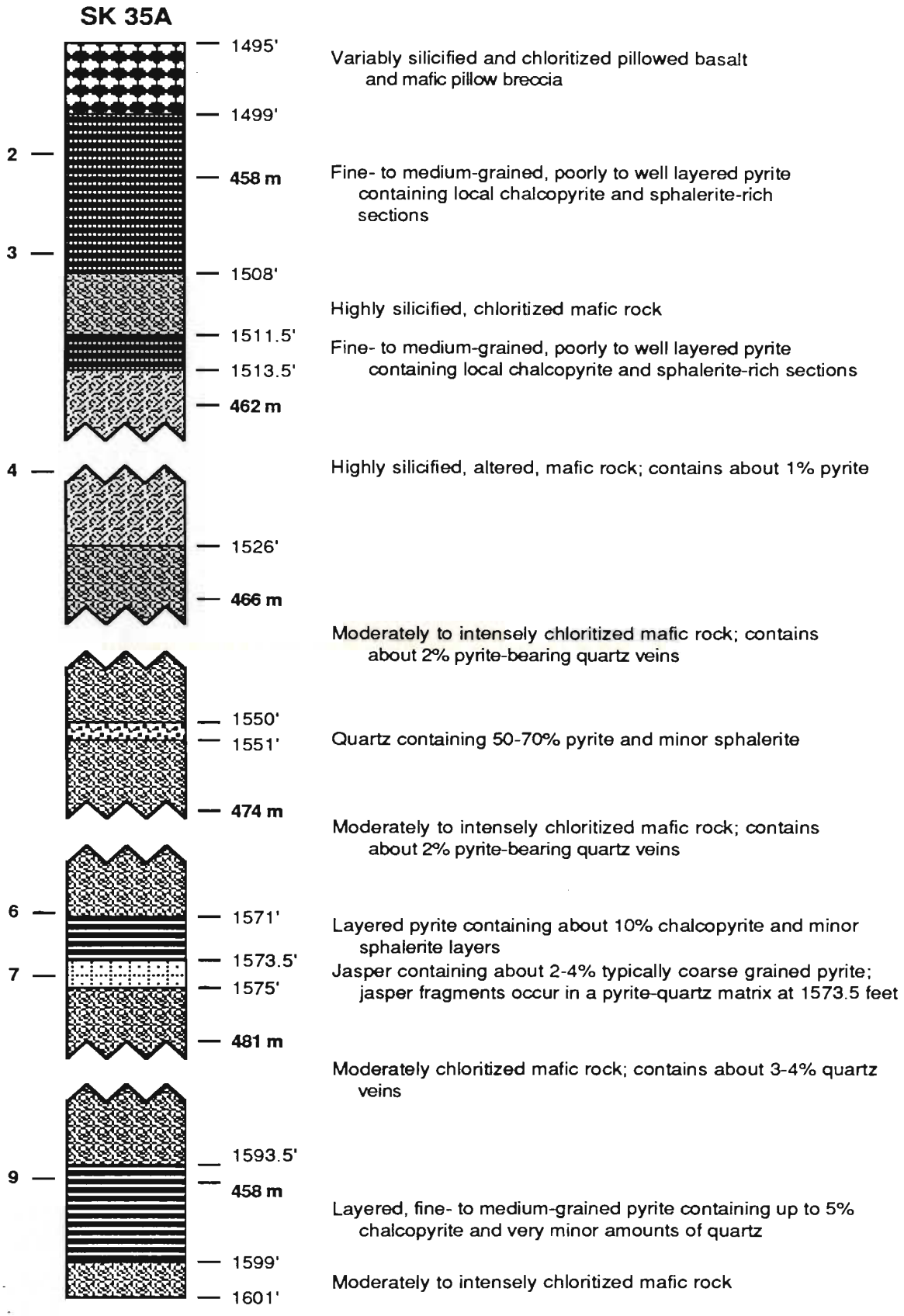

Figure 6-23: Stratigraphic column showing sulphide-bearing units noted in core from diamond drill hole SK 35A. Sample locations and numbers indicated on left side of stratigraphic column; hole-depths, in feet and metres, on right.

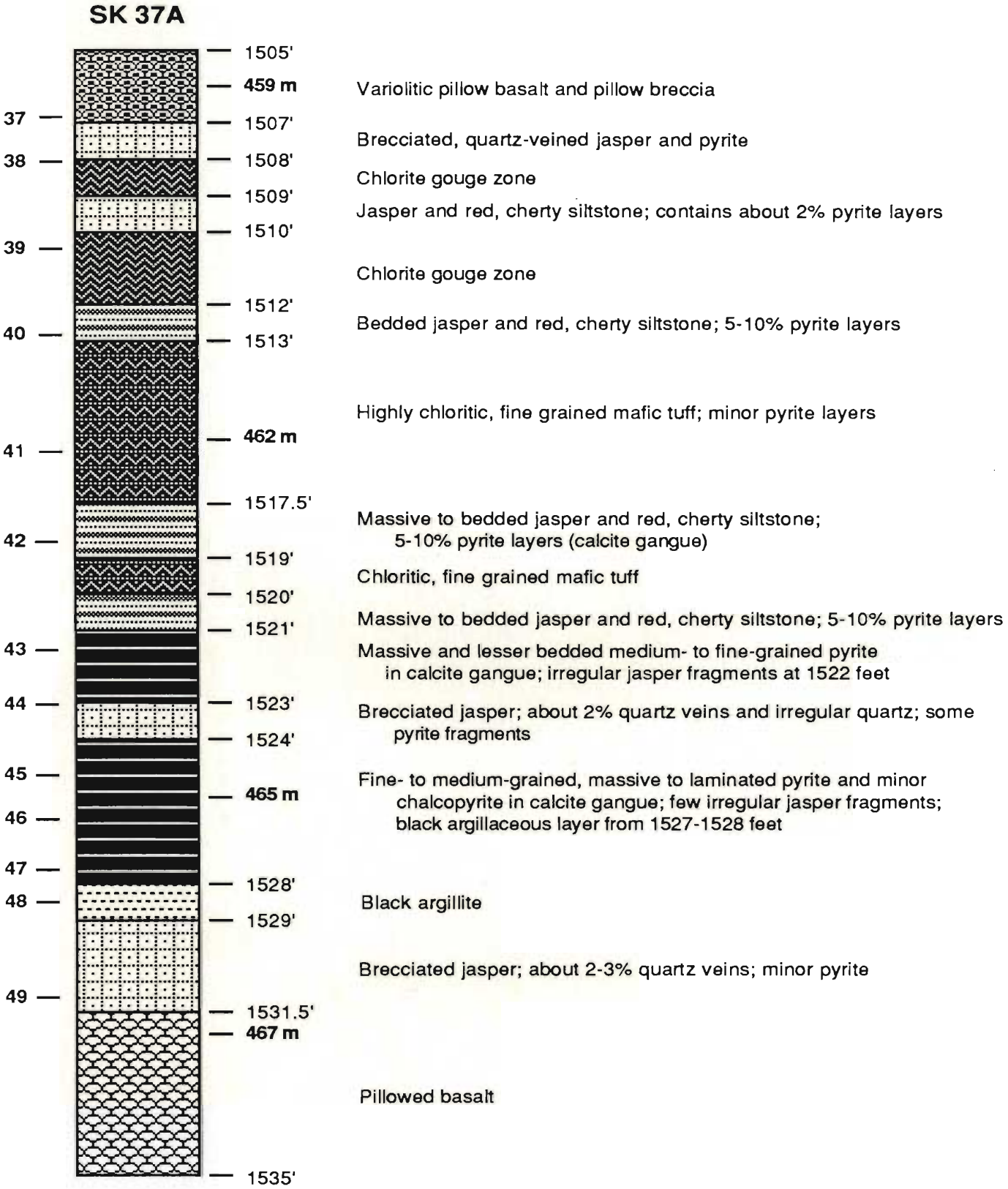

Figure 6-24: Stratigraphic column showing sulphide-bearing units noted in core from diamond drill hole SK 37A. Sample locations and numbers indicated on left side of stratigraphic column; hole-depths, in feet and metres, on right.

Sulphides intersected in drill holes SK 30 and SK 34 occur as disseminations and veins in highly silicified and/or chloritized rocks (Figure 6-19 and 6-20). The sulphide-bearing zone has a cored width of 220' (67.0 m) in DDH SK 30, and 323' (98.5 m) in SK 34. Pyrite and minor chalcopyrite and sphalerite comprise from 10 to 80% of the rocks. A trondhjemite dyke cuts intensely silicified rock in SK 30. The dyke is brecciated, quartz veined and contains finely disseminated pyrite throughout.

Sulphide-rich units related to Lens 1 were also intersected in diamond drill holes SK 29 and SK 31. Highly silicified rock overlies massive pyrite in the upper portion of the sulphide-bearing zone intersected in SK 29 (Figure 6-21). A chlorite-rich gouge zone separates this upper zone from interlayered brecciated jasper and layered massive sulphides below. In SK 31, pyrite-rich, highly altered, silicified and chloritized rock is underlain by mafic tuff, some of the latter being composed of medium green chlorite-talc fragments in a black chlorite matrix (Figure 6-22). Massive, medium grained, bedded pyrite directly underlies the tuff. A chlorite/talc gouge zone separates the bedded pyrite from underlying chlorite "tuff".

Massive sulphides of Lens 2, as intersected in drill holes SK 35A and SK 37A, comprise several zones of massive and layered sulphides, which occur within variably chloritized, silicified, pyrite-bearing rocks (Figures 6-23 and 6-24). Mafic chlorite-rich tuffs in SK 37A include some pyrite layers. Brecciated and layered jasper is spatially associated with the sulphides in places.

6.3.2 Jasper-chert

Brecciated, quartz veined, unlayered and lesser bedded jasper and jasper-rich siltstone are spatially associated with the massive sulphides in several places (Figures 6-16 to 6-24). The jasper, in units which range from 0.3 to 8 m thick, occurs as brecciated, irregular inclusions embedded in pyrite, as semicontinuous layers interbedded with pyrite, and as massive to layered bodies consisting predominantly of jasper but in places

containing medium- to coarse-grained pyrite, either as disseminations or in irregular masses and lenses.

A photograph of drill core samples presented as Figure 6-25 illustrates the different modes of occurrence of the jasper. Drill core sample 1 comprises brecciated quartz-veined jasper; sample 2 shows disseminated medium grained pyrite in unlayered jasper; samples 3 and 4 are of interlayered jasper and jasper-rich siltstone and pyrite; and samples 5, 6 and 7 show irregular clasts of jasper embedded in fine- to medium-grained pyrite. Note that an irregular mass of sphalerite-bearing quartz partially surrounds one of the jasper fragments in sample 7, and abundant quartz accompanies the pyrite and partially comprises one of the jasper fragments in sample 6. Note also that much of the jasper is composed of rounded bright red masses about 2-10 mm across; in places the masses have dull red, relatively more silica-rich, central portions. In several areas, the jasper is cut by "late" quartz veins.

Pyrite-bearing quartz-veined grey chert occurs between jasper and laminated sulphides in SK 28. A photograph of a sample of this unit is shown below (sample 6 in Figure 6-28).

6.3.3 Semimassive to massive sulphides

Both layered and unlayered semimassive to massive sulphides occur in the Skidder Prospect (Figures 6-16 to 6-24). The unlayered sulphides typically consist of semimassive to massive, medium- to coarse-grained pyrite with 5-15 per cent quartz and lesser calcite gangue. Rare, fine grained chalcopyrite and sphalerite-rich zones occur within the massive pyrite. The layered sulphides consist of laminated, fine- to medium-grained pyrite with 10 to 15 per cent interlaminated chalcopyrite and sphalerite.

A photograph of drill core samples showing features typical of the semimassive to massive sulphides is presented as Figure 6-26. Sample 1 shows layered, massive, fine- to medium-grained pyrite; the layering is defined by variations in the grain size of the pyrite. Sample 2 shows fine grained pyrite interlayered with chalcopyrite (light gold) and

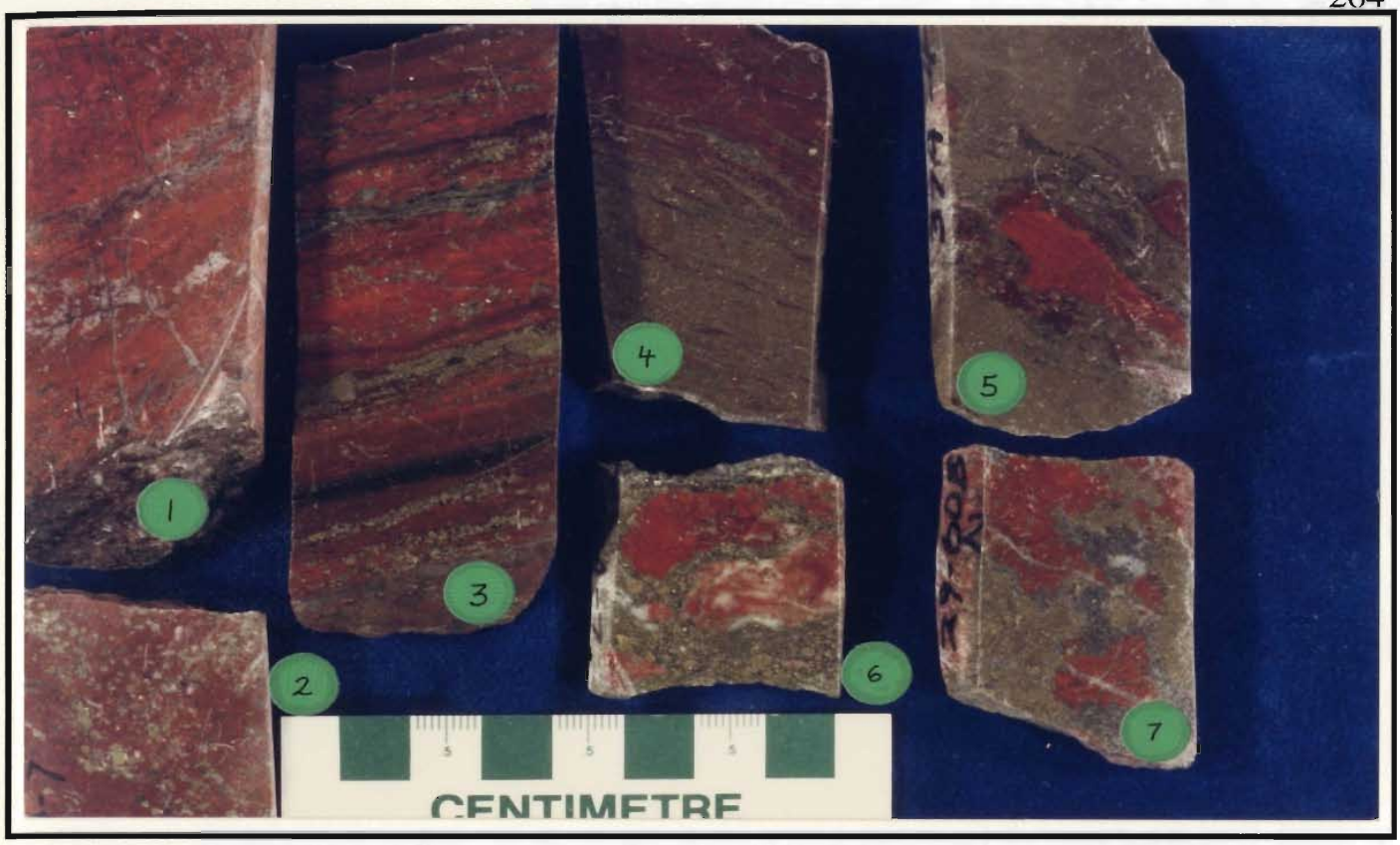

Figure 6-25: Photograph of drill core samples illustrating different modes of occurrence of jasper associated with the Skidder Prospect. Sample 1 is from DDH SK 32 at 707' (215.5 m); sample 2, DDH SK 35A at 1571' (478.8 m); sample 3, DDH SK 27 at 632' (192.6 m); sample 4, DDH SK 37A at 1518.5' (462.8 m); sample 5, DDH SK 37A at 1521.5' (463.8 m); sample 6, DDH SK 35A at 1573.5' (479.6 m); and sample 7, DDH SK 29 at 858' (261.5 m).

Figure 6-26: Photograph of drill core samples showing features of the Skidder Prospect semimassive to massive sulphides. Sample 1 is from DDH SK 28 at 700' (213.5 m); sample 2, DDH SK 27 at 579' (176.5 m); sample 3, DDH SK 37A at 1508' (459.6 m); sample 4, DDH SK 27 at 580' (176.8 m); sample 5, DDH SK 30 at 938' (285.9 m); sample 6, DDH SK 28 at 532.5' (162.3 m); sample 7, DDH SK 28 at 526' (160.3 m); and sample 8, DDH SK 29 at 802.5' (244.6 m).

sphalerite (dark grey). Sample 3 shows layered, fine grained pyrite; "dendritic" chalcopyrite (light gold) fills interstices between pyrite grains. Note the presence of small jasper fragments (dull red) elongated parallel to the layering in this sample. Discontinuous, convoluted layers of fine grained pyrite and sphalerite (dark grey) accompanied by discontinuous layers and "dendrites" of chalcopyrite are shown in sample 4. Sample 5 is of typical massive, medium grained pyrite. Samples 6 and 7 show medium- to coarse-grained pyrite in a predominantly chlorite gangue. In places, fractured, subhedral pyrite grains reach up to 2.5 cm across in units similar to that displayed in sample 7. Sample 8 shows medium- to coarse-grained pyrite in predominantly quartz gangue.

6.3.4 Disseminated and vein sulphides

6.3.4.1 Chlorite-quartz-pyrite type

Black chlorite containing various amounts (20-80%) of quartz and medium- to coarse-grained pyrite characterize this type of sulphide-bearing unit. In places the pyrite occurs as disseminations in chlorite, but more typically it is associated with quartz, either in vein networks or irregular masses. A photograph of drill core samples showing features typical of this type of sulphide-bearing unit is presented as Figure 6-27. The sample at the bottom left of the photograph shows medium- to coarse-grained pyrite in black chlorite. Network pyrite-bearing quartz veins cutting black chlorite, seen in samples at the top and bottom centre of the photograph, give the rock a brecciated appearance. The bottom-right sample shows abundant medium- and coarse-grained pyrite in black chlorite and quartz gangue.

6.3.4.2 Quartz-pyrite-chlorite type

The quartz-pyrite-chlorite sulphide-bearing units consist of 30 to 70 per cent pyrite, plus rare chalcopyrite and sphalerite, in quartz-veined to massive silicified rock. A continuum exists between the chlorite-pyrite-quartz type of sulphide-bearing unit and this

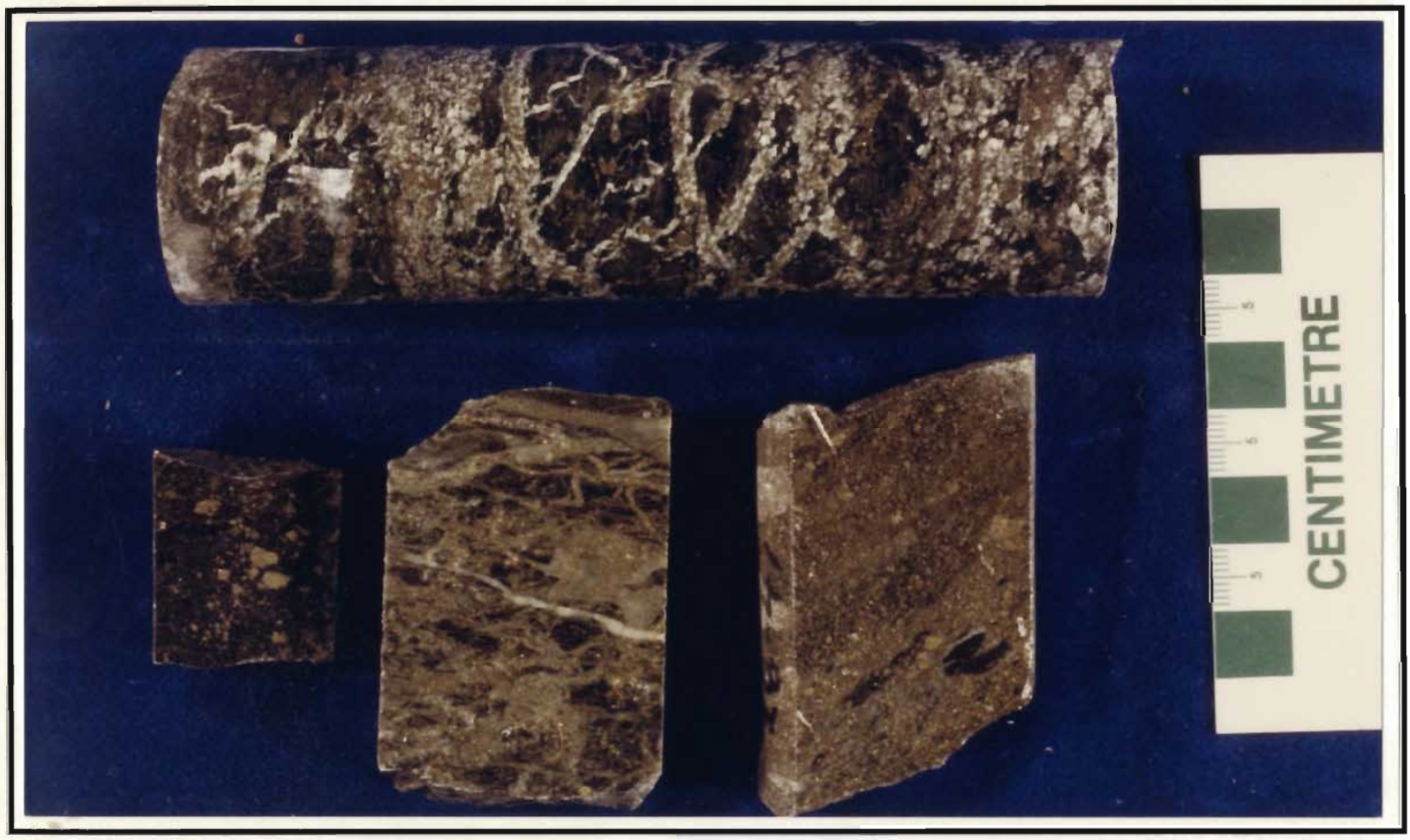

Figure 6-27: Photograph of drill core samples showing features of the chlorite, pyrite, quartz sulphide-bearing zone. Sample at top of photograph is from DDH SK 30 at 959' (292.3 m); sample at bottom-left of photograph is from DDH SK 28 at 530.5' (161.7 m); sample at bottom-centre of photograph is from DDH SK 30 at 821' (250.2 m); and sample at bottom-right of photograph is from DDH SK 28 at 532.5' (162.3 m). See text for discussion.

type. Quartz and pyrite make up approximately 80 per cent of the rocks, the remaining 20 per cent consisting of scattered, discontinuous chlorite-rich masses, some of which contain extremely altered varioles. The pyrite is generally medium to coarse grained and occurs as veins, massive bodies and disseminated cubes within the quartz. The chalcopyrite and sphalerite occur typically along the outside portions of quartz veins.

Figure 6-28 is a photograph of core samples typical of this type of sulphide-bearing unit. Note the varying proportions of quartz to pyrite in the samples and the occurrence of small amounts of very dark green chlorite in sample 7. The dark mineral surrounding the irregular quartz mass at the bottom of sample 5 is sphalerite. Alternating quartz- and pyrite-rich areas in sample 2 impart a poorly developed "layering". Sample 4 is rich in sphalerite (dark grey) and chalcopyrite (light gold), the sulphides occur as discontinuous, contorted layers in quartz.

Sample 6 is of a pyrite-bearing quartz-veined grey chert unit present in DDH SK 28. Note that the chert is hematite stained in its central portion.

6.4 Local Alteration

6.4.1 Secondary mineral assemblages

Distinct alteration zones, characterized by changes in the components and proportion of components comprising secondary mineral assemblages, envelop the Skidder Prospect sulphide-bearing zones. The secondary mineral assemblages are: chlorite, calcite, epidote ± hematite; chlorite, quartz, calcite, epidote; chlorite, quartz, calcite; chlorite, quartz, pyrite; and quartz, pyrite, chlorite — arranged in order from farthest away to closest to the sulphide-bearing zones. The distribution of the various secondary mineral assemblages is shown on Figures 6-3 to 6-10.

The secondary mineral assemblage chlorite, calcite, epidote ± hematite, which is typical of spilitized Skidder basalts, marks the outer limit of mineralogical changes associated with the Skidder Prospect alteration zone. On this basis, the outer limit of the

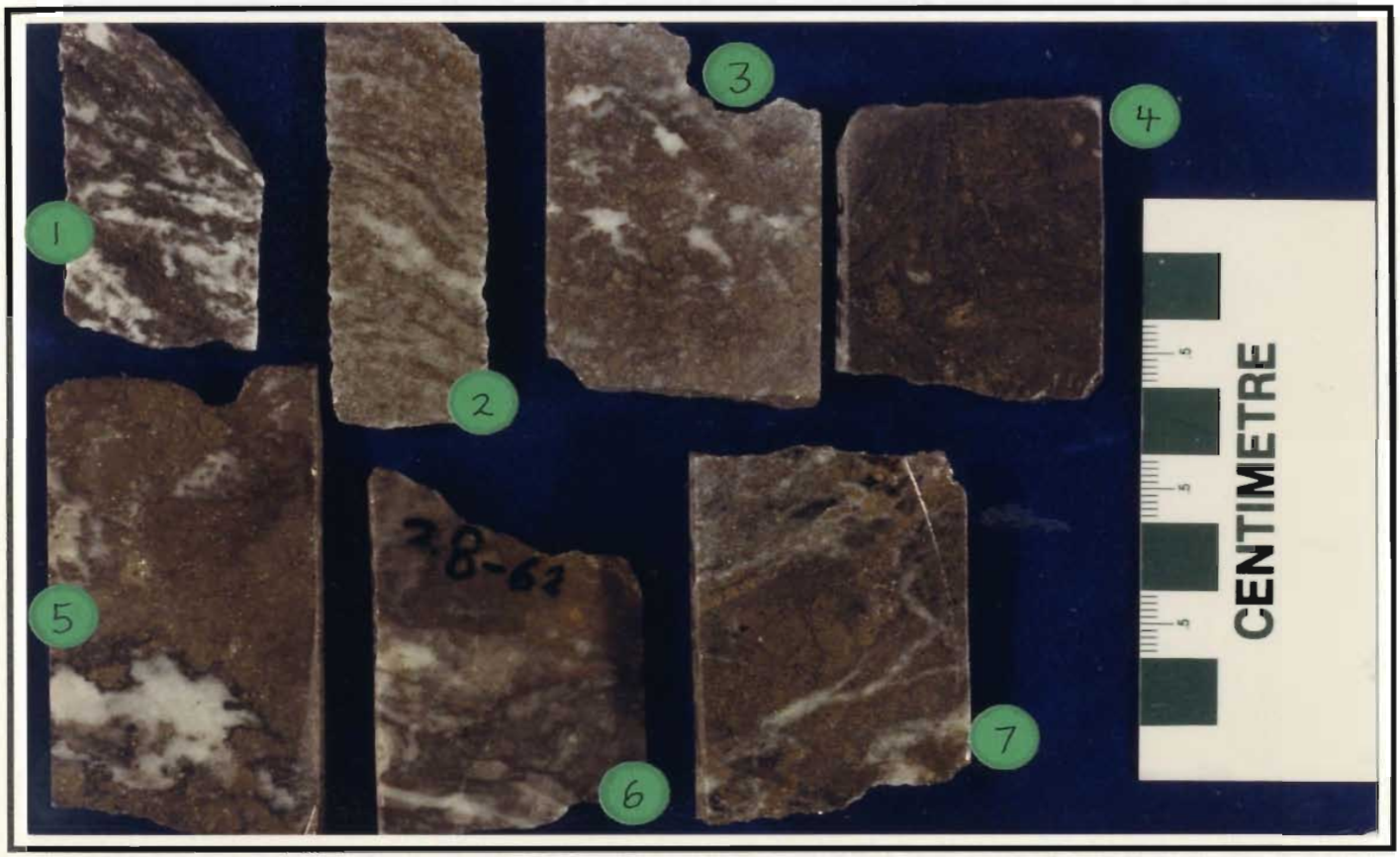

Figure 6-28: Photograph of drill core samples showing features of the quartz, pyrite, chlorite sulphide-bearing zone. Sample 1 is from DDH SK 31 at 138' (42.1 m); sample 2 from DDH SK 30 at 912.5' (278.1 m); sample 4 from DDH SK 27 at 579.5' (176.6 m); sample 6 from DDH SK 28 at 666' (203.0 m); and sample 7 is from DDH SK 30 at 908.5' (276.9 m). It is unknown from which diamond drill hole(s) samples 3 and 5 were collected. See text for discussion.

alteration is between 100 and 300 m away from the sulphide-bearing zones. The modes of occurrence of the various secondary minerals are described below. Calcite and epidote occur in veinlets and amygdules. "Blotches" of epidote, typically 5-15 cm in diameter, are also present in some areas. Hematite is less abundant than epidote and calcite, and is more prevalent in pillow breccia zones. Hematite occurs as veins and, in some areas, is disseminated throughout the rock. Figure 6-29 is a photograph of drill core samples that show the typical mode of occurrence of the secondary minerals in this alteration zone. The sample at the top shows a hematite veinlet cut by epidote veins, which are, in turn, cut by calcite veins. In the sample at the centre of the photograph, an epidote-rich area is cut by calcite-hematite veins. An epidote "blotch", containing white-pink calcite-filled amygdules, is shown in the bottom sample.

The absence of hematite, and the occurrence of quartz ± calcite in veins and amygdules define the chlorite, quartz, calcite, epidote alteration zone, this being the outermost alteration assemblage associated with the Skidder Prospect. The change in secondary mineral assemblage is typically noted about 50 to 75 m away from the massive sulphide zones and 100 to 300 m removed from the disseminated and vein sulphides, e.g. those present in holes SK 30 and SK 34.

An increase in the amount of chlorite, the lack of epidote, and the presence of fine grained, grey siliceous areas mark the chlorite, quartz, calcite alteration zone. This mineral assemblage occurs typically between 30 and 70 m away from the massive sulphide zones and 70 to 150 m away from the disseminated and vein sulphide zones. The siliceous sections characteristically have quartz veinlets throughout and range from 5 to 20 cm across (as estimated from the length of the silicious areas in drill core). Figure 6-30 is a photograph of drill core samples showing characteristics of this alteration zone. The light grey area at the centre of the variolitic pillow in the drill core sample at the top of the photograph, and the brown and grey pillow breccia fragments in the centre and bottom-left drill core samples, have been pervasively silicified and cut by later quartz veins. Note that

Figure 6-29: Photograph of drill core samples showing modes of occurrence of secondary mineral assemblages characteristic of the chlorite, calcite, epidote ± hematite alteration zone. Sample at top of photograph is from DDH SK 28 at 189' (57.6 m); sample in centre of photograph is from DDH SK 35 at 992.5' (302.5 m); and sample at the bottom of the photograph is from DDH SK 28 at 190' (57.9 m). See text for discussion.

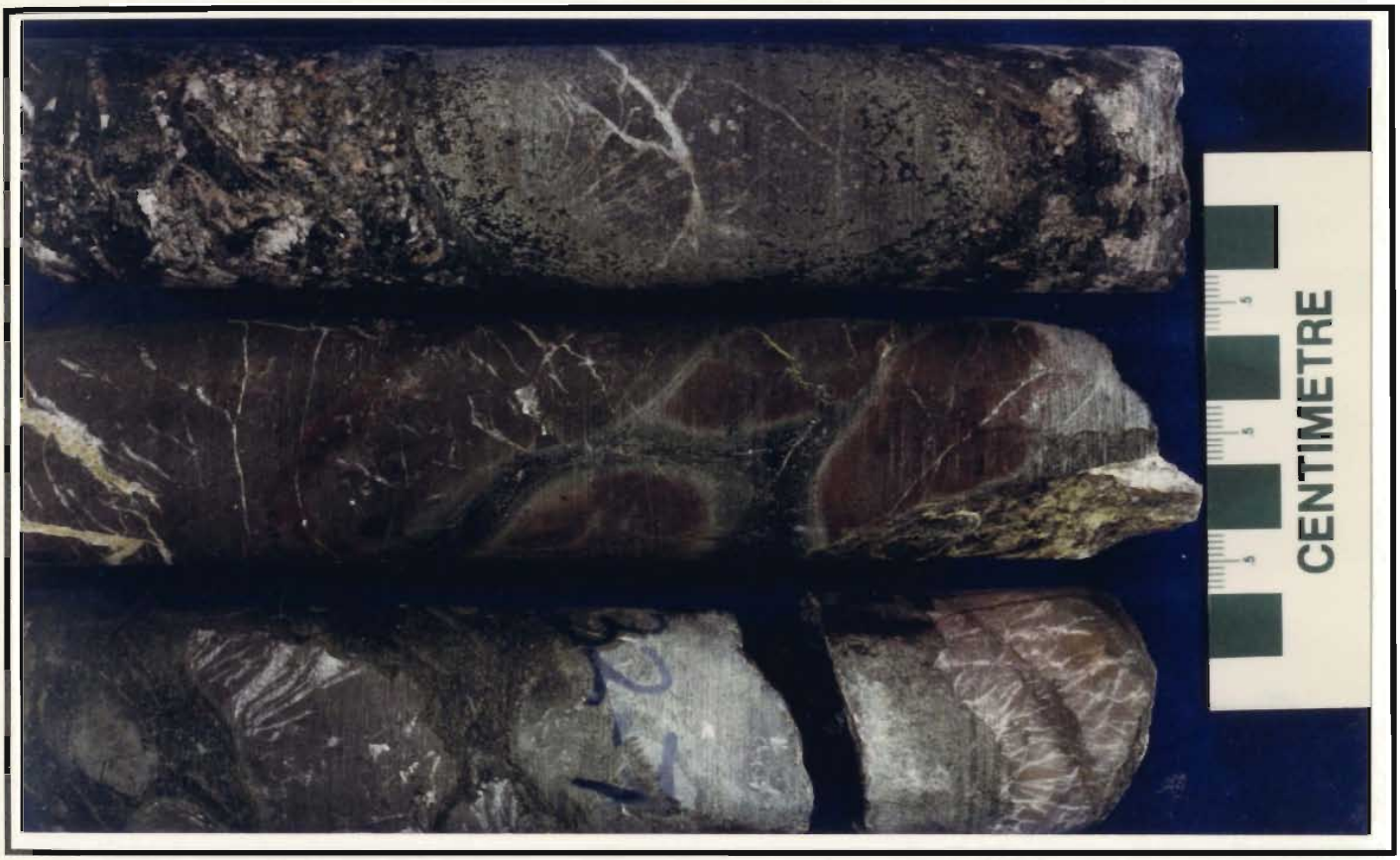

Figure 6-30: Photograph of drill core samples showing modes of occurrence of secondary mineral assemblages characteristic of the chlorite, quartz, calcite alteration zone. Sample at top of photograph is from DDH SK 34 at 982' (299.3 m); sample in centre of photograph is from DDH SK 30 at 77.5' (23.6 m); sample at the bottom-left of the photograph is from DDH SK 32 at 196' (59.7 m); and sample at the bottom-right is from DDH SK 30 at 612' (186.5 m). See text for discussion.

the pillow and pillow breccia fragments have been preferentially silicified, in contrast to the matrix, which has been highly chloritized. Grey, fine grained quartz veins cut by white veinlets, which are at right angles to the walls of the larger veins, are also characteristic of this type of alteration (bottom-right drill core sample). Note that pyrite occurs in the centre of the large vein.

A marked increase in chlorite, quartz and pyrite, accompanied by a decrease in calcite relative to zones one and two characterize the chlorite, quartz, pyrite and quartz, chlorite, pyrite alteration zones. Rocks displaying these secondary mineral assemblages are the most intensely altered, typically occurring less than 50 m away from the sulphide-bearing zones. Chlorite and quartz have an antithetic relationship in these alteration zones, and a continuum exists between rocks that contain an estimated 60 to 90 per cent chlorite and those that contain similar percentages of quartz. Rocks in these alteration zones also contain between 10 and 80 per cent pyrite, ± minor chalcopyrite and sphalerite. Drill core samples showing features typical of this alteration zone are shown in Figure 6-31. The sample at the top of the photograph is of highly silicified rock; note that bleaching and silicification has permeated outward from fractures (now filled with pyrite) such that isolated patches of medium green-grey less silicified material are preserved away from the fractures. The sample in the bottom of the photograph illustrates characteristics of the chlorite-rich end member of this alteration zone; in this sample highly chloritized basalt is cut by pyrite-bearing quartz veins. Note again that pyrite occurs in the centre of the quartz veins. Other examples of rocks that have been almost completely altered to chlorite ± talc are shown in Figures 6-32 and 6-33. In places, these rocks are composed of very fine grained, light green, elongate, chlorite-rich "fragments" in a black chlorite matrix (sample at right in Figure 6-32), in other areas the chlorite ± talc rock has an autobrecciated appearance (sample at left in Figure 6-32). Abundant pyrite occurs between "fragments" in places (sample at left in Figure 6-32), and in black chlorite (sample at right in Figure 6-32). Note that the fragments in the sample on the left in Figure 6-32 can be fitted back together.

Figure 6-31: Photograph of drill core samples showing modes of occurrence of secondary mineral assemblages characteristic of the quartz, pyrite, chlorite; and the chlorite, quartz, pyrite alteration zones. Sample at top of photograph is from DDH SK 29 at 707.5' (215.6 m); and sample at the bottom of the photograph is from DDH SK 28 at 632' (192.6 m). See text for discussion.

Figure 6-32: Photograph showing features of chlorite/talc-rich rocks as noted in the Skidder Prospect drill core. Sample at left of photograph is from DDH SK 30 at 578.5' (176.3 m); sample at right of photograph is from DDH SK 34 at 1454.5' (443.3 m). See text for discussion.

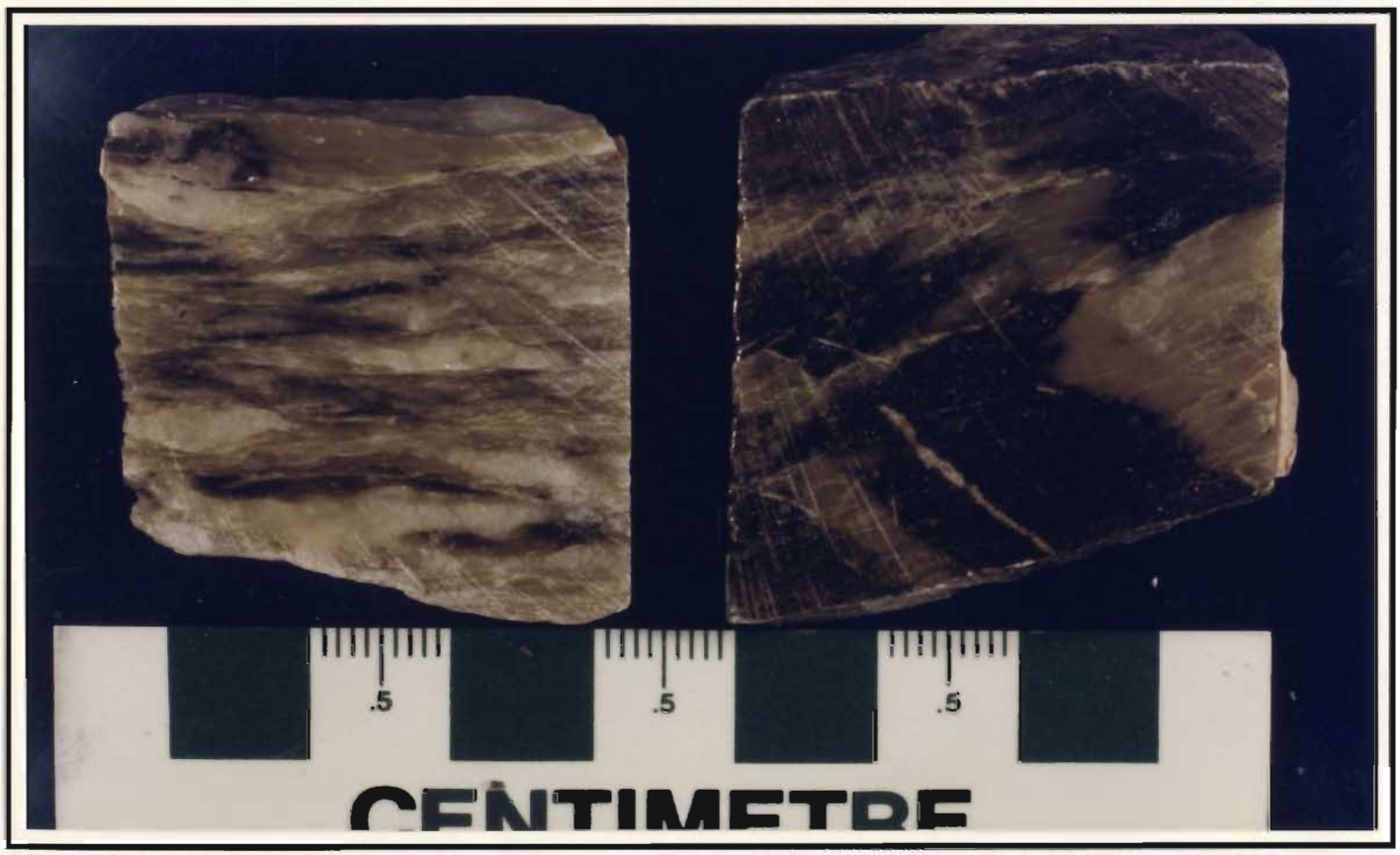

Figure 6-33: Photograph of Skidder Prospect drill core samples composed almost entirely of talc (very light green) and black chlorite. Sample at left of photograph is from DDH SK 31 at 93' (28.3 m); and sample at right of photograph from DDH SK 30 at 967.5' (294.9). See text for discussion.

In places, the light green chlorite-rich material, black chlorite and pyrite occur in distinct layers. In other places, the rocks are composed entirely of black chlorite and/or light green talc (Figure 6-33). Sulphide-rich end members of the chlorite, quartz, pyrite; and quartz, chlorite, pyrite alteration zones are described above in Section 6.3.4 (disseminated and vein sulphides). Examples of pyrite-rich samples are shown in Figures 6-27 and 6-28, which accompany Section 6.3.4.

6.4.2 Preserved host-rock textures

In most areas alteration is not intense enough in the chlorite, calcite, epidote ± hematite; chlorite, quartz, calcite, epidote; and chlorite, quartz, calcite alteration zones to obliterate original textures of the rock. In contrast, original textures have been completely obliterated in large portions of the most intensely altered rocks that occupy the chlorite, quartz, pyrite; and pyrite, quartz, chlorite alteration zones. Hence, for example, the chlorite- ± talc-rich rocks have been variably labelled chlorite-talc rock, chlorite tuff or chlorite-rich aquagene tuff on Figures 6-3 to 6-10 and Figures 6-16 to 6-24. Nevertheless, in places, some macroscopic features such as pillow outlines and varioles are preserved, even though the rocks have been almost completely replaced by various combinations of quartz, black chlorite and pyrite. Photographs showing preserved host-rock textures are presented in Figures 6-34 and 6-35. Pillow selvages and amygdules are preserved in drill core samples at the top and bottom of Figure 6-34, and in sample 1 on Figure 6-35. Note that the selvages are marked by abundant pyrite-bearing black chlorite. Highly altered varioles are evident in the centre-right sample on Figure 6-34 and in samples 1 to 4 on Figure 6-35. Buff angular fragments of highly altered host rock occur in quartz in sample 6 on Figure 6-35. Note that the rock is intensely silicified.

Figure 6-34: Photograph of drill core samples showing preserved host rock textures from the chlorite, quartz, pyrite; and the quartz, pyrite, chlorite alteration zones. Sample at top of photograph is from DDH SK 30 at 674' (205.4 m); sample in centre-left of photograph is from DDH SK 31 at 28' (8.5 m); sample in centre-right of the photograph is from SK 34 at 1243' (378.9 m); and sample at bottom of the photograph is from DDH SK 34 at 1339' (408.1 m). See text for discussion.

Figure 6-35: Photograph of drill core samples showing preserved host rock textures (particularly varioles) from the chlorite, quartz, pyrite and quartz, pyrite, chlorite alteration zones. Sample 1 is from DDH SK 35 at 1499' (456.9 m); sample 2 is from DDH SK 32 at 572' (174.3 m); sample 3 is from DDH SK 30 at 821' (250.2 m); sample 4 is from DDH SK 30 at 822' (250.5 m); sample 5 is from DDH SK 30 at 848' (258.5 m); and sample 6 is from DDH SK 30 at 893' (272.2 m). See text for discussion.

6.5 Structure

The strike of rock units in the vicinity of the Skidder Prospect varies from north-northeasterly, as shown in the southwestern portion of Figure 6-2, to northeasterly, as indicated in the northeastern part of Figure 6-2. Foliations trend predominantly northeasterly and dip steeply to the southeast. One outcrop in the east-central portion of Figure 6-2, however, shows an east-northeasterly striking, steep southerly dipping foliation.

As shown in Figure 6-3, variolitic pillow basalt occurs both above and below sulphide-bearing, intensely altered rocks in SK 30 and SK 34, and highly altered varioles are preserved in the sulphide-bearing zones in both holes. In contrast, variolitic pillow basalt occurs only below the massive sulphides in drill holes SK 27 and 28. This suggests that the disseminated and vein sulphide-bearing alteration zones in SK 30 and 34 crosscut stratigraphy (Figure 6-3), and supports Barbour's (Barbour, 1977) interpretation that these zones represent a stockwork or feeder zone to the overlying massive sulphides. This relationship between the massive sulphides and related alteration, and the contact between variolitic and nonvariolitic pillow basalts shown on Figure 6-3, suggest that the rock units are gently dipping and facing toward the southeast. Caution is warranted here however since the very presence of an intense alteration zone indicates a zone of high permeability and probable faulting. Pillowed basalt in outcrop shown in the east-central portion of Figure 6-2 also faces southeast but is steeply dipping. This southeast facing of units is in contrast to northwest-facing directions typical of the Skidder Basalt elsewhere and suggests local folding and/or faulting in the area (see Figure 3-4). Pillows indicate that units to the southeast of the fault shown in the southeast portion of Figure 6-2 are steeply southeast dipping and face to the northwest.

A large number of gouge zones are noted in the Skidder Prospect drill core. They are particularly common in the highly altered, intensely chloritized rocks, as would be

expected since these rocks are very soft and thus susceptible to deformation. The amount of movement, if any, that has occurred along the gouge zones is unknown.

The Skidder Prospect semimassive to massive sulphides occur predominantly in two lens-shaped bodies termed Lenses 1 and 2 (Barbour, 1977) (Figure 6-1). Lens 1 extends from surface to a depth of 213 m. It plunges 37 degrees west having a known length of 380 m along the plunge. It has a maximum width of 90 m, a maximum known thickness of 11 m, and an average thickness of 4.1 m. Lens 2 extends from about 213 m to a depth of 412 m. It plunges 57 degrees west having a defined length along plunge of 243 m. It has a maximum width of 68 m, a maximum known thickness of 6.7 m, and an average thickness of 3.4 m (Barbour, 1977).

The occurrence of the sulphide-bearing zones at the contact between variolitic and overlying nonvariolitic basalts in Lens 1, and the reverse for Lens 2 suggests that, barring structural complexities, Lens 2 stratigraphically underlies Lens 1.

6.6 Petrography

The petrography of the Skidder Basalt has been presented in Chapter 4. Hence, the descriptions and discussion below concentrate mainly on changes in the petrography of the rocks as a result of interaction with hydrothermal fluids during the Skidder Prospect mineralizing event(s). The descriptions are arranged in order from the least altered rocks of the chlorite, calcite, epidote ± hematite alteration zone, which have a similar petrography to spilitized Skidder basalts elsewhere, to the highly altered rocks of the chlorite, quartz, pyrite; and quartz, chlorite, pyrite alteration zones, which are almost completely dominated by secondary minerals and textures related to hydrothermal alteration during the mineralizing event(s). Petrographic descriptions of the massive and heavily disseminated sulphide-bearing rocks, the spatially associated jasper, and the trondhjemites that intrude rocks in the immediate vicinity of the Skidder Prospect are also presented.

6.6.1 Petrography of the alteration zones

Summary tables showing the relative abundances of minerals in, and a partial geochemical analysis of rocks thin-sectioned from the various alteration zones are presented in Tables 6-1 to 6-6. Rocks analyzed show a considerable range of Zr concentrations in each of the alteration zones, suggesting that a variety of basaltic compositions are represented.

6.6.1.1 Chlorite, calcite, epidote ± hematite zone

Rocks having this secondary mineral assemblage are similar to spilitized basalts outside the Skidder Prospect alteration zone. Pillowed and massive basalts are composed predominantly of albite, intergranular sphene and subhedral opaque minerals (abundant in some rocks), and intersertal chlorite and quartz (Table 6-1).

Most samples have several 0.5 to 1 mm-long, albitized plagioclase phenocrysts, and a lesser number also contain relict clinopyroxene grains, which are up to 1 mm across.

Table 6-1: Petrographic table showing rock type, partial geochemical analysis and mineralogy of mafic rocks from the Skidder Prospect cl,cc,ep ± hm alteration zone

Key:	See Figure 6-1 for location of drill holes
	Abbreviations: Ab-albite, Cpx-clinopyroxene, Cl-chlorite, Cc-calcite, Ep-epidote, Qz-quartz, Chr-chromite Amph-amphibole, hm-hematite, py-pyrite, serp-serpentine, sc-sericite, opaques or opaq-opaque minerals acic-acicular minerals, bx-breccia
	Abundance of mineral relative to its average content in mafic rocks from the Skidder area: x-low, xx-medium, xxx-high
	See Appendix B for complete whole rock analyses and description of analytical methods

Sample Name	Rock Type	Depth feet	Depth m	SiO_2 %	TiO_2 %	MgO %	Zr ppm	Ab	Cpx	Cl	Sphene	Cc	Ep	Qz	Chr	Opaques	Other Minerals and Comments
SK 27 01	Pillow Bx	20	5.9	48.3	1.3	5.0	75	xx	x	xx	xx	xx	xx	x		xxx	hematite, acic. opaq.
SK 27 02	Massive	31	9.3	52.7	0.8	5.7	44	xxx	xx	xx	xx	x		xx		xxx	sericite (?)
SK 27 08	Pillowed	142	43.3	47.1	0.9	8.9	45	x	x	xx	xx	x	xxx	x		x	K-feldspar, amph. (?)
SK 28 06	Pillowed	99	30.0	51.5	0.8	9.2	41	xxx	x	xx	xx	x	xx	x		xx	
SK 28 153	Bx zone	153	46.6					x		x	x	xx		xxx			pyrite, sericite
SK 29 15	Diabase (?)	228	69.5	50.4	1.3	8.7	75	xx	xx	xx	xxx		x	x		x	
SK 30 20	Massive	244	74.2	53.1	1.0	5.4	48										
SK 30 245	Massive	245	74.7					xxx	xx	xx	xx		x	x		xxx	
SK 35 995	Pillowed	995	303.3					xx	xxx	xx	xx	xx	x	x	xx	x	
SK 36 113	Pillowed	113	34.4					xx	xx	xx	xx	xxx	x	x		x	amph. (x)

Table 6-2: Petrographic table showing rock type, partial geochemical analysis and mineralogy of mafic rocks from the Skidder Prospect cl,qz,cc,ep alteration zone

Key:	As per Table 6-1

Sample Name	Rock Type	Depth feet	Depth m	SiO_2 %	TiO_2 %	MgO %	Zr ppm	Ab	Cpx	Cl	Sphene	Cc	Ep	Qz	Chr	Opaques	Others + Comments
SK 14 543	Massive (?)	543	165.5					xxx		xx	xxx	xx	x	x		xxx	
SK 24 100	Pillow Bx	100	30.5					xxx	xx	xx	xx	xx	x	xx		xx	amph. (x)
SK 24 1180	Massive	1180	359.7					xx	xx	xx	xxx	xx	x	xx		xxx	
SK 24 1184	Massive	1184	360.9					xx		x	xx	xx	xxx	xx		xx	amph. (xx)
SK 32 74	Tuff (?)	74	22.6					?		xxx	xx			xx		xx	

A few plagioclase phenocrysts are carbonatized. Many samples have intergranular to subophitic intergrowths of 0.1-0.3 mm-long albitized plagioclase and stubby 0.05-0.2 mm-long prismatic clinopyroxene. Subhedral chromite is present in some thin sections. Hematization of subhedral opaque minerals imparts a pronounced reddish colouration to some of the rocks. In thin section SK 35 995, 0.5 mm-long, quench-textured clinopyroxene grains are intergrown with albitized plagioclase that does not exhibit quench-textured morphologies.

Clinopyroxene is typically altered to various combinations of amphibole, epidote and chlorite. In a few samples, K-feldspar replaces albitized plagioclase, particularly larger grains. Calcite ± chlorite ± quartz amygdules, and calcite and epidote veins occur in most samples; epidote also occurs as subhedral grains throughout some samples.

Thin section SK 28 153, of a breccia zone, is composed predominantly of anhedral quartz cut by coarse grained quartz veins and a few calcite and sericite veinlets.

6.6.1.2 Chlorite, quartz, calcite, epidote alteration zone

Pillowed and massive basalts from this alteration zone are composed predominantly of intergranular albite, sphene and subhedral opaque minerals; and intersertal chlorite and quartz (Table 6-2). Chloritized clinopyroxene grains are present in some samples and many samples have several 0.5 to 1 mm-long albitized plagioclase phenocrysts.

Calcite, epidote, quartz and chlorite occur in veinlets and amygdules, although subhedral epidote grains occur throughout some samples. Quartz has partially replaced intergranular albite laths in some areas, and, in thin section SK 24 100, has also partially replaced albite displaying fan-shaped and bowtie "quench-texture" morphologies (Lofgren, 1974).

6.6.1.3 Chlorite, quartz, calcite alteration zone

Macroscopically, this alteration zone is characterized by an overall increase in the amount of chlorite, lack of epidote and the presence of fine grained, grey siliceous areas. Quartz veins are common and the siliceous sections characteristically have quartz veinlets throughout.

Samples from this alteration zone that are richer in chlorite are composed predominantly of 0.2 to 0.5 mm-long, albitized plagioclase, accessory sphene and subhedral opaque minerals, and abundant intersertal chlorite (Table 6-3). Pyrite is abundant in some samples. A few 1 to 1.5 mm-long albitized plagioclase phenocrysts are present in most samples.

In many areas, albite laths, particularly the larger ones, have been partially to completely replaced by quartz, calcite and, locally, sericite. Alteration of albite to quartz in places results in two elongate single grains or aggregates of quartz separated by a thin sliver of chlorite or quartz along the original twin planes. Rounded quartz grains occur throughout some thin sections. Chlorite pseudomorphs grains that were probably originally clinopyroxene in some places, and, in some samples, sphene pseudomorphs skeletal grains that were probably originally ilmenite. A small number of quartz, chlorite or calcite veins are present in some samples, and a few contain "wispy" sericite veinlets. Pyrite occurs in some of the quartz veins. Anhedral masses of calcite occur throughout some samples.

Thin section SK 29 64 shows a cross-section through the outer portion of an altered variolitic pillow; including a portion of the nonvariolitic interior portion of the pillow, part of its outer variolitic rim and a portion of the chlorite-rich selvage. Varioles in the pillow rim contain a central core of chlorite and spherulitic albite concentrically surrounded by a an inner "ring" of albite and sphene, and an outer ring dominated by sphene (Figures 6-36 and 6-37). Brown birefringent chlorite and accessory sphene are the dominant minerals in the matrix to the varioles. The nonvariolitic inner portion of the pillow consists of partially

Table 6-3: Petrographic table showing rock type, partial geochemical analysis and mineralogy of mafic rocks from the Skidder Prospect cl,qz,cc alteration zone

Key:	As per Table 6-1

Sample Name	Rock Type	Depth feet	Depth m	SiO_2 %	TiO_2 %	MgO %	Zr ppm	Ab	Cpx	Cl	Sphene	Cc	Ep	Qz	Chr	Opaques	Other Minerals and Comments
SK 1 296	Massive (?)	296	90.2					xx		xx	xx	xx		x		xx	
SK 1 271	Tuff	271	82.6					xx		xx	xx	x		xxx		xx	
SK 1 312	?	312	95.1					xxx		xx	x	xx		xxx		x	autobrecciated, silicified
SK 3 49	Pillow Bx (?)	49	14.9					xxx		xx	xx			xxx		x	
SK 3 87	Pillow Bx (?)	87	26.5					x		xx	x	xxx		xx		xx	
SK 5 361	Pillow Bx (?)	361	110.0					xx		xx	xx	xxx		x		xx	
SK 7 105	Pillowed	105	32.0					xx		xx	xxx			xx		xxx	sericite or talc (xxx)
SK 7 159	Tuff (?)	159	48.5					xx		xx	xx	xxx		xx			foliated
SK 17 375	Massive (?)	375	114.3					xx		xx	x	xx		xx	x	xx	calcic plag. (?), sericite (x)
SK 18 52	Pillow Bx (?)	52	15.8					xx		xx	x	xxx		x		x	sericite (?)
SK 18 88	Diabase (?)	88	26.8					xx		xx	x	xx		x		x	
SK 18 299	Pillow Bx (?)	299	91.1					xx		xx	xx	xxx		x		x	
SK 18 357	Massive (?)	357	108.8					xx		xx	xx	xx		xx		x	
SK 19 114	Diabase (?)	114	34.7					xx		xx	xx	xxx		xx		x	
SK 20 403	Pillow Bx	403	122.8					xx		xxx	xx	xxx		x		xxx	pyrite, calcite vein
SK 27 18	Massive	316	96.3	71.4	0.3	2.5	94	xxx		xx	xx			xxx		x	
SK 27 33	Pillowed	517	157.6	46.5	1.1	12.7	77	xx		xx	xx			xx			pyrite
SK 28 17	Diabase (?)	335	102.1	46.7	0.9	9.2	48	xx		xxx	xx	xx		xx			sericite
SK 28 20	Massive	408	124.4	43.2	0.3	16.3	64	xx		xxx	x	xx		xx			pyrite
SK 28 58	Massive	640	195.1	47.9	1.2	12.3	74	xx		xxx	xx	x		xx		x	
SK 29 416	Diabase (?)	416	126.8					xx		xx	xxx	x		x			amphibole (x)
SK 29 506	Diabase (?)	506	154.2					xx		xx	xx	xx		xx		xxx	
SK 29 33	Diabase (?)	510	155.4	52.2	0.9	6.1	47										
SK 29 63	Pillowed	887	270.2	50.9	0.9	15.8	46	x	?	xxx	xx	x		xx		x	
SK 29 64	Pillowed	915	278.7	43.5	1.1	14.1	55	x		xxx		xx		x	xx		variolitic, pyrite

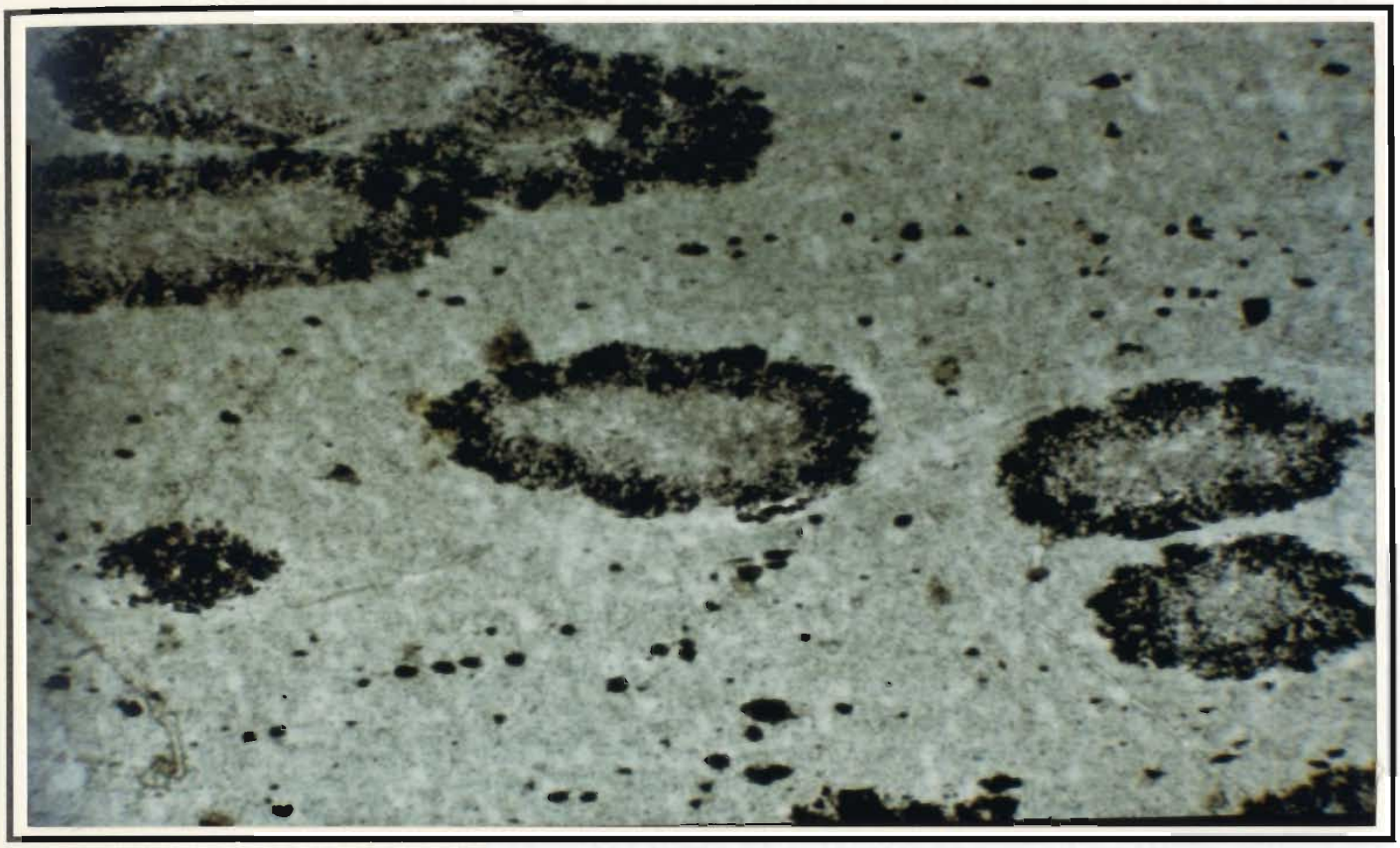

Figure 6-36: Transmitted light photomicrograph of chlorite-rich variolitic pillow rim. Thin section SK 29 64, plane polarized light, 3.2 x. **— 0.5 mm —**

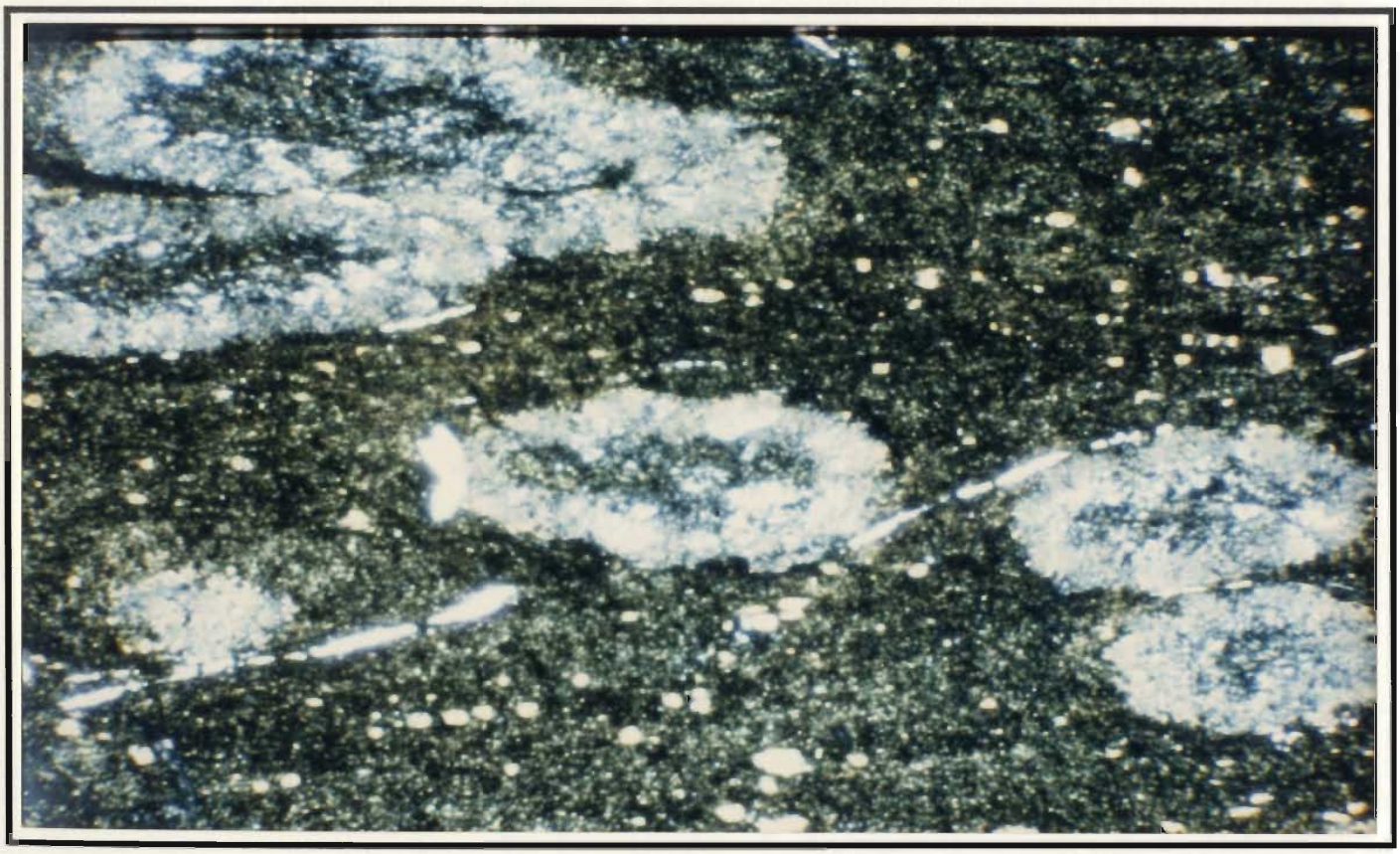

Figure 6-37: Transmitted light photomicrograph of same area shown in Figure 6-36 but under crossed nicols. Thin section SK 29 64, crossed nicols, 3.2 x. **— 0.5 mm —**

silicified albite, much of which displays fan-shaped quench textures; dense granular sphene; intersertal chlorite; and lesser amounts of opaque minerals and intersertal quartz.

Poorly aligned albite, flattened calcite amygdules, and intersertal chlorite define a foliation in thin section SK 7 159. Similarly, elongate quartz, calcite and poorly aligned carbonatized, silicified albite define a foliation in thin section SK 32 74.

Coarser grained massive units, interpreted as coarse grained massive flows or diabase, typically display intergranular to subophitic textures; they have a similar mineralogy, and show a similar style and degree of alteration to finer grained mafic units. Average grain size for albite, the predominant euhedral mineral, is about 0.5 mm in these rocks. Portions of 0.5 mm-long prismatic clinopyroxene grains are preserved in thin section SK 29 416. Most of the grains have been altered to chlorite and lesser amounts of fibrous actinolite (Figures 6-38 and 6-39). The grains are subophitically intergrown with albitized plagioclase that has been variably silicified, carbonatized and/or sericitized. Calcite completely replaces what were probably originally clinopyroxene grains in thin section SK 28 17, as indicated by preserved subophitic texture between the calcite masses and silicified, sericitized albite.

Quartz-rich samples from this alteration zone are similar in most respects to the nonvariolitic chlorite-rich samples, the major difference being that intersertal quartz rather than chlorite predominates in the groundmass. Albite laths are partially altered to quartz in most places. Glomeroporphyritic clusters, in addition to single grains, of silicified, plagioclase phenocrysts occur in some samples.

6.6.1.4 Chlorite, quartz, pyrite alteration zone

The chlorite, quartz, pyrite alteration zone is characterized by a marked increase in chlorite and decrease in calcite, relative to the chlorite, quartz, calcite zone. In some areas, chlorite makes up an estimated 50 to 60 per cent of the rock. Pervasively silicified areas cut by quartz veinlets, similar to those in the previously described zone, are present. All rocks

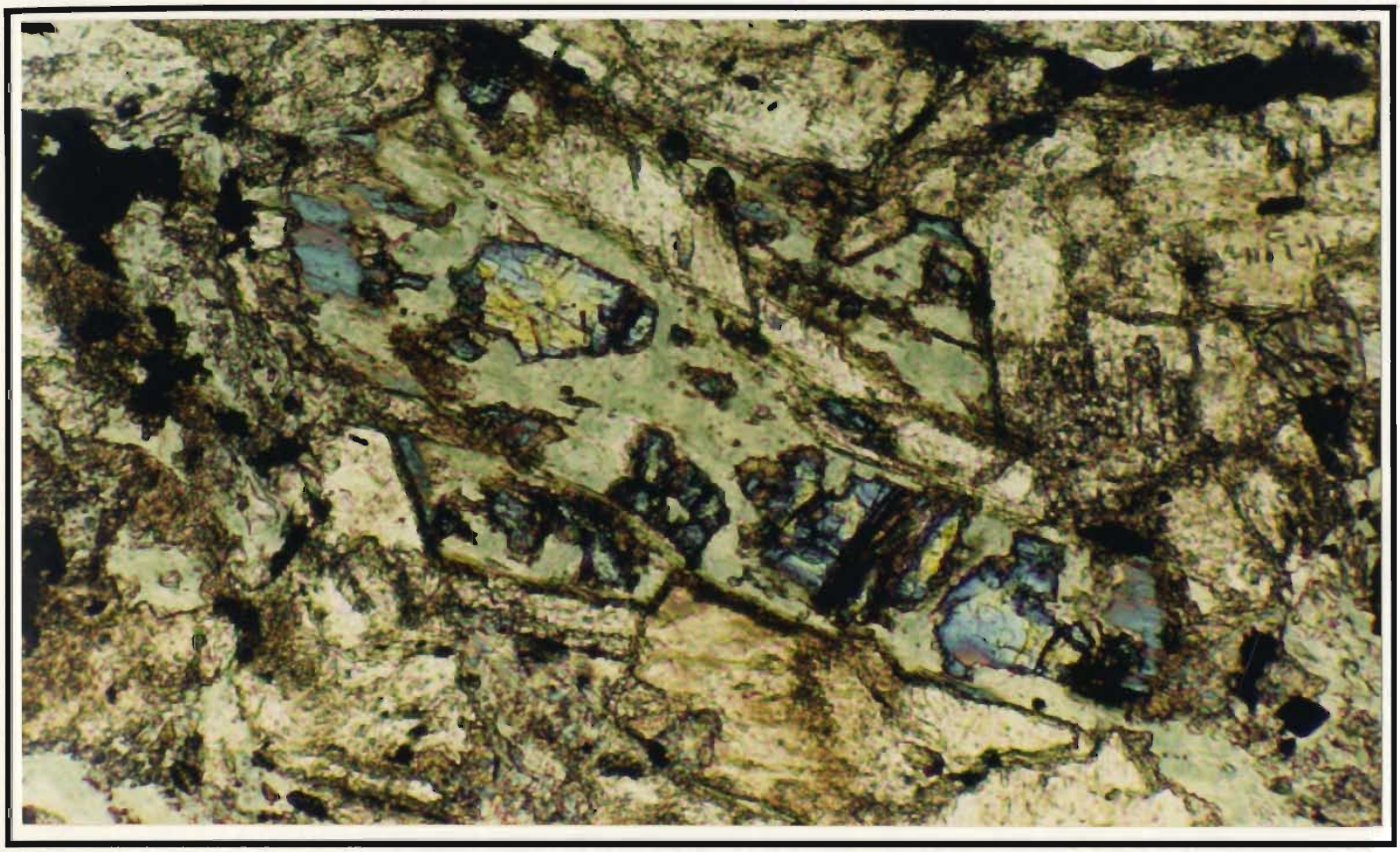

Figure 6-38: Transmitted light photomicrograph showing prismatic clinopyroxene grain partially altered to chlorite and fibrous actinolite, the latter being confined to the grain's extremities. Thin section SK 29 416 (416'), plane polarized light, 10 x. —— **0.2 mm** ——

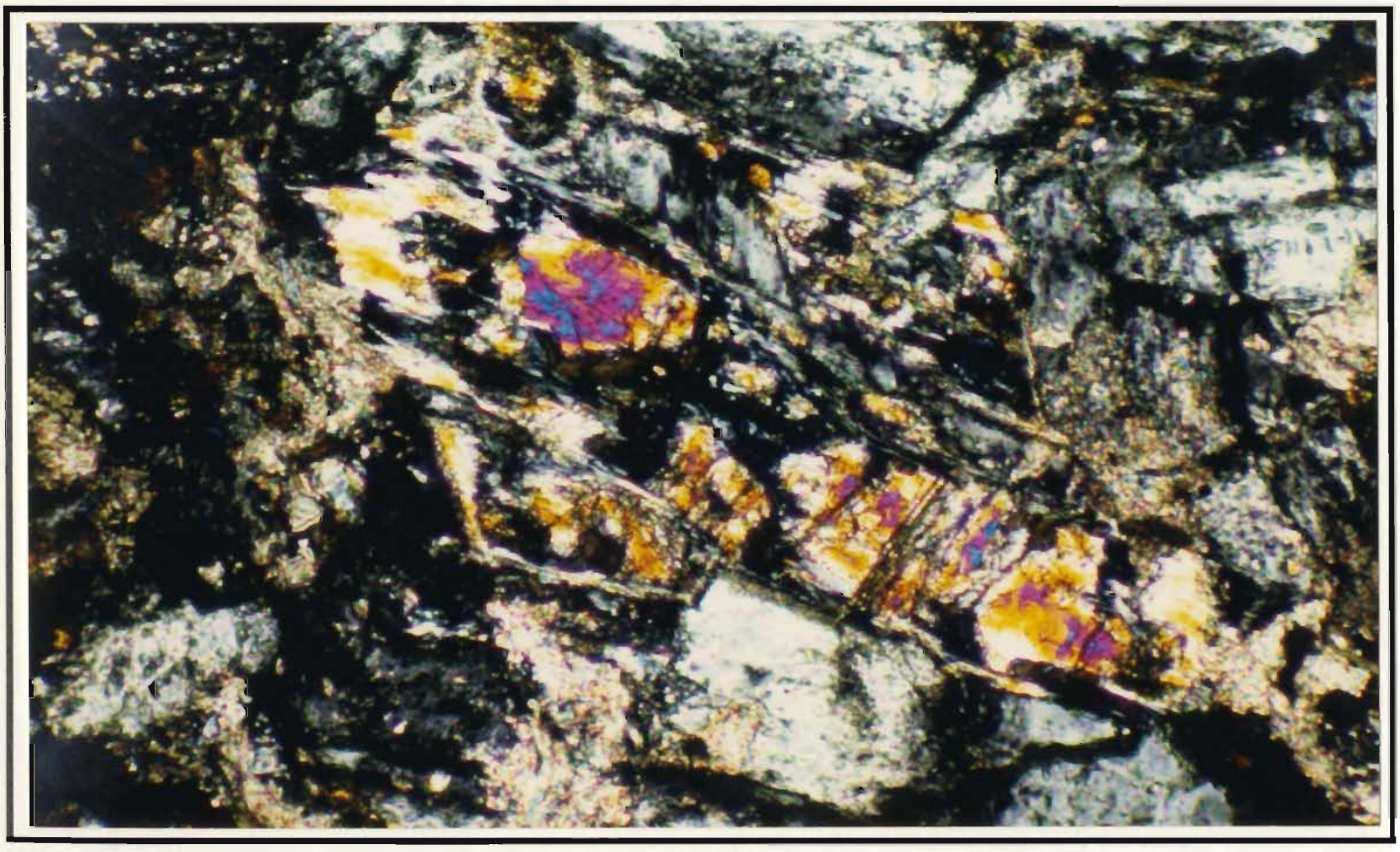

Figure 6-39: Transmitted light photomicrograph of same area shown in Figure 6-38 but under crossed nicols. Thin section SK 29 416 (416'), crossed nicols, 10 x. —— **0.2 mm** ——

in this alteration zone have been highly altered (some more intensely than others) to various combinations of chlorite, talc, quartz and, in some places, calcite (Tables 6-4 and 6-6).

Less intensely altered rocks from this alteration zone are composed of abundant chlorite, in many areas showing anomalous blue birefringence, and lesser amounts of 0.05 to 1-mm long quartz pseudomorphs of albite. Although in most places the albite has been completely replaced and pseudomorphed by quartz, in a few areas the replacement is not complete and some albite is preserved. Selective replacement of albite by quartz is suggested in thin section SK 29 49, where larger grains have been completely replaced by quartz whereas 0.1 mm-long albite grains in the groundmass are, in places, partially preserved. Parts of thin section SK 27 27 show fan-shaped or bow-tie shaped clusters of partially silicified albite, suggesting preserved quench textures. Chlorite pseudomorphs albite and clinopyroxene (?) in some places. Chlorite and quartz or, to a lesser extent, calcite fill amygdules. Intergranular sphene and pyrite make up most of the remainder of the rocks. Thin section SK 27 44, of a diabase dyke (?) that intrudes layered massive sulphides (Figure 6-17), shows similar mineralogy and degree of alteration as the less altered rocks in this zone. Some albite is preserved in this sample but much of the groundmass is composed of quartz and chlorite, pyrite is also noted.

More intensely altered samples from this alteration zone are composed almost entirely of chlorite, accompanied by lesser amounts of quartz and pyrite. Subhedral chromite is noted in some thin sections. Chlorite, in places showing spherulitic growth, occupies intersertal areas and fills amygdules, irregular-shaped vugs and veins. Quartz occurs as albite pseudomorphs, as irregular grains throughout the rock, and in amygdules and veins. Quartz that pseudomorphs albite has, in some thin sections, been partially to completely replaced by chlorite (Figures 6-40 and 6-41). Abundant pyrite occurs with quartz in veins, and as disseminations throughout the samples. Varioles in thin section SK 28 81 are completely replaced by quartz and minor chlorite. The matrix is predominantly

Table 6-4: Petrographic table showing rock type, partial geochemical analysis and mineralogy of mafic rocks from the Skidder Prospect cl,qz,py alteration zone

Key:	As per Table 6-1

Sample Name	Rock Type	Depth feet	Depth m	SiO_2 %	TiO_2 %	MgO %	Zr ppm	Ab	Cpx	Cl	Sphene	Cc	Ep	Qz	Chr	Opaques	Other Minerals and Comments
SK 5 154	Massive (?)	154	46.9					xx		xxx	xx			xx			pyrite
SK 7 280	Tuff (?)	280	85.3							xxx	xxx			x			pyrite, talc (xx)
SK 7 354	Massive (?)	354	107.9					xx		xxx	xx			xx			pyrite
SK 7 379	Massive (?)	379	115.5					xx		xx	xx	x		xx			pyrite
SK 7 392	Massive (?)	392	119.5					xx		xxx	xxx	x		xx			pyrite
SK 16 296	Pillow Bx (?)	296	90.2							xxx	x	x		xx			pyrite
SK 22 605	Pillowed	605	184.4					xx	?	xxx	xxx	x		x		xx	variolitic
SK 25 891	Pillow Bx	891	271.6					xx		xxx	xxx	x		xx			pyrite
SK 27 26	Massive	401	122.2	41.6	1.1	21.3	65	x		xxx	xx	x		xx		x	pyrite
SK 27 27	Massive	425	129.5	41.5	1.3	19.7	73	x		xxx	xx	x		x		x	
SK 27 44	Diabase (?)	636	193.9	48.0	1.2	15.0	68	x		xxx	xx			xx			pyrite
SK 27 48	Massive	666	203.0	40.2	0.5	23.1	64	x		xxx	xx			xx			pyrite
SK 28 27	Pillow Bx	477	145.2	28.6	0.6	27.2	58			xxx	xx	x		x			pyrite
SK 28 51	Massive	558	170.1	53.1	0.5	12.2	26	xx		xxx	xx			xx			minor pyrite
SK 28 71	Diabase (?)	709	216.1	43.7	1.0	18.0	65	xx		xxx	xx			xx			
SK 28 73	Tuff (?)	716	218.1	31.4	0.4	27.4	55			xxx	x	xx		x			pyrite, talc (xx)
SK 28 75	Massive (?)	741	225.9	53.7	0.6	16.7	50			xxx	xx			xx	xx		pyrite, serpentine (?)
SK 28 81	Pillowed	798	243.1	46.1	0.8	19.0	51	x		xxx	xx			xx	x		pyrite, serpentine (?)
SK 29 572	Massive	572	174.3					xx		xx	xx			xx			
SK 29 49	Pillowed	749	228.1	44.4	1.1	19.5	61	x		xxx	xx			xx			pyrite, serpentine (?)
SK 29 50	Pillowed	757	230.6	45.9	1.2	17.7	69	x		xxx	xx	x		xx			pyrite, talc (?).
SK 29 51	Pillowed	783	238.7	48.7	1.0	18.0	59	x		xxx	xx			xx	x		pyrite, talc (?)
SK 29 868	?	868	264.6							xxx	xx	xx		xx			
SK 30 950	Tuff (?)	950	289.6							xxx	x	xxx		x			pyrite
SK 31 188	Tuff (?)	188	57.3							xxx	xx	x		xxx			pyrite

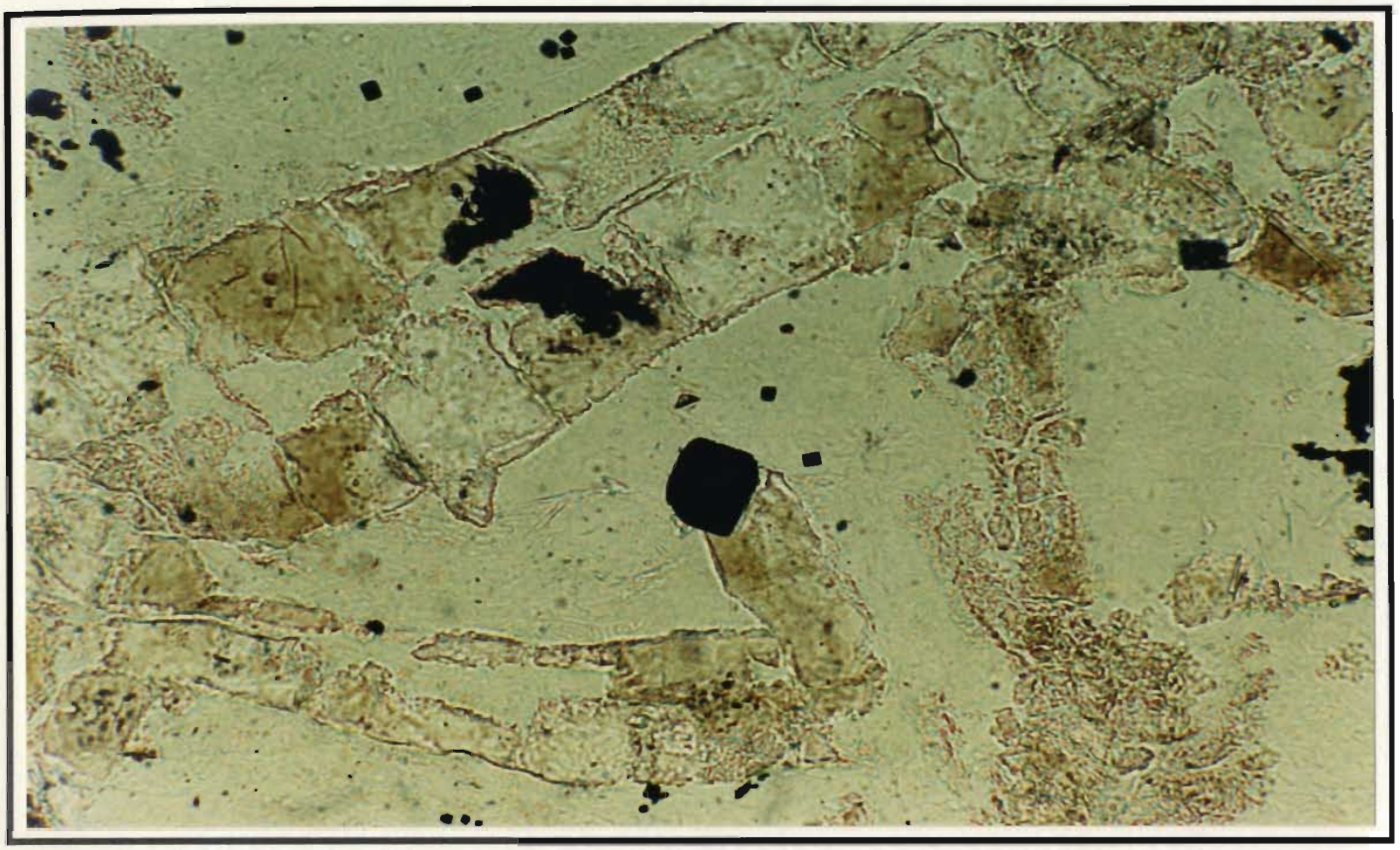

Figure 6-40: Transmitted light photomicrograph showing chlorite having partially replaced quartz pseudomorphs of albite. Note that the matrix has been almost completely chloritized. Thin section SK 5 154 (154'), plane polarized light, 20 x. —— **0.1 mm** ——

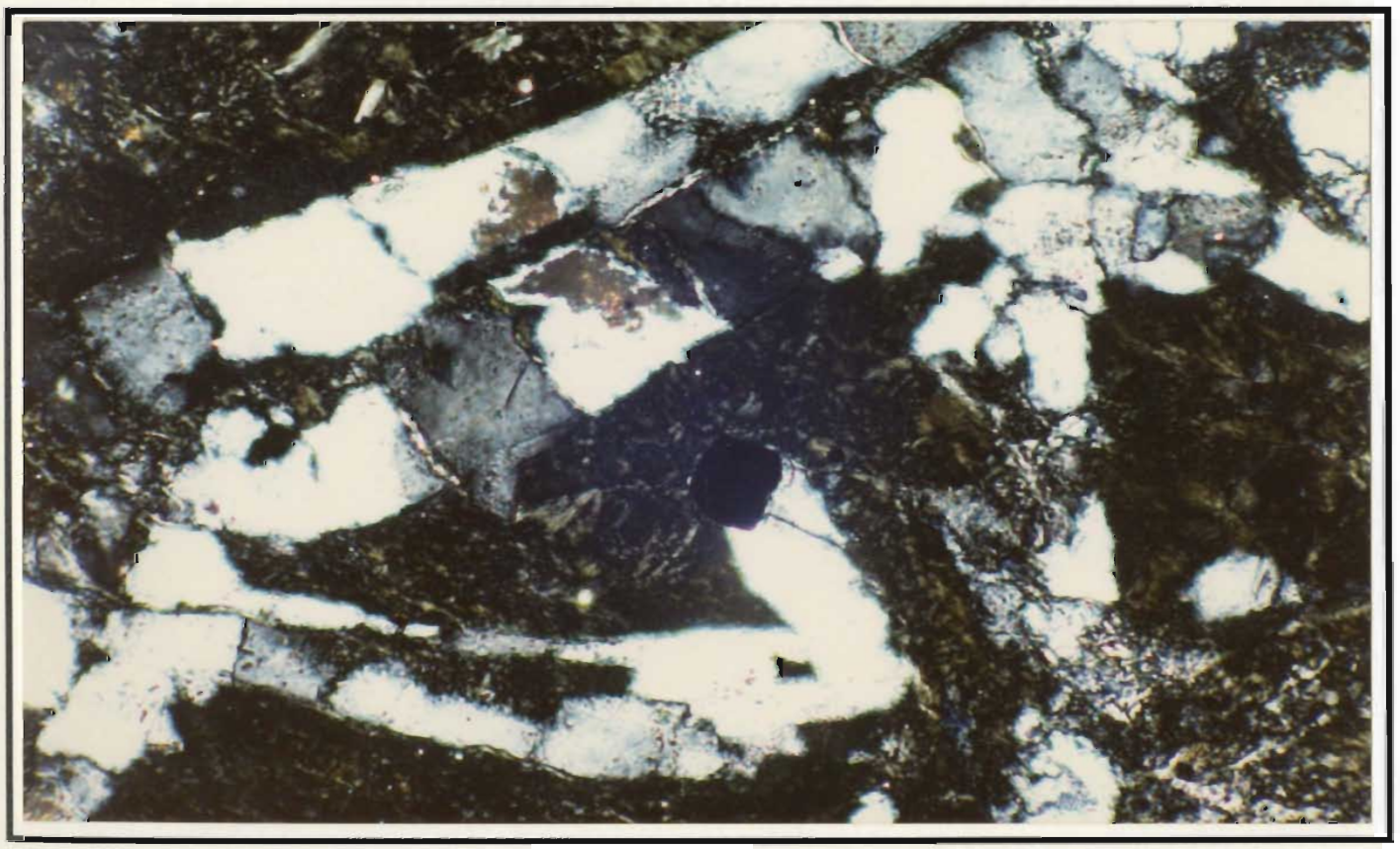

Figure 6-41: Transmitted light photomicrograph of same area shown in Figure 6-40 but under crossed nicols. Thin section SK 5 154 (154'), crossed nicols, 10 x. —— **0.2 mm** ——

chlorite. Elsewhere in this thin section, plumose and fan-shaped quartz-pseudomorphed albite clusters are present.

Some of the rocks in this alteration zone have been so intensely altered that even pseudomorphs of host-rock textures have been destroyed. In thin section, these extremely altered rocks are shown to consist predominantly of veins and elongate masses of chlorite, accompanied by lesser amounts of quartz, talc, and, in some thin sections, calcite. A minor amount of sphene is also present. In places, parallel alignment of the veins and elongate masses produce a foliation (sensu lato) in the rocks (Figure 6-42). Some samples, e.g. SK 27 39 and SK 28 27, are composed almost totally of chlorite and lesser pyrite (Figure 6-42), often containing a small amount of quartz or talc in "pressure shadows". Talc typically occurs as intergrowths of elongate platy grains, occurring either in veins or as irregular masses (Figure 6-43). Pyrite occurs with quartz, calcite or talc, in veins, or as disseminations throughout the samples. Even though chlorite is the predominant mineral in these rocks, pyrite grains are typically not in direct contact with chlorite anywhere but are surrounded by a small amount of quartz, calcite or talc (cf. Figure 6-42).

Intersertal quartz rather than chlorite predominates in the groundmass of more quartz-rich samples from this alteration zone. Quartz veins are abundant in these rocks, and many contain sericite veinlets. Pyrite ± quartz veins, and disseminated pyrite are present in most places. Subhedral chromite occurs in several samples.

6.6.1.5 Quartz, chlorite, pyrite alteration zone

In this alteration zone, an estimated 90 per cent of the rock has been replaced by various combinations of quartz, chlorite and pyrite (Table 6-5 and 6-6). Quartz is the predominant mineral in these rocks, occurring as equigranular anhedral grains throughout the sample, or as elongate anhedral grains protruding inward from the walls of veins, or outward away from pyrite grains (cf. Figure 6-45). Quartz pseudomorphs of plagioclase are noted in thin section SK 29 57. Sericite typically occurs as intergranular, elongate

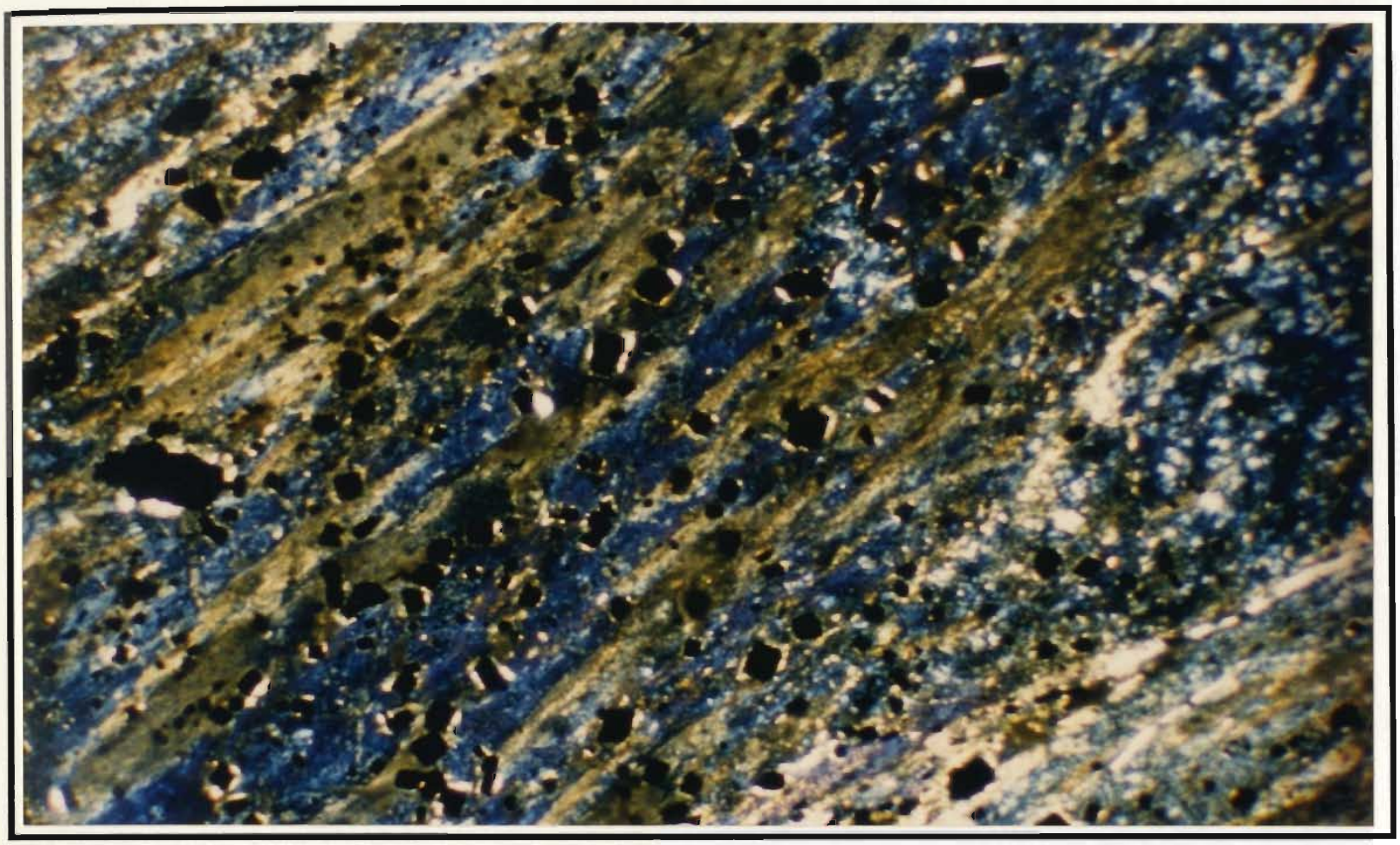

Figure 6-42: Transmitted light photomicrograph showing parallel alignment of elongate chlorite masses (olive green and blue) and calcite and/or quartz veins. Note that the abundant disseminated pyrite grains are not in direct contact with chlorite, but are surrounded by a small amount of quartz or calcite. Thin section SK 28 27, crossed nicols, 3.2 x. **— 0.5 mm —**

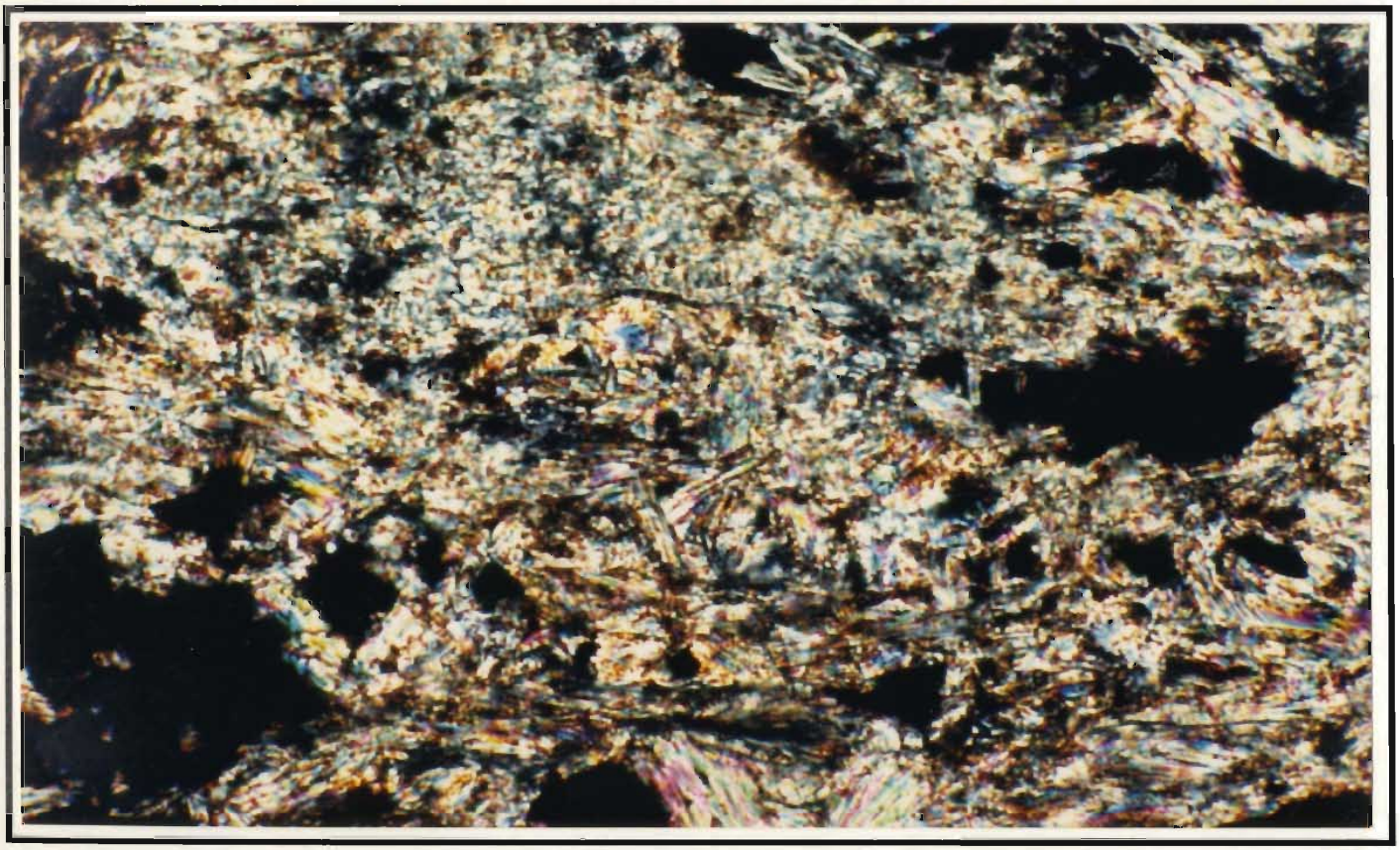

Figure 6-43: Transmitted light photomicrograph showing a fibrous, platy talc intergrowth. Thin section SK 28 73, crossed nicols, 20 x. **—— 0.1 mm ——**

Table 6-5: Petrographic table showing rock type, partial geochemical analysis and mineralogy of rocks from the Skidder Prospect qz,cl,py alteration zone

Key:	As per Table 6-1

Sample Name	Rock Type	Depth feet	Depth m	SiO_2 %	TiO_2 %	MgO %	Zr ppm	Ab	Cpx	Cl	Sphene	Cc	Ep	Qz	Chr	Opaques	Other Minerals and Comments
SK 7 186	Pillow Bx (?)	186	56.7					xx		xx	xx			xxx			py, serp. (?), talc (?), sc (?)
SK 7 206	Pillow Bx	206	62.8					xx		xx	xx			xxx			sericite (xx)
SK 28 78	Pillowed	778	237.1	63.1	0.9	9.1	51			xx	xx			xxx	xxx		pyrite, sericite (xx)
SK 34 1254	Stockwork	1254	382.2					?		x	x	x		xxx			pyrite, sericite (x)
SK 34 1260	Diabase (?)	1260	384.0					xx		xx	xx			xxx			pyrite
SK 25 969	Quartz	969	295.4					x			x	xx		xxx			

Table 6-6: Petrographic table showing rock type, partial geochemical analysis and mineralogy of sulphide-rich rocks from the cl,qz,py and qz,cl,py alteration zones

Key:	See Figure 6-1 for location of drill holes
	Abbreviations: Ab-albite, Cl-chlorite, Cc-calcite, Qz-quartz, hm-hematite, sc-sericite, Py-pyrite, Cp-chalcopyrite, Sph-sphalerite F - fine grained, M - medium grained, C - coarse grained
	Abundance of mineral as estimated from examination of the polished thin sections using transmitted and reflected light microscopy: x-low, xx-medium, xxx-high.
	See Appendix B for complete whole rock analyses and description of analytical methods

Sample	Depth		Alteration	SiO_2	TiO_2	MgO	Zr	Grain	Py	Cp	Sph	Sphene	Qz	Cl	Cc	Other Minerals
Name	feet	m	zone	%	%	%	ppm	Size								and Comments
SK 28 37	520.5	158.6	qz,cl,py	11.7	0.1	3.7	31	M	xx		x	x	xxx	xx	xx	
SK 28 39	530.5	161.7	cl,qz,py					F/M	xx				xx	xxx		
SK 28 40	532.0	162.2	qz,cl,py					F/M	xx	x	xxx	x	xxx	xx	x	
SK 28 41	532.5	162.3	cl,py,qz					M	xx		x	x	xxx	xxx	x	
SK 28 62	666.0	203.0	qz,cl,py					F/M	xx				xxx			
SK 29 57	823.0	250.9	qz,cl,py					F/M	x	x	x	x	xxx	xx		sph, cp, qz vein; sericite (xx)
SK 30 73	917.5	279.7	qz,cl,py					F/M	xx	x	xx		xxx			
SK 31 12	138.0	42.1	qz,cl,py	39.9	0.1	8.7	12	F/M	xx	x	x	x	xx	xx	xxx	talc

fibrous grains but in places occurs as clusters of radially aligned grains. Sericite pseudomorphs a large plagioclase grain in thin section SK 7 206 (Figure 6-44). Pyrite occurs as subhedral to euhedral grains or, locally, as tiny spheroidal grains. The pyrite is present in veins or is disseminated throughout the samples. Lesser chlorite and calcite are intersertal to quartz. Minor amounts of sphene are preserved in some samples. Anhedral chalcopyrite and/or sphalerite occur with pyrite ± quartz in veins or, in some areas, intersertal to pyrite. Calcite is the dominant mineral in thin section SK 31 12; it is accompanied by lesser amounts of quartz, pyrite, chlorite and talc. About equal amounts of quartz, calcite, pyrite and chlorite make up thin sections SK 28 37 and SK 28 41.

6.6.2 Jasper petrography

As seen in thin section, the jasper consists of quartz and very fine grained hematite (Table 6-7), which defines rounded to irregular, translucent to opaque masses intergrown with pyrite. In places, the rounded masses have a core of specular hematite. Quartz occurs as very fine grained intergrowths; as elongate grains that define myrmekite-like texture, in places nucleating on pyrite (Figure 6-45); and as spherulites.

In thin and polished sections of jasper interlayered with pyrite, the jasper consists of fine grained hematite that forms opaque to, in some areas, translucent masses; fine grained quartz is interlayered with the hematite in some areas. Elongate, wispy chlorite and hematite form discontinuous layers in some places. In polished section SK 37A 42, flaky specular hematite, in jasper and to a lesser extent in pyrite, parallels layering defined by pyrite elsewhere in the sample.

Jasper fragments in thin sections of brecciated jasper and pyrite are composed of fine grained anhedral quartz and tiny grains of hematite, the latter occurring as red translucent to opaque masses. Coarser grained quartz ± calcite and, to a lesser extent, calcite ± quartz veins crosscut the jasper fragments. Subhedral to euhedral pyrite, in places surrounded by coarser grained quartz, also occurs throughout the fragments. In thin

Table 6-7: Petrographic table showing rock type, partial geochemical analysis and mineralogy of sulphide-rich, jasper-bearing rocks; petrographic information either from polished thin sections or from polished sections

Key:	See Figure 6-1 for location of drill holes
	Abbreviations: Ab-albite, Cl-chlorite, Cc-calcite, Qz-quartz, hm-hematite, sc-sericite, py-pyrite, cp-chalcopyrite, sph-sphalerite L - layered, F- fine grained, M - medium grained, C - coarse grained T - thin section, PT - polished thin section
	Abundance of mineral as estimated from examination of the polished thin or polished sections: x-low, xx-medium, xxx-high
	See Table 6-34 for complete whole rock analyses and Appendix B for description of analytical methods

Sample Name	Depth feet	Depth m	Sulphide Type		Grain Size	SiO_2 %	TiO_2 %	MgO %	Zr ppm	Py	Cp	Sph	Hm	Sphene	Qz	Cl	Cc	Other Minerals and Comments
SK 7 329	329	100.3		L						xx			xxx	x	xxx	xx	x	T - specular hm magnetite (?)
SK 27 39	605.0	184.4	brecciated		F/M	85.8	0.0	0.1	8	xx			xx		xxx	x	xx	PT.
SK 27 42	633.0	192.9	semimassive	L	F/M					xxx		x	xx		xxx	xx	x	PT - jasper inclusions
SK 29 60B	858.0	261.5	semimassive		M/C					xxx	x	xx	xx		xxx			PT - Qz veins
SK 35A 7	1574.0	479.8	jasper, qz and py		F/M	71.0	0.0	0.6	13	xx	x	x	xx		xxx	x	xx	PT - jasper
SK 37A 38	1508.0	459.6	semimassive	L	F/M					xx	xx	x	xx	x	xxx	xx	x	specular hm.
SK 37A 42	1518.5	462.8	semimassive	L	F/M					xxx			xxx		xx	x	xxx	specular hm., magnetite (xx)
SK 37A 43	1521.5	463.8	semimassive	L	F/M					xx	x	x	xx		xxx		xx	jasper
SK 37A 44	1523.0	464.2	massive		F/M					xxx	xx	x	x		x	x	xx	minor jasper
SK 37A 45	1525.0	464.8	massive	L	F/M					xxx	x	x	xx		xx	x	xxx	jasper inclusion
SK 37A 46	1526.0	465.1	massive	L	F/M					xxx	xx	xx	xxx		xxx	x	xx	jasper inclusion

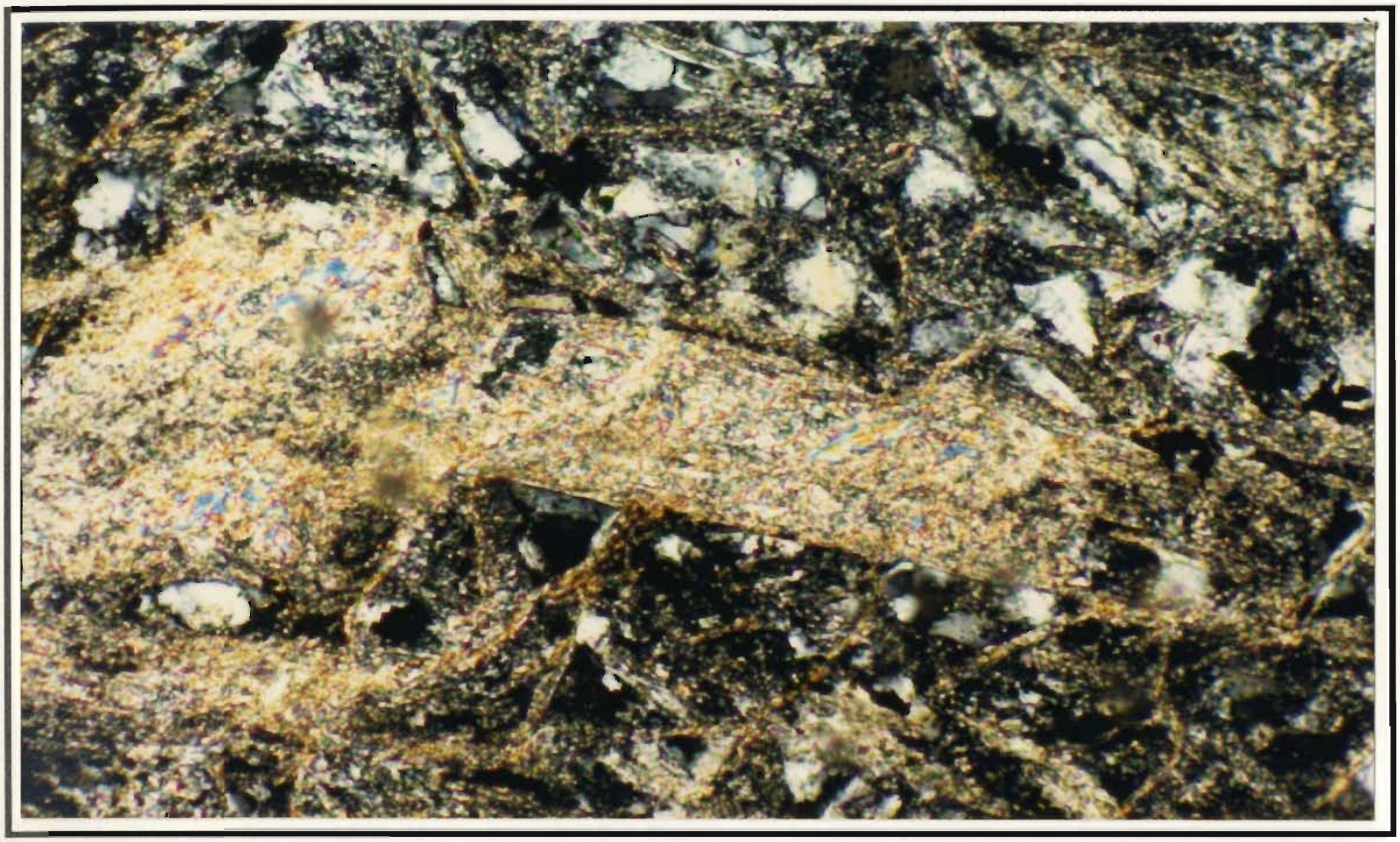

Figure 6-44: Transmitted light photomicrograph showing interconnected network of fibrous sericite, which also pseudomorphs a large plagioclase grain. Abundant rounded anhedral quartz grains are also present. Thin section SK 7 206 (206'), crossed nicols, 10 x. —— **0.2 mm** ——

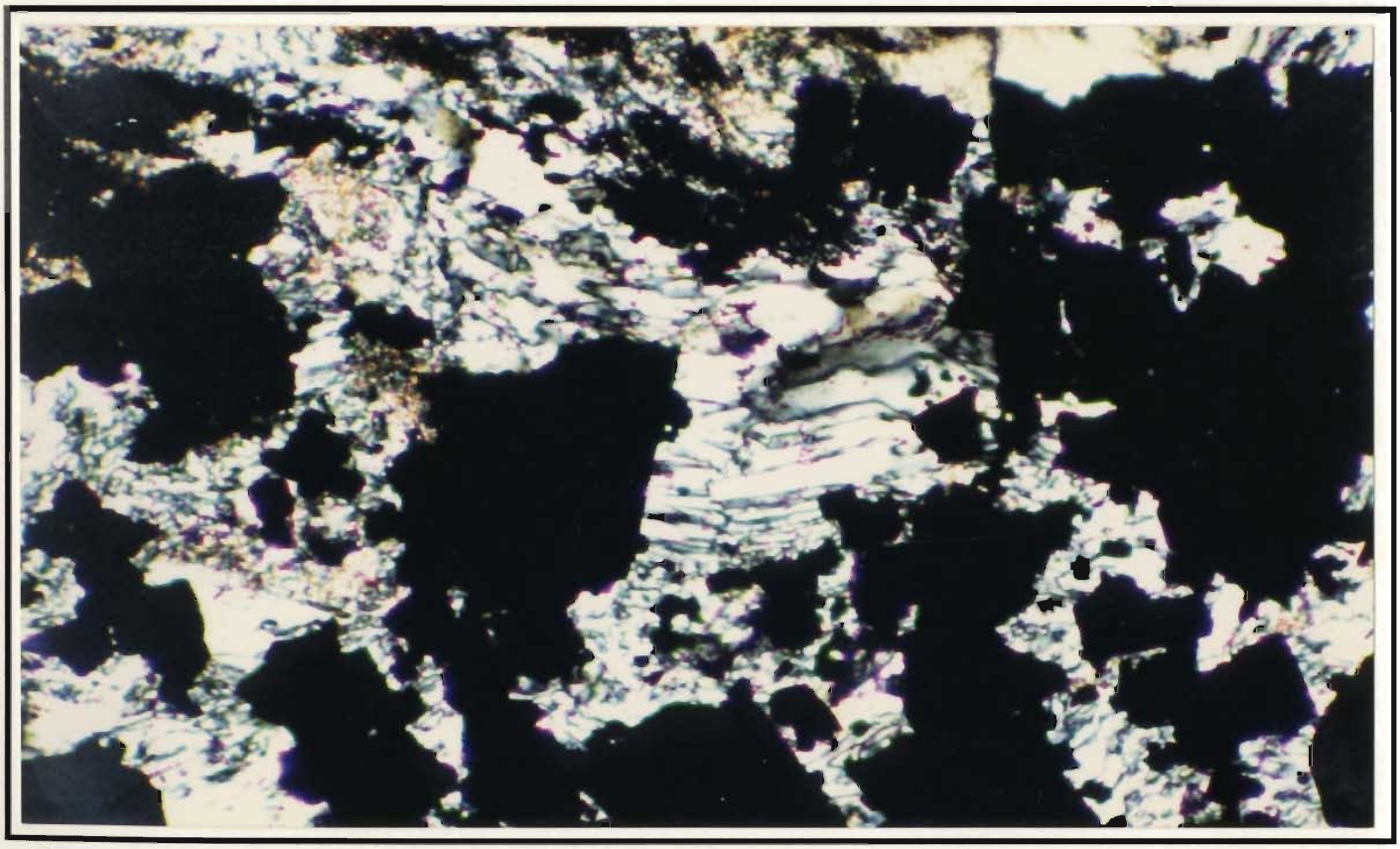

Figure 6-45: Transmitted light photomicrograph showing elongate anhedral myrmekite-like grains of quartz that radiate outward from pyrite grains (black), the quartz grains are typically interlocked with grains of similar habit protruding from adjacent pyrite grains. Thin section SK 37A 43, crossed nicols, 10 x. —— **0.2 mm** ——

section SK 27 39, coarser grained, red translucent to opaque hematite, and quartz grains partially to completely fill vugs. Colloform (?) masses of hematite, consisting of concentrically layered silica and coarser hematite cores that are surrounded by brilliant red, very fine grained hematite, are displayed in polished section SK 37A 46 (Figures 6-46 and 6-47).

Quartz in veins cutting sulphides and jasper occurs as fine grained equigranular intergrowths, and, in places, as elongate, interlocking myrmekite-like intergrowths displaying cockade structure. In some areas, quartz grains show undulatory extinction. Possibly four generations of quartz are shown in sample SK 28 62. Early ubiquitous quartz is cut by quartz veins, which are cut by pyrite-bearing quartz veins; the pyrite-bearing quartz veins are, in turn, crosscut by barren quartz veins.

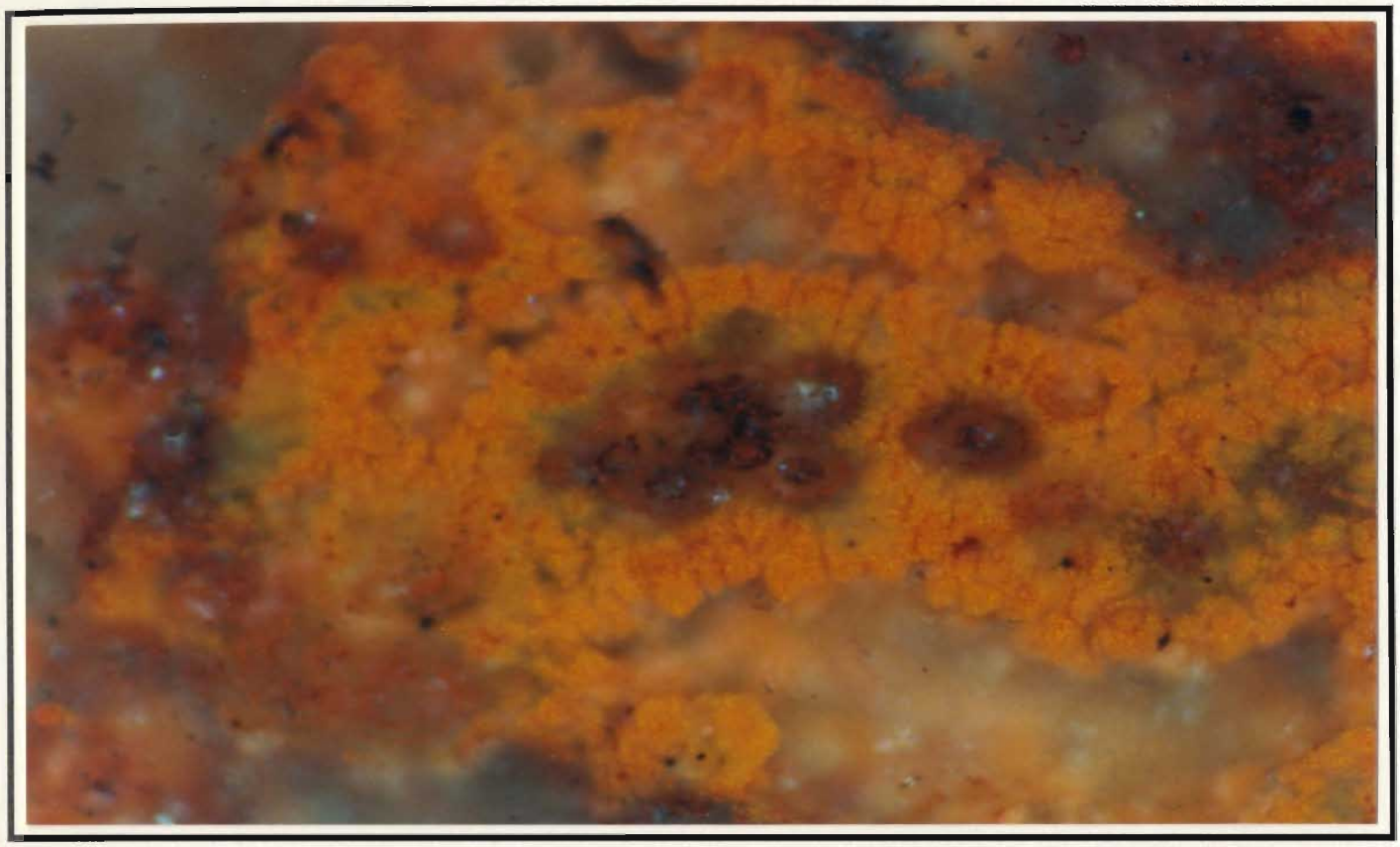

Figure 6-46: Reflected light photomicrograph of hematite showing colloform (?) structure. Polished section SK 37A 46, plane polarized light, 20 x. —— **0.1 mm** ——

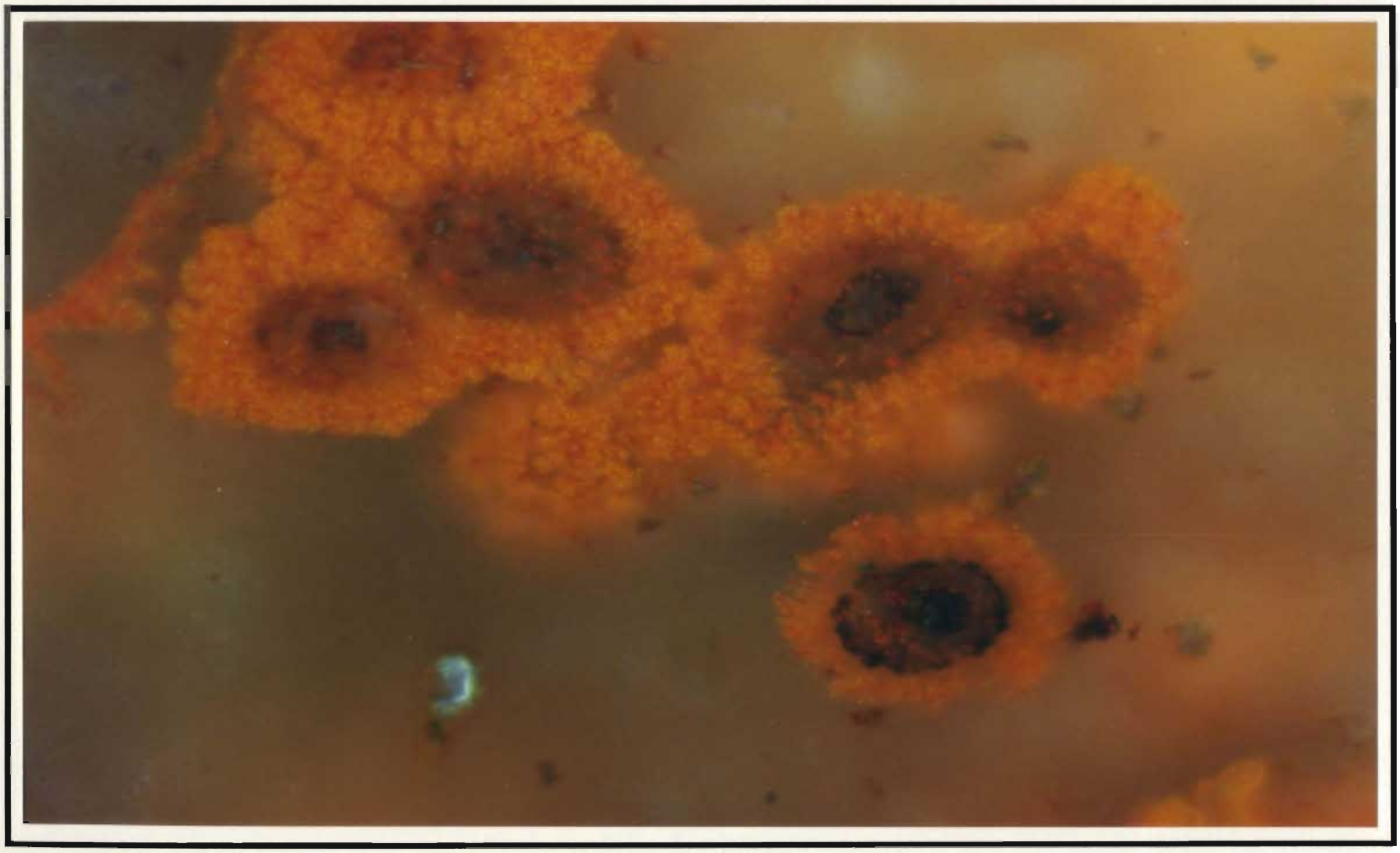

Figure 6-47: Reflected light photomicrograph of hematite showing colloform (?) structure. Polished section SK 37A 46, plane polarized light, 50 x. —— **0.04 mm** ——

6.6.3 Petrography of the trondhjemite dykes

Trondhjemite dykes that intrude the rocks in the vicinity of the Skidder Prospect, in places separate rocks that have been affected by different intensities of alteration (Figure 6-3). In other areas, particularly in the most intensely altered zones, the trondhjemite dykes have highly altered rocks on either side and are typically altered themselves (Figure 6-19).

The least altered trondhjemite dykes have similar mineralogy and texture to trondhjemites that occur in rocks unaffected by the mineralizing solutions that formed the Skidder Prospect (Section 4.2). In some samples, 1-3 mm-long albitized plagioclase and lesser quartz phenocrysts occur in a matrix of ≤ 0.05 mm anhedral quartz grains and 0.05-0.1 mm-long albite laths (Table 6-8). In places, the albitized plagioclase ± quartz (phenocrysts (?)) occur as glomeroporphyritic clusters. Minor amounts of chlorite occur as elongate anhedral masses intersertal to quartz and albite. Quartz ± lesser chlorite or calcite fill veinlets. Minor amounts of pyrite, sphene, and rare tiny subhedral zircon are finely disseminated throughout the rocks.

Relative to the unaltered trondhjemite dykes, the more altered ones are characterized by: an increase in the number of quartz veins; the occurrence, in most samples, of abundant sericite veins, in places forming an interconnected network; and an increase in the size of groundmass anhedral quartz grains to an average of about 0.3 mm across, this increase being at the expense of albite. Many larger plagioclase phenocrysts are replaced by quartz (Figure 6-48) and quartz pseudomorphs of tiny albite laths are present in many samples. Subhedral pyrite, in places abundant, is finely disseminated throughout the rocks.

Table 6-8: Petrographic table showing rock type, partial geochemical analysis and mineralogy of trondhjemite dykes intruding the Skidder Basalt in the Skidder Prospect area

Key:	As per Table 6-1 Complete whole rock analyses are presented in Tables 5-12 and 6-37

Sample Name	Depth feet	Depth m	Alteration zone	SiO_2 %	TiO_2 %	MgO %	Zr ppm	Ab	Cpx	Cl	Sphene	Cc	Ep	Qz	Opaques	Other Minerals and Comments
SK 3 64	64	19.5	qz,cl,cc					?		x	x			xxx		silicified; py, sericite (xx)
SK 4 346	346	105.5						xx		x	x	x		xxx		porphyritic; sericite (x)
SK 8 215	215	65.5						xx		x	x			xxx		
SK 17 332	332	101.2						x		x		x		xxx		pyrite, sericite (x)
SK 18 307	307	93.6						x		x	x			xxx		pyrite, sericite (x)
SK 26 510	510	155.4						xx		x	x	x		xxx	xx	zircon
SK 27 25	380	115.7	qz,cl,py	76.9	0.2	2.4	163	xx		x	x	x		xxx		zircon
SK 29 45	691	210.6	cl,qz,py	70.3	0.3	4.9	211									
SK 29 695	695	211.8	qz,cl,py	70.3	0.3	4.9	211	x		x	x			xxx		sericite (xx), zircon
SK 30 09	9	2.7	cl,cc,ep ± hm					xxx		x	x		x	xxx	xxx	zircon
SK 30 01	11	3.4	cl,cc,ep ± hm	75.0	0.2	0.9	199									
SK 30 747	747	227.7	qz,cl,py					xx		x	x			xxx		silicified, pyrite
SK 30 51	753	229.4	qz,cl,py	83.5	0.1	0.2	159									
SK 30 901	901	274.6	qz,cl,py					xx		x	x					pyrite, sericite (x)
SK 34 799	799	243.5						xx		x	x			xxx	xx	

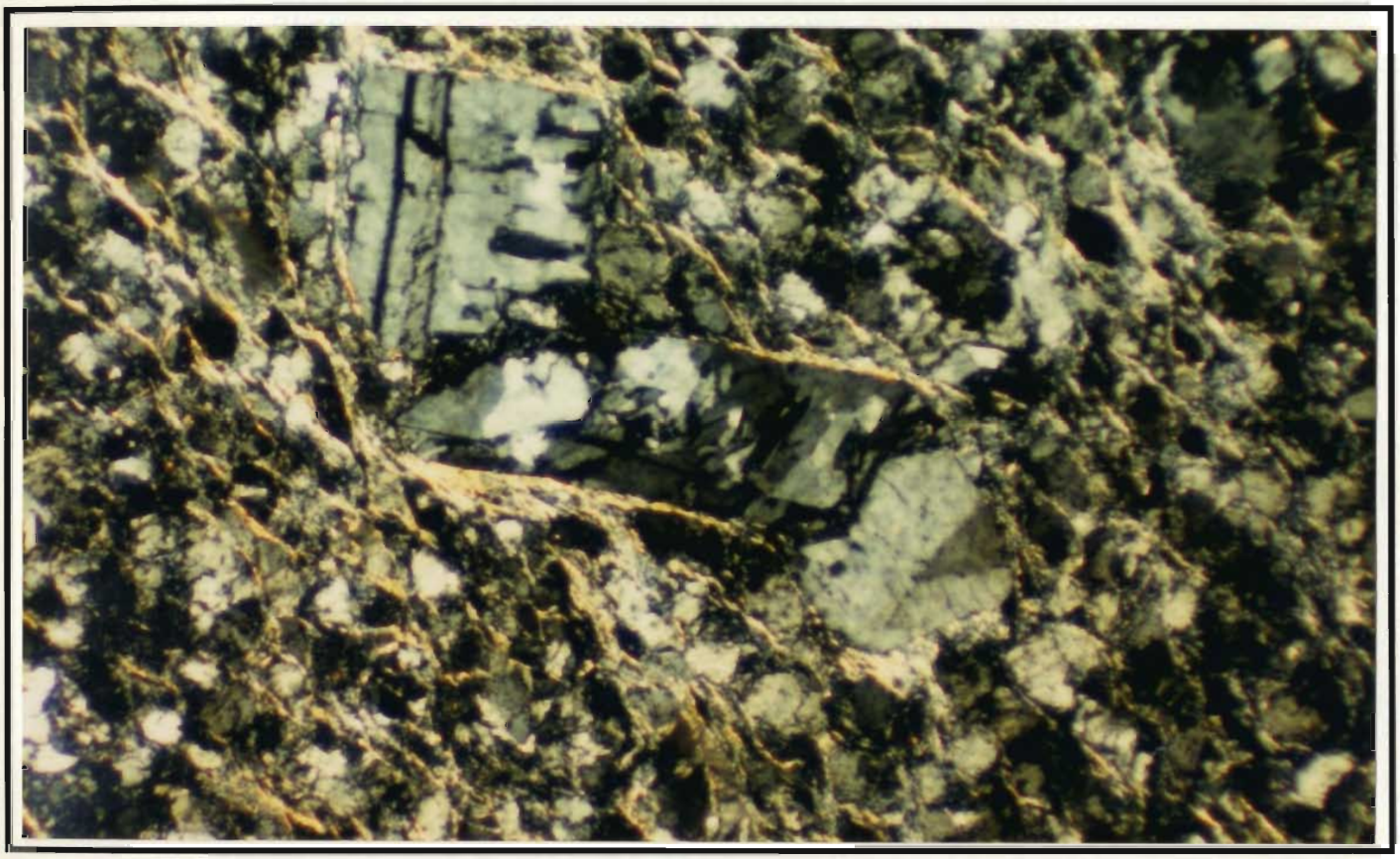

Figure 6-48: Transmitted light photomicrograph showing quartz that has pseudomorphed glomeroporphyritic plagioclase grains in altered trondhjemite. Fibrous sericite forms an interconnected network of grains surrounding anhedral quartz. Thin section SK 29 695 (695'), crossed nicols, 3.2 x. **— 0.5 mm —**

6.7 Mineral Chemistry

6.7.1 Chlorite

Electron microprobe analyses of chlorites that occur in rocks from the various Skidder Prospect alteration zones, and as gangue to the semimassive and massive sulphides, are listed in Table A-4, Appendix A; selected analyses are presented in Table 6-9. Averages of chlorites proximal to the Skidder Prospect are compared to the average of chlorites in spilitized Skidder Basalt unaffected by the Skidder Prospect mineralizing event in Table 6-10.

As shown in Tables 6-9 and 6-10, most chlorites from rocks proximal to the Skidder Prospect are significantly enriched in Mg, and depleted in Fe and Mn relative to the chlorites from the Skidder Basalt unaffected by the mineralizing event. Chlorites from the less altered rocks included in the cl,cc,ep ± hm alteration zone are less enriched in Mg and depleted in Fe than those from rocks in the more intensely altered cl,qz,cc; cl,qz,py and qz,cl,py alteration zones. Only limited variation in chlorite composition is evident in rocks from the latter three alteration zones; all are Mg-enriched and Fe-depleted, including those from quartz-rich rocks in the qz,cl,py alteration zone. Chlorites that occur as gangue in semimassive sulphides are similar to those from rocks included in the three most intense alteration zones. Chlorite gangue in massive sulphides is, on average, slightly enriched in iron relative to chlorite gangue in the semimassive sulphides and to chlorites from the most intensely altered rocks. Chlorites associated with jasper or jasper-rich sulphides are the only chlorites (of those analyzed from rocks proximal to the Skidder Prospect) that are relatively enriched in Fe and depleted in Mg. These chlorites have Fe, Mn and Mg contents similar to chlorites from typical spilitized Skidder Basalt.

The Mg-enriched, Fe-depleted character of most chlorites from rocks proximal to the Skidder Prospect is further illustrated on Figure 6-49. The Skidder Prospect chlorites show a range of compositions on the basis of atomic Si (Figure 6-49). According to the classification scheme of Hey (1954) most of the chlorites are classified as clinochlore and

Table 6-9: Electron microprobe analyses of chlorites from rocks in the Skidder Prospect area; analyses that have been averaged are presented in Table A-4, Appendix A

	cl,cc, ep±hm	cl,qz, cc	cl,qz,py					qz,cl,py		semimassive sulphides			semimassive sulphides		
	SK	SK	SK	SK	SK	SK	SK	SK	SK	SK	SK	SK	SK	SK	SK
Weight %	27 8	27 33	28 27	28 39	28 41	28 73	28 75	28 40	29 57	27 37	29 60	30 67	30 80	30 822A	31 13
SiO_2	28.18	29.43	31.53	27.79	29.39	33.46	29.00	30.23	30.82	32.79	28.92	27.12	26.94	25.86	27.46
TiO_2	0.00	0.02	0.02	0.01	0.01	0.01	0.00	0.03	0.03	0.03	0.02	0.02	0.01	0.02	0.01
Al_2O_3	18.60	22.17	17.81	20.41	18.86	15.61	19.67	19.99	20.47	17.48	19.83	19.80	21.36	20.72	18.84
Cr_2O_3	0.04	0.07	0.05	0.08	0.08	0.06	0.05	0.04	0.07	0.01	0.02	0.08	0.04	0.09	0.57
FeO*	16.62	8.25	9.95	13.24	9.92	8.39	12.57	11.01	10.32	9.04	8.32	12.88	11.36	15.03	9.73
MnO	0.38	0.23	0.23	0.23	0.21	0.11	0.26	0.25	0.21	0.19	0.16	0.26	0.14	0.15	0.17
NiO	0.07	0.04	0.03	0.04	0.01	0.01	0.02	0.03	0.03	0.02	0.02	0.03	0.04	0.02	0.03
MgO	21.63	26.22	26.51	22.72	24.29	28.26	23.80	24.95	20.51	27.51	26.23	22.91	23.16	21.05	24.57
CaO	0.09	0.06	0.10	0.06	0.06	0.15	0.04	0.08	0.07	0.11	0.05	0.03	0.02	0.03	0.01
Na_2O	0.04	0.07	0.02	0.02	0.04	0.03	0.00	0.04	0.05	0.04	0.05	0.01	0.02	0.02	0.00
K_2O	0.02	0.01	0.02	0.01	0.02	0.05	0.02	0.02	0.93	0.03	0.01	0.02	0.01	0.01	0.00
Total	85.64	86.57	86.27	84.61	82.86	86.14	85.42	86.66	83.48	87.24	83.60	83.16	83.10	82.97	81.38
Atomic Proportions (based on 28 oxygens)															
Si	5.804	5.705	6.182	5.675	6.008	6.501	5.838	5.936	6.250	6.312	5.816	5.645	5.549	5.460	5.744
Al	4.516	5.058	4.116	4.914	4.544	3.577	4.668	4.623	4.896	3.967	4.702	4.853	5.187	5.159	4.644
Fe	2.863	1.337	1.631	2.261	1.695	1.365	2.115	1.807	1.752	1.456	1.399	2.242	1.957	2.654	1.703
Mn	0.067	0.037	0.038	0.040	0.035	0.018	0.044	0.041	0.037	0.032	0.026	0.046	0.024	0.026	0.029
Mg	6.639	7.574	7.745	6.930	7.392	8.186	7.140	7.296	6.197	7.892	7.860	7.101	7.110	6.625	7.663
Others	0.053	0.058	0.043	0.042	0.043	0.057	0.021	0.046	0.052	0.046	0.038	0.031	0.028	0.032	0.103
K	0.004	0.003	0.004	0.004	0.004	0.013	0.004	0.005	0.240	0.006	0.002	0.005	0.003	0.003	0.001
Total	19.95	19.77	19.76	19.87	19.72	19.72	19.83	19.75	19.42	19.71	19.84	19.92	19.86	19.96	19.89
Fe/Fe+Mg	0.30	0.15	0.17	0.25	0.19	0.14	0.23	0.20	0.22	0.16	0.15	0.24	0.22	0.29	0.18
Analyses	2	3	5	3	4	5	2	3	2	3	2	3	1	2	4
Whole Rock (complete analyses presented in Appendix B)															
Zr (ppm)	45	77	58			55	50				61		20	48	
Fe_2O_3 (%)**	10.54	10.38	14.93			14.07	10.36				31.00		35.05	23.10	
MgO (%)	8.87	12.74	27.18			27.38	16.68				16.52		0.63	10.61	

* Total iron as FeO

** Total iron as Fe_2O_3

Table 6-9 **(continued)**: Electron microprobe analyses of chlorites from rocks in the Skidder Prospect area; analyses that have been averaged are presented in Table A-4, Appendix A

	massive sulphides						jasper-rich sulphides		
Weight %	SK 27 46	SK 28 38	SK 28 67	SK 30 58	SK 30 81	SK 35A 6	SK 27 42	SK 27 45	SK 37A 46
SiO_2	26.36	28.80	31.18	27.90	30.75	30.36	27.84	25.87	21.95
TiO_2	0.02	0.02	0.00	0.00	0.01	0.01	0.00	0.03	0.02
Al_2O_3	16.52	22.00	16.36	22.34	15.10	16.82	18.57	17.13	17.75
Cr_2O_3	0.02	0.02	0.01	0.04	0.03	0.02	0.01	0.03	0.02
FeO*	15.87	10.12	10.59	13.26	9.92	6.00	22.35	20.32	26.33
MnO	0.25	0.15	0.14	0.16	0.10	0.18	0.29	0.22	0.38
NiO	0.04	0.04	0.05	0.03	0.00	0.03	0.03	0.03	0.04
MgO	21.73	23.89	26.64	22.48	26.51	28.34	17.68	18.58	12.62
CaO	0.04	0.01	0.16	0.02	0.11	0.00	0.08	0.02	0.02
Na_2O	0.02	0.04	0.03	0.00	0.04	0.00	0.00	0.04	0.01
K_2O	0.00	0.01	0.03	0.02	0.00	0.00	0.03	0.01	0.02
Total	80.87	85.09	85.17	86.25	82.56	81.74	86.87	82.26	79.12
Atomic Proportions (based on 28 oxygens)									
Si	5.773	5.732	6.227	5.574	6.319	6.163	5.820	5.701	5.270
Al	4.260	5.140	3.850	5.262	3.656	4.028	4.577	4.451	5.031
Fe	2.908	1.684	1.768	2.216	1.704	1.019	3.908	3.746	5.293
Mn	0.046	0.026	0.023	0.027	0.018	0.030	0.050	0.041	0.077
Mg	7.078	7.089	7.927	6.694	8.115	8.575	5.507	6.101	4.519
Others	0.030	0.031	0.055	0.015	0.046	0.008	0.025	0.035	0.021
K	0.001	0.002	0.008	0.005	0.000	0.000	0.007	0.003	0.005
Total	20.10	19.70	19.86	19.79	19.86	19.82	19.89	20.08	20.21
Fe/Fe+Mg	0.29	0.19	0.18	0.25	0.17	0.11	0.42	0.38	0.54
Analyses	3	3	2	1	2	2	2	2	2
Whole Rock (complete analyses presented in Appendix B)									
Zr (ppm)						19			
Fe_2O_3 (%)**						42.72			
MgO (%)						0 63			

* Total iron as FeO

** Total iron as Fe_2O_3

Table 6-10: Average of chlorites from the Skidder Basalt outside the Skidder Prospect alteration zone (1) compared to chlorites from rocks proximal to the Skidder Prospect (2); also listed are the averages of chlorites from the various alteration zones; the average of chlorites that are gangue to the semimassive and massive sulphides and the average of chlorites from jasper-bearing sulphides

Weight %	Skidder Basalt 1 Mean	Skidder Prospect 2 Mean	cl,cc, ep±hm SK 27 8	cl,qz,cc SK 27 33	cl,qz,py Mean	qz,cl,py Mean	Semi massive sulphides Mean	Massive sulphides Mean	Jasper-rich sulphides Mean
SiO_2	28.40	29.15	28.18	29.43	30.73	30.47	28.40	28.65	24.89
TiO_2	0.01	0.01	0.00	0.02	0.01	0.03	0.02	0.01	0.01
Al_2O_3	18.76	18.71	18.60	22.17	18.06	20.18	19.31	17.91	18.16
Cr_2O_3	0.04	0.08	0.04	0.07	0.06	0.05	0.18	0.02	0.01
FeO*	22.93	11.95	16.62	8.25	10.33	10.73	10.85	12.32	24.34
MnO	0.35	0.21	0.38	0.23	0.20	0.23	0.18	0.18	0.33
NiO	0.04	0.03	0.07	0.04	0.02	0.03	0.03	0.03	0.03
MgO	17.65	24.00	21.63	26.22	25.62	23.17	24.48	23.96	15.15
CaO	0.10	0.06	0.09	0.06	0.09	0.08	0.04	0.05	0.05
Na_2O	0.03	0.03	0.04	0.07	0.02	0.04	0.02	0.03	0.00
K_2O	0.03	0.05	0.02	0.01	0.03	0.38	0.01	0.01	0.02
Total	88.34	84.26	85.64	86.57	85.16	85.39	83.53	83.17	82.99
Atomic Proportions (based on 28 oxygens)									
Si	5.847	5.924	5.804	5.705	6.113	6.062	5.796	5.927	5.545
Ti	0.002	0.002	0.000	0.003	0.002	0.004	0.003	0.002	0.002
Al	4.554	4.495	4.516	5.058	4.248	4.732	4.663	4.362	4.804
Cr	0.006	0.013	0.006	0.011	0.010	0.008	0.031	0.004	0.002
Fe	3.954	2.068	2.863	1.337	1.725	1.785	1.864	2.164	4.600
Mn	0.061	0.036	0.067	0.037	0.033	0.039	0.032	0.031	0.064
Ni	0.007	0.005	0.012	0.006	0.003	0.004	0.004	0.005	0.006
Mg	5.408	7.253	6.639	7.574	7.594	6.856	7.447	7.375	5.013
Ca	0.021	0.014	0.020	0.013	0.019	0.016	0.009	0.011	0.012
Na	0.014	0.010	0.016	0.025	0.009	0.016	0.008	0.010	0.001
K	0.007	0.012	0.004	0.003	0.006	0.099	0.003	0.002	0.006
Total	19.882	19.831	19.945	19.771	19.764	19.621	19.860	19.894	20.054
Fe/Fe+Mg	0.42	0.22	0.30	0.15	0.19	0.21	0.20	0.23	0.48
Analyses	49	63	2	3	19	5	15	15	4

* Total iron as FeO

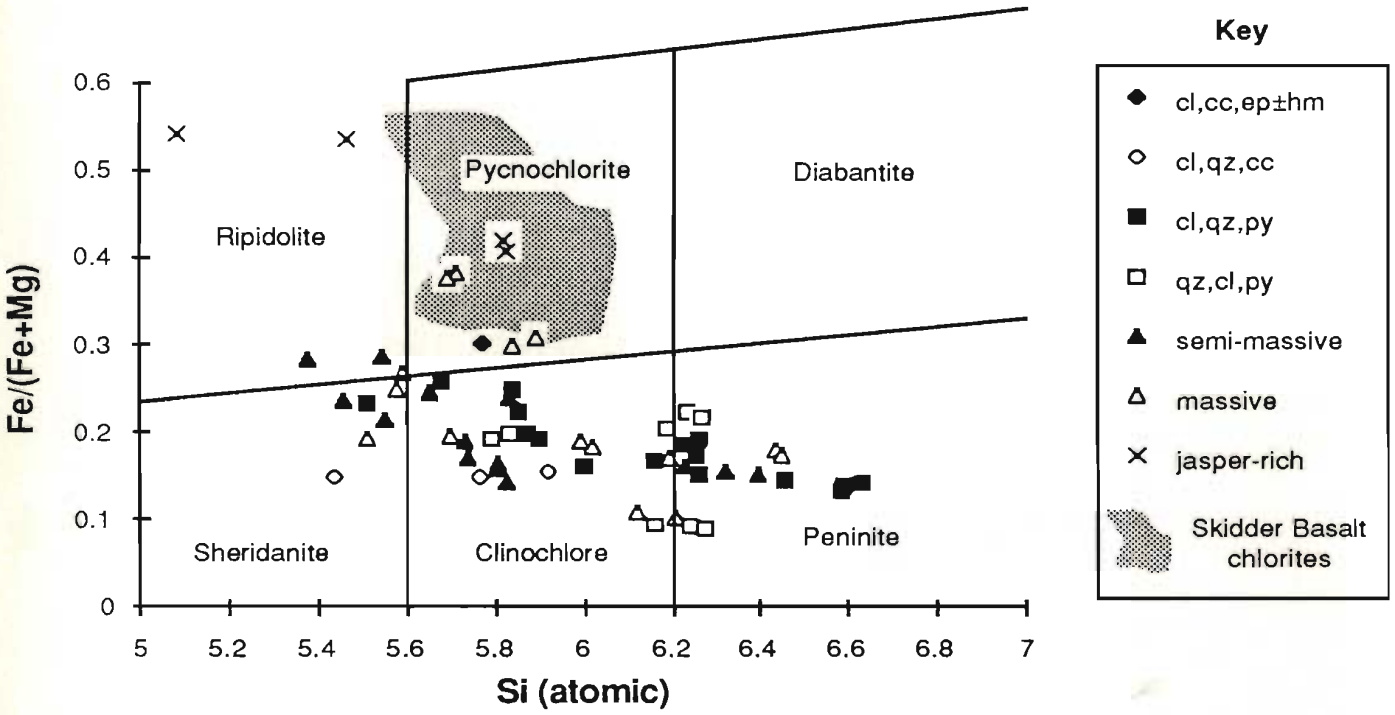

Figure 6-49: Chlorites from rocks proximal to the Skidder Prospect plotted on classification diagram after Hey (1954).

penninite; a few are classified as sheridanite, ripidolite and pycnochlorite. Chlorites in jasper and jasper-rich sulphides are classified as ripidolite and pycnochlorite; these latter chlorites represent the only compositions that overlap the field for spilitized Skidder Basalt chlorites on this diagram (Figure 6-49).

Chlorites in jasper and jasper-bearing massive sulphides plot in the fields defined by typical spilitized Skidder Basalt chlorites on Figure 6-50. Four of these chlorite compositions plot in the typical metabasalt field, and two in the field of quartz chlorite breccias (fields after Mottl, 1983a). The remainder of the Skidder Prospect chlorite compositions define a curved path which trends away from the FeO apex (and the field for chlorite-quartz metabasalt) and then toward the MgO apex. This trend matches very well that predicted by the model of Mottl (1983a) for variation in chlorite compositions as a result of increasing seawater/rock ratios. The trend defined by the Skidder Prospect chlorites, however, extends toward the MgO apex of the diagram well beyond the chlorite composition that, according to Mottl (1983a), would result from a seawater/rock ratio of 125 (the highest seawater/rock ratio used in his model). In fact, phyllosilicates, analyzed in SK 28 73, that have compositions intermediate between high-magnesium chlorite and talc provide an almost complete link between the high magnesian chlorites and Skidder Prospect talcs (Table 6-11), which plot very close to the MgO apex on this diagram.

Variations in the compositions of chlorites discussed above are effected by interatomic substitutions, as described, for example, by Deer et al. (1962). Hence, substitution of Mg for Fe and Mn is reflected by the marked negative correlations between MgO and FeO, and the positive correlation between FeO and MnO (Table 6-12 and Figure 6-51). A reduction in the substitution of Al for Si and Mg in the higher magnesian chlorites is supported by the negative correlations of Si and Mg with Al, and by the positive correlation between Si and Mg (Table 6-12 and Figure 6-51). The high-magnesium, high-silica chlorites have a lower hydrous component as indicated by positive correlations of SiO_2 and MgO with analytical totals (Figure 6-51).

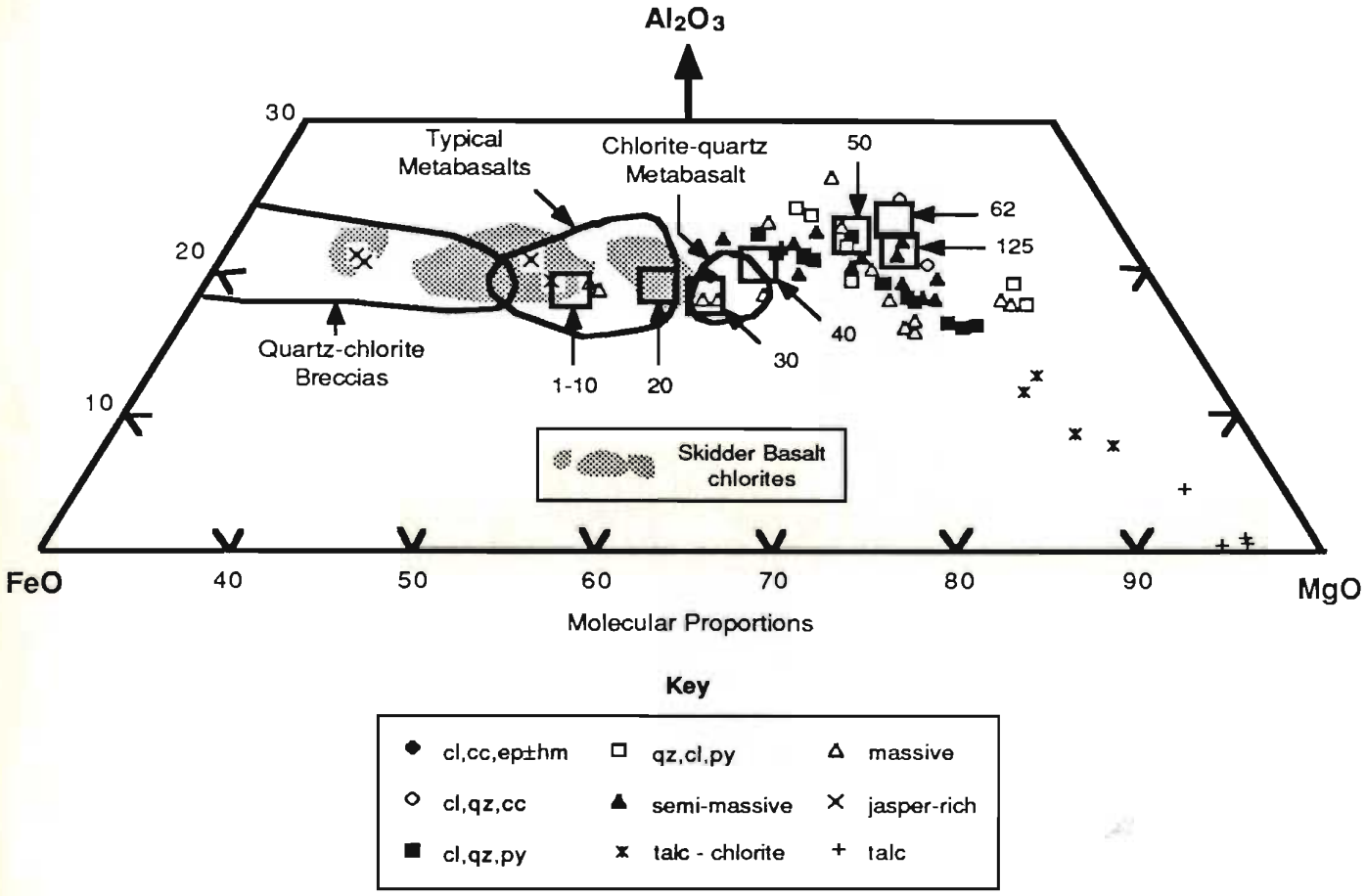

Figure 6-50: Chlorites, talc-chlorites and talc from rocks proximal to the Skidder Prospect compared to Skidder Basalt chlorite compositions; and to those of typical metabasalts, quartz-chlorite breccias and a chlorite-quartz metabasalt (after Melson and van Andel, 1966; Humphris and Thompson, 1978; Mottl 1983a). Large open squares represent chlorite compositions for different seawater/rock ratios from model predictions of Mottl (1983a).

Table 6-11: Electron microprobe analyses of chlorite, talc, and minerals intermediate in composition between chlorite and talc, in rocks proximal to the Skidder Prospect; analyses that have been averaged are presented in Table A-4, Appendix A

Mineral	Chlorite	Talc	Chlorite	Talc/Chlorite			Talc
	SK	SK	SK	SK	SK	SK	SK
Weight %	31 12	31 12	28 73	28 73	28 73	28 73	28 73
SiO_2	31.67	62.94	33.46	39.51	48.58	50.00	56.22
TiO_2	0.02	0.00	0.01	0.03	0.00	0.00	0.01
Al_2O_3	17.46	0.64	15.61	10.88	10.18	6.72	1.81
Cr_2O_3	0.03	0.02	0.06	0.03	0.00	0.00	0.02
FeO*	5.39	2.17	8.39	5.97	6.94	5.34	3.14
MnO	0.03	0.03	0.11	0.11	0.12	0.06	0.03
NiO	0.01	0.00	0.01	0.05	0.06	0.01	0.03
MgO	29.22	28.78	28.26	27.61	28.31	28.87	28.24
CaO	0.05	0.05	0.15	0.16	0.04	0.05	0.05
Na_2O	0.03	0.05	0.03	0.02	0.01	0.02	0.02
K_2O	0.02	0.02	0.05	0.03	0.01	0.03	0.02
Total	83.94	94.69	86.14	84.40	94.25	91.07	89.57
Atomic Proportions							
Si	6.225	8.059	6.501	7.639	8.326	8.778	7.698
Ti	0.002	0.000	0.002	0.004	0.000	0.000	0.001
Al	4.046	0.095	3.577	2.480	2.057	1.389	0.299
Cr	0.005	0.002	0.010	0.005	0.000	0.000	0.002
Fe	0.887	0.232	1.365	0.965	0.995	0.783	0.360
Mn	0.005	0.003	0.018	0.018	0.017	0.008	0.003
Ni	0.002	0.000	0.002	0.008	0.008	0.001	0.003
Mg	8.556	5.486	8.186	7.955	7.231	7.555	5.773
Ca	0.011	0.007	0.031	0.033	0.007	0.008	0.007
Na	0.012	0.012	0.012	0.007	0.003	0.005	0.005
K	0.006	0.003	0.013	0.007	0.002	0.006	0.003
Total	19.756	13.900	19.716	19.122	18.648	18.533	14.154
Analyses	3	2	5	1	1	2	2
Fe/(Fe+Mg)	0.09	0.04	0.14	0.11	0.12	0.09	0.06
Mg/(Mg+Fe+Mn)	0.91	0.96	0.86	0.89	0.88	0.91	0.94
XMg/(1-XMg)	9.60	23.30	5.92	8.09	7.14	9.55	15.89
Kd(Mg) talc-chlorite	2.43	2.43	2.68				2.68
Oxygens	28	22	28	28	28	28	22
Alteration	qz,cl,py		cl,qz,py				

* Total iron as FeO

XMg - ionic fraction of Mg in chlorite or talc = Mg/(Mg+Fe+Mn) (cf. McLeod and Stanton, 1984)

Kd(Mg) - distribution coefficient of Mg between coexisting talc and chlorite

= [XMg(talc)/(1-XMg(talc))]/[XMg(chlorite)/(1-XMg(chlorite))]

Table 6-12: Correlation matrix for Skidder Prospect chlorite compositions

	SiO_2	Al_2O_3	Cr_2O_3	FeO*	MnO	MgO	CaO
Al_2O_3	-0.17						
Cr_2O_3	-0.17	0.04					
FeO*	**-0.74**	-0.04	-0.13				
MnO	**-0.50**	0.14	-0.11	**0.67**			
MgO	**0.82**	-0.13		**-0.91**	**-0.63**		
CaO	**0.64**	**-0.41**	-0.26	-0.24	-0.18	**0.40**	
Total	**0.67**	0.37	-0.28	-0.30	-0.09	**0.48**	**0.42**

* Total iron as FeO

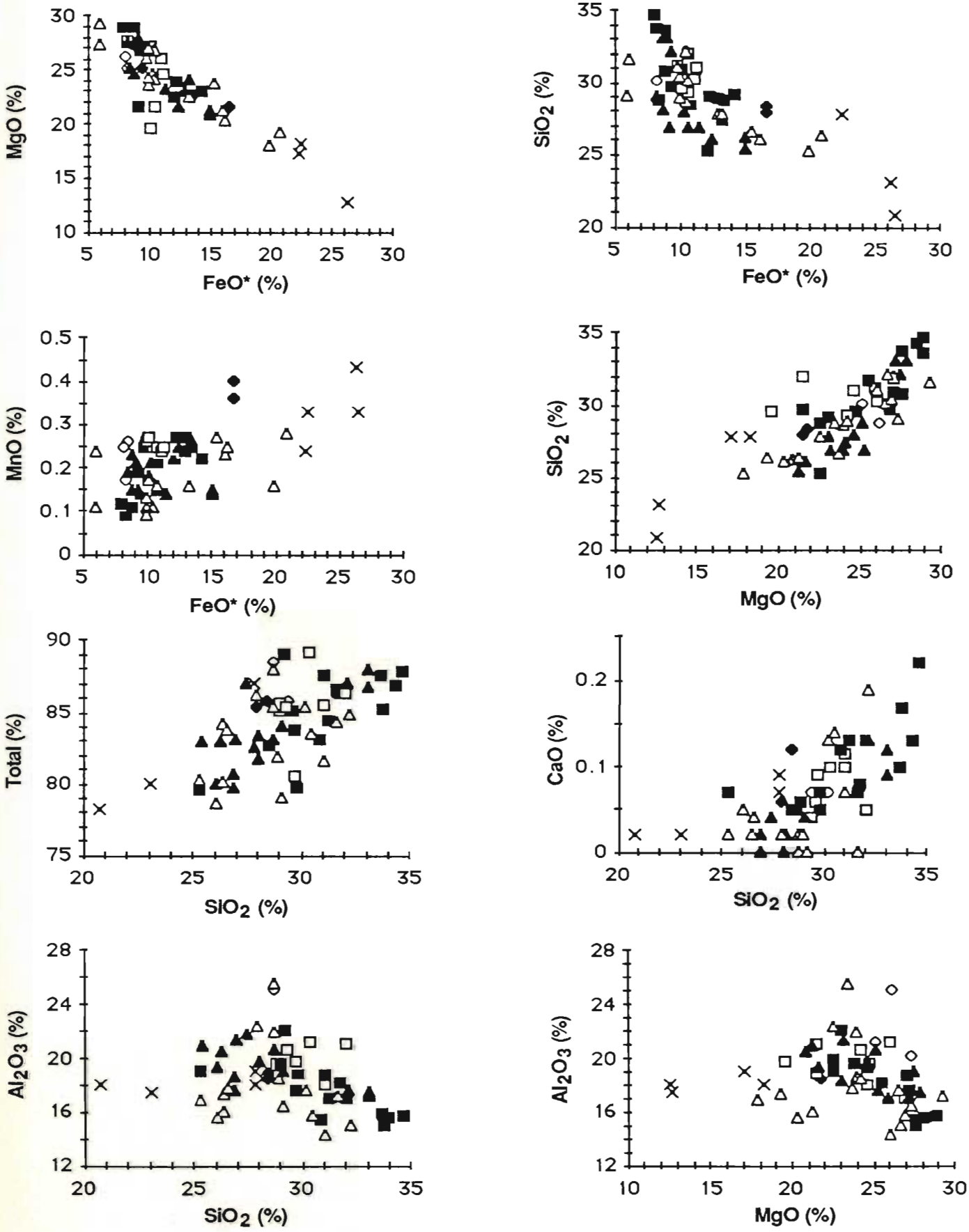

Figure 6-51: Miscellaneous X-Y plots for chlorites from rocks proximal to the Skidder Prospect. FeO* - total iron as FeO. Key as per Figure 6-49. See text for discussion.

Deer et al. (1962) indicate that Ca, which occurs in small amounts in most chlorites, occurs as structural ions or impurities. The positive correlation of CaO with SiO_2 and MgO, and its negative correlation with Al_2O_3 in the Skidder Prospect chlorites suggests that its occurrence in the chlorites is not random but is favoured by higher amounts of Si and Mg, and by lower amounts of Al.

6.7.2 Muscovite

Limited amounts of sericite (muscovite) have been noted in rocks from all alteration zones, except the very highly chloritic rocks of the chlorite, quartz, pyrite zone. Electron microprobe analyses of muscovites from rocks proximal to the Skidder Prospect are presented in Table 6-13 (analyses that have been averaged are presently individually in Table A-5, Appendix A). Muscovites analyzed include some from rocks included in the quartz, chlorite, pyrite alteration zone, and muscovites that are gangue to semimassive and massive sulphides. The muscovites are phengitic, containing up to 2.42% FeO and 3.56% MgO. On the portion of a triangular plot of atomic Si vs. atomic Al vs. atomic (Fe + Mn + Mg) shown in Figure 6-52, they show a trend that is parallel to the muscovite (sensu stricto) to celadonite line but offset to higher silica values (cf. McNamara, 1965).

6.7.3 Other minerals

Albite is abundant in the less intensely altered rocks proximal to the Skidder Prospect, but much of the albite in the more intensely altered rocks has been altered to quartz (see Section 6.6). Albite analyzed in sample SK 27 33 from the cl,qz,py alteration zone is similar to the average of albites from typical spilitized Skidder Basalt (Table 6-14).

The potassium-bearing mineral in more intensely altered rocks proximal to the Skidder Prospect is muscovite, but, as shown in Table 6-14, at least some of the potassium in less intensely altered rocks proximal to the Skidder Prospect is present in orthoclase. Note that K-feldspar may be more abundant than shown in the petrographic tables

Table 6-13: Electron microprobe analyses of muscovites from rocks proximal to the Skidder Prospect; analyses that have been averaged are presented in Table A-5, Appendix A

Weight %	SK 28 78	SK 29 57	SK 30 58	SK 30 80	SK 30 B
SiO_2	49.18	47.32	45.75	49.89	44.53
TiO_2	0.20	0.03	0.05	0.22	0.13
Al_2O_3	30.91	33.22	31.72	25.35	31.80
Cr_2O_3	0.05	0.02	0.03	0.05	0.09
FeO*	1.11	0.48	0.77	2.42	0.96
MnO	0.02	0.01	0.00	0.03	0.01
NiO	0.03	0.05	0.03	0.01	0.02
MgO	2.23	1.25	1.40	3.56	1.17
CaO	0.05	0.02	0.12	0.00	0.03
Na_2O	0.09	0.22	0.14	0.02	0.15
K_2O	9.40	9.88	9.45	10.06	9.67
Total	93.24	92.50	89.46	91.61	88.56
Atomic Proportions (based on 22 oxygens)					
Si	6.606	6.414	6.421	6.912	6.340
Ti	0.020	0.003	0.005	0.023	0.013
Al	4.895	5.309	5.248	4.140	5.339
Cr	0.005	0.002	0.003	0.005	0.010
Fe	0.124	0.054	0.090	0.280	0.115
Mn	0.002	0.001	0.000	0.004	0.002
Ni	0.003	0.005	0.003	0.001	0.002
Mg	0.445	0.253	0.293	0.735	0.248
Ca	0.007	0.003	0.018	0.000	0.004
Na	0.022	0.058	0.038	0.005	0.042
K	1.611	1.709	1.692	1.778	1.757
Total	13.741	13.811	13.813	13.884	13.872
Fe/(Fe+Mn+Mg)	0.22	0.18	0.24	0.28	0.32
Analyses	2	1	1	1	3
Alteration/ sulphide type	qz,cl,py	qz,cl,py	massive sulphides	semi-massive sulphides	qz,cl,py

* Total iron as FeO

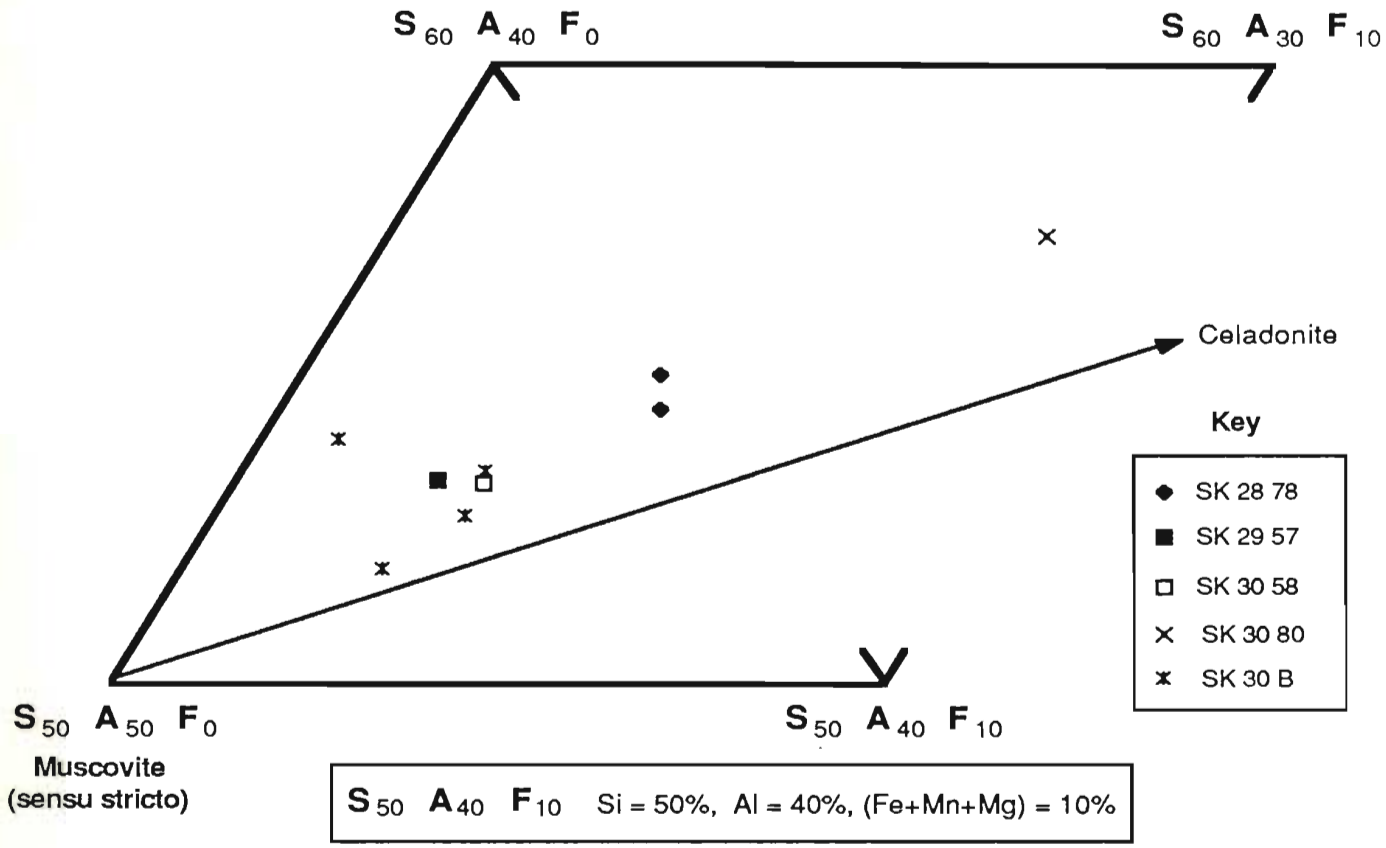

Figure 6-52: Portion of atomic Si-Al-(Fe+Mn+Mg) triangular plot (after McNamara, 1965) showing celadonite component of muscovites from rocks proximal to Skidder Prospect.

Table 6-14: Electron microprobe analyses of albite and K-feldspar from rocks proximal to the Skidder Prospect; average of albite from Skidder Basalt samples unaffected by alteration associated with the Skidder Prospect mineralizing event(s) shown for comparison

	Albite	Albite	Large Grain Albite - Orthoclase		Orthoclase
	Average Skidder Basalt	cl,qz,cc alteration zone	Centre	Rim	cl,cc,ep ± hm alteration zone
Weight %		SK 27 33	SK 27 8	SK 27 8	SK 27 8
SiO_2	68.41	66.75	68.60	65.81	65.13
TiO_2	0.02	0.00	0.03	0.13	0.00
Al_2O_3	19.51	19.38	19.86	18.59	18.51
FeO*	0.27	0.05	0.21	0.22	0.18
MnO	0.02	0.04	0.01	0.04	0.00
MgO	0.02	0.02	0.10	0.00	0.00
CaO	0.28	0.48	0.65	0.21	0.21
Na_2O	11.84	12.66	12.02	0.71	1.61
K_2O	0.05	0.05	0.64	15.06	14.11
Total	100.44	99.44	102.17	100.77	99.75
Atomic Proportions (based on 8 oxygens)					
Si	2.983	2.955	2.958	3.001	2.996
Ti	0.001	0.000	0.001	0.004	0.000
Al	1.003	1.011	1.010	0.999	1.004
Fe	0.010	0.002	0.008	0.008	0.007
Mn	0.001	0.001	0.000	0.002	0.000
Mg	0.001	0.001	0.006	0.000	0.000
Ca	0.013	0.023	0.030	0.010	0.010
Na	1.001	1.087	1.005	0.063	0.144
K	0.003	0.003	0.035	0.876	0.828
Total	5.017	5.084	5.055	4.964	4.988
Analyses	14	1	1	1	1
Molecular %					
Ab	96.5	97.7	93.9	6.6	14.6
An	1.3	2.0	2.8	1.1	1.1
Or	0.3	0.3	3.3	92.3	84.3
Whole Rock (complete analyses presented in Appendix B)					
Zr (ppm)		77	45	45	45
K_2O (%)		0.05	2.36	2.36	2.36

* Total iron as FeO

presented in Section 6.6 since, in thin sections of Skidder Basalt where its presence has been confirmed by electron microprobe analysis, the K-feldspar is optically indistinguishable from albite. K-feldspar analyzed in SK-27 8 from the cl,cc,ep,±hm alteration zone contains about 6.6 and 14.6 molecular per cent albite and 1.1 molecular per cent anorthite. Multiple analyses performed on one grain in this sample showed it to have an albite core and almost pure orthoclase rim (Table 6-14) (cf. Skidder Basalt sample S 16, Section 4.4.4).

Electron microprobe analyses of calcites from the Skidder Prospect area are compared to those of typical spilitized Skidder Basalt on Table 6-15. The Skidder Prospect calcites have, on average, similar $FeCO_3$ components but slightly higher $MgCO_3$, and a somewhat higher component of $MnCO_3$ compared to those of typical Skidder Basalt. Calcites in thin section SK 28 27 are particularly enriched in $MnCO_3$.

Table 6-15: Electron microprobe analyses of calcite from rocks in the vicinity of the Skidder Prospect; average of calcite from rocks unaffected by the Skidder Prospect mineralizing event(s) shown for comparison

	Average Skidder Basalt	Average Skidder Prospect	Jasper + sulphides	Jasper + sulphides	cl,qz,py	cl,qz,py	qz,cl,py	cl,qz,py	semi-massive sulphides	qz,cl,py	Sulphides + jasper
			SK	SK	SK	SK	SK	SK	SK	SK	SK
Weight %			27 42	27 42	28 27	28 27	28 40	28 41	28 66	31 12	37A 46
SiO_2	0.30	0.20	1.07	0.05	0.03	0.29	0.00	0.01	0.32	0.01	0.04
TiO_2	0.01	0.03	0.02	0.00	0.03	0.22	0.00	0.00	0.00	0.00	0.02
Al_2O_3	0.20	0.18	1.21	0.03	0.20	0.11	0.03	0.03	0.00	0.02	0.00
Cr_2O_3	0.02	0.01	0.00	0.00	0.00	0.02	0.00	0.00	0.02	0.01	0.01
FeO*	0.44	0.43	1.14	0.39	0.38	0.51	0.43	0.13	0.38	0.23	0.30
MnO	0.41	0.96	0.29	0.43	1.91	2.41	0.94	0.58	0.93	0.59	0.59
MgO	0.33	0.45	0.60	0.03	0.65	0.85	0.63	0.33	0.38	0.47	0.11
CaO	58.97	57.60	51.93	53.07	50.28	58.25	61.79	63.16	59.25	60.06	60.63
Na_2O	0.10	0.04	0.10	0.22	0.00	0.00	0.00	0.02	0.00	0.00	0.00
K_2O	0.01	0.01	0.02	0.00	0.00	0.01	0.01	0.01	0.00	0.01	0.00
Total	60.80	59.94	56.39	54.28	53.52	62.68	63.83	64.32	61.33	61.40	61.74
Atomic Proportions (based on 1 cation)											
Fe	0.006	0.006	0.015	0.006	0.006	0.006	0.005	0.002	0.005	0.003	0.004
Mn	0.005	0.013	0.004	0.006	0.028	0.030	0.012	0.007	0.012	0.008	0.008
Mg	0.007	0.010	0.014	0.001	0.017	0.019	0.014	0.007	0.009	0.011	0.002
Ca	0.965	0.958	0.895	0.980	0.941	0.928	0.968	0.982	0.964	0.978	0.984
Others	0.017	0.014	0.059	0.014	0.011	0.015	0.006	0.003	0.010	0.004	0.005
Total	0.995	0.995	0.973	1.003	0.997	0.992	1.000	1.000	0.995	1.000	0.999
Analyses	9	9	1	1	1	1	1	1	1	1	1
Molecular %											
$FeCO_3$	0.67	0.66	1.91	0.65	0.65	0.74	0.61	0.18	0.56	0.34	0.44
$MnCO_3$	0.62	1.47	0.49	0.72	3.26	3.54	1.34	0.82	1.39	0.87	0.87
$MgCO_3$	0.64	0.89	1.30	0.07	1.43	1.61	1.16	0.60	0.73	0.90	0.21
$CaCO_3$	98.07	96.98	96.30	98.56	94.66	94.11	96.89	98.39	97.32	97.89	98.48

* Total iron as FeO

cl,qz,py - alteration zone characterized by secondary mineral assemblage chlorite and lesser amounts of quartz and pyrite

qz,cl,py - alteration zone characterized by secondary mineral assemblage quartz and lesser amounts of chlorite and pyrite

6.7.4 Discussion

McLeod and Stanton (1984) show that coexisting talc and chlorite in several southeastern Australia stratiform mineral deposits have distribution coefficients for Mg relative to Mn and Fe between talc and chlorite that range from 2.45 to 3.15, averaging 2.84. As shown on Table 6-11, coexisting talc and chlorite in Skidder Prospect sample SK 31 12 and SK 28 73 are 2.43 and 2.68 respectively, somewhat similar to those presented by McLeod and Stanton (1984). Intermediate compositions between talc and chlorite in SK 28 73 may represent preserved compositions during the formation of which deposition was so rapid as to prevent attainment of equilibrium between the two minerals.

In the Woodlawn deposit, chlorites associated with sphalerite-rich sulphide assemblage are significantly enriched in Mg than those associated with a chalcopyrite-rich sulphide assemblage (McLeod and Stanton, 1984). The dividing line is at a Fe / (Fe + Mg + Mn) ratio of about 0.2 (McLeod and Stanton, 1984). As shown on Figure 6-49 most Skidder Prospect chlorites are similar to those associated with the Zn-rich sulphides, in that they have a Fe / (Fe + Mg + Mn) ratios less than 0.2. McLeod and Stanton (1984) also show that, in the Woodlawn deposit, sphalerites associated with Mg-rich chlorites have lower FeS contents than those associated with Fe-rich chlorites. As noted in Section 6.9, sphalerites in the Skidder Prospect have low concentrations of FeS.

Muscovites in southeastern Australia stratiform mineral deposits are phengitic (McLeod and Stanton, 1984), like those of the Skidder Prospect. Phengitic muscovite (1-3% FeO and MgO) and talc have also been noted in the hydrothermal sulphide deposits located on the East Pacific Rise at 21°N (Hekinian et al., 1980; Spiess et al., 1980).

McLeod and Stanton (1984) suggest that phyllosilicates that are interlayered with, and immediately surround the sulphide minerals in stratiform sulphide deposits in southeastern Australia were deposited as chemical precipitates from hydrothermal fluids during formation of the mineral deposits. A similar origin is plausible for the Skidder Prospect phyllosilicates.

6.8 Ore Petrography

6.8.1 Introduction

Polished thin sections of samples representative of the semimassive to massive nonbedded sulphides consist of subhedral to euhedral pyrite, and anhedral sphalerite and chalcopyrite in a gangue of quartz and chlorite ± calcite; in some samples the gangue consists of approximately equal amounts of quartz and calcite plus lesser chlorite (Table 6-16). Minor amounts of sphene are also present. Equigranular quartz occurs throughout the samples as dense masses of tiny anhedral grains, and as coarser grained anhedral grains, 0.1 mm across, accompanied by calcite. In some areas, quartz occurs as elongate, anhedral, myrmekite-like grains that radiate around pyrite grains; the quartz grains are typically interlocked with other quartz grains of similar habit protruding from adjacent pyrite grains (cf. Figure 6-45). Calcite and lesser chlorite occur in areas intersertal to pyrite and as irregular anhedral masses intergrown with quartz.

Polished thin sections of the layered massive sulphides show fine- to medium-grained pyrite interlayered with anhedral chalcopyrite and sphalerite, and, in polished thin section SK 27 42C, interlayered with magnetite and hematite. Gangue is typically quartz, which displays similar habit and textures to that occurring in the unlayered sulphides. Some thin sections show anhedral calcite as the principal gangue mineral. It typically occurs as anhedral masses intersertal to the sulphide minerals.

6.8.2 Petrography of the sulphide minerals

Pyrite, chalcopyrite, sphalerite and galena are the only sulphide minerals identified in the Skidder Prospect. Pyrite is ubiquitous and is by far the dominant sulphide. It ranges in content from 5 to 10% as disseminated grains and pyrite-bearing veins in less altered rocks, from 10 to 80% in quartz within the most intensely altered portion of the alteration pipe; and from 80 to 90% in massive sulphide portions of the prospect. Lesser amounts of

Table 6-16: Ore petrography table showing partial geochemical analysis and mineralogy of semimassive to massive sulphides

Key:	See Figure 6-1 for location of drill holes
	Abbreviations: Ab-albite, Cl-chlorite, Cc-calcite, Qz-quartz, hm-hematite, sc-sericite, Py-pyrite, Cp-chalcopyrite Sph-sphalerite; L - layered, F - fine grained, M - medium grained, C - coarse grained semimass. - semimassive; PT - polished thin section
	Abundance of mineral as estimated from examination of polished sections: x-low, xx-medium, xxx-high.
	See appendix B for complete whole rock analyses and description of analytical methods.

Sample Name	Depth feet	Depth m	Sulphide Type		Grain Size	SiO_2 %	TiO_2 %	MgO %	Zr ppm	Py	Cp	Sph	Hm	Qz	Cl	Cc	Other Minerals and Comments
SK 27 37	579.5	176.6	semimass.	L	F					xxx	xx	xx		xxx	x	xxx	PT; folded layers; galena (x)
SK 27 42C	633.0	192.9	semimass.	L	F/M					xxx	x	x	x	xxx			magnetite
SK 27 43	635.0	193.5	massive	L	F/M					xxx	xx	xx	x	xx	xx		
SK 27 45	639.5	194.9	massive		M/F					xxx	xx	xx		xx	xx		
SK 27 46	644.8	196.5	massive	L	F/M					xxx	xxx	xxx		xx	xx		
SK 28 38	526.0	160.3	massive		M/C					xxx	x	x		xx	xx	x	
SK 28 44	541.0	164.9	semimass.	L	F/M					xxx	xx	xx		xx	xx	x	
SK 28 61	661.8	201.7	massive	L	F/M					xxx				x	x		
SK 28 66	691.0	210.6	semimass.		F/M					xxx	xx	x		xxx	x	x	
SK 28 67	697.0	212.4	massive	L	F/M					xxx	xx	x		x	x	xxx	
SK 29 52	788.5	240.3	massive		F/M					xxx	xxx	xx		xxx	x		sph-qz veins, framboidal py
SK 29 55	802.5	244.6	semimass.		M					xxx	x	x		xxx	x		
SK 29 59	847.5	258.3	massive	L	M/C	**14.0**	**0.2**	**0.3**	**28**	xxx	x	x		x	x		
SK 29 60	849.5	258.9	semimass.		M	**20.0**	**0.2**	**16.5**	**61**	xxx				xx	xx		
SK 30 58	804.0	245.1	massive		M/C					xxx	x	x		xx	x	x	pyrite fractured
SK 30 59	811.0	247.2	semimass.		M					xxx	xx	xxx		xx	x		qz-sph vein
SK 30 822A	822.0	250.5	semimass.		M	**41.9**	**0.2**	**10.6**	**48**	xxx				xxx	xxx	x	
SK 30 63	837.0	255.1	massive		M/C					xxx				xx	x	x	pyrite fractured
SK 30 B	863.5	263.2	qz,cl,py		F/M					xx	x			xxx			
SK 30 67	872.0	265.8	semimass.		M/C					xxx		x		xxx	x	x	
SK 30 75	938.0	285.9	massive		M/C	**7.1**	**0.1**	**3.6**	**37**	xxx	x	x		x	x	xx	pyrite fractured

Table 6-16 (continued):

Sample Name	Depth feet	Depth m	Sulphide Type		Grain Size	SiO_2 %	TiO_2 %	MgO %	Zr ppm	Py	Cp	Sph	Hm	Qz	Cl	Cc	Other Minerals and Comments
SK 30 76	940.5	286.7	semmass.		F/M					xxx	xx	xxx		xx	x		qz-sph-cp vein
SK 30 80	973.5	296.7	semmass.		F/M	39.3	0.1	0.6	20	xxx	xxx	x		xxx	x		qz-cp-sph vein
SK 30 81	985.5	300.4	massive	L	M					xxx	x	x		x	x	xxx	
SK 31 11	137.0	41.8	semmass.		M					xxx	xx	xx		xx	xx	xxx	PT
SK 31 13	142.5	43.4	semimass.		M					xxx	x	x		xx	xx		
SK 31 17C	174.0	53.0	massive	L	F/M					xxx	xx	x		x	x	xxx	
SK 33 20	346.0	105.5	semimass.		M					xxx				xx	x		
SK 35A 2	1501.0	457.5	massive	L	F/M					xxx	xx	xx		xx	x		
SK 35A 3	1507.0	459.3	massive	L	F/M					xxx	xx	x		xx	x		
SK 35A 6	1570.5	478.7	massive	L	F/M	4.4	n.d.	0.6	19	xxx	xx	xxx		x	x		

n.d. - not detected

sphalerite and chalcopyrite occur interstitial to pyrite, or in quartz veins that cut the massive sulphides.

Pyrite occurs typically as subhedral grains that show a range of grain sizes up to about 2 mm across (Figure 6-53). It reaches a maximum size in the semimassive to massive unlayered sulphides, where, in rare instances, grains up to 2 cm across are present. In most places, pyrite grains show well developed cleavage, and, in many places, irregular fractures. Cleavage cracks occur in two directions mostly at right angles to each other; irregular fractures in a third direction often result in angular wedge-shaped grains (Figure 6-54). Where not surrounded by other sulphide minerals, pyrite is typically surrounded by quartz, even where the gangue is predominantly chlorite. Pyrite most frequently occurs as subhedral grains where surrounded by quartz but it tends to occur as angular anhedral grains in the very few places where it is immediately surrounded by chlorite (Figure 6-55). In a few areas, e.g. in polished section SK 29 59, pyrite grains in contact with each other show equilibrium 120° triple point junctions. Pyrite, where surrounded by sphalerite or chalcopyrite is typically more anhedral than where surrounded by quartz and in many areas is embayed along grain edges and cleavage cracks (Figures 6-56, 6-57 and 6-58). Fractures in the pyrite are cemented by the chalcopyrite (Figure 6-54) or sphalerite. Chalcopyrite or sphalerite or both occur as rounded inclusions in the pyrite (Figure 6-59). Rounded inclusions of chalcopyrite or sphalerite also occur in pyrite surrounded by gangue. Subhedral pyrite pseudomorphs feldspar in polished sections SK 29 52 and SK 37A 47. Pyrite grains are replaced by calcite in SK 27 39.

Numerous tiny framboidal grains of pyrite or "mineralized bacteria" (Ramdohr, 1980) occur in quartz adjacent to a sphalerite-bearing quartz vein in polished section SK 29 52 (Figure 6-60). Pyrite elsewhere in the sample occurs as typical subhedral grains. In places, the framboidal grains coalesce to form anhedral masses with cuspate rounded edges. Detailed examination of the pyrite spheres show them to be composed of tiny subhedral pyrite grains cemented by a dark-coloured material, possibly very fine grained

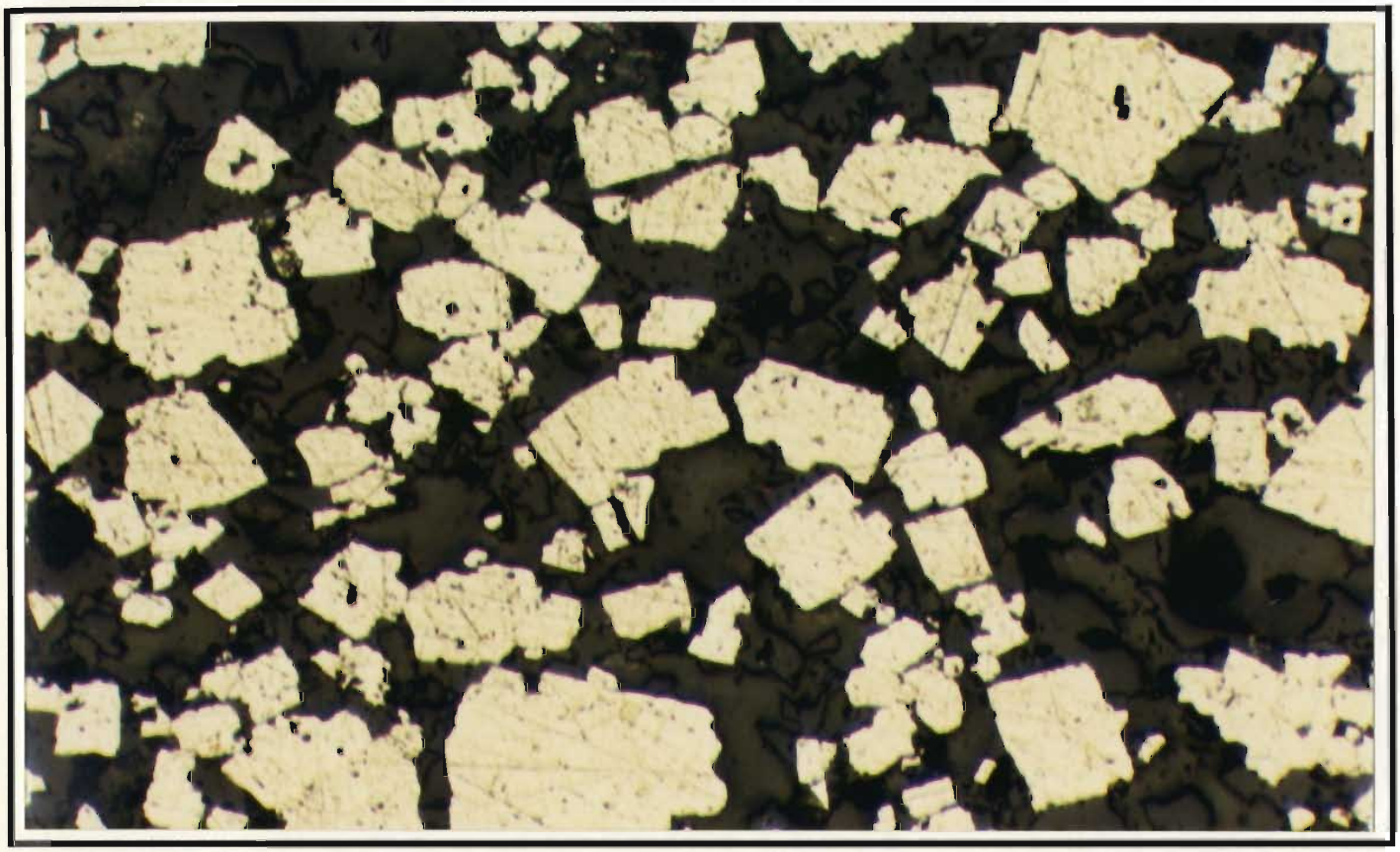

Figure 6-53: Reflected light photomicrograph of subhedral pyrite grains in quartz. Polished section SK 31 17C, plane polarized light, 10 x. —— 0.2 mm ——

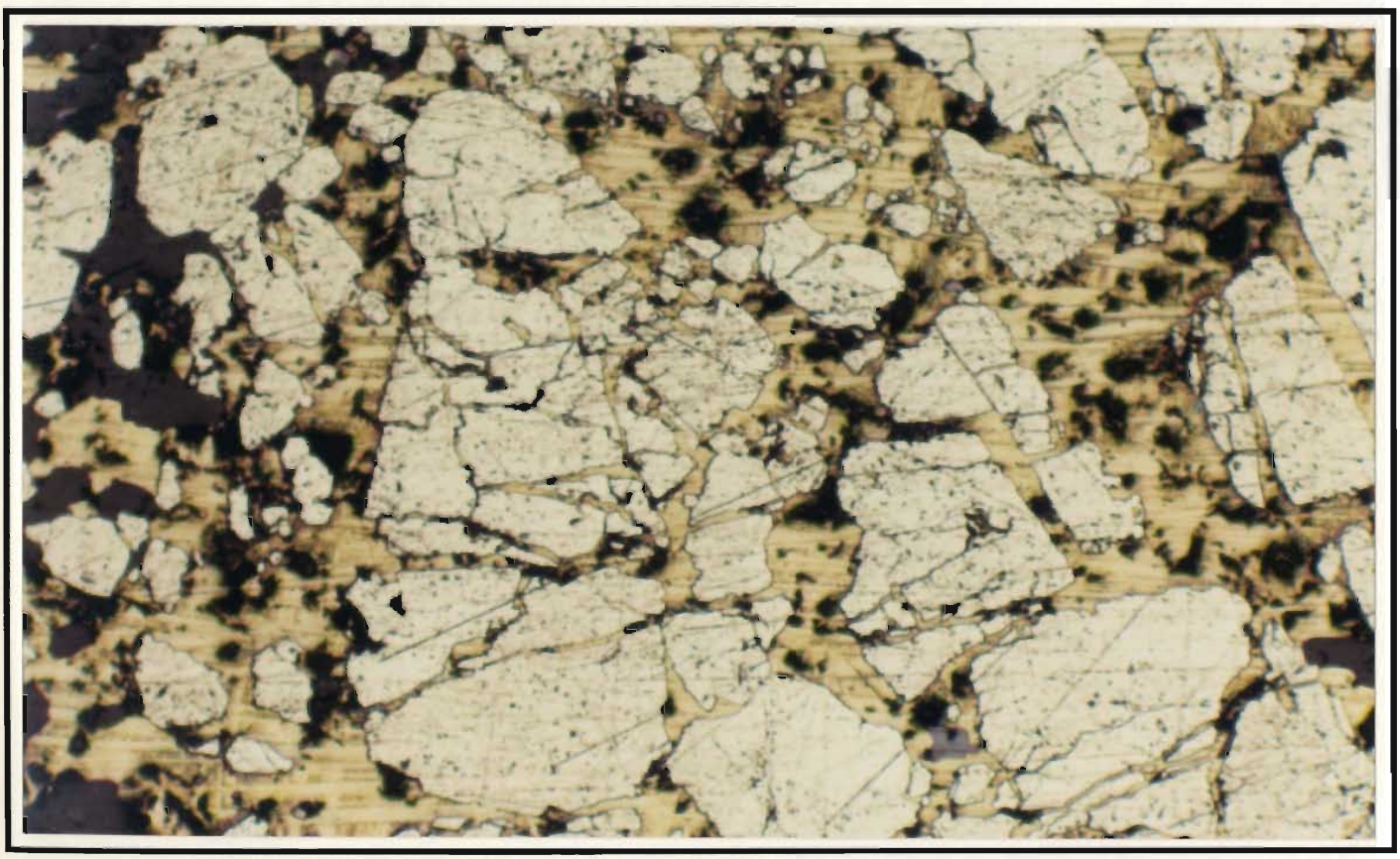

Figure 6-54: Reflected light photomicrograph of fractured pyrite. Chalcopyrite fills fractures and cleavage cracks. Note rounded anhedral sphalerite inclusion in the chalcopyrite. Polished section SK 27 45, plane polarized light, 10 x. —— 0.2 mm ——

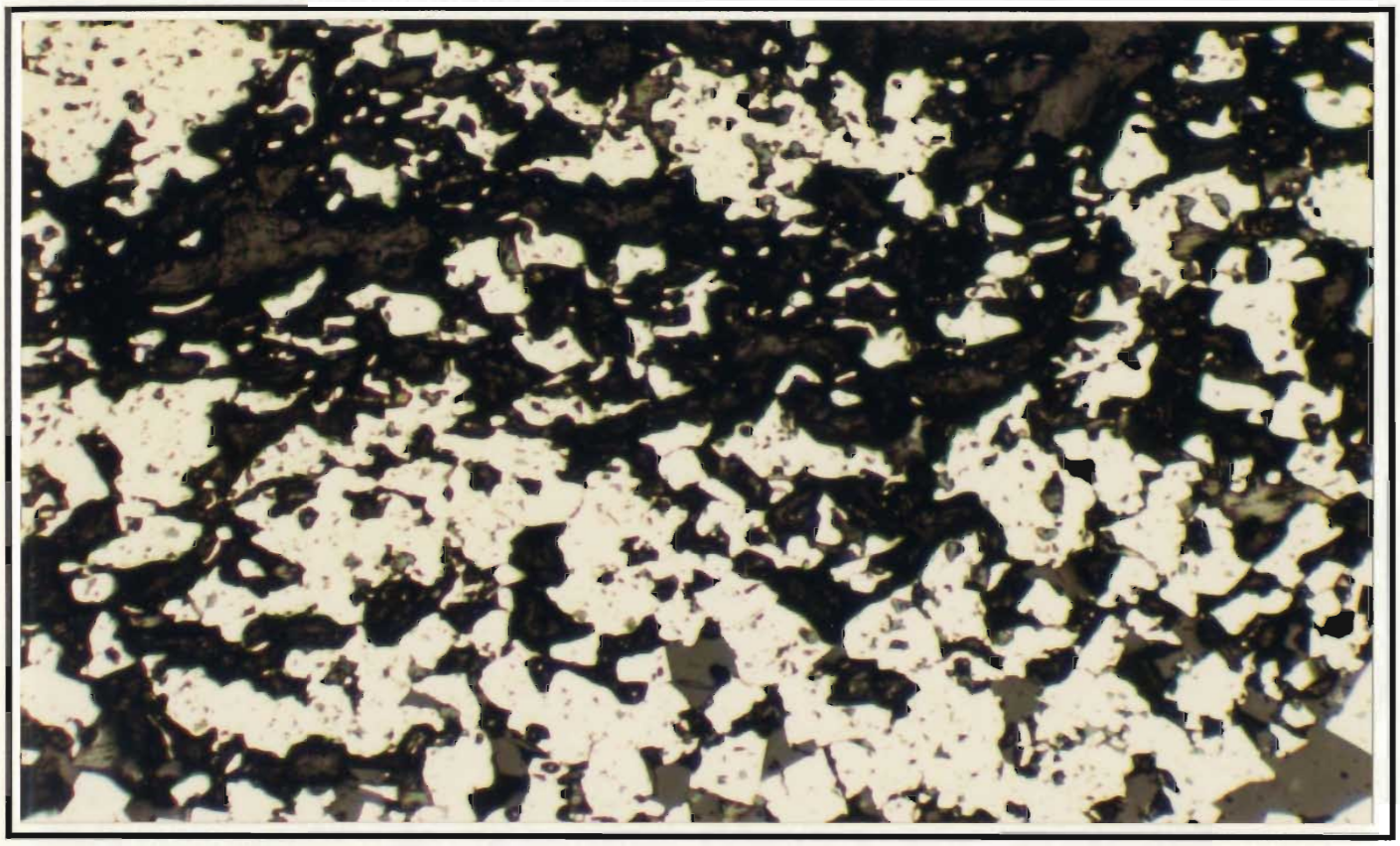

Figure 6-55: Reflected light photomicrograph showing contrast between subhedral pyrite grains in quartz (medium grey) at the bottom of the photograph, and anhedral, angular pyrite grains in chlorite (dark brown) in the central and top portions of the photograph. Polished section SK 27 43, plane polarized light, 10 x. —— 0.2 mm ——

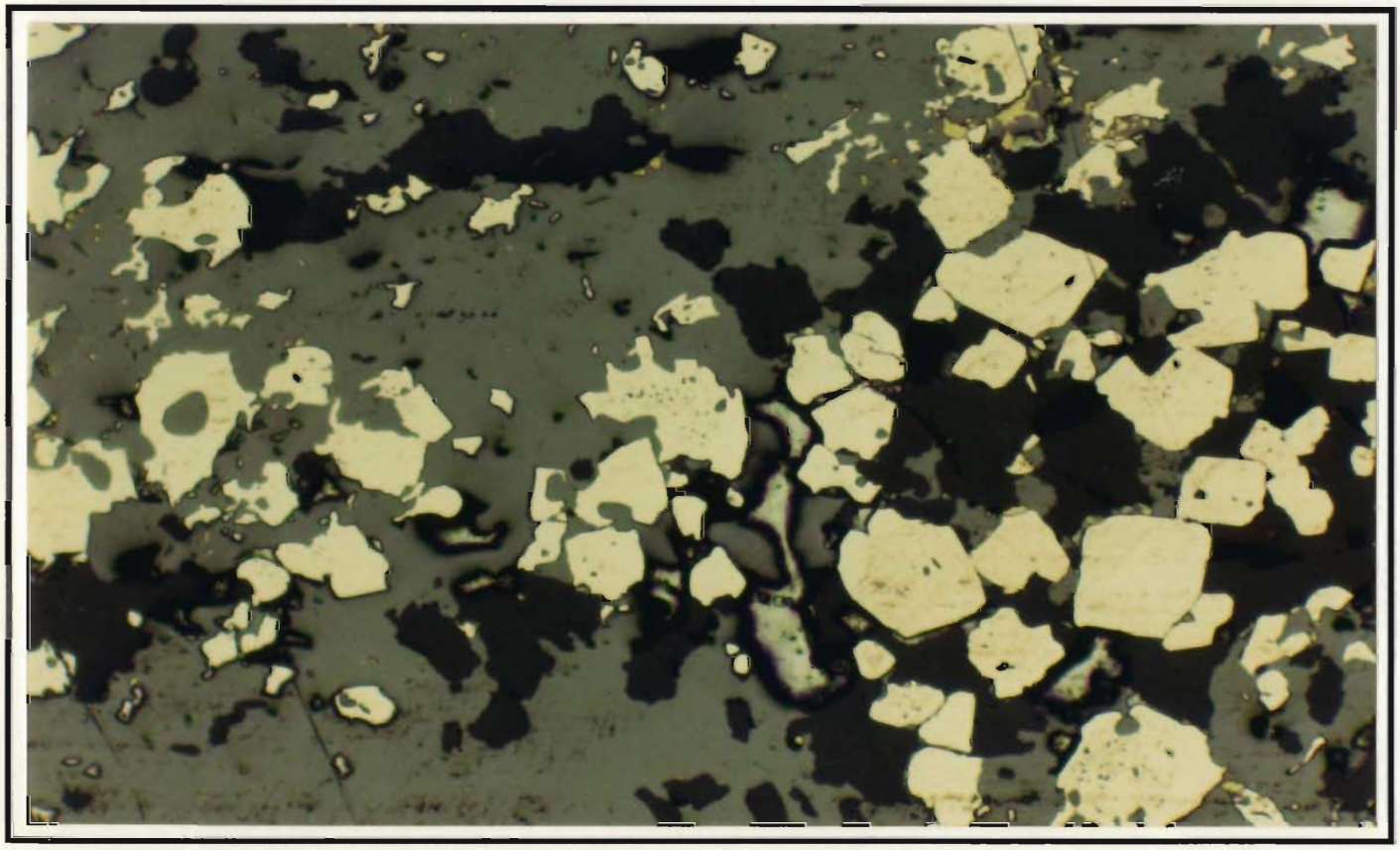

Figure 6-56: Reflected light photomicrograph showing subhedral pyrite in quartz (dark grey) at the right of the photograph, and anhedral pyrite in sphalerite (medium grey) at the left of the photograph. Polished section SK 35A 6, plane polarized light, 10 x. —— 0.2 mm ——

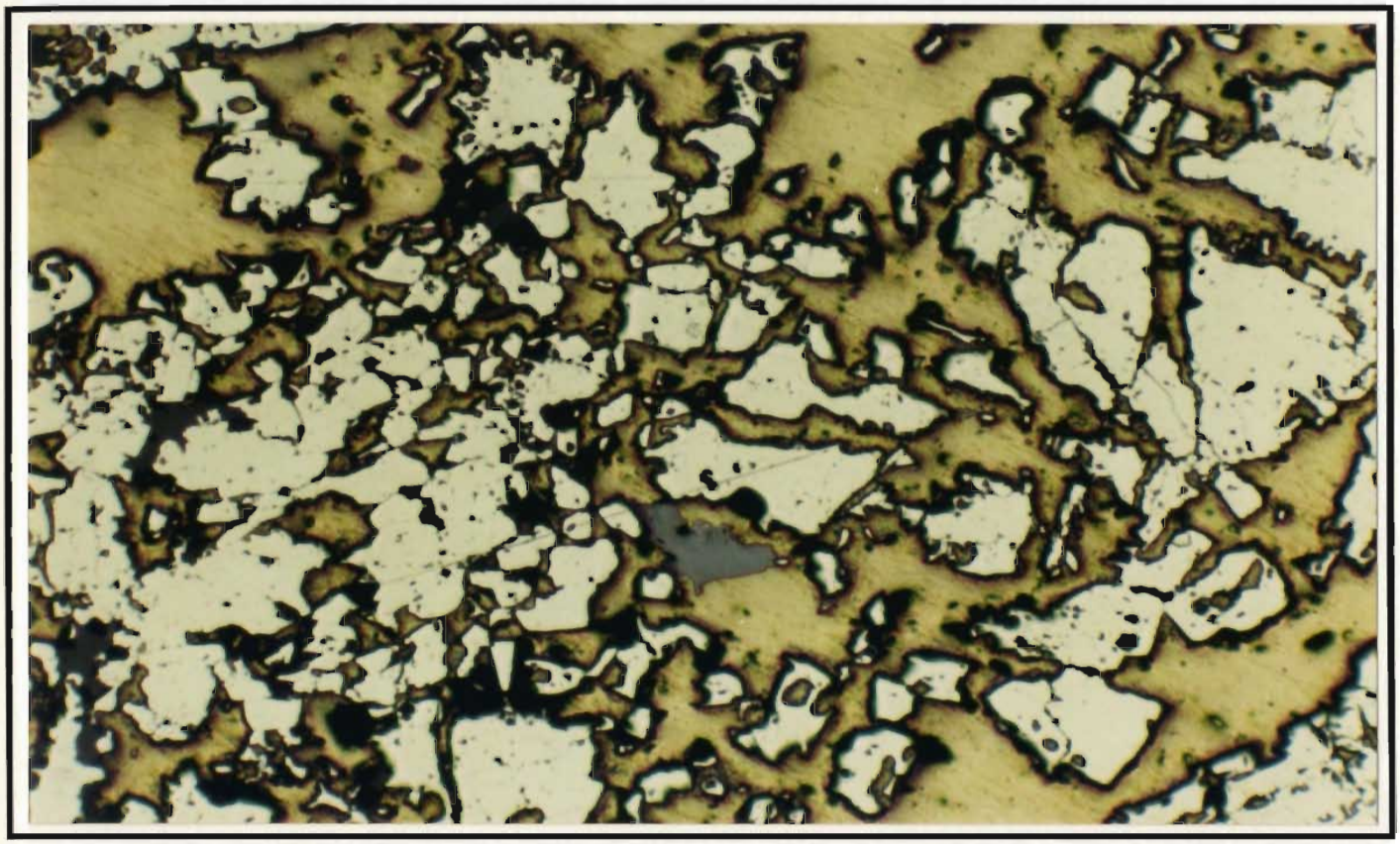

Figure 6-57: Reflected light photomicrograph of anhedral resorbed pyrite in chalcopyrite. Note anhedral sphalerite inclusion (grey) in the chalcopyrite. Polished section SK 29 52, plane polarized light, 10 x. —— **0.2 mm** ——

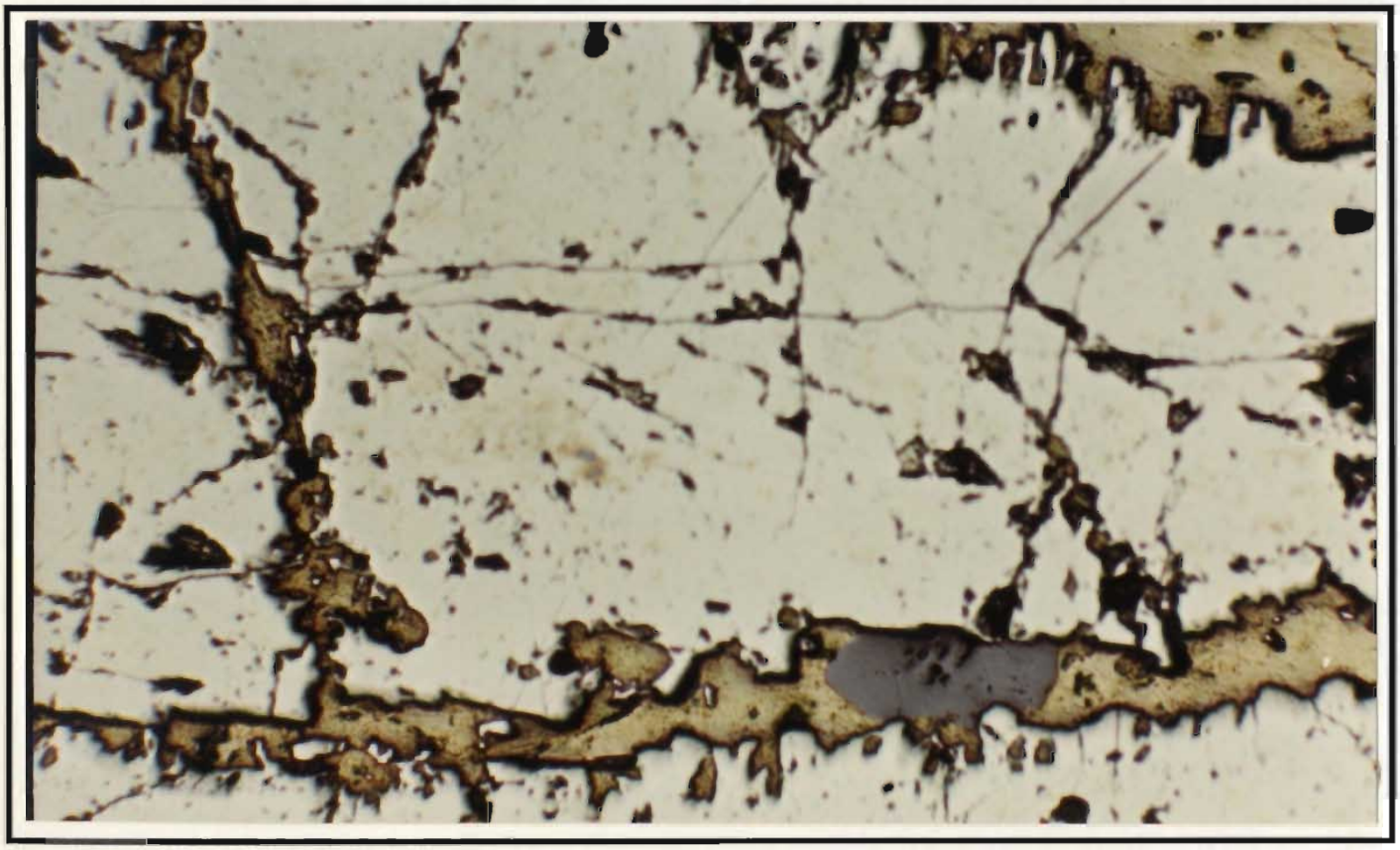

Figure 6-58: Reflected light photomicrograph of pyrite, which is embayed along chalcopyrite-filled fractures. Note anhedral sphalerite inclusion (grey) in the chalcopyrite. Polished section SK 29 52, plane polarized light, 20 x. —— **0.1 mm** ——

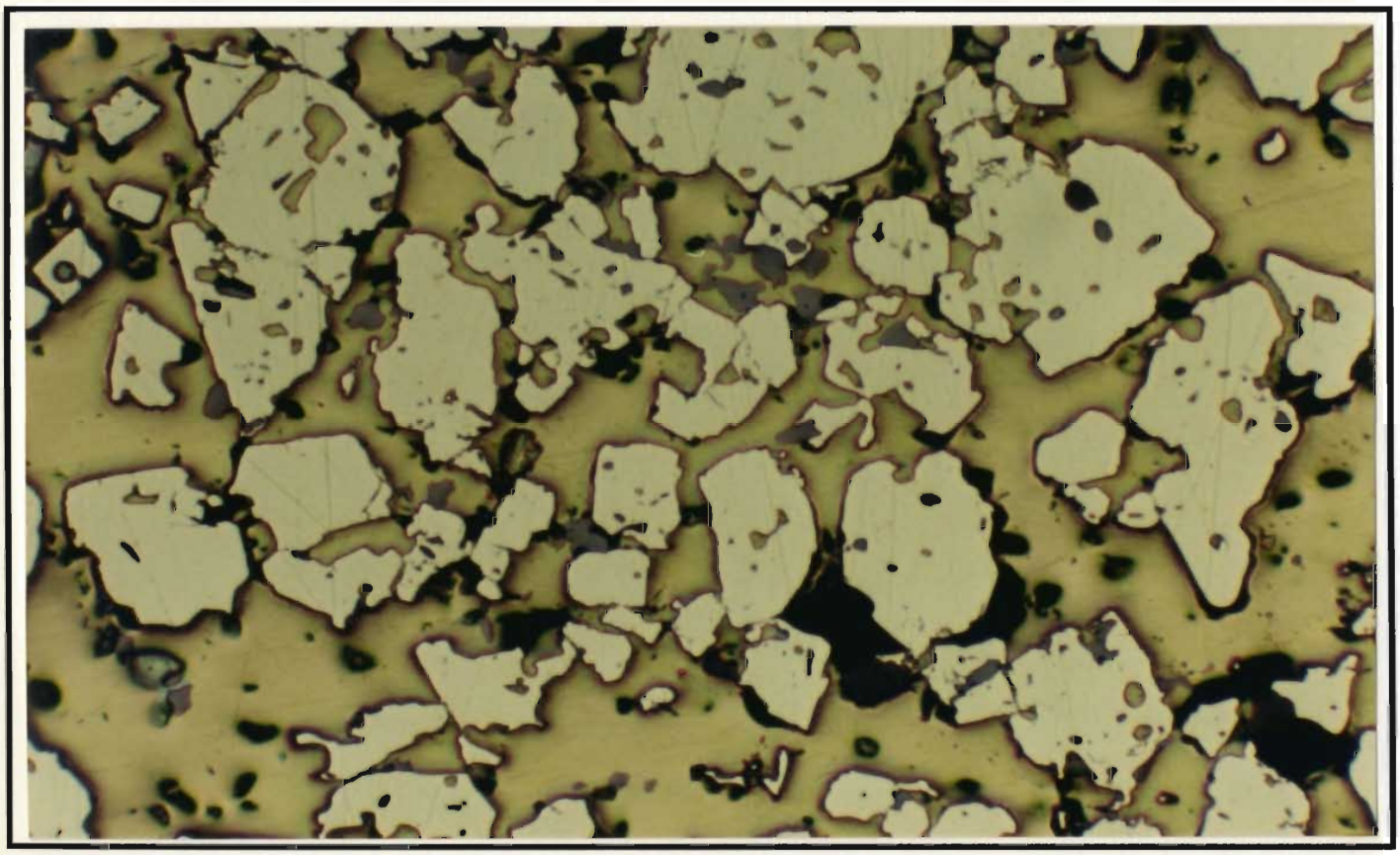

Figure 6-59: Reflected light photomicrograph of subhedral to anhedral, partially resorbed pyrite grains in chalcopyrite. Rounded chalcopyrite inclusions occur in the pyrite, and rounded anhedral sphalerite occurs in both chalcopyrite and pyrite. Polished section SK 35A 6, plane polarized light, 10 x. —— 0.2 mm ——

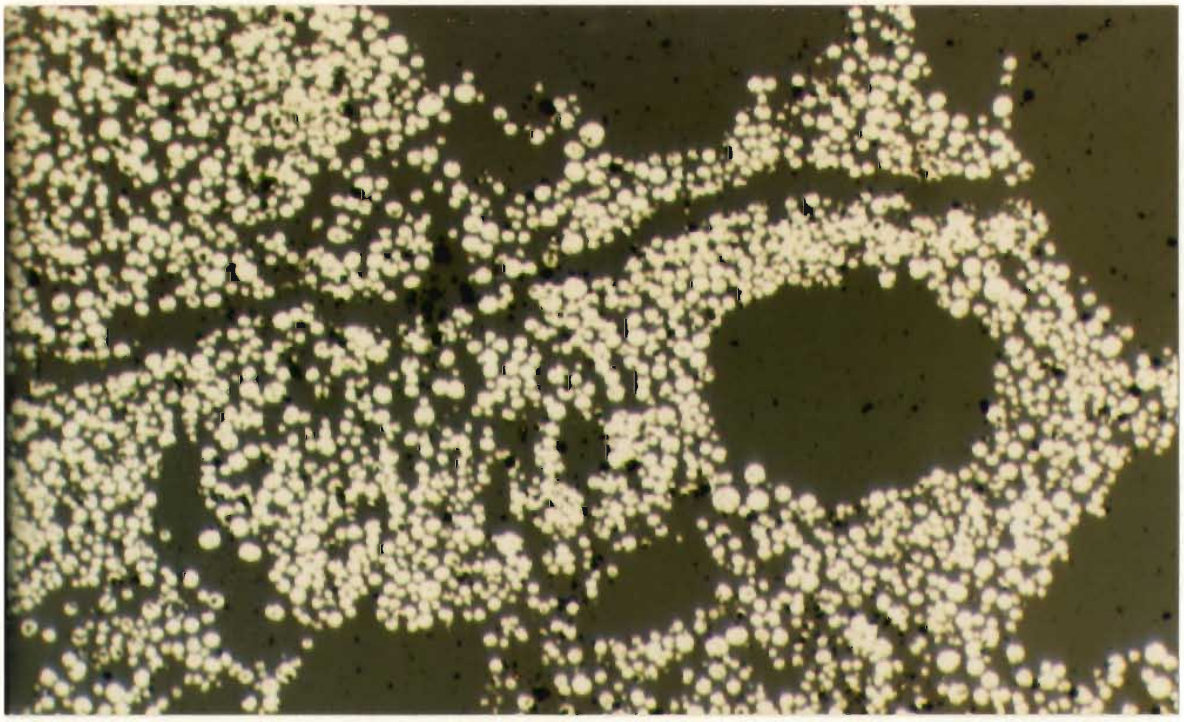

Figure 6-60: Reflected light photomicrograph of framboidal pyrite in quartz. Polished section SK 29 52, plane polarized light, 10 x. —— **0.2 mm** ——

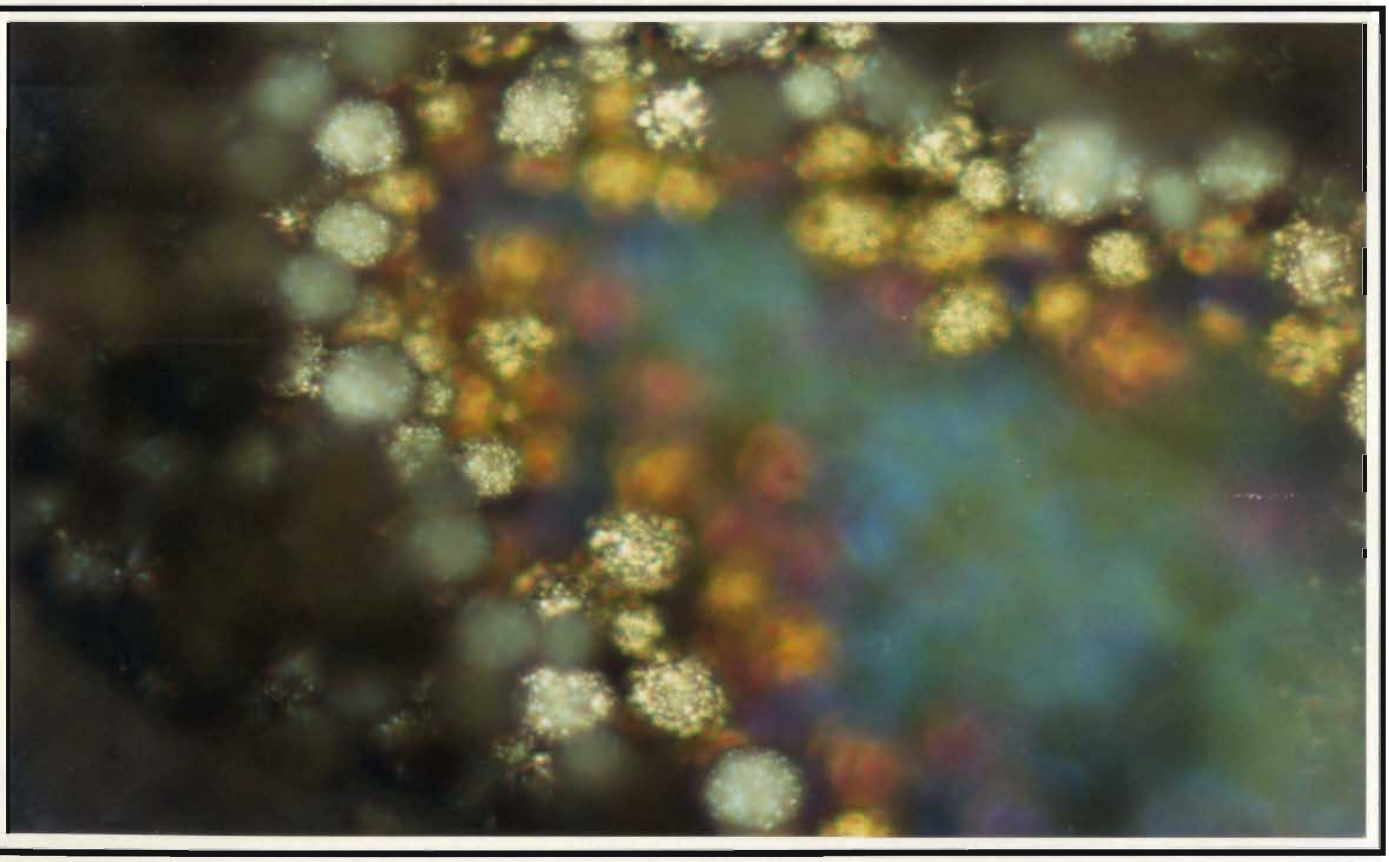

Figure 6-61: Reflected light photomicrograph of framboidal pyrite grains showing them to be composed of tiny subhedral pyrite grains cemented by a dark-coloured material. Microscope has been focussed on framboidal grains slightly beneath surface of polished section. Polished section SK 29 52, plane polarized light, 50 x. —— **0.04 mm** ——

sulphide grains (Figure 6-61). In some places the framboidal pyrite occurs as inclusions in sphalerite, however no inclusions of framboidal pyrite are noted in chalcopyrite (Figure 6-62).

Chalcopyrite most typically occurs as anhedral masses interstitial to, or, to a lesser extent, as rounded inclusions in pyrite (Figures 6-54, 6-57, 6-58 and 6-59). Chalcopyrite and sphalerite are typically intricately intergrown, having cuspate irregular boundaries, and, in many instances, containing irregular anhedral inclusions of one mineral within the other (Figure 6-63). Chalcopyrite is also present in quartz veins, where it occurs as anhedral, dendritic masses. Anhedral chalcopyrite cements pyrite grains, and fills cleavage cracks and fractures within the grains themselves (Figures 6-54, 6-57, 6-58 and 6-59). In places, the chalcopyrite occurs around the edges of pyrite grains adjacent to gangue. Minor amounts of chalcopyrite also occur in jasper fragments embedded in pyrite, e.g. in SK 37A 45.

Sphalerite occurs in thin units interlayered with pyrite or in quartz veins cutting pyrite. It also fills interstitial areas between pyrite grains and cleavage cracks in the grains themselves (Figure 6-64), but to a lesser extent than chalcopyrite. Some sphalerite is intergrown with chalcopyrite in areas interstitial to pyrite (Figures 6-57, 6-58 and 6-59). In quartz veins, sphalerite occurs as anhedral grains (Figure 6-65) (less dendritic than chalcopyrite) and in places preferentially occurs on the flanks of the vein.

Polished section SK 35A 6 contains a 2 cm thick layer of sphalerite. The sphalerite contains ubiquitous elongate rounded inclusions of gangue. Anhedral to subhedral pyrite inclusions in the sphalerite parallel layering in the remainder of the sample. In one area, the sphalerite contains chalcopyrite inclusions, the largest of which display intricate intergrowth textures with the sphalerite.

Occurrences of galena are rare in the Skidder Prospect. Where present, it occurs as anhedral grains intergrown with chalcopyrite, sphalerite or a combination of these minerals (Figures 6-66 and 6-67). In places, it shows characteristic triangular pits. Dihedral angles

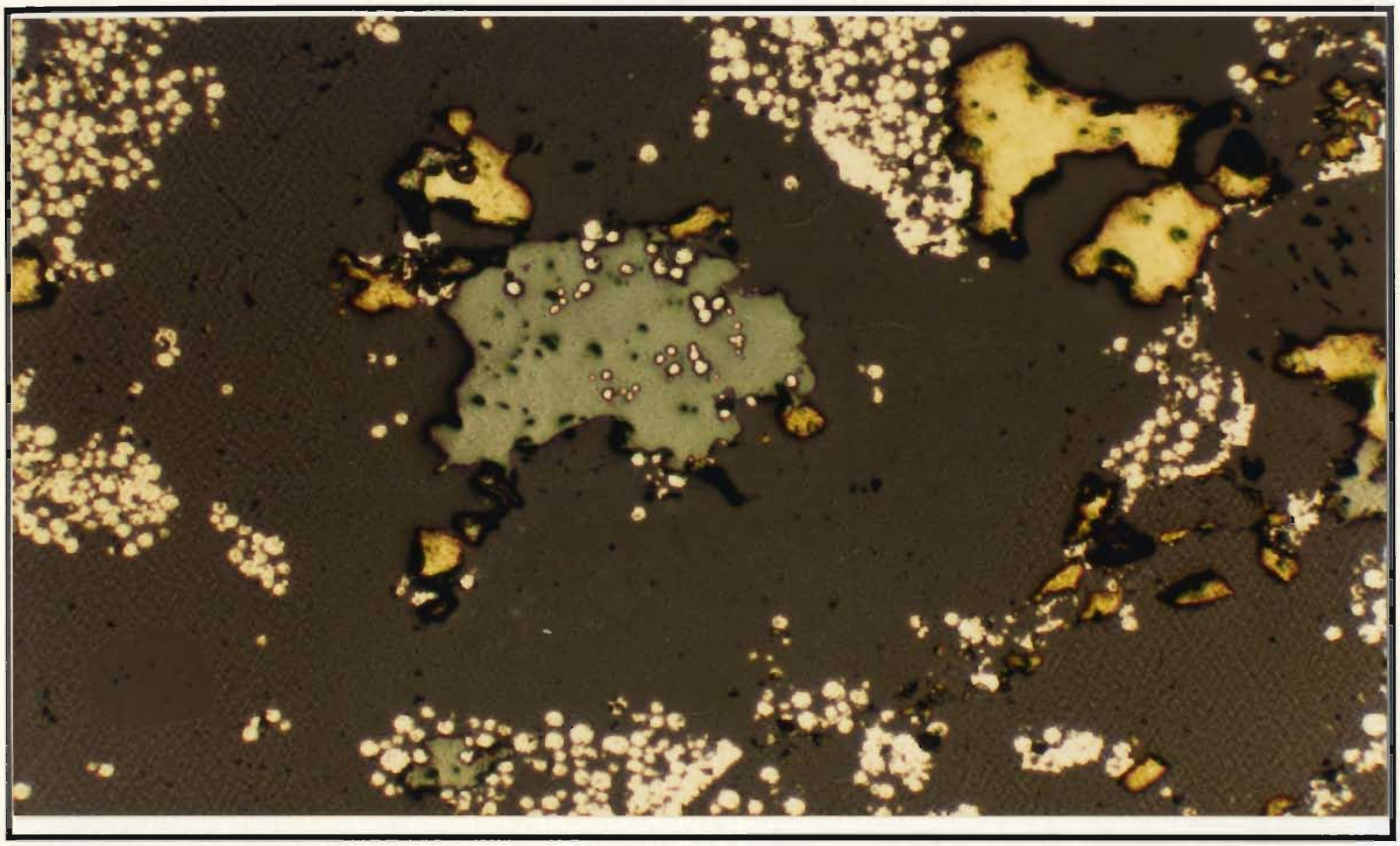

Figure 6-62: Reflected light photomicrograph of framboidal pyrite in quartz and sphalerite (light grey). Note the lack of framboidal pyrite in the anhedral chalcopyrite masses. Polished section SK 29 52, plane polarized light, 10 x. —— 0.2 mm ——

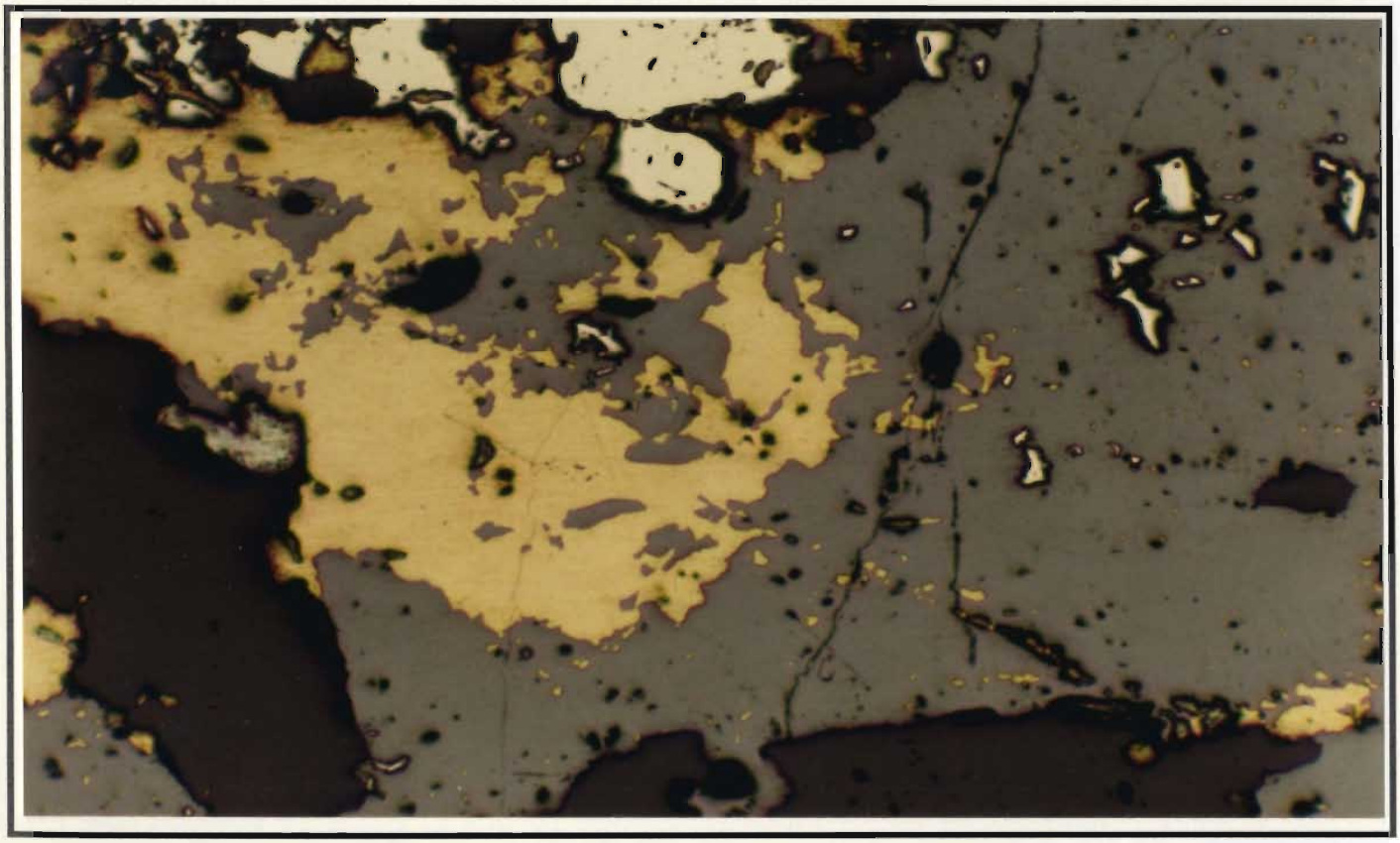

Figure 6-63: Reflected light photomicrograph showing intricately intergrown chalcopyrite and sphalerite, each containing irregular anhedral inclusions of the other. Polished section SK 29 52, plane polarized light, 10 x. —— 0.2 mm ——

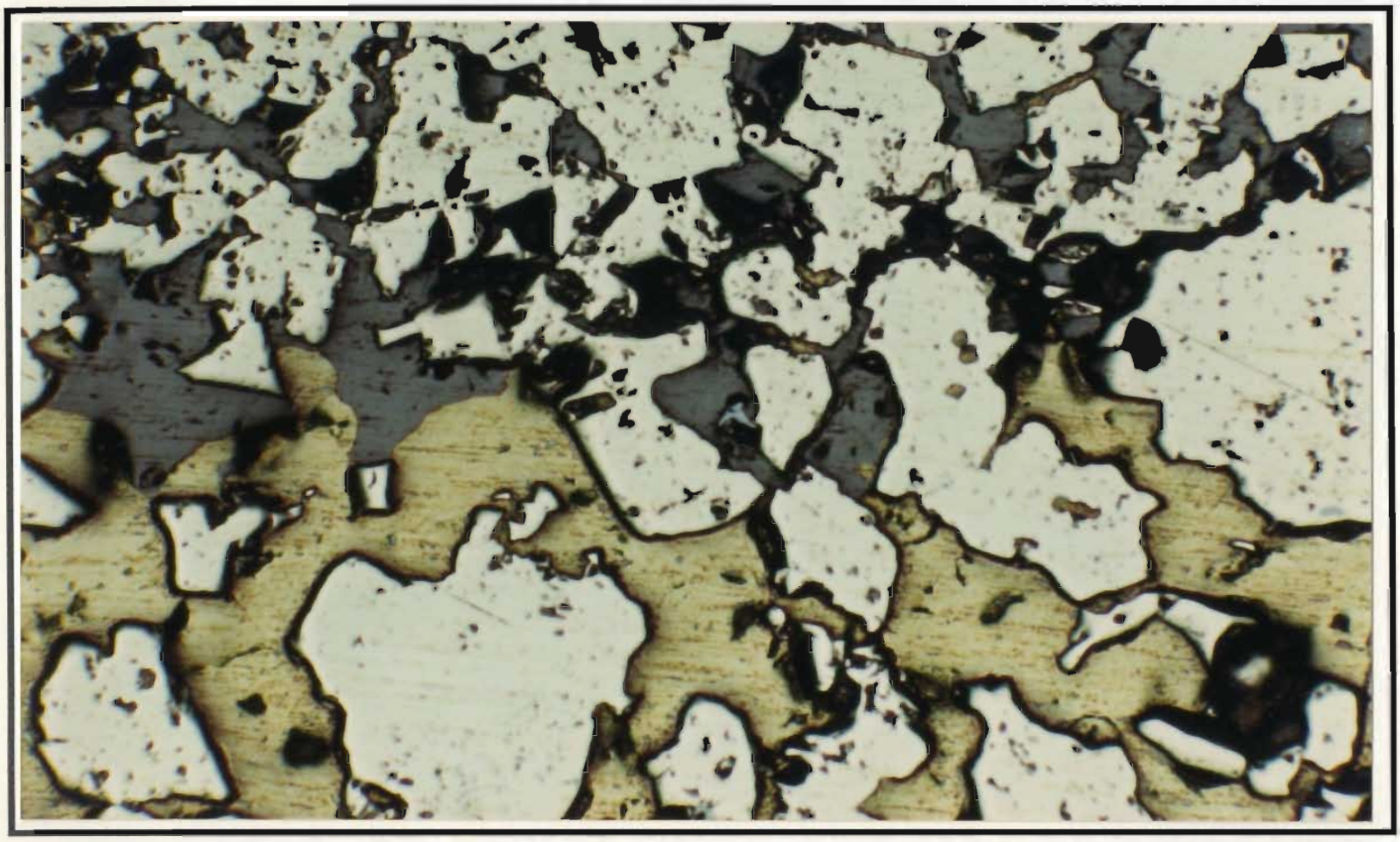

Figure 6-64: Reflected light photomicrograph of anhedral pyrite, chalcopyrite and sphalerite. Sphalerite occupies areas between pyrite grains at the top of the photograph, chalcopyrite occupies intergranular areas at the bottom. Polished section SK 27 43, plane polarized light, 20 x.
—— 0.1 mm ——

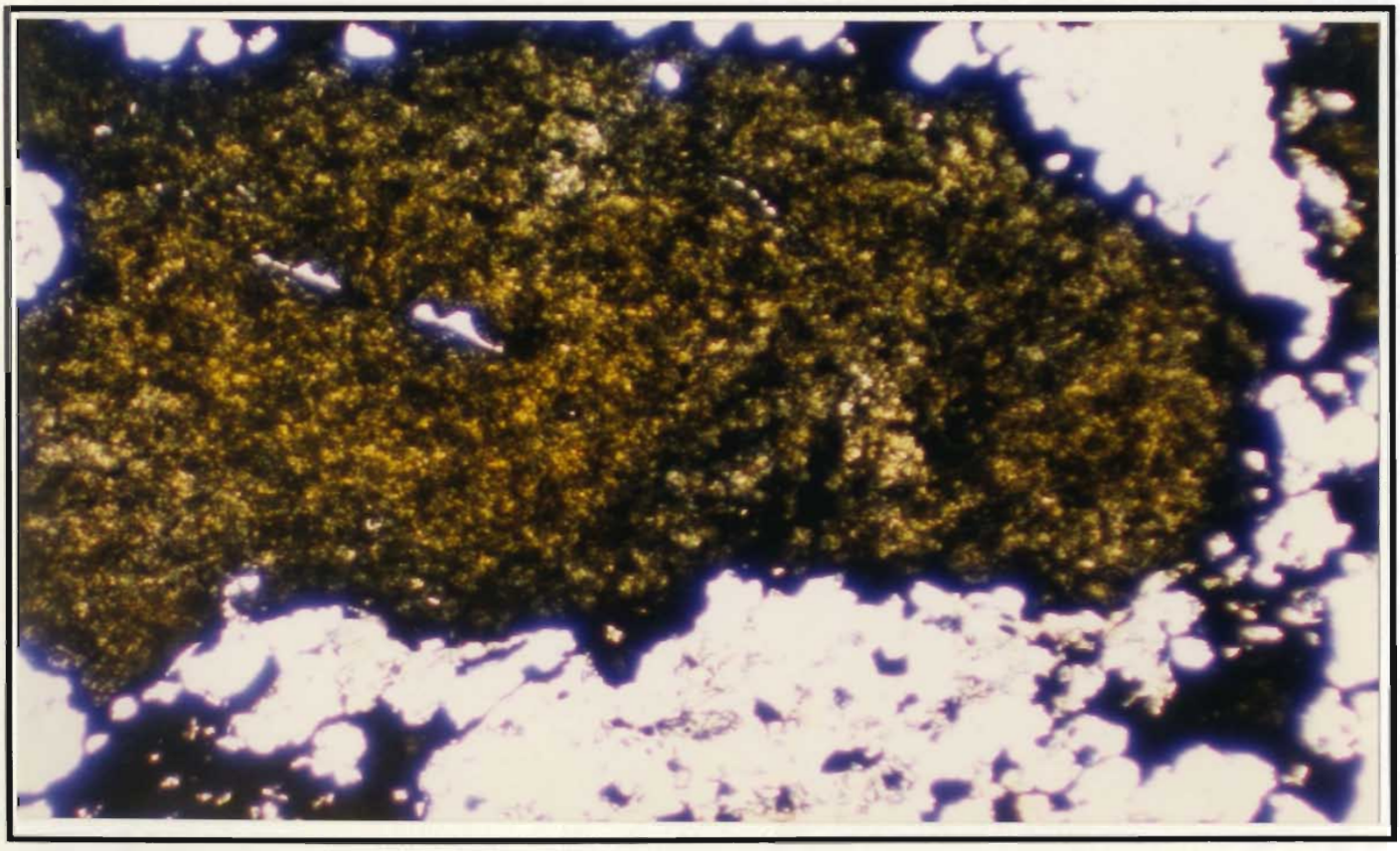

Figure 6-65: Transmitted light photomicrograph of an anhedral mass of sphalerite in a quartz vein. Polished thin section SK 29 57, plane polarized light, 3.2 x. — 0.5 mm —

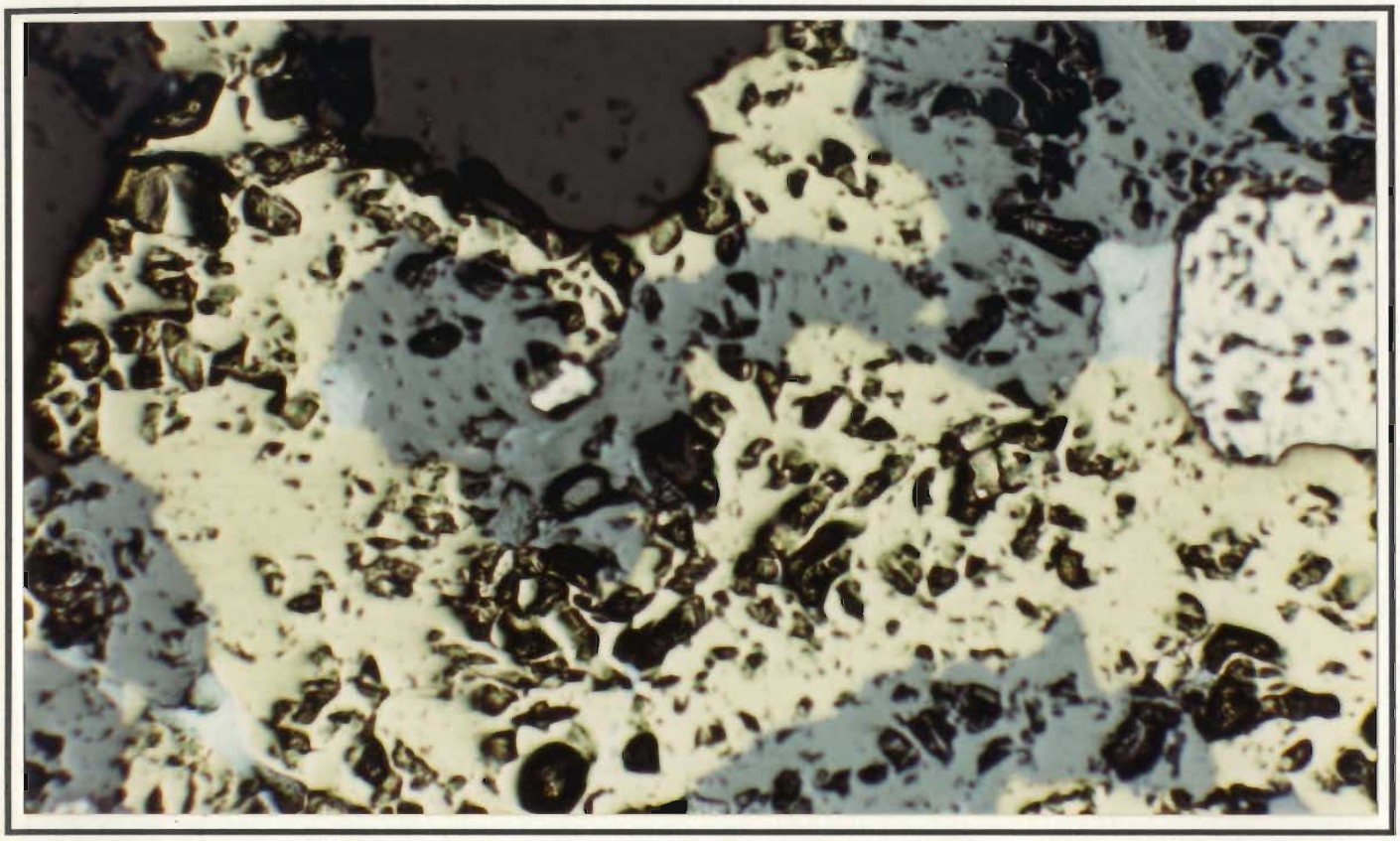

Figure 6-66: Reflected light photomicrograph showing small anhedral masses of galena (silver grey) intergrown with chalcopyrite (golden yellow), sphalerite (medium grey) and pyrite (white). Polished thin section SK 27 37, plane polarized light, 20 x. —— **0.1 mm** ——

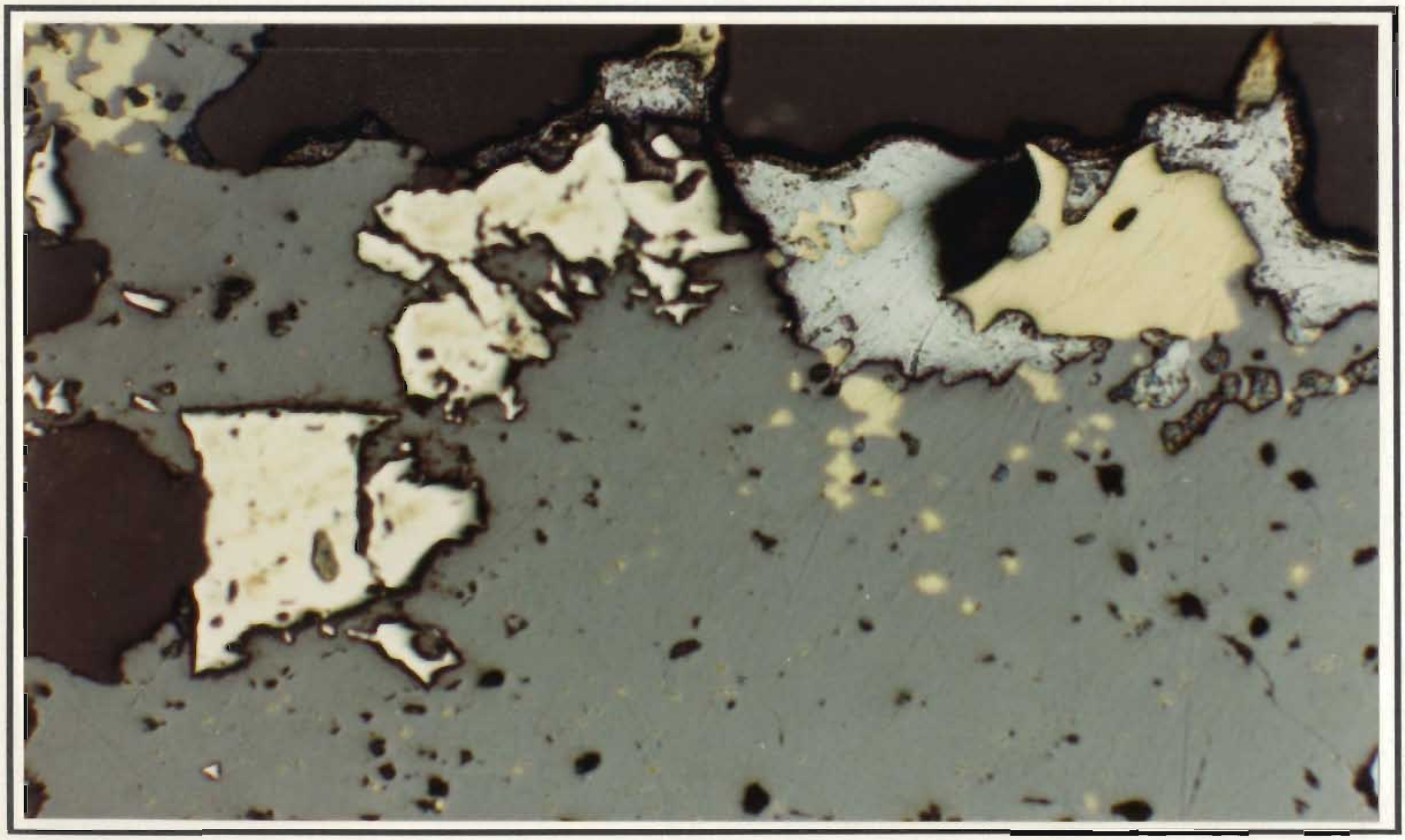

Figure 6-67: Reflected light photomicrograph showing anhedral sphalerite (medium grey), chalcopyrite (golden yellow), galena (silver grey) and subhedral pyrite (white). Note rounded anhedral chalcopyrite inclusions in sphalerite and galena. Polished section SK 29 52, plane polarized light, 20 x. —— **0.1 mm** ——

exhibited by three phase triple point junctions between galena, chalcopyrite and sphalerite are roughly characteristic of equilibrium minimum surface energy boundaries reported by Stanton (1972), i.e. the smallest dihedral angle exhibited by galena, an intermediate angle by chalcopyrite and the largest by sphalerite (Figure 6-66).

Layering in the sulphides is, in places, produced by alternating coarser and finer grained pyrite. Although a large range of pyrite grain sizes is usually represented, in some samples pyrite shows a predominantly bimodal grain size distribution, consisting of smaller grains less than 0.5 mm across interlayered with larger grains about 1-2 mm across. Layering may also result from areas alternately enriched in pyrite, chalcopyrite, sphalerite or gangue. Note for example in Figure 6-64 where sphalerite occupies interstitial areas between pyrite grains at the top of the photograph, and chalcopyrite occupies interstitial areas in the bottom of the photograph.

6.8.3 Petrography of the oxide minerals

Hematite and magnetite are the only oxide minerals noted in the sulphide-rich zones. Very fine grained hematite and lesser specular hematite, the latter typically occurring as elongate laths, are an essential component of the jasper-rich units as described in Section 6.6.2. In thin section SK 7 329, specular-hematite-rich layers occur between layered pyrite and jasper.

When viewed using reflected light microscopy, hematite occurs as irregular anhedral masses or as rectangular laths, which occur singly or as intergrown groups of grains (Figures 6-68 and 6-69). In poorly polished sections, the hematite shows a "pockmarked" appearance.

Magnetite is noted as occurring in significant amounts in only one polished section, i.e. SK 27 42C, where textures indicate that some of it has resulted from replacement of hematite (Figures 6-70 and 6-71). Hematite laths have been almost perfectly pseudomorphed by the magnetite in some places (Figures 6-71 and 6-72). Magnetite also

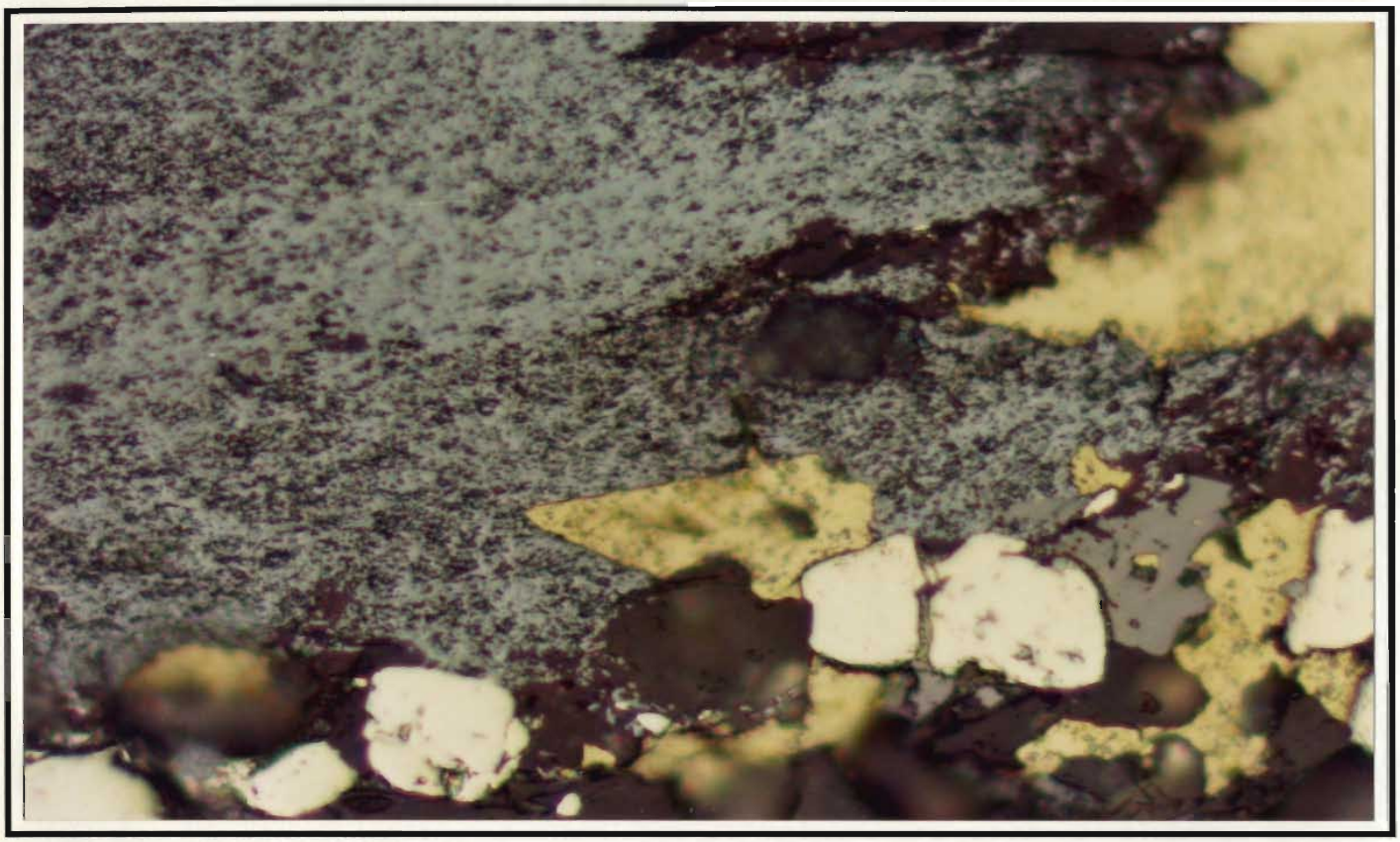

Figure 6-68: Reflected light photomicrograph showing anhedral masses of "pockmarked" hematite (blue grey) accompanied by chalcopyrite, pyrite and sphalerite. Polished section SK 27 42C, plane polarized light, 50 x. —— **0.04 mm** ——

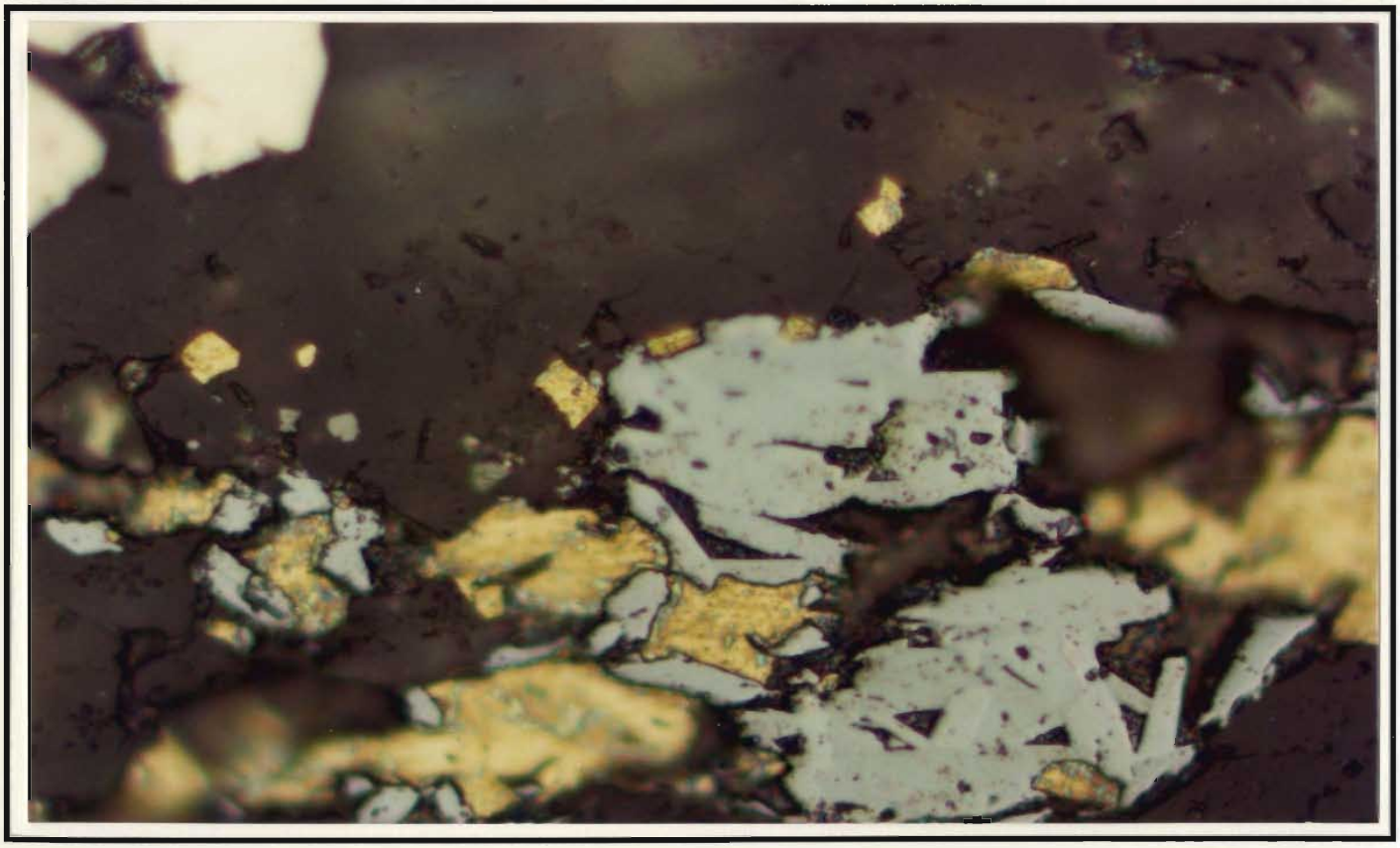

Figure 6-69: Reflected light photomicrograph showing anhedral masses and elongate rectangular laths of hematite (blue grey) in gangue and intergrown with chalcopyrite. Polished section SK 27 42C, plane polarized light, 50 x. —— **0.04 mm** ——

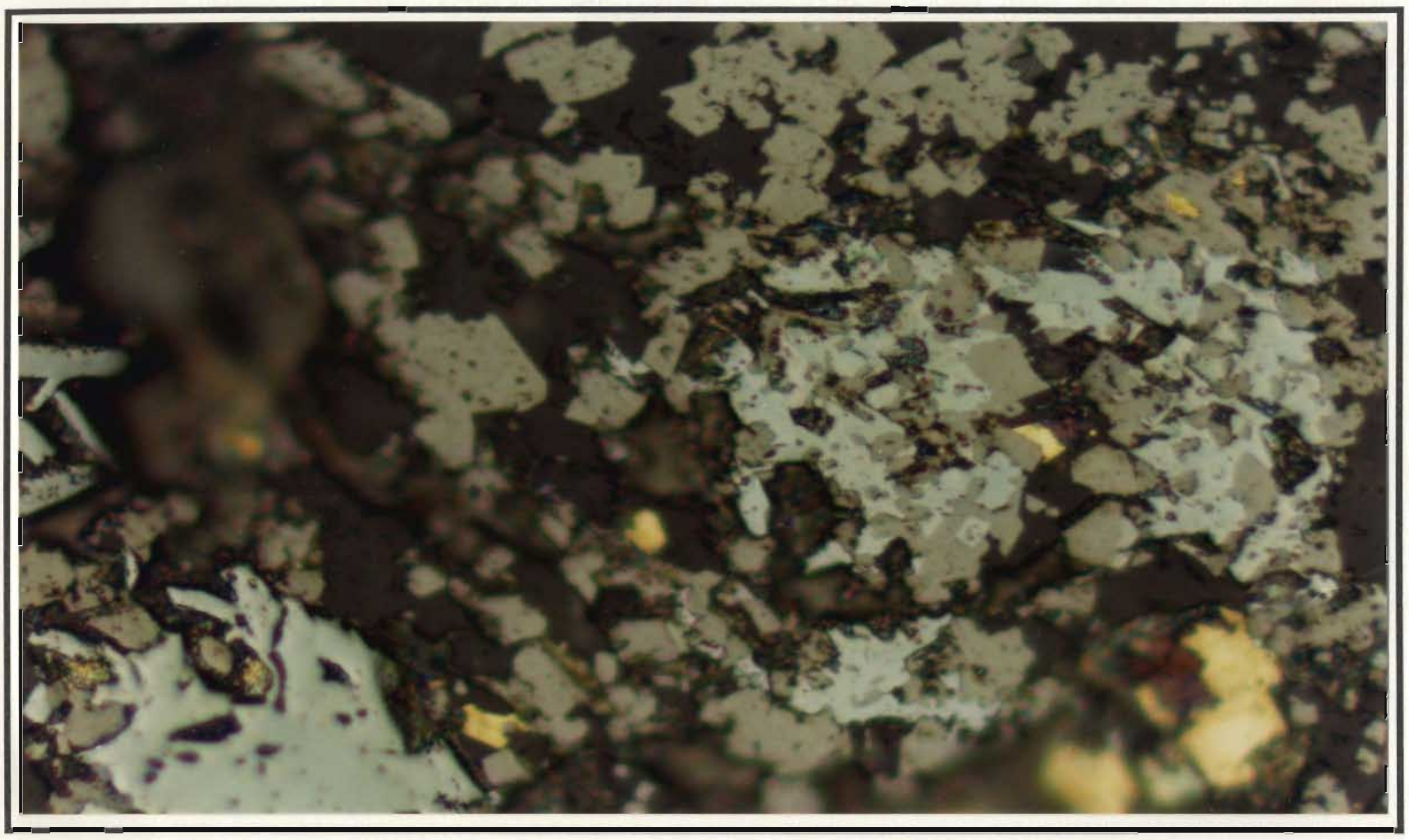

Figure 6-70: Reflected light photomicrograph showing partial to complete replacement of hematite (blue grey) by magnetite (steel grey). Polished section SK 27 42C, plane polarized light, 50 x.
—— **0.04 mm** ——

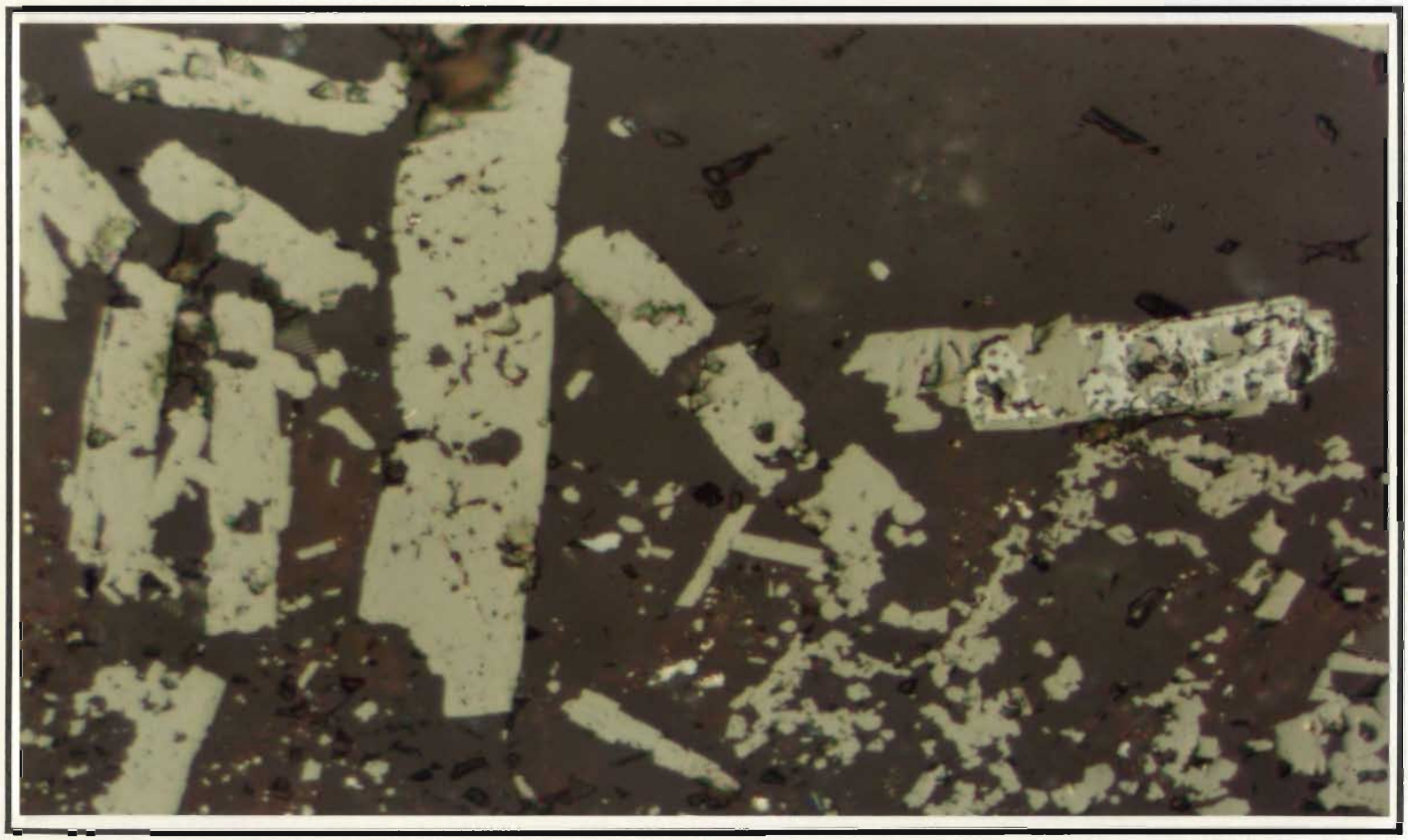

Figure 6-71: Reflected light photomicrograph showing partial to complete replacement and pseudomorphing of hematite laths by magnetite (steel grey). A small amount of hematite (blue grey) remains in the lath shown in the right portion of the photograph. Polished section SK 27 42C, plane polarized light, 50 x. —— **0.04 mm** ——

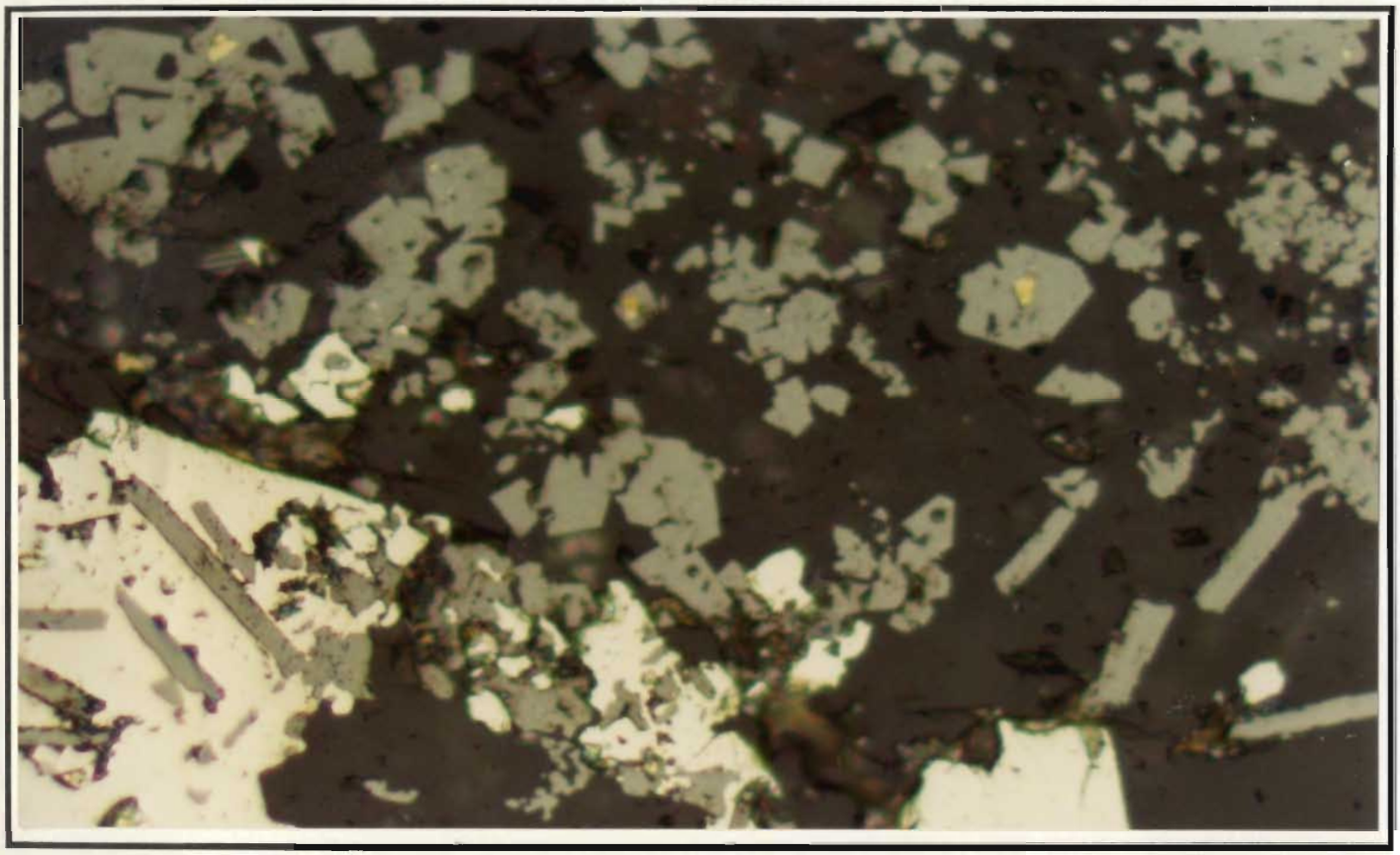

Figure 6-72: Reflected light photomicrograph showing equant masses of magnetite (steel grey) in gangue and magnetite pseudomorphs of hematite laths in pyrite. Polished section SK 27 42C, plane polarized light, 50 x. —— 0.04 mm ——

occurs as subhedral equant masses, some of which contain small anhedral chalcopyrite inclusions (Figure 6-72). The equant masses of magnetite may be pseudomorphs of intergrown hematite laths (compare grains in the top left portion of Figure 6-72 to intergrown hematite laths in the bottom right portion of Figure 6-69).

Hematite is accompanied by chalcopyrite, sphalerite or pyrite or some combination of these minerals in portions of SK 27 42 (Figure 6-68). It is intergrown with chalcopyrite in parts of polished section SK 29 42C (Figure 6-69). In other parts of this section, magnetite-pseudomorphed hematite laths occur as inclusions in pyrite (Figure 6-72).

6.9 Ore Mineral Chemistry

Electron microprobe analyses of Skidder Prospect pyrite, chalcopyrite, sphalerite and galena compositions are presented in Tables 6-17 to 6-20. Analytical procedures are described in Appendix A.

Skidder Prospect pyrite compositions are relatively uniform (Table 6-17). The pyrite contains only trace amounts of Ni. Slightly elevated contents of Zn and Cu in analyzed pyrites proximal to sphalerite and chalcopyrite respectively are probably due to minute inclusions of these latter minerals in the pyrite (cf. Deer et al., 1966; Ramdohr, 1980).

Chalcopyrite in the Skidder Prospect also has somewhat uniform composition (Table 6-18). Minor amounts of Zn present in chalcopyrite that is proximal to, or occurs as inclusions in sphalerite is most probably a result of admixed sphalerite since solid solution of zinc in chalcopyrite at low temperatures is unlikely (cf. Ramdohr, 1980).

Skidder Prospect sphalerites have low Fe contents (less than 2 weight per cent (wt%)) and contain only minor amounts of Cd (less than 0.4 wt%) (Tables 6-19 and 6-20). The iron contents depend to a certain extent on the mode of occurrence of the sphalerite. For example, sphalerite comprising a 1 cm-thick layer in sample SK 35A 6 is extremely low in Fe (less than 0.2 wt%). Also, sphalerites that are not in close proximity to pyrite or chalcopyrite have lower iron contents (less than 1 wt%) than those that are proximal to these minerals (these sphalerites typically contain 1.5 to 2 wt% Fe). Analyses of sphalerites that are proximal to, or intergrown with chalcopyrite show up to 2 wt% Cu and typically 1 to 2 wt% Fe. This, like the increased contents of Zn in chalcopyrite proximal to sphalerite, is probably due to admixing of these two minerals.

The Skidder Prospect galenas analyzed contain minor amounts of bismuth and only trace amounts of silver (Table 6-20).

Table 6-17: Electron microprobe analyses of Skidder Prospect pyrite

	Unlayered Massive Sulphides			Layered Massive Sulphides						
			1					2	3	3
	SK	SK	SK	SK	SK	SK	SK	SK	SK	SK
Weight %	28 38	29 52	29 52	28 44	27 43	31 17C	35A 6	35A 6	35A 6	35A 6
S	53.01	52.43	52.54	53.73	53.68	53.84	52.43	53.88	54.15	53.34
Fe	48.56	48.92	50.02	49.21	48.43	48.79	50.33	47.22	48.00	48.31
Ni	0.03	0.02	0.05	0.02	0.03	0.05	0.07	0.04	0.02	0.12
Cu	0.06	0.00	0.08	0.13	0.05	0.12	0.10	0.22	0.05	0.01
Zn	0.09	0.13	0.05	0.07	0.16	0.05	0.09	0.10	0.21	0.62
Cd	0.02	0.02	0.04	0.00	0.01	0.03	0.04	0.02	0.00	0.05
Total	101.76	101.52	102.77	103.16	102.36	102.88	103.04	101.48	102.43	102.45
Atomic Proportions (Formula Base = 3)										
S	1.964	1.952	1.937	1.964	1.974	1.971	1.931	1.991	1.985	1.964
Fe	1.033	1.045	1.059	1.032	1.022	1.025	1.064	1.002	1.010	1.021
Ni	0.001	0.000	0.001	0.000	0.001	0.001	0.001	0.001	0.000	0.002
Cu	0.001	0.000	0.001	0.002	0.001	0.002	0.002	0.004	0.001	0.000
Zn	0.002	0.002	0.001	0.001	0.003	0.001	0.002	0.002	0.004	0.011
Cd	0.000	0.000	0.000	0.000	0.000	0.000	0.000	0.000	0.000	0.001
Analyses	2	1	2	1	2	1	2	1	1	1

1 - framboidal pyrite
2 - cemented by chalcopyrite
3 - proximal to sphalerite

Table 6-18: Electron microprobe analyses of Skidder Prospect chalcopyrite

	Unlayered Massive		Layered Semi-massive Sulphides				Layered Massive Sulphides				
		1			1	2				1	2
	SK	SK	SK	SK	SK	SK	SK	SK	SK	SK	SK
Weight %	29 52	29 52	27 37	28 44	28 44	28 44	27 43	31 17C	35A 6	35A 6	35A 6
S	34.87	34.92	34.54	34.14	34.09	33.70	34.30	34.55	34.11	34.09	34.30
Fe	31.98	30.71	32.00	31.37	31.31	30.19	31.55	31.44	32.02	31.74	31.50
Ni	0.01	0.05	0.03	0.03	0.03	0.01	0.03	0.03	0.02	0.03	0.03
Cu	34.07	33.91	34.41	33.99	33.97	33.73	33.40	33.89	33.76	33.85	33.67
Zn	0.07	0.71	0.18	0.11	0.19	1.17	0.13	0.12	0.10	0.15	1.21
Cd	0.05	0.02	0.01	0.06	0.02	0.03	0.04	0.03	0.02	0.01	0.07
Total	101.05	100.31	101.16	99.69	99.60	98.81	99.44	100.04	100.03	99.86	100.76
Atomic Proportions (Formula Base = 4)											
S	1.979	1.995	1.963	1.968	1.967	1.964	1.979	1.981	1.961	1.963	1.960
Fe	1.042	1.007	1.044	1.038	1.037	1.010	1.045	1.035	1.057	1.049	1.033
Ni	0.000	0.001	0.001	0.001	0.001	0.000	0.001	0.001	0.001	0.001	0.001
Cu	0.976	0.977	0.987	0.989	0.989	0.992	0.972	0.980	0.979	0.983	0.971
Zn	0.002	0.020	0.005	0.003	0.005	0.033	0.004	0.003	0.003	0.004	0.034
Cd	0.001	0.000	0.000	0.001	0.000	0.000	0.001	0.000	0.000	0.000	0.001
Analyses	1	2	2	2	3	2	2	2	4	2	2

1 - proximal to sphalerite
2 - inclusion in sphalerite

Table 6-19: Electron microprobe analyses of Skidder Prospect sphalerite

	Unlayered Massive Sulphides				Layered Semimassive Sulphides				Layered Massive Sulphides				
			1					2		3		4	3
	SK	SK	SK	SK	SK	SK	SK	SK	SK	SK	SK	SK	SK
Weight %	28 38	29 52	29 52	29 52	27 37	28 44	28 44	28 44	27 43	27 43	35A 6	35A 6	35A 6
S	33.55	33.18	33.27	33.37	33.27	32.65	33.29	32.89	31.87	32.81	32.80	33.82	32.88
Fe	0.44	1.01	1.53	1.99	0.90	0.40	0.46	1.50	1.20	2.12	0.11	0.81	1.47
Ni	0.01	0.00	0.04	0.03	0.02	0.02	0.04	0.02	0.01	0.05	0.02	0.03	0.02
Cu	0.18	1.68	0.56	2.39	0.35	0.50	0.40	1.30	0.46	0.17	0.10	0.21	0.17
Zn	70.46	66.21	68.77	66.89	69.89	70.58	70.58	68.00	69.38	68.26	69.98	69.88	69.58
Cd	0.25	0.26	0.38	0.28	0.25	0.23	0.30	0.28	0.39	0.38	0.11	0.17	0.14
Total	104.88	102.33	104.55	104.94	104.67	104.38	105.06	104.00	103.31	103.77	103.12	104.92	104.24
Atomic Proportions (Formula Base = 2)													
S	0.979	0.988	0.974	0.973	0.974	0.963	0.972	0.970	0.952	0.969	0.975	0.984	0.967
Fe	0.007	0.017	0.026	0.033	0.015	0.007	0.008	0.025	0.021	0.036	0.002	0.014	0.025
Ni	0.000	0.000	0.001	0.000	0.000	0.000	0.001	0.000	0.000	0.001	0.000	0.000	0.000
Cu	0.003	0.025	0.008	0.035	0.005	0.007	0.006	0.019	0.007	0.002	0.002	0.003	0.002
Zn	1.009	0.967	0.988	0.956	1.003	1.021	1.011	0.983	1.017	0.989	1.020	0.997	1.004
Cd	0.002	0.002	0.003	0.002	0.002	0.002	0.002	0.002	0.003	0.003	0.001	0.001	0.001
Analyses	2	2	1	2	2	2	2	3	1	2	4	3	2

1 - Sphalerite inclusion in chalcopyrite
2 - Proximal to chalcopyrite
3 - Sphalerite inclusion in pyrite
4 - Sphalerite cementing pyrite

Table 6-20: Electron microprobe analyses of Skidder Prospect sphalerite and galena

Sphalerite Analyses

	SM	SM	SM	SM	M	M/L	M/L
				1	1		
	SK	SK	SK	SK	SK	SK	SK
Weight %	28 66	30 59	30 80	30 80	27 45	27 43	35A 6
S	33.23	32.64	33.05	32.89	32.63	33.10	33.01
Fe	0.63	1.01	0.05	0.33	1.02	1.04	0.09
Zn	69.26	71.60	72.85	69.78	73.70	67.91	69.36
Total	103.12	105.24	105.95	103.00	107.35	102.05	102.46
Atomic Proportions (Formula Base = 2)							
S*	0.984	0.955	0.961	0.977	0.941	0.988	0.985
Fe	0.011	0.017	0.001	0.006	0.017	0.018	0.002
Zn	1.005	1.028	1.039	1.017	1.042	0.994	1.013
Analyses	2	2	1	1	1	1	2

* Formula base = 2
SM - unlayered semimassive sulphides
M - unlayered massive sulphides
M/L - layered massive sulphides

1 - Sphalerite proximal to chalcopyrite

Galena Analyses

	SM/L	M/L
	SK	SK
	27 37	35A 6
S*	13.09	13.24
Pb	86.59	86.83
Bi	1.33	0.90
Ag	0.00	0.01
Total	101.00	100.97
S**	0.981	0.987
Pb	1.004	1.002
Bi	0.015	0.010
Ag	0.000	0.000
Analyses	2	2

* Weight %
** Atomic Proportions (Formula base = 2)
SM/L - layered semimassive sulphides
M/L - layered massive sulphides

6.10 Geochemistry of the Alteration Zone

6.10.1 Presentation of results

A total of 152 Skidder Prospect drill core samples, comprising basalts from each of the Skidder Prospect alteration zones (see Section 6.4) and semimassive and massive sulphides from the prospect, were analyzed for whole rock contents and trace element concentrations. Details of the methods used are presented in Appendix B. Samples having different amounts and proportions of the various secondary mineral assemblages were chosen in an attempt to show the geochemical variation within, as well as between the various alteration zones. Individual analyses are listed in Tables B-11 to B-16, Appendix B. The mean, standard deviation, minimum and maximum for the samples representative of each alteration zone are presented in Table 6-21.

The geochemistry of the Skidder Basalt is presented in Chapter 5 and will not be discussed in detail here. Thus, following a brief description of the "alteration-resistant element" geochemistry of the rocks in the immediate vicinity of the prospect, this section will concentrate on the geochemical effects of hydrothermal alteration associated with the Skidder Prospect mineralizing event(s). It is shown below that the incompatible elements Zr, Ti and Y, and the compatible elements Cr and Ni are relatively unaffected by all except the most intense alteration associated with the Skidder Prospect.

Zr concentrations for each of the analyzed samples are plotted on Figures 6-3 to 6-10. Variolitic pillow basalts that underlie massive sulphide Lens 1 have low to intermediate Zr concentrations, typically 30 to 60 ppm. Massive portions of the overlying interlayered pillowed and massive basalt (diabase dykes (?)) unit tend to have lower Zr concentrations (typically 40-60 ppm) than the pillowed basalt or mafic pillow breccia portions (typically 60-90 ppm Zr). Note, however, that massive units in much of the upper portion of SK 34 have high Zr concentrations > 100 ppm. Massive and pillowed basalts immediately adjacent to Lens 2, as shown in drill holes SK 35, 35A, 37 and 37A, and variolitic pillow basalts which overlie Lens 2 contain intermediate Zr concentrations (typically 50-80 ppm).

Table 6-21: Mean, standard deviation, minimum and maximum for whole rock analyses from the various Skidder Prospect alteration zones

	Alteration zone - cl,cc,ep ± hm				Alteration zone - cl,cc,qz,ep				Alteration zone - cl,qz,cc			
weight %	Mean	Standard Deviation	Minimum	Maximum	Mean	Standard Deviation	Minimum	Maximum	Mean	Standard Deviation	Minimum	Maximum
SiO_2	49.41	2.38	44.20	53.30	52.46	7.36	39.20	69.10	51.71	5.37	43.40	65.50
TiO_2	1.11	0.27	0.66	1.79	1.20	0.37	0.54	2.00	1.11	0.26	0.48	1.86
Al_2O_3	15.67	0.98	14.20	18.00	14.88	1.59	10.80	16.90	15.83	1.89	12.30	22.50
Fe_2O_3*	11.40	1.35	8.65	14.58	10.98	2.50	4.86	14.80	9.50	2.08	3.65	12.40
MnO	0.17	0.04	0.07	0.24	0.14	0.05	0.05	0.20	0.13	0.07	0.01	0.33
MgO	7.52	2.20	3.13	12.05	6.54	2.79	0.49	11.10	6.49	3.19	1.14	13.03
CaO	5.20	1.62	1.16	9.52	3.73	1.43	2.16	7.54	3.18	2.29	1.00	11.22
Na_2O	4.82	1.18	1.49	6.65	5.22	0.94	2.71	6.78	4.88	0.90	3.23	6.66
K_2O	0.69	0.77	0.05	2.70	0.35	0.41	0.06	1.50	0.80	1.18	0.05	5.09
P_2O_5	0.14	0.07	0.01	0.30	0.18	0.08	0.08	0.36	0.22	0.13	0.01	0.58
LOI	3.71	1.35	1.84	8.03	3.16	1.61	0.62	8.39	5.21	2.00	2.40	10.76
Total	99.82	0.76	98.01	100.84	98.84	1.56	92.75	100.15	99.06	0.95	95.59	100.66
ppm												
Pb	3	3	n.d.	10	5	3	n.d.	14	7	7	n.d.	27
Rb	7	8	n.d.	35	3	4	n.d.	11	13	22	n.d.	84
Sr	114	72	41	331	92	49	34	194	75	31	32	163
Y	28	8	10	50	38	14	19	62	31	10	17	59
Zr	65	21	24	106	79	32	35	144	72	20	27	125
Nb	5	2	2	10	5	2	2	9	6	2	2	10
Zn	84	16	52	121	86	34	25	150	82	32	37	161
Cu	38	22	7	75	29	15	3	56	41	28	1	98
Ni	53	42	n.d.	151	31	51	n.d.	215	58	44	n.d.	143
Ba	131	218	n.d.	987	74	117	n.d.	406	86	124	n.d.	490
V	339	65	237	533	352	113	179	579	320	101	54	493
Ce	66	36	3	129	76	36	15	141	71	39	9	166
Cr	171	124	26	496	103	144	4	628	218	156	n.d.	533
Ga	16	2	12	21	18	4	9	28	17	4	7	25
	n.d. - not detected											
Distance	207.7	107.1	78.2	444.7	143.2	94.5	26.0	316.1	79.8	79.4	14.0	469.7
Samples	28				21				34			

* Total iron as Fe_2O_3

Distance - distance from massive sulphides or most intense alteration

Table 6-21 (continued):

	Alteration zone - cl,qz,py				Alteration zone - qz,cl,py				Semimassive and massive sulphides			
weight %	Mean	Standard Deviation	Minimum	Maximum	Mean	Standard Deviation	Minimum	Maximum	Mean	Standard Deviation	Minimum	Maximum
SiO_2	42.25	7.82	28.50	53.70	60.18	11.10	41.90	78.80	24.15	13.08	4.35	47.00
TiO_2	0.82	0.33	0.08	1.25	0.63	0.43	0.04	1.34	0.17	0.19	n.d.	0.78
Al_2O_3	14.76	2.07	8.09	18.40	11.52	4.46	2.30	18.70	4.69	4.23	0.40	12.80
Fe_2O_3*	9.91	2.74	3.15	15.60	10.69	6.73	0.85	23.10	37.89	9.16	23.10	54.64
MnO	0.16	0.04	0.07	0.27	0.06	0.05	n.d.	0.22	0.06	0.05	0.00	0.14
MgO	20.10	5.61	10.96	31.35	4.42	3.15	0.10	10.61	4.90	5.99	0.11	16.52
CaO	1.07	1.02	0.18	5.04	1.16	2.00	0.01	8.62	1.24	2.62	0.04	7.96
Na_2O	1.62	1.42	0.01	3.74	1.82	2.14	n.d.	5.66	0.02	0.02	n.d.	0.06
K_2O	0.15	0.27	n.d.	1.19	1.85	1.77	n.d.	4.64	0.42	0.48	n.d.	1.71
P_2O_5	0.14	0.05	0.01	0.27	0.11	0.07	n.d.	0.23	0.04	0.07	n.d.	0.24
LOI	8.87	2.28	5.66	13.76	6.60	3.31	1.56	12.73	20.78	4.23	12.73	28.53
Total	99.84	0.93	98.25	100.89	99.03	0.69	98.06	100.35	94.37	7.39	74.92	100.43
ppm												
Pb	13	22	n.d.	116	52	75	4	293	166	154	14	443
Rb	3	4	n.d.	19	27	25	1	81	14	7	2	27
Sr	26	18	4	76	25	26	1	75	11	18	1	54
Y	20	6	8	33	17	10	n.d.	33	13	13	n.d.	39
Zr	56	15	22	73	57	26	5	113	33	15	14	61
Nb	5	2	1	9	6	2	2	10	9	3	4	15
Zn	490	658	66	3817	192	202	24	937	26731	46218	31	137221
Cu	52	75	7	464	38	29	12	113	13856	25613	14	94181
Ni	92	72	23	390	56	54	n.d.	232	37	32	5	111
Ba	35	110	n.d.	604	262	463	n.d.	1861	43	50	n.d.	141
V	387	61	209	528	224	129	6	418	120	127	9	362
Ce	57	27	15	111	56	34	n.d.	132	22	23	n.d.	65
Cr	332	240	72	1294	234	189	1	773	159	133	n.d.	402
Ga	16	3	10	22	13	5	5	21	24	23	2	85
	n.d. - not detected											
Distance	25.3	21.7	0.0	79.8	20.1	20.6	0.0	78.8	24.1	13.1	4.4	47.0
Samples	34				20				15			

* Total iron as Fe_2O_3

Distance - distance from massive sulphides or most intense alteration

Pillowed basalts overlying the variolitic basalt in these drill holes have intermediate to high Zr concentrations (70-130 ppm Zr). Diabase dykes intruding these units have much lower Zr concentrations (40-45 ppm).

The averages for mafic rocks from each of the alteration zones is compared to the average of the Skidder basalts not affected by the Skidder Prospect alteration event on Table 6-22. The alteration zones from left to right represent increasing intensity of alteration of the rocks and closer proximity to the sulphide-bearing units. The higher average Cr and Ni concentrations in samples from the cl,qz,cc; cl,qz,py and qz,cl,py alteration zones relative to the others may represent a primary magmatic feature, since, in the case of the cl,qz,py and qz,cl,py alteration zones, the higher Cr and Ni is accompanied by lower Ti, Zr and Y in the samples. Caution is advised however since these represent some of the most intensely altered rocks associated with the Skidder Prospect.

Table 6-23 shows the results of dividing the mean and standard deviation of average contents of major and minor elements in each alteration zone by those of typical Skidder Basalt[1]. A qualitative summary of these results is presented in Table 6-24. To augment these tables, scattergrams of major oxide and selected minor elements versus distance from most intense alteration are presented in Figures 6-73 to 6-80.

Sporadic enrichment of K_2O, Rb and Ba relative to typical Skidder basalt is evident in the cl,cc,ep±hm alteration zone and marks the outermost geochemical effects of alteration associated with the Skidder Prospect mineralizing event. Sporadic enrichment of these elements is recognizable up to 400 m away from the most intensely altered rocks (Figures 6-75, 6-76, 6-77 and 6-79), and is evident to varying degrees in all the alteration zones (except the cl,qz,py zone). Electron microprobe analyses presented in Section 6.7 indicate that the potassium is present in two different mineral phases, i.e. in K-feldspar in the less altered rocks but in muscovite in more intensely altered rocks.

---

[1] Note that mass changes have not been taken into account, thus these ratios only show a semi-quantitative estimate of the actual change.

Table 6-22: Averages of analyses from the various Skidder Prospect alteration zones compared to the average of those of typical spilitized Skidder Basalt

weight %	Skidder Basalt	cl,cc,ep ± hm	cl,cc,qz,ep	cl,qz,cc	cl,qz,py	qz,cl,py	sulphides
SiO_2	50.39	49.41	52.46	51.71	42.25	60.18	24.15
TiO_2	1.09	1.11	1.20	1.11	0.82	0.63	0.17
Al_2O_3	15.11	15.67	14.88	15.83	14.76	11.52	4.69
Fe_2O_3*	10.76	11.40	10.98	9.50	9.91	10.69	37.89
MnO	0.15	0.17	0.14	0.13	0.16	0.06	0.06
MgO	6.93	7.52	6.54	6.49	20.10	4.42	4.90
CaO	5.43	5.20	3.73	3.18	1.07	1.16	1.24
Na_2O	4.94	4.82	5.22	4.88	1.62	1.82	0.02
K_2O	0.17	0.69	0.35	0.80	0.15	1.85	0.42
P_2O_5	0.17	0.14	0.18	0.22	0.14	0.11	0.04
LOI	4.43	3.71	3.16	5.21	8.87	6.60	20.78
Total	99.57	99.82	98.84	99.06	99.84	99.03	94.37
ppm							
Pb	3	3	5	7	13	52	166
Rb	2	7	3	13	3	27	14
Sr	82	114	92	75	26	25	11
Y	31	28	38	31	20	17	13
Zr	68	65	79	72	56	57	33
Nb	5	5	5	6	5	6	9
Zn	83	84	86	82	490	192	26731
Cu	40	38	29	41	52	38	13856
Ni	47	53	31	58	92	56	37
Ba	29	131	74	86	35	262	43
V	327	339	352	320	387	224	120
Ce	65	66	76	71	57	56	22
Cr	146	171	103	218	332	234	159
Ga	16	16	18	17	16	13	24
Distance (m)		207.7	143.2	79.8	25.3	20.1	
Samples	114	28	21	34	34	20	15

* Total iron as Fe_2O_3

Distance - average distance from massive sulphides or most intense alteration

Table 6-23: Mean and standard deviation of samples from the various Skidder Prospect alteration zones and massive sulphides divided by that of typical spilitized Skidder Basalt samples

1 Mean of alteration zone samples divided by mean of unaltered Skidder Basalt samples
2 Log of 1
3 Standard deviation of alteration zone samples divided by standard deviation of unaltered Skidder Basalt samples
4 Log of 3

	cl,cc,ep ± hm alteration zone				cl,cc,qz,ep alteration zone				cl,qz,cc alteration zone			
	Mean		Standard Deviation		Mean		Standard Deviation		Mean		Standard Deviation	
weight %	1	2	3	4	1	2	3	4	1	2	3	4
SiO_2	0.98	-0.01	**0.52**	**-0.28**	1.04	0.02	**1.61**	**0.21**	1.03	0.01	1.18	0.07
TiO_2	1.02	0.01	0.81	-0.09	1.10	0.04	1.14	0.06	1.02	0.01	*0.79*	*-0.10*
Al_2O_3	1.04	0.02	0.85	-0.07	0.98	-0.01	*1.37*	*0.14*	1.05	0.02	**1.63**	**0.21**
Fe_2O_3*	1.06	0.03	*0.72*	*-0.14*	1.02	0.01	*1.34*	*0.13*	0.88	-0.05	1.11	0.05
MnO	1.10	0.04	0.93	-0.03	0.93	-0.03	*1.35*	*0.13*	0.89	-0.05	**1.64**	**0.22**
MgO	1.08	0.04	0.94	-0.03	0.94	-0.03	1.19	0.07	0.94	-0.03	*1.36*	*0.13*
CaO	0.96	-0.02	**0.50**	**-0.30**	*0.69*	*-0.16*	**0.44**	**-0.36**	**0.59**	**-0.23**	*0.70*	*-0.15*
Na_2O	0.98	-0.01	1.23	0.09	1.06	0.02	0.98	-0.01	0.99	-0.01	0.94	-0.03
K_2O	**4.04**	**0.61**	**4.54**	**0.66**	**2.06**	**0.31**	**2.44**	**0.39**	**4.69**	**0.67**	**6.91**	**0.84**
P_2O_5	0.81	-0.09	*0.53*	*-0.28*	1.04	0.02	**0.61**	**-0.21**	*1.32*	*0.12*	0.97	-0.01
LOI	0.84	-0.08	*0.58*	*-0.24*	*0.71*	*-0.15*	*0.69*	*-0.16*	1.18	0.07	0.85	-0.07
ppm												
Pb	1.02	0.01	1.07	0.03	*1.60*	*0.20*	1.11	0.05	**2.25**	**0.35**	**2.20**	**0.34**
Rb	**3.46**	**0.54**	***2.66***	***0.42***	*1.52*	*0.18*	1.21	0.08	**6.29**	**0.80**	**7.19**	**0.86**
Sr	*1.39*	*0.14*	*1.42*	*0.15*	1.12	0.05	0.95	-0.02	0.92	-0.04	**0.60**	**-0.22**
Y	0.89	-0.05	*0.70*	*-0.15*	1.23	0.09	1.17	0.07	1.00	0.00	0.84	-0.07
Zr	0.96	-0.02	0.83	-0.08	1.16	0.07	*1.29*	*0.11*	1.05	0.02	*0.80*	*-0.10*
Nb	1.09	0.04	1.04	0.02	1.03	0.01	0.80	-0.10	1.13	0.05	0.93	-0.03
Zn	1.01	0.01	***0.49***	***-0.31***	1.03	0.01	1.04	0.02	0.99	-0.01	0.98	-0.01
Cu	0.96	-0.02	*0.72*	*-0.14*	*0.72*	*-0.14*	**0.51**	**-0.29**	1.03	0.01	0.92	-0.03
Ni	1.12	0.05	0.86	-0.06	*0.67*	*-0.18*	1.05	0.02	1.24	0.09	0.89	-0.05
Ba	**4.51**	**0.65**	***5.08***	***0.71***	**2.57**	**0.41**	**2.72**	**0.43**	**2.98**	**0.47**	**2.88**	**0.46**
V	1.04	0.02	*0.66*	*-0.18*	1.08	0.03	1.16	0.06	0.98	-0.01	1.03	0.01
Ce	1.01	0.00	1.15	0.06	1.17	0.07	1.17	0.07	1.09	0.04	1.24	0.09
Cr	1.17	0.07	0.90	-0.04	*0.71*	*-0.15*	1.05	0.02	*1.49*	*0.17*	1.14	0.06
Ga	1.02	0.01	*0.76*	*-0.12*	1.10	0.04	*1.40*	*0.15*	1.03	0.01	1.22	0.09

* Total iron as Fe_2O_3

Table 6-23 (continued):

1 Mean of alteration zone samples divided by mean of unaltered Skidder Basalt samples
2 Log of 1
3 Standard deviation of alteration zone samples divided by standard deviation of unaltered Skidder Basalt samples
4 Log of 3

	cl,qz,py alteration zone				qz,cl,py alteration zone				Semi-massive and massive sulphides			
	Mean		Standard Deviation		Mean		Standard Deviation		Mean		Standard Deviation	
weight %	1	2	3	4	1	2	3	4	1	2	3	4
SiO_2	**0.84**	**-0.08**	**1.71**	**0.23**	**1.19**	**0.08**	**2.43**	**0.39**	**0.48**	**-0.32**	**2.87**	**0.46**
TiO_2	*0.75*	*-0.12*	1.01	0.00	**0.58**	**-0.24**	1.31	0.12	**0.16**	**-0.80**	**0.58**	**-0.23**
Al_2O_3	0.98	-0.01	**1.78**	**0.25**	*0.76*	*-0.12*	**3.85**	**0.59**	**0.31**	**-0.51**	**3.65**	**0.56**
Fe_2O_3*	0.92	-0.04	*1.47*	*0.17*	0.99	0.00	**3.60**	**0.56**	**3.52**	**0.55**	**4.90**	**0.69**
MnO	1.04	0.02	1.10	0.04	**0.38**	**-0.42**	1.20	0.08	**0.39**	**-0.41**	*1.31*	*0.12*
MgO	**2.90**	**0.46**	**2.39**	**0.38**	**0.64**	**-0.20**	1.34	0.13	*0.71*	*-0.15*	**2.55**	**0.41**
CaO	**0.20**	**-0.70**	**0.31**	**-0.50**	**0.21**	**-0.67**	**0.61**	**-0.21**	**0.23**	**-0.64**	0.80	-0.10
Na_2O	**0.33**	**-0.48**	*1.48*	*0.17*	**0.37**	**-0.43**	**2.23**	**0.35**	**0.00**	**-2.44**	**0.02**	**-1.72**
K_2O	0.86	-0.06	**1.57**	**0.20**	**10.89**	**1.04**	**10.41**	**1.02**	**2.48**	**0.39**	**2.85**	**0.46**
P_2O_5	0.83	-0.08	**0.42**	**-0.38**	**0.62**	**-0.21**	0.53	-0.28	**0.24**	**-0.61**	**0.51**	**-0.30**
LOI	**2.00**	**0.30**	0.97	-0.01	*1.49*	*0.17*	1.41	0.15	**4.69**	**0.67**	**1.81**	**0.26**
ppm												
Pb	**4.34**	**0.64**	**7.17**	**0.86**	**17.32**	**1.24**	**25.03**	**1.40**	**55.49**	**1.74**	**51.20**	**1.71**
Rb	*1.44*	*0.16*	*1.33*	*0.12*	**13.30**	**1.12**	**8.39**	**0.92**	**6.80**	**0.83**	**2.32**	**0.36**
Sr	**0.31**	**-0.50**	**0.36**	**-0.45**	**0.30**	**-0.52**	**0.51**	**-0.29**	**0.13**	**-0.68**	**0.35**	**-0.46**
Y	0.65	-0.18	**0.53**	**-0.27**	**0.54**	**-0.27**	0.81	-0.09	**0.42**	**-0.37**	1.06	0.02
Zr	0.82	-0.09	**0.60**	**-0.22**	0.84	-0.08	1.05	0.02	**0.49**	**-0.31**	**0.60**	**-0.22**
Nb	0.97	-0.01	0.99	-0.01	1.14	0.06	1.14	0.06	**1.77**	**0.25**	**1.62**	**0.21**
Zn	**5.91**	**0.77**	**19.94**	**1.30**	**2.32**	**0.37**	**6.12**	**0.79**	**322.05**	**2.51**	**1400.53**	**3.15**
Cu	*1.30*	*0.12*	**2.51**	**0.40**	0.94	-0.03	0.96	-0.02	**346.41**	**2.54**	**853.75**	**2.93**
Ni	**1.96**	**0.29**	*1.47*	*0.17*	1.20	0.08	1.11	0.04	*0.79*	*-0.10*	*0.65*	*-0.19*
Ba	1.21	0.08	**2.57**	**0.41**	**9.04**	**0.96**	**10.78**	**1.03**	*1.48*	*0.17*	1.16	0.06
V	1.18	0.07	**0.62**	**-0.21**	*0.68*	*-0.16*	*1.32*	*0.12*	**0.37**	**-0.44**	*1.29*	*0.11*
Ce	0.88	-0.05	0.89	-0.05	0.86	-0.06	1.10	0.04	**0.34**	**-0.47**	*0.75*	*-0.12*
Cr	**2.28**	**0.36**	**1.76**	**0.24**	**1.60**	**0.21**	*1.38*	*0.14*	1.09	0.04	0.97	-0.01
Ga	0.98	-0.01	1.01	0.01	*0.80*	*-0.10*	*1.52*	*0.18*	*1.52*	*0.18*	**7.55**	**0.88**

* Total iron as Fe_2O_3

Table 6-24: Table summarizing data presented in Tables 6-22 and 6-23

Alteration Zone	Enrichment relative to typical Skidder Basalt		Depletion relative to typical Skidder Basalt		Standard deviation relative to typical Skidder Basalt	
	Extensive	Slight	Extensive	Slight	Greater	Lesser
Cl, cc, cp ± hm	K, Rb, Ba	Sr			K, Rb, Sr,Ba	Si, Fe, Ca, P, LOI, Y, Zn, Cu, V, Ga
Cl, cc, qz, ep	K, Ba	Pb, Rb		Ca, LOI, Cu, Ni, Cr	Si, Al, Fe, Mn, K, Zr, Ga	Ca, P, LOI, Cu
Cl, qz, cc	K, Pb, Rb, Ba	P, Cr	Ca		Al, Mn, Mg, K, Pb, Rb, Ba	Ti, Ca, Sr, Zr
Cl, qz, py	Mg, LOI, Pb, Zn, Ni, Cr	Rb, Cu	Si, Ca, Na, Sr	Ti, Y	Si, Al, Fe, Mg, Na, K, Pb, Rb, Zn, Cu, Ni, Ba, Cr	Ca, P, Sr Y, Zr, V
Qz, cl, py	Si, K, Pb, Rb, Zn, Ba, Cr	LOI	Ti, Mn, Mg, Ca, Na, P, Sr, Y	Al, V, Ga	Si, Ti, Al, Fe, Mg, Na, K, LOI, Pb, Rb, Zn, Ba, V, Cr, Ga	Ca, P, Sr
Semimassive and massive sulphides	Fe, K, LOI, Pb, Rb, Nb, Zn, Cu	Ba, Ga	Si, Ti, Al, Mn, Ca, Na, P, Sr, Y	Mg, Ni	Si, Al, Fe, Mg, Mn, K, LOI, Pb, Rb, Nb, Zn, Cu, V, Ga	Ti, Ca, Na, P, Sr, Zr, Ni, Ce

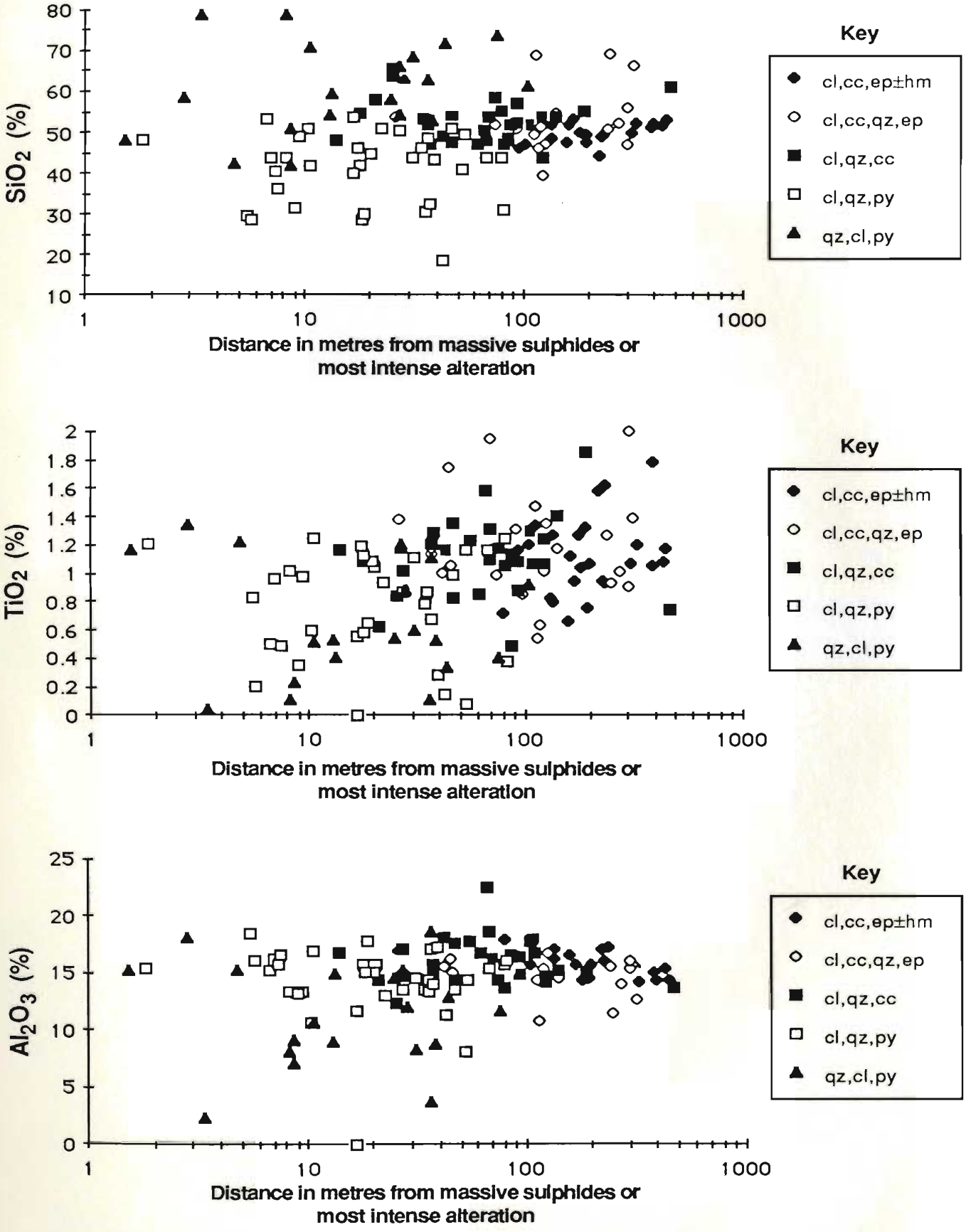

Figure 6-73: Major oxide contents of samples from the various Skidder Prospect alteration zones versus distance from massive sulphides or most intense alteration.

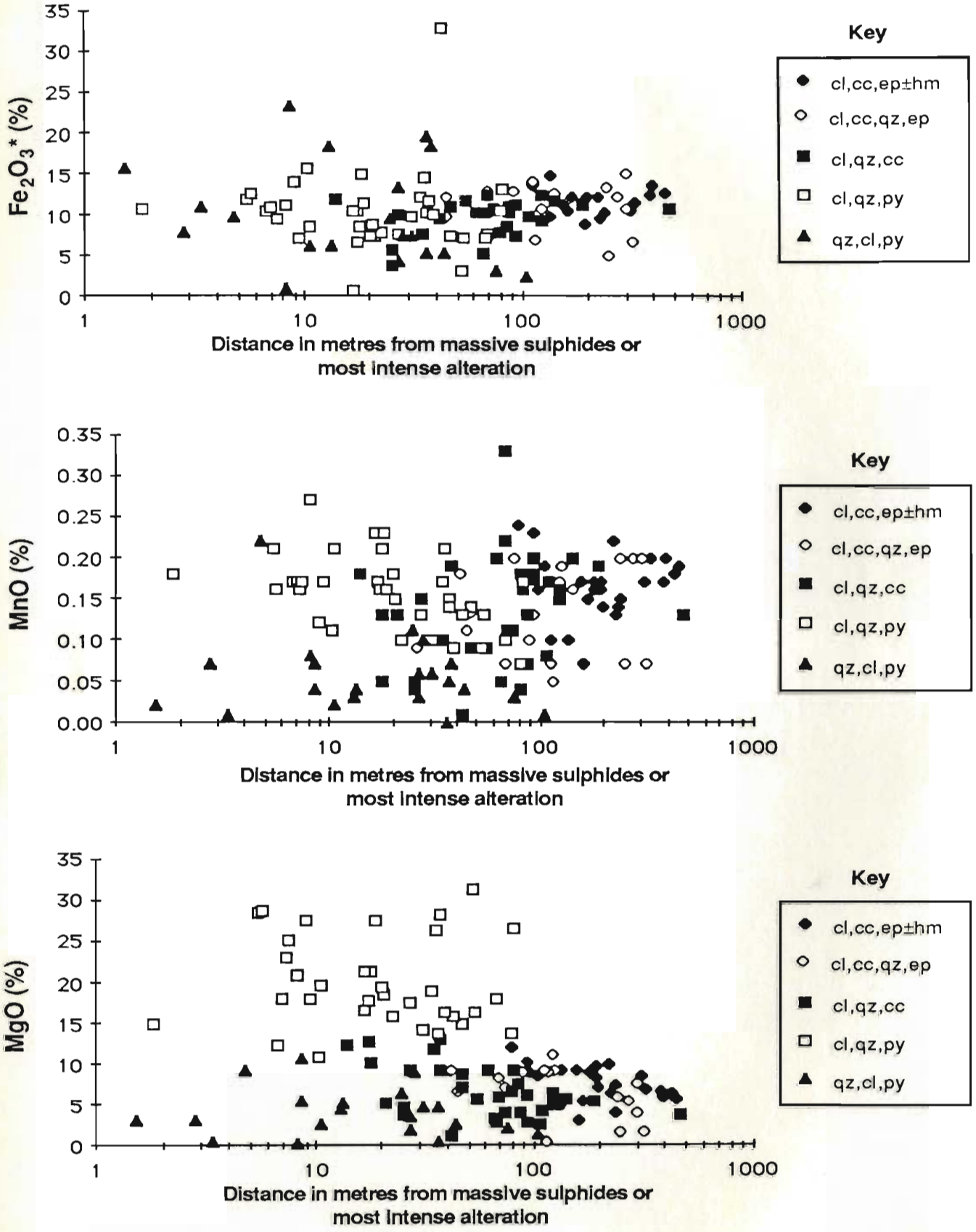

Figure 6-74: Major oxide contents of samples from the various Skidder Prospect alteration zones versus distance from massive sulphides or most intense alteration. * Total iron as Fe_2O_3.

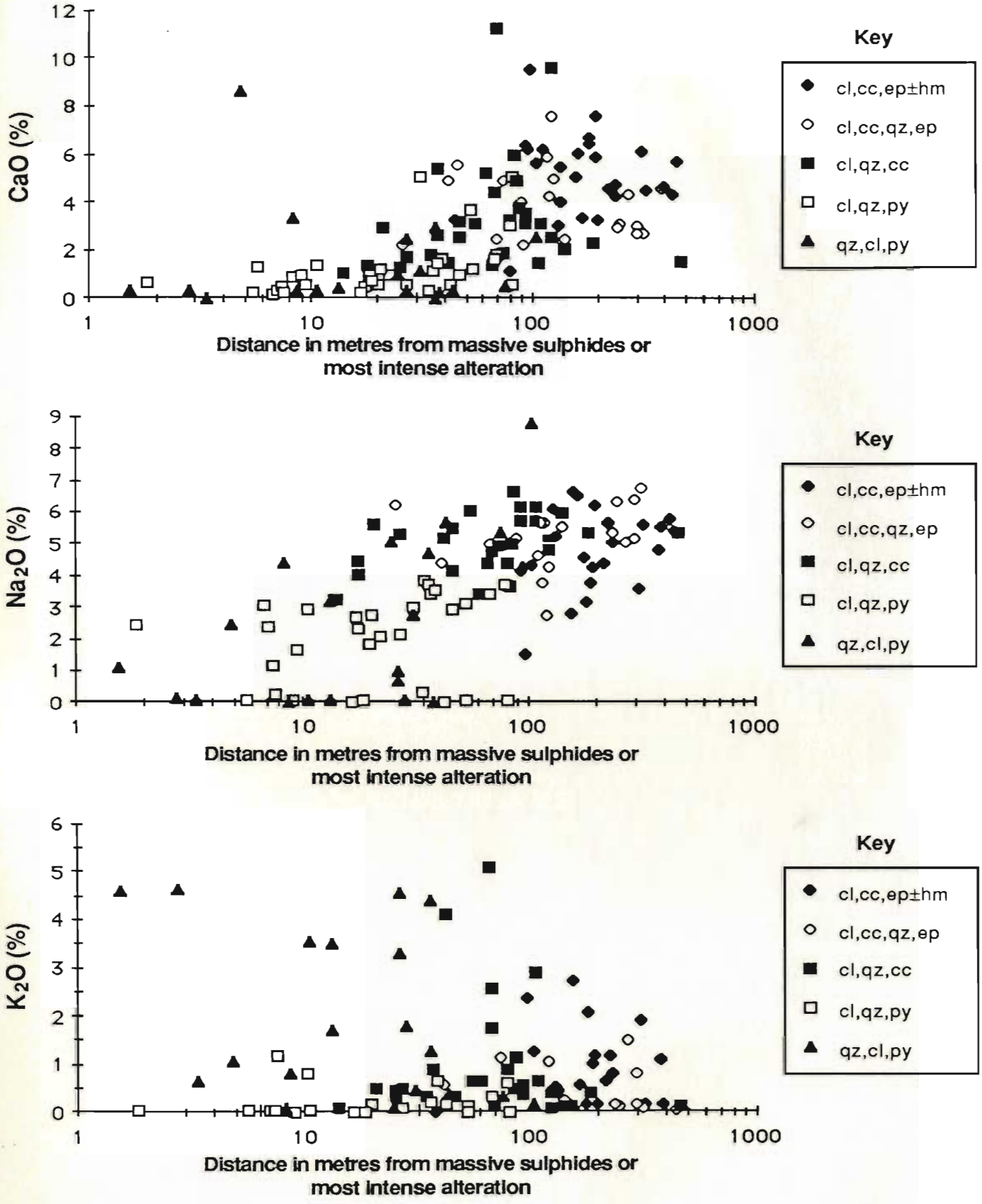

Figure 6-75: Major oxide contents of samples from the various Skidder Prospect alteration zones versus distance from massive sulphides or most intense alteration.

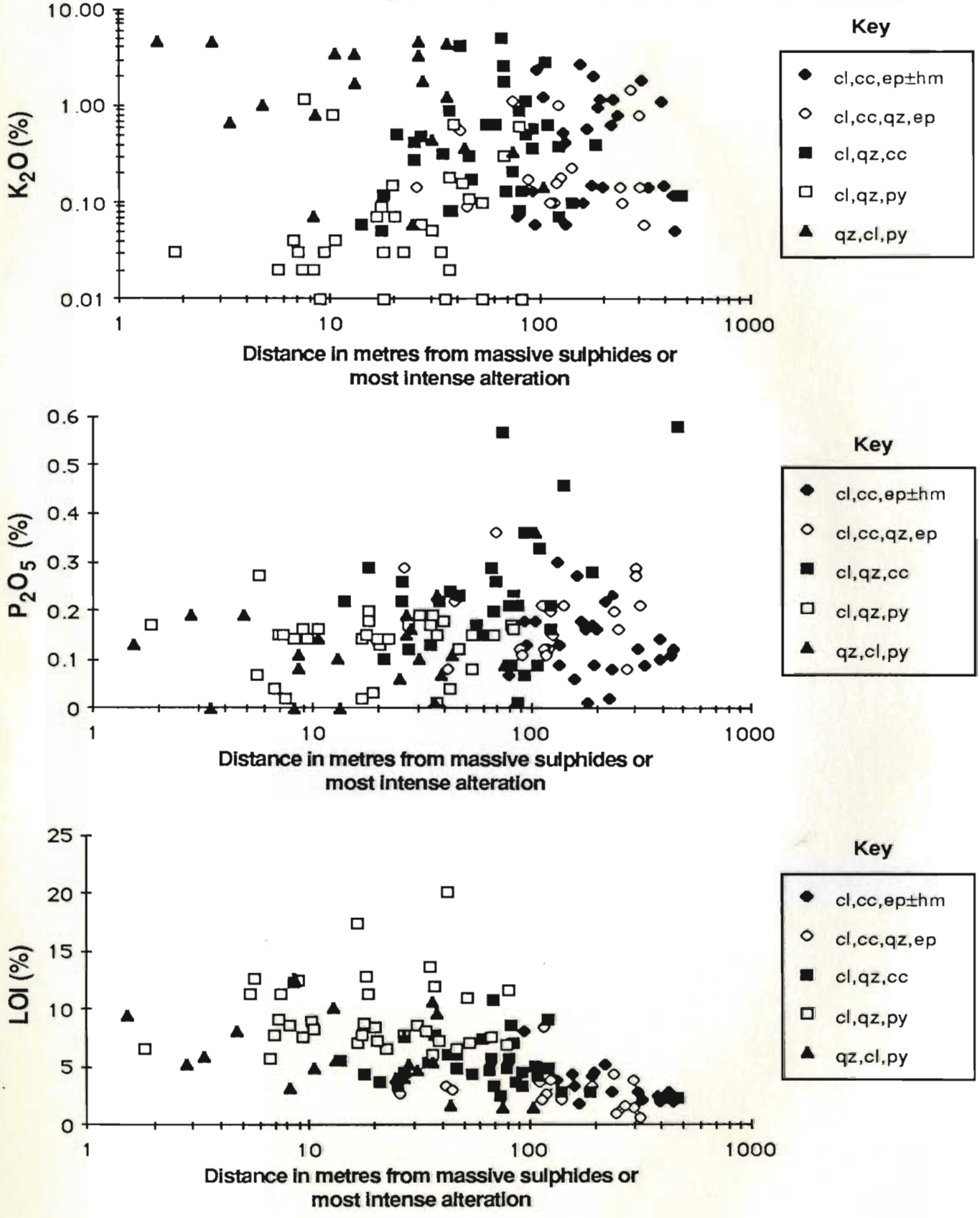

Figure 6-76: Major oxide contents and loss on ignition of samples from the various Skidder Prospect alteration zones versus distance from massive sulphides or most intense alteration.

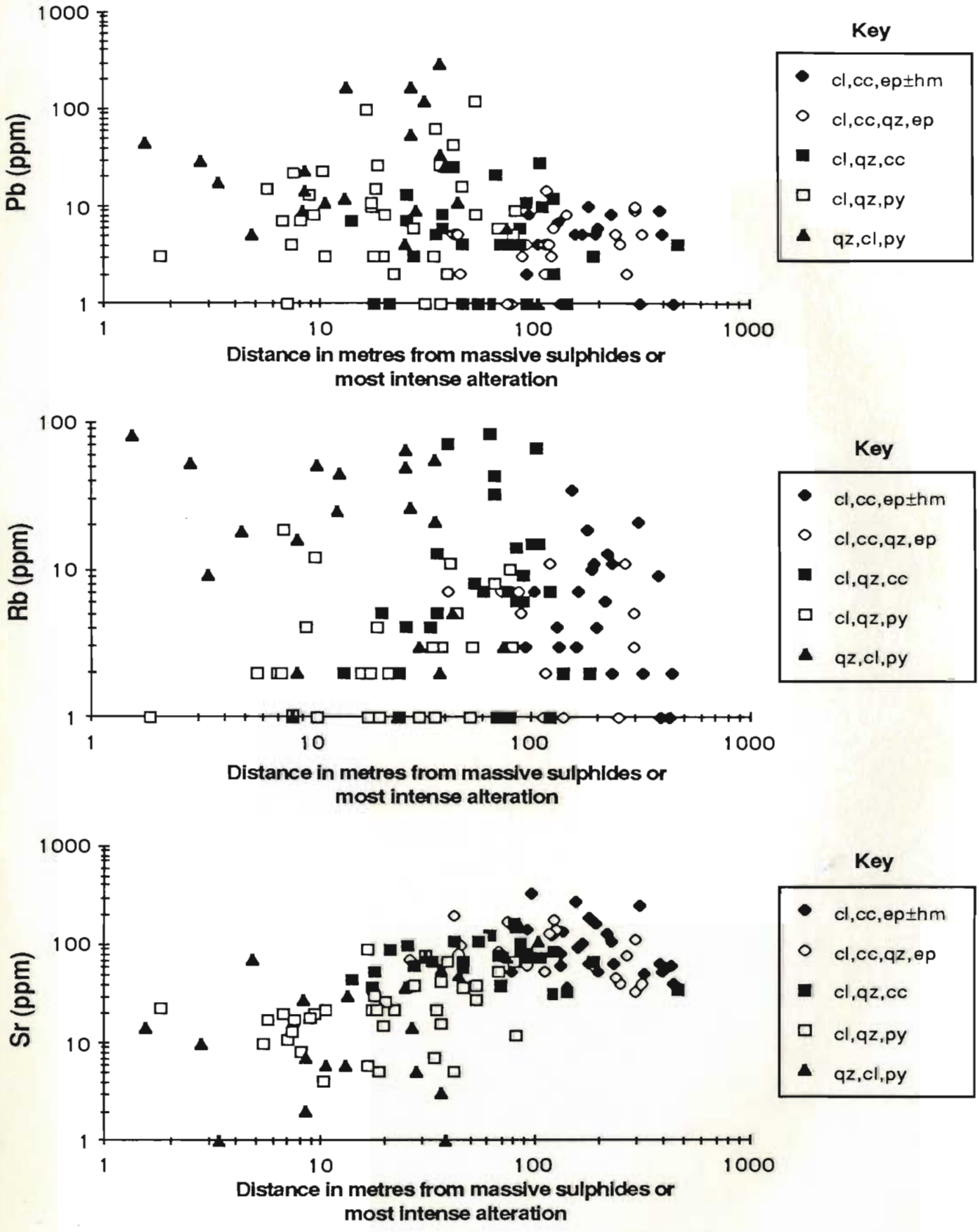

Figure 6-77: Trace element concentrations of samples from the various Skidder Prospect alteration zones versus distance from massive sulphides or most intense alteration.

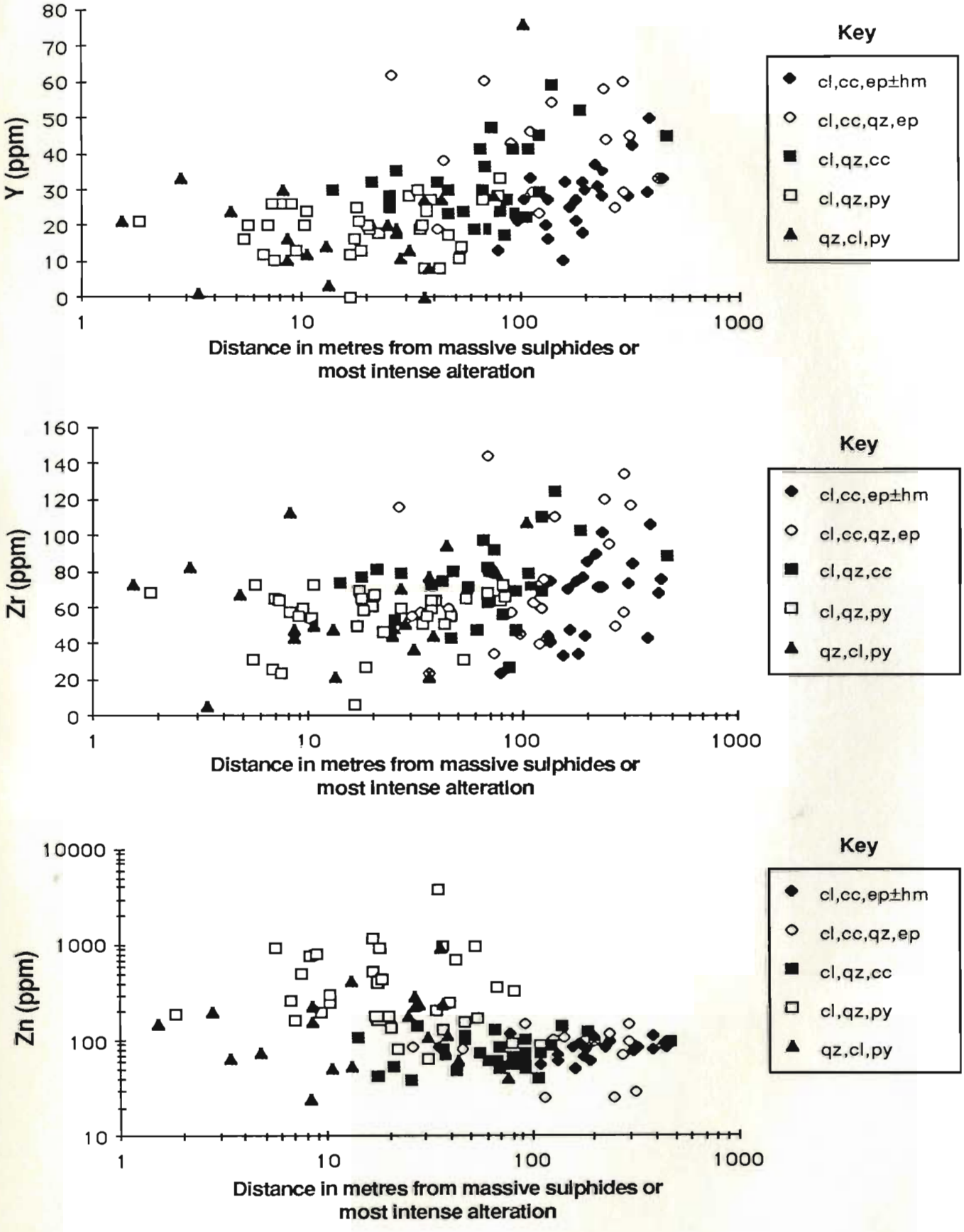

Figure 6-78: Trace element concentrations of samples from the various Skidder Prospect alteration zones versus distance from massive sulphides or most intense alteration.

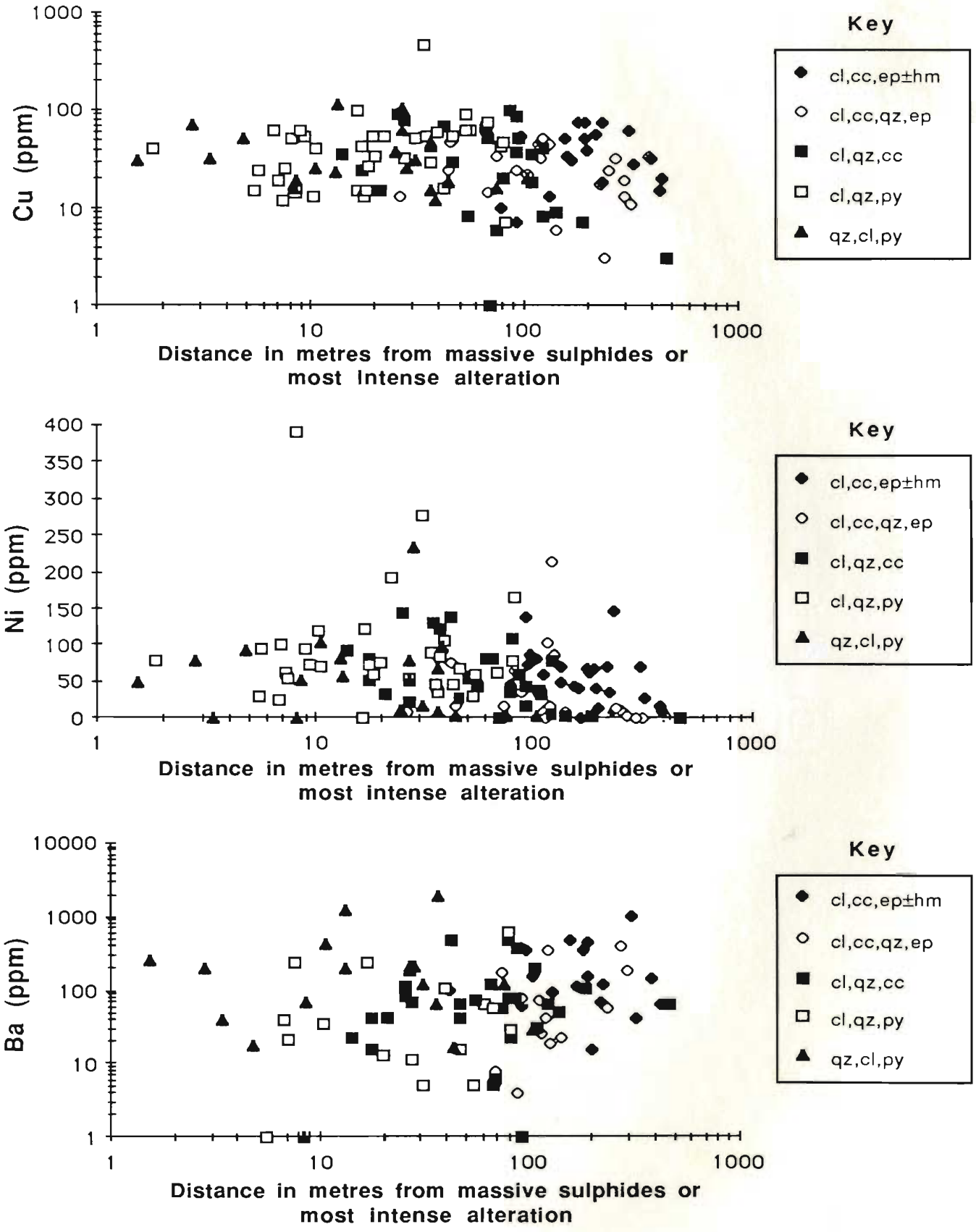

Figure 6-79: Trace element concentrations of samples from the various Skidder Prospect alteration zones versus distance from massive sulphides or most intense alteration.

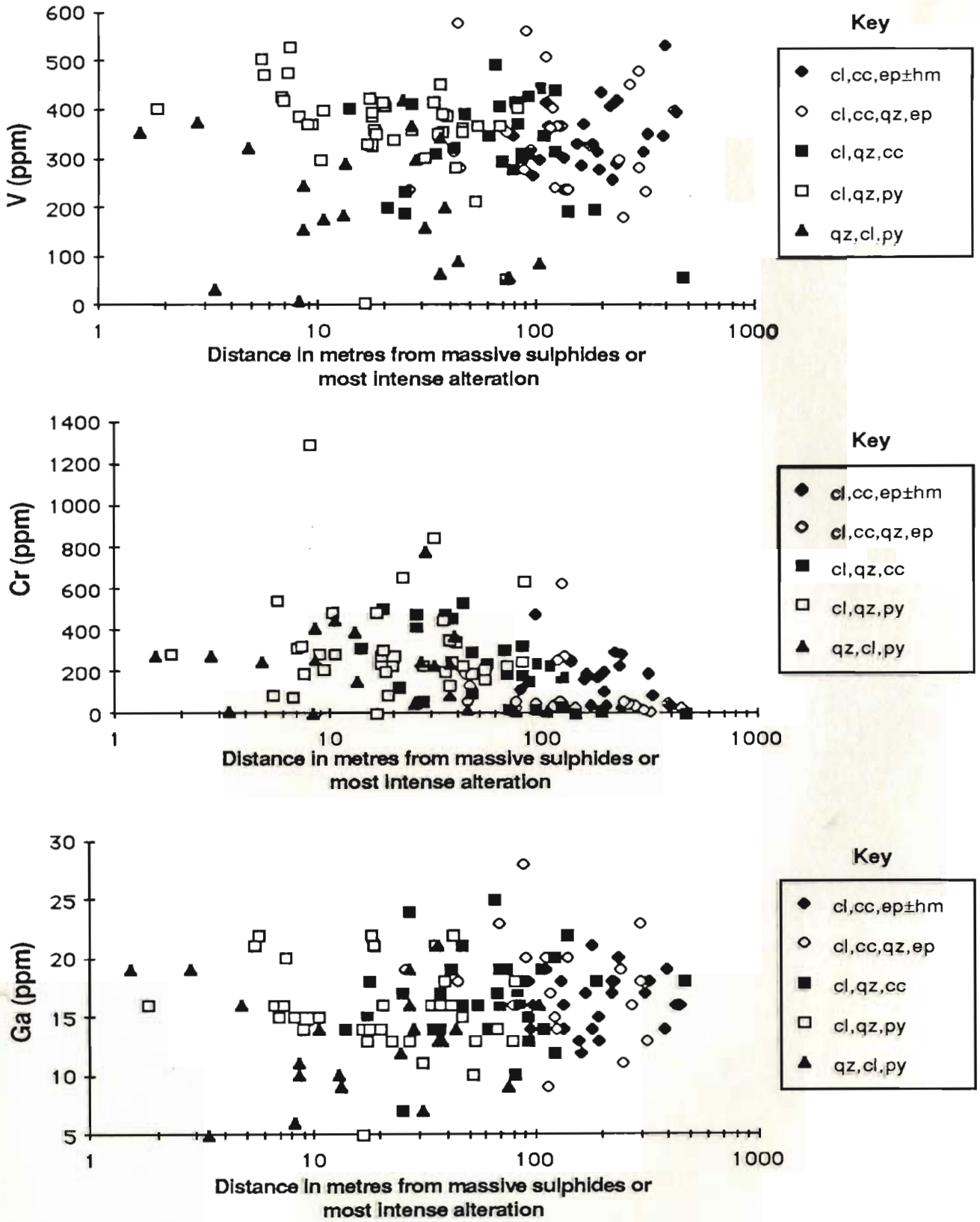

Figure 6-80: Trace element concentrations of samples from the various Skidder Prospect alteration zones versus distance from massive sulphides or most intense alteration.

Slight depletion of CaO and slight enrichment of Pb accompanies enrichment of K_2O, Rb and Ba in the cl,cc,qz,ep alteration zone, and extensive depletion of CaO and enrichment of Pb accompanies K_2O, Rb and Ba enrichment in the more altered rocks from the cl,qz,cc alteration zone. Depletion of Na_2O and Sr accompanies depletion of CaO and enrichment of Pb and Zn in the cl,qz,py alteration zone; all of which is accompanied by enrichment of K_2O, Rb and Ba in the qz,cl,py alteration zone. As mentioned previously, the cl,qz,py and qz,cl,py alteration zones are end members of a continuum marked by a predominance of chlorite for the former and quartz for the latter. It is not surprising therefore that enrichment of MgO and depletion of SiO_2 marks the former, and the reverse is true for the latter (Table 6-24). As shown in Figures 6-73 to 6-80, the alteration effects described in this paragraph are evident only within about 100 to 150 m of the most intensely altered rocks related to the sulphide-bearing zones.

Enrichment of Fe, Pb, Zn and Cu, which are common constituents of sulphide minerals, and depletion of elements that occur in silicate minerals characterize the semimassive and massive sulphide samples, as would be expected. Note however that the massive and semimassive sulphide samples are enriched in K_2O, Rb and Nb, and depleted in Ni relative to typical spilitized Skidder Basalt.

Comparison of the standard deviations of the elements for each of the various alteration zones to those of typical Skidder Basalt shows that in most areas the alteration-resistant incompatible and compatible elements have standard deviations similar to, or lesser than typical Skidder Basalt. In contrast to this, elements that are susceptible to alteration have standard deviations that are greater in the alteration zones than in typical Skidder Basalt. This serves to illustrate that, although trends toward increases or decreases of the various elements are statistically evident, the effects are sporadic (cf. Figures 6-73 to 6-80). A notable exception to this is CaO, which is depleted in almost all samples analyzed from the more intensely altered zones.

6.10.2 Principal component analysis

6.10.2.1 Introduction

Pearson correlation coefficient matrices for the samples from each of the alteration zones are presented in Tables B-17 to B-22, Appendix B. In order to better illustrate groupings of interelement correlations for the whole rock and trace element geochemical data, and to determine the effects of alteration on the various groupings, factor analysis was undertaken (see Appendix C for description of method used). Nine groupings of analyses were chosen: 1) Skidder Basalt samples unaffected by the Skidder Prospect alteration event (Group 1) (see Section 5.2.2); 2) all analyses of drill core from the Skidder Prospect, excluding trondhjemite and jasper, but including sulphide-rich samples (Group 2); 3) Group 2 excluding sulphide-rich samples (Group 3); the chlorite, calcite, epidote ± hematite (cl,cc,ep±hm) alteration zone (Group 4); the chlorite, calcite, quartz and epidote (cl,cc,qz,ep) alteration zone (Group 5); the chlorite, quartz and calcite (cl,qz,cc) alteration zone (Group 6); the chlorite, quartz and pyrite (cl,qz,py) alteration zone (Group 7); the quartz, chlorite, and pyrite (qz,cl,py) alteration zone (Group 8); and the sulphide-rich samples (Group 9).

Varimax-rotated factors determined for each of the data groupings are presented in Tables C-1 to C-9, Appendix C. Factors having similar loadings in the various data sets have been grouped together and presented in Tables 6-25 to 6-32.

6.10.2.2 Factor grouping 1

Factor 1 of Group 1, the Skidder Basalt samples unaffected by the Skidder Prospect alteration event, is typified by large positive loadings for TiO_2, P_2O_5, Y, Zr, Nb, Ce and Ga (Table 6-25) (cf. Section 5.2.2). This factor, with slight modification, occurs in all alteration zones. Modifications of the factor in the the qz,cl,py alteration zone (Group 8) involve lesser loadings for TiO_2, and exclusion of Ga, Nb and Ce from the factor. The factor has positive loadings for SiO_2, Al_2O_3, Na_2O, Fe_2O_3, and "distance from most

Table 6-25: Factor Grouping 1 - "Incompatible elements" factors extracted from the various data groupings

Data Grouping	Skidder Basalt	All drill core data	All except sulphides	Cl,cc,ep ± hm	Cl,cc,qz,ep	Cl,qz,cc	Cl,qz,py	Qz,cl,py	Sulphides
Factor	1 of 8	1 of 7	1 of 7	1 of 7	4 of 5	5 of 6	4 of 8	2 of 6	1 of 7
% variance	21.7%	25.5%	20.7%	20.3%	19.0%	16.5%	13.6%	20.9%	30.6%
SiO_2		.213				.242			-.375
TiO_2	.678	.627	.451	.865	.564	.170	.271	.226	.624
Al_2O_3		.348	.154			-.266		.458	.777
Fe_2O_3*	.296			.213				-.212	
MnO					-.195				.687
MgO		-.297		-.232		-.338			.876
CaO				.210	-.198	.194			
Na_2O		.444						.743	
K_2O								-.274	-.250
P_2O_5	.432	.744	.737	.239	.751	.712	.792	.626	
LOI		-.324						-.318	
Pb		-.185							-.346
Rb								-.306	-.321
Sr					-.359			.640	
Y	.532	.756	.611	.782	.630	.405	.612	.714	.251
Zr	.685	.831	.725	.861	.745	.297	.806	.447	.829
Nb	.807	.518	.734	.783	.640	.453	.748		.202
Zn			.158		.156	-.241	.171		-.277
Cu				.271	-.513			-.179	
Ni				.201		.150			.380
Ba		-.260	-.209						
V				.295	-.304	-.646			.843
Ce	.683	.670	.573	.437	.188	.184	.547		.669
Cr							.241	-.201	.553
Ga	.542	.172	.351	.429	.292	-.163		.335	
Distance		.269		.348	.299	.402		.852	

* Total iron as Fe_2O_3

Skidder Basalt - Skidder Basalt samples relatively unaffected by Skidder Prospect alteration event(s)

Distance - distance from massive sulphides or most intense alteration

intense alteration" (distance); and negative loadings for MgO and Ba in some of the groupings. Loadings for other elements are inconsistent. In the sulphide-rich samples, the factor has positive loadings for Al_2O_3, MnO, MgO, V, and Cr in addition to most of those typical of the factor, and it has negative loadings for Pb and Zn.

The principal components of this factor (in most of the data groupings) are all incompatible with early crystallizing minerals in a basaltic magma (see discussion in Section 5.2.2). Significantly, this "incompatible element" factor, with slight modification, occurs in even the most intensely altered rocks, a testimony to the resistance of these elements to alteration. Positive loadings for distance from most intense alteration for this factor suggest lower contents of the incompatible elements in rocks closer to the most intense alteration. Higher concentrations of the compatible elements Cr and Ni in the cl,qz,py and qz,cl,py alteration zone suggests that the lower contents of the incompatible elements may reflect primary low incompatible and high compatible element concentrations in the original basalt rather than the effects of alteration. This factor, in the sulphide-rich samples grouping, is better interpreted as a "silicate-minerals factor" rather than an "incompatible elements factor" since the components having large positive loadings occur in silicate minerals whereas the elements Pb and Zn, which have negative loadings, are present in the sulphide minerals.

6.10.2.3 Factor grouping 2

Large positive loadings for Ni and Cr, and moderate positive loadings for MgO, LOI and Na_2O characterize another factor that is present in all alteration zone data groupings; the components of this factor are included in the "silicate minerals factor" of the sulphide-rich samples (Table 6-26). Positive loadings for Al_2O_3, CaO, P_2O_5 and Sr, and negative loadings for SiO_2, Y, Zn, and "distance" are evident in some groupings.

Positive intercorrelations between the principal components of this factor, i.e. Cr, Ni and MgO, and negative correlations of these elements with Na_2O are influenced by the

Table 6-26: Factor Grouping 2 - "Compatible elements" factors extracted from the various data groupings

Data Grouping	Skidder Basalt	All drill core data	All except sulphides	Cl,cc,ep ± hm	Cl,cc,qz,ep	Cl,qz,cc	Cl,qz,py	Qz,cl,py	Sulphides
Factor	4 of 8	4 of 7	5 of 7	2 of 7	1 of 5	4 of 6	5 of 8	6 of 6	1 of 7
% variance	17.1%	11.1%	13.0%	21.8%	29.3%	17.0%	10.7%	12.4%	30.6%
SiO_2	-.347			-.727	-.520			-.378	-.375
TiO_2						.260			.624
Al_2O_3	.267			.256					.777
Fe_2O_3*		-.179		-.243				.252	
MnO						-.229	.174	.245	.687
MgO	.647	.248	.194	.433	.594	.512		.773	.876
CaO				.414	.718	-.198			
Na_2O	-.460	-.268	-.303	-.387	-.789	-.598	-.203		
K_2O								-.162	-.250
P_2O_5						.150	.304	.213	
LOI	.331		.184	.606	.689	.209		.229	
Pb			-.273			.158	-.249	-.233	-.346
Rb				-.171	.169			-.163	-.321
Sr	.145			.218	.508				
Y	-.256			-.236	-.235		.424		.251
Zr							.176	-.173	.829
Nb	.152			.186	.251	.317	-.141	-.259	.202
Zn			-.167	-.273					-.277
Cu					.511				
Ni	.744	.924	.910	.791	.911	.669	.948	.703	.380
Ba	-.152			-.217				.157	
V				-.526	-.291			.307	.843
Ce	.238		.161	.214	.267	.200	-.242	-.161	.669
Cr	.825	.905	.908	.875	.896	.685	.924	.709	.553
Ga						-.220			
Distance		-.369	-.406	-.699	-.254	-.302			

* Total iron as Fe_2O_3

Skidder Basalt - Skidder Basalt samples relatively unaffected by Skidder Prospect alteration event(s)

Distance - distance from massive sulphides or most intense alteration

compatibility of Cr, Ni and MgO with early formed minerals from a basaltic magma (see discussion in Section 5.2.2). The strong positive correlation of Cr and Ni, in even the most intensely altered rocks, supports the resistance of these elements to alteration. The exclusion of MgO from this factor in the cl,qz,py alteration zone is probably due to the dominance of MgO as a component of the rocks in this alteration zone. The negative loading of "distance" in this factor suggests higher compatible element concentrations in rocks more proximal to the Skidder Prospect sulphide-bearing zones (see discussion in Section 6.10.2.2).

6.10.2.4 Factor grouping 3

Strong positive loadings for K_2O, Rb and Ba characterize a third factor evident in all groupings (Table 6-27). In this factor, positive loadings for Sr and Al_2O_3 are shown by the less altered rocks and negative loadings for MnO and MgO are evident in several of the groupings. The cl,qz,cc and/or qz,cl,py alteration zones show positive loadings for TiO_2, Al_2O_3, Na_2O, P_2O_5, Zr, Nb, V, Ce and Ga. A large negative loading for Na_2O is shown by the cl,cc,ep±hm alteration zone data.

Intercorrelations between the principal components of this "potassium" factor, i.e. K_2O, Rb and Ba, are readily explained by substitution of the latter elements for potassium in the potassium-bearing minerals (cf. Section 5.2.2). Similarly, Sr and Pb substitute for potassium. The large negative loading for Na_2O in the cl,cc,ep±hm alteration zone data is probably reflects the replacement of Na by K in alkali feldspar in these rocks. Potassium and its substitutes behave independently in the less altered rocks but share positive loadings with the incompatible elements in the cl,qz,cc and qz,cl,py alteration zones.

6.10.2.5 Factor grouping 4

A fourth factor distinguishable in all data groupings is characterized by large positive loadings for MgO, MnO (except for the cl,qz,cc alteration zone) and Zn (except for

Table 6-27: Factor Grouping 3 - "Potassium" factors extracted from the various data groupings

Data Grouping	Skidder Basalt	All drill core data	All except sulphides	Cl,cc,ep ± hm	Cl,cc,qz,ep	Cl,qz,cc	Cl,qz,py	Qz,cl,py	Sulphides
Factor	3 of 8	3 of 7	3 of 7	3 of 7	3 of 5	2 of 6	3 of 8	1 of 6	2 of 7
% variance	13.9%	13.2%	14.3%	21.5%	19.9%	21.2%	10.5%	28.1%	13.7%
SiO_2			.152	*-.206*		*-.239*		*-.243*	
TiO_2						.413		.875	
Al_2O_3	.432	.217				.806		.748	
Fe_2O_3*						*-.181*		*-.178*	
MnO		*-.253*	*-.380*		.384	*-.161*	*-.238*		*-.193*
MgO		*-.299*	*-.356*			*-.583*		*-.194*	
CaO				.398					
Na_2O	.159			*-.659*		.207			.888
K_2O	.902	.949	.940	.870	.839	.949	.931	.801	.714
P_2O_5	.164			*-.160*				.605	.194
LOI				*-.165*	*-.447*				
Pb			.463		*-.207*	.717			
Rb	.802	.914	.906	.834	.683	.950	.816	.793	.578
Sr	.359	.167	.149	.795					
Y			*-.165*		*-.154*			.368	
Zr					*-.199*	.275		.482	
Nb			.223		*-.238*	.343		.794	
Zn									
Cu				.504		.231		*-.217*	
Ni								.195	
Ba	.710	.730	.738	.783	.835	.478	.653	.258	.834
V						.402		.665	
Ce	*-.151*			*-.221*	*-.711*	.182		.605	*-.283*
Cr									
Ga						.480		.819	
Distance				.196	.411				*-.303*

* Total iron as Fe_2O_3

Skidder Basalt - Skidder Basalt samples relatively unaffected by Skidder Prospect alteration event(s)

Distance - distance from massive sulphides or most intense alteration

the qz,cl,py and sulphide-rich samples) (Table 6-28). Positive loadings for TiO_2, Fe_2O_3, LOI, V and Ga, and negative loadings for SiO_2, Na_2O, Ni, Ce and Cr are evident in some alteration zone data groupings.

Most elements that have large positive loadings for this factor are components of chlorite, a ubiquitous phase in most of the Skidder Basalt (see discussion in Section 5.2.2). Zinc, another component of this factor, correlates positively with MgO in several of the sample groupings, but particularly in the high-MgO cl,qz,py zone (see discussion in Section 6.10.3). Chlorite is the major mineral of rocks in that alteration zone. The negative loadings for SiO_2 and Na_2O in several of the alteration zone groupings, particularly in the high-MgO cl,qz,py zone, are probably a result of volumetric effects regarding the major mineral components of the rock, for example, samples having high chlorite contents would have lesser contents of albite and quartz. Groupings having large positive loadings for TiO_2, Fe_2O_3 and V may result from incorporation of an Fe-Ti oxide component along with the chlorite component in this factor. Ga and Zn correlate positively in all data groupings, but whether Ga substitutes for Fe or Mg in chlorite or for iron in Fe-Ti oxide is uncertain.

6.10.2.6 Factor grouping 5

Large positive loadings for CaO and Sr, a moderate positive loading for MnO, and generally negative loadings for SiO_2 define a fifth factor (Table 6-29). This factor is independent in all data groupings except those of the cl,cc,ep±hm, cl,cc,qz,ep and qz,cl,py alteration zones. In the cl,cc,ep±hm alteration zone data, it is incorporated into the "compatible elements factor" and the "potassium factor" (Tables 6-26 and 6-27); in the cl,cc,qz,ep it is incorporated into the "compatible elements factor" (Table 6-26); and, in the qz,cl,py data grouping, it is incorporated into the "chlorite factor" (Table 6-28). Positive loadings for LOI, Ba and "distance", and negative loadings for Ce and Ga are shown in some data groupings.

Table 6-28: Factor Grouping 4 - "Chlorite/Zinc" factors extracted from the various data groupings

Data Grouping	Skidder Basalt	All drill core data	All except sulphides	Cl,cc,ep ± hm	Cl,cc,qz,ep	Cl,qz,cc	Cl,qz,py	Qz,cl,py	Sulphides
Factor	2 of 8	6 of 7	2 of 7	4 of 7	2 of 5	1 of 6	2 of 8	3 of 6	1 of 7
% variance	10.5%	12.9%	18.3%	12.7%	23.3%	20.7%	20.9%	15.9%	30.6%
SiO_2	.180	*-.398*	***-.628***	*-.302*	***-.582***	***-.429***	***-.884***	***-.561***	*-.375*
TiO_2		.212			.362	**.519**	***-.419***		**.624**
Al_2O_3		**.491**			**.716**				**.777**
Fe_2O_3*	**.462**				**.872**	**.717**	.365		
MnO	**.738**	**.565**	.309	**.922**	**.542**		.396	**.807**	**.687**
MgO	.366	**.649**	**.668**	**.700**	**.424**	*-.455*	**.867**	**.408**	**.876**
CaO				*-.332*		*-.257*		.956	
Na_2O	***-.428***		*-.398*	*-.280*		*-.155*	***-.753***		
K_2O			*-.099*						*-.250*
P_2O_5		*-.170*	.178	*-.239*					
LOI			**.595**	.174	.375		**.749**	.225	
Pb		*-.283*	.293				.365	*-.167*	*-.346*
Rb	*-.157*								*-.321*
Sr			*-.222*			*-.310*	*-.310*	**.504**	
Y						.195			.251
Zr						**.417**			**.829**
Nb		*-.171*	.186			.181		.184	.202
Zn	**.644**		**.822**	**.827**	**.838**	**.608**	**.709**		*-.277*
Cu					*-.142*	*-.577*		**.804**	
Ni					*-.186*	*-.277*		*-.175*	.380
Ba	.350								
V		**.761**		.431	**.703**	.287			**.843**
Ce	*-.177*				*-.180*	*-.178*		*-.178*	**.669**
Cr	*-.184*				*-.195*	*-.177*		*-.215*	**.553**
Ga	.185	.219	.290	.274	**.505**	.264	.565	*-.207*	
Distance			*-.162*		*-.154*			*-.286*	

* Total iron as Fe_2O_3

Skidder Basalt - Skidder Basalt samples relatively unaffected by Skidder Prospect alteration event(s)

Distance - distance from massive sulphides or most intense alteration

Table 6-29: Factor Grouping 5 - "Calcite" factors extracted from the various data groupings

Data Grouping	Skidder Basalt	All drill core data	* All except sulphides	Cl,qz,cc	Cl,qz,py	Sulphides
Factor	5 of 8	5 of 7	4 of 7	3 of 6	6 of 8	5 of 7
% variance	11.9%	9.5%	10.4%	14.2%	10.3%	11.8%
SiO_2	*-.597*	*-.169*	*-.301*	*-.572*	.246	*-.194*
TiO_2		.158			.296	
Al_2O_3	*-.266*					
Fe_2O_3*				.218	***-.782***	
MnO	.148	**.434**	**.511**	**.650**	.178	**.564**
MgO	*-.261*	*-.156*				
CaO	**.797**	**.868**	**.891**	**.880**	**.400**	**.832**
Na_2O		.236		*-.228*	.293	
K_2O						*-.177*
P_2O_5						*-.155*
LOI	**.539**			**.669**	*-.312*	
Pb			*-.163*	*-.179*		
Rb					*-.202*	*-.282*
Sr	.210	**.770**	**.693**	.380	**.553**	**.842**
Y					.164	
Zr						
Nb	.181			.218	***-.518***	*-.156*
Zn	*-.318*			*-.166*		
Cu			**.429**			
Ni						
Ba		.211	.205		**.472**	
V						
Ce	*-.155*	*-.176*	*-.190*		*-.155*	
Cl				*-.160*		
Ga	*-.250*			*-.236*	*-.373*	
Distance		.363	.309	.196		***-.609***

* Total iron as Fe_2O_3

Skidder Basalt - Skidder Basalt samples relatively unaffected by Skidder Prospect alteration event(s)

Distance - distance from massive sulphides or most intense alteration

This factor is interpreted as a "calcite factor" since both Mn and Sr substitute for Ca in calcite (see discussion in Section 5.2.2). Positive loadings for distance in this factor attest to the depletion of calcite, and calcium overall, in the more intensely altered rocks; note however that calcite is a gangue mineral in the sulphide-rich samples, this being reflected in "distance" having a large negative loading in this data grouping.

6.10.2.7 Other factors

A factor defined by large positive loadings for Al_2O_3, and moderate negative loadings for SiO_2 and CaO is evident in four of the data groupings (Table 6-30). The factor has positive loadings for TiO_2, Fe_2O_3 and V in three of the groupings.

This factor is interpreted as a combination of an "alumina" and an "Fe-Ti oxide" factor.

An independent factor having large loadings for lead occurs in the "typical spilitized Skidder Basalt", cl,cc,ep±hm and cl,cc,qz,ep data groupings (Table 6-30). A second independent factor having large positive loadings for copper is shown by the cl,cc,ep±hm and cl,qz,py alteration zone data groupings (Table 6-31). Other independent factors, each of which occurs in only one of the data groupings, are listed in Table 6-31.

6.10.2.8 - Sulphide-related factors

Three factors that are probably sulphide related are evident in the data groupings (Table 6-32). These are: 1) a factor defined by positive loadings for Pb, Zn and Cu in the "all drill core" and "sulphides" groupings; 2) one defined by positive loadings for Fe_2O_3, LOI and Nb, and negative loadings for SiO_2 and Ba in the "all drill core", "all except sulphides" and "sulphides" groupings; and 3) one in the qz,cl,py data grouping defined by positive loadings for Fe_2O_3, LOI, Pb and Zn, and negative loadings for SiO_2 and Zr.

The first factor is interpreted as a "sulphide factor". The three principal components of this factor strongly intercorrelate in the sulphide rich-samples, and they form a distinct

Table 6-30: "Alumina" and "Lead" factors extracted from the various data groupings

	Alumina				Lead		
Data Grouping	Skidder Basalt	All except sulphides	Cl,cc,ep ± hm	Cl,qz,py	Skidder Basalt	Cl,cc,ep ± hm	Cl,cc,qz,ep
Factor	6 of 8	6 of 7	5 of 7	1 of 8	7 of 8	6 of 7	5 of 5
% variance	10.7%	16.1%	10.0%	19.3%	6.9%	7.3%	8.6%
SiO_2	*-.351*	***-.470***	*-.245*	*-.243*			
TiO_2	.166	.369	*-.161*	.249			*-.241*
Al_2O_3	**.533**	**.766**	**.783**	**.899**		*-.166*	
Fe_2O_3*	**.491**	.142		.252			
MnO		.358	*-.167*				**.480**
MgO	.237	.357		.243			*-.248*
CaO	*-.137*	*-.254*	***-.602***	***-.762***	*-.173*		
Na_2O			.257				
K_2O							
P_2O_5	***-.440***		.315			***-.482***	
LOI			.398	*-.239*	.358	.315	.189
Pb		*-.360*		***-.617***	**.807**	**.910**	**.733**
Rb					.273	.192	
Sr				***-.480***	***-.485***		
Y			*-.275*	.322			
Zr				.178			
Nb						.197	*-.233*
Zn	.175		.301		.156	.128	.161
Cu		***-.417***					*-.168*
Ni							
Ba	*-.248*			*-.165*	*-.165*		
V	**.846**	**.861**		**.890**			
Ce			**.442**	.192			.215
Cr							
Ga		**.603**		**.729**		*-.357*	*-.249*
Distance			*-.325*				**.418**

* Total iron as Fe_2O_3

Skidder Basalt - Skidder Basalt samples relatively unaffected by Skidder Prospect alteration event(s)

Distance - distance from massive sulphides or most intense alteration

Table 6-31: Miscellaneous factors extracted from the various data groupings

Data Grouping	Copper		Negative Copper	Mn, Ce	Distance	Barium	P_2O_5	Zn,Y,Ga
	Cl,cc,ep ± hm	Cl,qz,py	Skidder Basalt	Cl,qz,cc	Cl,qz,py	Qz,cl,py.	Sulphides	Sulphides
Factor	7 of 7	7 of 8	8 of 8	6 of 6	8 of 8	5 of 6	7 of 7	4 of 7
% variance	6.4%	5.6%	7.3%	10.5%	9.1%	10.0%	5.6%	11.9%
SiO_2	.172	.204			-.156	.302	.161	
TiO_2		-.164	.150					
Al_2O_3			.260	.164		.182		
Fe_2O_3*	-.703	-.197		-.266	.158	-.558		-.374
MnO		-.200		.441	-.548			
MgO		.161	-.197	.049				
CaO								
Na_2O	.161	-.225	.382	-.270	.299	.169		
K_2O						.320		
P_2O_5	.253		.239				.890	
LOI	.238	-.177				-.422		
Pb				-.207				
Rb						.243		
Sr		-.196	.320	-.251	.420			
Y		.217	.202	.151	.199	-.215		.728
Zr			.179					
Nb		-.192		.328	-.188	-.446	.233	
Zn					-.147			.676
Cu	.598	.817	-.680	.282				
Ni						.247	-.218	-.168
Ba	.161			-.691	.264	.735		
V					-.163			
Ce		.228	-.234	.732	-.617	-.489	.260	
Cr								-.276
Ga			-.292	.215				.817
Distance		.151		-.163	.796		-.480	-.564

* Total iron as Fe_2O_3

Skidder Basalt - Skidder Basalt samples relatively unaffected by Skidder Prospect alteration event(s)

Distance - distance from massive sulphides or most intense alteration

Table 6-32: Sulphide-related factors extracted from the various data groupings

	Sulphide		Pyrite			Pb, Zn
Data Grouping	All drill core data	Sulphides	All drill core data	All except sulphides	Sulphides	Qz,cl,py
Factor	2 of 7	6 of 7	7 of 7	7 of 7	3 of 7	4 of 6
% variance	13.3%	9.1%	14.5%	7.3%	17.4%	12.8%
SiO_2			*-.654*	*-.267*	*-.808*	*-.354*
TiO_2						
Al_2O_3			*-.158*			
Fe_2O_3*			**.609**	**.816**	**.753**	**.498**
MnO			.172			*-.241*
MgO						
CaO			.159			
Na_2O			*-.290*	*-.211*		
K_2O		*-.196*				
P_2O_5				*-.207*		
LOI			**.544**	.243	**.828**	**.457**
Pb	.336	**.679**	.189			**.792**
Rb		*-.399*	.150		.209	
Sr						
Y	.158	*-.161*			*-.249*	*-.180*
Zr						*-.332*
Nb		.311	**.700**	.389	**.702**	
Zn	**.830**	.163				**.822**
Cu	**.642**	**.684**		.266		
Ni		**.465**			*-.517*	*-.234*
Ba		.217	*-.189*	*-.292*	*-.156*	.176
V				.186		
Ce				.177		*-.366*
Cr		.258			-.351	*-.183*
Ga	**.831**					
Distance						.202

* Total iron as Fe_2O_3

Distance - distance from massive sulphides or most intense alteration

grouping dominated by sulphide mineralogy as opposed to silicate, oxide or carbonate mineralogy in the "all drill core" data grouping. The second factor is interpreted as a "pyrite factor". Niobium, which, along with Fe_2O_3 and LOI, has large positive loadings in this factor, is slightly enriched in the sulphide-rich rocks (Table 6-32). It is uncertain, however, whether the inclusion of Nb in this factor implies that it can be incorporated into pyrite or whether its enrichment in the sulphide-rich rocks is due to analytical error. The third sulphide-related factor probably reflects enrichment of Zn and Pb relative to copper in the qz,cl,py alteration zone.

6.10.2.9 Discussion and summary

Two factors that probably reflect magmatic processes can be distinguished in all data groupings, these being the "incompatible elements factor" and the "compatible elements factor". Of the elements having the largest positive loadings in the "incompatible elements" factor, Zr, Y and P_2O_5 remain strongly positively correlated in even the most intensely altered rocks. However, TiO_2 and Ce have only weak positive loadings in the more altered rock groupings. In the "compatible elements factor", Ni an Cr have strong positive correlations in all alteration zones, even the most intensely altered. The lack of contribution of a sulphide component to the Ni content of the samples, including those that are sulphide rich, is implied.

Alteration-related factors evident in several of the data groupings include two factors related to specific minerals, i.e. the "calcite" and "chlorite" factors. Spilitization and the Skidder Prospect alteration event has masked the positive correlations of the alkalis to other incompatible elements such that potassium, and elements that substitute for it, form an independent factor in all the data groupings. Na_2O has a large positive loading in the "incompatible elements factor" only in the qz,cl,py data grouping. Like SiO_2, the contributions of Na_2O to the variance in most of the data groupings are through negative loadings in the "compatible elements factor" and the "chlorite factor".

Independent factors for lead and Al_2O_3 occur in some of the data groupings. An Fe-Ti "subfactor" is discernible in the "alumina factor" in three data groupings, and in other factors elsewhere.

Factors related to sulphides include a Pb, Zn and Cu "sulphide factor" in the "all drill core" and "sulphides" groupings, and a "pyrite" factor in the "all drill core", "all except sulphides" and "sulphides" groupings. Note that several factors or factor components are unique to the "sulphides" data grouping. For instance, Factor 1 in this grouping includes a combination of factor components to form a "silicate factor"; elsewhere these components are separated into the "incompatible elements", "compatible elements", "chlorite", and "alumina" factors. Also, the "potassium factor" in the "sulphides" grouping has a positive loading with respect to Na_2O; and P_2O_5 is not included in the "incompatible elements" factor in the "sulphides" grouping, but occurs as an independent factor.

6.10.3 Zinc enrichment in magnesium-rich rocks

Zn shows a strong positive correlation with MgO in rocks proximal to the Skidder Prospect (Figure 6-81). It is particularly enriched in the high-MgO rocks of the cl,qz,py alteration zone; several of these rocks having Zn concentrations greater than 900 ppm. Electron microprobe analysis for S, Fe and Zn was done on several chlorites in thin and polished sections of rocks proximal to the Skidder Prospect in an effort to determine whether the zinc occurs in minute sphalerite grains or whether it is directly incorporated into the high-Mg-chlorite structure. Several quartz grains were analyzed for S, Fe and Zn for use as controls. The mean, standard deviation, maximum and minimum for the S, Fe and Zn contents of the various minerals analyzed are presented in Table 6-33; individual analyses are listed in Table A-7, Appendix A. The analyses show that Zn contents are indeed higher in chlorite than in quartz and muscovite. Zn contents are also higher in the very few analyses carried out on talc, calcite and magnetite relative to those of quartz and muscovite. As shown on Figure 6-82, despite extensive scattering of the data points, there

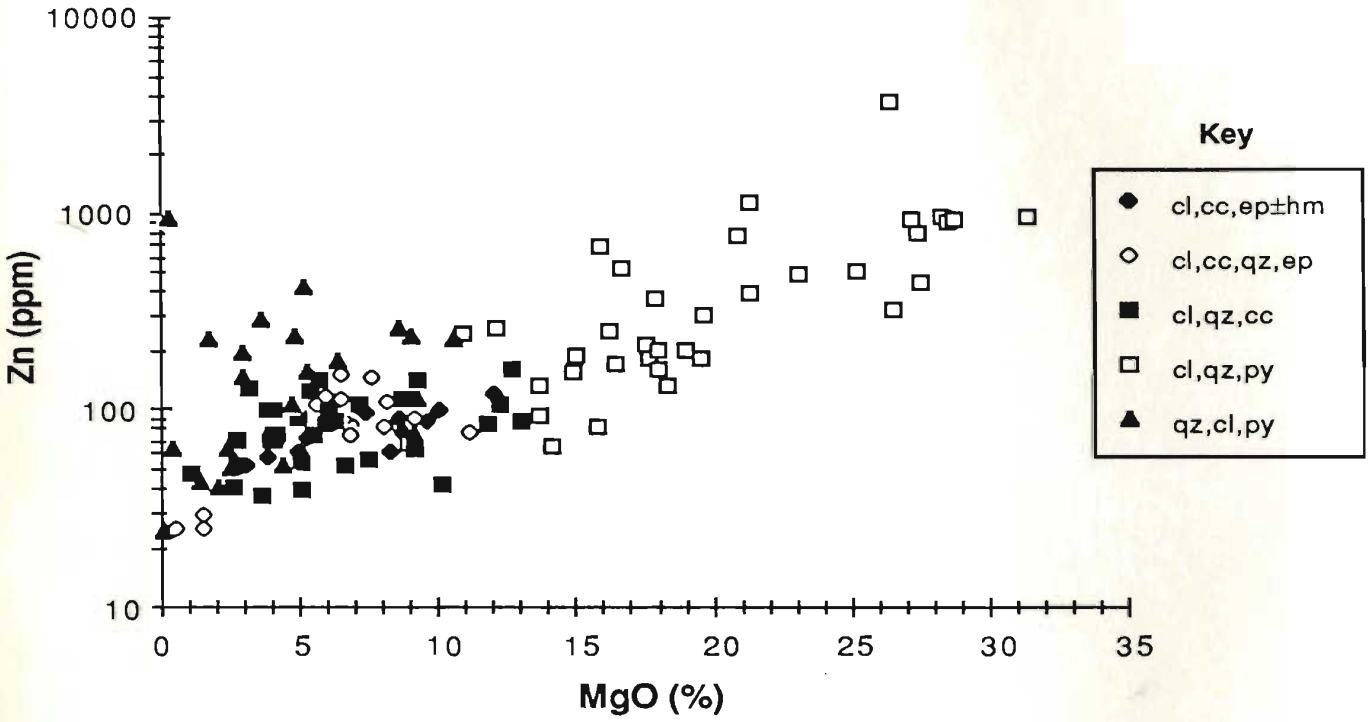

Figure 6-81: Per cent MgO versus parts per million Zn in samples from the various Skidder Prospect alteration zones.

Table 6-33: Averages of electron microprobe analyses for S-Fe-Zn in non-sulphide minerals from rocks proximal to the Skidder Prospect

Mineral	Chlorite	Quartz	Muscovite	Talc	Calcite	Magnetite
Average						
S	0.06	0.02	0.03	0.03	n.d.	0.15
Fe	8.74	0.05	0.82	2.61	0.68	98.98
Zn	0.30	0.16	0.15	0.24	0.21	0.23
Analyses	41	11	3	2	1	1
Standard Deviation						
S	0.05	0.02	0.01	0.01		
Fe	4.10	0.05	0.54	0.99		
Zn	0.12	0.03	0.06	0.05		
Minimum						
S	0.01	0.01	0.02	0.02		
Fe	3.16	0.01	0.34	1.91		
Zn	0.15	0.09	0.09	0.20		
Maximum						
S	0.20	0.05	0.04	0.03		
Fe	21.09	0.17	1.41	3.31		
Zn	0.68	0.21	0.20	0.27		

n.d. - not detected

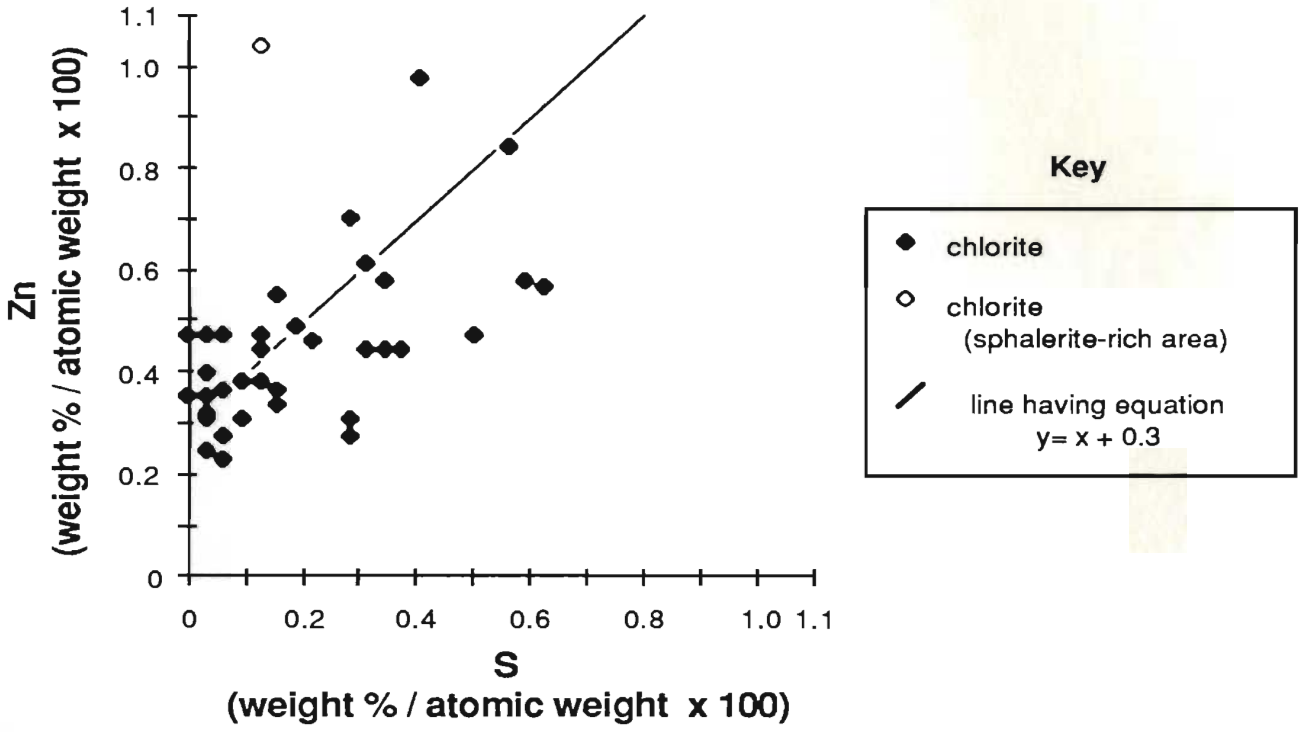

Figure 6-82: Zn vs. S in chlorites from rocks proximal to the Skidder Prospect.

is a crude one to one correspondence between atomic S and Zn in the chlorite analyses. The data scattering, and the indicated presence of greater amounts of atomic Zn at a given atomic S content, is probably a result of analytical uncertainty, since the contents of both elements being measured is close to the detection limit for the electron microprobe.

The one to one correspondence between atomic S and Zn in the chlorite analyses suggests that the Zn is present in minute sphalerite inclusions in the chlorites rather than directly incorporated into the chlorite structure.

6.11 Jasper Geochemistry

Jasper analyses listed in Table 6-34 include one from the jasper unit at sample location S 71 (Figures 3-3 and 3-4); and six of jasper associated with the Skidder Prospect. Silica and iron comprise the bulk of sample S 71, accompanied by a very small amount of Ca and Al. The reciprocal relationship between silica and iron in the Skidder Prospect jasper samples reflects the presence of varying proportions of quartz and hematite in the samples. High LOI values for samples SK 28 48, SK 35A 7 and SK 37A 40 indicate the presence of sulphides, mostly pyrite. Chalcopyrite accompanies the pyrite in sample SK 28 48 (Cu = 8313 ppm), and chalcopyrite and sphalerite occur with pyrite in sample SK 37A 40 (Cu = 7936 ppm, Zn = 909 ppm). Disproportionately high contents of Al_2O_3, MgO, Y, Zr and V in sample SK 37A 40 relative to the others are probably due to the presence of silicates other than quartz in the sample, e.g. silicates comprising an incorporated basalt fragment. The high P_2O_5 and CaO contents of this sample probably reflect the presence of apatite, with or without calcite. The apatite may be part of a basalt fragment incorporated into the jasper, or alternatively, it may be of sedimentary origin (?).

Table 6-34: Whole rock analyses of jasper from the Skidder area

	Outcrop	Skidder Prospect Drill Core						Average
		SK	SK	SK	SK	SK	SK	(Drill
weight %	S 71	27 39	28 48	32 30	35A 7	37A 40	37A 49	Core)
SiO_2	86.80	85.80	64.90	79.80	71.00	40.00	93.40	72.48
TiO_2	n.d.	n.d.	0.04	n.d.	n.d.	0.03	n.d.	0.04
Al_2O_3	0.10	0.20	0.60	n.d.	0.50	1.70	n.d.	0.75
Fe_2O_3*	11.79	6.60	21.97	16.26	17.12	45.20	4.33	18.58
MnO	0.01	0.04	0.01	0.01	0.04	0.04	0.01	0.03
MgO	0.01	0.10	0.17	0.02	0.55	1.61	0.05	0.42
CaO	0.21	2.14	0.12	1.74	1.56	2.60	0.98	1.52
Na_2O	0.02	n.d.	0.05	n.d.	0.01	0.01	n.d.	0.02
K_2O	0.01	n.d.	0.06	n.d.	0.01	0.03	0.01	0.03
P_2O_5	0.06	0.03	0.06	0.05	0.06	1.10	n.d.	0.26
LOI	0.43	4.03	11.43	1.02	8.12	6.72	0.92	5.37
Total	99.44	98.94	99.41	98.90	98.97	99.04	99.70	99.16
ppm								
Pb	2	6	69	9	10	236	1	55
Rb	2	n.d.	6	2	2	11	n.d.	5
Sr	3	12	2	11	8	28	6	11
Y	2	1	n.d.	2	1	32	n.d.	9
Zr	8	8	15	8	13	29	4	13
Nb	3	3	8	2	3	10	3	5
Zn	n.d.	n.d.	43	n.d.	19	909	4	244
Cu	38	33	8313	n.d.	84	7936	32	3280
Ni	n.d.	n.d.	4	n.d.	n.d.	2	n.d.	3
Ba	n.d.	n.d.	6	n.d.	n.d.	5	n.d.	6
V	10	1	15	56	16	221	16	54
Ce	27	27	12	13	43	10	68	29
Cr	11	3	n.d.	11	n.d.	33	8	14
Ga	2	2	2	2	6	14	3	5
Depth (feet)		605	544.5	707	1574	1513	1531	
Depth (metres)		184.4	166.0	215.5	479.6	461.1	466.6	
Distance		11.3	2.6	30.5	0.5	5.5		10.1
Comment			Bx			L	Bx	

* Total iron as Fe_2O_3
n.d. - not detected
Depth - drill hole depth at which sample was taken
Distance - distance from massive sulphides or most intense alteration
Bx - brecciated
L - layered

6.12 Miscellaneous Geochemical Analyses

6.12.1 Diabase dyke intruding massive sulphides

Sample SK 27 44, of a diabase dyke intruding massive sulphides, shows moderate enrichment of MgO and Zn, and depletion of CaO, Sr and Na_2O relative to typical spilitized Skidder Basalt (Table 6-35). These geochemical effects are similar to those of less altered rocks from the cl,qz,py alteration zone. This would suggest that Mg-metasomatism continued in the Skidder Prospect area after deposition of the sulphides (see Section 6.15).

6.12.2 K-feldspar-rich masses

Sample SK 37A 39 (Table 6-35), from a chlorite gouge zone, is of rounded masses composed of K-feldspar and quartz in a chlorite matrix (Figure 6-15 is a photograph of the sample). These K-feldspar-rich areas are discussed briefly in Section 6.2.2.5. The sample is enriched in K_2O, Rb and Ba, as would be expected. Surprisingly however, it also has unusually high Zr (415 ppm) and Y (129 ppm) concentrations. These concentrations are much higher than in any other sample analyzed from the Skidder area, e.g. trondhjemite dyke SK 68, which has the next highest Zr and Y concentrations of the Skidder Basalt samples, has a Zr concentration of 220 ppm and an Y concentration of 74 ppm. Trace element concentrations in sample SK 37A 39 are similar to those in some samples of the Silurian Topsails peralkaline granite suite exposed to the northwest of the Skidder Basalt (Taylor et al., 1980; Whalen and Currie, 1983; 1987) (Figure 3-1). These K-feldspar-rich masses may therefore have formed later than the Skidder Basalt; possibly having crystallized from magmatic fluids related to the Topsails igneous event.

Table 6-35: Miscellaneous whole rock geochemical analyses of rocks proximal to the Skidder Prospect

Diabase dyke intruding massive sulphides	
weight %	SK 27 44
SiO_2	48.00
TiO_2	1.20
Al_2O_3	15.40
Fe_2O_3*	10.74
MnO	0.18
MgO	15.01
CaO	0.65
Na_2O	2.45
K_2O	0.03
P_2O_5	0.17
LOI	6.57
Total	100.40
ppm	
Pb	3
Th	0
U	0
Rb	1
Sr	23
Y	21
Zr	68
Nb	7
Zn	188
Cu	41
Ni	78
La	3
Ba	0
V	400
Ce	71
Cr	285
Ga	16
Depth (f)	636.0
Depth (m)	193.9
Distance**	1.8

K-feldspar-rich mass	
weight %	SK 37A 39
SiO_2	54.80
TiO_2	0.56
Al_2O_3	18.20
Fe_2O_3*	5.65
MnO	0.05
MgO	4.43
CaO	1.12
Na_2O	0.28
K_2O	9.30
P_2O_5	0.05
LOI	3.76
Total	98.20
ppm	
Pb	8
Th	7
U	0
Rb	135
Sr	19
Y	129
Zr	415
Nb	9
Zn	156
Cu	8
Ni	4
La	16
Ba	972
V	57
Ce	41
Cr	10
Ga	26
Depth (f)	1510.5
Depth (m)	460.4
Distance**	6.2

(f) feet
(m) metres
* Total iron as Fe_2O_3
** Distance from most intense alteration or massive sulphides

6.13 Rare-Earth Element Geochemistry

6.13.1 Presentation of results

Rare-earth element (REE) concentrations of eight rock samples from the Skidder Prospect are listed in Table 6-36. The REE concentrations were determined according to the method of Fryer (1977) (see Appendix D). Samples chosen for analysis include: an epidotized basalt from the cl,cc,ep±hm alteration zone (sample SK 27 8); a silicified basalt from the cl,cc,qz,ep alteration zone (sample SK 31 522); a basalt from the cl,qz,cc alteration zone (sample SK 28 58); and an intensely chloritized basalt from the cl,qz,py alteration zone (sample SK 27 27). The remaining samples are sulphide rich and comprise: a silicified, pyrite-rich rock from the qz,cl,py alteration zone (sample SK 30 61); semimassive pyrite in chlorite (sample SK 30 74); semimassive pyrite, chalcopyrite and sphalerite in quartz (sample SK 30 80); and massive pyrite, sphalerite and chalcopyrite (sample SK 28 69).

Chondrite-normalized REE patterns for the Skidder Prospect samples presented on Figure 6-83 show two distinct groupings. Analyzed basalts that do not contain appreciable amounts of sulphides have rare-earth element concentrations (Table 6-36), and display chondrite-normalized REE patterns (Figures 6-83 and 6-84) similar to typical spilitized Skidder basalts not affected by the Skidder Prospect mineralizing event(s) (cf. Section 5.3.3). Note that silicified basalt sample SK 31 522 and highly chloritized basalt sample SK 27 27, which analyzed 19.65% MgO in whole rock (Table 6-36), are included in this group.

The sulphide-rich samples are depleted in REE concentrations relative to the others, and their chondrite-normalized REE patterns show different characteristics than the sulphide-poor samples. Some characteristics shown by samples SK 30 74 and SK 28 69, i.e. depletion of Ce relative to La and Nd, and the depletion of Sm, Eu and Gd relative to the light and heavy REE, are similar to those of the REE patterns of hydrothermal crusts sampled from the FAMOUS and TAG areas of the northern Mid-Atlantic ridge

Table 6-36: Representative suite of altered Skidder basalts and sulphide-rich rocks proximal to the Skidder Prospect; rare-earth element chondrite-normalizing values used are those of Taylor and Gorton (1977)

Alteration	Cl,cc,ep ± hm	Cl,cc,qz,ep	Cl,qz,cc	Cl,qz,py
Weight %	SK 27 8	SK 31 522	SK 28 58	SK 27 27
SiO_2	47.10	68.80	47.90	41.50
TiO_2	0.85	0.54	1.16	1.25
Al_2O_3	16.00	10.80	16.70	16.90
Fe_2O_3*	10.54	6.72	11.89	8.54
MnO	0.16	0.05	0.18	0.21
MgO	8.87	0.49	12.25	19.65
CaO	9.52	2.82	1.03	1.34
Na_2O	1.49	5.65	3.23	2.92
K_2O	2.36	0.09	0.06	0.04
P_2O_5	0.13	0.12	0.22	0.16
LOI	3.76	2.19	5.61	8.19
Total	100.78	98.27	100.23	100.70
ppm				
Pb	0	14	7	3
Rb	15	1	2	1
Sr	331	81	45	22
Y	21	29	30	24
Zr	45	68	74	73
Nb	5	4	8	5
Zn	72	25	106	308
Cu	54	41	35	41
Ni	86	0	91	69
Ba	345	25	22	35
V	263	366	404	398
Cr	215	25	307	286
Ga	16	9	14	15

* Total iron as Fe_2O_3

RARE EARTH ELEMENT CONCENTRATIONS

	SK 27 8		SK 31 522		SK 28 58		SK 27 27	
	ppm	chondrite normalized	ppm	chondrite normalized	ppm	chondrite normalized	ppm	chondrite normalized
La	5.4	17.1	6.1	19.4	10.6	33.7	4.2	13.3
Ce	13.7	16.9	17.0	20.9	30.2	37.1	14.9	18.3
Nd	10.5	17.6	14.4	24.1	22.7	38.0	12.4	20.8
Sm	3.2	16.7	4.3	22.4	6.7	34.9	4.0	20.8
Eu	1.2	16.6	1.5	20.8	2.6	36.0	1.2	16.6
Gd	4.2	16.2	4.5	17.4	7.4	28.6	5.2	20.1
Dy	5.5	16.9	4.5	13.8	7.5	23.1	5.4	16.6
Er	2.6	12.2	2.1	9.9	3.0	14.1	2.2	10.3
Total	46.3		54.4		90.7		49.5	
Ratios (chondrite normalized)								
La/Ce		1.0		0.9		0.9		0.7
La/Sm		1.0		0.9		1.0		0.6
Eu/Eu*		1.0		1.0		1.1		0.8

Eu* = (Sm+Gd)/2

Table 6-36 (continued):

	Qz,cl,py	Semimassive pyrite in chlorite	Semimassive pyrite, chalcopyrite and sphalerite in quartz	Massive pyrite, sphalerite and chalcopyrite
Weight %	SK 30 61	SK 30 74	SK 30 80	SK 28 69
SiO_2	50.50	18.30	39.30	15.60
TiO_2	0.22	0.14	0.13	0.02
Al_2O_3	7.07	11.35	2.00	0.50
Fe_2O_3*	22.90	32.80	35.05	44.29
MnO	0.04	0.13	0.01	0.11
MgO	5.32	15.88	0.63	1.10
CaO	0.32	0.54	0.06	7.36
Na_2O	0.02	0.00	0.02	0.02
K_2O	0.80	0.16	0.59	0.00
P_2O_5	0.08	0.04	0.01	0.00
LOI	12.35	20.11	17.78	22.44
Total	99.62	99.45	95.58	91.44
ppm				
Pb	23	43	439	330
Rb	16	11	13	7
Sr	7	5	1	54
Y	10	8	n.d.	n.d.
Zr	43	51	20	20
Nb	5	10	7	10
Zn	158	693	4253	22363
Cu	19	16	26140	16053
Ni	55	45	111	19
Ba	71	0	48	n.d.
V	154	279	40	26
Cr	256	230	248	n.d.
Ga	10	22	2	22

* Total iron as Fe_2O_3
n.d. - not detected

RARE-EARTH ELEMENT CONCENTRATIONS

	ppm	chondrite normalized	ppm	chondrite normalized	ppm	chondrite normalized	ppm	chondrite normalized
La	1.2	3.8	1.1	3.5	0.5	1.6	1.6	5.1
Ce	2.8	3.4	2.1	2.6	0.6	0.7	3.5	4.3
Nd	3.3	5.5	2.0	3.4	0.6	1.0	3.3	5.5
Sm	0.6	3.1	0.2	1.0	n.d.		n.d.	
Eu	0.2	2.8	0.4	5.5	0.1	1.4	n.d.	
Gd	0.9	3.5	1.1	4.2	0.2	0.8	0.4	1.5
Dy	1.5	4.6	2.2	6.8	0.7	2.2	1.5	4.6
Er	1.0	4.7	1.0	4.7	0.4	1.9	0.7	3.3
Total	11.5		10.1		3.1		11.0	
Ratios (chondrite normalized)								
La/Ce		1.1		1.4		2.2		1.2
La/Sm		1.2		3.4				
Eu/Eu*		0.8		2.1				

Eu* = (Sm+Gd)/2

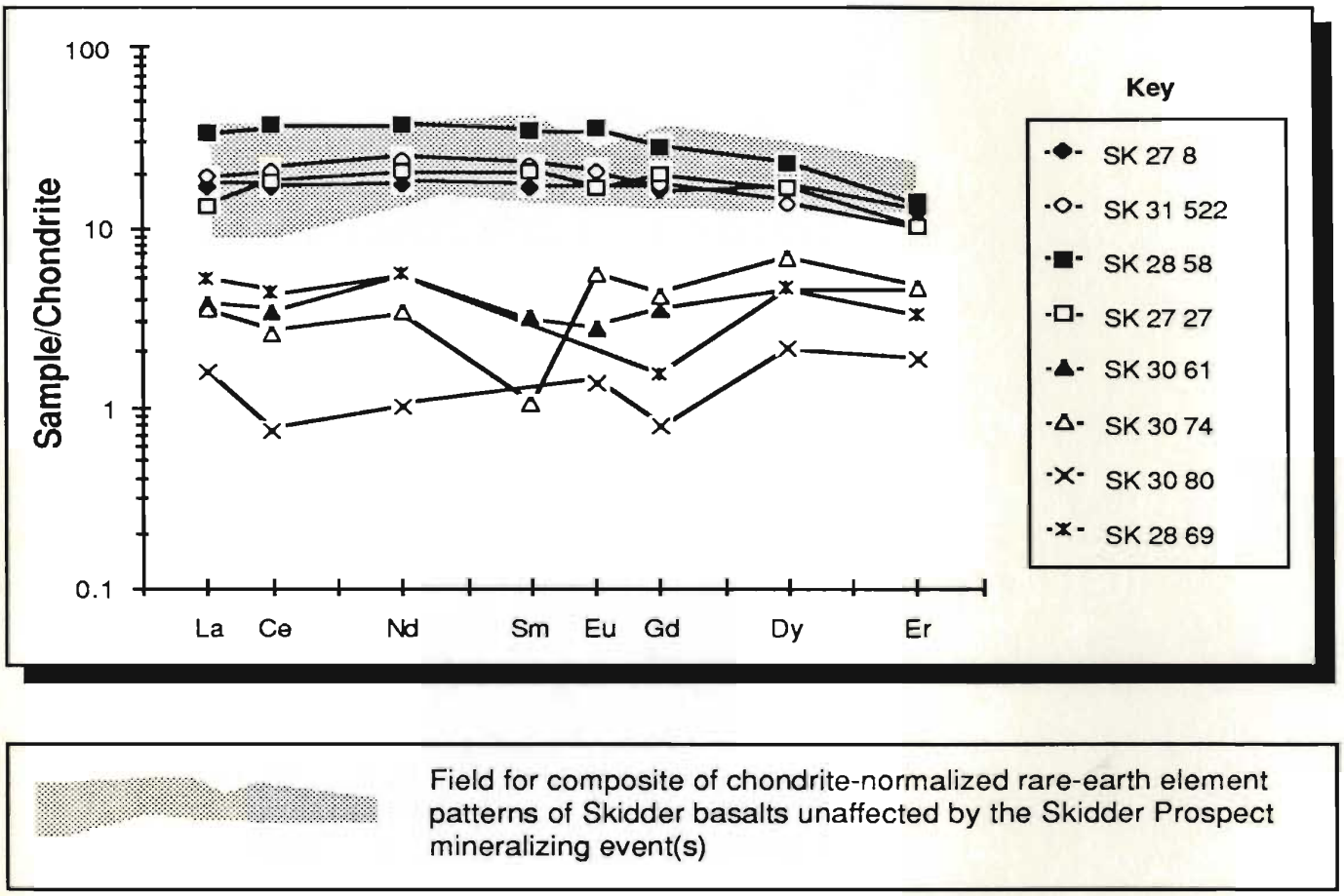

Figure 6-83: Composite of chondrite-normalized rare-earth element patterns of altered rocks proximal to the Skidder Prospect, and sulphide-rich rocks from the prospect itself.

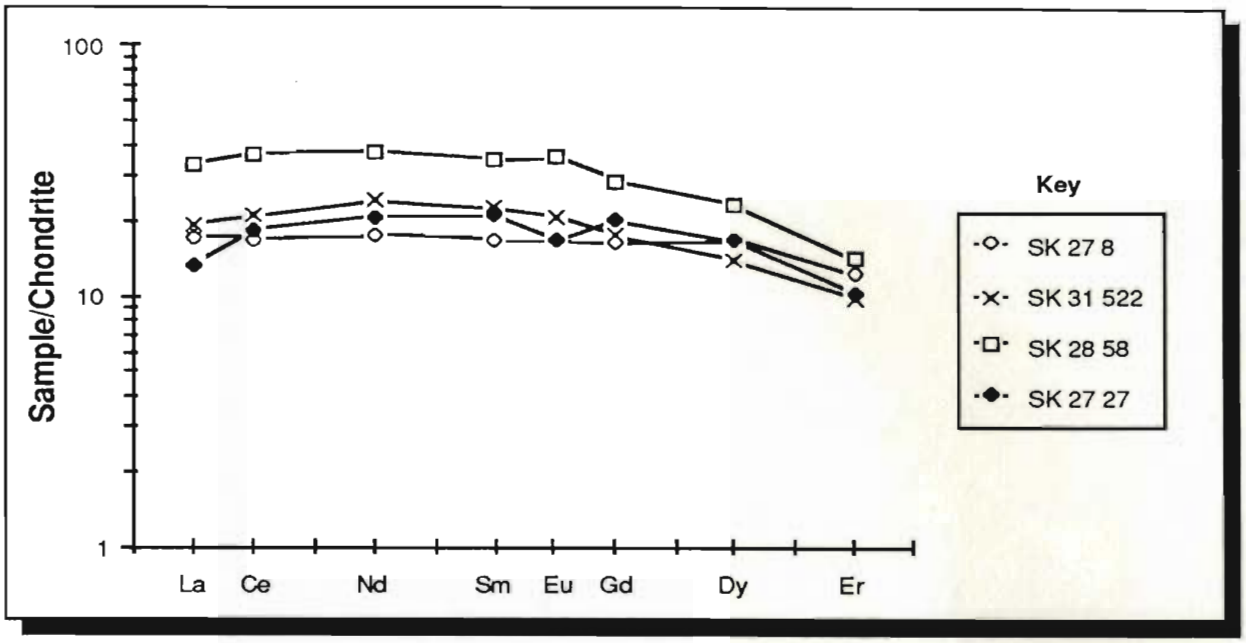

Figure 6-84: Chondrite-normalized rare-earth element patterns for altered, sulphide-poor rocks proximal to the Skidder Prospect.

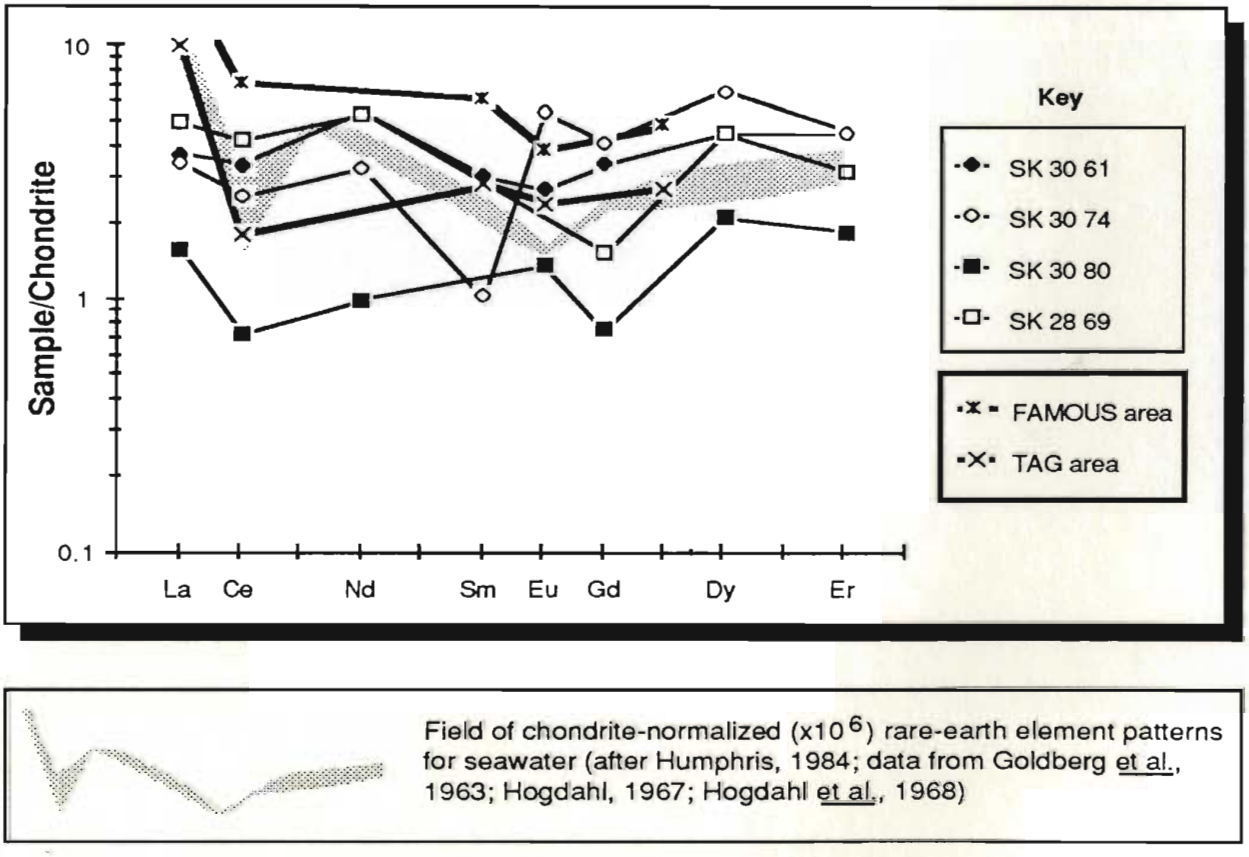

Figure 6-85: Chondrite-normalized rare-earth element patterns for altered, sulphide-rich rocks of the Skidder Prospect. Chondrite-normalized (Taylor and Gorton, 1977) REE patterns for hydrothermal crusts from the FAMOUS and TAG areas calculated from North American shales-normalized (Haskin et al., 1968) REE patterns presented as **Figure 10.10 by Fleet (1984), from original** data of Toth (1980).

(Toth, 1980; Fleet, 1984) (Figure 6-85). Note that the depletion of Ce relative to La is not as pronounced in the Skidder Prospect samples as in those from the FAMOUS and TAG areas. Depletion of Ce and the middle REE are also characteristics of chondrite-normalized REE plots for seawater (Figure 6-85). Samples SK 30 74 and SK 30 80 also show relative Ce depletion and enrichment of the heavy REE, but, unlike the others, they have positive Eu anomalies.

6.13.2 Discussion

The chondrite-normalized REE pattern for SK 31 522 suggests that, where significant amounts of sulphides are not present, the REE have not been mobilized as a result of pervasive silicification and quartz veining.

The similarity of the chondrite-normalized REE pattern for highly chloritized sample SK 27 27 to those of typical spilitized Skidder Basalt samples suggests that the REE have not been leached from the rock, even though the high MgO content of SK 27 27 is suggestive of its interaction with large amounts of heated seawater (e.g. Mottl, 1983a). Menzies et al. (1979) report that glassy tholeiitic basalt completely transformed to a mixed layer chlorite-smectite phase at temperatures of 150-350°C and seawater/rock ratios of 10-125 produced a REE profile very similar to the unaltered basalt. Thus, hydrothermal fluids circulating through a basalt may not be able to effectively leach the REE, even under fluid-dominated conditions, and therefore, the hydrothermal fluid could retain its original relative concentrations of the various REE. The REE characteristics of the hydrothermal fluid may, in this way, be preserved in sulphide-rich rocks where the dominant products are hydrothermal precipitates. The chondrite-normalized REE patterns for the Skidder Prospect sulphide-rich rocks could therefore reflect interaction of Skidder basalts (which show relatively flat chondrite-normalized REE patterns) with hot upwelling hydrothermal fluids having the overall REE depletion, and relative Ce and middle REE depleted characteristics of seawater.

6.13.3 REE characteristics of an altered Skidder trondhjemite dyke

Trondhjemite dyke sample SK 30 51 contains abundant disseminated pyrite, and is from the most intensely altered portion of the Skidder Prospect alteration zone; it was analyzed to check the effects of hydrothermal alteration on REE concentrations in the trondhjemites.

Altered sample SK 30 51 has lower concentrations of all the REE than trondhjemite dyke sample SK 30 1, which has not been extensively altered by the Skidder Prospect mineralizing event(s) (Table 6-37; Figure 6-86). However, compared to trondhjemite pod sample S 68, it has similar concentrations of most of the REE. The altered sample has a much more pronounced negative Eu anomaly than the others.

Table 6-37: Geochemistry of a sulphide-bearing trondhjemite dyke that intrudes intensely altered rocks of the Skidder Prospect

weight %	SK 30 51
SiO_2	83.50
TiO_2	0.10
Al_2O_3	8.84
Fe_2O_3*	0.18
MnO	0.01
MgO	0.16
CaO	0.18
Na_2O	3.75
K_2O	0.75
P_2O_5	0.02
LOI	1.00
Total	98.49
ppm	
Pb	3
Rb	10
Sr	37
Y	51
Zr	159
Nb	6
Zn	40
Cu	20
Ni	0
La	3
Ba	45
V	7
Ce	82
Cr	10
Ga	11
Depth (feet)	752.5
Depth (metres)	229.4
Distance**	12.6

* Total iron as Fe_2O_3

** Distance from most intensely altered rocks in the drill hole

RARE-EARTH ELEMENT CONCENTRATIONS

	SK 30 51	
	ppm	chondrite normalized
La	14.2	45.1
Ce	39.4	48.5
Nd	26.4	44.2
Sm	6.8	35.4
Eu	0.4	5.5
Gd	6.6	25.5
Dy	7.0	21.5
Er	3.9	18.3
Total	104.7	
Ratios (chondrite normalized)		
La/Ce		0.9
La/Sm		1.3
Eu/Eu*		0.2

Eu* = (Sm+Gd)/2

Chondrite-normalizing values used are those of Taylor and Gorton (1977)

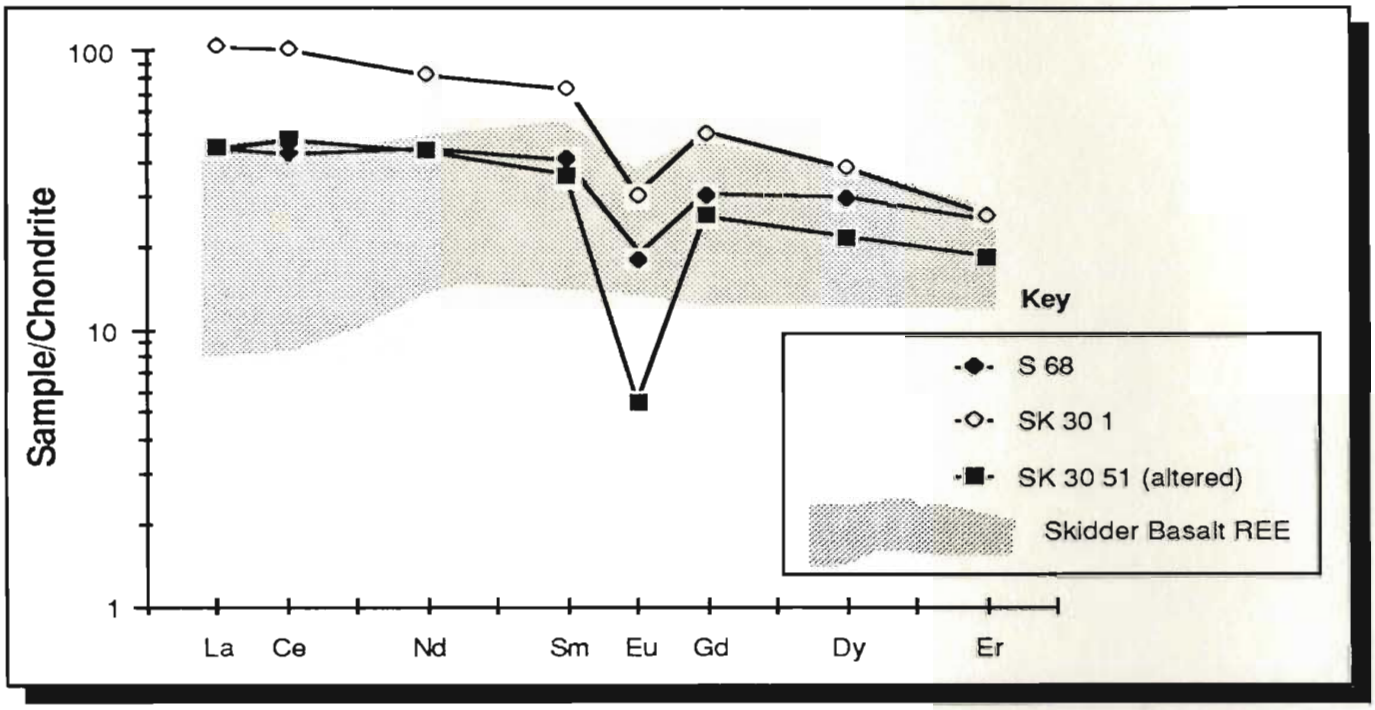

Figure 6-86: Chondrite-normalized (Taylor and Gorton, 1977) rare-earth element pattern for pyrite-rich altered trondhjemite sample SK 30 51 compared to other Skidder area trondhjemites; range of Skidder Basalt REE concentrations shown for comparison.

6.14 Lead Isotopes

6.14.1 Preamble

Three of the four isotopes of lead, i.e. ^{206}Pb, ^{207}Pb and ^{208}Pb, are radiogenic, produced from radioactive breakdown of ^{238}U, ^{235}U and ^{232}Th respectively. Hence, within a closed system, the amounts of each of the radiogenic Pb isotopes will increase with time relative to the stable Pb isotope ^{204}Pb, the amount of the increase being dependent on the amounts of ^{238}U, ^{235}U and ^{232}Th initially present, and their decay constants. The Holmes-Houtermans lead evolution model (Holmes, 1946; 1947; 1949; Houtermans, 1946) assumed such a closed system and presented a series of growth curves originating at time T, which represented the age of the earth as determined from lead in the troilite phase of the Canyon Diablo meteorite. Lead isotope ratios from several massive sulphide deposits were found by Stanton and Russell (1959) to fit reasonably well such a single-stage growth curve. The model ages determined for these deposits from the lead-lead isotope ratios also corresponded relatively well with ages determined for the deposits by other methods.

Improvements in the determinations of lead isotopes, including the redetermination of lead isotopes in the Canyon Diablo meteorite (Tatsumoto et al., 1973), and refinements in the decay constants of uranium and thorium, shifted the growth curves such that they did not fit the stratabound sulphides lead isotope data; and model ages for the deposits no longer matched ages determined by other methods (see review by Köppel and Grünenfelder, 1979). To adjust the revised lead isotope growth curves such that they again accommodated the stratabound sulphides data, Stacey and Kramers (1975) proposed a two-stage lead isotope growth curve; the first stage ending at 3.7 billion years ago, at which time they propose a major differentiation of the earth into a crust and mantle, the former enriched in Th and U relative to the latter. Cumming and Richards (1975) (cf. Sinha and Tilton, 1973) proposed an alternative to the Stacey and Kramers (1975) model. Cumming and Richards (1975) used a linear increase in the $^{238}U / ^{204}Pb$ ratio and the $^{232}Th / ^{204}Pb$

ratio with time to adjust the lead evolution curve such that it fits the stratabound sulphide data. By forcing their curve through the Canyon Diablo meteorite lead isotope data and through the lead isotope data of the Captains Flat, Australia stratabound massive sulphide deposit, and by using an age of 430 million years for the latter, they found that their model yielded acceptable ages for the other sulphide deposits investigated by them.

The plumbotectonics lead isotope evolution models of Doe and Zartman (1979) (version I) and Zartman and Doe (1981) (version II) involves a more complex, multistage model, which differentiates between leads from three environments, i.e. the mantle, upper crust and lower crust. They suggest that oceanic tholeiite basalts, which probably best represent mantle leads, have lead isotope ratios notably deficient in both ^{206}Pb and ^{207}Pb compared to continental-crust-derived leads. They explain the more radiogenic upper-crustal lead isotope ratios as having resulted from their derivation from material having a high in situ ^{238}U / ^{204}Pb ratio, and by this ratio gradually increasing with time. According to them, the lower crust is somewhat depleted in uranium but only slightly depleted in Pb and Th, consequently, leads from this environment have a lower ^{238}U / ^{204}Pb ratio, and are depleted in ^{206}Pb and ^{207}Pb but not in ^{208}Pb relative to the upper crust and mantle. The fourth environment included in the plumbotectonics model, i.e. the orogene, represents a mixed medium with contributions from the upper and lower crust, and the mantle. Island arc volcanic rocks, according to Zartman and Doe (1981), represent mixtures of MORB and continent-derived material brought together in an orogenic environment. They suggest that primitive island arcs away from continents will have Pb isotope ratios similar to MORB, but more mature arcs close to continents will have Pb isotope ratios that are influenced by adjacent continental crust.

6.14.2 Presentation of data

Lead isotope ratios of Skidder Prospect sulphide mineral samples described in Table 6-38 are presented by Cumming and Krstic (1987), and reproduced in Table 6-39.

Table 6-38: Descriptions of Skidder Prospect samples analyzed for lead isotope ratios.

Sample	Depth feet	Depth metres	Description
SK 35A 6	1570.9'	478.8 m	Layered massive sulphides
SK 27 37	578.5'	176.3 m	Layered massive sulphides
SK 28 63	669.0'	203.9 m	Layered massive sulphides
SK 29 52	788.5'	240.3 m	Sphalerite- and chalcopyrite-bearing quartz veins plus pyrite
SK 35A 3	1507.0'	459.3 m	Layered massive sulphides

Table 6-39: Lead isotope ratios of the Skidder Prospect sulphide samples (after Cumming and Krstic, 1987).

Sample Number	GSC Sample Number	$^{206}Pb / ^{204}Pb$	$^{207}Pb / ^{204}Pb$	$^{208}Pb / ^{204}Pb$	Comment
SK 35A 6	KQ 83 72	17.639	15.457	37.458	
SK 27 37	KQ 83 73	17.586	15.445	37.498	
SK 28 63	KQ 83 77	17.638	15.452	37.491	leach
		17.644	15.445	37.464	residue
SK 29 52	KQ 83 78	17.634	15.445	37.461	leach
		17.629	15.442	37.463	residue
SK 35A 3	KQ 83 80	17.685	15.455	37.481	leach
		17.684	15.455	37.492	residue

6.14.3 ^{207}Pb / ^{204}Pb vs. ^{206}Pb / ^{204}Pb ratios

On Figure 6-87, the Skidder Prospect ^{206}Pb / ^{204}Pb and ^{207}Pb / ^{204}Pb lead isotope ratios are compared to those of other Newfoundland mineral deposits. Of the deposits compared, the Skidder Prospect leads, along with those of Catchers Pond, have the lowest ^{206}Pb / ^{204}Pb and ^{207}Pb / ^{204}Pb ratios, and plot at the low radiogenic lead portion of a discontinuous linear trend defined by leads from the various Newfoundland mineral deposits (cf. Swinden and Thorpe, 1984). The Skidder Prospect leads plot along the mantle lead evolution curve (version II) of Zartman and Doe (1981), below their orogene and upper crustal lead evolution curves, and below the lead evolution curve of Stacey and Kramers (1975) (Figure 6-87).

Examination of Figure 6-87 shows that a gap exists in the trend defined by the Newfoundland mineral deposit leads at a ^{207}Pb / ^{204}Pb ratio of 15.7. Of the Newfoundland mineral deposit leads having a ^{207}Pb / ^{204}Pb ratio above 15.7, the Victoria Lake, Wild Bight and Pacquet Harbour Group deposits plot close to the orogene evolution curve of Zartman and Doe (1981), and leads of the Barasway de Cerf deposit (Baie d'Espoir Group) and the Strickland deposit (Baie du Nord Group) plot close to their upper crustal lead evolution curve (Figure 6-87). Swinden and Thorpe (1984) make two alternative suggestions to account for this variation in the lead isotope ratios. They suggest that contemporaneous volcanic activity may have occurred, in an oceanic environment for the less radiogenic Victoria Lake Group mineral deposits, and at or near a continental margin for the more radiogenic Baie d'Espoir and Baie du Nord Group deposits. As an alternative, they suggest that volcanic activity may have been slightly diachronous, whereby early ensimatic volcanism, with which the less radiogenic lead-bearing mineral deposits are associated, was followed by migration of the volcanic centres toward the continental margin, resulting in some incorporation of more radiogenic continental crustal leads in the more radiogenic lead-bearing mineral deposits. Swinden and Thorpe (1984) propose that the mineral deposits having ^{207}Pb / ^{204}Pb ratios above 15.7 may have

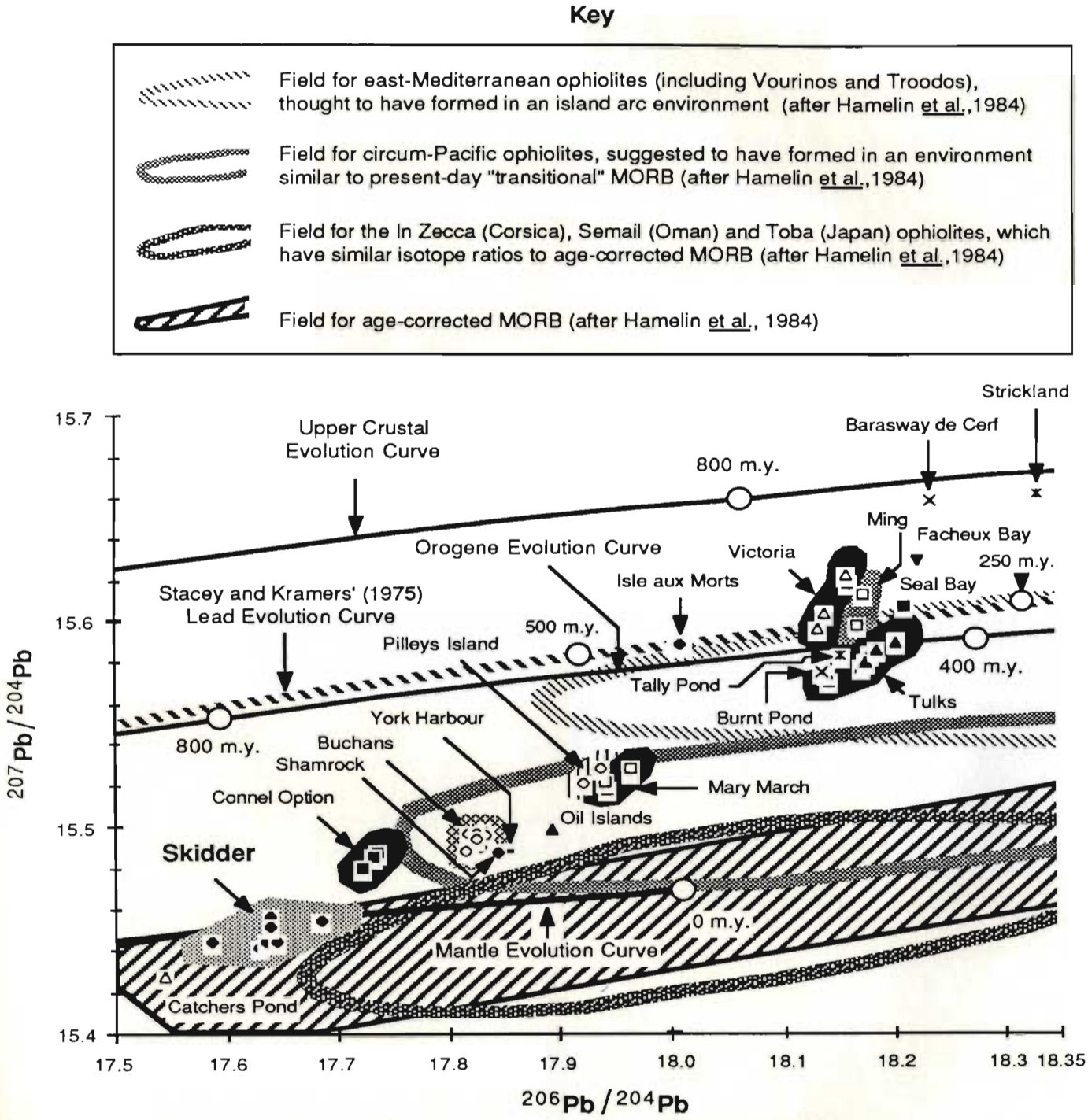

Figure 6-87: $^{207}Pb/^{204}Pb$ vs. $^{206}Pb/^{204}Pb$ for the Skidder Prospect leads compared to those of other Newfoundland mineral deposits. Data for the Skidder Prospect, Connel Option and Mary March deposits; and some for the Buchans, Tulks and Victoria deposits taken from Cumming and Krstic (1987); the Isles aux Morts data is from O'Neill (1985), and the remainder from Swinden and Thorpe (1984). Lines for mantle, orogene, upper crustal and lower crustal evolution curves from data presented in Zartman and Doe (1981) (version II of their model). Abbreviation: m.y. - million years.

incorporated relatively radiogenic lead from the Precambrian Avalon terrane continental crust; whereas the less radiogenic Buchans, Roberts Arm and Cutwell Group deposits, which have ^{207}Pb / ^{204}Pb ratios below 15.7, have incorporated leads from a less radiogenic source, such as the Grenvillian continental crust of the North American craton (cf. Fletcher and Farquhar, 1977; Bell and Blenkinsop, 1981).

The Skidder Prospect leads are less radiogenic than those of the Buchans Group deposits, which, with the exception of those of the Connel Option deposit, form a tight cluster. The linear trend between the Catchers Pond/Skidder Prospect leads and the Mary March/Pilleys Island leads may represent a mixing line resulting from incorporation of material from increasingly more radiogenic lead sources.

The relatively radiogenic-lead-depleted nature of the Skidder Prospect lead isotopes suggests their derivation from a relatively radiogenic-lead-depleted source, but whether this source was the Early Ordovician mantle is uncertain; for instance, leads from the York Harbour deposit of the Bay of Islands Ophiolite Complex, which represent a possible example of Early Ordovician mantle, are more radiogenic than those of the Skidder Prospect.

Results of a study by Hamelin et al. (1984) of lead isotope ratios from samples of eleven Mediterranean and circum-Pacific ophiolites showed three groupings on the basis of ^{207}Pb content. The In Zecca (Corsica), Semail (Oman) and Toba (Japan) ophiolite complexes have ^{207}Pb / ^{204}Pb ratios similar to those of the least radiogenic present-day MORB; the circum-Pacific ophiolite complexes have higher ^{207}Pb / ^{204}Pb ratios, which are comparable to transitional portions of oceanic ridges; and the Troodos, Vourinos and Antaly ophiolites have the highest ^{207}Pb / ^{204}Pb ratios, suggesting incorporation of continental-crustal-lead component, and possible origin in an island arc environment (Hamelin et al., 1984) (Figure 6-87). The Skidder Prospect leads plot within the field for age-corrected MORB leads, and along the trend of the field for leads of the In Zecca, Semail and Toba ophiolite complexes. Note that leads from the Newfoundland Victoria

Lake Group mineral deposits (Swinden and Thorpe, 1984) plot in the field defined by the most radiogenic lead-bearing ophiolites (Figure 6-87).

6.14.4 $^{208}Pb / ^{204}Pb$ vs. $^{206}Pb / ^{204}Pb$ ratios

As shown on Figure 6-88, the Skidder Prospect leads are also depleted in ^{208}Pb compared to most other Newfoundland mineral deposit leads. The two groups of more and less radiogenic Newfoundland mineral deposit leads, separated by a gap in the trend of $^{207}Pb / ^{204}Pb$ ratios at 15.7, are similarly separated by a gap in the trend of $^{208}Pb / ^{204}Pb$ ratios at 37.8 (Figure 6-88).

Of the mineral deposits having $^{208}Pb / ^{204}Pb$ ratios less than 37.8, the Skidder Prospect leads, most of the Buchans Group deposit leads (except those from the Mary March area) and the Catchers Pond leads plot to the left of the orogene, mantle and upper crustal evolution curves of Zartman and Doe (1981), and to the left of the lead evolution curve of Stacey and Kramers (1975) (Figure 6-88). Compared to the Buchans and most of the other data, the Pilleys Island, Mary March and Oil Island leads are offset to a higher $^{206}Pb / ^{204}Pb$ ratio at a given $^{208}Pb / ^{204}Pb$ ratio; they plot on the mantle orogene curve of Zartman and Doe (1981). The York Harbour deposit is offset to lower $^{206}Pb / ^{204}Pb$ and $^{208}Pb / ^{204}Pb$ ratios relative to the others and plots between the upper crustal and mantle evolution curves of Zartman and Doe (1981).

Of the Newfoundland mineral deposits having $^{208}Pb / ^{204}Pb$ ratios greater than 37.8, leads from the Tally Pond and Burnt Pond deposits plot to the right of the orogene curve of Zartman and Doe (1981), in a similar position, relative to this curve, as the leads from the Pilleys Island and Mary March deposits. Leads from the Tulks deposits plot on Zartman and Doe's (1981) orogene curve; leads from the remainder of the deposits plot to the left of the orogene curve, in a similar relative position as the Buchans Group, etc., deposits.

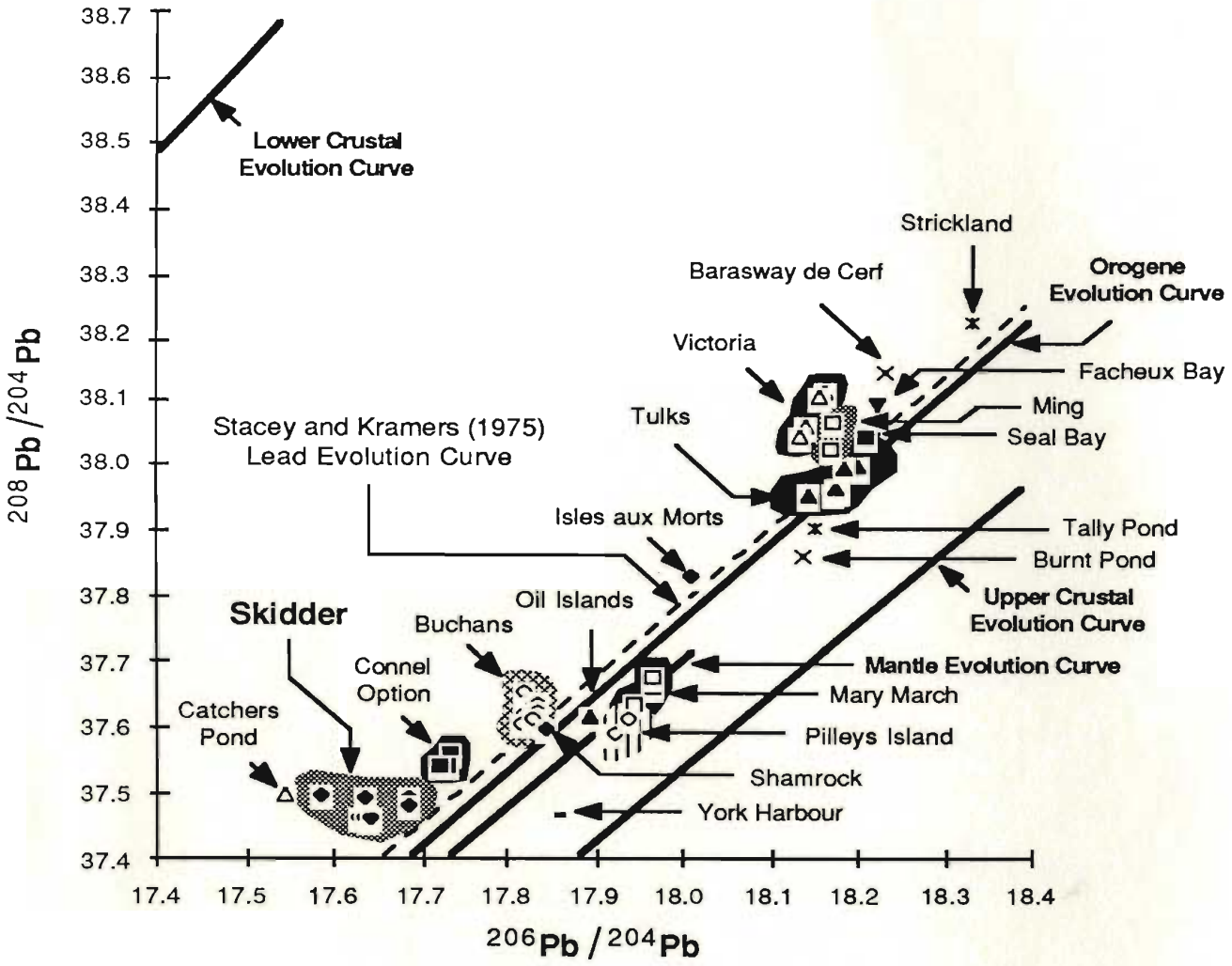

Figure 6-88: $^{208}Pb / ^{204}Pb$ vs. $^{206}Pb / ^{204}Pb$ ratios for the Skidder Prospect leads compared to those of other Newfoundland mineral deposits. Data for the Skidder Prospect, Connel Option and Mary March deposits; and some for the Buchans, Tulks and Victoria deposits taken from Cumming and Krstic (1987); the Isles aux Morts data is from O'Neill (1985), and the remainder from Swinden and Thorpe (1984). Lines for mantle, orogene, upper crustal and lower crustal evolution curves from data presented in Zartman and Doe (1981), their model version II; note that the mantle and orogene evolution curves are slightly different from those shown on Figure 5 of Zartman and Doe (1981). Since, using their numerical data, the curves plot as shown above, not as shown on their Figure 5, an error is suggested in their plot.

The offset of several Newfoundland mineral deposit leads, including those of the Skidder Prospect, to the left of Zartman and Doe's (1981) orogene, mantle and upper crustal lead evolution curves, and the lead evolution curve of Stacey and Kramers (1975) suggest that they have been derived from a slightly uranium-depleted/thorium-enriched source relative to sources used in the calculation of these model curves. Lead isotope ratios used by Zartman and Doe (1981) to calculate their lower crustal evolution curve show a somewhat more extreme effect of lead evolution in a uranium-depleted/thorium-enriched environment.

6.14.5 Model ages

A linear regression line through the Skidder Prospect ^{207}Pb / ^{204}Pb vs. ^{206}Pb / ^{204}Pb data confirms the suggestion by Cumming and Krstic (1987) that the data lie along a line of shallow slope. This line intersects Zartman and Doe's (1981) mantle evolution curve at an unrealistically young age of 230 million years (Figure 6-89). The line intersects Zartman and Doe's (1981) mantle lead evolution curve again at 1.6 billion years on a plot of ^{207}Pb / ^{204}Pb vs. ^{206}Pb / ^{204}Pb; it intersects the Stacey and Kramers (1975) lead evolution curve at 2.09 billion years on this plot. Between-sample point scatter for the Skidder Prospect lead isotope ratios results in model age estimates between 210 and 290 million years according to the model of Zartman and Doe (1981), and between 530 and 580 million years using the lead evolution model presented by Swinden and Thorpe (1984). Ages determined by U-Pb in zircons for rocks in the Skidder Area include 473^{+3}_{-2} Ma for the Buchans Group (Dunning et al., 1987), and $477{:}5^{+2.6}_{-2}$ or $481.4^{+4}_{-1.9}$ Ma for the Annieopsquotch Ophiolite Complex (Dunning and Krogh, 1985). Assuming that the Skidder Basalt is similar in age to the Annieopsquotch ophiolite, model lead ages for the Skidder Prospect based on Zartman and Doe's (1981) model are unrealistically young, and ages based on Swinden and Thorpe's (1984) model are probably too old. The discrepancy

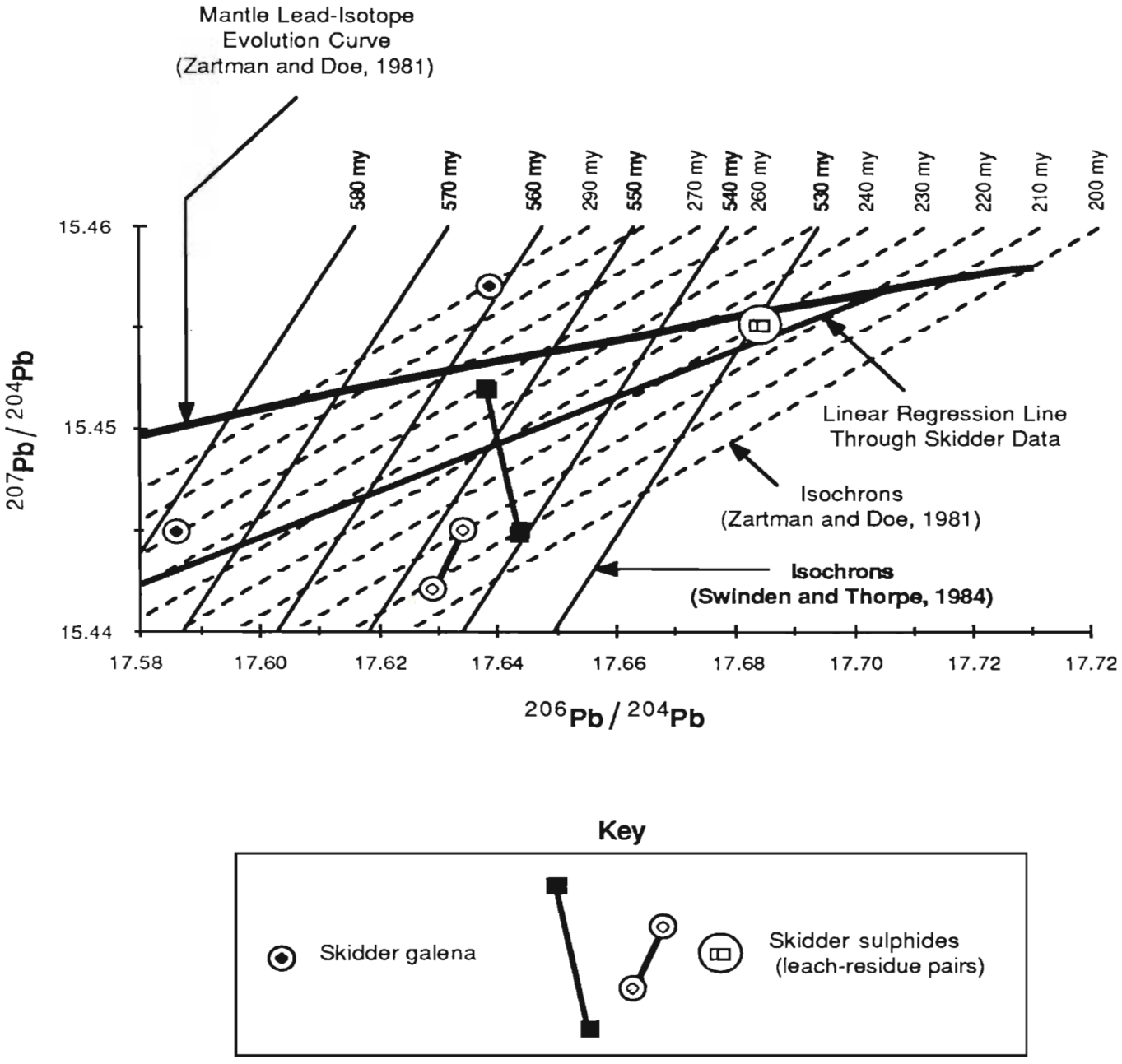

Figure 6-89: $^{207}Pb/^{204}Pb$ vs. $^{206}Pb/^{204}Pb$ for the Skidder Prospect leads. Data taken from Cumming and Krstic (1987). The Zartman and Doe (1981) isochrons have been determined by proportionately dividing into 10 million-year intervals the time between their 0 and 400 million-year mantle and orogene isochrons. The Swinden and Thorpe (1984) isochrons have been extrapolated to older ages on the basis of 10 million-year intervals determined by proportionately dividing the time between the 300 and 500 million year isochrons shown on their Figure 10.

between the age estimates according to the two different models serves to illustrate the model dependency and unreliability of model lead ages.

Cumming and Krstic (1987) suggest two alternative explanations for the scatter of Pb-isotope ratios shown by the Skidder Prospect leads, viz. accumulation of radiogenic lead in the sulphides from the time of ore formation to the present day, or an episodic addition of lead for a short period some time after its initial deposition, e.g. recrystallization of the leads during the Topsails igneous episode. The latter explanation is supported by the presence of small K-feldspar-rich masses noted in one or two areas in the Skidder Prospect drill core; these masses have high Zr (415 ppm) and Y (129 ppm) concentrations and may be related to later magmatic activity associated with the Topsails igneous episode.

6.15 General Discussion and Summary

6.15.1 Geologic setting

The Skidder Prospect has more similarities to massive sulphide deposits in ophiolite sequences (e.g. Constantinou and Govett, 1973; Constantinou, 1980; Franklin et al., 1981; and references therein) than do other deposits in the Buchans area, which are considered similar to the Kuroko ore deposits of Japan (Thurlow, 1973; Thurlow et al., 1975). The massive and disseminated sulphides, and spatially related jasper comprising the Skidder Prospect are hosted within basaltic pillow lavas, mafic pillow breccias and aquagene tuffs of the Skidder Basalt, shown in Chapters 4 and 5 to be of ophiolitic affinity. Variolitic pillowed basalts, typically having Zr concentrations less than 60 ppm, are immediate hosts to most of the sulphide-rich units.

Massive pyrite, chalcopyrite and lesser sphalerite bodies occur as stratiform lenses and stockwork zones within pillow lava sequences in ophiolites throughout the world. Examples are documented from Cyprus, Newfoundland, Turkey, Oman, and from the Norwegian Caledonides. The massive sulphide deposits typically occur within the lower part of the pillow lavas, immediately above the sheeted dykes, as at Betts Cove Newfoundland (Upadhyay and Strong, 1973; Saunders and Strong, 1986); or between two, often chemically distinct, pillow lava sequences, as do most of the deposits within the Troodos ophiolite, Cyprus. The Skouriotissa orebody of Cyprus is an exception in that it occurs at the top of the pillow lavas, beneath overlying sedimentary rocks.

In Newfoundland, ophiolite-associated massive sulphide deposits (other than the Skidder Prospect) occur in the Lushs Bight Group, and in the Betts Cove and Bay of Islands ophiolites. In the Lushs Bight Group, which is composed of spilitized pillow lavas and sheeted dykes considered to be of ophiolite affinity (e.g. Strong, 1973; Kean, 1983; 1984), the sulphide deposits are associated with chlorite shear zones (Peters, 1967; Kean, 1983; 1984). Several small sulphide showings occur in chlorite shear zones within the sheeted diabase dykes (Kean, 1984); the larger deposits, however, occur either in pillow

lavas within a few hundred metres of sheeted dykes, e.g. in the Little Bay area, or in pillow lavas and intercalated tuffs that show no obvious spatial relationship with the sheeted dykes, e.g. the Whalesback and Little Deer deposits (Kean, 1984). The Tilt Cove and Betts Cove deposits (Upadhyay and Strong, 1973; Saunders and Strong, 1986; Strong and Saunders, in press) occur near the base of the Betts Cove Ophiolite pillow lavas. Massive sulphide mineralization at York Harbour in the Bay of Islands Ophiolite occurs at the contact between two mafic pillow lava units, the lower of which is more altered and less magnetic than the upper (Duke and Hutchinson, 1974).

Several of the massive sulphide deposits associated with the Oman Ophiolite occur in the upper portion of the Geotimes basalt unit, near the contact with the overlying Lasail Unit (Alabaster and Pearce, 1985). The Geotimes Unit is compositionally intermediate between mid-ocean ridge basalts and island arc tholeiites, and is interpreted to have formed in a marginal basin setting (Alabaster et al., 1982; Alabaster and Pearce, 1985). The overlying Lasail Unit comprises a sequence of basic to felsic volcanic rocks that have geochemical characteristics of the island arc tholeiite series, and are interpreted to represent off-axis seamount volcanism (Alabaster and Pearce, 1985). The Lasail massive sulphide deposit, one of the massive sulphide deposits that occurs at the top of the Geotimes Unit, is interpreted to have formed from hydrothermal circulation localized around an isolated magma cupola, from which the Lasail Unit volcanic lavas later erupted (Alabaster and Pearce, 1985).

Authors of earlier papers generally concluded that ophiolite-related sulphide deposits were formed on or near ridge axes associated with major oceanic spreading centres; a notable exception being Miyashiro (1973), who suggested that the Troodos ophiolite, Cyprus, probably formed in an island arc environment. Malpas and Robinson (1983) state that the extrusive suite of the Troodos ophiolite in Cyprus is composed of two distinct magmatic suites, viz. a lower arc tholeiitic suite composed of andesite and rhyodacite, and an upper boninitic suite of basalts and basaltic andesites. These two

distinct magmatic suites are also present in the sheeted dyke complex. Malpas and Robinson (1983) also state that structural relationships suggest that the plutonic sequence was formed from a series of relatively small, isolated magma chambers. They conclude that the ophiolite formed in a supra-subduction zone environment, not at a mid-ocean ridge spreading centre (cf. Miyashiro, 1973).

Alabaster (1983) concludes that massive sulphide deposits of the Oman ophiolite were formed above magma chambers undergoing "closed system fractionation and periodic expulsion away from the ridge axis". He further states that the ridge axis was located in a marginal basin environment.

On the basis of mineral and whole rock geochemistry presented in Chapters 4 and 5 the Skidder Basalt is suggested to have formed in a slow spreading oceanic or back-arc-basin ridge environment.

6.15.2 Structure

A northeast-trending lineament passing through the Skidder Prospect and through a pyrite-rich zone about 2.5 km to the northeast of it is suggested in Section 3.9 to represent a locus for hydrothermal fluids related to formation of the Skidder Prospect. Many of the Cyprus orebodies are immediately adjacent to steep normal faults and are interpreted to have been formed in fault-controlled basins (Adamides, 1980). Hutchinson and Searle (1971) suggest the faults there may be synvolcanic features, which, according to Oudin et al. (1981), may be reactivated after ore deposition. Adamides (1980) indicates that the tectonic zones in which the Cyprus ore deposits occur typically have large length to width ratios, being bounded on one side by faults and on the other by premineralization lavas.

6.15.3 Composition

Most ophiolite-type massive sulphide deposits are mineralogically simple.

Pyrite, chalcopyrite, sphalerite and very minor galena are the only sulphide minerals identified in the Skidder Prospect. Pyrite is ubiquitous, occurring as disseminated grains, in veins and as massive intergrowths. It is by far the dominant sulphide, ranging in content from 5 to 10% in less altered rocks; from 10 to 80% in quartz within the most intensely altered portion of the stockwork zone; and from 80 to 90% in massive sulphide portions of the prospect. Lesser amounts of sphalerite and chalcopyrite occur either interstitial to pyrite, or in quartz veins that cut massive sulphides.

Massive sulphide deposits in the Lushs Bight Group, Newfoundland consist mostly of pyrite accompanied by lesser amounts of chalcopyrite, sphalerite and, in contrast to the Skidder Prospect, pyrrhotite (Kean, 1984). Pyrite, chalcopyrite and irregularly dispersed sphalerite comprise massive sulphide deposits in the Betts Cove Ophiolite (Upadhyay and Strong, 1973; Saunders and Strong, 1986). Irregular masses of pyrite containing lesser sphalerite and chalcopyrite comprise the York Harbour Deposit in the Bay of Islands Ophiolite (Duke and Hutchinson, 1974).

Oudin et al. (1981) describe the Cyprus deposits as having a disseminated pyritic stockwork zone underlying the ore that becomes massive near the top, where it is enriched in copper and locally in zinc. Constantinou (1980) indicates that the Cyprus ores typically contain a massive sulphide zone, a sulphide with silica zone and a lower stockwork zone. The sulphide with silica zone contains variable amounts of Zn, Cu and Fe sulphides intimately mixed with chalcedony and jasper, the latter two components being younger than the sulphides. The massive sulphide section of the orebodies typically consists of massive, porous, colloform-banded blocks of pyrite, marcasite, chalcopyrite and sphalerite within a finer grained sand-sized sulphide matrix. Constantinou (1976) attributes the conglomeratic nature of the ore to secondary leaching during oxidation of pyrite by sea water.

Intensely silicified units, consisting of massive and vein quartz and lesser pyrite, are in contact with massive sulphides in Skidder Prospect drill holes SK 28 (Figure 6-18) and SK 29 (Figure 6-21). Constantinou (1980) suggests that the silica with sulphide zone in the Cyprus deposits is formed by replacement of the sulphides by silica. Hekinian and Fouquet (1985) report that, in the modern hydrothermal deposits located at 13°N on the East Pacific Rise, silica completely replaces pyrite in places. It is plausible therefore that the pyrite-bearing silicified units in immediate proximity to the massive sulphides in the Skidder Prospect formed in a similar manner, i.e. by replacement of the sulphides by silica during continued hydrothermal activity, after sulphide deposition. Intensely silicified, sulphide-bearing zones that underlie the massive sulphide units of the Skidder Prospect, e.g. those noted in drill holes SK 30 and SK 34 (Figure 6-3), probably formed in a different manner, i.e. by replacement of basalt (not previously deposited sulphides) by silica and pyrite, which was deposited from upwelling hydrothermal fluids (see further discussion in Section 6.15.10 below).

6.15.4 Ore petrography

In the Skidder Prospect, pyrite typically occurs as subhedral grains where surrounded by quartz, and as angular anhedral grains in the very few places where it is immediately surrounded by chlorite. Pyrite, where surrounded by sphalerite or chalcopyrite, is typically more anhedral than where surrounded by quartz, and in many areas is embayed along grain edges and cleavage cracks. Fractures in the pyrite are cemented by the chalcopyrite or sphalerite. Chalcopyrite and sphalerite are typically intricately intergrown, and, in many areas, contain irregular anhedral inclusions of one mineral within the other (Figure 6-59). Chalcopyrite is also present in quartz veins where it occurs as anhedral, dendritic masses. The minor amounts of galena occur as anhedral grains intergrown with chalcopyrite, sphalerite or a combination of these minerals. Hematite and magnetite occur in polished section SK 27 42C. Hematite laths have been

almost perfectly pseudomorphed by magnetite in some places. The hematite is, in places, intergrown with chalcopyrite, and, in some areas, magnetite-pseudomorphed hematite laths are enclosed in pyrite.

Several of the ore mineral textures in massive sulphide deposits within the Semail ophiolite, Oman, as reported by Ixer et al. (1984), are similar to those of the Skidder Prospect. These include fractured subhedral pyrite cemented by chalcopyrite, intimate intergrowth of chalcopyrite and sphalerite, intergrowth of chalcopyrite and hematite, and enclosure of hematite in pyrite. Colloform pyrite textures reported by Ixer et al. (1984) were not observed in the Skidder Prospect ores. However, botryoidal hematite in jasper associated with the Skidder Prospect show textures similar to colloform pyrite (see further discussion in Section 6.15.10.6 below).

6.15.5 Paragenesis

Caution is advised when suggesting an ore mineral paragenesis for massive sulphide deposits since, as discussed below, modern massive sulphide deposits, which are possible analogs to ancient massive sulphide deposits, form in a dynamic environment where physical and chemical conditions and changing fluid compositions within the deposit subject early formed sulphides to recrystallization, and replacement by later-forming sulphides. Brecciation and sometimes transportation of the ore as well as submarine weathering are also an integral part of the process.

The form energy of the minerals themselves can also result in a mistaken paragenetic sequence, e.g. it may be concluded, by mistake, that pyrite, which has a strong tendency to form euhedral crystals (Craig, 1983), has formed before chalcopyrite and sphalerite, which typically occur as anhedral masses.

Pyrite, magnetite and sphalerite are refractory enough to retain original growth features through mild metamorphism (Craig, 1983). McClay and Ellis (1983) demonstrate that primary textures are preserved by pyrite up to mid-upper-greenschist facies

metamorphism. Due to the hardness and brittleness of pyrite, it often exhibits cataclastic textures as a result of dynamic metamorphism; recrystallization and development of 120° triple junctions, which are characteristic of equilibrated annealed textures, are common during thermal metamorphism (Craig, 1983; McClay and Ellis, 1983).

According to Upadhyay and Strong (1973), pyrite is the earliest phase to crystallize in mineral occurrences of the Betts Cove area; chalcopyrite occurs next, as disseminated stringers and as anhedral masses interstitial to euhedral pyrite crystals, it also fills fractures within highly brecciated pyrite grains; sphalerite appears last, filling fractures in both chalcopyrite and pyrite.

Ixer et al. (1984) indicate a paragenesis for the Oman massive sulphide deposits of: i) early euhedral pyrite ± hematite, magnetite and chalcopyrite; ii) colloform pyrite ± marcasite; iii) chalcopyrite, sphalerite ± bornite; and iv) late rhythmic hematite and quartz. They also indicate a generalized paragenesis for ophiolite-related deposits to be: i) early euhedral, zoned pyrite, which contains numerous inclusions, and is extensively shattered, recemented and replaced by chalcopyrite and locally sphalerite and ii) later, more anhedral or colloform-textured pyrite.

Early formation of at least some of the pyrite in the Skidder Prospect is suggested by its occurrence as fractured subhedral grains, the fractures being filled by chalcopyrite in several places. Note however that Craig (1983) interprets the occurrence of chalcopyrite in fractures and cracks in pyrite grains to be due to migration of chalcopyrite to zones of low pressure during metamorphism. The contrast between subhedral pyrite grains in quartz, and, proximal to these grains, anhedral pyrite surrounded by chlorite, chalcopyrite or sphalerite suggests dissolution or replacement of parts of the pyrite. In some areas, replacement of pyrite by chalcopyrite or sphalerite is also supported by embayment of the pyrite grains where in contact with these minerals. Intimate intergrowth of chalcopyrite, sphalerite and rare galena suggest contemporaneous deposition of these minerals in most areas.

In polished section SK 27 42C (the only polished section where hematite-magnetite textures were studied), hematite is intergrown with chalcopyrite, and magnetite-pseudomorphed hematite laths are intergrown with, and enclosed by pyrite suggesting contemporaneous deposition of chalcopyrite and pyrite with the hematite. Most magnetite in the sample has formed by replacement of hematite. Sphalerite has not been noted in contact with the oxide minerals.

6.15.6 Sphalerite chemistry

Skidder Prospect sphalerites have low Fe contents (less than 2 wt%) and contain only minor amounts of Cd (less than 0.4 wt%).

Craig et al. (1984) point out that sulphide deposits of the Norwegian Caledonides containing pyrite as the most abundant iron sulphide have sphalerites that are low in iron (typically less than 3 wt%). The Fe content of sphalerite in equilibrium with pyrite or pyrrhotite increases with increasing temperature and a_{S_2} (e.g Barton and Skinner, 1979). At any given temperature, over the temperature range 250°C to 700°C, sphalerites having atomic Fe contents less than about 0.1 are in equilibrium with pyrite in the Zn-Fe-S system, those having atomic Fe greater than about 0.2 are in equilibrium with pyrrhotite (Barton and Skinner, 1979). Barton and Skinner (1979) point out the relationship between FeS in sphalerite and pyrite as follows:

$$2\ FeS\ (\text{in sphalerite}) + S_2 = 2\ FeS_2\ (\text{pyrite}).$$

At a given temperature of formation (at least between 250°C and 700°C), the Fe content of sphalerite can be used to estimate the a_{S_2}. Figure 6-90 shows sulphide and oxide mineral stability fields on a plot of activity O_2 versus activity S_2 at 250°C and H_2O pressure of 40 bars (after Barton and Skinner, 1979). The shaded region shows the range of atomic Fe contents of the Skidder Prospect sphalerites, which indicate formation of the sphalerite under log a_{S_2} conditions of -10 to -11 assuming a temperature of 250°C. If higher temperatures of formation are assumed, the Fe contents indicate higher log a_{S_2} conditions,

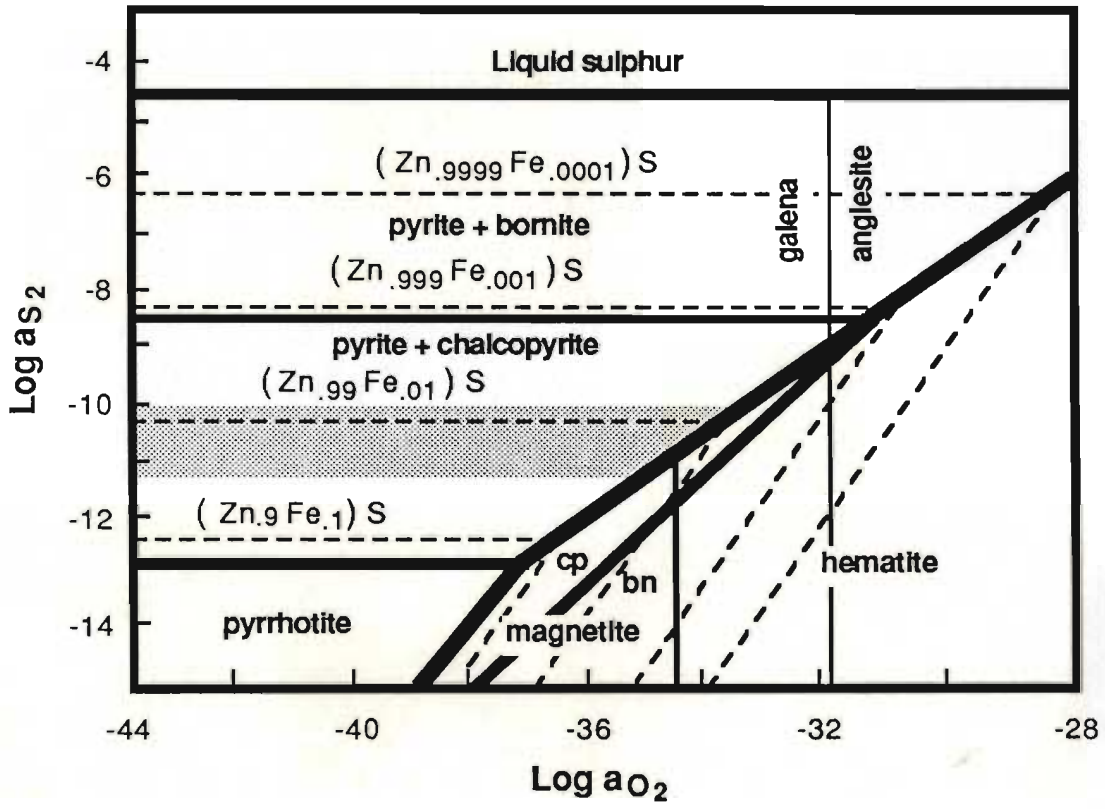

Figure 6-90: Activity O_2 versus activity S_2 diagram after Barton and Skinner (1979) calculated for 250°C and H_2O pressure of 40 bars. Shaded area indicates range of iron contents in Skidder Prospect sphalerites. Abbreviations: cp - chalcopyrite, bn - bornite.

e.g. approximately -8.5 to -9.7 at 300°C, or -6.3 to -7.5 at 350°C (estimated from Figure 7.14 of Barton and Skinner, 1979). For comparison, Janecky and Seyfried (1984) calculate a log f_{S_2} of -9.6 at 350°C and 250 bars for an end member solution determined from observed compositions of East Pacific Rise (EPR) hydrothermal fluids.

Figure 6-90 also shows that the Skidder Prospect sphalerites are in equilibrium with chalcopyrite and pyrite but not pyrrhotite at 250°C and 40 bars H_2O. At appropriate log a_{O_2} conditions, i.e. approximately -33.5 to -35, hematite or magnetite is in equilibrium with the Skidder Prospect sulphide mineral assemblage (Figure 6-90). A slight reduction in log a_{S_2} accompanied by a slight reduction in log a_{O_2} could result in magnetite replacing hematite as the equilibrium Fe-oxide phase (cf. textures shown in thin section SK 27 42C, Section 6.8.3). Calculations performed by Janecky and Seyfried (1984) show that, due to the abundance of reducing agents (e.g. ferrous iron and sulphides), the oxygen fugacity of mixtures of their calculated EPR end member solution and seawater decreases from about 10^{-30} at 350°C to about 10^{-70} at about 20°C; it rises to that of seawater only at very low temperatures, and after mixing of the calculated end member solution with very large amounts of seawater. Thus, any equilibrium between the sulphide minerals and hematite and/or magnetite would probably be short lived, occurring during initial stages of mixing between the hydrothermal fluid and seawater. Note, however, that hematite is the stable iron-bearing phase under the high log f_{O_2} (-0.64) (Janecky and Seyfried, 1984) conditions of ambient seawater; magnetite and the sulphide minerals are unstable under these conditions.

6.15.7 Alteration

Rocks which are immediate hosts to the Skidder Prospect massive sulphides are typically chlorite (± talc) rich and/or silicified. Distinct alteration zones, characterized by changes in the components and proportion of components comprising secondary mineral assemblages, envelop the Skidder Prospect sulphide-bearing zones. Arranged in order

from farthest away to closest to the sulphide-bearing units, the mineral assemblages are: chlorite, calcite, epidote ± hematite; chlorite, quartz, calcite, epidote; chlorite, quartz, calcite; chlorite, quartz, pyrite; and quartz, pyrite, chlorite (Section 6.4).

Mineralogical changes associated with the alteration of rocks in the vicinity of the Skidder Prospect relative to typical spilitized Skidder Basalt include: an increase in the amount of intersertal chlorite or quartz; silicification and, to a lesser extent, chloritization or sericitization of albitized plagioclase (phenocrysts seem to have been more susceptible to alteration than grains in the matrix); and the absence of epidote, clinopyroxene, actinolite and subhedral opaque minerals — all having been replaced by chlorite. K-feldspar replaces albitized plagioclase, particularly larger grains, in a few samples. In more intensely altered zones, albite laths, particularly the larger ones, have been partially to completely replaced by some combination of quartz, calcite and/or sericite.

Replacement of quartz pseudomorphs by chlorite in places suggests that the intense chloritization evident in some samples may have been produced at the expense of quartz, in addition to chloritization of other minerals. Excess silica produced by massive chloritization has probably been locally redistributed to other areas which are now quartz rich. The abundant quartz gangue in the massive sulphides, and some quartz in rocks from the qz,cl,py alteration zone was probably deposited from upwelling hydrothermal solutions that had transported silica leached from rocks at depth (see further discussion in Section 6.15.10). Calcite is rare in most of the altered rocks, but is ubiquitous as gangue in the sulphide-rich areas. This suggests that calcium, having been released by alteration of epidote, actinolite, clinopyroxene and calcite, has moved upward in the system and redeposited with the bulk of the sulphide-bearing minerals. Iron released from various minerals presumably has combined with sulphur to form pyrite.

Most chlorites from rocks proximal to the Skidder Prospect are significantly enriched in Mg, and depleted in Fe and Mn relative to the chlorites from the Skidder Basalt unaffected by the mineralizing event(s). Chlorites associated with jasper or jasper-rich

sulphides are the only chlorites (of those analyzed from rocks proximal to the Skidder Prospect) that are relatively enriched in Fe and depleted in Mg. These chlorites have Fe, Mn and Mg contents similar to chlorites from typical spilitized Skidder Basalt.

Mottl (1983a) suggested the following sequences of mineral assemblages to be characteristic of increasing seawater/basalt ratios within the temperature range 250°C to 450°C: 1) chlorite-albite-epidote-actinolite, 2) chlorite-albite-epidote-actinolite-quartz, 3) chlorite-albite-quartz, and 4) chlorite-quartz (Figure 5-19). These assemblages match reasonably well those enveloping the Skidder Prospect sulphide-bearing zones, and indicate that greater volumes of hydrothermal fluids passed through the rocks that are more intensely altered (cf. Saunders and Strong, 1986). Large-scale interaction with seawater is also supported by the high Mg and relatively low Fe and Mn contents of chlorites in rocks proximal to the Skidder Prospect. The trend defined by the Skidder Prospect chlorites on Figure 6-70 extends toward the MgO apex of the diagram, well beyond the chlorite composition that, according to Mottl (1983a), would result from a seawater/rock ratio of 125 (the highest seawater/rock ratio used in his model). In fact, phyllosilicates in SK 28-73 that have compositions intermediate between high-magnesium chlorite and talc provide an almost complete link between the high-magnesium chlorites and the Skidder Prospect talcs, which plot very close to the MgO apex on this diagram.

6.15.8 Geochemistry of the alteration zones — discussion

Sporadic enrichment of K, Rb and Ba marks the outermost whole rock geochemical effect of alteration associated with the Skidder Prospect mineralizing event(s). This geochemical effect is typically recognizable about 200 m away from the sulphide-bearing zones but, in places, is noted up to 400 m away. Sporadic enrichment of K and related elements is accompanied by enrichment of Pb, and depletion of Ca in more altered rocks. This geochemical signature, characteristic of the cl,cc,qz,ep and cl,qz,cc alteration zones, is generally recognizable about 75 to 150 m away from the sulphide-bearing zones, but

locally is noted up to 200 m away. The most altered rocks are represented by the cl,qz,py and qz,cl,py alteration zones. The former is characterized by enrichment of Mg, Zn and Pb, and depletion of Na, Si, Ca and Sr. The latter shows enrichment of Si, K, Rb, Ba, Pb and Zn, and depletion of Na, Ca, Sr, Mg, Mn, Ti, P, and Y. These geochemical effects are evident less than 50 m away from the sulphide-bearing zones. Zinc is enriched in high MgO rocks, which are composed predominantly of high-Mg chlorite. The Zn probably occurs in tiny sphalerite grains intimately associated with the chlorite (Section 6.10.3).

Principal component analysis on the whole rock geochemical data from rocks proximal to the Skidder Prospect shows that "incompatible element" (Zr, Y, P ± Ti) and "compatible element" (Cr and Ni) factors are evident even in the most intensely altered rocks, which would suggest that these elements have been little affected by the alteration associated with the Skidder Prospect mineralizing event (Section 6.10.2). Factors interpreted to be related to alteration include the "chlorite", "calcite", "potassium" and "sulphide" factors (Section 6.10.2).

6.15.9 Alteration associated with ophiolite-related deposits

According to Constantinou (1980), the alteration of basalts adjacent to the stockwork zone beneath the Cyprus deposits is characterized mineralogically by destruction of plagioclase, clinopyroxene, magnetite and the zeolite minerals. Quartz, chlorite and illite are the most abundant minerals present in the zone of alteration. Chemically, the alteration zone is characterized by loss of CaO, Na_2O and K_2O; and enrichment of MgO, except in the sulphide-rich core of the stockwork zone, where MgO is volumetrically depleted.

Bachinski (1977) describes similar alteration effects at the Whalesback Mine, Notre Dame Bay, Newfoundland. He reports intense chloritization and silicification of basalts surrounding the deposits. Chemically, rocks in the alteration zone have been almost completely leached of Na_2O and CaO; SiO_2 and MgO have been redistributed.

Saunders and Strong (1986) describe mineralogical alteration assemblages in footwall rocks to the Betts Cove ophiolite massive sulphide deposits that are similar to those of the Skidder Prospect. They note the presence of an inner Cu-enriched chlorite-quartz core alteration zone surrounded by a Zn-enriched chlorite-albite-quartz halo. In contrast to the chlorites in the most intensely altered rocks proximal to the Skidder Prospect which are Mg rich, chlorites in the central core of the Betts Cove alteration zone are Fe rich. Whole rock geochemical effects at Betts Cove include extreme depletion of Ca and Na in the "core" alteration zone and variable depletion of these elements in the surrounding alteration "halo". No potassium enrichment is indicated in the alteration pipe beneath the Betts Cove deposits however, in contrast to that of the Skidder Prospect.

Franklin et al. (1981) summarize the alteration zones associated with ophiolite-hosted massive sulphide deposits as being characterized by "pervasive feldspar destruction as well as introduction and redistribution of MgO and FeO to form chlorite". Sericite may also be present, but no clear zonation pattern of sericite relative to chlorite is reported. Silica, according to Franklin et al. (1981), has been redistributed; having been leached from surrounding basalts and deposited within the stockwork zone.

6.15.10 Genetic model

6.15.10.1 Introduction

Genetic models for the formation of ophiolite-related massive sulphide deposits have been proposed by several authors, including: Constantinou and Govett (1972); Sillitoe (1972; 1973); Upadhyay and Strong (1973); Bonatti et al. (1976); Spooner (1977); Constantinou (1980); and Franklin et al. (1981). All of the models have somewhat similar characteristics. Typically, the models involve convection of seawater through the oceanic crustal sequence, and, due to interaction with surrounding rocks, evolution of the seawater into a chloride-rich brine. Metals are leached from the surrounding rocks and transported in solution as chloride complexes. The convecting solution, which is being driven by heat from sub-axis and off-axis magma chambers, eventually rises along zones of high permeability, e.g. fault zones (Spooner and Fyfe, 1973). Permeability is, in part, controlled by fracture systems developed above the magma chambers as a result of intrusive pressures (Alabaster and Pearce, 1985). Materials being carried in the solution are deposited as a result of some combination of the following: cooling of the fluid during ascent; reaction with surrounding wall rock; mixing with sea water; or, in a shallow seawater environment, boiling of the fluids. Various components of the above model, combined with results of studies on East Pacific Rise hydrothermal deposits are discussed below as a possible analog to the mode of formation of the Skidder Prospect.

6.15.10.2 Modern hydrothermal deposits

6.15.10.2.1 General description

Since 1979, massive sulphide deposits have been discovered associated with inactive and, in places, active hydrothermal vents on several fast spreading ridges in the Pacific Ocean. These include: the East Pacific Rise (EPR) at 21°N (Francheteau et al., 1979; Spiess et al., 1980), and at 13°N (Hekinian and Fouquet, 1985); the Galapagos Ridge (Malahoff, 1981; 1982); and along the Juan de Fuca Ridge (Normark et al., 1982;

Koski et al., 1982). These sulphide deposits provide a plausible modern analog to the method of formation of the Skidder Prospect massive sulphide deposit, and of other ophiolitic deposits. For example, Adamides (1983) and Constantinou and Robinson (1983) compare the massive sulphide deposits of Cyprus with those being formed at present on the East Pacific Rise; Ixer et al. (1984) suggest a similar comparison for the Oman ophiolite sulphide deposits.

At the time of writing, information available on the physical appearance, mineral composition and chemistry of actively forming sulphide deposits, and on the composition of the mineralizing hydrothermal solutions comes mainly from the East Pacific Rise at 21°N (e.g. Spiess et al., 1980; Hekinian et al., 1980; Haymon and Kastner, 1981; and Goldfarb et al., 1983). Vent deposits at 21°N on the EPR comprise basal mounds that are 15-30 m in area and up to 2 m high surmounted by elongate chimney edifices that reach up to 5 m in height (Spiess et al., 1980; Hekinian et al., 1980; Haymon and Kastner, 1981). The surface of basal mounds is composed of partially oxidized sulphides (predominantly sphalerite, pyrite, and lesser chalcopyrite), which are "honeycombed" by worm channels; soft, fine grained sulphide mud is also present in various amounts (Hekinian et al., 1980; Goldfarb et al., 1983). Chimneys are of two types: 1) "black smokers", from which emanate plumes of high temperature (350°C) fluids that precipitate pyrrhotite and minor Zn-sulphide, pyrite, Cu-sulphide, anhydrite, barite, silica and graphite as particulate matter suspended in solution; and 2) "white smokers", emitting cooler (≤ 32°C to 300°C) fluids precipitating white particulate matter (including anhydrite, barite and amorphous silica) and pyrite (Spiess et al., 1980; Haymon and Kastner, 1981). Abundant animal life is associated with the white smoker chimneys.

Most black smoker chimneys are concentrically zoned; they have an outer zone composed of anhydrite and rare magnesium hydroxysulphate hydrate (MHSH), and other sulphates; an intermediate zone comprising pyrite and sphalerite; and an inner zone composed predominantly of chalcopyrite — the chimneys show no axial variability

(Haymon and Kastner, 1981). In thin chimneys, a sequence of successively more Cu-rich sulphides, including bornite, covellite and chalcocite, replace chalcopyrite radially outward from the centre of the chimney (Haymon and Kastner, 1981; Goldfarb et al., 1983). The concentric zoning is thought to result from gradients in temperature, pH, oxygen and sulphur fugacity, and solution composition between the inner and outer portions of the chimneys. The white smoker chimneys have slower flow rates and are composed of sphalerite and/or wurtzite, pyrite, anhydrite, barite and amorphous silica; they lack Cu-sulphides (Spiess et al., 1980; Haymon and Kastner, 1981).

Lonsdale et al., (1982) report active hydrothermal vents, which are forming Fe and Cu sulphides, on two seamounts about 10-20 km west of the EPR at 21°N. Also, Hekinian and Fouquet (1985) describe recent hydrothermal deposits forming in an axial graben located on a fast moving section (12 cm/yr) of the EPR at 13°N, and on off-axis seamounts that occur about 7 km from the ridge crest. Hydrothermal material formed on the flank and summit of the off-axis seamounts at 13°N comprise about 62% goethite, which overlies material composed of about 24% Fe-rich massive sulphides, 13% silica-rich sulphides and 1% massive Fe-Cu sulphides.

Massive sulphide stacks, 3-4 m high, occur along a 2 km stretch of the Galapagos Ridge (Malahoff, 1981; 1982; Bischoff et al., 1983). Samples dredged from the area are composed of coarsely crystalline pyrite with significant amounts of chalcopyrite (Malahoff, 1981; 1982; Bischoff et al., 1983). Visual estimates of the massive sulphide deposits (Malahoff, 1982) suggest a possible 20 million tonnes of massive sulphide to be present (Bischoff et al., 1983).

Dredged sulphides from the Juan de Fuca ridge include slabs of crudely layered, coarsely crystalline sulphide aggregates composed primarily of Zn sulphides and lesser pyrite; other samples are of hard but spongy-textured light grey Zn-sulphide similar to that forming basal mounds at 21°N EPR (Koski et al., 1982; Normark et al., 1982; Bischoff et al., 1983).

6.15.10.2.2 Mineral composition

In samples of massive sulphides from 21°N on the East Pacific Rise, pyrite occurs as framboidal masses and euhedral crystals; sphalerite as irregular octahedrons and dodecahedrons accompanied, in places, by hexagonal wurtzite; and chalcopyrite occurs as botryoidal masses (Haymon and Kastner, 1981). The sulphide minerals are typically intergrown, mineral banding being a common feature (Haymon and Kastner, 1981).

Modern hydrothermal sulphide samples typically have insignificant amounts of Au and platinum group elements, and low contents of Ni (Bischoff et al., 1983). Zn-rich samples from 21°N EPR and the Juan de Fuca Ridge are enriched in As, Cd, Tl, and Ge (Bischoff et al., 1983). The Galapagos samples are relatively enriched in Co and Mo.

Amorphous silica occurs as globules on sulphide surfaces, and as layers intercalated with sulphide lamellae in fossil worm-tubes at 21°N on the East Pacific Rise (Haymon and Kastner, 1981). Native sulphur, accompanied by amorphous silica and barite, fills inactive chimneys in some areas (Haymon and Kastner, 1981). Minor amounts of hydrothermal talc is intermixed with chalcopyrite in disaggregated mound material (Haymon and Kastner, 1981).

Wurtzite is the more common Zn-sulphide in active chimneys of modern hydrothermal sulphide deposits, but sphalerite is most common in inactive off-axis chimneys (Hekinian et al., 1980; Haymon and Kastner, 1981). Wurtzite and sphalerite have Fe contents of 2-22 wt% (Hekinian et al., 1980; Zierenberg et al., 1984). Their sulphur isotope compositions indicate that the sulphur is primarily basaltic in origin (Styrt et al., 1981; Janecky and Seyfried, 1984).

Hekinian and Fouquet (1985) suggest a mineral paragenesis for the seamount related sulphides at 13°N as follows: early formed colloform pyrite; Zn-sulphides + pyrite; chalcopyrite; barite; opal encrustations; quartz; cobaltiferous pyrite; framboidal pyrite; and finally, Cu-rich sulphides. In places, silica completely replaces pyrite in the sulphides

deposited at 13°N EPR. Framboidal pyrite is associated with the replacing amorphous silica in some areas (Hekinian and Fouquet, 1985).

Anhydrite and MHSH precipitate from seawater due to their reduced solubility at high temperatures, e.g. in water depths of 2600 m, anhydrite solubility is exceeded in seawater above 130°C (Haymon and Kastner, 1981; Janecky and Seyfried, 1984). Precipitation of anhydrite from seawater is supported by the fact that the $\partial^{34}S$ of chimney anhydrite in modern hydrothermal sulphide deposits is close to that of seawater (Hekinian et al., 1980; Zierenberg et al., 1984). The anhydrite forms the leading edge of chimneys, which grow upward and outward as sulphide replaces previously deposited anhydrite and a new layer of anhydrite forms by precipitation from seawater immediately surrounding the chimney (Haymon and Kastner, 1981).

6.15.10.3 Source of the metals

Bischoff et al. (1983) indicate that, although the heavy metals are enriched in East Pacific Rise sulphide samples, the relative abundances of Zn, Cu, Co, and Ag in the sulphides are similar to the relative abundances of these metals in MORB. Calculations based on enrichment factors of the heavy metals in the sulphides relative to MORB indicate that seawater, in "reasonable" amounts, could leach the metals contained in the EPR, Juan de Fuca, Galapagos and Cyprus massive sulphide deposits from the underlying rocks (Bischoff et al., 1983).

Rosenbauer and Bischoff (1983) report that heated seawater can leach significant amounts of heavy metals from basalt between 150°C and 360°C, mainly due to the reduction in pH from precipitation of MHSH, but the metals are not retained in solution at low water/rock ratios since silicate hydrolysis increases the pH once all the Mg is removed. Rosenbauer and Bischoff (1983) illustrate by the following reaction how removal of Mg can decrease the pH of the solution, note that clinochlore represents the smectite/chlorite alteration phase:

$$5\,Mg^{2+} + \text{anorthite} + 8\,H_2O + SiO_2 = \text{clinochlore} + Ca^{2+} + 8\,H^+.$$

Basalt-seawater interaction at temperatures ≥ 400°C produce similar results to that at lower temperatures with the important exception that heavy metals are retained in solution under low water/rock conditions (Rosenbauer and Bischoff, 1983). Rosenbauer and Bischoff (1983) suggest that a fluid produced experimentally by interaction with basalt at 400°C and 600 bars, or a fluid at 375°C interpolated between their results at 250 and 500 bars most resemble 21°N EPR vent fluid.

Graf (1977) suggests that the metal content of a sulphide deposit should be related to the relative amounts of mafic vs. felsic volcanic rocks in the underlying volcanic pile from which the metals have been leached. According to Stephens (1982), Zn and Cu are concentrated in Fe-Ti oxides and, to a lesser extent, in pyroxene and plagioclase; Zn is also present in biotite; Pb replaces K in K-feldspar, and, to a lesser extent, is present in plagioclase and biotite (cf. Graf, 1977). Hence, Cu-rich deposits would be expected to be underlain by mostly mafic rocks and Pb-rich deposits underlain by mostly felsic rocks (cf. Solomon, 1976; Stephens, 1982). Stephens (1982) stresses that ophiolite massive sulphide deposits are lead free, and that lead-rich massive sulphide deposits require not just felsic but lead-rich felsic source rocks.

The York Harbour Deposit, which occurs well up in the pillow lava sequence of the Bay of Islands ophiolite in mafic lavas that have MORB-like chemistry (e.g. Suen et al., 1979), is relatively Zn-rich (Duke and Hutchinson, 1974) (like the Skidder Prospect) but the Tilt Cove and Betts Cove deposits (Upadhyay and Strong, 1973; Strong and Saunders, in press), which occur near the base of the Betts Cove Ophiolite within pillow lavas that have boninite-like geochemistry, are Cu rich. One explanation for this is that the Zn-rich portions of the Betts Cove and Tilt Cove deposits have been removed by submarine weathering. An alternative to this is that the source rocks for these deposits is enriched in copper relative to Zn. The average Zn and Cu concentrations in 114 nonmineralized Skidder Basalt samples are: Zn (83 ppm), and Cu (40 ppm), for a Zn/Cu ratio of 2.08; in

contrast, the average concentrations of Zn and Cu in 50 nonmineralized Betts Cove basalts in the vicinity of the Betts Cove Mine (data in Saunders, 1985) are: Zn (59 ppm), and Cu (83 ppm), for a Zn/Cu ratio of 0.71. This suggests that, locally at least, the host rocks to the Betts Cove deposit are copper rich and Zn poor relative to those of the Skidder Prospect.

Although local differences in the Cu and Zn concentrations of host rocks to the Betts Cove and Skidder Prospect are apparent, another consideration is the concentrations of these metals in the rocks at depth, from which the metals can be effectively leached and held in solution. Rosenbauer and Bischoff (1983) indicate, on the basis of buoyancy constraints, that seawater circulating through a section of oceanic crust having an underlying magma chamber would be restricted to about 420°C at 450 bars, the latter being the probable pressure at the base of the sheeted dyke zone, but, after crystallization of the magma was complete, could reach 500°C at 700 bars pressure if circulation occurred to the base of the gabbro zone. Thus, the thickness of the pillow lava and sheeted dykes portion of an ophiolite, as well as the timing of the hydrothermal circulation, play a role in which rocks are being leached of their metals.

Lead isotope ratios of the Skidder Prospect sulphides, which are some of the least radiogenic of Newfoundland mineral deposits, plot along the mantle lead evolution curve of Zartman and Doe (1981) on the $^{207}Pb / ^{204}Pb$ vs. $^{206}Pb / ^{204}Pb$ diagram. Stephens (1982) indicates that Pb-isotope systematics in massive sulphide deposits ultimately reflect the material that undergoes partial melting to produce the source rocks. The radiogenic-lead-depleted nature of the Skidder Prospect sulphides may therefore be attributed to derivation of the lead from a radiogenic-lead-depleted source, one such source being the mantle (see Section 6.14).

6.15.10.4 Ore fluid composition

On the basis of fluid inclusion studies, Solomon and Walshe (1979) concluded that the hydrothermal solutions from which the Cyprus massive sulphide deposits formed contained about 0.6 m NaCl and were at 300°C when they were emitted onto the sea floor.

Janecky and Seyfried (1984) summarize compositional ranges determined for hydrothermal solutions emanating from vents at 21°N on the East Pacific Rise (cf. Edmond, 1981; Rona et al., 1983; Janecky and Seyfried, 1984; and references therein). They indicate that the solutions are acidic (pH = 3.5), have H_2S concentrations of 6-9 mM, Fe concentrations of 0.7-2.5 mM, and Zn and Cu concentrations of 0.01-0.1 mM; the solutions contain Cl as the only anion (no sulphate), and are strongly enriched in the alkalies and barium, and variably so in calcium. Relative to seawater, the solutions have similar salinity, are depleted in Mg and SO_4, but are enriched in most other components.

6.15.10.5 Sulphide precipitation on the seafloor

Buoyancy constraints indicate that high temperature brines emitted from the sea floor should be less dense, but not necessarily less saline, than seawater (Campbell et al., 1984). Solomon and Walshe (1979) predicted from the density-temperature curves of Haas (1971) that the hydrothermal solutions associated with formation of the Cyprus massive sulphide deposits were probably about 25% lighter than seawater when they emerged onto the sea floor, and that they were likely emitted at seawater depths exceeding 750 m, which would have prevented boiling (Haas, 1971; Ridge, 1973; Solomon and Walshe, 1979).

With the exception of stratified brine pools in the Red Sea, modern hydrothermal sulphide deposits, e.g. the EPR deposits, are deposited from brines that are less dense than seawater (cf. Type III brines of Sato, 1972). Campbell et al. (1984) calculate that a typical EPR black smoker will probably rise to about 300 m before attaining neutral density with seawater. They indicate that the fine particulate matter precipitated within the plume will be

dispersed several hundred kilometres before settling the 300 m. Hence, particulate matter from the plumes is unlikely to form massive sulphide deposits — unless the plumes are emitted in a narrow seafloor depression having walls greater than 300 m high.

Several authors have proposed models for the formation of EPR-type massive sulphide mounds (e.g. Haymon and Kastner, 1981; Goldfarb et al., 1983; Hekinian and Fouquet, 1985); and for the formation of off-axis seamount sulphide mounds (Hekinian and Fouquet, 1985). Campbell et al., (1984) have suggested that a similar model may be appropriate for the formation of some ancient volcanogenic massive sulphide deposits. The salient features stressed in some or all of the models include: i) the importance of anhydrite precipitation from heated seawater due to its reduced solubility at elevated temperatures — the anhydrite forms a protective cap and a porous infrastructure through which some of the hydrothermal fluid and seawater mix, resulting in precipitation of sulphides; ii) zonation of chimney edifices and possibly basal mounds — a central zone of Cu-rich sulphides, which are precipitated at high temperatures, is surrounded by an outer zone dominated by Zn-rich sulphides, which precipitate at lower temperatures; iii) hydrothermal fluids venting at lower temperatures may precipitate Zn-rich sulphides only, at surface; Cu-rich sulphides probably precipitate below the seawater/basalt interface as a result of mixing with shallow convecting seawater; iv) the sulphide mounds are a dynamic system in which minerals that precipitate at higher temperatures replace those at lower temperatures and vice versa, depending upon the temperature of the ascending hydrothermal fluids, and the stage of development of the mounds themselves; v) cessation of hydrothermal activity results in dissolution of anhydrite and oxidation of the sulphide minerals.

Haymon and Kastner (1981) summarize the evolution of vent deposits as follows: metal sulphide-sulphate chimneys are formed by mixing of ambient seawater with a metal-bearing evolved-seawater hydrothermal solution, which emanates from vents on the sea floor — the metal-bearing hydrothermal solution is sulphur rich, oxygen poor and of low-pH; mixing results in rapid precipitation of a non-equilibrium assemblage of pyrrhotite +

pyrite and wurtzite + sphalerite from vent solutions, and Ca-Mg sulphates from heated seawater. Janecky and Seyfried (1984) modeled mixing of 21°N EPR hydrothermal fluid and seawater. According to their calculations, chalcopyrite, quartz, anhydrite and talc should precipitate at high temperatures, followed by pyrite and sphalerite at lower temperatures. Barite and dolomite would be expected to precipitate at temperatures less than 60°C. The calculated mixing model suggests that quartz, and not amorphous silica, should be present in the vent materials, and that both quartz and talc should be present in greater amounts than are noted. Janecky and Seyfried (1984) suggest that kinetic effects must play a role in the small amounts of talc being precipitated relative to that predicted by the mixing model, and that the presence of amorphous silica instead of quartz is probably a result of cooling of the solution by conductive heat loss in addition to mixing.

Pyrrhotite is the observed iron-sulphide phase that precipitates from EPR-type hydrothermal solutions (e.g. Haymon and Kastner, 1981), although the mixing model of Janecky and Seyfried (1984) predicts that pyrite should be the iron sulphide phase to precipitate. Pyrrhotite precipitating in the discharging fluids is probably a metastable phase, its disordered structure favoured kinetically over more structured pyrite as a result of the sudden change in chemical environment experienced by the fluid (Haymon and Kastner, 1981). Janecky and Seyfried (1984) indicate that the metastable precipitation of pyrrhotite in the vents would result in an increase in the temperature at which sphalerite would precipitate, from about 180°C to about 255°C; high-iron sphalerites could precipitate at even higher temperatures (about 265°C) — if pyrite precipitation is suppressed. In this way, Zn-sulphide precipitation could precede precipitation of pyrite, which could, in turn, replace anhydrite and pyrrhotite in the chimney walls — such a paragenesis is consistent with textures observed in some areas, e.g. Haymon and Kastner (1981) report that pyrite replaces pyrrhotite in the outer walls of chimneys (cf. Goldfarb et al., 1983; Janecky and Seyfried, 1984). The early, high-temperature crystallization of chalcopyrite provides an explanation for its forming the central portion of many chimneys, and its absence as a

major phase in the lower-temperature Zn-rich chimneys (Haymon and Kastner, 1981; Janecky and Seyfried, 1984).

Mixing models for 21°N EPR hydrothermal fluid and ambient seawater presented by Janecky and Seyfried (1984) show that the pH of the solution will remain at about 1.5 units more acid than neutral until the temperature reaches about 160°C, below which the pH would gradually rise toward that of seawater. Note however that the pH remains below 5 until the temperature falls to about 125°C, and does not increase to 6 until the temperature of the mixed solution reaches about 50°C (Janecky and Seyfried, 1984). Precipitation of sulphides in black smoker chimneys, which occurs at temperatures between 350°C and 250°C, cannot therefore be attributed to an increase in pH of the solution. Janecky and Seyfried (1984) indicate that the pH buffering capacity of the hydrothermal solution is a result of complex interactions between activities of various carbonate, sulphate and hydroxide species; precipitation of the sulphide minerals will also help keep the pH of the solution low.

Calculated precipitates resulting from mixing of 21°N EPR hydrothermal solution and seawater at 150°C, (Janecky and Seyfried, 1984), compare well to the average metal composition of the Skidder Prospect massive sulphides.

6.15.10.6 Origin of the jasper

Brecciated, quartz-veined, unlayered jasper, and lesser amounts of bedded jasper and jasper-rich siltstone are spatially associated with the Skidder Prospect massive sulphides in several places. As indicated above, authors reporting studies of modern hydrothermal deposits on the East Pacific Rise suggest that cessation of hydrothermal activity results in dissolution of anhydrite and oxidation of the sulphide minerals. These workers suggest that, unless they are buried by sediments or lava flows, the sulphide mounds would probably be completely oxidized leaving metal-enriched ocherous residues. Weathered sulphide samples from the East Pacific Rise have a 5 mm-thick rusty layer

composed of amorphous iron oxyhydroxides and crystalline goethite (Haymon and Kastner, 1981). Hematite can form from dehydration of amorphous ferric hydroxide according to the following reaction:

$$2Fe(OH)_3 = 2FeOOH + 2H_2O = Fe_2O_3 + 3H_2O$$

goethite hematite

(Fischer and Schwertmann, 1975; Cole, 1983). The massive to layered goethite, maghemite, quartz, illite sedimentary rock termed "ochre", which typically caps the Cyprus orebodies, is considered by Constantinou and Govett (1972) to have formed by submarine oxidative leaching of sulphide minerals that were exposed on the sea floor (cf. Constantinou, 1980; Bischoff et al., 1983).

Some of the jasper that is present in the Skidder Prospect area may also have formed by oxidative leaching of sulphide minerals that were, at one time, exposed on the sea floor. Supportive of this premise is that Hekinian and Fouquet (1985) show photographs illustrating pseudomorphic textures of amorphous silica and Fe-hydroxide after pyrite that are similar to those shown in some jasper fragments associated with the Skidder Prospect massive sulphides (Section 6.6.2).

The presence of several jasper units in spatial association with the Skidder Prospect massive sulphides (e.g. seven brecciated and layered jasper units were intersected in the mineralized portion of SK 37A; Figure 6-24) suggests that formation of the massive sulphides may have been episodic. Thus, deposition of massive sulphides was possibly followed by oxidative leaching of portions of the sulphides to produce jasper, this, in turn, was followed by deposition of more sulphides and so on. Highly altered chlorite-rich basalts occur between two jasper and massive sulphide-bearing zones in drill hole SK 28 (Figure 6-18). This would suggest that volcanic activity proceeded during the sulphide deposition and further supports episodic introduction of metal-bearing hydrothermal fluids into the area.

6.15.10.7 Sub-seafloor precipitation of sulphides, and alteration effects

Janecky and Seyfried (1984) suggest that mixing of upwelling hydrothermal solutions with entrained seawater could result in precipitation of Cu- and Fe-sulphides in altered basalt beneath the zinc-rich chimneys of East Pacific Rise massive sulphide mounds. They suggest that this could provide a mechanism for formation of stockwork zones that are present beneath most massive sulphide deposits (cf. Franklin et al., 1981; and references therein).

Figure 6-91 presents a schematic model for formation of the Skidder Prospect sulphides and related alteration effects. On Figure 6-91 it is suggested that alteration effects associated with the Skidder Prospect, and stockwork sulphide deposition have resulted from mixing of an upwelling, metal-bearing, modified seawater hydrothermal fluid and cool, shallow-circulating seawater. Roberts and Reardon (1978) propose a similar mixing model to explain alteration associated with the Mattagami Lake Mine massive sulphide deposit, Quebec.

6.15.10.7.1 Magnesium metasomatism

Metal-bearing upwelling hydrothermal fluids, such as those forming modern hydrothermal sulphide deposits on the East Pacific Rise, are devoid of Mg. This is probably due to removal of Mg from the fluid upon interaction with basalt during its downward circulation (cf. Mottl, 1983a; 1983b; Rosenbauer and Bischoff, 1983). Thus, the secondary, shallow-circulating seawater hydrothermal circulation suggested on Figure 6-91 is necessary in order to provide a source of Mg for the intense magnesium metasomatism characteristic of the Skidder Prospect alteration zone.

Chondrite-normalized rare-earth element patterns associated with the Skidder Prospect area rocks indicate that the hydrothermal fluid that caused the Mg metasomatism was probably not effective in leaching "stable elements" from the rocks, e.g. sulphide-poor samples, even those that have been intensely chloritized, show chondrite-normalized REE

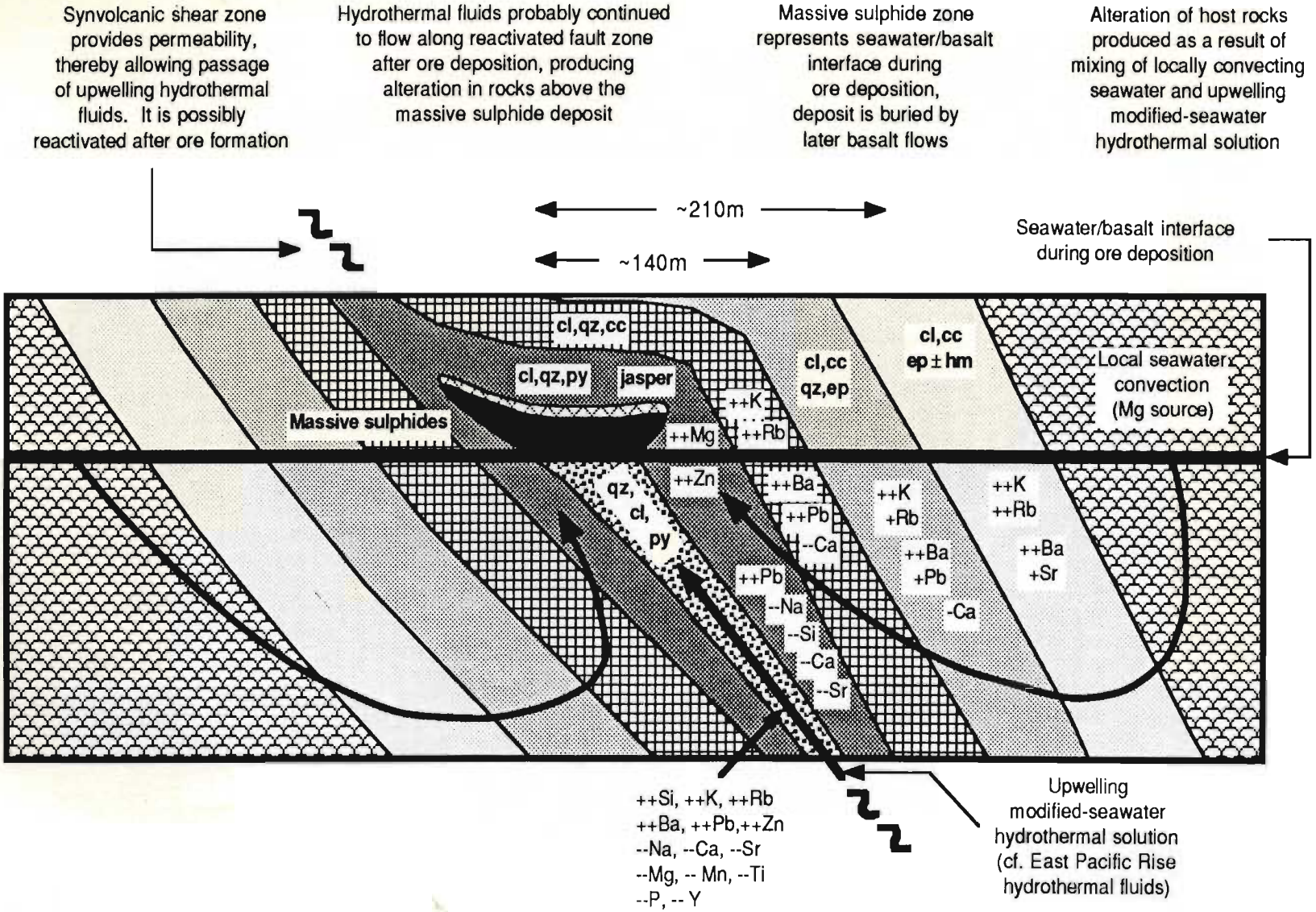

Figure 6-91: Schematic diagram (not to scale) illustrating Skidder Prospect alteration zones, and a possible model for formation of the sulphides (cf. Saunders and Strong (1986) model for ore formation at Betts Cove). See text for discussion. Key: enrichment or depletion relative to typical spilitized Skidder Basalt; "+" slight enrichment, "++" extensive enrichment, "-" slight depletion, and "--" extensive depletion.

patterns similar to typical spilitized Skidder Basalt. In contrast, sulphide-rich samples have much lower REE concentrations than those of typical spilitized Skidder Basalt, and some have REE patterns showing relative depletion of Ce and the middle REE; characteristics shown by REE patterns for seawater. These sulphide-rich samples probably reflect the REE characteristics of the metal-rich, upwelling, modified seawater hydrothermal fluid.

In several areas, crosscutting textural relationships suggest that formation of the black chlorite in rocks proximal to the Skidder Prospect occurred before deposition of pyrite-bearing quartz veins (cf. Figures 6-27 and 6-31). Roberts and Reardon (1978) report that formation of Mg-rich chlorite beneath the Mattagami Lake deposit occurred during the early stages of alteration. Note that, unlike several other massive sulphide deposits, no Fe-rich chlorites are noted in the alteration pipe beneath the Mattagami Lake deposit; in this respect the deposit is similar to the Skidder Prospect. Magnesium metasomatism of rocks beneath the Skidder Prospect may have occurred in stages. Secondary circulating seawater, in the early stages of hydrothermal activity, may have been able to reach the focal point for upwelling hydrothermal fluids before precipitating magnesium, whereas later, when the upwelling fluid flow was probably greater, the secondary circulating seawater would be heated and deposit the magnesium at a greater distance from the central focus for the upwelling fluids. In this way, quartz and pyrite being deposited from the upwelling fluid could overprint earlier-formed chlorite. Conversely, deposition of the pyrite-bearing quartz veins could have occurred during the waning stages of hydrothermal activity, possibly after deposition of the main sulphide lenses.

Zn is enriched in high-MgO rocks in the Skidder Prospect cl,qz,py alteration zone. The zinc probably occurs in tiny sphalerite grains intimately associated with high-Mg chlorite (see Section 6.10.3). Gale (1969) concludes from a study of Springdale peninsula sulphide deposits that Zn and Cu, introduced by epigenetic hydrothermal fluids, were dispersed into the wall rocks. The presence of anomalous values of Zn in the Mg-chlorite-

rich zone in the Skidder Prospect area could similarly be explained by precipitation of zinc from the upwelling hydrothermal solution, and of Mg from shallow-circulating seawater in a zone of mixing between the two solutions. Note that, since Zn-chloride complexes are more soluble than Cu-chloride complexes, Zn would probably diffuse farther outward from the focal area for the upwelling solutions than would Cu (e.g. Finlow-Bates, 1980). A problem with the mixing hypothesis is that, as long as Mg is precipitating, the pH of the solution should remain low, thereby increasing the solubility of Zn. Basalt/seawater interaction experiments, however, show that Zn, leached when the pH of the solution drops due to precipitation of MHSH, coprecipitates with the alteration products when the pH of the solution rises in response to silicate hydrolysis after complete removal of the Mg from the seawater (Rosenbauer and Bischoff, 1983; and references therein). This would imply that the Zn probably remains in solution in the zone of mixing until all the Mg is precipitated. It should be noted that the Mg may also have been precipitated in areas farther removed from the conduit than where the Zn precipitation occurs. This implies that the Mg metasomatism in the area of Zn precipitation could have occurred during prior influxes of hydrothermal fluids.

Chlorite-talc-rich rocks in the alteration pipe beneath the Skidder Prospect are shown to grade into recognizable pillow lava in places. However, in other areas, the chlorite-talc-rich rocks are interlayered with mafic tuff (e.g. in hole SK 31). In these latter areas, the chlorite-talc-rich rocks could have formed by intense alteration of selected layers within the mafic tuff, or alternatively, by primary deposition as a chemical sediment at the seawater interface. The latter hypothesis is supported by observations reported by Costa et al. (1983) who report that hydrothermal talc probably coprecipitated with sulphides in a sea-floor brine pool during formation of the Mattagami Lake Mine sulphide deposit.

6.15.10.7.2 Potassium metasomatism

Figure 6-91 shows that potassium enrichment has occurred in several of the alteration zones associated with the Skidder Prospect. Electron microprobe analyses presented in Section 6.7 indicate that potassium is present in two different mineral phases, i.e. in K-feldspar in the less altered rocks of the outer alteration zones, and in phengitic sericite in more intensely altered inner alteration zone rocks.

Figure 6-92 (after Urabe et al., 1983) shows the relationship between chlorite, kaolinite, sericite and albite on the basis of activities of $Mg^{2+} / (H^+)^2$ and (total alkalies) / H^+. Heating of shallow-circulating seawater as a result of mixing with an upwelling hydrothermal fluid and thereby deposition of magnesium in MHSH (probably a precursor to Mg-rich chlorite) would result in depletion of Mg in the solution, and a large increase in the activity of H^+ (Rosenbauer and Bischoff, 1983). This would tend to affect the activity ratios shown on Figure 6-92 such that the solution could eventually move away from the chlorite stability field (point A) and into that of sericite (point B).

Fluids emanating from hydrothermal conduits on the East Pacific Rise are enriched in K relative to seawater, and the solutions are acidic. Mixing of such a fluid with shallow circulating seawater, with resultant precipitation of Mg, would probably increase the acidity of the solution in the zone of mixing (see above). Figure 6-93 (after Helgeson, 1974) shows that high H^+ activity favours equilibrium of the solution with muscovite rather than K-feldspar (point A on Figure 6-93). However, dispersal of some of the K-bearing upwelling solution away from the conduit, and mixing with downwelling seawater could eventually result in a mixed solution having a temperature below 150°C. Magnesium removal, which is the main source of H^+ generation in heated seawater (e.g. Rosenbauer and Bischoff, 1983), is not effective below 150°C and therefore mixing between the K-bearing hydrothermal solution and low-temperature circulating seawater could raise the pH of the solution mixture, and thereby favour production of K-feldspar over muscovite (point B on Figure 6-93). This provides on explanation for the change from muscovite, the

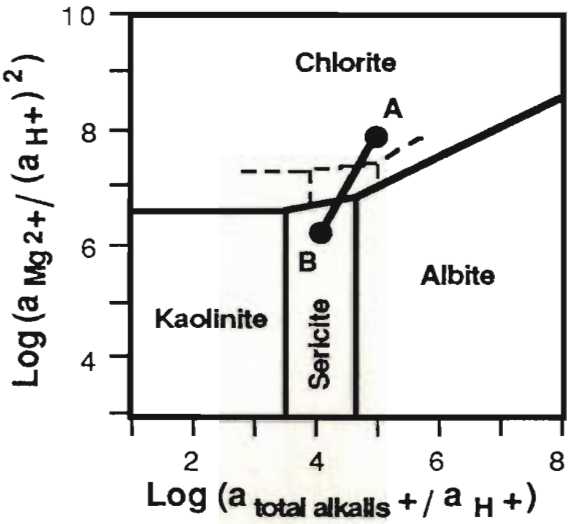

Figure 6-92: Activity diagram for the system Na-K-Mg-Al-Si-H-Cl-O at 300°C and a fixed K/(K+Na) ratio of 0.123 under the condition of quartz saturation (Na = 0.5 molal, K = 0.07 molal, and Mg = 0.01 molal) (after Urabe et al., 1983). Dashed lines are phase boundaries at 250°C. K-feldspar is not stable at the ionic concentrations on this diagram. See text for discussion.

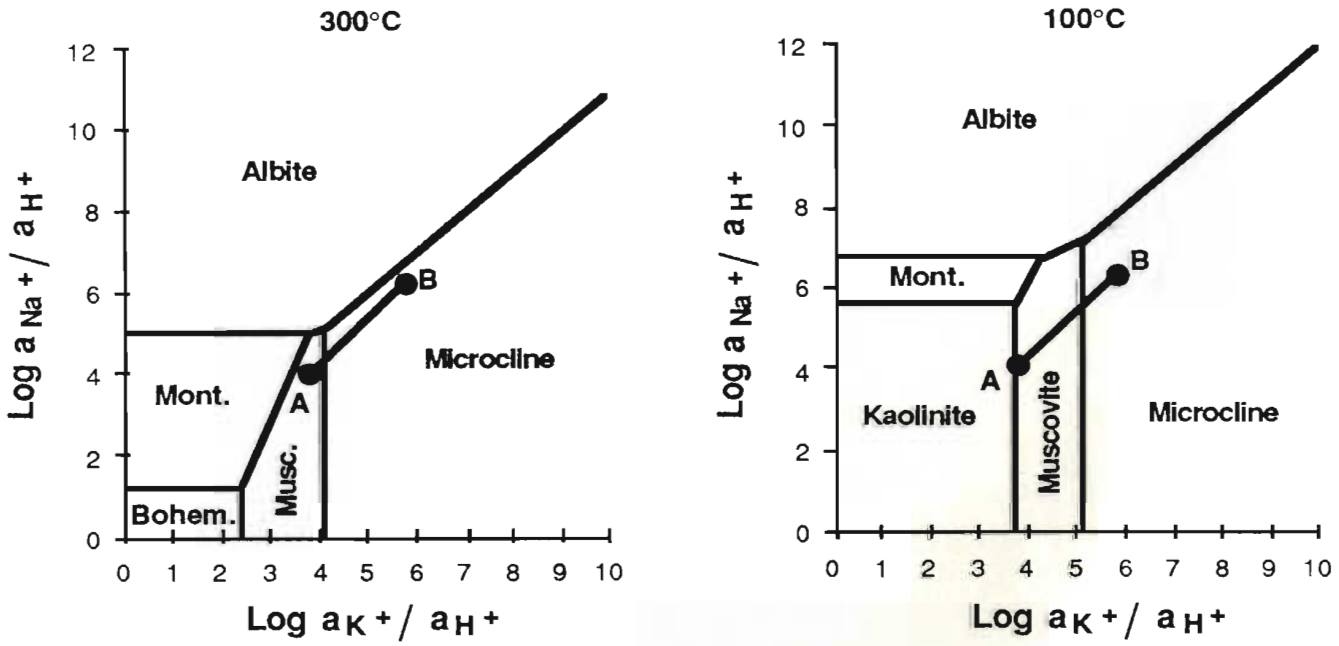

Figure 6-93: Equilibrium activity diagram for the system K_2O-Na_2O-Al_2O_3-SiO_2-H_2O-HCl at 100°C and 300°C, one bar, unit activity of H_2O, and in the presence of quartz (after Helgeson, 1974). See text for discussion.
Abbreviations: mont. - montmorillonite, musc.- muscovite, and bohem.-bohemite.

K-bearing phase in the more intensely altered rocks of the inner alteration zones, to K-feldspar in the less altered rocks of the outer alteration zones,

6.15.11 Diabase and trondhjemite dykes — discussion

Diabase dykes noted in the Skidder Prospect drill core presumably "fed" overlying mafic flows. The dykes are typically lower in Zr than the basalts they intrude, which would suggest a replenishment of the magma chamber(s) between extrusion of the basalts and intrusion of the dykes.

Massive sulphides in SK 27 are cut by post-ore diabase dykes (Figure 6-17), which are chlorite rich, and geochemically similar to less altered rocks of the cl,qz,py alteration zone. This would suggest that Mg-metasomatism continued in the area after deposition of the massive sulphides.

Host rocks to the Skidder Prospect are cut by trondhjemite dykes, which, in places, separate rocks showing different degrees of alteration, but, in other areas, are brecciated, silicified and pyrite bearing. This suggests that at least some of the trondhjemite dykes were emplaced prior to or during the sulphide-forming event while others were emplaced at a later time.

6.16 Conclusions

The Skidder Prospect is an ophiolite-type volcanogenic massive sulphide deposit hosted within basaltic pillow lavas, mafic pillow breccias and aquagene tuffs of the Skidder Basalt. Brecciated, quartz-veined, unlayered jasper and lesser bedded jasper and jasper-rich siltstone are spatially associated with the massive sulphides. Trondhjemite dykes intrude rocks in the Skidder Prospect area in several places.

The deposit contains possible and probable reserves of 200 000 tonnes grading 2% copper and 2% zinc, accompanied by very minor amounts of lead. The sulphides occur mainly in two lenses composed of semimassive to massive unlayered and layered pyrite containing lesser amounts of chalcopyrite and low-iron sphalerite. Rare galena, hematite and magnetite are also noted. Quartz, chlorite and lesser calcite are the predominant gangue minerals. Abundant disseminated sulphides, mostly pyrite, occur in a quartz- and/or chlorite- ± talc-rich stringer zone underlying the massive sulphides.

Distinct alteration zones, characterized by secondary mineral assemblages, envelop the massive sulphide lenses and flank the underlying stringer zone, typically up to 150 m away from the sulphide-bearing zones. The alteration primarily involves large increases in the amount of intersertal chlorite and quartz; replacement of mafic minerals by chlorite, and replacement of albitized plagioclase by quartz and lesser phengitic sericite. Chlorite also replaces quartz in places. Chlorites from the alteration zone are significantly enriched in magnesium relative to those of typical spilitized Skidder basalts. Calcite and epidote, which occur in abundance in typical spilitized Skidder basalt, are destroyed.

In most areas, the alteration is characterized by sporadic enrichment of K, Rb, Ba and Pb; depletion of Ca, Sr and Na; and redistribution of Si. Magnesium and Zinc are enriched in intensely chloritized zones. The Zn probably occurs in tiny sphalerite grains intimately associated with the high-Mg chlorite. The sporadic enrichment of K and related elements is evident up to 400 m away from the sulphide-bearing zones; the other geochemical effects are recognizable only about 150 m away. Incompatible elements Zr,

Y, P ± Ti, and compatible elements Cr and Ni have remained stable, even in intensely altered rocks. Chondrite-normalized rare-earth element patterns associated with sulphide-poor samples, ranging from relatively unaltered to silicified and intensely chloritized, are similar to those of typical spilitized Skidder Basalt. Sulphide-rich samples are depleted in REE concentrations relative to typical Skidder Basalt, and some show relative depletion of Ce and the middle REE; characteristics shown by chondrite-normalized REE patterns for seawater.

Lead isotope ratios of the Skidder Prospect sulphides are some of the least radiogenic of Newfoundland mineral deposits. On the $^{207}Pb / ^{204}Pb$ vs. $^{206}Pb / ^{204}Pb$ diagram, they plot along the mantle lead evolution curve of Zartman and Doe (1981).

The genetic model suggested for formation of the Skidder Prospect is similar to that proposed for other ophiolite-related deposits (Figure 6-91). Metals are suggested to have been leached from underlying rocks by heated, deep-circulating, modified seawater; possibly similar in composition to hydrothermal solutions emanating from vents on the East Pacific Rise. The metals were probably carried in solution as chloride complexes. Local faulting provided upward access to the seafloor for the metal-bearing hydrothermal fluids; there, the massive sulphides are suggested to have been deposited, possibly in a similar manner to those now forming on the East Pacific Rise. Mixing between the upwelling, metal-bearing hydrothermal fluid and cool, shallow-convecting seawater is suggested to have produced the associated alteration effects and the disseminated-sulphide stockwork zone. Much of the spatially associated jasper has probably been produced by oxidative leaching of sulphides exposed on the seafloor.

REFERENCES

Abbey, S., 1980: Studies in "standard samples" for use in the general analysis of silicate rocks and minerals. Part 6: 1979 edition of "usable" values. Geological Survey of Canada, Paper 80-14, 30p.

Adamides, N.G., 1980: The form and environment of formation of the Kalavasos ore deposits - Cyprus. In Panayiotou, A., ed., Ophiolites. Proceedings of the International Ophiolite Symposium, Cyprus, 1979; Cyprus Ministry of Agriculture and Natural Resources, Geological Survey Department, p. 117-178.

Adamides, N.G., 1983: Diverse modes of occurrence of Cyprus sulphide deposits and comparison with recent analogues [abs.]. GAC/MAC Joint Annual Meeting, Victoria 1983, Program with Abstracts, v. 8, p. A1.

Alabaster, T., 1983: Genesis of massive sulphide deposits in the Northern Oman ophiolite [abs.]. GAC/MAC Joint Annual Meeting, Victoria 1983, Program with Abstracts, v. 8, p. A1.

Alabaster, T., and Pearce, J.A., 1985: The interrelationship between magmatic and ore-forming hydrothermal processes in the Oman ophiolite. Economic Geology, v. 80, p. 1-16.

Alabaster, T., Pearce, J.A., and Malpas, J., 1982: The volcanic stratigraphy and petrogenesis of the Oman ophiolite complex. Contributions to Mineralogy and Petrology, v. 81, p. 168-183.

Allègre, C.J., and Minster, J.F., 1978: Quantitative models of trace element behaviour in magmatic processes. Earth and Planetary Science Letters, v. 38, p. 1-25.

Amstutz, G.C., ed, 1974: Spilites and Spilitic Rocks. International Union of Geological Sciences, Series A, Number 4, Springer-Verlag, Berlin/Heidelberg, 482p.

Arth, J.G., and Barker, F., 1976: Rare-earth partitioning between hornblende and dacitic liquid and implications for the genesis of trondhjemitic-tonalitic magmas. Geology, v. 4, p. 534-536.

ASARCO (American Smelting and Refining Company), 1972: Geology, Skidder Brook Sheet. Unpublished company map, scale 1:12 000.

ASARCO-Price, 1977: Skidder Prospect. Unpublished company map, scale 1:2400.

Bachinski, D.J., 1977: Alteration associated with metamorphosed ophiolitic cupriferous iron sulfide deposits: Whalesback mine, Notre Dame Bay, Newfoundland. Mineralium Deposita, v. 12, pp 48-63.

Baragar, W.R.A., Plant, A.G., Pringle, G.J., and Schau, M., 1977: Petrology and alteration of selected units of Mid-Atlantic Ridge basalts sampled from sites 332 and 335, DSDP. Canadian Journal of Earth Sciences, v. 14, p. 837-874.

Barbour, D., 1977: Geology and mineralization of the Skidder Prospect; Price-ASARCO co-tenancy. Unpublished company report for the Price Company Limited, Mineral Resources Division, 20 p.

Barker, F., 1979: Trondhjemite: definition, environment and hypotheses of origin. In Barker, F., ed., Trondhjemites, Dacites and Related Rocks. Developments in Petrology 6, Elsevier Scientific, Amsterdam, p. 1-12.

Barton, P.B., Jr., and Skinner, B.J., 1979: Sulfide mineral stabilities. In Barnes, H.L., ed., Geochemistry of Hydrothermal Ore Deposits; Second Edition. John Wiley and Sons, New York, p. 278-403.

Basaltic Volcanism Study Project (BVSP), 1981a: Ocean-floor basaltic volcanism. In Basaltic Volcanism Study Project, Basaltic Volcanism on the Terrestrial Planets. Pergamon Press, New York p. 132-160.

Basaltic Volcanism Study Project (BVSP), 1981b: Island arc basalts. In Basaltic Volcanism Study Project, Basaltic Volcanism on the Terrestrial Planets. Pergamon Press, New York p. 193-213.

Basaltic Volcanism Study Project (BVSP), 1981c: Experimental petrology of basalts and their source rocks; Introduction. In Basaltic Volcanism Study Project, Basaltic Volcanism on the Terrestrial Planets. Pergamon Press, New York p. 494-513.

Battey, M.H., 1974: Spilites as weakly metamorphosed tholeiites. In Amstutz, G.C., ed, Spilites and Spilitic Rocks. International Union of Geological Sciences, Series A, Number 4, Springer-Verlag, Berlin/Heidelberg, p. 365-372.

Beccaluva, L., Ohnenstetter, D., and Ohnenstetter, M., 1979: Geochemical discrimination between ocean-floor and island-arc tholeiites—application to some ophiolites. Canadian Journal of Earth Sciences, v. 16, p. 1874-1882.

Beccaluva, L., Piccardo, G.B., and Serri, G., 1980: Petrology of Northern Apennine ophiolites and comparison with other Tethyan ophiolites. In Panayiotou, A., ed., Ophiolites. Proceedings of the International Ophiolite Symposium, Cyprus, 1979; Cyprus Ministry of Agriculture and Natural Resources, Geological Survey Department, p. 314-331.

Bell, K., and Blenkinsop, J., 1981: A geochronological study of the Buchans area, Newfoundland. In Swanson E.A., Strong, D.F., and Thurlow, J.G., eds., The Buchans Orebodies: Fifty Years of Geology and Mining. Geological Association of Canada, Special Paper 22, p. 91-111.

Bence, A.E., and Albee, A.L., 1968: Empirical correction factors for the electron microanalysis of silicates and oxides. Journal of Geology, v. 76, p. 382-403.

Bence, A.E., and Bender, J.F., 1978: Clinopyroxenes in mid-ocean ridge basalts: experimental studies [abs.]. EOS, Transactions of the American Geophysical Union, v. 59, p. 410.

Bender, J.F., Hodges, F.N., and Bence, A.E., 1978: Petrogenesis of basalts from the project FAMOUS area: Experimental study from 0 to 15 kbars. Earth and Planetary Science Letters, v. 41, p. 277-302.

Best, M.G., 1975: Migration of hydrous fluids in the upper mantle and potassium variation in calc-alkalic rocks. Geology, v. 3, pp 429-432.

Binney, W.P., 1987: A sedimentological investigation of MacLean channel transported sulphide ores. In Kirkham, R.V, ed., Buchans Geology, Newfoundland. Geological Survey of Canada, Paper 86-24, Report 8, p. 107-147.

Bischoff, J.L., Rosenbauer, R.J., Aruscavage, P.J., Baedecker, P.A., and Crock, J.G., 1983: Sea-floor massive sulfide deposits from 21° N, East Pacific Rise; Juan de Fuca Ridge; and Galapagos Rift: Bulk chemical composition and economic implications. Economic Geology, v. 78, p. 1711-1720.

Blackwood, R.F., 1978: Northeastern Gander zone, Newfoundland. In Gibbons, R.V., ed., Report of Activities for 1977. Newfoundland Department of Mines and Energy, Mineral Development Division, Report 78-1, p. 72-79.

Blackwood, R.F., 1979: Geology of the Gander River area (2E/2), Newfoundland. In Gibbons, R.V., ed., Report of Activities for 1978. Newfoundland Department of Mines and Energy, Mineral Development Division, Report 79-1, p. 38-42.

Blackwood, R.F., 1980: Geology of the Gander (west) area (2D/15), Newfoundland. In O'Driscoll, C.F., and Gibbons R.V., eds., Current Research. Newfoundland Department of Mines and Energy, Mineral Development Division, Report 80-1, p. 53-61.

Blackwood, R.F., 1985: Geology of the Facheux Bay map area (11P/9), Newfoundland. Newfoundland Department of Mines and Energy, Mineral Development Division, Report 85-4.

Blackwood, R.F., and Kennedy, M.J., 1975: The Dover Fault: western boundary of the Avalon Zone in northeastern Newfoundland. Canadian Journal of Earth Sciences, v. 12, p. 320-325.

Blackwood, R.F., and O'Driscoll, C.F., 1976: The Gander-Avalon zone boundary in southeastern Newfoundland. Canadian Journal of Earth Sciences. v. 13, p. 1155-1159.

Bonatti, E., Zerbi, M., Kay, R., Rydell, H., 1976: Metalliferous deposits from the Apennine ophiolites: Mesozoic equivalents of modern deposits from oceanic spreading centers. Geological Society of America Bulletin, v. 87, p. 83-94.

Bostock, H.H., 1978: The Roberts Arm Group, Newfoundland: Geological notes on a Middle or Upper Ordovician island arc environment. Geological Survey of Canada, Paper 78-15, 21 p.

Bougault, H., Maury, R.C., El Azzouzi, M., Joron, J.L., Cotten, J., and Treuil, M., 1982: Tholeiites, basaltic andesites, and andesites from Leg 60 sites: Geochemistry, mineralogy, and low partition coefficient elements. In Lee, M., Watkins, J.S., et al., Initial Reports of the Deep Sea Drilling Project, v. 60, Washington (U.S. Government Printing Office), p. 657-677.

Brown, E.H., 1977: The crossite content of Ca-amphibole as a guide to pressure of metamorphism. Journal of Petrology, v. 18, p. 53-72.

Butler, A.J., and Davenport, P.H., 1978: Lake sediment geochemical survey in the Meelpaeg Lake area of central Newfoundland. Newfoundland Department of Mines and Energy, Mineral Development Division, Open File NFLD (986).

Calon, T.J., and Green, F.K., 1987: Preliminary results of detailed structural analysis of the Buchans Mine area. In Kirkham, R.V, ed., Buchans Geology, Newfoundland. Geological Survey of Canada, Paper 86-24, Report 17, p. 273-288.

Cameron, W.E., McCulloch, M.T., and Walker, D.A., 1983: Boninite petrogenesis: Chemical and Nd-Sr isotopic constraints. Earth and Planetary Science Letters, v. 65, p. 75-89.

Cameron, W.E., Nisbet, E.G., and Dietrich, V.J., 1980: Petrographic dissimilarities between ophiolitic and ocean floor basalts. In Panayiotou, A., ed., Ophiolites. Proceedings of the International Ophiolite Symposium, Cyprus, 1979; Cyprus Ministry of Agriculture and Natural Resources, Geological Survey Department, p. 182-192.

Campbell, I.H., McDougall, T.J., and Turner, J.S., 1984: A note on fluid dynamic processes which can influence the deposition of massive sulfides. Economic Geology. v. 79, pp 1905-1913.

Carlisle, D., 1963: . Pillow breccias and their aquagene tuffs, Quadra Island, British Columbia. Journal of Geology, v. 71, p. 48-71.

Carmichael, I.S.E., Turner, F.J., and Verhoogen, J., 1974: Igneous Petrology. McGraw-Hill, New York, 739p.

Chappell, B.W., and White, A.J.R., 1974: Two contrasting granite types. Pacific Geology, v. 8, p. 173-174.

Chorlton, L., 1980: Geology of the La Poile River area (11O/16), Newfoundland. Newfoundland Department of Mines and Energy, Mineral Development Division, Report 80-3.

Church, W.R., and Stevens, R.K., 1971: Early Paleozoic ophiolite complexes of the Newfoundland Appalachians as mantle-oceanic crust sequences. Journal of Geophysical Research, v. 76, p. 1460-1466.

Coish, R.A., and Church, W.R., 1979: Igneous geochemistry of mafic rocks in the Betts Cove ophiolite, Newfoundland. Contributions to Mineralogy and Petrology, v. 70, p. 29-39.

Coish, R.A., and Taylor, L.A., 1979: The effects of cooling rate on texture and pyroxene chemistry in DSDP Leg 34 basalt: A microprobe study. Earth and Planetary Science Letters, v. 42, p. 389-398.

Coish, R.A., Hickey, R., and Frey, F.A., 1982: Rare earth element geochemistry of the Betts Cove ophiolite, Newfoundland: complexities in ophiolite formation. Geochimica et Cosmochimica Acta, v. 46, p. 2117-2134.

Cole, T.G., 1983: Oxygen isotope geothermometry and origin of smectites in the Atlantis II Deep, Red Sea. Earth and Planetary Science Letters, v. 66, p. 166-176.

Coleman, R.G., and Donato, M.M., 1979: Oceanic plagiogranite revisited. In Barker, F., ed., Trondhjemites, Dacites and Related Rocks. Developments in Petrology 6, Elsevier Scientific, Amsterdam, p. 149-168.

Coleman, R.G., and Peterman, Z.E., 1975: Oceanic plagiogranite. Journal of Geophysical Research, v. 80, p. 1099-1108.

Collins, W.J., Beams, S.D., White, A.J.R., and Chappell, B.W., 1982: Nature and origin of A-type granites with particular reference to southeastern Australia. Contributions to Mineralogy and Petrology, v. 80, p. 189-200.

Colman-Sadd, S.P., 1980: Geology of south-central Newfoundland and evolution of the eastern margin of Iapetus. American Journal of Science, v. 280, p. 991-1017.

Colman-Sadd, S.P., and Swinden, H.S., 1984: A tectonic window in central Newfoundland? Geological evidence that the Appalachian Dunnage zone may be allochthonous. Canadian Journal of Earth Sciences, v. 21, p. 1349-1367.

Coney, P.J., Jones, D.L., and Monger, J.W.H., 1980: Cordilleran suspect terranes. Nature, v. 288, p. 329-333.

Constantinou, G., 1976: Genesis of the conglomerate structure, porosity and collomorphic textures of the massive sulphide ores of Cyprus. In Strong, D.F., ed., Metallogeny and Plate Tectonics. Geological Association of Canada, Special Paper 14, p. 187-210.

Constantinou, G., 1980: Metallogenesis associated with the Troodos ophiolite. In Panayiotou, A., ed., Ophiolites. Proceedings of the International Ophiolite Symposium, Cyprus, 1979; Cyprus Ministry of Agriculture and Natural Resources, Geological Survey Department, p. 663-674.

Constantinou, G., and Govett, G.J.S., 1972: Genesis of sulphide deposits, ochre and umber of Cyprus. Institution of Mining and Metallurgy Transactions, Section B, Applied earth science, v. 81, p. B34-B46.

Constantinou, G., and Govett, G.J.S., 1973: Geology, geochemistry and genesis of Cyprus sulfide deposits. Economic Geology, v. 68, p. 843-858.

Constantinou, G., and Robinson, P.T., 1983: The formative environment of the massive sulphide ores of the Troodos ophiolite complex, Cyprus [abs.]. GAC/MAC Joint Annual Meeting, Victoria 1983, Program with Abstracts, v. 8, p. A14.

Costa, U.R., Barnett, R.L., and Kerrich, R., 1983: The Mattagami Lake mine Archean Zn-Cu sulfide deposit, Quebec: Hydrothermal coprecipitation of talc and sulfides in a sea-floor brine pool—Evidence from geochemistry $^{18}O/^{16}O$, and mineral chemistry. Economic Geology v. 78, p. 1144-1203.

Coyle, M, and Strong, D.F., 1987: Geology of the Springdale Group: a newly recognized Silurian epicontinental-type caldera in Newfoundland. Canadian Journal of Earth Sciences, v. 24, p. 1135-1148.

Craig, J.R., 1983: Metamorphic features in Appalachian massive sulphides. Mineralogical Magazine, v. 47, p. 515-525.

Craig, J.R., Ljøkjell, P., and Vokes, F.M., 1984: Sphalerite compositional variations in sulfide ores of the Norwegian Caledonides. Economic Geology, v. 79, p. 1727-1735.

Crawford, A.J., and Cameron, W.E., 1985: Petrology and geochemistry of Cambrian boninites and low-Ti andesites from Heathcote, Victoria. Contributions to Mineralogy and Petrology, v. 91, p. 93-104.

Crawford, A.J., Beccaluva, L., and Serri, G., 1981: Tectono-magmatic evolution of the west Philippine-Mariana region and the origin of boninites. Earth and Planetary Science Letters, v. 54, p. 346-356.

Cullers, R.L., and Graf, J.L., 1984: Rare earth elements in igneous rocks of the continental crust: Predominantly basic and ultrabasic rocks. In Henderson, P., ed., Rare Earth Element Geochemistry; Developments in Geochemistry, No. 2. Elsevier, p. 237-274.

Cumming, G.L., and Krstic, D., 1987: Detailed lead isotope study of Buchans and related ores. In Kirkham, R.V., ed., Buchans Geology, Newfoundland. Geological Survey of Canada, Paper 86-24, Report 13, p. 227-233.

Cumming, G.L., and Richards, J.R., 1975: Ore lead isotope ratios in a continuously changing earth. Earth and Planetary Science Letters, v. 28, p. 155-171.

Currie, K.L., Pajari, G.E., and Pickerill, R.K., 1979: Tectono-stratigraphic problems in the Carmanville area, northeastern Newfoundland. In Current Research, Part A, Geological Survey of Canada, Paper 79-1A, p. 71-76.

Dallmeyer, R.D., Odom, A.L., O'Driscoll, C.F., and Hussey, E.M., 1981a: Geochronology of the Swift Current granite and host volcanic rocks of the Love Cove Group, southwestern Avalon zone, Newfoundland: evidence of a late Proterozoic volcanic-subvolcanic association. Canadian Journal of Earth Sciences, v. 18, p. 699-707.

Dallmeyer, R.D., Blackwood, R.F., and Odom, A.L., 1981b: Age and origin of the Dover fault: tectonic boundary between the Gander and Avalon zones of the northeastern Newfoundland Appalachians. Canadian Journal of Earth Sciences, v. 18, p. 1431-1442.

Dean, P.L., 1978: The volcanic stratigraphy and metallogeny of Notre Dame Bay, Newfoundland. Memorial University of Newfoundland, Geology Report 7, 205p.

Dean, P.L., and Strong, D.F., 1975: The volcanic stratigraphy, geochemistry and metallogeny of the central Newfoundland Appalachians. Geological Association of Canada, Annual Meeting, Waterloo, Ontario, 1975, Program with Abstracts, p. 745-746.

Deer, W.A., Howie, R.A., and Zussman, J., 1962: Rock-Forming Minerals, Volume 3, Sheet Silicates. Longmans, Green; London, 270 p.

Deer, W.A., Howie, R.A., and Zussman, J., 1966: An introduction to the rock-forming minerals. Longman Group Limited, London, 528 p.

Dewey, J.F., and Bird, J.M., 1971: Origin and emplacement of the ophiolite suite: Appalachian ophiolites in Newfoundland. Journal of Geophysical Research, v. 76, p. 3179-3206.

Dick, H.J.B., and Bryan, W.B., 1978: Variation of basalt phenocryst mineralogy and rock compositions in DSDP Hole 396B. In Dmitriev, L., Heirtzler, et al., Initial Reports of the Deep Sea Drilling Project, v. 46, Washington (U.S. Government Printing Office), p. 215-226.

Dick, H.J.B., and Bullen, T., 1984: Chromian spinel as a petrogenetic indicator in abyssal and alpine-type peridotites and spatially associated lavas. Contributions to Mineralogy and Petrology, v. 86, p. 54-76.

Dingwell, D.B., 1980: The geology, geophysics and geochemistry of the Port aux Basques Granite. Unpublished B.Sc. (Honours) thesis, Memorial University of Newfoundland, St. John's, Newfoundland. 126p.

Dixon, S., and Rutherford, M.J., 1979: Plagiogranites as late-stage immiscible liquids in ophiolite and mid-ocean ridge suites: an experimental study. Earth and Planetary Science Letters, v. 45, p. 45-60.

Dixon, T.H., and Batiza, R., 1979: Petrology and chemistry of recent lavas in the northern Marianas: implications for the origin of island arc basalts. Contributions to Mineralogy and Petrology, v. 70, p. 167-181.

Doe, B.R., and Zartman, R.E., 1979: Plumbotectonics, the Phanerozoic. In Barnes, H.L., ed., Geochemistry of Hydrothermal Ore Deposits; Second Edition. John Wiley and Sons, New York, p. 22-70.

Duke, N.A., and Hutchinson, R.W., 1974: Geological relationships between massive sulfide bodies and ophiolitic volcanic rocks near York Harbour, Newfoundland. Canadian Journal of Earth Sciences, v. 11, p. 53-69.

Dunning, G.R., 1984: The geology, geochemistry, geochronology and regional setting of the Annieopsquotch Complex and related rocks of southwest Newfoundland. Unpublished Ph.D. thesis, Memorial University of Newfoundland, St. John's, Newfoundland, 403p.

Dunning, G.R., 1986: Precise U/Pb zircon geochronology applied to Newfoundland ophiolites, granitoid and felsic volcanic rocks [abs.]. Isotopes, Geological Association of Canada, Newfoundland Section, Spring Meeting March 20-21, 1986, Program with Abstracts, pp 11-12.

Dunning, G.R., and Chorlton, L.B., 1985: The Annieopsquotch ophiolite belt of southwest Newfoundland: Geology and tectonic significance. Geological Society of America Bulletin, v. 96, p. 1466-1476.

Dunning, G.R., and Herd, R.K., 1980: The Annieopsquotch ophiolite complex, southwest Newfoundland, and its regional relationships. In Current Research, Part A, Geological Survey of Canada, Paper 80-1A, p. 227-234.

Dunning, G.R., and Krogh, T.E., 1985: Geochronology of ophiolites of the Newfoundland Appalachians. Canadian Journal of Earth Sciences, v. 22, No. 11, p. 1659-1670.

Dunning, G.R., Kean, B.F., Thurlow, J.G., and Swinden, H.S., 1987: Geochronology of the Buchans, Roberts Arm, and Victoria Lake groups and Mansfield Cove Complex, Newfoundland. Canadian Journal of Earth Sciences v. 24, p. 1175-1184.

Edmond, J.M., 1981: Hydrothermal activity at mid-ocean ridge axes. Nature, v. 290, p. 87-88.

Elders, W.A., Hoagland, J.R., McDowell, S.D., and Cobo, J.M., 1979: Hydrothermal mineral zones in the geothermal reservoir of Cerro Prieto. In Elders, W.A., ed., Geology and Geothermics of the Salton Trough, Geological Society of America Guidebook, U.C. Riverside Campus Museum Contribution, v. 5, p. 36-43. Also in Proceedings of the First Symposium On the Cerro Prieto Geothermal Field: Part 1, Geothermics, v. 8, No. 3-4, p. 201-209.

Erlank, A.J., and Kable, E.J.D., 1976: The significance of incompatible elements in Mid-Atlantic Ridge basalts from 45° N with particular reference to Zr/Nb. Contributions to Mineralogy and Petrology, v. 54, p. 281-291.

Evarts, R.C., and Schiffman, P., 1983: Submarine hydrothermal metamorphism of the Del Puerto Ophiolite, California. American Journal of Science, v. 283, p. 289-340.

Ewart, A., 1976: Mineralogy and chemistry of modern orogenic lavas—some statistics and implications. Earth and Planetary Science Letters, v. 31, p. 417-432.

Ewart, A., 1982: The mineralogy and petrology of Tertiary-Recent orogenic volcanic rocks: with special reference to the andesite-basaltic compositional range. In Thorpe, R.S., ed., Andesites: Orogenic Andesites and Related Rocks. John Wiley and Sons, Chichester, p. 25-95.

Ewart, A., Bryan, W.B., and Gill, J.B., 1973: Mineralogy and geochemistry of the younger volcanic islands of Tonga, S.W. Pacific. Journal of Petrology, v. 14, p. 429-465.

Feldman, D.S., Jr., Gagnon, J., Hofmann, R., and Simpson, J., 1986: Statview 512+. Abacus Concepts.

Finlow-Bates, T., 1980: The chemical and physical controls on the genesis of submarine exhalative orebodies and their implication for formulating exploration concepts. A review. Geologisches Jahrbuch, Reihe D, p. 131-168.

Fischer, W.R., and Schwertmann, U., 1975: The formation of hematite from amorphous iron(III) hydroxide. Clays and Clay Minerals, v. 23, p. 33-37.

Fleet, A.J., 1984: Aqueous and sedimentary geochemistry of the rare earth elements. In Henderson, P., ed., Rare Earth Element Geochemistry; Developments in Geochemistry, No. 2. Elsevier, p. 343-373.

Fletcher, I.R., and Farquhar, R.M., 1977: Lead isotopes in the Grenville and adjacent Palaeozoic formations. Canadian Journal of Earth Sciences, v. 14, p. 56-66.

Francheteau, J., Needham, H.D., Choukroune, P., Juteau, T., Séguret,M., Ballard, R.D., Fox, P.J., Normark, W., Carranza, A., Cordoba, D., Guerrero, J., Rangin, C., Bougault, H., Cambon, P., and Hekinian, R., 1979: Massive deep-sea sulphide ore deposits discovered on the East Pacific Rise. Nature, v. 277, pp 523-528.

Franklin, J.M., Lydon, J.W., and Sangster, D.F., 1981: Volcanic-associated massive sulfide deposits. Economic Geology, 75th Anniversary Volume, 1981, p. 485-627.

Frey, F.A., Dickey, J.S., Thompson, G., Bryan, W.B., and Davies, H.L., 1980: Evidence for heterogeneous primary MORB and mantle sources, N.W. Indian Ocean. Contributions to Mineralogy and Petrology, v. 74, p. 387-402.

Fryer, B.J., 1977: Rare earth evidence in iron-formations for changing Precambrian oxidation states. Geochimica et Cosmochimica Acta, v. 41, p. 361-367.

Gale, G.H., 1969: The primary dispersion of Cu, Zn, Ni, Co, Mn, and Na adjacent to sulfide deposits, Springdale Peninsula, Newfoundland. Unpublished M.Sc. thesis, Memorial University of Newfoundland, St. John's, Newfoundland, 143p.

Garcia, M.O., 1978: Criteria for the identification of ancient volcanic arcs. Earth Science Reviews, v. 14, p. 147-165.

Geological Survey of Canada, 1954a: Aeromagnetic map 177G, Buchans (NTS 12A/15), scale 1:63 360.

Geological Survey of Canada, 1954b: Aeromagnetic map 187G, Lake Ambrose (NTS 12A/10), scale 1:63 360.

Geological Survey of Canada, 1968: Aeromagnetic map 7049G, Red Indian Lake (NTS 12A), scale 1:253 440.

George, P.W., 1937: Geology of lead-zinc-copper deposits at Buchans, Newfoundland. Transactions of the American Institute of Mining and Metallurgical Engineers, v. 126, p. 488-511.

Gélinas, L., Brooks, C., and Trzcienski, W.E., Jr., 1976: Archean variolites—quenched immiscible liquids. Canadian Journal of Earth Sciences, v. 13, p. 210-230.

Giggenbach, W.F., 1984: Mass transfer in hydrothermal alteration systems—A conceptual approach. Geochimica et Cosmochimica Acta, v. 48, p. 2693-2711.

Goff, S.P., 1984: The magmatic and metamorphic history of the East Arm, Great Slave Lake, N.W.T. Unpublished Ph.D. thesis, University of Alberta, 295p.

Goldberg, E.D., Koide, M., Schmitt, R.A., and Smith, R.H., 1963: Rare-earth distributions in the marine environment. Journal of Geophysical Research, v. 68, p. 4209-4217.

Goldfarb, M.S., Converse, D.R., Holland, H.D., and Edmond, J.M., 1983: The genesis of hot spring deposits on the East Pacific Rise, 21°N. Economic Geology, Monograph 5, The Kuroko and Related Volcanogenic Massive Sulfide Deposits, p. 184-197.

Gorton, M.P., 1977: The geochemistry and origin of Quaternary volcanism in the New Hebrides. Geochimica et Cosmochimica Acta, v. 41, p. 1257-1270.

Graf, J.L., 1977: Rare earth elements as hydrothermal tracers during the formation of massive sulfide deposits in volcanic rocks. Economic Geology, v. 72, p. 527-548.

Gravenor, C.P., 1980: Heavy minerals and sedimentological studies on the glaciogenic Late Precambrian Gaskiers Formation of Newfoundland. Canadian Journal of Earth Sciences, v. 17, p. 1331-1341.

Greenough, J.D., and Papezik, V.S., 1985: Petrology and geochemistry of Cambrian volcanic rocks from the Avalon Peninsula, Newfoundland. Canadian Journal of Earth Sciences, v. 22, p. 1594-1601.

Griffin, B.J., and Varne, R., 1980: The Macquarie Island ophiolite complex: Mid-Tertiary oceanic lithosphere from a major ocean basin. Chemical Geology, v. 30, p. 285-308.

Grove, T.L., and Bence, A.E., 1977: Experimental study of pyroxene-liquid interaction in quartz-normative basalt 15597. In Merrill, R.B., Blanchard, D.D., and Lofgren, G.E., (eds.), Proceedings of the Eighth Lunar Science Conference. Pergamon Press, New York (Geochimica et Cosmochimica Acta, Supplement 8), p. 1549-1579.

Grove, T.L., and Bryan, W.B., 1983: Fractionation of pyroxene-phyric MORB at low pressure: An experimental study. Contributions to Mineralogy and Petrology, v. 84, p. 293-309.

Haas, J.L., Jr., 1971: The effect of salinity on the maximum thermal gradient of a hydrothermal system at hydrostatic pressure. Economic Geology, v. 66, p. 940-946.

Hajash, A., Jr., 1984: Rare earth element abundances and distribution patterns in hydrothermally altered basalts: experimental results. Contributions to Mineralogy and Petrology, v. 85, p. 409-412.

Hamelin, B., Dupré, B., and Allègre, C.J., 1984: The lead isotope systematics of ophiolite complexes. Earth and Planetary Science Letters, v. 67, p. 351-366.

Hanmer, S., 1981: Tectonic significance of the northeastern Gander Zone, Newfoundland: an Acadian ductile shear zone. Canadian Journal of Earth Sciences, v. 18, p. 120-135.

Haskin, L.A., Haskin, M.A., Frey, F.A., and Wildeman, T.R., 1968: Relative and absolute terrestrial abundances of the rare earths. In Ahrens, L.H., ed., Origin and Distribution of the Elements. Pergamon Press, Oxford, p. 889-912.

Hawthorne, F.C., 1983: The crystal chemistry of the amphiboles. Canadian Mineralogist, v. 21, part 2, p. 173-480.

Haymon, R.M., and Kastner, M., 1981: Hot spring deposits on the East Pacific Rise at 21°N: preliminary description of mineralogy and genesis. Earth and Planetary Science Letters, v. 53, p. 363-381.

Hekinian, R., and Fouquet, Y., 1985: Volcanism and metallogenesis of axial and off-axial structures on the East Pacific Rise near 13° N. Economic Geology, v. 80, p. 221-249.

Hekinian, R., Fevrier, M., Bischoff, J.L., Picot., P., and Shanks, W.C., 1980: Sulfide deposits from the East Pacific Rise near 21°N. Science, v. 207, p. 1433-1444.

Helgeson, H.C., 1974: Chemical interaction of feldspars and aqueous solutions. In Mackenzie, W.S., and Zussman, J., eds., The Feldspars. Manchester University Press, Manchester, England, p. 184-217.

Hellman, P.L., and Henderson, P., 1977: Are rare earth elements mobile during spilitization? Nature, v. 267, p. 38-40.

Henderson, P., 1984: General geochemical properties and abundances of the rare earth elements. In Henderson, P., ed., Rare Earth Element Geochemistry; Developments in Geochemistry, No. 2. Elsevier, p. 1-32.

Herrmann, A.G., Potts, M.J., and Knake, D., 1974: Geochemistry of the rare earth elements in spilites from the oceanic and continental crust. Contributions to Mineralogy and Petrology, v. 44, p. 1-16.

Hey, M.H., 1954: A new review of the chlorites. Mineralogical Magazine, v. 30, p. 277-292.

Hibbard, J., 1983: Geology of the Baie Verte Peninsula, Newfoundland. Newfoundland Department of Mines and Energy, Mineral Development Division, Memoir 2, 277p.

Hiscott, R.N., 1982: Tidal deposits of the Lower Cambrian Random Formation, eastern Newfoundland: facies and paleoenvironments. Canadian Journal of Earth Sciences, v. 19, p. 2028-2042.

Hofmann, R.J., 1978: The orthotran solution. Multivariate Behavioral Research, v. 13, p. 99-124.

Høgdahl, O.T., 1967: Distribution of the rare earth elements in seawater. NATO Research Grant No. 203. Semi-annual Progress Report 4 (unpublished), Central Inst. Ind. Res., Blindern.

Høgdahl, O.T., Melson, S., and Bowen, V.T., 1968: Neutron activation analysis of lanthanide elements in seawater. In Baker, R.A., ed., Trace Inorganics in Water. American Chemical Society, Advances in Chemistry Series, No. 73, p. 308-325.

Holloway, J.R., and Burnham, C.W., 1972: Melting relations of basalt with equilibrium water pressure less than total pressure. Journal of Petrology, v. 13, p. 1-29.

Holmes, A., 1946: An estimate of the age of the Earth. Nature, v. 157, p. 680-684.

Holmes, A., 1947: A revised estimate of the age of the earth. Nature, v. 159, p. 127-128.

Holmes, A., 1949: Lead isotopes and the age of the Earth. Nature, v. 163, p. 453-456.

Hotelling, H., 1933: Analysis of a complex of statistical variables into principal components. Journal of Educational Psychology, v. 24, p. 417 and 498.

Houtermans, F.G., 1946: The isotope ratios in natural lead and the age of uranium. Naturwissenschaften, v. 33, p. 185-186, addendum, p. 219.

Hughes, C.J., 1970: The late Precambrian Avalonian orogeny in Avalon, southeast Newfoundland. American Journal of Science, v. 269, p. 183-190.

Hughes, C.J., 1972: Geology of the Avalon Peninsula, Newfoundland, and its possible correspondence with Morocco. Notes et Mémoires du Service Géologique du Maroc, v. 236, p. 265-275.

Hughes, C.J., 1973: Spilites, keratophyres, and the igneous spectrum. Geological Magazine. v. 109, p. 513-527.

Humphris, S.E., 1984: The mobility of the rare earth elements in the crust. In Henderson, P., ed., Rare Earth Element Geochemistry; Developments in Geochemistry, No. 2. Elsevier, p. 317-342.

Humphris, S.E., and Thompson, G., 1978: Hydrothermal alteration of oceanic basalts by seawater. Geochimica et Cosmochimica Acta, v. 42, p. 107-125.

Hutchinson, R.W., and Searle, D.L., 1971: Stratabound pyrite deposits in Cyprus and relations to other sulphide ores. Society Mining Geologists, Japan, Special Issue 3, pp 198-205.

Hyde, R.S., 1984: Geology and mineralization of the Carboniferous Deer Lake Basin, western Newfoundland. In Swinden, H.S., compiler, Mineral Deposits of Newfoundland - A 1984 Perspective. Newfoundland Department of Mines and Energy, Mineral Development Division, Report 84-3, p. 19-26.

Irvine, T.N., 1965: Chromian spinel as a petrogenetic indicator: Part 1. theory. Canadian Journal of Earth Sciences, v. 2, p. 648-672.

Irvine, T.N., 1967: Chromian spinel as a petrogenetic indicator: Part 2, petrologic applications. Canadian Journal of Earth Sciences, v. 4, p. 71-103.

Irvine, T.N., 1976: Chromite crystallization in the join Mg_2SiO_4 — $CaMgSi_2O_6$ — $CaAl_2Si_2O_8$ — $MgCr_2O_4$ — SiO_2. Carnegie Institution of Washington, Yearbook, v. 76, p. 465-472.

Ixer, R.A., Alabaster, T., and Pearce, J.A., 1984: Ore petrography and geochemistry of massive sulphide deposits within the Semail ophiolite, Oman. Transactions of the Institution of Mining and Metallurgy, Section B, Applied earth science, v. 93, p. B114-B124.

Jacobi, R.D., and Wasowski, J.J., 1985: Geochemistry and plate-tectonic significance of the volcanic rocks of the Summerford Group, north-central Newfoundland. Geology, v. 13, p. 126-130.

Jakes, P., and Gill, J., 1970: Rare earth elements and the island arc tholeiitic series. Earth and Planetary Science Letters, v. 9, p. 17-28.

Jakes, P., and White, A.J.R., 1972: Major and trace element abundances in volcanic rocks of orogenic areas. Geological Society of America Bulletin, v. 83, p. 29-40.

Jamieson, R.A., 1977: A suite of alkali basalts and gabbros associated with the Hare Bay Allochthon of western Newfoundland. Canadian Journal of Earth Sciences, v. 14, p. 346-356.

Jamieson, R.A., 1979: The St. Anthony Complex, northwestern Newfoundland: A petrological study of the relationship between a peridotite sheet and its dynamothermal aureole (2 parts). Unpublished Ph.D. thesis, Memorial University of Newfoundland, St. John's, Newfoundland.

Jamieson, R.A., 1980: Formation of metamorphic aureoles beneath ophiolites - Evidence from the St. Anthony Complex, Newfoundland. Geology, v. 8, p. 150-154.

Jamieson, R.A., 1982: Metamorphism during ophiolite emplacement—the petrology of the St. Anthony Complex. Journal of Petrology, v. 22, p. 397-449.

Janecky, D.R., and Seyfried, W.E., Jr., 1984: Formation of massive sulfide deposits on oceanic ridge crests: Incremental reaction models for mixing between hydrothermal solutions and seawater. Geochimica et Cosmochimica Acta, v. 48, p. 2723-2738.

Jenner, G.A., 1981: Geochemistry of high-Mg andesites from Cape Vogel, Papua New Guinea. Chemical Geology, v. 33, p. 307-332.

Jenner, G.A., and Fryer, B.J., 1980: Geochemistry of the upper Snooks Arm Group basalts, Burlington Peninsula, Newfoundland: evidence against formation in an island arc. Canadian Journal of Earth Sciences, v 17, p. 888-900.

Jenness, S.E., 1963: Terra Nova and Bonavista map areas, Newfoundland. Geological Survey of Canada, Memoir 327, 184p.

Kaiser, H.F., 1958: The varimax criterion for varimax rotation in factor analysis. Psychometrika, v. 23, p. 187-200.

Karson, J., and Dewey, J.F., 1978: Coastal Complex, western Newfoundland: An Early Ordovician oceanic fracture zone. Geological Society of America Bulletin, v. 89, p. 1037-1049.

Kay, R., Hubbard, N.J., and Gast, P.W., 1970: Chemical characteristics and origin of ocean ridge volcanic rocks. Journal of Geophysical Research, v. 75, p. 1585-1613.

Kean, B.F., 1977: Geology of the Victoria Lake map area (12A/6), Newfoundland. Newfoundland Department of Mines and Energy, Mineral Development Division, Report 77-4, 11 p.

Kean, B.F., 1978: Geology of the Star Lake east half sheet (12A/11E), Newfoundland. In Gibbons, R.V., ed., Report of Activities for 1977. Newfoundland Department of Mines and Energy, Mineral Development Division, Report 78-1, p. 129-134.

Kean, B.F., 1979: Buchans, Newfoundland. Newfoundland Department of Mines and Energy, Mineral Development Division, Map 79-125 with marginal notes, scale 1: 50 000.

Kean, B.F., 1983: Geology and mineral deposits of the Lush's Bight Group in the Little Bay Head - Halls Bay Head area. In Murray, M.J., Saunders, P.D., Boyce, W.D., and Gibbons, R.V., compilers and editors, Current Research, Newfoundland Department of Mines and Energy, Mineral Development Division, Report 83-1, p. 157-174.

Kean, B.F., 1984: Geology and mineral deposits of the Lushs Bight Group, Notre Dame Bay, Newfoundland. In Murray, M.J., Whelan, J.G., and Gibbons, R.V., compilers and editors, Current Research, Newfoundland Department of Mines and Energy, Mineral Development Division, Report 84-1, p. 141-156.

Kean, B.F., and Jayasinghe, N.R., 1980: Geology of the Lake Ambrose (12A/10) - Noel Paul's Brook (12A/9) map areas, central Newfoundland. Newfoundland Department of Mines and Energy, Mineral Development Division, Report 80-2, 29 p.

Kean, B.F., Dean, P.L., and Strong, D.F., 1981: Regional geology of the Central Volcanic Belt of Newfoundland. In Swanson E.A., Strong, D.F., and Thurlow, J.G., eds., The Buchans Orebodies: Fifty Years of Geology and Mining. Geological Association of Canada, Special Paper 22, p. 65-78.

Kidd, W.S.F., 1974: The evolution of the Baie Verte lineament, Burlington Peninsula, Newfoundland. Unpublished Ph.D. thesis, Cambridge University, England, 329p.

King, A.F., 1986: Geology of the St. John's area, Newfoundland. In Blackwood, R.F., Walsh, D.G., and Gibbons, R.V., compilers and editors, Current Research, Newfoundland Department of Mines and Energy, Mineral Development Division, Report 86-1, p. 209-218.

King, A.F., Brückner, W.D., Anderson, M.M., and Fletcher, T.P., 1974: Late Precambrian and Cambrian sedimentary sequences of southeastern Newfoundland. Fieldtrip manual B-6, Annual Meeting, Geological, and Mineralogical Association of Canada, St. John's, Newfoundland, 59p.

Kirkham, R.V., 1987: Tectonic setting of the Buchans Group. In Kirkham, R.V, ed., Buchans Geology, Newfoundland. Geological Survey of Canada, Paper 86-24, Report 1, p. 23-34.

Kirkham, R.V., and Thurlow, J.G., 1987: Evaluation of a resurgent caldera and aspects of ore deposition and deformation at Buchans. In Kirkham, R.V, ed., Buchans Geology, Newfoundland. Geological Survey of Canada, Paper 86-24, Report 10, p. 177-194.

Knapp, D.A., 1980: The stratigraphy, structure, and metamorphism of central Glover Island, western Newfoundland. In Current Research, Part B, Geological Survey of Canada, Paper 80-1B, p. 89-96.

Koski, R.A., Goodfellow, R., and Bouse, R.M., 1982: Preliminary description of massive sulfide samples from the southern Juan de Fuca Ridge. United States Geological Survey, Open-File Report, No. 82-0200-B, 22p.

Köppel, V., and Grünenfelder, M., 1979: Isotope geochemistry of lead. In Jager, E., and Hunziltev, J.C., eds., Lectures in isotope geology. Springer-Verlag, Berlin, 329p.

Krauskopf, K.B., 1967: Introduction to Geochemistry. McGraw-Hill, New York, 721p.

Kushiro, I., 1960: Si-Al relation in clinopyroxenes from igneous rocks. American Journal of Science, v. 258, p. 548-554.

Langmyhr, F.J., and Paus, P.E., 1968: The analysis of inorganic siliceous materials by atomic absorption spectrophotometry and the hydrofluoric acid decomposition technique, Part I: The analysis of silicate rocks. Analytica Chimica Acta, v. 43, p. 397-408.

Langmuir, C.H., Bender, J.F., Bence, A.E., Hanson, G.N., and Taylor, S.R., 1977: Petrogenesis of basalts from the FAMOUS area: Mid-Atlantic Ridge. Earth and Planetary Science Letters, v. 36, p. 133-156.

Le Roex, A.P., Dick, H.J.B., Erlank, A.J., Reid, A.M., Frey, F.A., and Hart, S.R., 1983: Geochemistry, mineralogy and petrogenesis of lavas erupted along the southwest Indian Ridge between the Bouvet triple junction and 11 degrees east. Journal of Petrology, v. 24, p. 267-318.

Leake, B.E., 1978: Nomenclature of amphiboles. American Mineralogist, v. 63; p. 1023-1052.

LeBas, M.J., 1962: The role of aluminum in igneous clinopyroxenes with relation to their parentage. American Journal of Science, v. 260, p. 267-288.

Leterrier, J., Maury, R.C., Thonon, P., Girard, D., and Marshal., M., 1982: Clinopyroxene composition as a method of identification of the magmatic affinities of paleo-volcanic series. Earth and Planetary Science Letters, v. 59, p. 139-154.

Liou, J.G., 1973: Synthesis and stability relations of epidote, $Ca_2Al_2FeSi_3O_{12}(OH)$. Journal of Petrology, v. 14, p. 381-413.

Liou, J.G., and Ernst, W.G., 1979: Oceanic ridge metamorphism of the East Taiwan ophiolite. Contributions to Mineralogy and Petrology, v. 68, p. 335-348.

Lofgren, G., 1974: An experimental study of plagioclase crystal morphology: Isothermal crystallization. American Journal of Science, v. 274, p. 243-273.

Lonsdale, P., Batiza, R., and Simkin, T., 1982: Metallogenesis at seamounts on the East Pacific Rise. Marine Technology Society Journal, v. 16, p. 54-61.

Ludden, J.N., and Thompson, G., 1978: Behaviour of rare earth elements during submarine weathering of tholeiitic basalts. Nature v. 274, p. 147-149.

Ludden, J.N., and Thompson, G., 1979: An evaluation of the behaviour of the rare earth elements during the weathering of sea-floor basalt. Earth and Planetary Science Letters, v 43, pp 85-92.

Malahoff, A., 1981: Comparison between Galapagos and Gorda spreading centers. Proceedings, Offshore Technology Conference, Number 13, v. 4, p. 115-121.

Malahoff, A., 1982: A comparison of the massive submarine polymetallic sulfides of the Galapagos rift with some continental deposits. Marine Technology Society Journal, v. 16, p. 39-45.

Malpas, J., 1976: The petrology and petrogenesis of the Bay of Islands ophiolite suite, western Newfoundland (2 parts). Unpublished Ph.D. thesis, Memorial University of Newfoundland, St. John's, Newfoundland, 435p.

Malpas, J., 1979: Two contrasting trondhjemite associations from transported ophiolites in western Newfoundland: Initial report. In Barker, F., ed., Trondhjemites, Dacites and Related Rocks. Developments in Petrology 6, Elsevier Scientific, Amsterdam, p. 465-487.

Malpas, J., and Robinson, P.T., 1983: Geology of the Troodos ophiolite, Cyprus [abs.]. GAC/MAC Joint Annual Meeting, Victoria 1983, Program with Abstracts, v. 8, p. A44.

Malpas, J., and Strong, D.F., 1975: A comparison of chrome-spinels in ophiolites and mantle diapirs of Newfoundland. Geochimica et Cosmochimica Acta, v. 39, p. 1045-1060.

Marten, B.E., 1971a: Geology of the Western Arm Group, Green Bay, Newfoundland. Unpublished M.Sc. thesis, Memorial University of Newfoundland, St. John's, Newfoundland, 72p.

Marten, B.E., 1971b: Stratigraphy of volcanic rocks in the Western Arm area of the central Newfoundland Appalachians. Proceedings, Geological Association of Canada, v. 24, No. 1, p. 73-84.

Mattey, D.P., Marsh, N.G., and Tarney, J., 1980: The geochemistry, mineralogy, and petrology of basalts from the west Philippine and Parece Vela basins and from the Palau-Kyushu and west Mariana ridges, Deep Sea Drilling Project Leg 59. In Orlofsky, S., et al., Initial Reports of the Deep Sea Drilling Project, v. 59, Washington (U.S. Government Printing Office), p. 753-800.

McClay, K.R., 1987: Aspects of the structural geology of the Buchans area. In Kirkham, R.V, ed., Buchans Geology, Newfoundland. Geological Survey of Canada, Paper 86-24, Report 3, p. 47-57.

McClay, K.R., and Ellis, P.G., 1983: Deformation and recrystallization of pyrite. Mineralogical Magazine, v. 47, p. 527-538.

McLeod, R.L., and Stanton, R.L., 1984: Phyllosilicates and associated minerals in some Paleozoic stratiform sulfide deposits of southeastern Australia. Economic Geology, v. 79, p. 1-22.

McNamara, M., 1965: The lower greenschist in the Scottish Highlands. Geologiska Föreningens I Stockholm Förhandlingar, v. 87, p. 347-389.

Melson, W.G., and van Andel, T.H., 1966: Metamorphism in the Mid-Atlantic Ridge, 22°N latitude. Marine Geology, v. 4, p. 165-186.

Melson, W.G., Vallier, T.L., Wright, T.L., Byerly, G., and Nelen, J., 1976: Chemical diversity of abyssal volcanic glass erupted along Pacific, Atlantic and Indian Ocean sea-floor spreading centers. In American Geophysical Union, The Geophysics of the Pacific Ocean Basin and its Margin. Geophysics Monograph No. 19, p. 351-367.

Menzies, M., Blanchard, D., and Jacobs, J., 1977: Rare earth and trace element geochemistry of metabasalts from the Point Sal ophiolite, California. Earth and Planetary Science Letters, v. 37, p. 203-215.

Menzies, M., Seyfried, W., Jr., and Blanchard, D., 1979: Experimental evidence of rare earth element immobility in greenstones. Nature, v. 282, p. 398-399.

Miyashiro, A., 1973: The Troodos ophiolite complex was probably formed in an island arc. Earth and Planetary Science letters, v. 19, p. 218-224.

Moore-Biot, N., 1970: Petrologie des formations volcaniques de Permo-Carbonifere du nord de la France. Annals Scient., Univ. Besançon, Ser. 3, Geol., v. 10.

Mottl, M.J., 1983a: Metabasalts, axial hot springs, and the structure of hydrothermal systems at mid-ocean ridges. Geological Society of America Bulletin, v. 94, p. 161-180.

Mottl, M.J., 1983b: Hydrothermal processes at seafloor spreading centers: application of basalt-seawater experimental results. In Rona, P.A., Boström, K., Laubier, L., and Smith, K.L., Jr., eds., Hydrothermal Processes at Seafloor Spreading Centers. NATO Conference Series IV: Marine Sciences, v. 12., Plenum Press, New York, p. 199-224.

Murray, A., 1877: Geography and resources of Newfoundland. Royal Geographical Society Journal, p. 267-278.

Murray, A., 1881: Survey of Exploits River and Red Indian Lake. Geological Survey of Newfoundland, Report for 1871. In Murray, A., and Howley, J.P., Geological Survey of Newfoundland. Edward Stanford, London, p. 250-278.

Nelson, K.D., 1981: Mélange development in the Boones Point Complex, north-central Newfoundland. Canadian Journal of Earth Sciences, v. 18, p. 433-442.

Newhouse, W.H., 1931: Geology and ore deposits of Buchans, Newfoundland. Economic Geology, v. 26, p. 399-414.

Nisbet, E.G., and Pearce, J.A., 1977: Clinopyroxene composition in mafic lavas from different tectonic settings. Contributions to Mineralogy and Petrology, v 63, p. 149-160.

Normark, W.R., Lupton, J.E., Murray, J.W., Delaney, J.R., Johnson, H.P., Koski, R.A., Claque, D.A., and Morton, J.L., 1982: Polymetallic sulfide deposits and water-column tracers of active hydrothermal vents on the southern Juan de Fuca Ridge. Marine Technology Society Journal, v. 16, p. 46-53.

Nowlan, G.S., and Thurlow, J.G., 1984: Middle Ordovician conodonts from the Buchans Group, central Newfoundland, and their significance for regional stratigraphy of the Central Volcanic Belt. Canadian Journal of Earth Sciences, v. 21, p. 284-296.

O'Brien, S.J., Dickson, W.L., and Blackwood, R.F., 1986: Geology of the central portion of the Hermitage Flexure area, Newfoundland. In Blackwood, R.F., Walsh, D.G., and Gibbons, R.V., compilers and editors, Current Research, Newfoundland Department of Mines and Energy, Mineral Development Division, Report 86-1, p. 189-208.

O'Brien, S.J., Wardle, R.J., and King, A.F., 1983: The Avalon Zone: a Pan-African terrane in the Appalachian orogen of Canada. Geological Journal, v. 18, p. 195-222.

O'Connor, J.T., 1965: A classification for quartz-rich igneous rocks based on feldspar ratios. United States Geological Survey, Professional Paper 525-B, p. B79-B84.

O'Hara, M.J., 1977: Geochemical evolution during fractional crystallization of a periodically refilled magma chamber. Nature, v. 266, p. 503-507.

O'Neill, P.P., 1985: An economic, metamorphic, structural and geochemical study of the Isle aux Morts prospect, southwest Newfoundland. Unpublished M.Sc. thesis, Memorial University of Newfoundland, St. John's, Newfoundland, 263p.

O'Nions, R.K., Pankhurst, R.J., and Grönvold, K., 1976: Nature and development of basalt magma sources beneath Iceland and the Reykjanes Ridge. Journal of Petrology, v. 17, p. 315-338.

Oudin, E., Picot, P., and Pouit, G., 1981: Comparison of sulphide deposits from the East Pacific Rise and Cyprus. Nature, v. 291, p. 404-407.

Pajari, G.E., Pickerill, R.K., and Currie, K.L., 1979: The nature, origin and significance of the Carmanville ophiolitic mélange, northeastern Newfoundland. Canadian Journal of Earth Sciences, v. 16, p. 1439-1451.

Papezik, V.S., 1970: Petrochemistry of volcanic rocks of the Harbour Main Group, Avalon Peninsula, Newfoundland. Canadian Journal of Earth Sciences, v. 7, p. 1485-1498.

Papezik, V.S., and Hodych, J.P., 1980: Early Mesozoic diabase dikes of the Avalon Peninsula, Newfoundland: Petrochemistry, mineralogy, and origin. Canadian Journal of Earth Sciences, v. 17, p. 1417-1430.

Papike, J.J., Cameron, K.L., and Baldwin, K., 1974: Amphiboles and pyroxenes: Characterization of other than quadrilateral components and estimates of ferric iron from microprobe data [abs.]. Geological Society of America, Abstracts with Programs, v. 6, p. 1053-1054.

Payne, J.G., and Strong, D.F., 1979: Origin of the Twillingate trondhjemite, north-central Newfoundland: Partial melting in the roots of an island arc. In Barker, F., ed., Trondhjemites, Dacites and Related Rocks. Developments in Petrology 6, Elsevier Scientific, Amsterdam, p. 489-516.

Pearce, J.A., 1976: Statistical analysis of major element patterns in basalt. Journal of Petrology, v. 17, p. 15-43.

Pearce, J.A., 1980: Geochemical evidence for the genesis and eruptive setting of lavas from Tethyan ophiolites. In Panayiotou, A., ed., Ophiolites. Proceedings of the International Ophiolite Symposium, Cyprus, 1979; Cyprus Ministry of Agriculture and Natural Resources, Geological Survey Department, p. 261-272.

Pearce, J.A., 1982: Trace element characteristics of lavas from destructive plate boundaries. In Thorpe, R.S., ed., Andesites: Orogenic Andesites and Related Rocks. John Wiley and Sons, Chichester, p. 525-548.

Pearce, J.A., and Cann, J.R., 1973: Tectonic setting of basic volcanic rocks determined using trace element analyses. Earth and Planetary Science Letters, v. 19, p. 290-300.

Pearce, J.A., and Norry, M.J., 1979: Petrogenetic implications of Ti, Zr, Y and Nb variations in volcanic rocks. Contributions to Mineralogy and Petrology, v. 69, p. 33-47.

Pearce, J.A., Lippard, S.J., and Roberts, S., 1984: Characteristics and tectonic significance of supra-subduction zone ophiolites. In Kokelaar, B.P., and Howells, M.F., eds., Marginal Basin Geology: Volcanic and associated sedimentary and tectonic processes in modern and ancient marginal basins. Blackwell Scientific Publications, Oxford, p. 77-94.

Pederson, R.B., and Malpas, J., 1984: The origin of oceanic plagiogranites from the Karmoy ophiolite, Western Norway. Contributions to Mineralogy and Petrology v. 88, p. 36-52.

Perfit, M.R., Gust, D.A., Bence, A.E., Arculus, R.J., and Taylor, S.R., 1980: Chemical characteristics of island-arc basalts: implications for mantle sources. Chemical Geology, v. 30, p. 227-256.

Peters, H.R., 1967: Mineral deposits of the Halls Bay area, Newfoundland. In Neale, E.R.W., and Williams, Harold, eds., Collected Papers on Geology of the Atlantic Region. Hugh Lilly Memorial Volume, Geological Association of Canada., Special Paper 4, p. 171-179.

Philpotts, A.R., 1979: Liquid immiscibility in tholeiitic basalts. Journal of Petrology, v. 20, p. 99-118.

Philpotts, A.R., 1982: Compositions of immiscible liquids in volcanic rocks. Contributions to Mineralogy and Petrology, v. 80, p. 201-218.

Pickerill, R.K., Pajari, G.E., Jr., and Currie, K.L., 1981: Resedimented volcaniclastics in the Carmanville area, northeastern Newfoundland—depositional remnants of Early Palaeozoic oceanic islands. Canadian Journal of Earth Sciences, v. 18, p. 55-70.

Pickett, J.W., 1987: Geology and geochemistry of the Skidder Basalt. In Kirkham, R.V, ed., Buchans Geology, Newfoundland. Geological Survey of Canada, Paper 86-24, Report 11, p. 195-218.

Pickett, J.W., and Barbour, D.M., 1984: Geology of the Skidder Prospect, Buchans, Newfoundland. In Current Research, Part A., Geological Survey of Canada, Paper 84-1A, p. 581-586. Also in Current Research, Newfoundland Department of Mines and Energy, Mineral Development Division, Report 84-1, p. 190-197.

Poldervaart, A., and Hess, H.H., 1951: Pyroxenes in the crystallization of basaltic magma. Journal of Geology, v. 59, p. 472-489.

Ramdohr, P., 1980: The Ore Minerals and Their Intergrowths, Second Edition, Two Volumes. Akademie-Verlag Berlin, Pergamon Press, Frankfurt, 1207p.

Ranger, M.J., Pickerill, R.K., and Fillion, D., 1984: Lithostratigraphy of the Cambrian? - Lower Ordovician Bell Island and Wabana groups of Bell, Little Bell, and Kellys islands, Conception Bay, eastern Newfoundland. Canadian Journal of Earth Sciences, v. 21, p. 1245-1261.

Relly, B.H., 1960: The geology of the Buchans Mine, Newfoundland. Unpublished Ph.D. thesis, McGill University, Montreal, Quebec, 281p.

Ridge, J.D., 1973: Volcanic exhalations and ore deposition in the vicinity of the seafloor. Mineralium Deposita, v. 8,p. 332-348.

Ridley, W.I., Rhodes, J.M., Reid, A.M., Jakes, P., Shih, C., and Bass, M.N., 1974: Basalts from Leg 6 of the Deep Sea Drilling Project. Journal of Petrology, v. 15, p. 140-159.

Riley, G.C., 1957: Red Indian Lake (west half), Newfoundland. Geological Survey of Canada, Map 8 -1957, scale 1:253 440.

Roberts, R.G., and Reardon, E.J., 1978: Alteration and ore forming processes at Mattagami Lake Mine, Quebec. Canadian Journal of Earth Sciences, v. 15, p. 1-21.

Rodgers, J., 1965: Long Point and Clam Bank Formations, western Newfoundland. Proceedings of the Geological Association of Canada, v. 16, p. 83-94.

Rona, P.A., Boström, K., Laubier, L., and Smith, K.L., Jr., eds., 1983: Hydrothermal Processes at Seafloor Spreading Centers. NATO Conference Series IV: Marine Sciences, v. 12, Plenum Press, New York, 796p.

Rosenbauer, R.J., and Bischoff, J.L., 1983: Uptake and transport of heavy metals by heated seawater: a summary of experimental results. In Rona, P.A., Boström, K., Laubier, L, and Smith, K.L., Jr., eds., Hydrothermal Processes at Seafloor Spreading Centers. NATO Conference Series IV: Marine Sciences, v. 12, Plenum Press, New York. p. 177-197.

Sato, T., 1972: Behaviours of ore-forming solutions in seawater. Mining Geology, Society of Mining Geologists of Japan, v. 22, p. 31-42.

Saunders, A.D., 1983: Geochemistry of basalts recovered from the Gulf of California during Leg 65 of the Deep Sea Drilling Project. In Lewis, B.T.R., Robinson, P., et al., Initial Reports of the Deep Sea Drilling Project, v. 65, Washington (U.S. Government Printing Office), p. 591-621.

Saunders, A.D., 1984: The rare earth element characteristics of igneous rocks from the ocean basins. In Henderson, P., ed., Rare Earth Element Geochemistry; Developments in Geochemistry, No. 2. Elsevier, p. 205-236.

Saunders, A.D., and Tarney, J., 1979: The geochemistry of basalts from a back-arc spreading centre in the East Scotia Sea. Geochimica et Cosmochimica Acta, v. 43, p. 555-572.

Saunders, A.D., Tarney, J., and Weaver, S.D., 1980: Transverse geochemical variations across the Antarctic Peninsula: implications for the genesis of calc-alkaline magmas. Earth and Planetary Science Letters, v. 46, p. 344-360.

Saunders, C.M., 1985: Controls of mineralization in the Betts Cove Ophiolite. Unpublished M.Sc. thesis, Memorial University of Newfoundland, St. John's, Newfoundland, 215p.

Saunders, C.M., and Strong, D.F., 1986: Alteration-zonation related to variations in water/rock ratio at the Betts Cove ophiolitic massive sulphide deposit, Newfoundland, Canada. In Gallagher, M.J., et al., eds., Metallogeny of Basic and Ultrabasic Rocks. Institution of Mining and Metallurgy, Conference Proceedings, p. 161-175.

Schenk, P.E., 1971: Southeastern Atlantic Canada, northwestern Africa, and continental drift. Canadian Journal of Earth Sciences, v. 8, p. 1218-1251.

Schilling, J.G., 1975a: Rare-earth variations across "normal segments" of the Reykjanes Ridge, 60°-53°N, Mid-Atlantic Ridge, 29°S, and East Pacific Rise, 2°-19°S, and evidence of the composition of the underlying low-velocity layer. Journal of Geophysical Research, v. 80, p. 1459-1473.

Schilling, J.G., 1975b: Azores mantle blob: Rare earth evidence. Earth and Planetary Science Letters, v. 25, p. 103-115.

Seyfried, W.E., Jr., and Bischoff, J.L., 1979: Low temperature basalt alteration by seawater: an experimental study at 70°C and 150°C. Geochimica et Cosmochimica Acta, v. 43, p. 1937-1947.

Seyfried, W.E., Jr., and Bischoff, J.L., 1981: Experimental seawater-basalt interaction at 300°C, 500 bars, chemical exchange, secondary mineral formation and implications for the transport of heavy metals. Geochimica et Cosmochimica Acta, v. 45, p. 135-147.

Seyfried, W.E., Jr., and Mottl, M.J., 1982: Hydrothermal alteration of basalt by seawater under seawater-dominated conditions. Geochimica et Cosmochimica Acta, v. 46, p. 985-1002.

Seyfried, W.E., Jr., Mottl, M.J., and Bischoff, J.L., 1978: Seawater/basalt ratio effects on the chemistry and mineralogy of spilites from the ocean floor. Nature, v. 275, p. 211-213.

Shapiro, L., and Brannock, W.W, 1962: Rapid analysis of silicate, carbonate and phosphate rocks. United States Geological Survey Bulletin 1144A, p. A1-A56.

Shervais, J.W., 1982: Ti-V plots and the petrogenesis of modern and ophiolitic lavas. Earth and Planetary Science Letters, v. 59, p. 101-118.

Sigurdsson, H., and Schilling, J.G., 1976: Spinels in Mid-Atlantic Ridge basalts: Chemistry and occurrence. Earth and Planetary Science Letters, v. 29, p. 7-20.

Sillitoe, R.H., 1972: Formation of certain massive sulphide deposits at sites of sea-floor spreading. Transactions of the Institution of Mining and Metallurgy, Section B, Applied earth science, v. 81, p. B141-B148.

Sillitoe, R.H., 1973: Environments of formation of volcanogenic massive sulfide deposits. Economic Geology, v. 68, p. 1321-1325.

Sinha, A.K., and Tilton, G.R., 1973: Isotopic evolution of common lead. Geochimica et Cosmochimica Acta, v. 37, p. 1823-1849.

Sivell, W.J., and Waterhouse, J.B., 1984a: The Patuki intrusive suite: closed-system fractionation beneath a slow-spreading ridge. Lithos, v. 17, p. 1-17.

Sivell, W.J., and Waterhouse, J.B., 1984b: Oceanic ridge metamorphism of the Patuki Volcanics, D'Urville Island, New Zealand. Lithos, v. 17, p. 19-36.

Smith, R.E., 1967: Segregation vesicles in basaltic lava. American Journal of Science, v. 265, p. 696-713.

Smith, S.A., and Hiscott, R.N., 1984: Latest Precambrian to Early Cambrian basin evolution, Fortune Bay, Newfoundland: fault-bounded basin to platform. Canadian Journal of Earth Sciences, v. 21, p. 1379-1392.

Smitheringale, W.G., 1972: Low-potash Lush's Bight tholeiites: ancient oceanic crust in Newfoundland? Canadian Journal of Earth Sciences, v. 9, p. 574-588.

Snelgrove, A.K., 1928: The geology of the central mineral belt of Newfoundland. Canadian Mining and Metallurgical Bulletin, v. 21, p. 1057-1127.

Solomon, M., 1976: "Volcanic" massive sulphide deposits and their host rocks - a review and an explanation. In Wolf, K.H., ed., Handbook of Strata-bound and Stratiform Ore Deposits; Regional and Specific Deposits, Volume 6: Cu, Zn, Pb, and Ag Deposits. Elsevier, Amsterdam, p. 21-54.

Solomon, M., and Walshe, J.L., 1979: The formation of massive sulfide deposits on the sea floor. Economic Geology, v. 74, p. 797-813.

Spiess, F.N., MacDonald, K.C., Atwater, T., Ballard, R., Carranza, A., Cordoba, D., Cox, C., Diaz Garcia, V.M., Francheteau, J., Guerrero, J., Hawkins, J., Haymon, R., Hessler, R., Juteau, T., Kastner, M., Larson, R., Luyendyk, B., Macdougall, J.D., Miller, S., Normark, W., Orcutt, J., and Rangin, C., 1980: East Pacific Rise: hot springs and geophysical experiments. Science, v. 207, p. 1421-1444.

Spooner, E.T.C., 1977: Hydrodynamic model for the origin of the ophiolitic cupriferous pyrite ore deposits of Cyprus. In Volcanic Processes in Ore Genesis. Geological Society of London, Special Publication 7, pp 58-71.

Spooner, E.T.C., and Fyfe, W.S., 1973: Sub-sea-floor metamorphism, heat and mass transfer. Contributions to Mineralogy and Petrology, v. 42, p. 287-304.

Srivastava, R.K., Emmermann, R., and Puchelt, H., 1980: Petrology and geochemistry of basalts from Deep Sea Drilling Project Leg 54. In Rosendahl, B.R., Hekinian, R., et al., Initial Reports of the Deep Sea Drilling Project, v. 54, Washington (U.S. Government Printing Office), p. 671-694.

Stacey, J.S., and Kramers, J.D., 1975: Approximation of terrestrial lead isotope evolution by a two-stage model. Earth and Planetary Science Letters, v. 26, p. 207-221.

Staff, Buchans Mining Company Limited, 1955: Buchans operation, Newfoundland. Canadian Mining and Metallurgical Bulletin, v. 48, p. 349-353.

Stanton, R.L, 1972: Ore Petrology. McGraw-Hill, New York, 713p.

Stanton, R.L., and Russell, R.D., 1959: Anomalous leads and the emplacement of lead sulfide ores. Economic Geology, v. 54, p. 588-607.

Stauffer, M.R., Mukherjee, A.C., and Koo, J., 1975: The Amisk Group: an Aphebian(?) island arc deposit. Canadian Journal of Earth Sciences, v. 12, p. 2021-2035.

Stephens, M.B., 1982: Spilitization, volcanite composition and magmatic evolution—their bearing on massive sulphide composition and siting in some volcanic terrains. Transactions of the Institution of Mining and Metallurgy, Section B, Applied earth science, v. 91, p. B200-B213.

Stern, C., 1979: Open and closed system igneous fractionation within two Chilean ophiolites and the tectonic implication. Contributions to Mineralogy and Petrology, v. 68, p. 243-258.

Stern, C., and de Wit, M.J., 1980: The role of spreading centre magma chambers in the formation of Phanerozoic oceanic crust: Evidence from Chilean ophiolites. In Panayiotou, A., ed., Ophiolites. Proceedings of the International Ophiolite Symposium, Cyprus, 1979; Cyprus Ministry of Agriculture and Natural Resources, Geological Survey Department, p. 497-506.

Stevens, R.E., 1944: Composition of some chromites of the western hemisphere. American Mineralogist, v. 29, p. 1-34.

Stevens, R.K., 1970: Cambro-Ordovician flysch sedimentation and tectonics in west Newfoundland and their possible bearing on a proto-Atlantic ocean. In Lajoie, J., ed., Flysch Sedimentology in North America. Geological Association of Canada, Special Paper No. 7, p. 165-177.

Stevens, R.K., and Williams, Harold, 1973: The emplacement of the Humber Arm allochthon, western Newfoundland [abs.]. Northeastern Section, 8th Annual Meeting, Geological Society of America, Abstracts with Programs, v. 5, No. 2, p. 222.

Stewart, I.C.F., 1984: *P*-wave travel-time residuals in the Newfoundland Appalachians. Canadian Journal of Earth Sciences, v. 21, p. 1278-1285.

Stewart, P.W., 1987: Geology and genesis of granitoid clasts in the MacLean Extension transported orebody. In Kirkham, R.V., ed., Buchans Geology, Newfoundland. Geological Survey of Canada, Paper 86-24, Report 9, p. 149-176.

Stolper, E., 1980: A phase diagram for mid-ocean ridge basalts: preliminary results and implications for petrogenesis. Contributions to Mineralogy and Petrology, v. 74, p. 13-27.

Stouge, S., 1980: Lower and Middle Ordovician conodonts from central Newfoundland and their correlatives in western Newfoundland. In O'Driscoll, C.F., and Gibbons R.V., eds., Current Research.Newfoundland Department of Mines and Energy, Mineral Development Division, Report 80-1, p. 134-142.

Stout, J.H., 1972: Phase petrology and mineral chemistry of coexisting amphiboles from Telemark, Norway. Journal of Petrology, v. 13, p. 99-145.

Strong, D.F., 1973: Lushs Bight and Roberts Arm Groups of central Newfoundland: possible juxtaposed oceanic and island-arc volcanic suites. Geological Society of America Bulletin, v. 84, p. 3917-3928.

Strong, D.F., 1974: An "off-axis" alkali volcanic suite associated with the Bay of Islands ophiolites, Newfoundland. Earth and Planetary Science Letters, v. 21, p. 301-309.

Strong, D.F., 1977: Volcanic regimes of the Newfoundland Appalachians. In Baragar, W.R.A., Coleman, L.C., and Hall, J.M., eds., Volcanic Regimes in Canada. Geological Association of Canada, Special Paper 16, p. 61-90.

Strong, D.F., 1979a: Proterozoic tectonics of northwestern Gondwanaland: new evidence from eastern Newfoundland. Tectonophysics, v. 54, p. 81-101.

Strong, D.F., 1979b: The Mount Peyton batholith, central Newfoundland: A bimodal calc-alkaline suite. Journal of Petrology, v. 20, p. 119-138.

Strong, D.F., 1980: Granitoid rocks and associated mineral deposits of eastern Canada and western Europe. In Strangway, D.W., ed., The Continental Crust and Its Mineral Deposits. Geological Association of Canada, Special Paper 20, p. 741-769.

Strong, D.F., 1982: Carbothermal metasomatism of alaskitic granite, St. Lawrence, Newfoundland, Canada. Chemical Geology, v. 35, p. 97-114.

Strong, D.F., and Dickson, W.L., 1978: Geochemistry of Paleozoic granitoid plutons from contrasting tectonic zones of northeast Newfoundland. Canadian Journal of Earth Sciences, v. 15, p. 145-156.

Strong, D.F., and Dupuy, C., 1982: Rare earth elements in the bimodal Mount Peyton batholith: Evidence of crustal anatexis by mantle-derived magma. Canadian Journal of Earth Sciences, v. 19, p. 308-315.

Strong, D.F., and Harris, A., 1974: The petrology of Mesozoic alkaline intrusives of central Newfoundland. Canadian Journal of Earth Sciences, v. 11, p. 1208-1219.

Strong, D.F., and Minatidis, D.G., 1975: Geochemistry and tectonic setting of the late Precambrian Holyrood plutonic series of eastern Newfoundland. Lithos, v. 8, p. 283-295.

Strong, D.F., and Saunders, C.M., in press: Ophiolitic sulfide mineralization at Tilt Cove, Newfoundland: controls by upper mantle and crustal precesses. Economic Geology.

Strong, D.F., and Williams, Harold, 1972: Early Paleozoic flood basalts of northwestern Newfoundland: their petrology and tectonic significance. Geological Association of Canada, Proceedings, v. 24, No. 2, p. 43-54.

Strong, D.F., Dickson, W.L., O'Driscoll, C.F., Kean, B.F., and Stevens, R.K., 1974: Geochemical evidence for an east-dipping Appalachian subduction zone in Newfoundland. Nature, v. 248, p. 37-39.

Strong, D.F., O'Brien, S.J., Taylor, S.W., Strong, P.G., and Wilton, D.H., 1978: Aborted Proterozoic rifting in eastern Newfoundland. Canadian Journal of Earth Sciences, v. 15, p. 117-131.

Styrt, M.M., Brackmann, A.J., Holland, H.D., Clark, B.C, Pisutha-Arnond, V., Eldridge, C.S., and Ohmoto, H., 1981: The mineralogy and the isotopic composition of sulfur in hydrothermal sulfide/sulfate deposits on the East Pacific Rise, 21° N latitude. Earth and Planetary Science Letters, v. 53, p. 382-390.

Suen, C.J., Frey, F.A., and Malpas, J., 1979: Bay of Islands ophiolite suite, Newfoundland: Petrologic and geochemical characteristics with emphasis on rare earth element geochemistry. Earth and Planetary Science Letters, v. 45, p. 337-348.

Sun, S.S., and Nesbitt, R.W., 1978: Chemical regularities and genetic significance of ophiolitic basalts. Geology, v. 6, p. 689-693.

Sun, S.S., Nesbitt, R.W., and Sharaskin, A., 1979: Geochemical characteristics of mid-ocean ridge basalts. Earth and Planetary Science Letters, v. 44, p. 119-138.

Swanson, E.A., and Brown, R.L., 1962: Geology of the Buchans orebodies. Canadian Mining and Metallurgical Bulletin, v. 55, p. 618-626.

Swanson, E.A., Strong, D.F., and Thurlow, J.G., eds., 1981: The Buchans Orebodies: Fifty Years of Geology and Mining. Geological Association of Canada, Special Paper 22, 350 p.

Swinden, H.S., 1982: Metallogenesis in the Bay d'Espoir area, southern Newfoundland: Summary and implications for regional metallogeny in the Newfoundland central mobile belt. CIM Bulletin, v. 75, p. 172-183.

Swinden, H.S., and Thorpe, R.I., 1984: Variation in style of volcanism and massive sulphide deposition in early to Middle Ordovician island-arc sequences of the Newfoundland central mobile belt. Economic Geology, v. 79, p. 1596-1619.

Tatsumoto, M., Knight, R.J., and Allègre, C.J., 1973: Time differences in the formation of meteorites as determined from the ratio of lead-207 to lead-206. Science, v. 180, p. 1279-1283.

Taylor, R.P., Strong, D.F., and Kean, B.F., 1980: The Topsails igneous complex: Silurian-Devonian peralkaline magmatism in western Newfoundland. Canadian Journal of Earth Sciences, v. 17, p. 425-439.

Taylor, S.R., and Gorton, M.P., 1977: Geochemical application of spark source mass spectrometry—III. Element sensitivity, precision and accuracy. Geochimica et Cosmochimica Acta, v. 41, p. 1375-1380.

Taylor, S.R., Capp, A.C., Graham, A.L., and Blake, D.H., 1969: Trace element abundances in andesites. Contributions to Mineralogy and Petrology, v. 23, p. 1-26.

Teng, H.C., and Strong, D.F., 1976: Geology and geochemistry of the St. Lawrence peralkaline granite and associated fluorite deposits, southeast Newfoundland. Canadian Journal of Earth Sciences, v. 13, p. 1374-1385.

Thayer, T.P., 1970: Chromite segregations as petrogenetic indicators. Geological Society of South Africa, Special Publication No. 1, p. 380-390.

Thompson, G., 1983: Basalt- seawater interaction. In Rona, P.A., Boström, K., Laubier, L., and Smith, K.L., Jr., eds., Hydrothermal Processes at Seafloor Spreading Centers. NATO Conference Series IV: Marine Sciences, v. 12., Plenum Press, New York, p. 225-278.

Thompson, G., Bryan, W.B., Frey, F.A., Dickey, J.S., and Suen, C.J., 1976: Petrology and geochemistry of basalts from DSDP Leg 34, Nazca Plate. In Yeats, R.S., Hart, S.R., et al., Initial Reports of the Deep Sea Drilling Project, v. 34, Washington (U.S. Government Printing Office), p. 215-226.

Thurlow, J.G., 1973: Lithogeochemical studies in the vicinity of the Buchans massive sulphide deposits, central Newfoundland. Unpublished M.Sc. thesis, Memorial University of Newfoundland, St. John's, Newfoundland, 171p.

Thurlow, J.G., 1974: Geology, geochemistry and ore deposits of the Buchans area. In Strong, D.F., ed., Plate Tectonic Setting of Newfoundland Mineral Occurrences. A Guidebook for the NATO Advanced Studies Institute On Metallogeny and Plate Tectonics, p. 72-80.

Thurlow, J.G., 1975: Buchans area report. In Kean, B.F., and Thurlow, J.G., Geology, Mineral Deposits and Mineral Potential of the Buchans Volcanic Belt. Report submitted to the Buchans Task Force, p. 6-38.

Thurlow, J.G., 1981a: Geology, ore deposits and applied rock geochemistry of the Buchans Group, Newfoundland. Unpublished Ph.D. thesis, Memorial University of Newfoundland, St. John's, Newfoundland, 305 p.

Thurlow, J.G., 1981b: The Buchans Group: its stratigraphic and structural setting. In Swanson E.A., Strong, D.F., and Thurlow, J.G., eds., The Buchans Orebodies: Fifty Years of Geology and Mining. Geological Association of Canada, Special Paper 22, p. 79-89.

Thurlow, J.G., and Swanson, E.A., 1981: Geology and ore deposits of the Buchans area, central Newfoundland. In Swanson E.A., Strong, D.F., and Thurlow, J.G., eds., The Buchans Orebodies: Fifty Years of Geology and Mining. Geological Association of Canada, Special Paper 22, p. 113-142.

Thurlow, J.G., and Swanson, E.A., 1987: Stratigraphy and structure of the Buchans Group. In Kirkham, R.V, ed., Buchans Geology, Newfoundland. Geological Survey of Canada, Paper 86-24, Report 2, p. 35-46.

Thurlow, J.G., Swanson, E.A., and Strong, D.F., 1975: Geology and lithogeochemistry of the Buchans polymetallic sulfide deposits, Newfoundland. Economic Geology, v. 70, p. 130-144.

Thurstone, L.L., 1947: Multiple Factor Analysis. McGraw Hill, New York.

Toth, J.R., 1980: Deposition of submarine crusts rich in manganese and iron. Geological Society of America Bulletin, v. 91, p. 44-54.

Tómasson, J., and Kristmannsdóttir, H., 1972: High temperature alteration minerals and thermal brines, Reykjanes, Iceland. Contributions to Mineralogy and Petrology, v. 36, p. 123-134.

Tuach, J., Davenport, P.H., Dickson, W.L., and Strong, D.F., 1986: Geochemical trends in the Ackley Granite, southeast Newfoundland: their relevance to magmatic-metallogenic processes in high-silica granitoid systems. Canadian Journal of Earth Sciences, v. 23, p. 747-765.

Twenhofel, W.H., and MacClintock, P., 1940: Surface of Newfoundland. Geological Society of America Bulletin, v. 51, p. 1665-1728.

Upadhyay, H.D., 1973: The Betts Cove ophiolite and related rocks of the Snooks Arm Group, Newfoundland. Unpublished Ph.D. thesis, Memorial University of Newfoundland, St. John's, Newfoundland, 224 p.

Upadhyay, H.D., and Smitheringale, W.G., 1972: Geology of the Gullbridge copper deposit, Newfoundland: Volcanogenic sulfides in cordierite-anthophyllite rocks. Canadian Journal of Earth Sciences, v. 9, p. 1061-1073.

Upadhyay, H.D., and Strong, D.F., 1973: Geological setting of the Betts Cove copper deposits, Newfoundland: an example of ophiolite sulfide mineralization, Economic Geology, v. 68, p. 161-167.

Upton, B.G.J., and Wadsworth, W.J., 1971: Rhyodacite glass in Réunion basalt. Mineralogical Magazine, v. 38, p. 152-159.

Urabe, T., Scott, S.D., and Hattori, K., 1983: A comparison of footwall-rock alteration and geothermal systems beneath some Japanese and Canadian volcanogenic massive sulfide deposits. Economic Geology, Monograph 5, The Kuroko and Related Volcanogenic Massive Sulfide Deposits, p. 345-364.

Vallance, T.G., 1974: Pyroxenes and the basalt-spilite relation. In Amstutz, G.C., ed, Spilites and Spilitic Rocks. International Union of Geological Sciences, Series A, Number 4, Springer-Verlag, Heidelberg, p. 59-68.

Vanderveer, D.G., and Sparkes, B.G., 1979: Geochemistry of glacial till samples from the Lake Ambrose (12A/10) - Noel Paul's Brook (12A/9) map areas, Newfoundland. Newfoundland Department of Mines and Energy, Mineral Development Division, Open File 12A(212).

Venturelli, G., Thorpe, R.S., and Potts, P.J., 1981: Rare earth and trace element characteristics of ophiolitic metabasalts from the Alpine-Apennine belt. Earth and Planetary Science Letters, v. 53, p. 109-123.

Wasowski, J.J., and Jacobi, R.D., 1985: Geochemistry and tectonic significance of the mafic volcanic blocks in the Dunnage mélange, north central Newfoundland. Canadian Journal of Earth Sciences, v. 22, p. 1248-1256.

Watson, E.B., 1976: Two-liquid partition coefficients: experimental data and geochemical implications. Contributions to Mineralogy and Petrology, v. 56, p. 119-134.

Watson, E.B., 1979: Zircon saturation in felsic liquids: experimental results and applications to trace element geochemistry. Contributions to Mineralogy and Petrology, v. 70, p. 407-419.

Whalen, J.B., and Currie, K.L., 1983: Geology of the Topsails igneous terrane, western Newfoundland. Geological Survey of Canada, Open File 923.

Whalen, J.B., and Currie, K.L., 1987: The relationship of the Topsails igneous terrane to the Buchans Group. In Kirkham, R.V., ed., Buchans Geology, Newfoundland. Geological Survey of Canada, Paper 86-24, Report 6, p. 69-73.

White, W.M., and Patchett, J., 1984: Hf-Nd-Sr isotopes and incompatible element abundances in island arcs: implications for magma origins and crust-mantle evolution. Earth and Planetary Science Letters, v. 67, p. 167-185.

White, W.M., Tapia, M.D.M., and Schilling, J.G., 1979: The petrology and geochemistry of the Azores Islands. Contributions to Mineralogy and Petrology, v. 69, p. 201-213.

Whitford, D.J., Nicholls, I.A., and Taylor, S.R., 1979: Spatial variations in the geochemistry of Quaternary lavas across the Sunda Arc in Java and Bali. Contributions to Mineralogy and Petrology, v. 70, p. 341-356.

Williams, Harold, 1964: The Appalachians in northeastern Newfoundland—a two-sided symmetrical system. American Journal of Science, v. 262, p. 1137-1158.

Williams, Harold, 1967: Silurian rocks of Newfoundland. In Neale, E.R.W., and Williams, Harold, eds., Collected Papers on Geology of the Atlantic Region. Hugh Lilly Memorial Volume, Geological Association of Canada., Special Paper 4, p. 93-137.

Williams, Harold, 1970: Red Indian Lake (east half), Newfoundland. Geological Survey of Canada, Map 1196A, scale 1:250 000.

Williams, Harold, 1978: Tectonic Lithofacies Map of the Appalachian Orogen. Memorial University of Newfoundland, Map No. 1a, scale 1:2 000 000.

Williams, Harold, 1979: Appalachian orogen in Canada. Canadian Journal of Earth Sciences, v. 16, p. 792-807.

Williams, Harold, 1980: Structural telescoping across the Appalachian orogen and the minimum width of the Iapetus ocean. In Strangway, D.W., ed., The Continental Crust and Its Mineral Deposits. Geological Association of Canada, Special Paper 20, p. 421-440.

Williams, Harold, and Hatcher, R.D., Jr., 1982: Suspect terranes and accretionary history of the Appalachian orogen. Geology, v. 10, p. 530-536.

Williams, Harold, and Hatcher, R.D., Jr., 1983: Appalachian suspect terranes. In Hatcher, R.D., Jr., Williams, Harold, and Zietz, I., eds., Contributions to the Tectonics and Geophysics of Mountain Chains. Geological Society of America, Memoir 158, p. 33-53.

Williams, Harold, and King, A.F., 1976: Southern Avalon Peninsula, Newfoundland: Trepassey map-area (1K). Geological Survey of Canada, Paper 76-1A, p. 179-182.

Williams, Harold, and St. Julien, P., 1982: The Baie Verte-Brompton Line: Early Paleozoic continent-ocean interface in the Canadian Appalachians. In St. Julien, P., and Béland, J., eds., Major Structural Zones and Faults of the Northern Appalachians. Geological Association of Canada, Special Paper 24, p. 177-207.

Williams, Harold, and Stevens, R.K., 1969: Geology of Belle Isle—northern extremity of the deformed Appalachian miogeosynclinal belt. Canadian Journal of Earth Sciences, v. 6, p. 1145-1157.

Williams, Harold, Kennedy, M.J., and Neale, E.R.W., 1972: The Appalachian structural province. In Price, R.A., and Douglas, R.J.W., eds., Variations in Tectonic Styles in Canada. Geological Association of Canada Special Paper 11, p. 181-261.

Williams, Harold, Kennedy, M.J., and Neale, E.R.W., 1974: The northeastward termination of the Appalachian Orogen. In Nairn, A.E.M., and Stehli, F.G., The Ocean Basins and Margins, Volume 2, The North Atlantic. Plenum Press, New York, p. 79-123.

Williams, Harold, Gillespie, R.T., and van Breemen, O., 1985: A late Precambrian rift-related igneous suite in western Newfoundland. Canadian Journal of Earth Sciences, v. 22, p. 1727-1735.

Williams, Howel, Turner, F.J., and Gilbert, C.M., 1982: Petrography: An Introduction to the Study of Rocks in Thin Sections, Second Edition. W.H. Freeman and Company, San Francisco, 626p.

Wilson, J.T., 1966: Did the Atlantic close and then re-open? Nature, v. 211, p. 676-681.

Wilton, D.H.C., 1985: Tectonic evolution of southwestern Newfoundland as indicated by granitoid petrogenesis. Canadian Journal of Earth Sciences, v. 22, p. 1080-1092.

Winchester, J.A., and Floyd, P.A., 1976: Geochemical magma type discrimination: application to altered and metamorphosed basic igneous rocks. Earth and Planetary Science Letters, v. 28, p. 459-469.

Winchester, J.A., and Floyd, P.A., 1977: Geochemical discrimination of different magma series and their differentiation products using immobile elements. Chemical Geology, v. 20, p. 325-343.

Wonderley, P.F., and Neuman, R.B., 1984: The Indian Bay Formation: fossiliferous Early Ordovician volcanogenic rocks in the northern Gander Terrane, Newfoundland, and their regional significance. Canadian Journal of Earth Sciences, v. 21, p. 525-532.

Wood, D.A., Tarney, J., Varet, J., Saunders, A.D., Bougault, H., Joron, J.L., Treuil, M., and Cann, J.R., 1979: Geochemistry of basalts drilled in the North Atlantic by IPOD Leg 49: Implications for mantle heterogeneity. Earth and Planetary Science Letters, v. 42, p. 77-97.

Zartman, R.E., and Doe, B.R., 1981: Plumbotectonics—the model. Tectonophysics, v. 75, p. 135-162.

Zierenberg, R.A., Shanks, W.C, III, and Bischoff, J.L., 1984: Massive sulfide deposits at 21°N, East Pacific Rise: Chemical composition, stable isotopes, and phase equilibria. Geological Society of America Bulletin, v. 95, p. 922-929.

APPENDIX A

ELECTRON MICROPROBE TECHNIQUES AND ANALYSES

Silicate, carbonate and sulphide minerals were analyzed at Memorial University of Newfoundland using a JEOL JXA-50A electron probe microanalyzer with three wavelength dispersive spectrometers run automatically by the Krisel control system through a PDP-11 computer. An operating voltage of 15 kv and a beam current of 0.22 mA were used during all analyses. Counts were made for 30 seconds or until 30 000, whichever came first.

Silicate data reduction was performed with the Alpha correction program, using the correction scheme of Bence and Albee (1968); sulphide analyses were corrected using the Krisel MAGIC program.

Pyroxene standard FCPX (Frisch pyroxene) was used for calibration when silicates were analyzed. Sulphide standards used for calibration were PYR 242 (CANMET), CUBS (cubanite from Strathcona), CdS (CANMET), PbS (U.S.G.S.), $AgBiSe_2$ (CANMET), sphalerite SP 20 (Taylor sulphide block), and sphalerite 20 (CANMET).

Statistical parameters for replicate analyses of FCPX are presented in Table A-1. Averaged analyses for clinopyroxenes, albites, chlorites and muscovites presented in Tables 4-7, 4-9, 4-10, 4-12, 4-14, 6-9 and 6-13 are listed in Tables A-2 to A-5. Replicate analyses of the sulphide standards are presented in Table A-6. Analyses of various minerals for S, Fe and Zn are listed in Table A-7.

Table A-1: Statistical parameters for analyses of pyroxene standard FCPX (Frisch pyroxene)

Weight %	Mean (m)	Standard Deviation (∂)	Minimum	Maximum	Range	M/∂ (%)	Accepted Value (v)	m-v	(m-v)/v (%)
SiO_2	50.41	0.92	48.55	51.97	3.42	2%	49.85	0.56	1%
TiO_2	0.77	0.03	0.68	0.81	0.13	4%	0.83	-0.06	-7%
Al_2O_3	7.85	0.14	7.61	8.24	0.63	2%	7.86	-0.01	0%
Cr_2O_3	0.02	0.02	0.00	0.05	0.05	71%			
FeO*	5.95	0.22	5.32	6.26	0.94	4%	6.17	-0.22	-4%
MnO	0.11	0.03	0.04	0.17	0.13	28%	0.14	-0.03	-20%
NiO	0.05	0.02	0.00	0.10	0.10	54%			
MgO	15.43	0.27	14.98	15.95	0.97	2%	15.47	-0.04	0%
CaO	17.99	0.48	16.98	18.83	1.85	3%	17.75	0.24	1%
Na_2O	1.31	0.11	1.12	1.63	0.51	8%	1.27	0.04	3%
K_2O	0.01	0.01	0.00	0.02	0.02	86%			
Total	99.90	1.05	97.95	101.60	3.65	1%	99.34	0.56	1%

Atomic Proportions (based on 6 oxygens)

Si	1.838	0.016	1.805	1.864	0.059
Ti	0.021	0.001	0.019	0.022	0.004
Al	0.337	0.005	0.329	0.352	0.023
Cr	0.001	0.000	0.000	0.001	0.001
Fe	0.181	0.006	0.165	0.192	0.027
Mn	0.003	0.001	0.001	0.005	0.004
Ni	0.001	0.001	0.000	0.003	0.003
Mg	0.838	0.013	0.814	0.865	0.051
Ca	0.703	0.023	0.665	0.750	0.085
Na	0.093	0.007	0.079	0.116	0.036
K	0.000	0.000	0.000	0.001	0.001
Total	4.018	0.015	3.995	4.057	0.061

Analyses	29

Table A-2: Averaged clinopyroxene analyses presented in Table 4-7

Weight %	S 59	S 59	S 59	S 59	Mean S 59	S 81	S 81	S 81	Mean S 81	S 19	S 19	S 19	Mean S 19	S 19	S 19	S 19	S 19	Mean S 19
SiO_2	48.26	50.02	47.16	49.14	48.65	50.91	49.39	51.28	50.53	50.05	48.95	47.71	48.90	47.88	48.39	48.08	48.39	48.19
TiO_2	0.71	0.72	0.79	0.70	0.73	0.64	0.66	0.72	0.67	1.28	1.48	1.52	1.43	1.94	2.01	2.13	2.25	2.08
Al_2O_3	6.69	5.68	6.51	5.26	6.04	4.93	3.96	3.38	4.09	6.06	6.16	6.84	6.35	6.46	7.05	7.11	6.82	6.86
Cr_2O_3	0.25	0.19	0.19	0.42	0.26	0.07	0.05	0.27	0.13	0.16	0.09	0.07	0.11	0.09	0.08	0.09	0.14	0.10
FeO*	6.72	7.09	7.11	8.68	7.40	7.90	10.54	9.99	9.48	8.36	10.63	11.91	10.30	10.92	9.18	9.87	10.51	10.12
MnO	0.14	0.11	0.13	0.23	0.15	0.21	0.28	0.32	0.27	0.16	0.14	0.57	0.29	0.14	0.16	0.15	0.20	0.16
NiO	0.02	0.00	0.03	0.05	0.03	0.05	0.04	0.07	0.05	0.00	0.01	0.05	0.02	0.03	0.02	0.05	0.03	0.03
MgO	12.96	13.55	13.70	12.87	13.27	15.93	15.12	15.32	15.46	13.09	11.11	11.47	11.89	11.59	12.69	12.18	11.53	12.00
CaO	21.38	21.85	21.89	21.51	21.66	20.02	20.05	20.34	20.14	21.39	21.83	20.50	21.24	21.34	21.88	21.41	21.68	21.58
Na_2O	0.25	0.23	0.23	0.40	0.28	0.05	0.38	0.24	0.22	0.28	0.39	0.51	0.39	0.33	0.50	0.34	0.24	0.35
K_2O	0.00	0.01	0.00	0.02	0.01	0.01	0.00	0.00	0.00	0.01	0.01	0.00	0.01	0.00	0.00	0.01	0.00	0.00
Total	97.38	99.45	97.74	99.28	98.46	100.72	100.47	101.93	101.04	100.84	100.80	101.15	100.93	100.72	101.96	101.42	101.79	101.47
Atomic proportions (based on 6 oxygens)																		
Si	1.833	1.861	1.797	1.851	1.836	1.866	1.849	1.882	1.866	1.845	1.830	1.790	1.822	1.796	1.781	1.782	1.792	1.788
Ti	0.020	0.020	0.023	0.020	0.021	0.018	0.019	0.020	0.019	0.035	0.042	0.043	0.040	0.055	0.056	0.059	0.063	0.058
Al	0.300	0.249	0.293	0.234	0.269	0.213	0.175	0.146	0.178	0.263	0.272	0.303	0.279	0.286	0.306	0.311	0.298	0.300
Cr	0.008	0.006	0.006	0.013	0.008	0.002	0.001	0.008	0.004	0.005	0.003	0.002	0.003	0.003	0.002	0.003	0.004	0.003
Fe	0.214	0.221	0.227	0.273	0.234	0.242	0.330	0.307	0.293	0.258	0.332	0.374	0.321	0.343	0.283	0.306	0.326	0.314
Mn	0.005	0.003	0.004	0.007	0.005	0.007	0.009	0.010	0.008	0.005	0.004	0.018	0.009	0.004	0.005	0.005	0.006	0.005
Ni	0.001	0.000	0.001	0.002	0.001	0.001	0.001	0.002	0.002	0.000	0.000	0.002	0.001	0.001	0.001	0.001	0.001	0.001
Mg	0.734	0.751	0.778	0.723	0.746	0.870	0.843	0.838	0.851	0.719	0.619	0.641	0.660	0.648	0.696	0.673	0.636	0.663
Ca	0.870	0.871	0.894	0.868	0.876	0.786	0.804	0.800	0.797	0.845	0.875	0.824	0.848	0.858	0.863	0.850	0.860	0.858
Na	0.018	0.017	0.017	0.029	0.020	0.004	0.028	0.017	0.016	0.020	0.028	0.037	0.028	0.024	0.036	0.024	0.017	0.025
K	0.000	0.000	0.000	0.001	0.000	0.000	0.000	0.000	0.000	0.000	0.000	0.000	0.000	0.000	0.000	0.000	0.000	0.000
Total	4.002	4.000	4.039	4.021	4.015	4.010	4.058	4.030	4.033	3.996	4.005	4.033	4.012	4.017	4.027	4.015	4.003	4.015
Analyses					4				3				3					4

* Total iron as FeO

Table A-2 (continued):

Weight %	S 53	S 53	S 53	Mean S 53	S 25	S 25	S 25	Mean S 25	S 25	S 25	S 25	Mean S 25
SiO_2	53.30	54.82	52.18	53.43	51.55	52.47	52.01		52.65	51.70	51.11	51.82
TiO_2	0.46	0.27	0.68	0.47	0.64	0.69	0.67		0.82	0.86	0.94	0.87
Al_2O_3	2.89	2.12	4.22	3.08	4.13	3.05	3.59		4.00	3.77	4.16	3.98
Cr_2O_3	0.68	0.38	0.79	0.62	0.05	0.05	0.05		0.08	0.11	0.05	0.08
FeO*	6.11	6.57	6.68	6.45	9.24	8.03	8.64		7.86	8.93	8.21	8.33
MnO	0.11	0.19	0.17	0.16	0.23	0.22	0.23		0.12	0.21	0.17	0.17
NiO	0.03	0.07	0.00	0.03	0.03	0.00	0.02		0.04	0.03	0.00	0.02
MgO	17.29	18.07	16.22	17.19	14.49	15.34	14.92		15.66	15.07	15.82	15.52
CaO	18.92	18.80	20.47	19.40	19.07	20.12	19.60		20.36	20.39	18.91	19.89
Na_2O	0.23	0.19	0.32	0.25	0.13	0.23	0.18		0.21	0.27	0.37	0.28
K_2O	0.01	0.01	0.01	0.01	0.01	0.00	0.01		0.00	0.01	0.00	0.00
Total	100.03	101.49	101.74	101.09	99.57	100.20	99.89		101.80	101.35	99.74	100.96
Atomic proportions (based on 6 oxygens)												
Si	1.942	1.967	1.887	1.932	1.915	1.932	1.923		1.906	1.895	1.890	1.897
Ti	0.013	0.007	0.018	0.013	0.018	0.019	0.018		0.022	0.024	0.026	0.024
Al	0.124	0.090	0.180	0.131	0.181	0.132	0.157		0.171	0.163	0.181	0.172
Cr	0.020	0.011	0.023	0.018	0.001	0.001	0.001		0.002	0.003	0.001	0.002
Fe	0.186	0.197	0.202	0.195	0.287	0.247	0.267		0.238	0.274	0.254	0.255
Mn	0.003	0.006	0.005	0.005	0.007	0.007	0.007		0.004	0.007	0.005	0.005
Ni	0.001	0.002	0.000	0.001	0.001	0.000	0.000		0.001	0.001	0.000	0.001
Mg	0.939	0.966	0.874	0.926	0.802	0.842	0.822		0.845	0.823	0.872	0.847
Ca	0.739	0.723	0.793	0.751	0.759	0.794	0.776		0.790	0.801	0.749	0.780
Na	0.016	0.013	0.022	0.017	0.009	0.016	0.013		0.015	0.019	0.027	0.020
K	0.000	0.000	0.000	0.000	0.000	0.000	0.000		0.000	0.000	0.000	0.000
Total	3.982	3.982	4.005	3.990	3.981	3.990	3.986		3.993	4.009	4.006	4.002
Analyses				3			2					3

* Total iron as FeO

Table A-2 (continued):

Weight %	S 79	S 79	Mean S 79	S 79	S 79	S 79	Mean S 79	S 60	S 60	S 60	Mean S 60	S 60	S 60	Mean S 60	S 60	S 60	Mean S 60
SiO_2	53.89	52.99	53.44	51.84	53.02	51.91	52.26	50.24	51.24	52.54	51.34	51.64	52.86	52.25	52.03	53.78	52.91
TiO_2	0.37	0.66	0.52	0.64	0.54	0.98	0.72	0.81	0.71	0.81	0.78	0.56	0.73	0.65	0.47	0.52	0.50
Al_2O_3	2.68	4.32	3.50	3.73	3.15	4.50	3.79	3.18	2.99	3.20	3.12	2.77	3.36	3.07	1.94	2.15	2.05
Cr_2O_3	0.13	0.09	0.11	0.01	0.05	0.05	0.04	0.02	0.04	0.02	0.03	0.18	0.14	0.16	0.04	0.02	0.03
FeO*	7.97	7.99	7.98	9.39	10.96	11.66	10.67	11.29	12.21	11.32	11.61	8.79	9.36	9.08	11.96	12.03	12.00
MnO	0.19	0.12	0.16	0.23	0.27	0.25	0.25	0.25	0.28	0.30	0.28	0.22	0.18	0.20	0.20	0.30	0.25
NiO	0.03	0.00	0.02	0.03	0.00	0.00	0.01	0.01	0.00	0.03	0.01	0.04	0.04	0.04	0.04	0.00	0.02
MgO	16.99	16.64	16.82	15.21	15.91	14.49	15.20	15.52	14.95	14.87	15.11	16.63	15.92	16.28	16.43	16.87	16.65
CaO	19.31	19.70	19.51	20.53	18.17	19.63	19.44	18.70	17.05	19.11	18.29	20.07	19.88	19.98	16.66	16.44	16.55
Na_2O	0.27	0.26	0.27	0.21	0.36	0.35	0.31	0.33	0.47	0.33	0.38	0.20	0.24	0.22	0.26	0.32	0.29
K_2O	0.00	0.02	0.01	0.02	0.01	0.00	0.01	0.01	0.03	0.00	0.01	0.01	0.00	0.01	0.01	0.01	0.01
Total	101.83	102.79	102.31	101.84	102.44	103.82	102.70	100.36	99.97	102.53	100.95	101.11	102.71	101.91	100.04	102.44	101.24
Atomic proportions (based on 6 oxygens)																	
Si	1.944	1.896	1.920	1.894	1.923	1.874	1.897	1.878	1.917	1.914	1.903	1.897	1.908	1.903	1.938	1.949	1.944
Ti	0.010	0.018	0.014	0.018	0.015	0.027	0.020	0.023	0.020	0.022	0.022	0.015	0.020	0.018	0.013	0.014	0.014
Al	0.114	0.182	0.148	0.161	0.135	0.191	0.162	0.140	0.132	0.137	0.136	0.120	0.143	0.131	0.085	0.092	0.089
Cr	0.004	0.003	0.003	0.000	0.001	0.001	0.001	0.001	0.001	0.001	0.001	0.005	0.004	0.005	0.001	0.001	0.001
Fe	0.240	0.239	0.240	0.287	0.332	0.352	0.324	0.353	0.382	0.345	0.360	0.270	0.283	0.276	0.373	0.365	0.369
Mn	0.006	0.004	0.005	0.007	0.008	0.008	0.008	0.008	0.009	0.009	0.009	0.007	0.006	0.006	0.006	0.009	0.008
Ni	0.001	0.000	0.000	0.001	0.000	0.000	0.000	0.000	0.000	0.001	0.000	0.001	0.001	0.001	0.001	0.000	0.001
Mg	0.913	0.887	0.900	0.828	0.860	0.779	0.823	0.865	0.834	0.807	0.835	0.911	0.857	0.884	0.912	0.911	0.912
Ca	0.746	0.755	0.751	0.804	0.706	0.759	0.756	0.749	0.684	0.746	0.726	0.790	0.769	0.780	0.665	0.638	0.652
Na	0.019	0.018	0.018	0.015	0.025	0.024	0.022	0.024	0.034	0.023	0.027	0.014	0.017	0.016	0.019	0.022	0.021
K	0.000	0.001	0.000	0.001	0.000	0.000	0.000	0.000	0.001	0.000	0.001	0.000	0.000	0.000	0.000	0.000	0.000
Total	3.997	4.003	4.000	4.016	4.007	4.016	4.013	4.041	4.014	4.006	4.020	4.032	4.007	4.019	4.015	4.002	4.008
Analyses			2				3				3			2			2

* Total iron as FeO

Table A-3: Electron microprobe analyses of averaged albites presented in Table 4-9

	Albite				Mean	Albite				Mean	Albite			Mean
Weight %	S 59	S 59	S 59	S 59	S 59	S 60	S 60	S 60	S 60	S 60	S 21A	S 21A	S 21A	S 21A
SiO_2	68.87	67.92	67.83	68.06	68.17	68.50	67.21	66.76	68.98	67.86	70.86	69.75	67.33	69.31
TiO_2	0.00	0.10	0.00	0.03	0.03	0.05	0.02	0.03	0.02	0.03	0.01	0.00	0.00	0.00
Al_2O_3	19.11	19.64	19.61	19.43	19.45	20.39	19.93	18.32	19.75	19.85	19.05	18.87	19.07	19.00
Cr_2O_3	0.02	0.02	0.02	0.00	0.02	0.02	0.00	0.03	0.00	0.01	0.00	0.00	0.00	0.00
FeO*	0.29	0.27	0.17	0.26	0.25	0.06	0.07	1.18	0.92	0.56	0.04	0.01	0.00	0.02
MnO	0.04	0.00	0.02	0.03	0.02	0.00	0.04	0.03	0.04	0.03	0.00	0.03	0.00	0.01
NiO	0.01	0.01	0.00	0.00	0.01	0.00	0.09	0.01	0.05	0.04	0.03	0.00	0.04	0.02
MgO	0.00	0.01	0.04	0.02	0.02	0.00	0.00	0.00	0.13	0.03	0.00	0.00	0.02	0.01
CaO	0.11	0.39	0.41	0.50	0.35	0.15	0.25	0.30	0.29	0.25	0.16	0.15	0.11	0.14
Na_2O	11.73	12.02	11.06	11.81	11.66	12.21	12.14	11.93	11.01	11.82	11.63	12.26	11.86	11.92
K_2O	0.02	0.03	0.07	0.09	0.05	0.04	0.05	0.07	0.07	0.06	0.03	0.03	0.05	0.04
Total	100.20	100.41	99.23	100.23	100.02	101.42	99.80	99.66	101.26	100.54	101.81	101.10	98.48	100.46
Atomic Proportions (based on 8 oxygens)														
Si	3.005	2.968	2.985	2.978	2.984	2.958	2.955	2.955	2.983	2.963	3.032	3.017	2.991	3.013
Ti	0.000	0.003	0.000	0.001	0.001	0.002	0.001	0.001	0.001	0.001	0.000	0.000	0.000	0.000
Al	0.983	1.012	1.017	1.002	1.004	1.038	1.033	1.008	1.007	1.022	0.961	0.962	0.999	0.974
Cr	0.001	0.001	0.001	0.000	0.001	0.001	0.000	0.001	0.000	0.000	0.000	0.000	0.000	0.000
Fe	0.011	0.010	0.006	0.010	0.009	0.002	0.003	0.044	0.033	0.020	0.001	0.000	0.000	0.001
Mn	0.001	0.000	0.001	0.001	0.001	0.000	0.001	0.001	0.001	0.001	0.000	0.001	0.000	0.000
Ni	0.000	0.000	0.000	0.000	0.000	0.000	0.003	0.000	0.002	0.001	0.001	0.000	0.001	0.001
Mg	0.000	0.001	0.003	0.001	0.001	0.000	0.000	0.000	0.008	0.002	0.000	0.000	0.001	0.000
Ca	0.005	0.018	0.019	0.023	0.017	0.007	0.012	0.014	0.013	0.012	0.007	0.007	0.005	0.007
Na	0.992	1.018	0.944	1.002	0.989	1.022	1.035	1.024	0.923	1.001	0.965	1.028	1.022	1.005
K	0.001	0.002	0.004	0.005	0.003	0.002	0.003	0.004	0.004	0.003	0.002	0.002	0.003	0.002
Total	5.000	5.033	4.980	5.023	5.009	5.033	5.046	5.053	4.976	5.027	4.970	5.017	5.022	5.003
Analyses					4					4				3
Molecular %														
Ab	99.37	98.08	97.59	97.24	98.07	99.11	98.61	98.26	98.16	98.53	99.08	99.17	99.22	99.15
An	0.51	1.76	2.00	2.27	1.64	0.67	1.12	1.37	1.43	1.15	0.75	0.67	0.51	0.64
Or	0.11	0.16	0.41	0.49	0.29	0.21	0.27	0.38	0.41	0.32	0.17	0.16	0.28	0.20

* Total iron as FeO

Table A-3 (continued): Electron microprobe analyses of averaged albites presented in Tables 4-10 and 4-12

	Albite				Mean	Albite		Mean
Weight %	S 63	S 63	S 63	S 63	S 63	S 16	S 16	S 16
SiO_2	66.67	67.92	67.57	68.44	67.65	68.49	68.28	68.39
TiO_2	0.00	0.00	0.00	0.00	0.00	0.00	0.00	0.00
Al_2O_3	19.36	20.13	19.39	19.45	19.58	18.94	18.45	18.70
Cr_2O_3	0.01	0.00	0.00	0.01	0.01	0.02	0.00	0.01
FeO*	0.04	0.04	0.07	0.04	0.05	0.00	0.04	0.02
MnO	0.00	0.01	0.00	0.03	0.01	0.00	0.01	0.01
NiO	0.03	0.03	0.02	0.03	0.03	0.01	0.00	0.01
MgO	0.00	0.00	0.00	0.00	0.00	0.00	0.02	0.01
CaO	0.33	0.00	0.46	0.35	0.29	0.06	0.00	0.03
Na_2O	11.69	11.68	11.98	10.91	11.57	11.92	12.40	12.16
K_2O	0.04	0.04	0.09	0.09	0.07	0.06	0.07	0.07
Total	98.17	99.85	99.58	99.35	99.24	99.50	99.27	99.39
Atomic Proportions (based on 8 oxygens)								
Si	2.974	2.972	2.976	3.002	2.981	3.008	3.012	3.010
Ti	0.000	0.000	0.000	0.000	0.000	0.000	0.000	0.000
Al	1.018	1.038	1.007	1.006	1.017	0.981	0.960	0.970
Cr	0.000	0.000	0.000	0.000	0.000	0.001	0.000	0.000
Fe	0.001	0.001	0.003	0.001	0.002	0.000	0.001	0.001
Mn	0.000	0.000	0.000	0.001	0.000	0.000	0.000	0.000
Ni	0.001	0.001	0.001	0.001	0.001	0.000	0.000	0.000
Mg	0.000	0.000	0.000	0.000	0.000	0.000	0.001	0.001
Ca	0.016	0.000	0.022	0.016	0.013	0.003	0.000	0.001
Na	1.011	0.991	1.023	0.928	0.988	1.015	1.061	1.038
K	0.002	0.002	0.005	0.005	0.004	0.003	0.004	0.004
Total	5.024	5.006	5.035	4.961	5.006	5.011	5.040	5.025
Analyses					4			2
Molecular %								
Ab	98.25	99.78	97.45	97.74	98.30	99.39	99.63	99.51
An	1.53	0.00	2.07	1.73	1.33	0.28	0.00	0.14
Or	0.22	0.22	0.48	0.53	0.36	0.33	0.37	0.35

* Total iron as FeO

Table A-4: Averaged electron microprobe analyses of chlorites presented in Table 4-14

Weight %	S 59	S 59	S 59	Mean S 59	S 59	S 59	S 59	Mean S 59	S 30	S 30	S 30	S 30	S 30	S 30	Mean S 30
SiO_2	28.49	30.73	27.98	29.07	28.99	27.42	27.82	28.08	26.92	28.47	27.58	27.72	27.61	28.78	27.85
TiO_2	0.00	0.00	0.00	0.00	0.00	0.01	0.04	0.02	0.00	0.00	0.00	0.01	0.00	0.00	0.00
Al_2O_3	19.38	19.60	19.62	19.53	18.90	19.41	20.19	19.50	18.31	17.12	18.98	18.46	18.21	17.46	18.09
Cr_2O_3	0.07	0.07	0.02	0.05	0.04	0.07	0.07	0.06	0.14	0.06	0.18	0.09	0.16	0.08	0.12
FeO*	18.02	18.52	18.59	18.38	18.67	19.11	19.38	19.05	21.38	21.50	22.14	22.52	22.75	23.16	22.24
MnO	0.34	0.25	0.32	0.30	0.34	0.32	0.27	0.31	0.23	0.20	0.23	0.18	0.18	0.21	0.21
NiO	0.02	0.06	0.08	0.05	0.08	0.10	0.07	0.08	0.09	0.07	0.10	0.06	0.14	0.10	0.09
MgO	18.91	21.00	20.30	20.07	20.65	18.46	20.04	19.72	17.95	17.82	17.41	19.24	17.30	18.48	18.03
CaO	0.13	0.08	0.09	0.10	0.09	0.13	0.15	0.12	0.04	0.12	0.08	0.14	0.08	0.07	0.09
Na_2O	0.03	0.09	0.00	0.04	0.01	0.03	0.02	0.02	0.00	0.05	0.01	0.05	0.00	0.01	0.02
K_2O	0.07	0.05	0.00	0.04	0.09	0.07	0.02	0.06	0.01	0.03	0.02	0.07	0.00	0.01	0.02
Total	85.46	90.45	87.00	87.64	87.86	85.13	88.07	87.02	85.07	85.44	86.73	88.54	86.43	88.36	86.76
Atomic Proportions (based on 28 oxygens)															
Si	5.904	5.998	5.722	5.875	5.867	5.759	5.643	5.756	5.739	6.028	5.772	5.700	5.823	5.934	5.833
Ti	0.000	0.000	0.000	0.000	0.000	0.002	0.006	0.003	0.000	0.000	0.000	0.002	0.000	0.000	0.000
Al	4.735	4.510	4.730	4.659	4.509	4.806	4.828	4.714	4.602	4.273	4.683	4.475	4.527	4.244	4.468
Cr	0.011	0.011	0.003	0.009	0.006	0.012	0.011	0.010	0.024	0.010	0.030	0.015	0.027	0.013	0.020
Fe	3.123	3.023	3.180	3.109	3.160	3.357	3.288	3.268	3.812	3.807	3.875	3.873	4.012	3.994	3.896
Mn	0.060	0.041	0.055	0.052	0.058	0.057	0.046	0.054	0.042	0.036	0.041	0.031	0.032	0.037	0.036
Ni	0.003	0.009	0.013	0.009	0.013	0.017	0.011	0.014	0.015	0.012	0.017	0.010	0.024	0.017	0.016
Mg	5.841	6.109	6.187	6.046	6.228	5.778	6.058	6.021	5.703	5.623	5.430	5.897	5.437	5.679	5.628
Ca	0.029	0.017	0.020	0.022	0.020	0.029	0.033	0.027	0.009	0.027	0.018	0.031	0.018	0.015	0.020
Na	0.012	0.034	0.000	0.015	0.004	0.012	0.008	0.008	0.000	0.021	0.004	0.020	0.000	0.004	0.008
K	0.019	0.012	0.000	0.010	0.023	0.019	0.005	0.016	0.003	0.008	0.005	0.018	0.000	0.003	0.006
Total	19.738	19.765	19.911	19.804	19.889	19.846	19.938	19.891	19.949	19.845	19.876	20.072	19.900	19.940	19.930
Analyses				3				3							6

* Total iron as FeO

Table A-4 (continued):

Weight %	S 35A	S 35A	Mean S 35A	S 81	S 81	Mean S 81	S 16	S 16	S 16	Mean S 16	S 19	S 19	S 19	S 19	S 19	Mean S 19
SiO_2	29.12	27.95	28.54	29.15	28.57	28.86	29.20	27.46	29.08	28.58	28.57	28.46	29.13	28.98	29.66	28.96
TiO_2	0.00	0.00	0.00	0.01	0.00	0.01	0.01	0.01	0.02	0.01	0.05	0.01	0.00	0.00	0.00	0.01
Al_2O_3	17.87	18.94	18.41	17.93	17.20	17.57	18.62	19.50	18.26	18.79	19.27	19.10	20.49	18.96	19.50	19.46
Cr_2O_3	0.08	0.03	0.06	0.00	0.00	0.00	0.01	0.02	0.03	0.02	0.02	0.02	0.01	0.06	0.05	0.03
FeO*	19.35	19.51	19.43	24.05	24.36	24.21	22.12	21.45	21.59	21.72	22.38	22.70	23.23	23.23	23.44	23.00
MnO	0.36	0.34	0.35	0.48	0.50	0.49	0.45	0.41	0.38	0.41	0.33	0.23	0.38	0.30	0.33	0.31
NiO	0.07	0.09	0.08	0.05	0.04	0.05	0.03	0.00	0.00	0.01	0.02	0.05	0.05	0.03	0.00	0.03
MgO	20.65	19.68	20.17	17.51	17.00	17.26	18.59	17.16	18.73	18.16	17.63	17.82	17.74	17.77	18.41	17.87
CaO	0.03	0.02	0.03	0.13	0.13	0.13	0.07	0.05	0.05	0.06	0.11	0.10	0.11	0.08	0.14	0.11
Na_2O	0.08	0.00	0.04	0.03	0.09	0.06	0.06	0.00	0.06	0.04	0.09	0.07	0.02	0.05	0.00	0.05
K_2O	0.04	0.02	0.03	0.03	0.02	0.03	0.07	0.04	0.08	0.06	0.03	0.02	0.03	0.02	0.01	0.02
Total	87.65	86.58	87.12	89.37	87.91	88.64	89.23	86.10	88.28	87.87	88.50	88.58	91.19	89.48	91.54	89.86
Atomic Proportions (based on 28 oxygens)																
Si	5.935	5.777	5.856	5.964	5.972	5.968	5.919	5.764	5.945	5.876	5.846	5.829	5.789	5.884	5.876	5.845
Ti	0.000	0.000	0.000	0.002	0.000	0.001	0.002	0.002	0.003	0.002	0.008	0.002	0.000	0.000	0.000	0.002
Al	4.294	4.615	4.454	4.324	4.238	4.281	4.449	4.826	4.401	4.559	4.649	4.612	4.801	4.539	4.554	4.631
Cr	0.013	0.005	0.009	0.000	0.000	0.000	0.002	0.003	0.005	0.003	0.003	0.003	0.002	0.010	0.008	0.005
Fe	3.298	3.372	3.335	4.115	4.258	4.187	3.750	3.766	3.691	3.736	3.830	3.889	3.861	3.945	3.884	3.882
Mn	0.062	0.060	0.061	0.083	0.089	0.086	0.077	0.073	0.066	0.072	0.057	0.040	0.064	0.052	0.055	0.054
Ni	0.011	0.015	0.013	0.008	0.007	0.007	0.005	0.000	0.000	0.002	0.003	0.008	0.008	0.005	0.000	0.005
Mg	6.272	6.062	6.167	5.339	5.296	5.317	5.616	5.369	5.706	5.563	5.377	5.440	5.254	5.377	5.435	5.377
Ca	0.007	0.004	0.005	0.028	0.029	0.029	0.015	0.011	0.011	0.012	0.024	0.022	0.023	0.017	0.030	0.023
Na	0.032	0.000	0.016	0.012	0.036	0.024	0.024	0.000	0.024	0.016	0.036	0.028	0.008	0.020	0.000	0.018
K	0.010	0.005	0.008	0.008	0.005	0.007	0.018	0.011	0.021	0.017	0.008	0.005	0.008	0.005	0.003	0.006
Total	19.933	19.916	19.924	19.883	19.930	19.906	19.875	19.825	19.872	19.857	19.841	19.878	19.817	19.854	19.844	19.847
			2			2				3						5

* Total iron as FeO

Table A-4 (continued):

Weight %	S 53	S 53	S 53	Mean S 53	S 22	S 22	S 22	S 22	Mean S 22	S 25	S 25	S 25	S 25	Mean S 25
SiO_2	27.81	27.93	29.19	28.31	29.57	30.86	30.36	28.98	29.94	28.76	28.21	28.23	28.07	28.32
TiO_2	0.00	0.01	0.02	0.01	0.05	0.00	0.02	0.01	0.02	0.03	0.00	0.00	0.04	0.02
Al_2O_3	18.30	18.55	19.16	18.67	18.34	19.04	18.23	17.40	18.25	20.48	18.84	18.95	19.79	19.52
Cr_2O_3	0.01	0.04	0.03	0.03	0.01	0.02	0.02	0.00	0.01	0.00	0.02	0.00	0.00	0.01
FeO*	23.36	23.55	24.00	23.64	18.52	19.29	19.29	19.01	19.03	22.81	24.68	24.89	24.98	24.34
MnO	0.17	0.25	0.28	0.23	0.46	0.43	0.42	0.34	0.41	0.29	0.23	0.21	0.17	0.23
NiO	0.03	0.03	0.06	0.04	0.02	0.01	0.05	0.01	0.02	0.06	0.05	0.05	0.05	0.05
MgO	16.55	16.89	16.80	16.75	21.54	21.45	21.83	21.19	21.50	16.36	16.84	16.48	16.64	16.58
CaO	0.10	0.19	0.15	0.15	0.04	0.10	0.08	0.03	0.06	0.08	0.11	0.07	0.04	0.08
Na_2O	0.04	0.07	0.04	0.05	0.01	0.01	0.01	0.03	0.02	0.02	0.00	0.04	0.07	0.03
K_2O	0.01	0.01	0.01	0.01	0.01	0.02	0.01	0.01	0.01	0.01	0.02	0.02	0.02	0.02
Total	86.38	87.52	89.74	87.88	88.57	91.23	90.32	87.01	89.28	88.90	89.00	88.94	89.87	89.18
Atomic Proportions (based on 28 oxygens)														
Si	5.876	5.831	5.926	5.878	5.926	6.000	5.979	5.941	5.961	5.850	5.814	5.825	5.729	5.805
Ti	0.000	0.002	0.003	0.002	0.008	0.000	0.003	0.002	0.003	0.005	0.000	0.000	0.006	0.003
Al	4.559	4.566	4.585	4.570	4.333	4.364	4.233	4.205	4.284	4.911	4.577	4.610	4.762	4.715
Cr	0.002	0.007	0.005	0.004	0.002	0.003	0.003	0.000	0.002	0.000	0.003	0.000	0.000	0.001
Fe	4.128	4.112	4.075	4.105	3.104	3.137	3.177	3.259	3.169	3.881	4.254	4.295	4.264	4.173
Mn	0.030	0.044	0.048	0.041	0.078	0.071	0.070	0.059	0.070	0.050	0.040*	0.037	0.029	0.039
Ni	0.005	0.005	0.010	0.007	0.003	0.002	0.008	0.002	0.004	0.010	0.008	0.008	0.008	0.009
Mg	5.212	5.256	5.083	5.183	6.433	6.215	6.407	6.474	6.382	4.960	5.172	5.068	5.061	5.065
Ca	0.023	0.043	0.033	0.033	0.009	0.021	0.017	0.007	0.013	0.017	0.024	0.015	0.009	0.016
Na	0.016	0.028	0.016	0.020	0.004	0.004	0.004	0.012	0.006	0.008	0.000	0.016	0.028	0.013
K	0.003	0.003	0.003	0.003	0.003	0.005	0.003	0.003	0.003	0.003	0.005	0.005	0.005	0.005
Total	19.853	19.896	19.785	19.845	19.902	19.821	19.903	19.962	19.897	19.695	19.899	19.880	19.901	19.844
				3					4					4

* Total iron as FeO

Table A-4 (continued):

Weight %	S 79	S 79	Mean S 79	S 60	S 60	S 60	S 60	Mean S 60	S 21A	S 21A	S 21A	Mean S 21A
SiO_2	27.82	27.97	27.90	27.04	29.18	26.81	30.15	28.30	26.84	26.72	27.39	26.98
TiO_2	0.02	0.00	0.01	0.00	0.00	0.02	0.05	0.02	0.01	0.05	0.00	0.02
Al_2O_3	18.32	17.41	17.87	18.47	17.24	18.98	18.68	18.34	18.36	17.64	19.03	18.34
Cr_2O_3	0.03	0.01	0.02	0.04	0.01	0.02	0.00	0.02	0.05	0.01	0.02	0.03
FeO*	27.23	27.34	27.29	23.82	24.18	24.29	25.06	24.34	25.71	23.98	23.61	24.43
MnO	0.39	0.36	0.38	0.29	0.27	0.24	0.27	0.27	0.63	0.57	0.57	0.59
NiO	0.08	0.00	0.04	0.01	0.03	0.05	0.03	0.03	0.00	0.05	0.04	0.03
MgO	14.81	15.52	15.17	16.99	17.25	16.03	17.60	16.97	15.57	15.55	15.14	15.42
CaO	0.10	0.09	0.10	0.07	0.10	0.07	0.11	0.09	0.49	0.08	0.11	0.23
Na_2O	0.00	0.05	0.03	0.11	0.02	0.06	0.02	0.05	0.08	0.02	0.00	0.03
K_2O	0.04	0.02	0.03	0.02	0.01	0.03	0.02	0.02	0.04	0.03	0.01	0.03
Total	88.84	88.77	88.81	86.86	88.29	86.60	91.99	88.44	87.78	84.70	85.92	86.13
Atomic Proportions (based on 28 oxygens)												
Si	5.836	5.880	5.858	5.715	6.044	5.694	5.987	5.860	5.689	5.818	5.836	5.781
Ti	0.003	0.000	0.002	0.000	0.000	0.003	0.007	0.003	0.002	0.008	0.000	0.003
Al	4.531	4.315	4.423	4.602	4.210	4.752	4.373	4.484	4.588	4.528	4.781	4.632
Cr	0.005	0.002	0.003	0.007	0.002	0.003	0.000	0.003	0.008	0.002	0.003	0.004
Fe	4.777	4.807	4.792	4.210	4.189	4.314	4.162	4.219	4.558	4.367	4.207	4.377
Mn	0.069	0.064	0.067	0.052	0.047	0.043	0.045	0.047	0.113	0.105	0.103	0.107
Ni	0.013	0.000	0.007	0.002	0.005	0.009	0.005	0.005	0.000	0.009	0.007	0.005
Mg	4.630	4.862	4.746	5.352	5.325	5.074	5.209	5.240	4.919	5.046	4.808	4.924
Ca	0.022	0.020	0.021	0.016	0.022	0.016	0.023	0.019	0.111	0.019	0.025	0.052
Na	0.000	0.020	0.010	0.045	0.008	0.025	0.008	0.021	0.033	0.008	0.000	0.014
K	0.011	0.005	0.008	0.005	0.003	0.008	0.005	0.005	0.011	0.008	0.003	0.007
Total	19.898	19.975	19.937	20.006	19.855	19.941	19.825	19.907	20.032	19.918	19.773	19.908
			2					4				3

* Total iron as FeO

Table A-4 (continued):

Weight %	S 29	S 29	S 29	S 29	Mean S 29	S 82A	S 82A	S 82A	Mean S 82A
SiO_2	27.98	28.15	26.84	27.27	27.56	27.39	27.96	28.14	27.83
TiO_2	0.02	0.03	0.05	0.03	0.03	0.02	0.00	0.01	0.01
Al_2O_3	20.04	19.60	20.30	19.15	19.77	18.45	19.32	18.57	18.78
Cr_2O_3	0.01	0.03	0.03	0.02	0.02	0.02	0.00	0.03	0.02
FeO*	28.00	28.78	29.34	29.77	28.97	19.93	19.31	19.27	19.50
MnO	0.54	0.52	0.53	0.56	0.54	0.38	0.43	0.38	0.40
NiO	0.03	0.00	0.00	0.00	0.01	0.09	0.09	0.05	0.08
MgO	13.41	13.52	13.33	13.43	13.42	18.62	20.23	18.90	19.25
CaO	0.04	0.08	0.04	0.04	0.05	0.08	0.13	0.15	0.12
Na_2O	0.00	0.00	0.04	0.00	0.01	0.01	0.06	0.06	0.04
K_2O	0.04	0.03	0.00	0.01	0.02	0.02	0.04	0.04	0.03
Total	90.11	90.74	90.50	90.28	90.41	85.01	87.57	85.60	86.06
Atomic Proportions (based on 28 oxygens)									
Si	5.786	5.804	5.582	5.702	5.719	5.793	5.713	5.877	5.794
Ti	0.003	0.005	0.008	0.005	0.005	0.003	0.000	0.002	0.002
Al	4.886	4.764	4.978	4.721	4.837	4.601	4.654	4.573	4.609
Cr	0.002	0.005	0.005	0.003	0.004	0.003	0.000	0.005	0.003
Fe	4.843	4.963	5.104	5.206	5.029	3.525	3.300	3.366	3.397
Mn	0.095	0.091	0.093	0.099	0.094	0.068	0.074	0.067	0.070
Ni	0.005	0.000	0.000	0.000	0.001	0.015	0.015	0.008	0.013
Mg	4.133	4.154	4.132	4.185	4.151	5.869	6.160	5.883	5.971
Ca	0.009	0.018	0.009	0.009	0.011	0.018	0.028	0.034	0.027
Na	0.000	0.000	0.016	0.000	0.004	0.004	0.024	0.024	0.017
K	0.011	0.008	0.000	0.003	0.005	0.005	0.010	0.011	0.009
Total	19.772	19.811	19.927	19.933	19.861	19.906	19.978	19.850	19.911
					4				3

* Total iron as FeO

Table A-4 (continued): Averaged chlorite analyses presented in Table 6-9

	SK	SK	Mean SK	SK	SK	SK	Mean SK	SK	SK	SK	SK	SK	Mean SK	SK	SK	SK	Mean SK
Weight %	27 8	27 8	27 8	27 33	27 33	27 33	27 33	28 27	28 27	28 27	28 27	28 27	28 27	28 39	28 39	28 39	28 39
SiO_2	28.41	27.94	28.18	29.39	30.17	28.73	29.43	31.25	32.04	31.59	31.77	31.01	31.53	29.25	25.32	28.81	27.79
TiO_2	0.00	0.00	0.00	0.00	0.02	0.04	0.02	0.05	0.02	0.00	0.02	0.01	0.02	0.01	0.01	0.02	0.01
Al_2O_3	18.52	18.67	18.60	20.18	21.23	25.11	22.17	17.10	17.13	17.82	18.16	18.85	17.81	22.15	19.14	19.93	20.41
Cr_2O_3	0.04	0.03	0.04	0.09	0.09	0.04	0.07	0.02	0.05	0.04	0.09	0.05	0.05	0.05	0.08	0.11	0.08
FeO*	16.60	16.63	16.62	8.45	8.21	8.09	8.25	9.82	9.70	9.73	10.35	10.15	9.95	14.24	12.11	13.37	13.24
MnO	0.36	0.40	0.38	0.26	0.17	0.25	0.23	0.19	0.25	0.20	0.25	0.26	0.23	0.22	0.22	0.25	0.23
NiO	0.02	0.12	0.07	0.03	0.04	0.05	0.04	0.00	0.00	0.03	0.07	0.04	0.03	0.03	0.05	0.03	0.04
MgO	21.70	21.55	21.63	27.36	25.18	26.13	26.22	25.90	26.99	27.11	25.55	27.02	26.51	23.04	22.52	22.59	22.72
CaO	0.12	0.06	0.09	0.07	0.07	0.04	0.06	0.13	0.13	0.07	0.08	0.11	0.10	0.04	0.07	0.06	0.06
Na_2O	0.05	0.03	0.04	0.00	0.11	0.09	0.07	0.00	0.04	0.01	0.02	0.01	0.02	0.00	0.01	0.05	0.02
K_2O	0.01	0.02	0.02	0.02	0.01	0.00	0.01	0.02	0.01	0.02	0.02	0.02	0.02	0.00	0.02	0.02	0.01
Total	85.83	85.45	85.64	85.85	85.30	88.57	86.57	84.48	86.36	86.62	86.38	87.53	86.27	89.03	79.55	85.24	84.61
Atomic Proportions (based on 28 oxygens)																	
Si	5.834	5.774	5.804	5.765	5.917	5.433	5.705	6.252	6.265	6.161	6.225	6.006	6.182	5.678	5.512	5.836	5.675
Ti	0.000	0.000	0.000	0.000	0.003	0.006	0.003	0.008	0.003	0.000	0.003	0.001	0.003	0.001	0.002	0.003	0.002
Al	4.484	4.548	4.516	4.667	4.908	5.598	5.058	4.033	3.949	4.097	4.195	4.304	4.116	5.069	4.913	4.759	4.914
Cr	0.006	0.005	0.006	0.014	0.014	0.006	0.011	0.003	0.008	0.006	0.014	0.008	0.008	0.008	0.014	0.018	0.013
Fe	2.851	2.874	2.863	1.386	1.347	1.279	1.337	1.643	1.586	1.587	1.696	1.644	1.631	2.312	2.205	2.265	2.261
Mn	0.063	0.070	0.067	0.043	0.028	0.040	0.037	0.032	0.041	0.033	0.041	0.043	0.038	0.036	0.041	0.043	0.040
Ni	0.003	0.020	0.012	0.005	0.008	0.008	0.006	0.000	0.000	0.005	0.011	0.006	0.004	0.005	0.009	0.005	0.006
Mg	6.641	6.637	6.639	7.998	7.359	7.364	7.574	7.722	7.865	7.880	7.460	7.799	7.745	6.665	7.307	6.819	6.930
Ca	0.026	0.013	0.020	0.015	0.015	0.008	0.013	0.028	0.027	0.015	0.017	0.023	0.022	0.008	0.016	0.013	0.012
Na	0.020	0.012	0.016	0.000	0.042	0.033	0.025	0.000	0.015	0.004	0.008	0.004	0.006	0.000	0.004	0.020	0.008
K	0.003	0.005	0.004	0.005	0.003	0.000	0.003	0.005	0.002	0.005	0.005	0.005	0.004	0.000	0.006	0.005	0.004
Total	19.932	19.958	19.945	19.897	19.641	19.776	19.771	19.725	19.763	19.792	19.674	19.842	19.759	19.782	20.028	19.785	19.865
Analyses			2				3						5				3

* Total iron as FeO

Table A-4 (continued): Averaged chlorite analyses presented in Table 6-9

Weight %	SK 28 41	SK 28 41	SK 28 41	SK 28 41	Mean SK 28 41	SK 28 73	SK 28 73	SK 28 73	SK 28 73	SK 28 73	Mean SK 28 73	SK 28 75	SK 28 75	Mean SK 28 75	SK 28 40	SK 28 40	SK 28 40	Mean SK 28 40
SiO_2	29.58	29.76	28.48	29.72	29.39	34.32	33.68	34.66	30.85	33.79	33.46	28.96	29.04	29.00	30.33	29.31	31.06	30.23
TiO_2	0.00	0.02	0.02	0.01	0.01	0.02	0.02	0.02	0.00	0.00	0.01	0.00	0.00	0.00	0.04	0.03	0.02	0.03
Al_2O_3	19.97	18.95	18.89	17.61	18.86	15.66	15.89	15.84	15.54	15.10	15.61	19.68	19.66	19.67	21.18	20.69	18.09	19.99
Cr_2O_3	0.04	0.14	0.11	0.03	0.08	0.09	0.01	0.03	0.11	0.08	0.06	0.00	0.10	0.05	0.07	0.02	0.04	0.04
FeO*	10.52	9.13	10.76	9.25	9.92	8.14	8.80	7.98	8.79	8.22	8.39	12.86	12.27	12.57	11.07	10.69	11.26	11.01
MnO	0.21	0.21	0.21	0.19	0.21	0.09	0.13	0.12	0.11	0.09	0.11	0.24	0.27	0.26	0.24	0.25	0.25	0.25
NiO	0.00	0.00	0.03	0.01	0.01	0.00	0.03	0.00	0.01	0.02	0.01	0.03	0.01	0.02	0.03	0.03	0.02	0.03
MgO	24.71	21.52	24.10	26.82	24.29	28.45	28.82	28.88	27.52	27.61	28.26	23.81	23.79	23.80	26.05	24.26	24.54	24.95
CaO	0.06	0.05	0.05	0.07	0.06	0.13	0.10	0.22	0.12	0.17	0.15	0.04	0.04	0.04	0.10	0.04	0.10	0.08
Na_2O	0.01	0.00	0.06	0.07	0.04	0.02	0.00	0.04	0.04	0.06	0.03	0.00	0.00	0.00	0.01	0.02	0.08	0.04
K_2O	0.01	0.00	0.02	0.03	0.02	0.02	0.05	0.07	0.04	0.08	0.05	0.01	0.02	0.02	0.02	0.02	0.02	0.02
Total	85.11	79.78	82.73	83.81	82.86	86.94	87.53	87.86	83.13	85.22	86.14	85.63	85.20	85.42	89.14	85.36	85.48	86.66
Atomic Proportions (based on 28 oxygens)																		
Si	5.899	6.257	5.874	6.001	6.008	6.585	6.455	6.578	6.261	6.626	6.501	5.824	5.851	5.838	5.789	5.834	6.185	5.936
Ti	0.000	0.003	0.003	0.002	0.002	0.003	0.003	0.003	0.000	0.000	0.002	0.000	0.000	0.000	0.006	0.004	0.003	0.004
Al	4.695	4.697	4.593	4.192	4.544	3.542	3.591	3.544	3.718	3.491	3.577	4.666	4.670	4.668	4.766	4.855	4.247	4.623
Cr	0.006	0.023	0.018	0.005	0.013	0.014	0.002	0.005	0.018	0.012	0.010	0.000	0.016	0.008	0.011	0.003	0.006	0.007
Fe	1.755	1.606	1.856	1.562	1.695	1.306	1.411	1.267	1.492	1.348	1.365	2.163	2.067	2.115	1.767	1.779	1.875	1.807
Mn	0.035	0.037	0.037	0.032	0.035	0.015	0.021	0.019	0.019	0.015	0.018	0.041	0.046	0.044	0.039	0.042	0.042	0.041
Ni	0.000	0.000	0.005	0.002	0.002	0.000	0.005	0.000	0.002	0.003	0.002	0.005	0.002	0.004	0.005	0.005	0.003	0.004
Mg	7.344	6.744	7.407	8.071	7.392	8.136	8.232	8.169	8.323	8.069	8.186	7.136	7.143	7.140	7.410	7.196	7.283	7.296
Ca	0.013	0.011	0.011	0.015	0.013	0.027	0.021	0.045	0.026	0.036	0.031	0.009	0.009	0.009	0.020	0.009	0.021	0.017
Na	0.004	0.000	0.024	0.027	0.014	0.007	0.000	0.015	0.016	0.023	0.012	0.000	0.000	0.000	0.004	0.008	0.031	0.014
K	0.003	0.000	0.005	0.008	0.004	0.005	0.012	0.017	0.010	0.020	0.013	0.003	0.005	0.004	0.005	0.005	0.005	0.005
Total	19.754	19.379	19.833	19.917	19.721	19.640	19.752	19.661	19.884	19.643	19.716	19.845	19.809	19.827	19.821	19.739	19.703	19.754
Analyses					4						5			2				3

* Total iron as FeO

Table A-4 (continued): Averaged chlorite analyses presented in Table 6-9

			Mean				Mean			Mean					Mean	
	SK	SK	SK	SK	SK	SK	SK	SK	SK	SK	SK	SK	SK	SK	SK	SK
Weight %	29 57	29 57	29 57	27 37	27 37	27 37	27 37	29 60	29 60	29 60	30 67	30 67	30 67	30 67	30 80
SiO_2	29.64	31.99	30.82	32.16	33.11	33.10	32.79	29.08	28.76	28.92	26.11	27.81	27.43	27.12	26.94
TiO_2	0.03	0.02	0.03	0.02	0.04	0.02	0.03	0.01	0.02	0.02	0.02	0.03	0.02	0.02	0.01
Al_2O_3	19.86	21.08	20.47	17.69	17.53	17.21	17.48	19.04	20.62	19.83	19.34	18.31	21.76	19.80	21.36
Cr_2O_3	0.06	0.07	0.07	0.02	0.00	0.00	0.01	0.01	0.02	0.02	0.13	0.10	0.00	0.08	0.04
FeO*	10.09	10.55	10.32	9.36	9.03	8.74	9.04	8.23	8.40	8.32	12.46	12.89	13.29	12.88	11.36
MnO	0.27	0.15	0.21	0.14	0.21	0.23	0.19	0.12	0.19	0.16	0.25	0.27	0.27	0.26	0.14
NiO	0.05	0.00	0.03	0.03	0.02	0.00	0.02	0.01	0.03	0.02	0.04	0.03	0.03	0.03	0.04
MgO	19.55	21.46	20.51	27.44	27.84	27.24	27.51	27.39	25.07	26.23	21.58	23.01	24.14	22.91	23.16
CaO	0.09	0.05	0.07	0.13	0.09	0.12	0.11	0.04	0.05	0.05	0.02	0.02	0.04	0.03	0.02
Na_2O	0.07	0.02	0.05	0.04	0.03	0.05	0.04	0.10	0.00	0.05	0.01	0.00	0.01	0.01	0.02
K_2O	0.89	0.96	0.93	0.02	0.03	0.03	0.03	0.01	0.00	0.01	0.00	0.06	0.00	0.02	0.01
Total	80.60	86.35	83.48	87.05	87.93	86.74	87.24	84.04	83.16	83.60	79.96	82.53	86.99	83.16	83.10
Atomic Proportions (based on 28 oxygens)															
Si	6.236	6.264	6.250	6.223	6.321	6.393	6.312	5.824	5.807	5.816	5.647	5.831	5.456	5.645	5.549
Ti	0.005	0.003	0.004	0.003	0.006	0.003	0.004	0.002	0.003	0.003	0.003	0.005	0.003	0.004	0.002
Al	4.926	4.866	4.896	4.035	3.946	3.919	3.967	4.495	4.909	4.702	4.931	4.526	5.103	4.853	5.187
Cr	0.010	0.011	0.011	0.003	0.000	0.000	0.001	0.002	0.003	0.003	0.022	0.017	0.000	0.013	0.007
Fe	1.775	1.728	1.752	1.515	1.442	1.412	1.456	1.378	1.419	1.399	2.254	2.260	2.211	2.242	1.957
Mn	0.048	0.025	0.037	0.023	0.034	0.038	0.032	0.020	0.032	0.026	0.046	0.048	0.045	0.046	0.024
Ni	0.008	0.000	0.004	0.005	0.003	0.000	0.003	0.002	0.005	0.004	0.007	0.005	0.005	0.006	0.007
Mg	6.130	6.263	6.197	7.913	7.921	7.841	7.892	8.175	7.544	7.860	6.956	7.190	7.156	7.101	7.110
Ca	0.020	0.010	0.015	0.027	0.018	0.025	0.023	0.009	0.011	0.010	0.005	0.004	0.009	0.006	0.004
Na	0.029	0.008	0.019	0.015	0.011	0.019	0.015	0.039	0.000	0.020	0.004	0.000	0.004	0.003	0.008
K	0.239	0.240	0.240	0.005	0.007	0.007	0.006	0.003	0.000	0.002	0.000	0.016	0.000	0.005	0.003
Total	19.425	19.418	19.422	19.765	19.709	19.657	19.710	19.947	19.734	19.841	19.875	19.901	19.991	19.922	19.858
Analyses			2				3			2				3	

* Total iron as FeO

Table A-4 (continued): Averaged chlorite analyses presented in Table 6-9

Weight %	SK 30 822A	SK 30 822A	Mean SK 30 822A	SK 31 13	SK 31 13	SK 31 13	SK 31 13	Mean SK 31 13	SK 27 46	SK 27 46	SK 27 46	Mean SK 27 46	SK 28 38	SK 28 38	SK 28 38	Mean SK 28 38
SiO_2	26.27	25.44	25.86	26.87	28.08	28.03	26.86	27.46	26.57	26.42	26.10	26.36	28.76	28.70	28.93	28.80
TiO_2	0.01	0.02	0.02	0.00	0.03	0.00	0.00	0.01	0.02	0.02	0.03	0.02	0.02	0.02	0.01	0.02
Al_2O_3	20.55	20.89	20.72	17.59	19.39	19.78	18.59	18.84	17.74	16.13	15.70	16.52	25.58	21.96	18.46	22.00
Cr_2O_3	0.09	0.09	0.09	0.68	0.66	0.46	0.46	0.57	0.00	0.02	0.03	0.02	0.03	0.04	0.00	0.02
FeO*	14.99	15.06	15.03	9.23	8.73	10.28	10.68	9.73	15.41	16.05	16.14	15.87	9.89	10.45	10.01	10.12
MnO	0.14	0.15	0.15	0.15	0.15	0.21	0.15	0.17	0.27	0.23	0.25	0.25	0.13	0.16	0.17	0.15
NiO	0.03	0.00	0.02	0.04	0.04	0.03	0.01	0.03	0.03	0.05	0.05	0.04	0.03	0.05	0.03	0.04
MgO	20.83	21.27	21.05	25.19	24.62	24.56	23.91	24.57	23.68	21.20	20.30	21.73	23.44	23.98	24.25	23.89
CaO	0.03	0.02	0.03	0.02	0.02	0.00	0.00	0.01	0.04	0.02	0.05	0.04	0.02	0.00	0.02	0.01
Na_2O	0.00	0.03	0.02	0.01	0.00	0.00	0.00	0.00	0.01	0.04	0.00	0.02	0.00	0.09	0.03	0.04
K_2O	0.00	0.02	0.01	0.00	0.00	0.00	0.01	0.00	0.01	0.00	0.00	0.00	0.00	0.00	0.02	0.01
Total	82.94	82.99	82.97	79.78	81.72	83.35	80.67	81.38	83.78	80.18	78.65	80.87	87.90	85.45	81.93	85.09
Atomic Proportions (based on 28 oxygens)																
Si	5.541	5.378	5.460	5.739	5.805	5.729	5.704	5.744	5.592	5.837	5.889	5.773	5.509	5.697	5.989	5.732
Ti	0.002	0.003	0.003	0.000	0.005	0.000	0.000	0.001	0.003	0.003	0.005	0.004	0.003	0.003	0.002	0.003
Al	5.110	5.207	5.159	4.429	4.725	4.766	4.654	4.644	4.402	4.201	4.176	4.260	5.776	5.139	4.505	5.140
Cr	0.015	0.015	0.015	0.115	0.108	0.074	0.077	0.094	0.000	0.003	0.005	0.003	0.005	0.006	0.000	0.004
Fe	2.644	2.663	2.654	1.649	1.509	1.757	1.897	1.703	2.713	2.966	3.045	2.908	1.584	1.735	1.733	1.684
Mn	0.025	0.027	0.026	0.027	0.026	0.036	0.027	0.029	0.048	0.043	0.048	0.046	0.021	0.027	0.030	0.026
Ni	0.005	0.000	0.003	0.007	0.007	0.005	0.002	0.005	0.005	0.009	0.009	0.008	0.005	0.008	0.005	0.006
Mg	6.547	6.702	6.625	8.018	7.585	7.482	7.567	7.663	7.428	6.981	6.826	7.078	6.691	7.094	7.481	7.089
Ca	0.007	0.005	0.006	0.005	0.004	0.000	0.000	0.002	0.009	0.005	0.012	0.009	0.004	0.000	0.004	0.003
Na	0.000	0.012	0.006	0.004	0.000	0.000	0.000	0.001	0.004	0.017	0.000	0.007	0.000	0.035	0.012	0.016
K	0.000	0.005	0.003	0.000	0.000	0.000	0.003	0.001	0.003	0.000	0.000	0.001	0.000	0.000	0.005	0.002
Total	19.895	20.017	19.956	19.992	19.774	19.850	19.931	19.887	20.207	20.066	20.015	20.096	19.598	19.744	19.766	19.703
Analyses			2					4				3				3

* Total iron as FeO

Table A-4 (continued): Averaged chlorite analyses presented in Table 6-9

Weight %	SK 28 67	SK 28 67	Mean SK 28 67	SK 30 81	SK 30 81	Mean SK 30 81	SK 35A 6	SK 35A 6	Mean SK 35A 6	SK 27 42	SK 27 42	Mean SK 27 42	SK 27 45	SK 27 45	Mean SK 27 45	SK 37A 46	SK 37A 46	Mean SK 37A 46
SiO_2	30.19	32.17	31.18	31.05	30.45	30.75	31.60	29.12	30.36	27.84	27.84	27.84	25.34	26.39	25.87	20.78	23.11	21.95
TiO_2	0.00	0.00	0.00	0.01	0.01	0.01	0.00	0.02	0.01	0.00	0.00	0.00	0.02	0.03	0.03	0.02	0.01	0.02
Al_2O_3	17.59	15.12	16.36	14.39	15.81	15.10	17.19	16.45	16.82	19.12	18.02	18.57	16.92	17.33	17.13	18.00	17.50	17.75
Cr_2O_3	0.00	0.02	0.01	0.02	0.04	0.03	0.00	0.03	0.02	0.02	0.00	0.01	0.02	0.04	0.03	0.01	0.02	0.02
FeO*	10.69	10.48	10.59	9.88	9.95	9.92	6.02	5.97	6.00	22.28	22.42	22.35	19.87	20.77	20.32	26.43	26.22	26.33
MnO	0.16	0.11	0.14	0.11	0.09	0.10	0.24	0.11	0.18	0.24	0.33	0.29	0.16	0.28	0.22	0.33	0.43	0.38
NiO	0.04	0.05	0.05	0.00	0.00	0.00	0.00	0.05	0.03	0.01	0.05	0.03	0.03	0.03	0.03	0.04	0.03	0.04
MgO	26.59	26.68	26.64	26.05	26.96	26.51	29.32	27.36	28.34	17.14	18.21	17.68	17.90	19.26	18.58	12.54	12.69	12.62
CaO	0.13	0.19	0.16	0.07	0.14	0.11	0.00	0.00	0.00	0.09	0.07	0.08	0.02	0.02	0.02	0.02	0.02	0.02
Na_2O	0.00	0.06	0.03	0.03	0.05	0.04	0.00	0.00	0.00	0.00	0.00	0.00	0.06	0.01	0.04	0.01	0.00	0.01
K_2O	0.04	0.02	0.03	0.00	0.00	0.00	0.00	0.00	0.00	0.03	0.02	0.03	0.01	0.01	0.01	0.02	0.01	0.02
Total	85.43	84.90	85.17	81.61	83.50	82.56	84.37	79.11	81.74	86.77	86.96	86.87	80.35	84.17	82.26	78.20	80.04	79.12
Atomic Proportions (based on 28 oxygens)																		
Si	6.021	6.432	6.227	6.446	6.192	6.319	6.208	6.117	6.163	5.816	5.824	5.820	5.713	5.689	5.701	5.078	5.462	5.270
Ti	0.000	0.000	0.000	0.002	0.002	0.002	0.000	0.003	0.002	0.000	0.000	0.000	0.003	0.005	0.004	0.004	0.002	0.003
Al	4.136	3.564	3.850	3.522	3.790	3.656	3.981	4.074	4.028	4.709	4.444	4.577	4.497	4.404	4.451	5.186	4.876	5.031
Cr	0.000	0.003	0.002	0.003	0.006	0.005	0.000	0.005	0.003	0.003	0.000	0.002	0.004	0.007	0.006	0.002	0.004	0.003
Fe	1.783	1.752	1.768	1.715	1.692	1.704	0.989	1.049	1.019	3.893	3.923	3.908	3.747	3.744	3.746	5.402	5.183	5.293
Mn	0.027	0.019	0.023	0.019	0.016	0.018	0.040	0.020	0.030	0.042	0.058	0.050	0.031	0.051	0.041	0.068	0.086	0.077
Ni	0.006	0.008	0.007	0.000	0.000	0.000	0.000	0.008	0.004	0.002	0.008	0.005	0.005	0.005	0.005	0.008	0.006	0.007
Mg	7.904	7.950	7.927	8.060	8.170	8.115	8.584	8.565	8.575	5.337	5.677	5.507	6.014	6.187	6.101	4.567	4.470	4.519
Ca	0.028	0.041	0.035	0.016	0.031	0.024	0.000	0.000	0.000	0.020	0.016	0.018	0.005	0.005	0.005	0.005	0.005	0.005
Na	0.000	0.023	0.012	0.012	0.020	0.016	0.000	0.000	0.000	0.000	0.000	0.000	0.026	0.004	0.015	0.005	0.000	0.003
K	0.010	0.005	0.008	0.000	0.000	0.000	0.000	0.000	0.000	0.008	0.005	0.007	0.003	0.003	0.003	0.006	0.003	0.005
Total	19.916	19.798	19.857	19.796	19.918	19.857	19.802	19.841	19.822	19.831	19.956	19.894	20.048	20.104	20.076	20.330	20.097	20.214
Analyses			2			2			2			2			2			2

* Total iron as FeO

Table A-5: Averaged electron microprobe analyses of muscovites presented in Table 6-13

Weight %	SK 28 78	SK 28 78	Mean SK 28 78	SK 30 B	SK 30 B	SK 30 B	Mean SK 30 B
SiO_2	49.29	49.06	49.18	45.55	43.77	44.26	44.53
TiO_2	0.18	0.21	0.20	0.24	0.09	0.05	0.13
Al_2O_3	31.22	30.60	30.91	21.38	32.64	31.38	31.80
Cr_2O_3	0.05	0.05	0.05	0.18	0.04	0.04	0.09
FeO*	1.13	1.08	1.11	0.89	0.93	1.07	0.96
MnO	0.00	0.03	0.02	0.01	0.02	0.01	0.01
NiO	0.05	0.00	0.03	0.01	0.03	0.02	0.02
MgO	2.32	2.13	2.23	1.29	0.97	1.25	1.17
CaO	0.03	0.07	0.05	0.08	0.00	0.00	0.03
Na_2O	0.03	0.14	0.09	0.21	0.11	0.14	0.15
K_2O	9.48	9.32	9.40	9.61	9.45	9.95	9.67
Total	93.78	92.69	93.24	89.45	88.05	88.17	88.56
Atomic Proportions (based on 22 oxygens)							
Si	6.585	6.627	6.606	6.413	6.259	6.348	6.340
Ti	0.018	0.021	0.020	0.025	0.010	0.005	0.013
Al	4.917	4.873	4.895	5.208	5.503	5.306	5.339
Cr	0.005	0.005	0.005	0.020	0.005	0.005	0.010
Fe	0.126	0.122	0.124	0.105	0.111	0.128	0.115
Mn	0.000	0.003	0.002	0.001	0.002	0.001	0.002
Ni	0.005	0.000	0.003	0.001	0.003	0.002	0.002
Mg	0.462	0.429	0.445	0.271	0.207	0.267	0.248
Ca	0.004	0.010	0.007	0.012	0.000	0.000	0.004
Na	0.008	0.037	0.022	0.057	0.031	0.039	0.042
K	1.616	1.606	1.611	1.726	1.724	1.821	1.757
Total	13.747	13.734	13.741	13.840	13.855	13.922	13.872
Analyses			2				3

* Total iron as FeO

Table A-6: Electron microprobe analyses conducted on sulphide standards during this study

Standard: PYR 242 (CANMET)

Weight %	Mean m	Standard Deviation ∂	Accepted Value v	m-v	(m-v)/v (%)
S	36.03	0.08	36.47	-0.44	-1%
Fe	65.86	1.21	63.03	2.83	4%
Ni	0.82	0.29	0.50	0.32	63%
Total	102.71	1.38	100.00	2.71	3%
Analyses	2				

Standard: CUBS (cubanite from Strathcona)

Weight %	Mean m	Standard Deviation ∂	Accepted Value v	m-v	(m-v)/v (%)
S	35.31	0.06	35.44	-0.14	0%
Fe	42.40	0.23	41.15	1.25	3%
Cu	23.03	0.09	23.41	-0.39	-2%
Total	100.73	0.35	100.00	0.72	1%
Analyses	2				

Standard: CdS (CANMET)

Weight %	This Study m	Accepted Value v	m-v	(m-v)/v (%)
S	20.63	22.20	-1.57	-7%
Cd	76.35	77.80	-1.45	-2%
Total	97.34	100.00	-2.66	-3%
Analyses	1			

Standard: PbS (U.S.G.S.)

Weight %	This Study m	Accepted Value v	m-v	(m-v)/v (%)
S	13.27	13.40	-0.13	-1%
Pb	86.95	86.60	0.35	0%
Total	100.22	100.00	0.22	0%
Analyses	1			

Standard: $AgBiSe_2$ (CANMET)

Weight %	This Study m	Accepted Value v	m-v	(m-v)/v (%)
Bi	39.83	44.03	-4.20	-10%
Ag	22.86	22.72	0.14	1%
Se		33.25		
Analyses	1			

Table A-6 (continued): Electron microprobe analyses conducted on sulphide standards during this study

Standard: sphalerite SP 20 (Taylor sulphide block)

Weight %	Mean (M)	Standard Deviation (∂)	∂/m (%)	Minimum	Maximum	Range	Accepted Value v	m-v	(m-v)/v (%)
S	32.66	0.44	1%	32.09	33.66	1.57	32.92	-0.26	-1%
Fe	11.55	0.39	3%	10.69	12.21	1.52	11.75	-0.20	-2%
Zn	55.89	1.87	3%	54.04	60.85	6.81	55.57	0.32	1%
Total	100.15	1.81	2%	98.38	104.52	6.14	100.24	-0.09	0%
Analyses	13								

Standard: Sphalerite 20 (CANMET)

Weight %	Mean (M)	Standard Deviation (∂)	∂/m (%)	Minimum	Maximum	Range	Accepted Value v	m-v	(m-v)/v (%)
S	33.38	0.25	1%	33.18	33.73	0.55	33.18	0.20	1%
Fe	4.80	0.14	3%	4.62	4.92	0.30	4.75	0.05	1%
Zn	66.47	0.42	1%	66.05	67.03	0.98	62.07	4.40	7%
Total	104.65	0.70	1%	104.28	105.78	1.50	100.00	4.65	5%
Analyses	4								

Table A-7: Electron microprobe analyses of various minerals for S, Fe and Zn (weight %)

	Chlorite										
	S 22	S 22	S 30	S 30	S 68B	SK 27 33	SK 27 33	SK 27 45	SK 27 46	SK 27 46	SK 27 46
S	0.01	0.02	0.02	0.01	0.02	0.02	0.02	0.11	0.18	0.13	0.09
Fe	12.69	11.98	15.20	15.29	21.09	5.22	5.27	13.12	10.60	9.75	11.04
Zn	0.20	0.24	0.17	0.16	0.24	0.18	0.15	0.38	0.55	0.64	0.46
Total	12.90	12.24	15.39	15.46	21.35	5.42	5.44	13.61	11.33	10.52	11.59

	Chlorite										
	SK 28 38	SK 28 38	SK 28 67	SK 28 73	SK 28 73	SK 28 73	SK 28 73	SK 28 73	SK 28 73	SK 28 75	SK 28 75
S	0.11	0.09	0.10	0.05	0.02	0.02	0.05	0.01	nd	nd	0.01
Fe	5.73	5.94	6.93	5.21	5.42	5.02	5.74	5.59	5.31	8.39	8.05
Zn	0.29	0.20	0.29	0.22	0.24	0.31	0.36	0.21	0.31	0.23	0.23
Total	6.13	6.23	7.32	5.48	5.68	5.35	6.15	5.81	5.62	8.62	8.29

	Chlorite										
	SK 28 75	SK 28 75	SK 28 78	SK 29 60	SK 30 58	SK 30 67	SK 30 67	SK 30 67	SK 30 81	SK 30 81	SK 30 822A
S	0.01	0.01	0.03	0.09	0.04	0.04	0.04	0.05	0.10	0.06	0.03
Fe	8.21	8.35	7.54	5.56	8.87	8.64	8.30	6.63	5.86	6.54	9.76
Zn	0.31	0.26	0.20	0.18	0.25	0.31	0.31	0.36	0.40	0.32	0.25
Total	8.53	8.62	7.77	5.83	9.16	8.99	8.65	7.04	6.36	6.92	10.04

	Chlorite								Calcite
	SK 30 822A	SK 30 822A	SK 31 13	SK 31 13	SK 35A 6	SK 35A 6	SK 37A 46	SK 37A 46	S 30
S	0.04	0.05	0.07	0.12	0.16	0.04	0.19	0.20	nd
Fe	9.77	9.85	6.87	6.21	3.82	3.16	17.86	17.96	0.68
Zn	0.29	0.24	0.30	0.29	0.31	0.68	0.38	0.37	0.21
Total	10.10	10.14	7.24	6.62	4.29	3.88	18.43	18.53	0.89

	Quartz										
	SK 27 46	SK 27 46	SK 28 75	SK 28 75	SK 28 75	SK 28 75	SK 28 78	SK 28 78	SK 37A 46	SK 37A 46	SK 37A 46
S	0.05	0.04	nd	nd	0.01	0.01	nd	nd	0.02	0.01	0.01
Fe	0.17	0.11	0.05	0.01	0.04	0.08	0.01	0.02	0.05	0.04	0.01
Zn	0.16	0.15	0.16	0.21	0.15	0.17	0.14	0.18	0.16	0.09	0.14
Total	0.38	0.30	0.21	0.22	0.20	0.26	0.15	0.20	0.23	0.14	0.16

	Phlogopite		Muscovite			Talc		Magnetite
	SK 29 55	SK 29 55	SK 29 55	SK 28 78	SK 30 58	SK 28 73	SK 28 73	SK 28 38
S	0.02	0.02	0.03	0.02	0.04	0.03	0.02	0.15
Fe	4.41	5.07	1.41	0.72	0.34	1.91	3.31	98.98
Zn	0.18	0.22	0.20	0.09	0.15	0.20	0.27	0.23
Total	4.61	5.31	1.64	0.83	0.53	2.14	3.60	99.36

nd - not detected

APPENDIX B

MAJOR AND TRACE ELEMENT ANALYTICAL PROCEDURES AND ANALYSES

B.1 Sample Preparation and Geochemical Methods for Major and Trace Element Analyses

Samples chosen for analysis were slabbed to remove weathered material and veins. The slabbed samples were crushed into chips and then pulverized for 2-3 minutes using a tungsten carbide puck mill to produce a powder of approximately -100 mesh.

With the exception of phosphorus and loss on ignition, the major element analyses were performed by atomic absorption spectrophotometry. Samples were prepared in a manner similar to that described by Langmyhr and Paus (1968); the elements were analyzed on a Perkin-Elmer Model 370 atomic absorption spectrometer with digital readout. Phosphorus was determined colorimetrically using a Bausch and Lomb Spectronic 20 Colorimeter, based on a modification of the method described by Shapiro and Brannock (1962). Loss on ignition was determined by weighing approximately 1 g of the powdered sample into a porcelain crucible and heating it to approximately 1000°C for about 90 minutes to volatilize S, CO_2, H_2O etc.

Statistical parameters for replicate major element analyses of Skidder Basalt sample S 60 are shown in Table B-1.

Sample pellets for trace element analysis were made by mixing 10 g of powdered sample with approximately 1.5 g of bakelite binding resin, the mixture was pressed and then baked for 10 minutes at 200°C. Analyses were made using a Phillips 1450 X-Ray fluorescence (XRF) spectrometer with a rhodium tube.

Samples were run in batches of nine with U.S.G.S. standard W-1 run as a tenth sample. A monitor that is saturated with trace elements was used to calibrate the machine against standard values and correct for instrument drift.

Table B-2 shows statistical parameters for 26 repeat analyses of W-1. Also, the accepted trace element values for W-1 according to Abbey (1980) and the detection limits of

Table B-1: Replicate major element analyses of Skidder Basalt sample S-60

weight %	Mean	Standard Deviation	Minimum	Maximum
SiO_2	51.48*	0.43	50.90	51.90
TiO_2	1.31*	0.06	1.27	1.40
Al_2O_3	14.93*	0.21	14.70	15.20
Fe_2O_3	13.64*	0.06	13.57	13.71
MnO	0.13*	0.01	0.13	0.14
MgO	6.60*	0.08	6.52	6.66
CaO	4.02*	0.01	4.00	4.03
Na_2O	5.57*	0.07	5.50	5.63
K_2O	0.09*	0.00	0.09	0.09
P_2O_5	0.14**	0.03	0.10	0.17
LOI	2.35***	0.11	2.25	2.48
Total	100.26			
Analyses	4			

Total iron as Fe_2O_3
* Analyzed by atomic absorption spectrophotometry
** Analyzed by colorimetry
*** Determined by weight difference after heating to 1000°C for 90 minutes

Table B-2: Replicate trace element analyses of U.S.G.S. standard W 1 by X-ray fluorescence spectrometry

Number of analyses: 26
m Mean
s Standard Deviation
Min Minimum
Max Maximum
v Accepted Value (Abbey, 1980)
d Detection Limit (D. Press, personal communication, 1984)

ppm	m	s	Min	Max	s/m %	v	m-v	(m-v)/v %	d
Pb	9	3.4	3	18	36%	7.8	1.5	19%	6.4
Th	5	2.6	0	10	57%	2.4	2.2	92%	4.4
U	1	1.4	0	6	207%	0.6	0.1	19%	1.7
Rb	22	2.6	17	27	12%	21	1.4	7%	3.4
Sr	183	2.8	176	188	2%	190	-7.0	-4%	3.1
Y	25	1.6	21	28	6%	25	-0.5	-2%	3.8
Zr	95	2.5	90	100	3%	105	-10.5	-10%	4.6
Nb	11	1.6	7	13	15%	9.5	1.1	12%	3.5
Zn	84	4.9	65	89	6%	86	-1.8	-2%	2.3
Cu	117	5.1	100	124	4%	110	6.5	6%	2.5
Ni	77	4.2	62	82	5%	76	0.5	1%	2.8
La	13	5.7	0	23	42%	9.8	3.6	37%	6.3
Ba	161	37.8	46	208	23%	160	1.0	1%	5.4
V	253	4.1	242	261	2%	260	-6.7	-3%	2.0
Ce	71	20.4	30	132	29%	23	47.5	207%	6.5
Cr	121	2.8	113	126	2%	115	6.2	5%	1.8
Ga	19	2.8	14	29	15%	16	2.7	17%	2.1

the elements (D. Press, personal communication, 1984) are listed. The elements Sr, Y, Zn, Cu, Ni, V, and Cr have low standard deviations relative to the mean, have a limited range, are close to accepted values, and concentrations of these elements in the Skidder Basalt are generally well above the detection limits by the XRF method. Zirconium values are also consistent but are approximately 10 ppm lower than the accepted value for W-1. Gallium, rubidium, and niobium have acceptable range and standard deviation relative to the mean, and are similar to the accepted values for W-1. However, concentrations of Rb and Nb within the Skidder Basalt are close to the detection limits for these elements by the XRF method. Lead values obtained are extremely variable and Pb concentrations in the Skidder Basalt are close to or below the detection limit. Barium analyses are highly variable but the mean is close to the accepted value for Ba in W-1.

B.2 Histograms and Probability Plots

Histograms and probability plots are presented in Figures B-1 to B-14 for analyses of mafic Skidder Basalt outcrop samples, and mafic Skidder Prospect drill core samples relatively unaffected by the mineralizing event(s). Histograms on the left in Figures B-1 to B-7 compare outcrop samples to relatively unaltered Skidder Prospect drill core samples and those on the right compare samples of massive flows to samples of pillow lavas.

Probability plots on the left in Figures B-8 to B-14 have per cent major oxide or ppm minor element on the y-axis and cumulative frequency plotted as probits on the x-axis. The scale on the x-axis is graduated such that a cumulative percent frequency plot of data having a normal distribution would be a straight line. Nearly linear segments separated by curved lines having an inflection point on such plots indicate the presence of more than one population of data. Plots on the right have $\log_{10}$ of the per cent major oxide or ppm minor element on the y-axis and cumulative frequency plotted as probits on the x-axis. Data having a lognormal distribution would plot as a straight line on this graph and different populations would be indicated in a manner similar to that described above. Arrows on these plots indicate per cent or ppm values at which there are changes in slope.

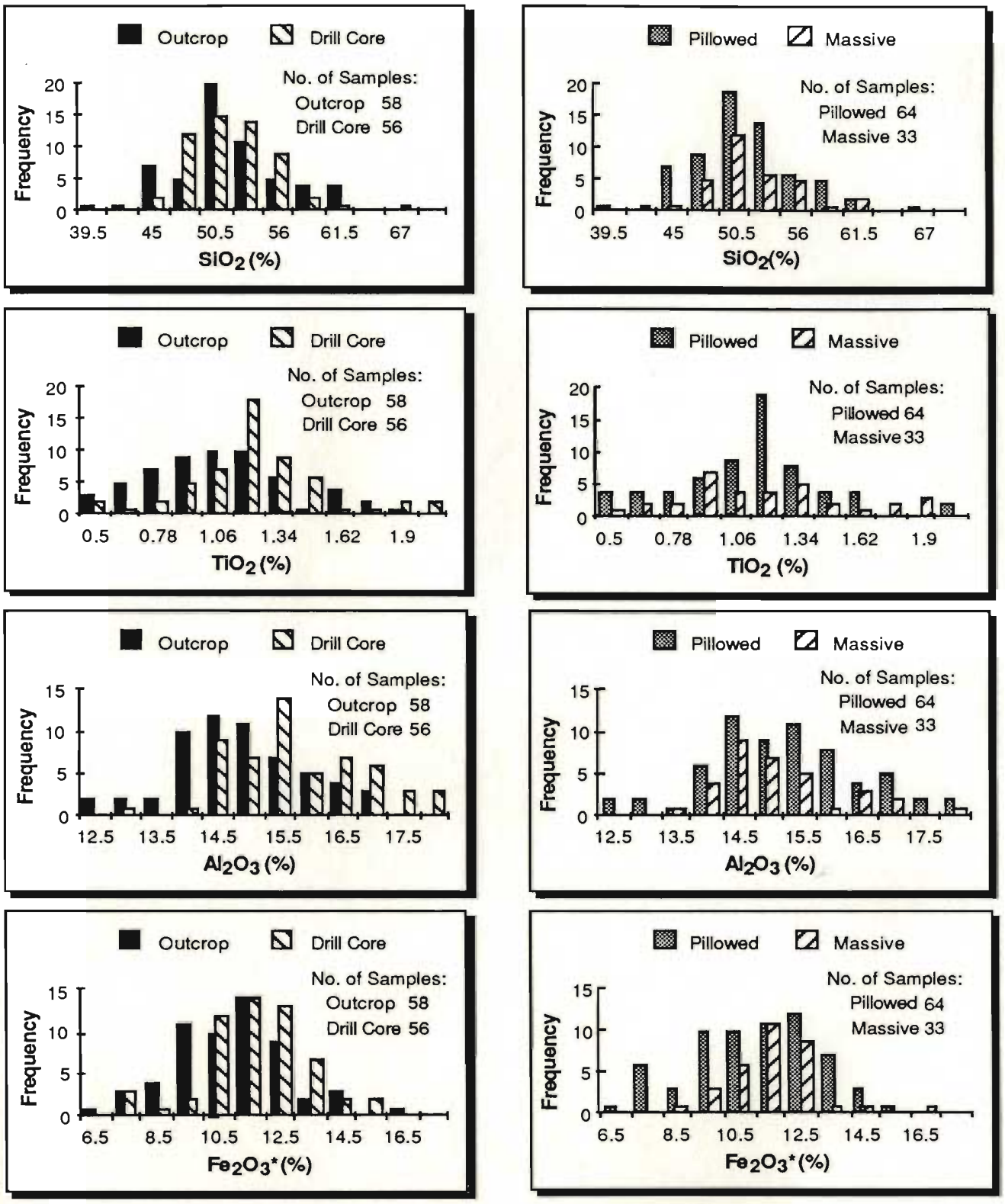

Figure B-1: Histograms showing distribution of SiO_2, TiO_2, Al_2O_3, and Fe_2O_3 in the Skidder Basalt. Outcrop samples include pillowed basalt, massive flows and a few diabase dykes. Drill core samples are of relatively unaltered pillowed and massive flows from the vicinity of the Skidder Prospect. Pillowed and massive flows shown in histograms on the right include samples from both drill core and outcrop. Values along the x-axis represent the maximum for the interval in which the value is shown. * Total iron as Fe_2O_3.

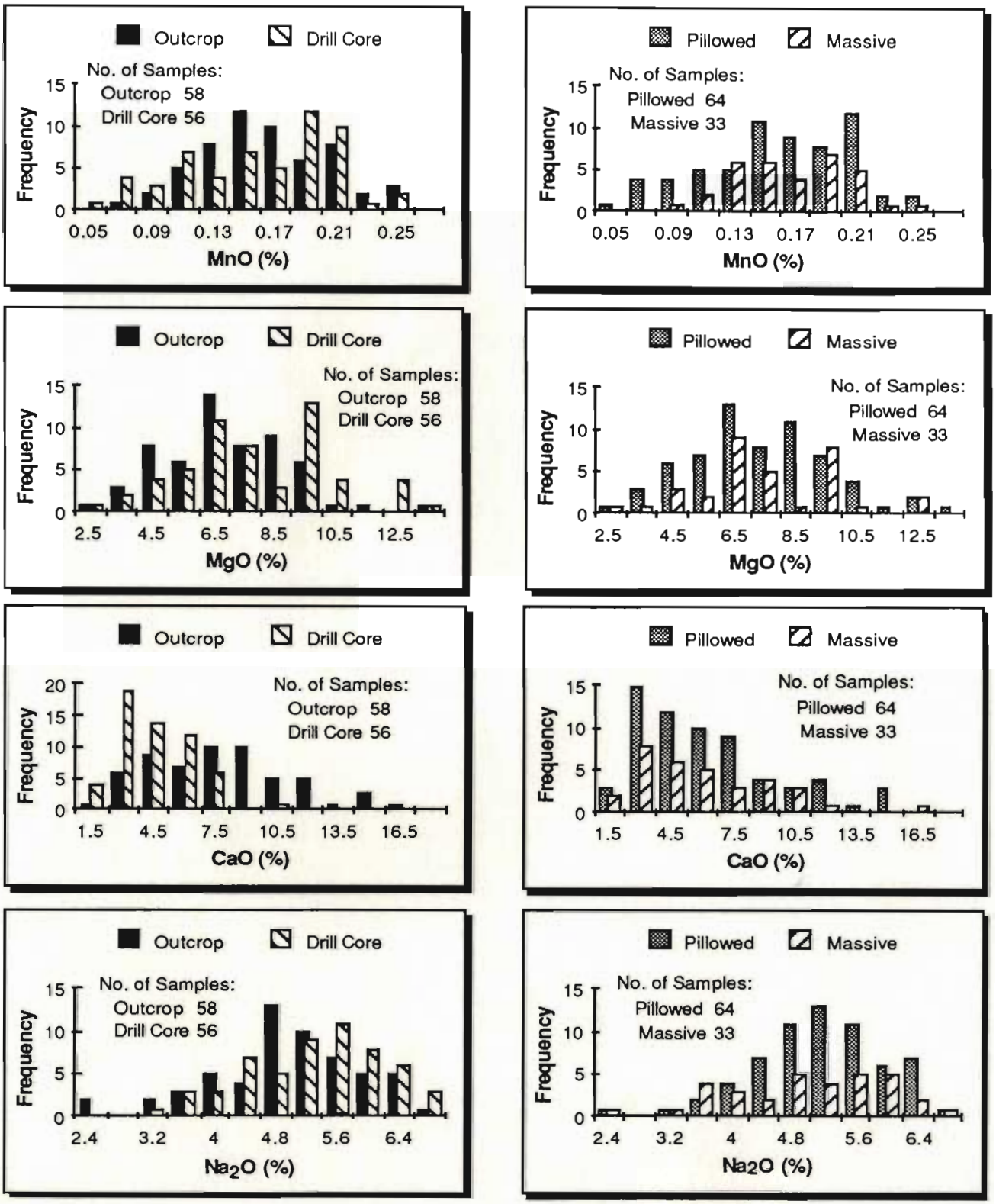

Figure B-2: Histograms showing distribution of MnO, MgO, CaO, and Na_2O in the Skidder Basalt. Outcrop samples include pillowed basalt, massive flows and a few diabase dykes. Drill core samples are of relatively unaltered pillowed and massive flows from the vicinity of the Skidder Prospect. Pillowed and massive flows shown in histograms on the right include samples from both drill core and outcrop. Values along the x-axis represent the maximum for the interval in which the value is shown.

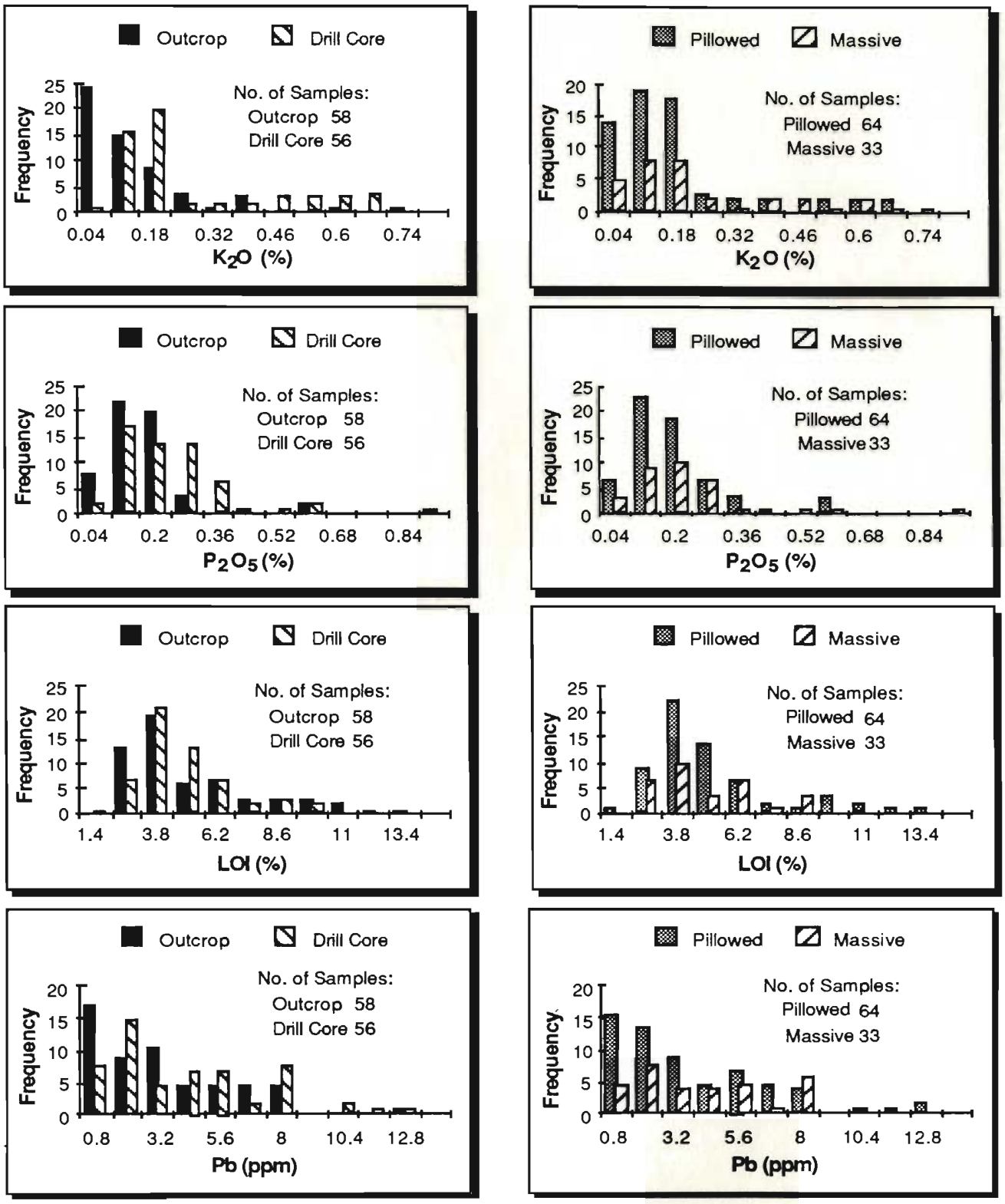

Figure B-3: Histograms showing distribution of K_2O, P_2O_5, LOI, and Pb in the Skidder Basalt. Outcrop samples include pillowed basalt, massive flows and a few diabase dykes. Drill core samples are of relatively unaltered pillowed and massive flows from the vicinity of the Skidder Prospect. Pillowed and massive flows shown in histograms on the right include samples from both drill core and outcrop. Values along the x-axis represent the maximum for the interval in which the value is shown.

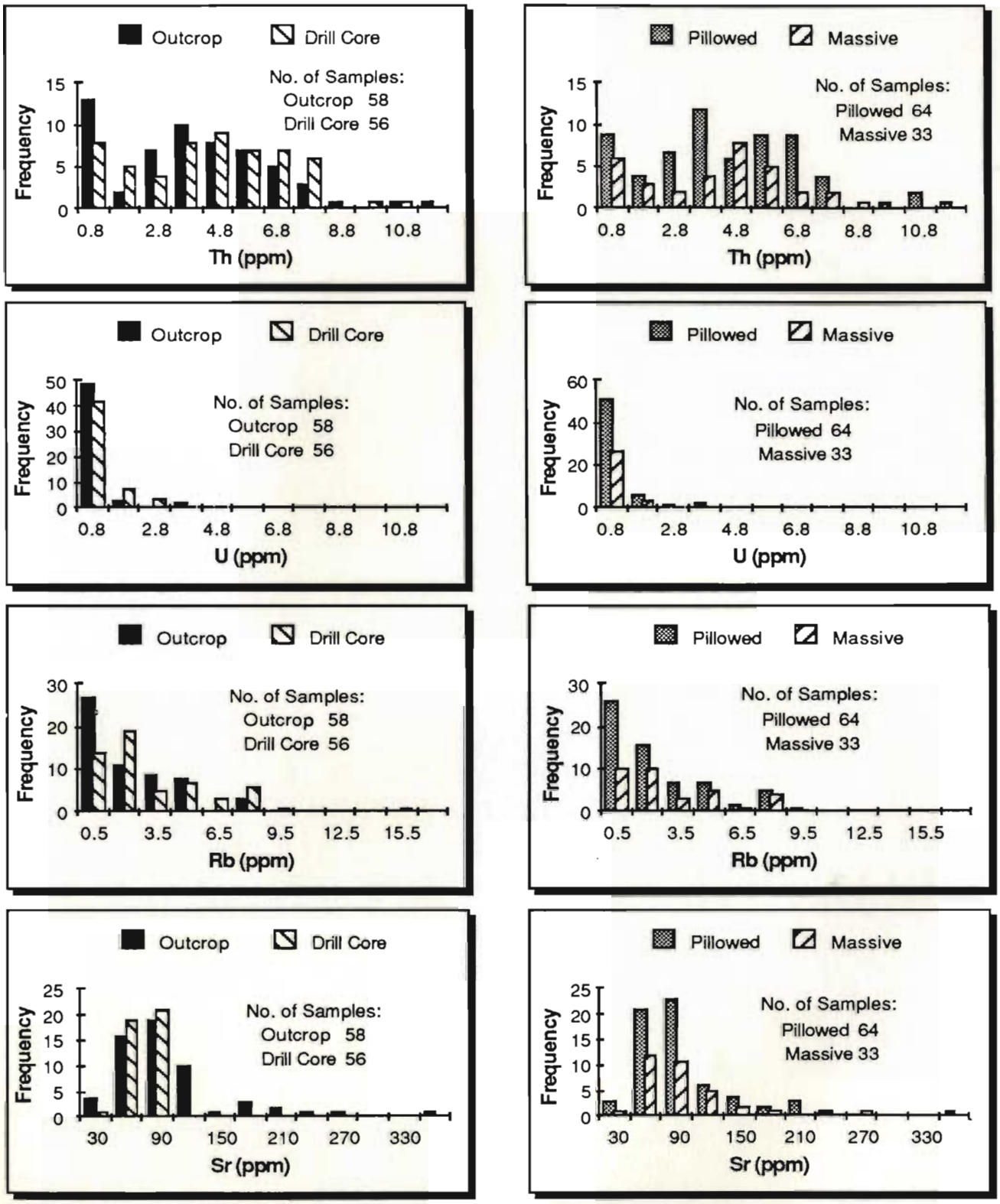

Figure B-4: Histograms showing distribution of Th, U, Rb, and Sr in the Skidder Basalt. Outcrop samples include pillowed basalt, massive flows and a few diabase dykes. Drill core samples are of relatively unaltered pillowed and massive flows from the vicinity of the Skidder Prospect. Pillowed and massive flows shown in histograms on the right include samples from both drill core and outcrop. Values along the x-axis represent the maximum for the interval in which the value is shown.

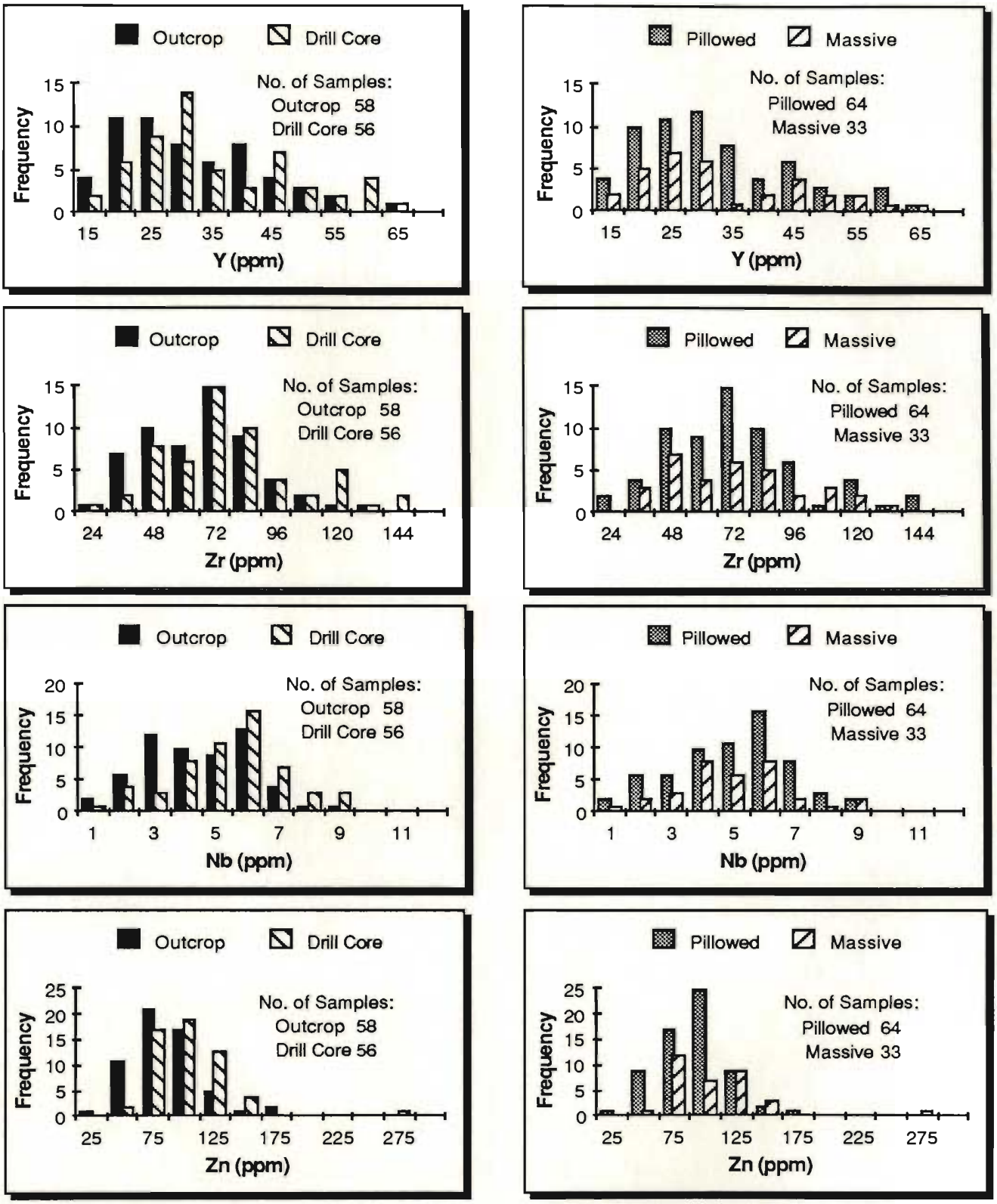

Figure B-5: Histograms showing distribution of Y, Zr, Nb, and Zn in the Skidder Basalt. Outcrop samples include pillowed basalt, massive flows and a few diabase dykes. Drill core samples are of relatively unaltered pillowed and massive flows from the vicinity of the Skidder Prospect. Pillowed and massive flows shown in histograms on the right include samples from both drill core and outcrop. Values along the x-axis represent the maximum for the interval in which the value is shown.

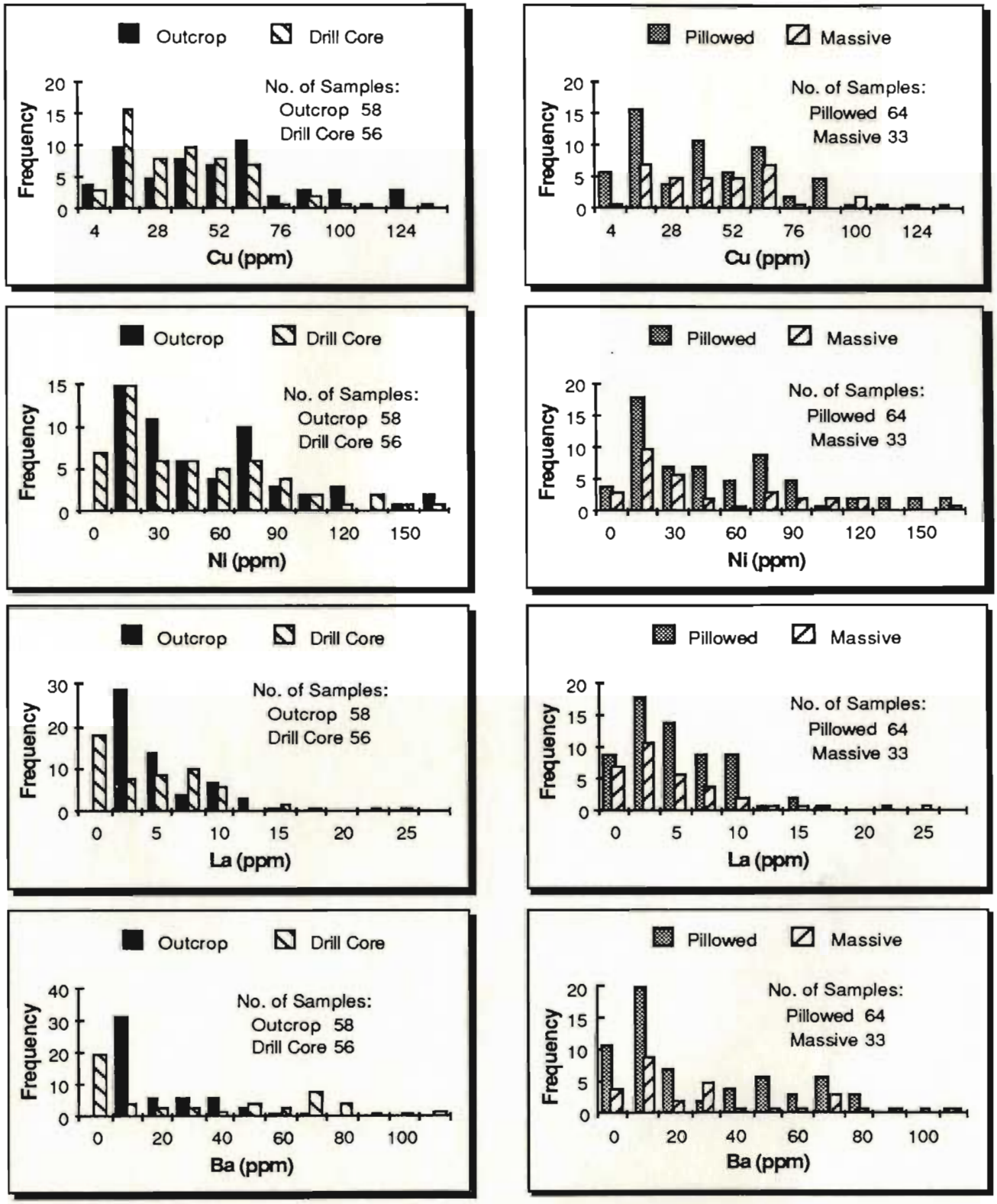

Figure B-6: Histograms showing distribution of Cu, Ni, La, and Ba in the Skidder Basalt. Outcrop samples include pillowed basalt, massive flows and a few diabase dykes. Drill core samples are of relatively unaltered pillowed and massive flows from the vicinity of the Skidder Prospect. Pillowed and massive flows shown in histograms on the right include samples from both drill core and outcrop. Values along the x-axis represent the maximum for the interval in which the value is shown.

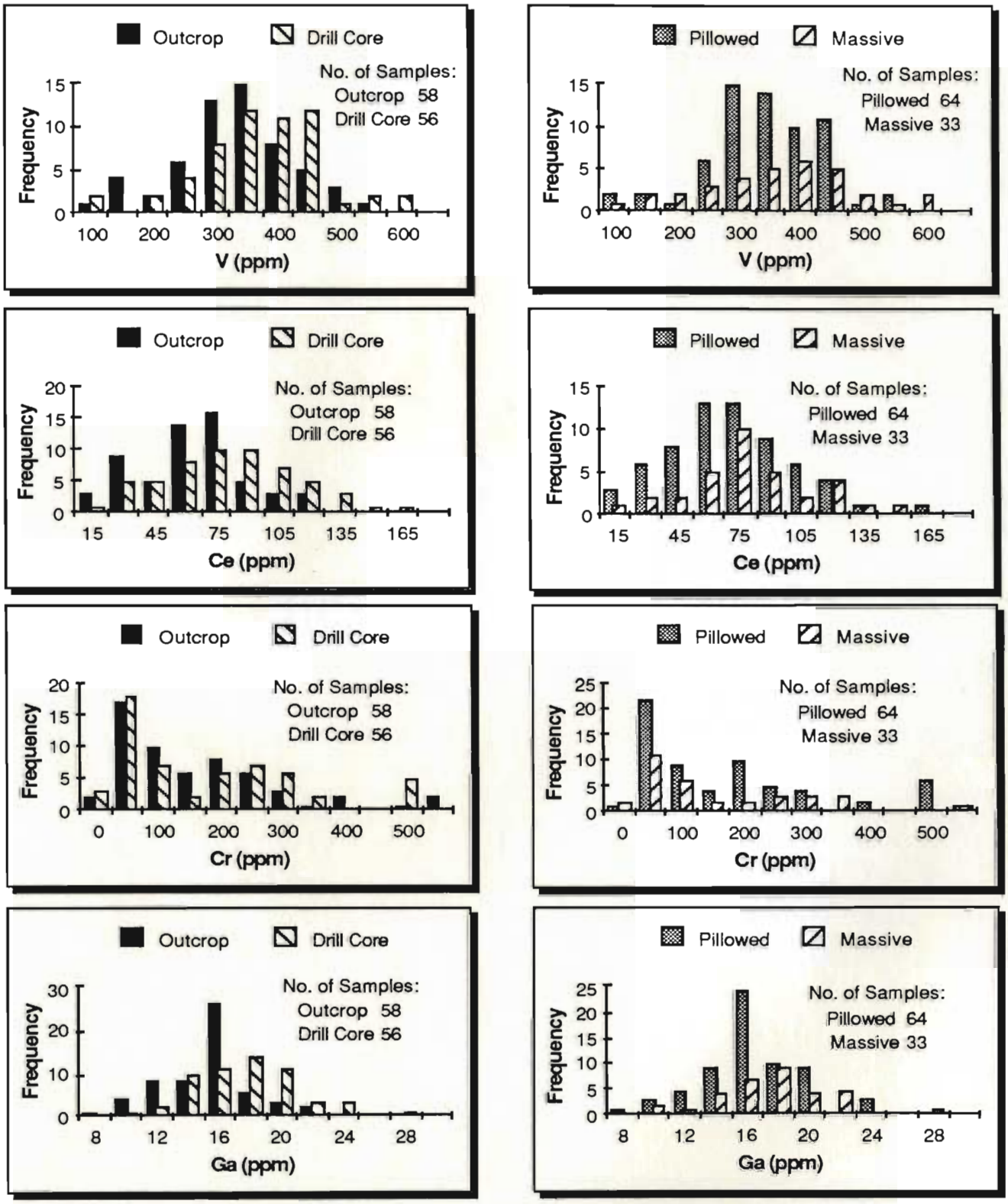

Figure B-7: Histograms showing distribution of V, Ce, Cr, and Ga in the Skidder Basalt. Outcrop samples include pillowed basalt, massive flows and a few diabase dykes. Drill core samples are of relatively unaltered pillowed and massive flows from the vicinity of the Skidder Prospect. Pillowed and massive flows shown in histograms on the right include samples from both drill core and outcrop. Values along the x-axis represent the maximum for the interval in which the value is shown.

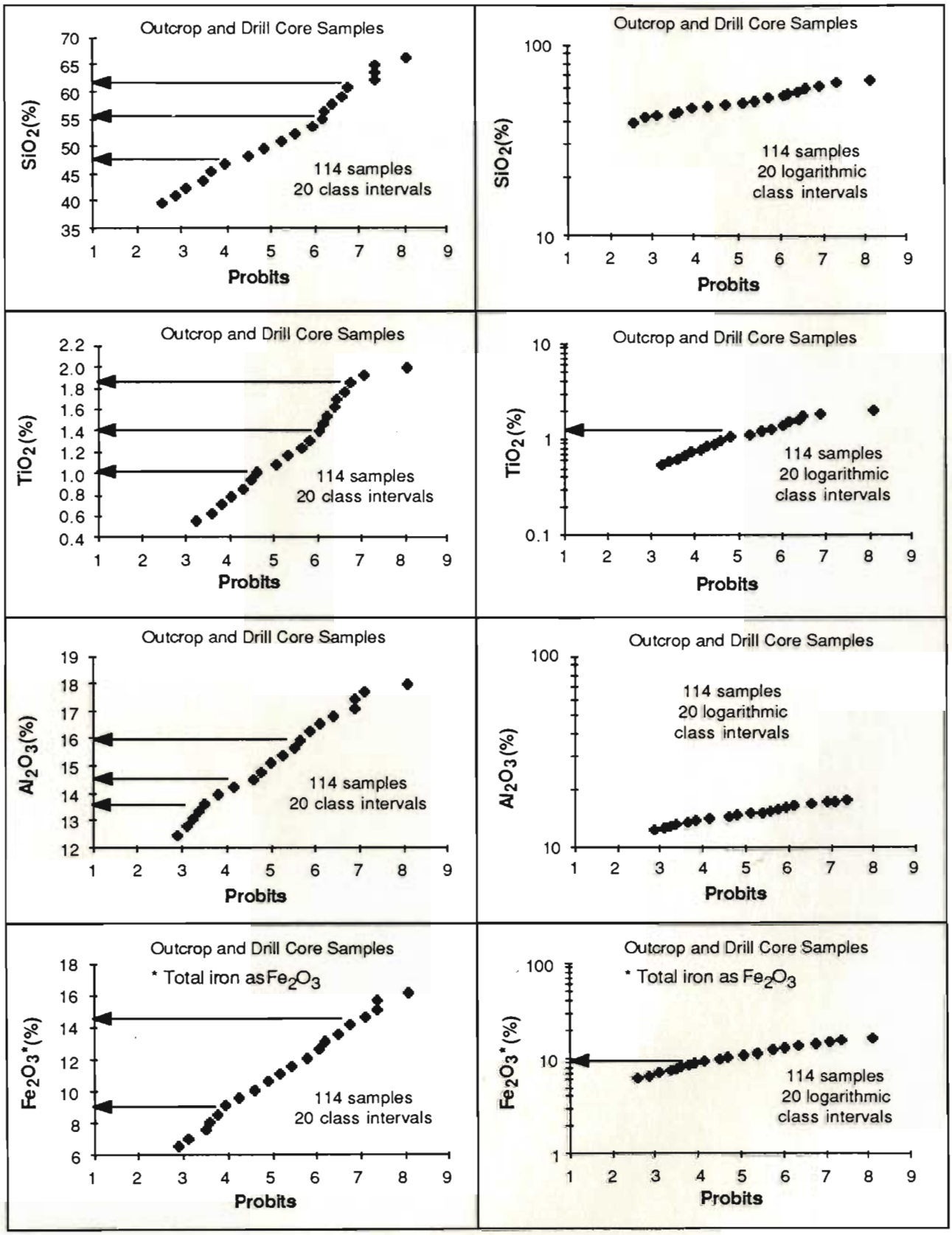

Figure B-8: Probability plots for SiO_2, TiO_2, Al_2O_3 and Fe_2O_3 in the Skidder Basalt. The X-axis, entitled probits, is equivalent to a cumulative frequency plot on probability paper; a normal distribution would give a straight line on plots to the left and a log normal distribution would give a straight line on the plots shown to the right.

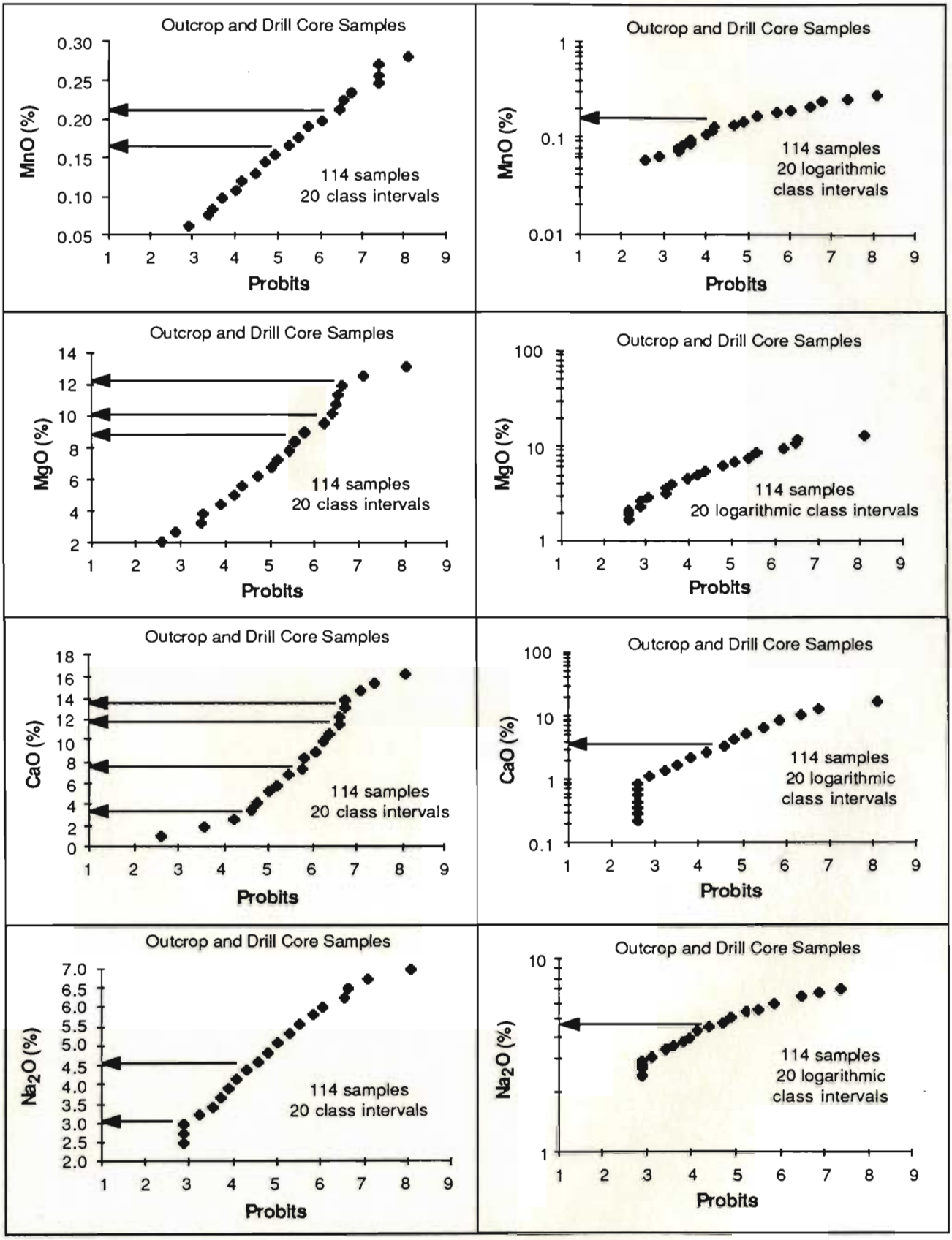

Figure B-9: Probability plots for MnO, MgO, CaO and Na_2O in the Skidder Basalt. The X-axis, labelled probits, is equivalent to a cumulative frequency plot on probability paper; a normal distribution would give a straight line on plots to the left and a log normal distribution would give a straight line on the plots shown to the right.

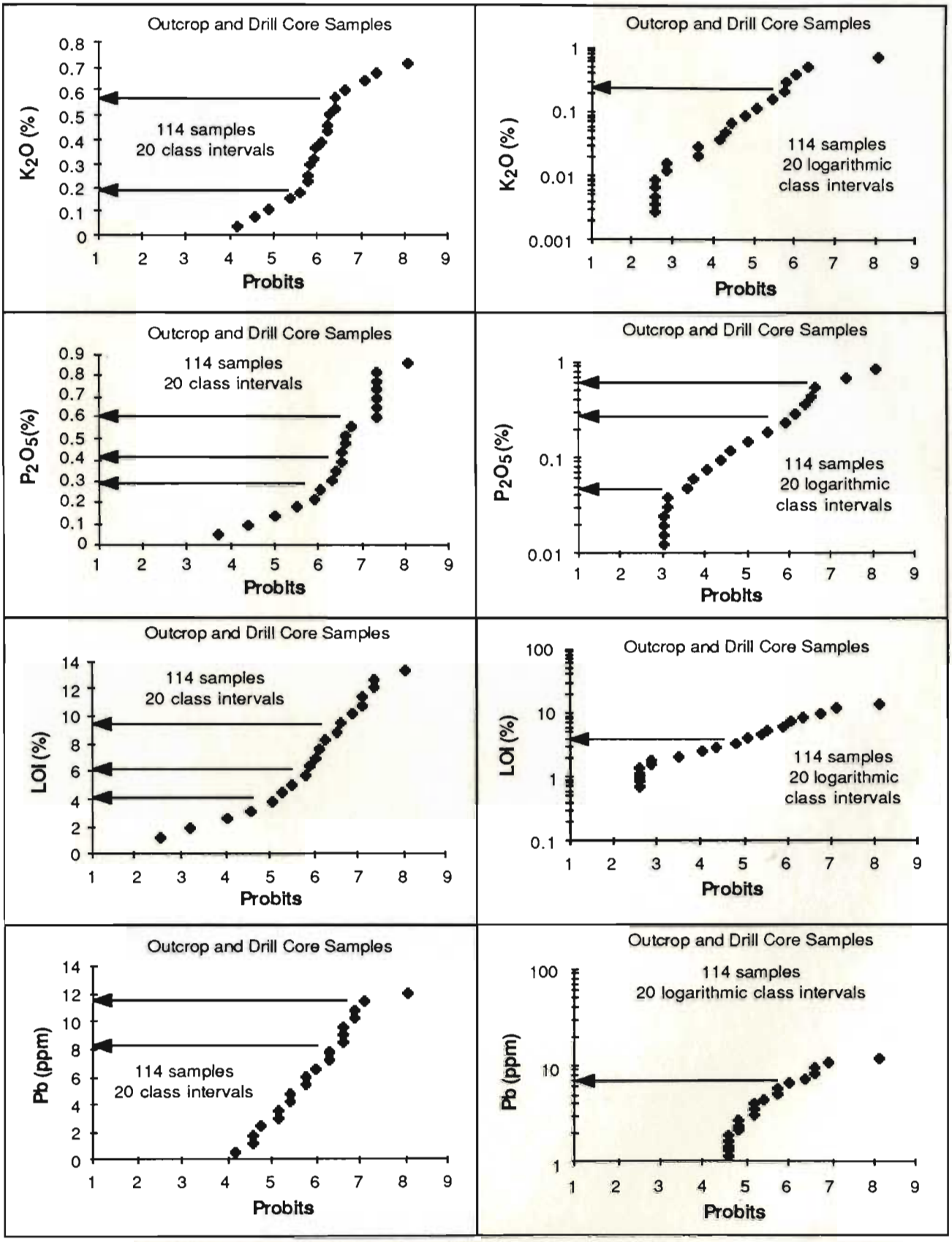

Figure B-10: Probability plots for K_2O, P_2O_5, LOI and Pb in the Skidder Basalt. The X-axis, labelled as probits, is equivalent to a cumulative frequency plot on probability paper; a normal distribution would give a straight line on plots to the left and a log normal distribution would give a straight line on the plots shown to the right.

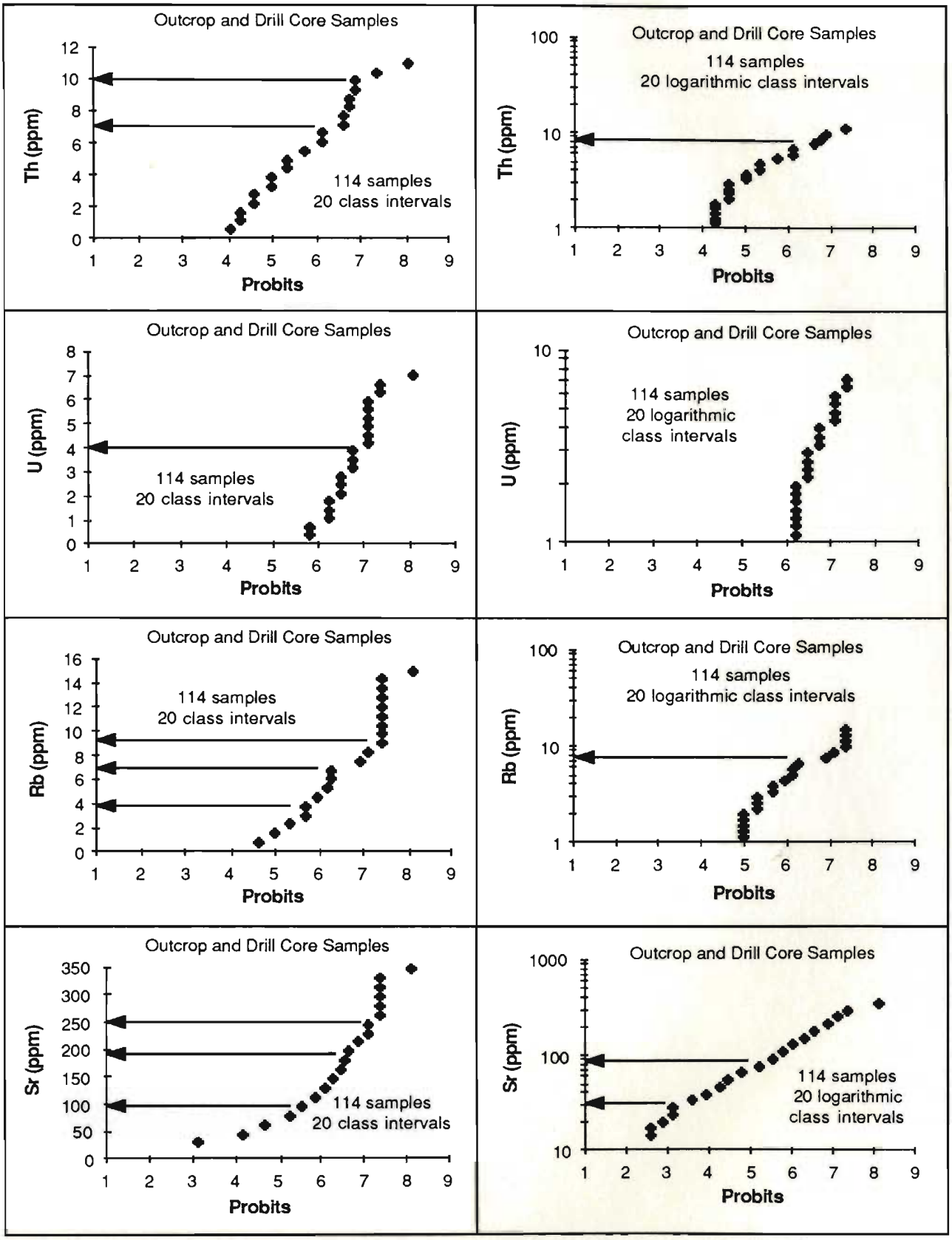

Figure B-11: Probability plots for Th, U, Rb and Sr in the Skidder Basalt. The X-axis, labelled as probits, is equivalent to a cumulative frequency plot on probability paper; a normal distribution would give a straight line on plots to the left and a log normal distribution would give a straight line on the plots shown to the right.

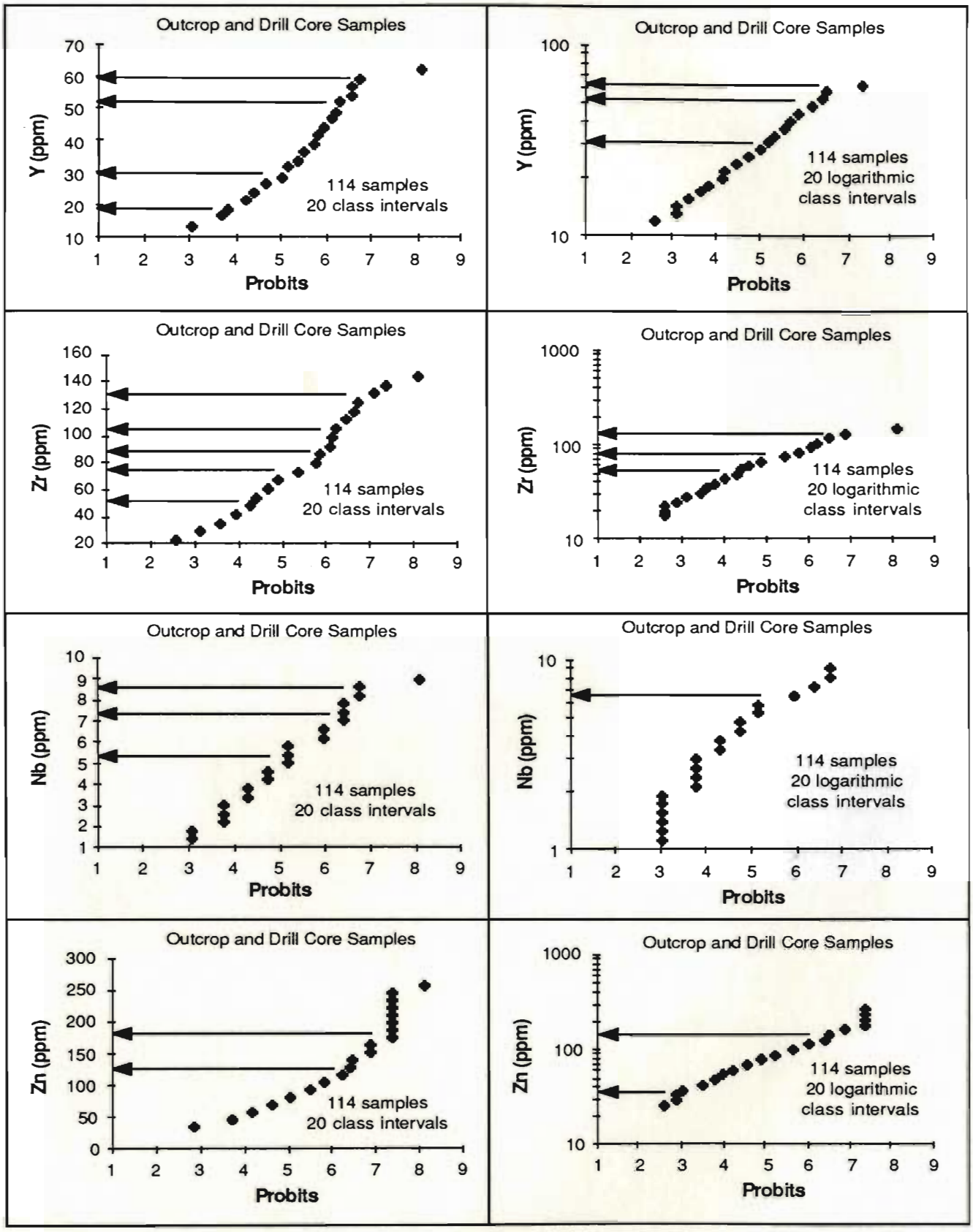

Figure B-12: Probability plots for Y, Zr, Nb and Zn in the Skidder Basalt. The X-axis, labelled probits, is equivalent to a cumulative frequency plot on probability paper; a normal distribution would give a straight line on plots to the left and a log normal distribution would give a straight line on the plots shown to the right.

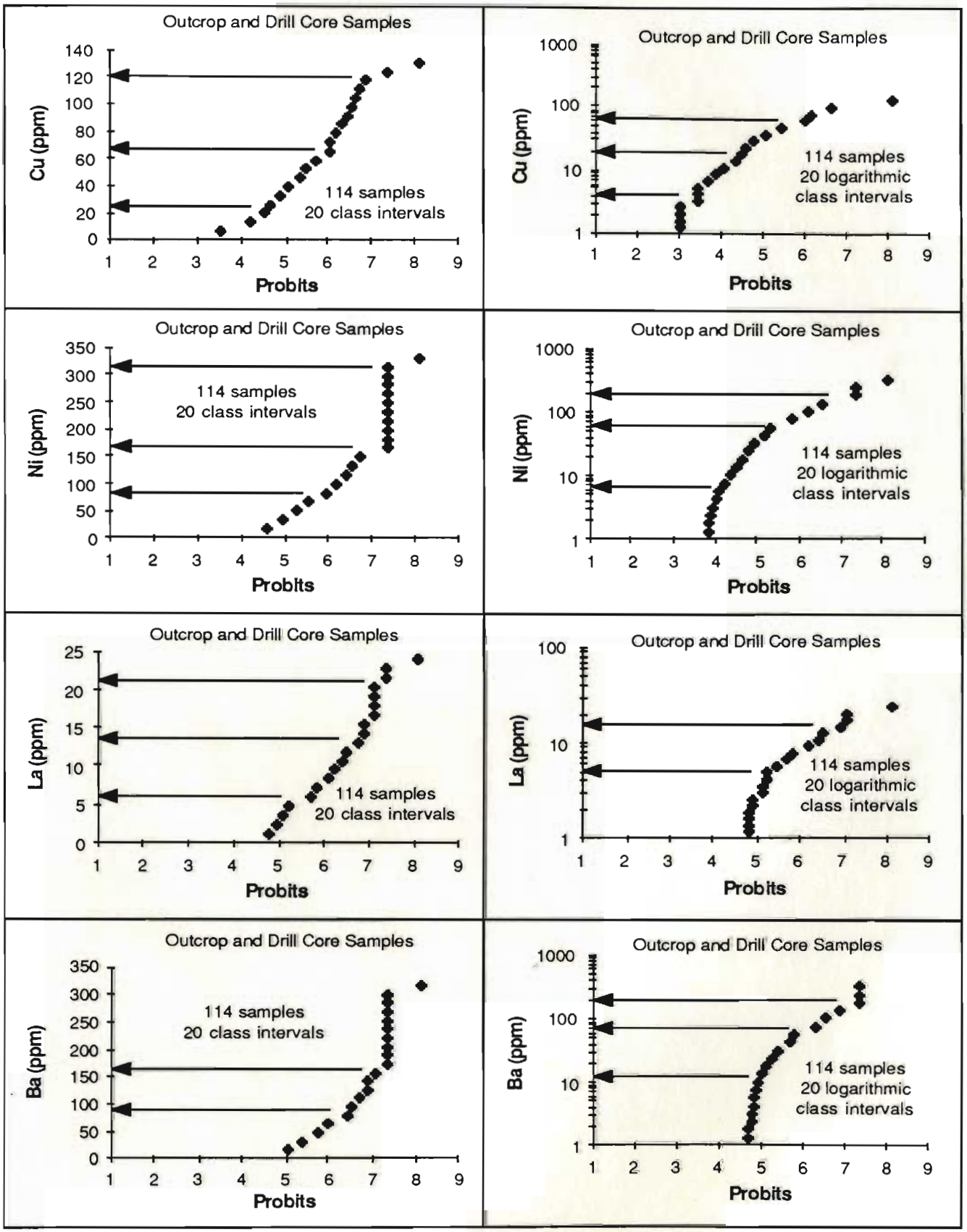

Figure B-13: Probability plots for Cu, Ni, La and Ba in the Skidder Basalt. The X-axis, labelled probits, is equivalent to a cumulative frequency plot on probability paper; a normal distribution would give a straight line on plots to the left and a log normal distribution would give a straight line on the plots shown to the right.

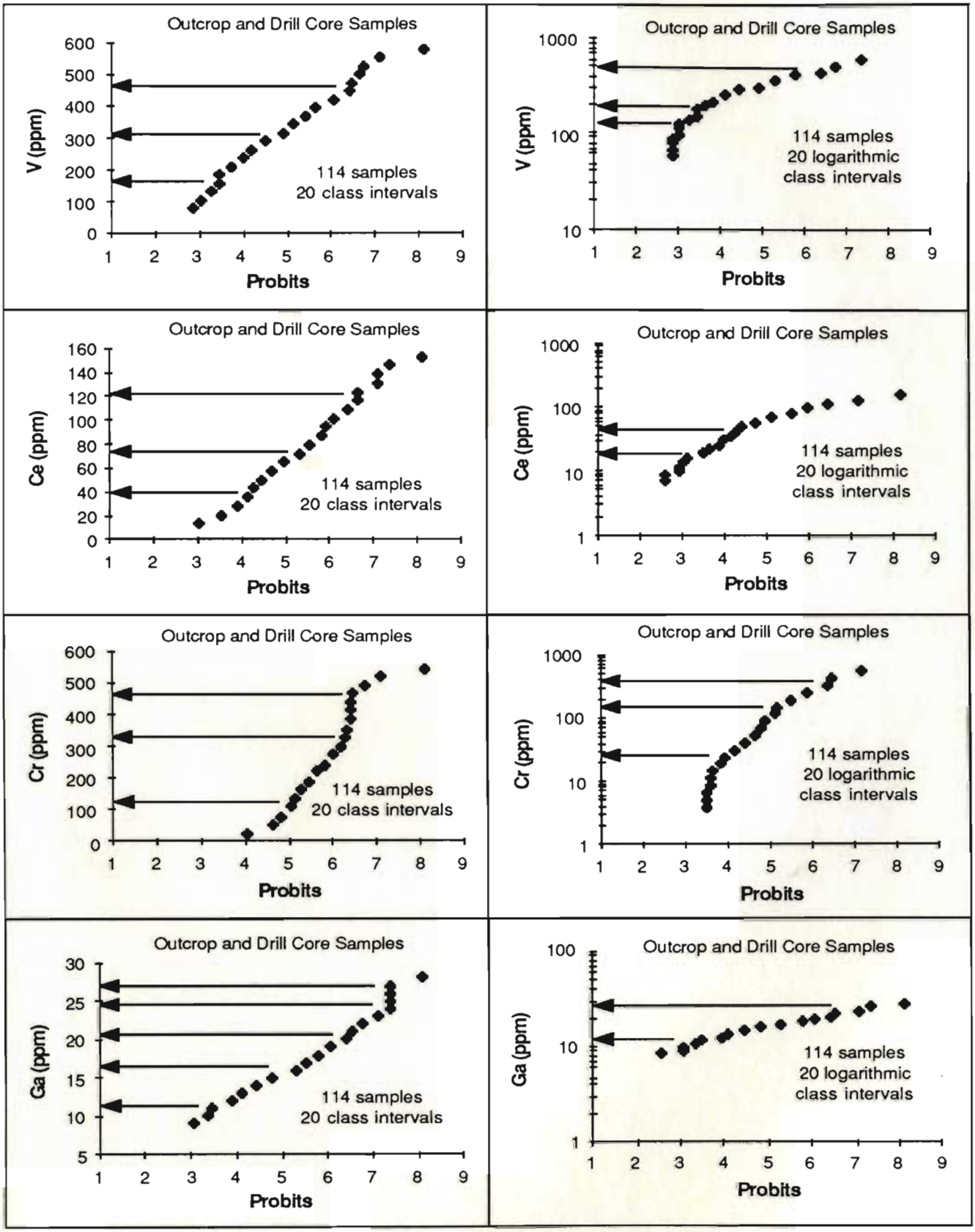

Figure B-14: Probability plots for V, Ce, Cr and Ga in the Skidder Basalt. The X-axis, labelled probits, is equivalent to a cumulative frequency plot on probability paper; a normal distribution would give a straight line on plots to the left and a log normal distribution would give a straight line on the plots shown to the right.

B.3 Major and Trace Element Analyses

Analyses of mafic Skidder Basalt outcrop samples and mafic Skidder Prospect drill core samples relatively unaffected by the mineralizing event(s) are presented in Tables B-3 to B-9. Analyses of miscellaneous altered Skidder Basalt flows and a mafic tuff; an altered Skidder trondhjemite; and Buchans Group samples are presented in Table B-10. Analyses of Skidder Prospect drill core samples from the various alteration zones are presented in Tables B-11 to B-15, and analyses of Skidder Prospect semimassive and massive sulphides are presented in Table B-16.

Table B-3: Analyses of pillowed Skidder Basalt outcrop samples having Zr concentrations ≤ 50 ppm

weight %	S 5B	S 7A	S 9A	S 11	S 31	S 32B	S 33	S 35A	S 39	S 45	S 47	S 51	S 59	S 78
SiO_2	42.40	47.80	48.90	48.00	48.60	60.90	43.30	48.50	50.60	45.90	47.80	51.40	47.90	50.60
TiO_2	0.72	0.74	0.82	1.11	0.67	0.90	0.62	0.62	0.79	0.57	0.79	0.56	0.49	0.87
Al_2O_3	14.00	15.80	13.80	16.90	15.00	12.20	12.60	14.50	16.60	16.30	14.40	14.80	15.10	14.60
Fe_2O_3*	6.84	9.02	7.88	10.03	6.07	10.02	7.45	8.86	10.75	9.65	11.34	11.33	10.12	9.35
MnO	0.14	0.28	0.09	0.13	0.08	0.06	0.18	0.16	0.15	0.17	0.17	0.19	0.16	0.18
MgO	4.24	6.18	3.14	5.00	4.50	3.98	6.08	8.94	7.43	6.45	7.72	7.88	11.13	9.12
CaO	12.31	11.19	9.60	6.07	14.17	3.15	13.98	7.07	4.66	10.95	10.58	6.79	8.03	5.91
Na_2O	5.87	3.59	6.17	6.13	4.36	4.69	4.63	4.89	5.14	3.93	3.80	4.30	3.68	4.63
K_2O	0.20	0.12	0.19	0.08	0.02	0.05	0.08	0.03	0.18	0.03	0.02	0.08	0.09	0.07
P_2O_5	0.08	0.08	0.18	0.18	0.01	0.56	0.04	0.03	0.12	0.16	0.04	0.06	0.01	0.07
LOI	11.80	3.56	8.63	5.47	5.23	2.92	10.37	5.56	3.25	5.32	3.31	2.33	3.75	4.14
Total	98.60	98.36	99.40	99.10	98.71	99.43	99.33	99.16	99.67	99.43	99.97	99.72	100.46	99.54
ppm														
Pb	6	n.d.	3	n.d.	n.d.	3	3	n.d.	n.d.	4	n.d.	12	n.d.	3
Th	3	2	5	1	2	5	5	n.d.	5	5	4	2	n.d.	6
U	n.d.	4	n.d.	2	n.d.	n.d.	n.d.	n.d.	n.d.	n.d.	n.d.	n.d.	n.d.	3
Rb	7	4	3	5	n.d.	n.d.	2	n.d.	n.d.	3	n.d.	3	n.d.	2
Sr	63	347	71	197	41	70	67	52	154	78	20	224	67	35
Y	15	20	25	23	11	43	15	19	22	16	28	17	17	16
Zr	33	38	50	47	34	46	41	38	50	39	44	36	16	46
Nb	2	1	2	2	3	5	4	1	5	6	3	4	4	4
Zn	45	166	39	102	23	54	48	87	77	69	71	41	68	71
Cu	3	n.d.	3	48	49	11	54	131	81	74	87	12	84	56
Ni	63	59	115	19	64	n.d.	119	151	88	43	44	35	148	69
La	8	1	10	8	n.d.	13	n.d.	n.d.	n.d.	3	n.d.	6	3	n.d.
Ba	36	45	32	159	6	23	n.d.	n.d.	9	3	n.d.	35	n.d.	13
V	229	245	251	398	304	286	223	302	379	277	298	278	1[illegible]	284
Ce	13	6	16	14	28	84	41	46	58	46	64	38	35	50
Cr	156	121	489	25	366	22	253	549	226	100	93	112	371	153
Ga	8	10	9	11	17	14	9	14	15	16	16	15	13	15

* Total iron as Fe_2O_3
n.d. - not detected

Table B-3 (continued): Outcrop samples of massive basalt flows and diabase dykes having Zr concentrations ≤ 50 ppm

	Massive				Diabase	
weight %	S 30	S 66B	S 76	S 81	S 27A	S 37
SiO_2	49.40	53.60	42.30	50.00	52.30	46.90
TiO_2	0.61	0.93	0.69	0.87	0.77	0.68
Al_2O_3	13.50	14.60	14.40	14.80	16.00	15.10
Fe_2O_3*	7.60	11.95	12.04	10.78	11.14	11.42
MnO	0.13	0.14	0.21	0.20	0.15	0.24
MgO	5.70	4.37	10.37	8.87	6.00	9.13
CaO	10.80	8.68	7.60	7.21	3.79	7.61
Na_2O	5.20	3.42	3.68	3.99	6.29	4.06
K_2O	0.02	0.03	0.03	0.71	0.03	0.03
P_2O_5	0.04	0.08	0.04	0.13	0.07	0.05
LOI	6.11	2.86	8.12	3.20	2.47	3.31
Total	99.11	100.66	99.48	100.76	99.01	98.53
ppm						
Pb	n.d.	n.d.	3	7	1	8
Th	6	4	n.d.	8	3	7
U	n.d.	n.d.	n.d.	n.d.	n.d.	n.d.
Rb	2	n.d.	n.d.	7	n.d.	n.d.
Sr	75	44	44	107	64	80
Y	16	19	16	15	20	28
Zr	30	41	30	44	32	30
Nb	4	4	2	5	3	3
Zn	43	82	92	81	65	167
Cu	90	45	15	91	33	114
Ni	156	5	331	65	18	56
La	4	2	n.d.	5	2	n.d.
Ba	n.d.	n.d.	2	157	2	n.d.
V	208	468	293	351	348	317
Ce	53	70	46	51	63	59
Cr	349	46	549	219	60	107
Ga	12	17	15	15	13	15

* Total iron as Fe_2O_3

n.d. - not detected

Table B-4: Drill core samples of pillowed flows, pillow breccia and massive flows having Zr concentrations ≤ 50 ppm

	Pillowed					Massive					
		1						2	2		
	SK	SK	SK	SK	SK	SK	SK	SK	SK	SK	SK
weight %	6 5	28 6	30 26	31 24	32 32	27 2	27 17	28 17	28 51	29 33	30 20
SiO_2	46.10	51.50	51.10	48.30	49.40	52.70	53.70	46.70	53.10	52.20	53.10
TiO_2	0.71	0.80	1.05	0.48	1.00	0.82	0.82	0.85	0.50	0.88	0.95
Al_2O_3	18.00	16.20	15.40	16.50	15.50	15.40	14.30	16.70	15.20	14.90	15.70
Fe_2O_3*	11.21	9.80	12.75	8.53	9.93	11.53	10.61	10.14	10.30	11.21	12.04
MnO	0.24	0.16	0.17	0.13	0.18	0.16	0.14	0.20	0.17	0.18	0.15
MgO	12.05	9.20	6.88	7.49	9.18	5.73	7.13	9.15	12.18	6.08	5.42
CaO	1.16	3.98	4.20	4.88	4.84	2.98	3.16	5.23	0.18	3.48	3.32
Na_2O	4.85	5.26	5.68	5.00	4.41	6.09	4.12	3.41	3.06	5.72	6.54
K_2O	0.07	0.06	0.16	0.50	0.56	0.53	0.30	0.63	0.04	0.36	0.58
P_2O_5	0.07	0.09	0.12	0.01	0.08	0.30	0.10	0.15	0.04	0.07	0.18
LOI	5.43	3.79	2.63	7.14	3.29	3.09	5.34	7.50	5.66	4.50	1.84
Total	99.89	100.84	100.14	98.96	98.37	99.33	99.72	100.66	100.43	99.58	99.82
ppm											
Pb	1	7	3	6	5	1	4	1	7	1	5
Th	4	4	3	5	4	5	1	n.d.	4	4	2
U	3	n.d.	n.d.	1	1	n.d.	n.d.	n.d.	n.d.	n.d.	n.d.
Rb	n.d.	1	2	6	7	4	5	7	n.d.	6	7
Sr	54	60	121	88	194	81	58	123	20	73	100
Y	13	16	27	17	19	20	23	19	12	23	25
Zr	24	41	40	27	46	44	43	48	26	47	48
Nb	2	3	2	2	3	3	4	5	1	2	6
Zn	121	72	74	56	63	97	105	63	258	101	93
Cu	10	13	32	98	56	44	55	60	60	37	30
Ni	46	70	17	60	75	n.d.	27	81	23	15	n.d.
La	n.d.	3	n.d.	2	6	5	n.d.	n.d.	n.d.	n.d.	24
Ba	n.d.	n.d.	42	78	102	92	42	65	40	1	116
V	346	299	403	299	314	366	379	345	428	426	368
Ce	70	46	41	30	59	80	55	67	33	9	66
Cr	116	256	55	153	197	35	96	261	72	15	36
Ga	16	14	17	16	16	18	16	14	16	13	17
Depth (f)	94	99	402	428	744	31	308	335	558	510	244
Depth (m)	28.7	30.0	122.4	130.5	226.6	9.3	93.7	102.1	170.1	155.4	74.2

1 - pillow breccia
2 - diabase dyke (?)
* Total iron as Fe_2O_3
n.d. - not detected
Depth represents footage in drill hole at which sample was taken
f - feet
m - metres

Table B-5: Outcrop samples of pillowed flows having Zr concentrations > 50 and ≤ 85 ppm

		1	1			1									
weight %	S 12	S 14A	S 14B	S 15A	S 23	S 27B	S 28	S 38	S 42	S 43	S 44	S 46	S 50	S 52	S 53
SiO_2	43.50	54.00	55.20	53.80	46.90	52.80	51.80	43.30	49.60	38.40	47.80	47.60	52.70	52.20	50.90
TiO_2	1.13	1.02	1.06	1.04	1.62	1.65	1.05	0.98	1.20	0.97	1.17	0.48	1.16	1.03	1.09
Al_2O_3	15.40	15.20	14.70	16.50	13.60	12.90	14.30	14.90	15.80	13.30	15.70	14.30	13.60	14.80	14.00
Fe_2O_3*	9.03	9.85	10.57	10.02	13.33	10.82	10.62	8.69	11.95	8.28	11.67	10.87	11.87	12.00	9.51
MnO	0.14	0.10	0.12	0.10	0.19	0.19	0.19	0.15	0.16	0.16	0.16	0.16	0.16	0.19	0.16
MgO	4.86	4.61	6.17	6.21	8.02	6.56	7.05	4.52	8.04	5.14	8.09	5.93	7.77	5.21	7.64
CaO	9.74	4.47	3.21	2.74	8.50	7.34	7.04	10.71	4.57	14.88	5.85	6.86	6.93	6.29	8.46
Na_2O	5.36	6.95	5.80	6.49	4.22	5.10	4.97	5.59	4.85	4.52	4.79	4.66	4.44	5.56	4.92
K_2O	0.27	0.17	0.15	0.20	0.03	0.02	0.03	0.11	0.05	0.17	0.04	0.02	0.02	0.03	0.03
P_2O_5	0.19	0.17	0.21	0.13	0.12	0.11	0.05	0.10	0.20	0.12	0.22	0.16	0.13	0.07	0.10
LOI	9.59	3.00	2.81	2.88	3.17	1.48	2.16	9.90	3.51	13.34	4.27	8.15	1.83	2.12	3.35
Total	99.21	99.54	100.00	100.11	99.70	98.97	99.26	98.95	99.93	99.28	99.76	99.19	100.61	99.50	100.16
ppm															
Pb	6	3	2	3	3	n.d.	n.d.	4	7	4	5	5	1	2	3
Th	6	2	6	0	n.d.	n.d.	2	2	n.d.	10	11	6	3	3	3
U	n.d.	0	0	0	n.d.	n.d.	n.d.	n.d.	n.d.	n.d.	3	n.d.	n.d.	n.d.	n.d.
Rb	7	4	3	4	n.d.	n.d.	1	3	n.d.	n.d.	2	n.d.	n.d.	n.d.	n.d.
Sr	97	72	102	96	66	32	98	76	46	69	158	32	89	57	67
Y	29	37	50	37	39	37	26	24	31	20	28	23	28	33	23
Zr	71	68	71	60	82	74	61	61	58	64	72	60	73	80	66
Nb	5	3	5	3	6	2	7	7	3	6	6	5	8	6	7
Zn	85	65	89	98	89	43	47	74	84	51	80	63	36	94	55
Cu	32	43	17	43	14	99	13	121	105	61	59	33	36	32	39
Ni	75	10	16	11	27	22	25	81	32	62	91	11	72	13	53
La	5	10	11	8	2	n.d.	4	1	n.d.	4	n.d.	4	10	n.d.	n.d.
Ba	29	32	31	30	n.d.	n.d.	34	n.d.	19	n.d.	45	n.d.	11	13	8
V	339	374	330	471	399	313	320	268	437	253	332	375	274	371	280
Ce	25	17	21	22	96	92	53	71	54	66	58	74	69	63	56
Cr	177	n.d.	41	n.d.	50	24	40	182	87	172	227	32	278	42	182
Ga	12	14	16	12	16	12	15	16	13	15	16	16	12	17	12

1 - pillow breccia

* Total iron as Fe_2O_3

n.d. - not detected

Table B-5 (continued): Outcrop samples of pillowed flows, massive flows and diabase having Zr concentrations > 50 and ≤ 85 ppm

	1	Pillowed				Massive							Diabase		
weight %	S 56	S 60	S 64	S 70	S 79	S 19	S 34B	S 41	S 57	S 61	S 65	S 75	S 22	S 25	S 49
SiO_2	44.40	51.80	43.80	50.90	49.40	48.10	49.60	49.80	49.80	49.10	46.70	39.80	48.50	49.80	58.80
TiO_2	1.07	1.27	1.11	1.53	1.15	1.13	0.84	1.23	0.90	1.60	1.22	1.02	0.96	1.45	0.76
Al_2O_3	16.20	14.80	15.80	15.20	15.30	14.50	14.50	14.00	13.90	13.80	16.10	15.00	15.10	14.00	14.90
Fe_2O_3*	13.77	13.68	9.32	14.35	13.49	9.23	9.65	11.95	9.18	16.16	10.59	9.77	11.19	11.68	8.2[illegible]
MnO	0.23	0.13	0.13	0.21	0.19	0.16	0.15	0.13	0.16	0.24	0.14	0.18	0.17	0.14	0.11
MgO	13.05	6.66	9.03	6.48	5.90	7.08	5.77	7.55	7.36	6.39	8.76	6.43	7.15	7.35	4.06
CaO	1.92	4.02	8.76	2.28	4.04	9.43	8.60	6.16	9.81	5.92	8.22	16.20	5.74	8.27	5.73
Na_2O	3.17	5.51	3.01	5.59	5.35	5.02	4.41	5.00	4.52	4.66	3.26	2.26	4.64	4.58	5.00
K_2O	0.00	0.09	0.38	0.09	0.06	0.12	0.14	0.11	0.06	0.24	0.13	0.57		0.02	0.02
P_2O_5	0.13	0.12	0.16	0.16	0.04	0.16	0.13	0.19	0.07	0.23	0.11	0.13	0.09	0.08	0.09
LOI	6.88	2.28	8.83	3.17	2.83	5.59	5.70	4.73	3.53	2.16	4.55	8.45	6.64	2.08	2.00
Total	100.82	100.36	100.33	99.96	97.75	100.52	99.49	100.85	99.29	100.50	99.78	99.81	100.56	99.45	99.76
ppm															
Pb	4	n.d.	2	8	4	1	5	7	1	3	n.d.	6	6	3	n.d.
Th	3	5	2	5	4	3	4	1	4	4	n.d.	3	4	n.d.	n.d.
U	1	1	n.d.	n.d.	n.d.	6	n.d.	1	n.d.	n.d.	n.d.	n.d.	n.d.	n.d.	n.d.
Rb	n.d.	1	2	n.d.	n.d.	3	2	5	[illegible]	3	3	4	[illegible]	1	n.d.
Sr	12	66	205	73	56	105	98	64	57	71	248	107	138	111	151
Y	22	41	24	36	35	27	21	39	23	41	32	25	29	36	36
Zr	74	82	59	69	78	62	52	68	58	80	70	62	68	73	64
Nb	6	6	6	3	6	3	4	4	3	6	4	5	3	5	2
Zn	72	90	59	123	106	66	60	75	55	134	65	74	95	[illegible]	40
Cu	7	32	73	45	20	51	56	14	54	26	62	57	59	118	19
Ni	94	12	71	6	5	67	37	20	28	16	87	114	75	42	26
La	1	3	11	6	n.d.	12	n.d.	3	n.d.	2	6	3	5	n.d.	n.d.
Ba	n.d.	10	n.d.	41	n.d.	17	2	28	15	27	30	316	[illegible]	1	n.d.
V	361	413	315	536	415	249	327	341	255	428	322	254	337	303	193
Ce	71	72	81	73	86	17	61	72	39	82	74	19	27	59	54
Cr	296	56	213	45	37	144	93	63	61	49	237	212	1[illegible]	75	103
Ga	15	20	15	16	17	10	14	15	16	22	16	21	12	16	16

1 - pillow breccia

* Total iron as Fe_2O_3

n.d. - not detected

Table B-6: Drill core samples of pillowed flows having Zr concentrations > 50 and ≤ 85 ppm

	1 SK	1 SK	1 SK	1 SK	1 SK	SK	SK	1 SK	SK	SK	SK	SK
weight %	27 1	27 11	28 1	28 8	28 11	28 18	29 24	29 28	29 66	29 69	30 25	33 1
SiO_2	48.30	45.70	51.80	48.60	45.80	48.90	43.40	51.60	46.70	50.70	47.00	57.10
TiO_2	1.27	1.12	1.12	1.34	1.08	1.23	1.07	1.07	1.21	1.06	1.35	1.08
Al_2O_3	17.10	15.40	16.30	16.80	15.10	17.80	14.70	16.80	15.10	15.10	16.70	16.40
Fe_2O_3*	14.58	10.55	10.46	13.16	10.46	11.57	9.27	9.90	10.80	10.01	12.13	7.2[illegible]
MnO	0.10	0.16	0.07	0.10	0.17	0.09	0.16	0.17	0.14	0.13	0.19	0.20
MgO	4.95	8.90	3.13	3.89	9.06	5.56	6.25	4.22	13.03	8.03	9.25	[illegible]'8
CaO	5.40	5.94	6.02	6.16	6.19	3.05	9.56	3.10	2.56	5.48	4.98	3.08
Na_2O	5.21	3.65	6.65	5.97	4.23	6.02	5.10	6.13	3.43	5.27	4.27	6.14
K_2O	0.42	0.13	0.10	0.09	0.06	0.63	0.38	0.63	0.08	0.09	0.18	0.58
P_2O_5	0.13	0.23	0.27	0.21	0.13	0.17	0.21	0.33	0.18	0.11	0.15	0.36
LOI	2.77	8.63	3.30	3.79	8.03	4.36	9.20	4.28	6.40	3.00	3.95	3.36
Total	100.23	100.41	99.12	100.11	100.31	99.38	99.30	98.23	99.63	98.98	100.15	98.31
ppm												
Pb	n.d.	4	n.d.	4	8	1	2	10	8	2	2	11
Th	4	n.d.	2	n.d.	7	1	1	7	6	3	n.d.	6
U	n.d.	n.d.	4	2	n.d.	n.d.	1	2	1	n.d.	n.d.	n.d.
Rb	3	1	3	1	3	8	7	15	5	n.d.	1	9
Sr	134	151	[illegible]3	78	89	105	85	80	49	98	145	82
Y	27	28	32	33	25	24	29	41	29	28	29	41
Zr	75	69	70	70	71	71	69	72	60	60	[illegible]	[illegible]
Nb	6	6	5	6	7	5	5	6	4	7	6	7
Zr	62	67	52	57	81	74	89	75	89	81	102	52
Cu	8	42	34	27	43	[illegible]	40	18	58	46	45	84
Ni	49	70	41	59	73	44	77	33	122	38	86	43
La	7	n.d.	2	1	3	n.d.	6	n.d.	n.d.	5	7	5
Ba	n.d.	22	n.d.	n.d.	n.d.	74	65	31	n.d.	n.d.	1[illegible]	n.d.
[illegible]	237	370	284	415	316	370	313	347	354	279	367	309
Ce	129	4	18	79	104	82	24	23	21	55	101	153
Cr	243	[illegible]13	187	226	214	236	170	215	456	131	277	232
Ga	16	17	12	19	14	16	12	14	14	18	14	15
Depth												
feet	20	190	10	173	224	355	409	458	935	962	382	46
metres	5.9	57.9	3.0	52.7	68.3	108.2	124.7	139.6	285.0	293.2	[illegible]16.4	14.0

1 - pillow breccia

* Total iron as Fe_2O_3

n.d. - not detected

Depth represents footage in drill hole at which sample was taken

Table B-6 (continued): Drill core samples of pillowed flows having Zr concentrations > 50 and ≤ 85 ppm

	SK	SK	SK	SK	SK	SK	SK	SK	SK	SK	SK	SK
weight %	33 4	34 14	34 69	34 81	34 127	35 12	35 34	35 70	37 2	37 27	37A 32	38 8
SiO_2	53.70	52.30	47.10	53.00	49.20	51 60	49.40	54.60	53.30	49.80	49.60	47.50
TiO_2	1.31	1.20	1.17	1.09	1.48	1.08	1.07	1.08	1.18	0.93	1.02	1.09
Al_2O_3	15.50	14.20	15.00	14.30	14.40	15.40	15.80	15.20	14.40	15.60	17.10	14.70
Fe_2O_3*	12.21	11.27	11.24	7.55	13.85	12.42	12.00	7.01	12.63	13.23	9.81	9.52
MnO	0.11	0.20	0.23	0.10	0.07	0.18	0.14	0.05	0.19	0.15	0.15	0.18
MgO	5.97	6.86	10.07	11.77	9.12	6.35	7.01	10.11	5.65	7.35	9.28	10.08
CaO	1.78	4.46	6.36	1.78	2.68	4.32	3.26	1.34	5.66	4.18	1.68	6.84
Na_2O	4 73	5.63	4.13	3.82	4.65	5.76	6.20	4.43	5.43	5.08	5.27	4.27
K_2O	0.13	0 14	0.13	0.32	0.10	0.12	0.14	0.12	0.05	0.14	0.48	0.14
P_2O_5	0.26	0.09	0.18	0.13	0.21	0.11	0.16	0.29	0.12	0.08	0.12	0.09
LOI	3.34	2.16	4.21	5.43	3.78	2.86	4.49	4.37	1.96	2.92	4.52	4.91
Total	99.02	98.51	99.82	99.29	99.54	100.20	99.67	98.60	100.57	99.46	99.03	99.32
ppm												
Pb	4	n.d.	2	5	2	1	6	1	1	n.d.	3	3
Th	7	7	3	6	5	3	6	1	3	3	n.d.	7
U	n.d.	n.d.	n.d.	n.d.	n.d.	n.d	n.d.	n.d.	n.d.	n.d.	n.d.	n.d.
Rb	1	2	n d.	4	n.d.	1	4	n d.	2	2	4	3
Sr	39	50	145	66	53	61	52	53	1	65	61	11
Y	36	42	25	19	26	33	30	25		28	35	24
Zr	80	84	66	57	63	68	85	58	7	71	79	62
Nb	6	5	8	4	6	4	9	4	6	4	7	4
Zn	84	84	99	95	91	90	107	42	86	97	141	71
Cu	1	28	7	48	32	15	39	15	20	18	77	62
Ni	n.d.	26	139	29	7	4	13	82	3	7	20	151
	9	6	7		n.d.	0	5	21	n.d.	n.d.	n.d.	8
	6	42	62		75	66	15	41	n.d.	n.d.	70	17
V	293	348	308	3	507	396	435	325	393	419	409	285
Ce	94	82	43	12	38	31	77	82	77	51	68	54
Cr	14	88	473	476	37	27	35	497	26	31	55	496
Ga	19	18	18	14	20	16	18	18	16	20	24	15
Depth												
feet	124	134	911	1101	1581	156	918	1512	72	757	1442	879
metres	37.8	40.8	277.7	335.4	481.9	47.5	279.7	460.7	21.9	230.7	439.5	267.8

* Total iron as Fe_2O

n.d. - not detected

Depth represents footage in drill hole at which sample was taken

Table B-6 (continued): Drill Core samples of massive flows having Zr concentrations > 50 and ≤ 85 ppm

	2 SK	SK	2 SK	Sk	SK	SK	SK	SK
weight %	28 19	28 58	29 15	30 34	30 88	31 532	37A 15	37A M
SiO_2	47.60	47.90	50.40	47.10	50.90	46.10	50.10	49.80
TiO_2	1.35	1.16	1.27	1.05	1.07	0.64	1.31	1.75
Al_2O_3	17.60	16.70	15.20	15.50	15.00	14.70	16.40	16.30
Fe_2O_3*	10.96	11.89	10.65	10.76	9.77	10.99	12.80	12.15
MnO	0.09	0.18	0.17	0.18	0.10	0.17	0.13	0.11
MgO	8.77	12.25	8.71	9.13	8.92	8.99	6.52	6.54
CaO	2.51	1.03	6.64	5.04	3.96	5.82	2.16	3.24
Na_2O	5.49	3.23	4.54	4.28	5.18	3.76	5.72	5.66
K_2O	0.17	0.06	0.15	0.08	0.17	0.10	0.40	0.10
P_2O_5	0.23	0.22	0.16	0.09	0.12	0.11	0.11	0.22
LOI	4.85	5.61	2.84	5.79	3.76	8.39	3.49	2.97
Total	99.62	100.23	100.73	99.10	98.95	99.77	99.14	98.84
ppm								
Pb	1	7	n.d.	7	3	4	4	5
Th	1	5	5	3	6	?	n.d.	5
U	n.d.	2	n.d.	n.d.	n.d.	n.c	n.d.	n.d.
Rb	n.d.	2	n.d.	1	7	2	5	n.d.
Sr	67	45	64	163	72	127	62	82
Y	30	30	27	24	28	28	43	38
Zr	80	74	75	56	57	69	68	75
Nb	6	8	5	4	5	6	6	5
Zn	113	106	67	69	67	70	150	113
Cu	29	35	73	20	41	44	24	24
Ni	53	91	66	109	36	102	8	17
La	6	n.d.	n.d.	1	13	6	2	n.d.
Ba	64	22	n.d.	84	4	n.d.	79	n.d.
V	338	404	325	416	275	363	560	579
Ce	101	78	124	60	71	141	68	107
Cr	293	307	169	320	151	258	43	52
Ga	21	14	21	10	28	17	20	18
Depth								
feet	383	640	228	530	1086	532	1231	1676
metres	116.7	195.1	69.5	161.5	330.9	162.2	375.2	510.8

2 - diabase (?)
* Total iron as Fe_2O_3
n.d. - not detected
Depth represents footage in drill hole at which sample was taken

Table B-7: Outcrop and drill core samples having Zr concentrations > 85 ppm but not included in Group 2

	Outcrop		Drill Core		
	Pillowed	Massive	Pillowed		Massive
weight %	S 48	S 80B	SK 30 6	SK 31 552	SK 37 7
SiO_2	57.50	48.	44.20	53.80	52.10
TiO_2	1.25	1.76	1.58	1.24	1.79
Al_2O_3	12.30	14.10	17.10	14.20	14.40
Fe_2O_3*	12.46	11.24	12.00	12.40	13.57
MnO	0.10	0.13	0.22	0.15	0.20
MgO	7.65	4.48	10.00	4.91	5.85
CaO	1.11	9.55	4.52	2.48	4.66
Na_2O	2.25	4. 6	4.36	4.81	5.56
K_2O	0.01	0.03	0.65	0.07	0.15
P_2O_5	0.18	0.2	22	0.16	0.14
LOI	4.20	6.53	.19	4.91	1.92
Total	99.01	100.70	00.04	99.13	100.34
ppm					
Pb	n.d.	5	n.d.	12	5
Th	n.d.	3	d.	9	4
U	n.d.	n.d.	n.d.	n.d.	1
Rb	n.d.	n.d.	6	1	1
Sr	17	45	127	32	52
Y	25	47	37	45	50
Zr	88	92	90	111	106
Nb	6	9	8	5	6
Zn		85	98	91	112
Cu	60	28	56	8	32
Ni	4	6	71		8
La	7	n.d.	5		1
Ba	n.d.	n.d.	70	n.d.	n.d.
V	441	480	406	438	533
Ce	103	113	96	108	94
Cr	32	34	289	29	40
Ga	13	18	17	20	19
Depth					
feet			76	552	247
metres			23.2	168.2	75.3

* Total iron as Fe_2O_3
n.d. - not detected

Depth represents footage in drill hole at which sample was taken

Table B-8: Group 2 outcrop samples

	Pillowed				Massive	
weight %	S 21A	S 40	S 54	S 77	S 29	S 58
SiO_2	58.70	53.50	59.80	57.70	56.70	61.30
TiO_2	1.60	0.49	0.84	1.34	1.88	1.22
Al_2O_3	14.30	16.90	13.70	14.10	14.40	14.10
Fe_2O_3*	9.45	8.91	7.20	10.95	10.20	9.49
MnO	0.15	0.15	0.10	0.19	0.12	0.14
MgO	4.09	6.49	4.32	3.07	2.37	3.17
CaO	2.09	2.47	4.35	3.38	3.39	1.65
Na_2O	5.98	6.11	5.42	5.64	6.18	5.93
K_2O	0.13	0.11	0.02	0.03	0.05	0.34
P_2O_5	0.38	0.07	0.[illegible]	0.59	0.86	0.17
LOI	2.39	3.06	4	2.89	2.16	1.84
Total	99.26	98.26	100.[illegible]3	99.88	98.31	99.31
ppm						
Pb	6	2	n.d.	5	1	n.d.
Th	3	4	7	n.d.	7	n.d.
U	7	n.d.	n.d.	n.d.	n.d.	n.d.
Rb	4	1	n.d.	3	n.d.	n.d.
Sr	131	118	30	38	40	32
Y	53	34	47	53	61	44
Zr	95	108	130	88	110	103
Nb	5	6	6	3	7	4
Zn	117	79	52	80	61	107
Cu	n.d.	40	61	11	10	14
Ni	n.d.	49	27	n.d.	n.d.	n.d.
La	9	5	n.d.	n.d.	2	5
Ba	52	n.d.	n.d.	62	2	1
V	131	223	149	30	145	124
Ce	33	76	69	69	116	106
Cr	n.d.	172	83	n.d.	116	3
Ga	16	15	16	20	18	19

* Total iron as Fe_2O_3

n.d. - not detected

Table B-9: Group 2 samples from drill core

	Pillowed						Massive			
	SK	SK	SK	SK	SK	SK	SK	SK	SK	SK
weight %	32 11	33 26	34 35	35 24	35 25	35 93	34 46	34 55	35 3	37 41
SiO_2	58.20	53.40	50.50	66.30	46.80	49.40	54.90	53.60	61.10	54.50
TiO_2	1.18	1.38	1.27	1.39	2.00	1.95	1.86	1.41	0.75	1.18
Al_2O_3	14.40	16.90	15.60	12.60	16.10	16.00	15.00	15.20	13.70	14.50
Fe_2O_3*	10.59	9.66	13.15	6.52	14.80	12.73	11.05	11.62	10.53	12.43
MnO	0.11	0.09	0.20	0.07	0.20	0.07	0.19	0.20	0.13	0.16
MgO	4.10	5.42	5.99	1.55	7.58	8.21	5.39	5.75	3.81	5.62
CaO	1.84	2.16	2.90	2.68	2.64	2.46	2.28	2.02	1.56	2.40
Na_2O	5.13	6.24	5.37	6.78	5.18	4.99	5.38	5.97	5.37	5.55
K_2O	0.21	0.14	0.14	0.06	0.14	0.13	0.40	0.10	0.12	0.23
P_2O_5	0.57	0.29	0.20	0.21	0.27	0.36	0.28	0.46	0.58	0.21
LOI	2.45	2.75	4.34	0.62	3.88	3.72	2.93	2.84	2.40	2.25
Total	98.78	98.43	99.66	98.78	99.59	100.02	99.66	99.17	100.05	99.03
ppm										
Pb	n.d.	7	5	5	10	n.d.	3	1	4	8
Th	6	4	10	2	3	6	7	4	n.d.	5
U	n.d.	n.d.	2	n.d.	1	n.d.	1	1	n.d.	n.d.
Rb	1	n.d.	n.d.	n.d.	3	n.d.	2	2	n.d.	1
Sr	66	69	46	40	34	86	68	34	35	36
Y	47	62	58	45	60	60	52	59	45	54
Zr	92	116	120	117	134	144	103	125	89	111
Nb	7	5	5	6	7	9	7	9	6	6
Zn	99	86	119	29	148	110	124	142	100	106
Cu	6	13	3	11	13	14	7	9	3	6
Ni	n.d.	7	12	n.d.	n.d.	2	1	1	n.d.	8
La	16	14	1	4	6	8	1	9	7	8
Ba	57	n.d.	57	n.d.	n.d.	8	109	52	64	23
V	254	234	296	233	479	410	195	191	57	235
Ce	99	114	46	84	114	108	76	61	72	81
Cr	n.d.	39	57	4	15	21	7	n.d.	n.d.	25
Ga	19	19	19	13	23	23	18	22	18	20
Depth										
feet	365	437	428	533	593	1794	599	752	29	1067
metres	111.3	133.0	130.3	162.5	180.7	546.8	182.6	229.2	8.8	325.2

* Total iron as Fe_2O_3
n.d. - not detected
Depth represents footage in drill hole at which sample was taken

Table B-10: Miscellaneous Skidder Basalt, Skidder trondhjemite, and Buchans Group samples

	Skidder Basalt								Altered Skidder	Buchans Group		
	Silicified Basalts				K-rich Basalts			Mafic Tuff	Trondhjemite	Sandy Lake Formation Basalt		Lundberg Hill Formation Dacite
weight %	S 7B	S 13C	S 49	S 66A	S 16A	S 62	S 74	S 10B	S 72	S 82A	S 82B	S 63
SiO_2	69.80	68.20	58.80	57.90	55.50	48.00	48.20	53.20	74.50	44.40	47.90	65.5
TiO_2	0.38	0.92	0.76	0.98	1.04	0.97	0.78	0.89	0.24	0.58	0.58	0.42
Al_2O_3	10.90	10.60	14.90	14.40	13.70	14.30	16.60	15.70	10.60	12.50	13.70	14.6
Fe_2O_3*	4.39	3.72	8.29	10.45	12.18	10.12	8.79	11.61	6.56	7.98	7.93	4.58
MnO	0.15	0.04	0.11	0.08	0.16	0.17	0.19	0.18	0.03	0.32	0.26	0.06
MgO	2.31	1.16	4.06	6.74	6.07	10.58	5.91	5.55	1.73	6.79	5.48	1.6
CaO	3.10	5.11	5.73	1.41	1.68	5.39	9.02	2.18	0.03	11.30	8.49	2.25
Na_2O	4.69	5.50	5.00	4.80	4.04	3.88	3.79	6.37	0.16	2.26	3.56	4.59
K_2O	0.13	0.09	0.02	0.24	1.45	1.54	1.64	0.49	2.18	1.26	1.14	2.1
P_2O_5	0.20	0.26	0.09	0.10	0.18	0.14	0.09	0.26	0.03	0.17	0.15	0.06
LOI	3.57	3.71	2.00	3.10	3.48	5.35	5.29	3.11	3.51	12.47	9.57	4.14
Total	99.62	99.31	99.76	100.20	99.48	100.44	100.30	99.54	99.57	100.03	98.76	99.90
ppm	* Total iron as Fe_2O_3											
Pb	2	0	0	3	2	0	11	0	2	3	12	3
Th	4	7	0	0	0	7	1	0	4	8	9	11
U	4	0	0	0	0	0	0	0	0	0	0	0
Rb	4	4	0	1	13	13	17	5	23	37	33	38
Sr	51	74	151	138	36	69	204	76	6	74	88	114
Y	35	48	36	19	22	22	18	27	60	19	19	24
Zr	92	80	64	39	51	66	50	46	182	53	59	142
Nb	4	3	2	3	3	6	5	2	6	4	6	9
Zn	115	49	40	69	134	72	56	82	17	124	98	44
Cu	7	7	19	38	15	45	76	3	13	41	13	25
Ni	0	0	26	5	0	148	36	0	0	181	149	1
La	4	5	0	0	1	0	2	4	7	18	16	13
Ba	28	42	0	71	231	274	220	106	669	188	118	236
V	44	117	193	515	386	299	318	368	12	240	249	97
Ce	15	18	54	58	17	53	29	14	16	61	101	85
Cr	0	0	103	50	0	371	156	0	0	455	521	12
Ga	8	7	16	11	13	14	15	13	13	12	13	14

Table B-11: Drill core samples from the Skidder Prospect chlorite, calcite, epidote ± hematite alteration zone

Weight %	SK 6 5	SK 27 1	SK 27 2	SK 27 6	SK 27 8	SK 28 1	SK 28 4	SK 28 6	SK 28 8	SK 28 11	SK 29 4	SK 29 12	SK 29 15	SK 30 5
SiO_2	46.10	48.30	52.70	47.60	47.10	51.80	47.50	51.50	48.60	45.80	49.90	47.50	50.40	48.80
TiO_2	0 71	1.27	0.82	1.21	0.85	1.12	0.66	0.80	1.34	1.08	1.62	1.32	1.27	0.94
Al_2O_3	18.00	17.10	15.40	15.80	16.00	16.20	16.60	16.20	16.80	15.10	17.20	15.40	15.20	16.10
Fe_2O_3*	11.21	14.58	11.53	11.10	10.54	10.46	11.70	9.80	13.16	10.46	10.11	11.71	10 65	9.56
MnO	0.24	0.10	0.16	0.19	0.16	0.07	0.17	0.16	0.10	0.17	0.14	0.17	0.17	0.13
MgO	12.05	4.95	5.73	8.60	8.87	3.13	9.17	9.20	3.89	9.06	3.96	9.64	8.71	6.26
CaO	1.16	5.40	2.98	5.56	9.52	6.02	4.99	3.98	6.16	6.19	4.72	5.82	6.64	4.34
Na_2O	4.85	5.21	6.09	4.34	1.49	6.65	2.82	5.26	5.97	4.23	5.37	3.75	4.54	5.65
K_2O	0.07	0.42	0.53	1.24	2.36	0.10	2.70	0.06	0.09	0.06	0.81	0.99	0.15	1.18
P_2O_5	0.07	0.13	0.30	0.18	0.13	0.27	0.06	0.09	0.21	0.13	0.23	0.17	0.16	0.02
LOI	5.43	2.77	3.09	4.96	3.76	3.30	4.33	3.79	3.79	8.03	4.42	3.34	2.84	5.03
Total	99.89	100.23	99.33	100.78	100.78	99.12	100.70	100.84	100.11	100.31	98.48	99.81	100.73	98.01
ppm														
Pb	1	n.d.	1	4	n.d.	n.d.	5	7	4	8	n.d.	5	n.d.	8
Th	4	4	5	6	n.d.	2	6	4	n.d.	7	n.d.	6	5	2
U	3	n.d.	n.d.	n.d.	n.d.	4	n.d.	n.d.	2	n.d.	n.d.	n.d.	n.d.	n.d.
Rb	n.d.	3	4	7	15	3	35	1	1	3	11	10	n.d.	13
Sr	54	134	81	112	331	93	271	60	78	89	65	171	64	108
Y	13	27	20	27	21	32	10	16	33	25	35	32	27	31
Zr	24	75	44	74	45	70	33	41	70	71	102	77	75	71
Nb	2	6	3	5	5	5	3	3	6	7	9	10	5	8
Zn	121	62	97	90	72	52	84	72	57	81	82	89	67	86
Cu	10	8	44	23	54	34	50	13	27	43	74	51	73	17
Ni	46	49	n.d.	80	86	41	43	70	59	73	145	68	66	36
La	n.d.	7	5	n.d.	10	2	2	3	1	3	4	20	n.d.	n.d.
Ba	n.d.	n.d.	92	153	345	n.d.	481	n.d.	n.d.	n.d.	n.d.	156	n.d.	120
V	346	237	366	296	263	284	329	299	415	316	288	313	325	255
Ce	70	129	80	96	43	18	53	46	79	104	127	66	124	101
Cr	116	243	35	222	215	187	160	256	226	214	282	195	169	230
Ga	16	16	18	16	16	12	13	14	19	14	19	15	21	18
Drill hole depth at which sample was taken														
feet	94.0	19.5	30.5	115.0	142.0	10.0	24.0	98.5	173.0	224.0	45.0	186.0	228.0	53.0
metres	28.7	5.9	9.3	35.1	43.3	3.0	7.3	30.0	52.7	68.3	13.7	56.7	69.5	16.2
Distance (m)	78.2	134.1	130.7	104.9	96.7	160.3	156.1	133.4	110.6	95.1	234.3	191.3	178.5	225.8

* Total iron as Fe_2O_3 n.d. - not detected

Distance - distance in metres from most intensely altered rocks in drill hole

Table B-11 (continued): Drill core samples from the Skidder Prospect: chlorite, calcite, epidote ± hematite alteration zone

Weight %	SK 30 6	SK 30 20	SK 32 1	SK 34 14	SK 34 69	SK 35 12	SK 35 16	SK 35 34	SK 37 2	SK 37 7	SK 37 16	SK 37 27	SK 37 30	SK 38 8
SiO_2	44.20	53.10	49.60	52.30	47.10	51.60	51.10	49.40	53.30	52.10	49.60	49.80	49.20	47.50
TiO_2	1.58	0.95	1.04	1.20	1.17	1.08	1.06	1.07	1.18	1.79	1.07	0.93	0.76	1.09
Al_2O_3	17.10	15.70	14.30	14.20	15.00	15.40	15.00	15.80	14.40	14.40	15.60	15.60	14.50	14.70
Fe_2O_3*	12.00	12.04	11.38	11.27	11.24	12.42	12.25	12.00	12.63	13.57	10.37	13.23	8.65	9.52
MnO	0.22	0.15	0.16	0.20	0.23	0.18	0.17	0.14	0.19	0.20	0.17	0.15	0.16	0.18
MgO	10.00	5.42	9.09	6.86	10.07	6.35	6.66	7.01	5.65	5.85	8.57	7.35	8.25	10.08
CaO	4.52	3.32	6.44	4.46	6.36	4.32	4.54	3.26	5.66	4.66	6.10	4.18	7.56	6.84
Na_2O	4.36	6.54	3.17	5.63	4.13	5.76	4.78	6.20	5.43	5.56	3.61	5.08	4.23	4.27
K_2O	0.65	0.58	2.08	0.14	0.13	0.12	1.10	0.14	0.05	0.15	1.90	0.14	1.16	0.14
P_2O_5	0.22	0.18	0.01	0.09	0.18	0.11	0.10	0.16	0.12	0.14	0.12	0.08	0.09	0.09
LOI	5.19	1.84	2.94	2.16	4.21	2.86	2.46	4.49	1.96	1.92	2.84	2.92	4.28	4.91
Total	100.04	99.82	100.21	98.51	99.82	100.20	99.22	99.67	100.57	100.34	99.95	99.46	98.84	99.32
ppm														
Pb	n.d.	5	10	n.d.	2	1	9	6	1	5	1	n.d.	n.d.	3
Th	n.d.	2	6	7	3	3	1	6	3	4	n.d.	3	4	7
U	n.d.	n.d.	n.d.	n.d.	n.d.	n.d.	6	n.d.	n.d.	1	1	n.d.	n.d.	n.d.
Rb	6	7	19	2	n.d.	1	9	4	2	1	21	2	11	3
Sr	127	100	192	50	145	61	64	52	41	52	244	65	162	119
Y	37	25	21	42	25	33	29	30	33	50	28	28	18	24
Zr	90	48	34	84	66	68	43	85	76	106	74	71	44	62
Nb	8	6	3	5	8	4	4	9	6	6	5	4	4	4
Zn	98	93	83	84	99	90	83	107	86	112	79	97	62	71
Cu	56	30	75	28	7	15	33	39	20	32	61	18	73	62
Ni	71	n.d.	61	26	139	4	15	13	3	8	71	7	41	151
La	5	24	1	6	7	n.d.	7	5	n.d.	1	n.d.	n.d.	n.d.	8
Ba	70	116	343	42	62	66	142	15	n.d.	n.d.	987	n.d.	453	17
V	406	368	327	348	308	396	345	435	393	533	312	419	274	285
Ce	96	66	3	62	43	31	28	77	77	94	8	51	11	54
Cr	289	36	167	88	473	27	44	35	26	40	184	31	107	496
Ga	17	17	14	18	18	16	14	18	16	19	17	20	13	15
Drill hole depth at which sample was taken														
feet	76.0	243.5	16.0	134.0	911.0	156.0	311.0	917.5	72.0	247.0	515.0	757.0	897.5	878.5
metres	23.2	74.2	4.9	40.8	277.7	47.5	94.8	279.7	21.9	75.3	157.0	230.7	273.6	267.8
Distance (m)	218.8	167.8	180.1	329.2	92.3	431.0	383.7	198.9	444.7	391.4	309.7	235.9	193.1	

* Total iron as Fe_2O_3 n.d. - not detected

Distance - distance in metres from most intensely altered rocks in drill hole

Table B-12: Drill core samples from the Skidder Prospect chlorite, calcite, quartz, epidote alteration zone

Weight %	SK 29 69	SK 30 25	SK 30 26	SK 30 88	SK 31 522	SK 31 532	SK 32 32	SK 33 26	SK 34 19	SK 34 28	SK 34 34	SK 34 35	SK 34 72	SK 34 127	SK 35 24	SK 35 25	SK 35 44	SK 35 93	SK 37 41	SK 37A 15	SK 37A M
SiO_2	50.70	47.00	51.10	50.90	68.80	46.10	49.40	53.40	55.80	52.00	69.10	50.50	51.60	49.20	66.30	46.80	39.20	49.40	54.50	50.10	49.80
TiO_2	1.06	1.35	1.05	1.07	0.54	0.64	1.00	1.38	0.91	1.02	0.93	1.27	0.99	1.48	1.39	2.00	1.01	1.95	1.18	1.31	1.75
Al_2O_3	15.10	16.70	15.40	15.00	10.80	14.70	15.50	16.90	15.40	14.10	11.50	15.60	14.90	14.40	12.60	16.10	14.60	16.00	14.50	16.40	16.30
Fe_2O_3*	10.01	12.13	12.75	9.77	6.72	10.99	9.93	9.66	10.58	12.08	4.86	13.15	12.13	13.85	6.52	14.80	10.59	12.73	12.43	12.80	12.15
MnO	0.13	0.19	0.17	0.10	0.05	0.17	0.18	0.09	0.20	0.20	0.07	0.20	0.20	0.07	0.07	0.20	0.17	0.07	0.16	0.13	0.11
MgO	8.03	9.25	6.88	8.92	0.49	8.99	9.18	5.42	4.10	5.33	1.58	5.99	6.97	9.12	1.55	7.58	11.10	8.21	5.62	6.52	6.54
CaO	5.48	4.98	4.20	3.96	2.82	5.82	4.84	2.16	3.02	4.32	3.08	2.90	4.86	2.68	2.68	2.64	7.54	2.46	2.40	2.16	3.24
Na_2O	5.27	4.27	5.68	5.18	5.65	3.76	4.41	6.24	6.41	5.07	6.32	5.37	4.83	4.65	6.78	5.18	2.71	4.99	5.55	5.72	5.66
K_2O	0.09	0.18	0.16	0.17	0.09	0.10	0.56	0.14	0.80	1.50	0.10	0.14	1.15	0.10	0.06	0.14	1.03	0.13	0.23	0.40	0.10
P_2O_5	0.11	0.15	0.12	0.12	0.12	0.11	0.08	0.29	0.29	0.08	0.16	0.20	0.08	0.21	0.21	0.27	0.20	0.36	0.21	0.11	0.22
LOI	3.00	3.95	2.63	3.76	2.19	8.39	3.29	2.75	1.51	1.73	1.06	4.34	2.35	3.78	0.62	3.88	4.60	3.72	2.25	3.49	2.97
Total	98.98	100.15	100.14	98.95	98.27	99.77	98.37	98.43	99.02	97.43	98.76	99.66	100.06	99.54	98.78	99.59	92.75	100.02	99.03	99.14	98.84
ppm																					
Pb	2	2	3	3	14	4	5	7	9	2	4	5	1	2	5	10	6	n.d.	8	4	5
Th	3	n.d.	3	6	4	2	4	4	5	5	5	10	n.d.	5	2	3	8	6	5	n.d.	5
U	n.d.	n.d.	n.d.	n.d.	n.d.	n.d.	1	n.d.	n.d.	n.d.	n.d.	2	n.d.	n.d.	n.d.	1	n.d.	n.d.	n.d.	n.d.	n.d.
Rb	n.d.	1	2	7	1	2	7	n.d.	5	11	1	n.d.	7	n.d.	n.d.	3	11	n.d.	1	6	n.d.
Sr	98	145	121	72	81	127	194	69	113	78	41	46	170	53	40	34	180	86	36	62	82
Y	28	28	27	28	29	28	19	62	29	35	44	58	26	46	45	60	23	60	54	43	38
Zr	60	76	40	57	68	69	46	116	57	50	95	120	35	63	117	134	59	144	111	68	75
Nb	7	6	2	5	4	6	3	5	4	4	4	5	3	6	6	7	5	9	6	6	5
Zn	81	102	74	67	25	70	63	86	97	72	25	119	97	91	29	148	77	110	106	150	113
Cu	46	45	32	41	41	44	56	13	19	32	24	3	33	32	11	13	51	14	6	24	24
Ni	38	86	17	36	n.d.	102	75	7	n.d.	2	11	12	16	7	n.d.	n.d.	215	2	8	8	17
La	5	7	n.d.	13	n.d.	6	6	14	5	n.d.	2	1	6	n.d.	4	6	1	8	8	2	n.d.
Ba	n.d.	19	42	4	25	n.d.	102	n.d.	185	406	n.d.	57	180	75	n.d.	n.d.	359	8	23	79	n.d.
V	279	367	403	275	366	363	314	234	279	452	179	296	353	507	233	479	238	410	235	560	579
Ce	55	101	41	71	95	141	59	114	51	15	141	46	30	38	84	114	42	108	81	68	107
Cr	131	277	55	151	25	258	197	39	20	37	42	57	52	37	4	15	628	21	25	43	52
Ga	18	14	17	28	9	17	16	19	18	16	11	19	16	20	13	23	15	23	20	20	18
Drill hole depth at which sample was taken																					
feet	962	382	402	1086	522	532	744	437	235	320	393	428	971	1581	533	593	1167	1794	1067	1231	1676
metres	293.2	116.4	122.4	330.9	159.1	162.2	226.6	133.0	71.6	97.4	119.8	130.3	296.0	481.9	162.5	180.7	355.7	546.8	325.2	375.2	510.8
Distance (m)	45.2	125.6	119.6	88.9	114.1	117.2	41.6	26.0	298.4	272.6	250.2	239.7	74.0	111.9	316.1	297.8	122.8	68.3	141.4	91.4	44.2

* Total iron as Fe_2O_3

n.d. - not detected

Distance - distance in metres from most intensely altered rocks in drill hole

Table B-13: Drill core samples from the Skidder Prospect chlorite, quartz, calcite alteration zone

Weight %	SK 6 12	SK 27 11	SK 27 17	SK 27 33	SK 28 16	SK 28 17	SK 28 18	SK 28 19	SK 28 58	SK 29 24	SK 29 28	SK 29 29	SK 29 33	SK 29 35	SK 29 37	SK 29 66	SK 30 34	SK 30 36
SiO_2	45.50	45.70	53.70	46.50	44.30	46.70	48.90	47.60	47.90	43.40	51.60	51.60	52.20	51.80	55.00	46.70	47.10	48.10
TiO_2	1.29	1.12	0.82	1.12	1.10	0.85	1.23	1.35	1.16	1.07	1.07	1.30	0.88	1.13	1.07	1.21	1.05	1.32
Al_2O_3	15.70	15.40	14.30	15.20	16.30	16.70	17.80	17.60	16.70	14.70	16.80	18.00	14.90	16.70	13.70	15.10	15.50	18.60
Fe_2O_3*	10.17	10.55	10.61	10.38	7.55	10.14	11.57	10.96	11.89	9.27	9.90	9.71	11.21	9.77	7.76	10.80	10.76	10.18
MnO	0.19	0.16	0.14	0.13	0.22	0.20	0.09	0.09	0.18	0.16	0.17	0.08	0.18	0.07	0.04	0.14	0.18	0.33
MgO	9.24	8.90	7.13	12.74	2.59	9.15	5.56	8.77	12.25	6.25	4.22	2.67	6.08	4.05	6.63	13.03	9.13	2.77
CaO	5.32	5.94	3.16	1.00	11.22	5.23	3.05	2.51	1.03	9.56	3.10	1.46	3.48	3.76	3.24	2.56	5.04	4.36
Na_2O	3.42	3.65	4.12	4.02	4.30	3.41	6.02	5.49	3.23	5.10	6.13	5.72	5.72	6.66	4.92	3.43	4.38	4.38
K_2O	0.89	0.13	0.30	0.05	1.76	0.63	0.63	0.17	0.06	0.38	0.63	2.90	0.36	1.12	0.90	0.08	0.08	2.57
P_2O_5	0.22	0.23	0.10	0.17	0.20	0.15	0.17	0.23	0.22	0.21	0.33	0.09	0.07	0.21	0.21	0.18	0.09	0.20
LOI	7.83	8.63	5.34	7.82	10.76	7.50	4.36	4.85	5.61	9.20	4.28	5.00	4.50	3.77	4.96	6.40	5.79	5.68
Total	99.77	100.41	99.72	99.13	100.30	100.66	99.38	99.62	100.23	99.30	98.23	98.53	99.58	99.04	98.43	99.63	99.10	98.49
ppm																		
Pb	6	4	4	10	6	1	1	1	7	2	10	27	1	4	9	8	7	4
Th	6	n.d.	1	n.d.	5	n.d.	1	1	5	1	7	1	4	1	3	6	3	8
U	4	n.d.	n.d.	n.d.	n.d.	n.d.	n.d.	n.d.	2	1	2	n.d.	n.d.	n.d.	4	1	n.d.	2
Rb	13	1	5	n.d.	33	7	8	n.d.	2	7	15	67	6	14	7	5	1	43
Sr	68	151	58	36	78	123	105	67	45	85	80	75	73	103	76	49	163	67
Y	28	28	23	24	19	19	24	30	30	29	41	22	23	27	23	29	24	30
Zr	73	69	43	77	63	48	71	80	74	69	72	79	47	67	59	60	56	82
Nb	10	6	4	7	6	5	5	6	8	5	6	6	2	4	3	4	4	8
Zn	71	67	105	161	50	63	74	113	106	89	75	41	101	70	52	89	69	69
Cu	57	42	55	24	50	60	8	29	35	40	18	35	37	50	48	58	20	61
Ni	82	70	27	51	63	81	44	53	91	77	33	38	15	50	36	122	109	58
La	5	n.d.	n.d.	3	n.d.	n.d.	n.d.	6	n.d.	6	n.d.	n.d.	n.d.	n.d.	n.d.	n.d.	1	5
Ba	n.d.	22	42	15	57	65	74	64	22	65	31	199	1	381	490	n.d.	84	5
V	369	370	379	367	297	345	370	388	404	313	347	442	426	309	276	354	416	408
Ce	123	74	55	64	64	67	82	101	78	24	23	21	9	16	24	21	60	117
Cr	248	213	96	239	184	261	236	293	307	170	215	228	15	193	183	456	320	250
Ga	17	17	16	15	16	14	16	21	14	12	14	19	13	18	13	14	10	17
Drill hole depth at which sample was taken																		
feet	228.0	190.0	307.5	517.0	312.0	335.0	355.0	383.0	640.0	409.0	458.0	463.0	510.0	528.5	553.0	935.0	530.0	572.5
metres	69.5	57.9	93.7	157.6	95.1	102.1	108.2	116.7	195.1	124.7	139.6	141.1	155.4	161.1	168.6	285.0	161.5	174.3
Distance (m)	-87.3	82.1	46.3	17.6	68.3	61.3	55.2	46.6	14.0	123.3	108.4	106.9	92.6	86.9	79.4	37.0	80.5	67.7

* Total iron as Fe_2O_3 n.d. - not detected

Distance - distance in metres from most intensely altered rocks in drill hole

Table B-13 (continued): Drill core samples from the Skidder Prospect chlorite, quartz, calcite alteration zone

Weight %	SK 30 38	SK 31 24	SK 31 552	SK 32 11	SK 33 1	SK 33 4	SK 34 46	SK 34 55	SK 34 81	SK 35 3	SK 35 63	SK 35 66A	SK 35 66B	SK 35 70	SK 37A 32	SK 37A 34
SiO_2	50.20	48.30	53.80	58.20	57.10	53.70	54.90	53.60	53.00	61.10	48.70	65.50	63.50	54.60	49.60	57.90
TiO_2	1.58	0.48	1.24	1.18	1.08	1.31	1.86	1.41	1.09	0.75	1.16	0.86	0.84	1.08	1.02	0.62
Al_2O_3	22.50	16.50	14.20	14.40	16.40	15.50	15.00	15.20	14.30	13.70	18.10	12.30	13.70	15.20	17.10	14.40
Fe_2O_3*	5.23	8.53	12.40	10.59	7.23	12.21	11.05	11.62	7.55	10.53	9.35	5.76	3.65	7.01	9.81	7.32
MnO	0.05	0.13	0.15	0.11	0.20	0.11	0.19	0.20	0.10	0.13	0.01	0.04	0.05	0.05	0.15	0.13
MgO	3.19	7.49	4.91	4.10	2.78	5.97	5.39	5.75	11.77	3.81	1.14	3.67	5.08	10.11	9.28	5.08
CaO	1.34	4.88	2.48	1.84	3.08	1.76	2.28	2.02	1.78	1.56	1.48	1.38	1.28	1.34	1.68	2.90
Na_2O	4.39	5.00	4.81	5.13	6.14	4.73	5.38	5.97	3.82	5.37	5.20	5.32	5.20	4.43	5.27	5.59
K_2O	5.09	0.50	0.07	0.21	0.58	0.13	0.40	0.10	0.32	0.12	4.12	0.42	0.28	0.12	0.48	0.50
P_2O_5	0.29	0.01	0.16	0.57	0.36	0.26	0.28	0.46	0.13	0.58	0.24	0.22	0.26	0.29	0.12	0.10
LOI	4.67	7.14	4.91	2.45	3.36	3.34	2.93	2.84	5.43	2.40	6.09	3.48	3.33	4.37	4.52	3.69
Total	98.53	98.96	99.13	98.78	98.31	99.02	99.66	99.17	99.29	100.05	95.59	98.95	97.17	98.60	99.03	98.23
ppm																
Pb	21	6	12	n.d.	11	4	3	1	5	4	25	13	7	1	3	1
Th	n.d.	5	9	6	6	7	7	4	6	n.d.	5	2	2	1	n.d.	3
U	n.d.	1	n.d.	n.d.	n.d.	n.d.	1	1	n.d.	n.d.	n.d.	n.d.	n.d.	n.d.	n.d.	n.d.
Rb	84	6	1	1	9	1	2	2	4	n.d.	72	2	1	n.d.	4	5
Sr	55	88	32	66	82	39	68	34	66	35	105	92	98	53	61	90
Y	41	17	45	47	41	36	52	59	19	45	32	28	25	25	35	32
Zr	97	27	111	92	69	80	103	125	57	89	75	49	63	58	79	81
Nb	7	2	5	7	7	6	7	9	4	6	8	5	5	4	7	4
Zn	129	56	91	99	52	84	124	142	85	100	48	37	39	42	141	54
Cu	64	98	8	6	84	1	7	9	48	3	68	89	87	15	77	15
Ni	80	60	4	n.d.	43	n.d.	1	1	129	n.d.	139	142	143	82	20	32
La	n.d.	2	8	16	5	9	1	9	4	7	5	n.d.	1	21	n.d.	4
Ba	123	78	n.d.	57	n.d.	6	109	52	n.d.	64	481	113	81	41	70	43
V	493	299	438	54	309	293	195	191	307	57	319	185	232	325	409	200
Ce	166	30	108	99	153	94	76	61	125	72	57	67	49	82	68	71
Cr	298	153	29	n.d.	232	14	7	n.d.	476	n.d.	533	419	473	497	55	124
Ga	25	16	20	19	15	19	18	22	14	18	19	7	17	18	24	16
Drill hole depth at which sample was taken																
feet	578.5	428.0	552.0	365.0	46.0	124.0	599.0	752.0	1100.5	29.0	1432.0	1487.0	1487.0	1511.5	1442.0	1462.5
metres	176.3	130.5	168.2	111.3	14.0	37.8	182.6	229.2	335.4	8.8	436.5	453.2	453.2	460.7	439.6	445.8
Distance (m)	65.7	85.5	123.2	73.7	93.0	69.2	187.4	140.8	34.6	469.7	42.1	25.3	25.3	17.8	27.1	20.9

* Total iron as Fe_2O_3 n.d. - not detected

Distance - distance in metres from most intensely altered rocks in drill hole

Table B-14: Drill core samples from the Skidder Prospect chlorite, quartz, pyrite alteration zone

Weight %	SK 6 16	SK 27 22	SK 27 26	SK 27 27	SK 27 44	SK 27 48	SK 28 20	SK 28 25	SK 28 27	SK 28 36	SK 28 51	SK 28 70	SK 28 71	SK 28 73	SK 28 75	SK 28 81	SK 29 36
SiO_2	45.20	30.20	41.60	41.50	48.00	40.20	43.20	50.30	28.60	29.40	53.10	28.50	43.70	31.40	53.70	46.10	43.80
TiO_2	1.04	0.86	1.12	1.25	1.20	0.50	0.28	0.86	0.58	0.92	0.50	0.20	0.96	0.35	0.55	0.78	1.24
Al_2O_3	15.80	13.40	15.70	16.90	15.40	15.70	17.30	13.50	15.10	18.40	15.20	16.00	16.30	13.20	11.60	13.50	15.80
Fe_2O_3*	8.79	14.42	8.53	8.54	10.74	9.40	9.99	7.45	14.93	11.74	10.30	12.48	10.93	14.07	10.36	12.06	10.34
MnO	0.15	0.21	0.21	0.21	0.18	0.16	0.09	0.13	0.23	0.21	0.17	0.16	0.17	0.12	0.17	0.17	0.07
MgO	18.38	26.40	21.30	19.65	15.01	23.08	16.26	17.50	27.18	28.45	12.18	28.70	17.98	27.38	16.68	18.96	13.73
CaO	1.19	1.16	1.03	1.34	0.65	0.47	1.58	0.52	0.96	0.20	0.18	1.29	0.33	0.93	0.23	0.32	2.98
Na_2O	2.72	0.06	2.33	2.92	2.45	1.14	3.53	2.10	0.06	0.03	3.06	0.03	2.37	0.06	0.03	0.29	3.73
K_2O	0.07	0.01	0.03	0.04	0.03	0.02	0.65	0.06	0.01	0.02	0.04	0.02	0.03	0.01	0.07	0.03	0.60
P_2O_5	0.13	0.19	0.18	0.16	0.17	0.15	0.18	0.17	0.20	0.07	0.04	0.27	0.15	0.16	0.14	0.17	0.17
LOI	7.29	13.76	8.86	8.19	6.57	9.20	7.33	7.75	12.90	11.34	5.66	12.63	7.77	12.59	7.13	8.13	6.97
Total	100.76	100.67	100.89	100.70	100.40	100.02	100.39	100.34	100.75	100.68	100.43	100.28	100.69	100.27	100.66	100.51	99.43
ppm																	
Pb	8	60	3	3	3	4	2	6	15	n.d.	7	15	1	13	n.d.	3	5
Th	4	n.d.	4	6	n.d.	2	n.d.	4	n.d.	n.d.	4	4	6	n.d.	4	9	2
U	n.d.	n.d.	n.d.	n.d.	n.d.	n.d.	n.d.	n.d.	n.d.	n.d.	n.d.	3	n.d.	n.d.	n.d.	2	3
Rb	1	3	n.d.	1	1	2	3	n.d.	1	n.d.	n.d.	2	2	n.d.	2	3	10
Sr	26	22	30	22	23	13	66	38	22	10	20	17	11	18	6	7	68
Y	19	20	25	24	21	26	27	17	21	16	12	20	20	26	12	30	28
Zr	67	55	65	73	68	64	64	60	58	31	26	73	65	55	50	51	72
Nb	8	8	6	5	7	8	4	6	4	1	1	7	6	4	6	4	5
Zn	135	3817	402	308	188	491	252	215	942	922	258	944	163	814	529	204	93
Cu	33	53	13	41	41	12	57	32	15	15	60	24	19	61	15	464	47
Ni	76	45	73	69	78	62	104	53	61	29	23	94	99	94	122	90	78
La	n.d.	n.d.	n.d.	n.d.	3	5	2	n.d.	3	n.d.	n.d.	3	2	n.d.	4	1	n.d.
Ba	n.d.	n.d.	n.d.	35	n.d.	n.d.	110	11	n.d.	1	40	n.d.	21	n.d.	n.d.	n.d.	604
V	406	348	393	398	400	477	387	352	357	505	428	471	419	369	329	413	402
Ce	111	69	109	54	71	86	79	76	54	47	33	72	51	56	76	77	20
Cr	274	198	301	286	285	320	337	228	201	84	72	539	311	287	483	447	242
Ga	16	21	14	15	16	16	18	13	22	21	16	22	15	14	14	16	13
Drill hole depth at which sample was taken																	
feet	284.0	344.0	401.0	425.0	636.0	666.0	408.0	447.0	476.5	518.0	558.0	704.5	709.0	715.5	741.0	797.5	552.0
metres	86.6	104.9	122.2	129.5	193.9	203.0	124.4	136.2	145.2	157.9	170.1	214.7	216.1	218.1	225.9	243.1	168.2
Distance (m)	20.3	35.1	17.8	10.5	1.8	7.3	39.0	27.1	18.1	5.5	6.7	5.6	7.0	9.0	16.8	34.0	79.8

* Total iron as Fe_2O_3 n.d. - not detected

Distance - distance in metres from most intensely altered rocks in drill hole

Table B-14 (continued): Drill core samples from the Skidder Prospect chlorite, quartz, pyrite alteration zone

Weight %	SK 29 40	SK 29 43	SK 29 44	SK 29 49	SK 29 50	SK 29 51	SK 29 63	SK 29 64	SK 30 79	SK 31 7	SK 31 10	SK 32 20B	SK 33 12	SK 34 118	SK 35 82	SK 35 88	SK 38 2
SiO_2	43.70	49.10	50.90	44.40	45.90	48.70	50.90	43.50	40.70	30.00	36.00	50.70	48.30	30.80	43.80	32.20	48.50
TiO_2	1.16	1.16	0.99	1.08	1.19	0.98	0.93	1.11	0.08	0.65	0.49	0.59	0.67	0.38	1.01	1.11	1.13
Al_2O_3	15.40	14.30	13.60	15.00	15.50	13.40	13.10	14.50	8.09	17.70	16.60	10.60	17.10	16.00	13.30	14.00	14.90
Fe_2O_3*	7.16	7.09	7.27	7.20	6.66	7.07	7.71	9.64	3.15	11.24	9.40	15.60	10.13	13.11	11.16	11.49	6.88
MnO	0.10	0.13	0.14	0.18	0.16	0.17	0.10	0.10	0.09	0.16	0.17	0.11	0.15	0.17	0.27	0.14	0.15
MgO	17.88	16.40	14.93	19.50	17.70	18.03	15.75	14.10	31.35	27.45	25.20	10.96	13.74	26.50	20.91	28.30	15.73
CaO	1.60	1.18	1.00	0.52	0.60	0.56	0.98	5.04	3.66	0.72	0.24	0.38	0.24	0.58	0.86	1.42	1.56
Na_2O	3.38	3.10	2.90	1.82	2.65	1.65	2.08	2.98	0.02	0.05	0.26	0.01	3.74	0.05	0.04	0.03	3.34
K_2O	0.30	0.10	0.11	0.15	0.09	0.03	0.03	0.05	0.01	n.d.	1.19	0.81	0.18	0.01	0.02	0.02	0.14
P_2O_5	0.15	0.15	0.12	0.14	0.15	0.14	0.14	0.19	0.08	0.03	0.02	0.15	0.01	0.16	0.14	0.15	0.16
LOI	7.66	7.02	6.52	8.36	7.75	7.54	6.54	8.64	11.02	11.35	11.25	8.99	6.04	11.62	8.57	11.99	6.56
Total	98.49	99.73	98.48	98.35	98.35	98.27	98.26	99.85	98.25	99.35	100.82	98.90	100.30	99.38	100.08	100.85	99.05
ppm																	
Pb	6	8	16	3	11	8	2	1	116	26	22	23	1	9	7	26	10
Th	5	8	2	3	10	3	6	n.d.	7	4	1	n.d.	2	3	6	3	5
U	1	n.d.	n.d.	4	1	n.d.	n.d.	n.d.	n.d.	n.d.	7	n.d.	n.d.	n.d.	n.d.	n.d.	1
Rb	8	3	5	4	n.d.	4	2	1	1	2	19	12	1	3	1	n.d.	1
Sr	54	39	36	15	22	20	22	76	27	5	17	4	42	12	8	16	42
Y	27	14	17	20	16	13	18	28	11	13	10	20	8	33	26	24	27
Zr	68	65	55	61	69	59	46	55	31	27	24	54	22	66	57	64	70
Nb	5	4	3	3	9	4	3	3	3	4	3	6	3	6	4	5	7
Zn	368	171	155	181	185	201	81	66	990	448	517	247	132	329	785	964	167
Cu	73	62	53	52	42	54	54	51	91	26	25	13	29	7	50	42	48
Ni	62	58	66	75	68	73	192	277	30	60	53	120	36	166	390	83	75
La	n.d.	n.d.	2	n.d.	1	n.d.	n.d.	n.d.	3	3	n.d.	1	n.d.	2	5	n.d.	n.d.
Ba	57	5	15	13	n.d.	n.d.	n.d.	5	n.d.	n.d.	245	n.d.	n.d.	28	1	n.d.	4
V	366	364	353	416	421	368	338	301	209	350	528	296	449	404	384	390	361
Ce	20	18	21	24	99	18	15	15	51	73	49	86	68	50	54	74	77
Cr	225	211	186	229	270	207	652	842	164	87	191	487	127	632	1294	345	258
Ga	14	13	15	14	13	15	13	11	10	21	20	14	16	18	15	16	15
Drill hole depth at which sample was taken																	
feet	592.0	638.0	662.0	748.5	756.5	783.0	886.5	914.5	967.5	86.5	123.0	573.0	231.0	1482.0	1597.0	1691.0	527.0
metres	180.4	194.5	201.8	228.1	230.6	238.7	270.2	278.7	294.9	26.4	37.5	174.7	70.4	451.7	486.8	515.4	160.6
Distance (m)	67.6	53.5	46.2	19.9	17.4	9.3	22.2	30.7	52.9	18.6	7.5	10.3	36.6	81.7	8.2	36.9	

* Total iron as Fe_2O_3 n.d. - not detected

Distance - distance in metres from most intensely altered rocks in drill hole

Table B-15: Drill core samples from the Skidder Prospect quartz, chlorite, pyrite alteration zone

Weight %	SK 27 18	SK 28 78	SK 29 38	SK 29 54	SK 30 48	SK 30 61	SK 30 63	SK 30 68A	SK 30 68B	SK 30 822B	SK 30 C
SiO_2	71.40	63.10	73.70	42.40	58.00	50.50	54.00	54.00	65.90	41.90	62.50
TiO_2	0.34	0.88	0.40	1.22	0.54	0.22	0.52	1.18	1.20	0.23	0.10
Al_2O_3	12.80	12.00	11.60	15.20	14.60	7.07	9.02	14.80	15.30	9.05	3.70
Fe_2O_3*	5.09	7.24	2.94	9.67	9.38	22.90	18.32	13.33	4.34	23.10	19.49
MnO	0.04	0.10	0.03	0.22	0.11	0.04	0.03	0.06	0.03	0.07	n.d.
MgO	2.46	9.08	2.04	9.20	6.44	5.32	4.38	3.60	1.75	10.61	0.34
CaO	0.33	0.28	0.44	8.62	0.92	0.32	0.28	0.34	2.46	0.32	0.02
Na_2O	5.66	0.03	5.37	2.42	5.07	0.02	0.04	0.96	0.65	n.d.	0.03
K_2O	0.37	1.78	0.33	1.03	0.06	0.80	1.69	3.30	4.54	n.d.	1.25
P_2O_5	0.11	0.16	0.09	0.19	0.06	0.08	0.10	0.19	0.15	0.11	0.01
LOI	1.67	5.19	1.56	8.15	4.04	12.35	10.08	7.59	4.03	12.73	10.62
Total	100.27	99.84	98.50	98.32	99.22	99.62	98.46	99.35	100.35	98.12	98.06
ppm											
Pb	11	9	6	5	4	23	12	164	52	14	293
Th	10	n.d.	4	2	9	7	5	3	6	5	6
U	2	n.d.	n.d.	n.d.	n.d.	3	1	n.d.	n.d.	n.d.	n.d.
Rb	5	26	3	18	1	16	25	50	65	2	21
Sr	49	5	73	71	36	7	6	14	14	2	3
Y	27	11	28	24	20	10	14	19	18	16	n.d.
Zr	94	51	79	67	44	43	48	71	70	48	21
Nb	6	3	4	10	2	5	8	9	9	6	5
Zn	63	236	41	74	177	158	53	285	229	230	937
Cu	18	25	16	51	36	19	23	104	60	14	15
Ni	1	232	2	92	11	55	81	79	50	50	8
La	5	n.d.	n.d.	11	7	n.d.	3	n.d.	n.d.	16	3
Ba	16	214	121	18	n.d.	71	200	190	213	n.d.	65
V	88	297	58	320	418	154	181	356	367	245	66
Ce	82	50	13	74	71	47	56	69	111	62	18
Cr	1?	773	5	244	49	256	385	247	241	402	85
Ga	14	14	9	16	12	10	10	19	16	11	13
Drill hole depth at which sample was taken											
feet	316.0	778.0	567.0	798.0	713.0	822.0	837.0	881.5	881.5	822.0	912.5
metres	96.3	237.1	172.8	243.2	217.3	250.5	255.1	268.7	268.7	250.5	278.1
Distance (m)	43.7	28.0	75.2	4.8	24.7	8.5	13.1	26.7	26.7	8.5	36.1

* Total iron as Fe_2O_3

n.d. - not detected

Distance - distance in metres from most intensely altered rocks in drill hole

Table B-15 (continued): Drill core samples from the Skidder Prospect quartz, chlorite, pyrite alteration zone

Weight %	SK 31 1	SK 31 9	SK 32 20A	SK 33 18	SK 33 19	SK 34 82	SK 34 94	SK 34 105	SK 35 78	1 SK 31 12	1 SK 34 125
SiO_2	51.90	59.50	70.80	78.80	78.80	68.20	58.10	52.40	47.70	39.90	61.20
TiO_2	1.11	0.40	0.51	0.10	0.04	0.60	1.34	0.52	1.16	0.10	0.92
Al_2O_3	18.70	14.90	10.70	8.15	2.30	8.29	18.10	8.82	15.30	2.70	17.70
Fe_2O_3*	5.12	6.23	6.13	0.85	10.84	7.27	7.84	18.16	15.53	12.88	2.37
MnO	0.05	0.04	0.02	0.08	0.01	0.06	0.07	0.07	0.02	0.19	0.01
MgO	4.81	5.22	2.52	0.10	0.44	4.76	3.01	9.32	2.96	8.66	1.43
CaO	2.90	0.36	0.34	3.32	0.01	1.16	0.34	0.20	0.28	13.18	2.48
Na_2O	4.67	3.19	0.05	4.37	0.02	2.71	0.13	n.d.	1.10	0.01	8.80
K_2O	4.37	3.49	3.53	0.07	0.66	0.45	4.64	0.08	4.60	n.d.	0.14
P_2O_5	0.23	n.d.	0.14	n.d.	n.d.	0.10	0.19	0.07	0.13	0.02	0.36
LOI	5.42	5.57	4.89	3.14	5.94	4.72	5.15	9.63	9.43	10.63	1.42
Total	99.28	98.90	99.63	98.98	99.06	98.32	98.91	99.27	98.21	88.27	96.83
ppm											
Pb	33	160	11	9	17	118	29	25	44	30	1
Th	5	1	1	6	4	1	5	1	9	5	3
U	1	9	n.d.	n.d.	5	n.d.	n.d.	n.d.	3	2	n.d.
Rb	55	45	51	1	9	3	53	2	81	1	n.d.
Sr	55	30	6	27	1	75	10	1	14	80	109
Y	27	3	12	30	1	13	33	8	21	5	76
Zr	77	22	50	113	5	37	82	44	73	12	107
Nb	6	4	4	4	4	4	9	5	7	4	5
Zn	239	417	51	24	64	108	198	115	148	261	43
Cu	46	113	25	16	31	30	69	12	30	20342	20
Ni	68	57	102	n.d.	n.d.	17	78	96	49	6	1
La	n.d.	n.d.	n.d.	n.d.	4	n.d.	n.d.	1	7	12	3
Ba	1861	1221	430	1	39	121	200	n.d.	260	138	29
V	340	288	176	6	31	156	375	200	355	71	85
Ce	n.d.	n.d.	82	50	26	51	132	48	80	n.d.	106
Cr	237	146	446	1	10	223	272	367	278	82	6
Ga	21	9	14	6	5	7	19	13	19	3	16
Drill hole depth at which sample was taken											
feet	28.0	104.0	572.0	324.0	340.0	1113.0	1223.0	1339.0	1575.0	138.0	1557.5
metres	8.5	31.7	174.3	98.8	103.6	339.2	372.8	408.1	480.1	42.1	474.7
Distance (m)	36.5	13.3	10.7	8.2	3.4	30.8	2.8	38.1	1.5	2.9	104.7

1 - Samples SK 31 12 and SK 34 125 are not included in the average for this alteration zone on Table 6-22

* Total iron as Fe_2O_3

n.d. - not detected

Distance - distance in metres from most intensely altered rocks in drill hole

Table B-16: Drill core samples from the Skidder Prospect semimassive and massive sulphide zones

	Massive Sulphides L					Semimassive Sulphides Pyrite-rich Basalt		Chlorite rich
Weight %	SK 28 37	SK 28 46	SK 28 69	SK 29 59	SK 29 60	SK 30 822B	SK 30 D	SK 30 74
SiO_2	11.70	27.20	15.60	14.00	20.00	41.90	34.30	18.30
TiO_2	0.10	n.d.	0.02	0.20	0.22	0.23	0.13	0.14
Al_2O_3	2.30	0.90	0.50	2.90	12.80	9.05	3.70	11.35
Fe_2O_3*	44.95	42.62	44.29	52.97	31.00	23.10	37.77	32.80
MnO	0.13	0.01	0.11	0.00	0.12	0.07	0.04	0.13
MgO	3.69	0.11	1.10	0.30	16.52	10.61	3.37	15.88
CaO	7.96	0.40	7.36	0.04	0.14	0.32	0.04	0.54
Na_2O	n.d.	0.01	0.02	0.06	0.04	n.d.	0.01	n.d.
K_2O	n.d.	0.29	n.d.	1.06	0.69	n.d.	0.34	0.16
P_2O_5	0.01	0.24	n.d.	n.d.	0.02	0.11	0.02	0.04
LOI	22.09	22.62	22.44	27.16	18.88	12.73	19.36	20.11
Total	92.93	94.40	91.44	98.69	100.43	98.12	99.08	99.45
ppm								
Pb	76	351	330	158	35	14	77	43
Th	n.d.	4	5	19	n.d.	5	10	8
U	8	n.d.	n.d.	2	n.d.	n.d.	n.d.	5
Rb	9	13	7	27	13	2	15	11
Sr	47	5	54	2	n.d.	2	1	5
Y	n.d.	3	n.d.	n.d.	9	16	n.d.	8
Zr	31	14	20	28	61	48	29	51
Nb	7	12	10	10	6	6	7	10
Zn	2,955	54,690	22,363	1,675	560	230	649	693
Cu	121	14,313	16,053	2,396	85	14	n.d.	16
Ni	5	n.d.	19	8	63	50	16	45
La	14	n.d.	3	12	4	16	9	n.d.
Ba	n.d.	19	n.d.	80	141	n.d.	9	n.d.
V	50	10	26	71	361	245	79	279
Ce	14	n.d.	n.d.	3	20	62	17	25
Cr	27	n.d.	n.d.	41	297	402	118	230
Ga	9	30	22	8	21	11	6	22
Drill hole depth at which sample was taken								
feet	521	543	703	848	849	822	908	933
metres	159	165	214	258	259	251	277	284
Distance (m)	5	2	5	10	11	9	35	42

* Total iron as Fe_2O_3
L - layered
n.d. - not detected
Distance - distance in metres from most intensely altered rocks in drill hole

Table B-16 (continued): Drill core samples from the Skidder Prospect semimassive and massive sulphide zones

	Massive Sulphides	Semimassive Sulphides		Pyrite-rich Basalt	Massive Sulphides		L
Weight %	SK 30 75	SK 30 944A	SK 30 80	SK 34 95	SK 35 75	SK 35 77	SK 35A 6
SiO_2	7.05	33.10	39.30	47.00	18.40	30.00	4.35
TiO_2	0.13	0.13	0.13	0.33	0.78	0.03	n.d.
Al_2O_3	4.10	1.90	2.00	5.79	10.80	1.90	0.40
Fe_2O_3*	54.64	37.93	35.05	28.84	32.88	26.82	42.72
MnO	0.04	0.01	0.01	0.01	0.14	0.04	0.02
MgO	3.61	0.30	0.63	0.91	13.33	2.55	0.63
CaO	0.12	0.04	0.06	0.10	0.24	0.52	0.74
Na_2O	0.01	0.01	0.02	0.05	0.02	0.01	0.01
K_2O	0.64	0.65	0.59	1.71	0.18	0.02	n.d.
P_2O_5	n.d.	0.01	0.01	0.04	0.11	0.01	n.d.
LOI	28.53	20.44	17.78	15.52	19.56	18.46	26.05
Total	98.87	94.52	95.58	100.30	96.44	80.36	74.92
ppm							
Pb	127	83	439	28	51	242	443
Th	4	7	n.d.	n.d.	9	6	4
U	n.d.	5	n.d.	n.d.	n.d.	n.d.	2
Rb	22	16	13	26	10	13	7
Sr	n.d.	2	1	4	8	3	8
Y	n.d.	n.d.	n.d.	7	23	39	n.d.
Zr	37	22	20	37	57	22	19
Nb	14	4	7	5	11	9	15
Zn	2,475	42,937	4,253	31	2,097	137,221	128,129
Cu	3,766	2,108	26,140	n.d.	3,106	17,833	94,181
Ni	5	11	111	39	74	39	n.d.
La	7	n.d.	6	3	1	n.d.	n.d.
Ba	21	n.d.	48	120	n.d.	n.d.	33
V	92	29	40	120	362	21	9
Ce	n.d.	n.d.	n.d.	15	65	n.d.	n.d.
Cr	68	n.d.	248	217	254	n.d.	n.d.
Ga	14	45	2	8	24	85	58
Drill hole depth at which sample was taken							
feet	938	944	974	1243	1563	1570	1571
metres	286	288	297	379	476	479	479
Distance (m)	44	46	55	9	2		

* Total iron as Fe_2O_3
L - layered
n.d. - not detected
Distance - distance in metres from most intensely altered rocks in drill hole

B.4 Pearson Correlation Coefficient Matrices

Pearson correlation coefficient (r) matrices for analyses from the various Skidder Prospect alteration zones are presented in Tables B-17 to B-22.

Table B-17: Pearson correlation coefficient (r) matrix for drill core samples from the Skidder Prospect chlorite, calcite, epidote ± hematite alteration zone

Number of samples = 26

* Total iron as Fe_2O_3

	SiO_2	TiO_2	Al_2O_3	Fe_2O_3*	MnO	MgO	CaO	Na_2O	K_2O	P_2O_5	LOI	Pb	Th	U	Rb	Sr	Y	Zr	Nb	Zn	Cu	Ni	La	Ba	V	Ce	Cr	Ga
SiO_2	1.00																											
TiO_2	.00	1.00																										
Al_2O_3	-.44	.00	1.00																									
Fe_2O_3*	.00	.31	.00	1.00																								
MnO	-.16	.00	.00	.00	1.00																							
MgO	-.59	-.26	.00	-.22	.70	1.00																						
CaO	-.04	.00	-.27	-.15	-.07	.00	1.00																					
Na_2O	.55	.07	.00	.14	-.26	-.65	-.58	1.00																				
K_2O	-.19	-.24	.00	-.19	.00	.18	.37	-.73	1.00																			
P_2O_5	.00	.36	.07	.00	-.08	-.36	.00	.32	-.27	1.00																		
LOI	-.74	.00	.34	-.39	.00	.38	.00	-.13	.00	.00	1.00																	
Pb	.00	.00	-.09	.00	.00	.00	.00	.00	.05	-.35	.00	1.00																
Th	.00	-.04	-.33	.00	.04	.24	.00	.00	.00	-.15	.00	.20	1.00															
U	.00	.00	.00	.00	.00	.00	.00	.00	.00	.00	.00	.00	-.26	1.00														
Rb	-.09	-.25	.00	-.18	.00	.00	.19	-.59	.93	-.28	.00	.15	.00	.00	1.00													
Sr	-.39	-.23	.00	-.12	.00	.30	.59	-.82	.86	.00	.00	.00	.00	-.03	.76	1.00												
Y	.19	.84	-.19	.31	.00	-.45	.00	.37	-.35	.18	-.26	.00	.00	.00	-.34	-.37	1.00											
Zr	.00	.85	.00	.15	.00	-.35	.00	.26	-.33	.31	.00	-.15	.00	-.11	-.26	-.28	.86	1.00										
Nb	-.17	.58	.00	.00	.00	.00	.00	.00	.00	.27	.08	.00	.00	-.17	.00	.00	.50	.70										
Zn	.00	.00	.00	.14	.68	.34	-.62	.00	.00	.00	.00	.00	.06	.00	.00	-.14	.00	.00										
Cu	.00	.00	.00	-.38	.00	.00	.40	-.39	.48	.00	.00	.00	.00	.00	.47	.37	.00	.00										
Ni	-.54	.16	.22	-.36	.00	.23	.39	-.43	.07	.00	.42	.00	-.03	.00	.00	.29	.00	.00										
La	.00	.00	.00	.00	.00	.00	.00	.00	.00	.17	-.10	.00	.00	.00	.00	.00	.00	.00										
Ba	.00	-.26	.00	-.28	.00	.21	.32	-.56	.76	-.20	.00	.00	.00	.00	.76	.74	-.25	-.21										
V	.18	.31	-.09	.54	.20	.00	-.34	.30	-.34	.00	-.20	.00	.00	.00	-.25	-.41	.45	.26										
Ce	.00	.45	.30	.15	.00	.00	-.09	.16	-.29	.21	.16	.00	.00	-.23	-.26	-.32	.22	.49										
Cr	-.58	.07	.29	-.23	.00	.18	.33	-.29	.00	.00	.42	.00	-.06	.00	.00	.27	.00	.00										
Ga	.00	.39	.00	.21	.00	.00	.00	.19	-.29	.06	-.07	-.23	.00	-.22	-.33	-.29	.41	.49										

	Nb	Zn	Cu	Ni	La	Ba	V	Ce	Cr	Ga
Zn	.00	1.00								
Cu	.00	-.16	1.00							
Ni	.30	-.06	.20	1.00						
La	.34	.00	.00	.00	1.00					
Ba	-.10	.00	.44	.00	.00	1.00				
V	.00	.52	.00	-.48	.00	-.19	1.00			
Ce	.42	.00	.00	.00	.00	-.53	.00	1.00		
Cr	.32	-.17	.00	.89	.00	.00	-.50	.00	1.00	
Ga	.23	.25	.00	.00	.00	-.21	.37	.50	.00	1.00

Table B-18: Pearson correlation coefficient (r) matrix for drill core samples from the Skidder Prospect chlorite, calcite, quartz, epidote alteration zone

Number of samples = 21

* Total iron as Fe_2O_3

	SiO_2	TiO_2	Al_2O_3	Fe_2O_3*	MnO	MgO	CaO	Na_2O	K_2O	P_2O_5	LOI	Pb	Th	U	Rb	Sr	Y	Zr
SiO_2	***1.00***																	
TiO_2	-.20	***1.00***																
Al_2O_3	***-.74***	***.50***	***1.00***															
Fe_2O_3*	***-.74***	***.48***	***.70***	***1.00***														
MnO	***-.51***	.00	***.40***	***.49***	***1.00***													
MgO	***-.93***	.07	***.63***	***.59***	***.33***	***1.00***												
CaO	***-.46***	***-.39***	.00	.00	***.38***	***.53***	***1.00***											
Na_2O	***.73***	.00	.00	-.27	***-.30***	***-.79***	***-.76***	***1.00***										
K_2O	-.11	-.18	.00	.00	***.51***	.00	***.36***	-.22	***1.00***									
P_2O_5	-.00	***.62***	.16	.00	-.07	.00	***-.44***	.10	-.18	***1.00***								
LOI	***-.65***	.00	***.30***	***.35***	.10	***.66***	***.38***	***-.69***	.00	.00	***1.00***							
Pb	.29	.00	-.22	-.12	.00	***-.43***	-.17	.11	.00	.00	.00	***1.00***						
Th	.00	.00	.00	.00	.00	.00	.00	.00	.00	***.30***	.00	.00	***1.00***					
U	.00	.00	.00	.17	***.34***	.00	.00	.00	.00	.00	.00	.00	***.37***	***1.00***				
Rb	-.28	-.24	.00	.00	***.44***	.21	***.49***	***-.40***	***.86***	***-.34***	.00	.00	.00	.00	***1.00***			
Sr	***-.40***	***-.31***	.00	.00	***.38***	***.47***	***.76***	***-.61***	***.43***	***-.30***	.17	.00	.00	.00	***.47***	***1.00***		
Y	.00	***.65***	.00	.00	-.20	.00	***-.72***	***.34***	***-.43***	***.70***	.00	.00	.07	.20	***-.55***	***-.72***	***1.00***	
Zr	.00	***.60***	.00	.00	-.17	-.03	***-.54***	.21	***-.46***	***.72***	.00	.00	.12	.23	***-.52***	***-.60***	***.89***	***1.00***
Nb	-.02	***.57***	.10	.11	-.17	.08	.00	.00	***-.35***	***.49***	.22	.00	.00	.00	***-.34***	***-.33***	***.52***	***.64***
Zn	***-.61***	***.59***	***.78***	***.85***	***.39***	***.41***	.00	.00	.00	.24	.21	.00	.00	.21	.00	.00	***.35***	.09
Cu	-.18	***-.47***	.00	.00	.00	***.41***	***.77***	***-.61***	.10	***-.62***	.24	.00	.00	-.12	***.40***	***.72***	***-.84***	***-.73***
Ni	***-.53***	-.16	.00	.00	.17	***.58***	***.84***	***-.82***	.09	.00	***.51***	.00	.00	.00	***.39***	***.65***	***-.44***	-.21
La	.00	.00	***.32***	.00	.00	.00	.00	.00	.00	.13	.00	.00	.00	.00	.00	.00	.08	.19
Ba	-.20	-.16	.00	.00	***.42***	.00	***.41***	***-.34***	***.94***	.00	.00	.00	.00	.00	***.83***	***.36***	***-.40***	***-.42***
V	-.26	***.38***	.28	***.60***	.00	.08	.00	.00	.00	.00	.00	.00	-.14	.00	.00	.00	.00	.00
Ce	.13	.00	.00	-.24	***-.34***	.00	-.11	.00	***-.61***	.25	.08	.09	.00	.00	***-.50***	-.18	***.33***	***.52***
Cr	***-.53***	-.14	.00	.00	.15	***.59***	***.84***	***-.81***	.13	.00	***.47***	.00	.00	.00	***.42***	***.63***	***-.44***	-.21
Ga	***-.48***	***.47***	***.59***	***.56***	.00	***.48***	.00	.00	.00	.24	.21	-.11	.00	.00	.00	-.10	.28	.00

	Nb	Zn	Cu	Ni	La	Ba	V	Ce	Cr	Ga
Zn	***.33***	***1.00***								
Cu	-.18	***-.28***	***1.00***							
Ni	.00	.00	***.62***	***1.00***						
La	.17	.00	.00	.00	***1.00***					
Ba	-.28	.00	.15	***.30***	-.28	***1.00***				
V	.00	***.51***	.00	-.07	***-.34***	.00	***1.00***			
Ce	***.33***	.00	.00	.00	.25	***-.66***	.00	***1.00***		
Cr	.00	.00	***.62***	***.99***	.00	***.33***	-.08	.00	***1.00***	
Ga	***.36***	.58	-.12	.00	.46	.00	.08	.00	.00	***1.00***

Table B-19: Pearson correlation coefficient (r) matrix for drill core samples from the Skidder Prospect chlorite, quartz, calcite alteration zone

Number of samples = 34

* Total iron as Fe_2O_3

	SiO_2	TiO_2	Al_2O_3	Fe_2O_3*	MnO	MgO	CaO	Na_2O	K_2O	P_2O_5	LOI	Pb	Th	U	Rb	Sr	Y	Zr
SiO_2	***1.00***																	
TiO_2	-.15	***1.00***																
Al_2O_3	**-.47**	*.37*	***1.00***															
Fe_2O_3*	*-.37*	.23	.00	***1.00***														
MnO	*-.34*	.00	.00	*.38*	***1.00***													
MgO	*-.33*	.00	-.11	.17	.00	***1.00***												
CaO	**-.53**	.00	.00	.00	**.44**	.00	***1.00***											
Na_2O	**.40**	.00	.00	.00	-.14	***-.62***	.00	***1.00***										
K_2O	-.05	.26	***.74***	-.27	-.09	**-.52**	.00	.00	***1.00***									
P_2O_5	*.37*	.20	.00	.00	.00	-.25	-.14	.14	.00	***1.00***								
LOI	*-.78*	.00	.00	.00	.23	.25	***.73***	**-.56**	.00	***-.43***	***1.00***							
Pb	.00	.06	*.35*	-.21	*-.35*	*-.32*	-.19	.00	***.70***	.00	.00	***1.00***						
Th	.00	.19	.00	.16	*.35*	.00	.00	.00	.00	.00	.00	.00	***1.00***					
U	-.10	.00	.00	.00	.17	.00	.00	-.13	.00	.00	.00	.00	*.31*	***1.00***				
Rb	-.14	.26	***.73***	-.19	.00	**-.50**	.00	.00	***.98***	.00	.00	***.75***	.00	.00	***1.00***			
Sr	-.05	-.18	.00	-.05	.00	.00	*.37*	.00	.00	-.26	.21	.00	-.19	.00	.00	***1.00***		
Y	.29	**.46**	.00	.19	.00	-.28	-.28	*.31*	.00	***.71***	**-.55**	.00	.26	.00	.00	*-.38*	***1.00***	
Zr	.00	***.65***	.08	.29	.00	-.20	-.20	.15	.00	**.52**	*-.31*	.00	.12	.00	.00	**-.42**	***.83***	***1.00***
Nb	.00	**.55**	.29	.07	.24	.00	.00	.00	.22	**.46**	.00	.08	.03	.16	.23	-.20	**.51**	***.63***
Zn	-.11	*.35*	.00	**.43**	.12	*.30*	-.19	.00	.00	.07	.00	-.14	.00	.00	.00	**-.50**	**.43**	**.49**
Cu	.00	*-.30*	.00	**-.56**	.00	.00	.00	.00	.26	*-.31*	.22	.25	.00	.00	.20	.20	**-.40**	**-.54**
Ni	.00	.00	.00	**-.50**	-.24	.16	.00	*-.37*	.12	-.22	*.31*	.27	.00	.00	.09	*.38*	**-.49**	**-.47**
La	.13	.00	-.07	.00	.00	.00	-.07	.00	-.07	**.49**	-.21	-.19	.05	.00	-.07	*-.33*	*.31*	.28
Ba	.00	.00	.00	-.08	**-.54**	*-.32*	.00	.26	**.44**	.00	.00	**.41**	-.07	.00	*.38*	.19	.00	.00
V	***-.60***	.12	.56	.00	.00	.18	.00	-.23	.28	***-.63***	*.39*	.27	.00	.00	*.33*	.00	*-.35*	.00
Ce	.00	*.33*	.26	.00	.00	.00	-.05	-.17	.12	.23	.00	.00	.10	.00	.00	-.11	.26	*.34*
Cr	.00	.00	.00	**-.49**	*-.35*	.16	.00	-.27	.20	-.12	.15	*.33*	.00	.00	.19	.24	**-.45**	*-.39*
Ga	.00	*.39*	**.50**	.00	.00	-.09	-.23	.00	*.33*	.22	-.17	.00	.00	.00	*.31*	*-.36*	**.44**	***.60***

	Nb	Zn	Cu	Ni	La	Ba	V	Ce	Cr	Ga
Zn	.28	***1.00***								
Cu	.00	-.29	***1.00***							
Ni	.00	**-.40**	.56	***1.00***						
La	.00	.00	*-.39*	-.13	***1.00***					
Ba	.00	-.23	.06	.00	-.05	***1.00***				
V	.00	.00	.11	.05	*-.33*	.00	***1.00***			
Ce	**.47**	.00	.00	.00	.27	*-.31*	.00	***1.00***		
Cr	.00	**-.42**	**.42**	***.92***	.00	.06	.17	.00	***1.00***	
Ga	**.40**	*.39*	.00	*-.38*	.22	.00	.00	*.32*	-.23	***1.00***

Table B-20: Pearson correlation coefficient (r) matrix for drill core samples from the Skidder Prospect chlorite, quartz, pyrite alteration zone

Number of samples = 34

* Total iron as Fe_2O_3

	SiO_2	TiO_2	Al_2O_3	Fe_2O_3*	MnO	MgO	CaO	Na_2O	K_2O	P_2O_5	LOI	Pb	Th	U	Rb	Sr	Y	Zr	Nb	Zn	Cu	Ni	La	Ba	V	Ce	Cr	Ga
SiO_2	1.00																											
TiO_2	.29	1.00																										
Al_2O_3	-.27	.08	1.00																									
Fe_2O_3*	**-.47**	-.23	.00	1.00																								
MnO	-.22	.00	.18	.24	1.00																							
MgO	**-.87**	**-.41**	.00	.11	.24	1.00																						
CaO	.00	.00	-.17	-.22	**-.47**	.00	1.00																					
Na_2O	**.57**	**.50**	.28	**-.49**	*-.32*	**-.72**	.15	1.00																				
K_2O	.00	.00	.00	.00	-.29	-.17	.00	.00	1.00																			
P_2O_5	.00	.00	.00	.13	.00	.00	.20	.00	-.14	1.00																		
LOI	**-.92**	**-.41**	.00	**.49**	.19	**.88**	.00	**-.78**	.00	.00	1.00																	
Pb	-.21	*-.36*	**-.56**	.00	.00	**.48**	*.32*	*-.37*	.00	.00	**.44**	1.00																
Th	.27	.16	.00	**-.49**	.00	.00	.00	.00	-.25	.00	-.27	.00	1.00															
U	.00	**.00**	.08	.00	.00	.00	.00	.00	**.60**	.00	.00	.00	.00	1.00														
Rb	.00	.00	.00	.00	-.18	.00	.00	.00	**.88**	-.10	.00	.00	-.15	**.68**	1.00													
Sr	.14	.20	.00	*-.30*	**-.55**	*-.38*	**.67**	**.72**	.15	.05	*-.32*	.00	.00	.00	.00	1.00												
Y	-.13	.07	.00	.23	.00	.00	.23	.00	.00	**.62**	.00	-.21	.00	.00	.00	.16	1.00											
Zr	.00	**.41**	.00	.00	.00	.00	.00	.20	.00	**.83**	.00	-.24	.00	.00	.00	.14	**.63**	1.00										
Nb	.00	.02	.00	.00	.00	.00	.00	.00	.00	**.50**	.00	.00	.00	.00	.00	.00	.23	**.64**										
Zn	**-.53**	-.10	.00	*.35*	.28	**.53**	.00	**-.47**	.00	.00	**.66**	**.52**	-.20	.00	.00	-.11	.00	.00	.08	1.00								
Cu	.00	.00	-.11	.00	.00	.00	.00	.00	.00	.00	.00	.00	*.37*	.00	.00	.00	.18	.00	.00	.00	1.00							
Ni	.00	.00	-.03	.00	.00	.00	.20	.00	.00	.20	.00	-.14	.00	.00	.00	.00	*.38*	.00	.00	.00	.00	1.00						
La	.00	*-.37*	.00	.00	.22	.17	.00	*-.37*	-.08	.00	.00	.00	.00	-.02	.00	*-.31*	.00	.00	.12	.00	.00	.00	1.00					
Ba	.00	.00	.10	.00	*-.31*	.00	.20	.20	**.58**	.00	.00	.00	.00	**.50**	**.56**	**.40**	.00	.00	.00	.00	.00	.00	.00	1.00				
V	-.18	.00	**.74**	.08	*.33*	.00	**-.50**	.00	.09	.00	.00	**-.49**	.00	**.45**	.00	-.10	.00	.00	.00	.00	.00	.00	.00	.00	1.00			
Ce	.00	.00	.00	.14	.16	.00	-.24	-.12	.00	.00	.00	.00	.00	.00	-.16	-.25	.00	.00	**.62**	.00	.00	.00	.00	.00	.00	1.00		
Cr	.00	.00	-.16	.10	.00	.00	.13	-.13	.00	*.34*	.00	-.08	.00	.00	.00	.00	**.43**	.18	.00	.00	.00	**.96**	*.33*	.00	.00	.00	1.00	
Ga	**-.66**	-.29	.51	**.57**	**.46**	**.47**	*-.38*	*-.39*	.00	.00	**.54**	.00	*-.35*	.08	.00	*-.30*	.00	-.05	.00	**.42**	.00	-.14	.07	.00	**.50**	.13	-.08	1.00

Table B-21: Pearson correlation coefficient (r) matrix for drill core samples from the Skidder Prospect quartz, chlorite, pyrite alteration zone

Number of samples = 20

* Total iron as Fe_2O_3

	SiO_2	TiO_2	Al_2O_3	Fe_2O_3*	MnO	MgO	CaO	Na_2O	K_2O	P_2O_5	LOI	Pb	Th	U	Rb	Sr	Y	Zr
SiO_2	1.00																	
TiO_2	-.37	1.00																
Al_2O_3	-.29	.81	1.00															
Fe_2O_3*	-.61	.00	-.35	1.00														
MnO	-.34	.29	.27	.00	1.00													
MgO	-.68	.00	.00	.30	.60	1.00												
CaO	-.04	.29	.21	-.19	.75	.00	1.00											
Na_2O	.17	.00	.27	-.60	.00	.00	.15	1.00										
K_2O	.00	.69	.61	.00	-.07	-.06	.00	.00	1.00									
P_2O_5	-.39	.83	.68	.00	.25	.20	.22	.00	.49	1.00								
LOI	-.71	.00	-.23	.94	.00	.35	.00	-.65	.00	.00	1.00							
Pb	.00	.00	.00	.00	-.23	-.16	.00	.00	.00	-.11	.00	1.00						
Th	.00	.00	.00	.00	.00	-.28	.00	.23	.00	.00	.00	.00	1.00					
U	.00	-.12	.00	.00	-.20	.00	.00	.00	.00	-.39	.00	.00	.00	1.00				
Rb	-.06	.67	.56	.00	-.11	.00	.00	-.14	.98	.46	.00	.00	.00	.00	1.00			
Sr	.00	.00	.25	-.50	.32	.00	.48	.77	.00	.00	-.48	.00	.00	.00	.00	1.00		
Y	.00	.42	.61	-.42	.27	.00	.31	.50	.00	.49	-.40	-.43	.29	-.37	.00	.43	1.00	
Zr	.00	.31	.49	-.42	.02	.00	.25	.42	.00	.38	-.36	-.31	.26	-.36	.00	.23	.91	1.00
Nb	-.42	.64	.37	.00	.00	.00	.35	-.14	.42	.56	.11	.00	.00	.00	.43	.00	.28	.27
Zn	.00	.00	.00	.21	-.11	.00	.00	.00	.00	.00	.24	.86	.00	.00	.00	-.13	-.41	-.33
Cu	.00	.47	.54	-.08	.00	.00	.00	.00	.57	.06	.00	.29	-.09	.35	.50	.00	.00	.00
Ni	-.27	.41	.16	.00	.24	.53	.00	-.42	.21	.47	.00	.00	-.53	.00	.21	-.21	.00	.00
La	-.47	.00	.00	.37	.32	.41	.14	.00	-.23	.00	.36	.00	.18	.00	-.08	.00	.00	.00
Ba	.00	.12	.44	-.18	.00	.00	.00	.12	.54	.15	.00	.00	.00	.33	.45	.00	.00	.00
V	-.59	.80	.78	.00	.31	.39	.00	.00	.56	.60	.00	.00	.00	.00	.56	.00	.03	.00
Ce	.00	.46	.28	.00	.00	.00	.00	-.13	.18	.38	.00	-.21	.10	-.35	.19	.00	.37	.33
Cr	-.35	.29	.00	.13	.00	.57	.00	-.57	.12	.44	.28	.00	-.46	-.08	.16	-.33	.00	.00
Ga	-.47	.81	.73	.00	.00	.00	.00	.00	.67	.80	.00	.00	.00	-.17	.68	.00	.34	.32

	Nb	Zn	Cu	Ni	La	Ba	V	Ce	Cr
Zn	.00	1.00							
Cu	.31	.00	1.00						
Ni	.00	.00	.00	1.00					
La	.00	.00	-.01	.00	1.00				
Ba	.00	.00	.38	.00	-.21	1.00			
V	.33	.00	.54	.39	.00	.21	1.00		
Ce	.48	-.18	.00	.00	.00	-.40	.36	1.00	
Cr	.00	.00	.00	.92	.00	.00	.32	.00	1.00
Ga	.56	.00	.26	.33	.00	.26	.69	.34	.23

Table B-22: Pearson correlation coefficient (r) matrix for drill core samples of Skidder Prospect massive and semimassive sulphides

Number of samples = 8

* Total iron as Fe_2O_3

	SiO_2	TiO_2	Al_2O_3	Fe_2O_3*	MnO	MgO	CaO	Na_2O	K_2O	P_2O_5	LOI	Pb	Th	U	Rb	Sr	Y	Zr	Nb	Zn	Cu	Ni	La	Ba	V	Ce	Cr	Ga
SiO_2	1.00																											
TiO_2	.00	1.00																										
Al_2O_3	.00	.68	1.00																									
Fe_2O_3*	-.57	.00	-.23	1.00																								
MnO	.00	.53	.64	-.35	1.00																							
MgO	.00	.62	.98	-.44	.75	1.00																						
CaO	.00	.00	.00	.00	.00	.00	1.00																					
Na_2O	.00	.00	.00	.00	.00	.00	.00	1.00																				
K_2O	.00	.00	.00	.31	.00	.00	-.25	.74	1.00																			
P_2O_5	.38	.00	.00	.00	.00	.00	.00	.00	.00	1.00																		
LOI	-.71	.00	-.30	.94	-.52	-.47	.00	.00	.16	.00	1.00																	
Pb	.00	-.64	-.84	.00	-.39	-.74	.02	-.30	-.47	.00	.00	1.00																
Th	.00	.00	.00	.07	.00	.00	.00	.53	.29	.00	.00	.00	1.00															
U	-.43	.00	.00	.20	-.44	-.18	.00	.20	.00	.00	.47	.00	.44	1.00														
Rb	.00	.00	.00	.46	-.31	.00	-.29	.45	.86	.00	.41	-.22	.51	.00	1.00													
Sr	.00	.00	.00	.00	.00	.00	.99	.00	-.31	.00	.00	.07	.00	.00	-.36	1.00												
Y	.58	.00	.00	-.77	.00	.00	.00	.00	.00	.00	-.69	.00	.00	-.13	.00	.00	1.00											
Zr	.00	.71	.98	.00	.66	.95	.00	.00	.00	.00	.00	-.87	.00	.00	.00	.00	.00	1.00										
Nb	-.51	.00	-.42	.44	-.32	-.43	.00	-.42	.00	.00	.63	.40	.00	.00	.00	.00	-.08	-.28	1.00									
Zn	.00	-.36	-.43	.00	-.23	-.25	.00	-.42	-.56	.00	.00	.62	.00	.00	-.20	.00	.14	-.49	.00	1.00								
Cu	-.28	-.08	-.31	.00	.00	-.09	.00	-.13	-.38	.00	.00	.70	.00	.48	-.34	.00	.00	-.29	.49	.66	1.00							
Ni	.00	.68	.82	-.70	.80	.87	.00	.00	.00	.00	-.75	-.65	.00	-.29	.00	.00	.55	.78	-.57	.00	-.19	1.00						
La	.00	.00	.00	.59	.00	.00	.00	.73	.86	-.21	.48	-.21	.55	.03	.84	.00	-.25	.00	.00	-.53	-.23	.00	1.00					
Ba	.00	.00	.40	.00	.00	.30	.00	.65	.63	.00	.00	-.22	.00	.00	.00	-.08	.00	.33	-.41	.00	.00	.00	.27	1.00				
V	.00	.77	.99	-.22	.72	.97	.00	.00	.00	.00	-.31	-.80	.00	.00	.00	.00	.00	.97	-.34	-.46	-.24	.84	.00	.27	1.00			
Ce	.00	.96	.71	-.22	.65	.71	.00	.00	.00	.00	-.29	-.52	.00	.00	.00	.00	.00	.71	.00	-.13	.00	.78	.00	.00	.81	1.00		
Cr	.00	.69	.99	-.19	.68	.98	.00	.00	.00	.00	-.28	-.79	.00	.00	.00	.00	.00	.97	-.37	-.45	-.21	.81	.00	.39	.99	.74	1.00	
Ga	.00	.00	.00	-.51	.00	.00	.00	-.41	-.60	.00	-.13	.27	.00	.00	-.26	.00	.59	-.03	.00	.94	.39	.00	-.60	.00	.00	.00	.00	1.00

APPENDIX C

PRINCIPAL COMPONENT ANALYSIS METHOD

Principal component analysis was performed utilizing the Statview 512+ (Feldman et al., 1986) statistical program on an Apple Macintosh microcomputer. The computational accuracy of the program was verified to twelve decimal places by a consultant to the program's creators (Feldman et al., 1986) using the SPSS program on an IBM 370 mainframe computer. The method chosen involves a varimax-rotated (Kaiser, 1958), reference-structured (Thurstone, 1947) orthotran (Hofmann, 1978) or oblique solution employing the principal component factor extraction method (Hotelling, 1933). The oblique solution was chosen since it allows factors to be correlated.

Varimax-rotated factors extracted from the various data groupings are presented in Tables C-1 to C-9.

Table C-1: Varimax-rotated factors extracted from Data Group 1 - Skidder Basalt samples unaffected by the Skidder Prospect alteration event(s)

Factor	1	2	3	4	5	6	7	8
Variance	21.7%	10.5%	13.9%	17.1%	11.9%	10.7%	6.9%	7.3%
SiO_2	-.098	.180	-.090	-.347	-.597	-.351	-.017	
TiO_2	.678	.052	-.017	-.090	.141	.166	-.056	.150
Al_2O_3		-.065	.432	.267	-.266	.533	-.135	.260
Fe_2O_3*	.296	.462	-.156	-.117	-.043	.491	-.101	.056
MnO	-.087	.738		.057	.148		.054	.055
MgO	.014	.366	-.132	.647	-.261	.237		-.197
CaO	-.085	-.024	-.040	-.081	.797	-.137	-.173	-.131
Na_2O	-.148	-.428	.159	-.460	-.126	.126	.072	.382
K_2O	.088	-.078	.902	-.014	-.068		.044	-.122
P_2O_5	.432	-.055	.164	-.019	-.145	-.440	.086	.239
LOI	.025	-.090	.096	.331	.539	-.031	.358	
Pb		.141	.146	.026	.022	.050	.807	.092
Rb	-.143	-.157	.802	-.081	.069	.050	.273	.102
Sr	-.135	.087	.359	.145	.210	.094	-.485	.320
Y	.532	.042	-.031	-.256	-.067	-.138	.074	.202
Zr	.685	-.027	-.061	-.080	.032	-.091	.040	.179
Nb	.807	-.077	.042	.152	.181	.024		.037
Zn	-.034	.644	.080	-.065	-.318	.175	.156	.073
Cu	-.107	-.119	.060	.025	.078	.077	-.010	-.680
Ni	-.056		-.060	.744	.148	-.124		.054
Ba		.350	.710	-.152	.048	-.248	-.165	-.064
V	.031	.071	-.043	-.121	.041	.846	.111	-.119
Ce	.688	-.177	-.151	.238	-.155	.089	.044	-.234
Cr	.019	-.184		.825	.017	-.082		.081
Ga	.542	.185	.104	-.047	-.250	.058	-.091	-.292

* Total iron as Fe_2O_3

Table C-2: Varimax-rotated factors extracted from Data Group 2 - all analyses of drill core from the Skidder Prospect, excluding trondhjemite and jasper, but including sulphide-rich samples

Factor	1	2	3	4	5	6	7
Variance	25.5%	13.3%	13.2%	11.1%	9.5%	12.9%	14.5%
SiO_2	.213	-.138	.068	-.010	-.169	-.398	-.654
TiO_2	.627	.038	.129		.158	.212	.045
Al_2O_3	.348		.217	.028	.028	.491	-.158
Fe_2O_3*	-.124		-.022	-.179		-.120	.609
MnO	-.015	-.021	-.253	.035	.434	.565	.172
MgO	-.297	-.044	-.299	.248	-.156	.649	.024
CaO	-.092	-.052	-.026	.042	.868	-.042	.159
Na_2O	.444	.093	-.038	-.268	.236	-.096	-.290
K_2O	.011	-.050	.949	.019			.039
P_2O_5	.744	.024	-.087	.144	-.010	-.170	.050
LOI	-.324		-.045	.036	-.085	.021	.544
Pb	-.185	.336	.081	-.032	-.011	-.283	.189
Rb	.019	-.048	.914		-.078	-.012	.150
Sr	-.015	.083	.167	.088	.770		-.092
Y	.756	.158	-.129	-.115	.025	-.033	-.076
Zr	.831	-.060	-.037	-.077	-.061	-.080	.123
Nb	.518	.100	.129		.023	-.171	.700
Zn	-.047	.830	-.044		.012	-.069	-.075
Cu	-.057	.642	-.053	.051	.129	-.146	.048
Ni	.014	.030		.924	.132		-.055
Ba	-.260	.087	.730	-.016	.211	.077	-.189
V	.094		.148	-.052	-.099	.761	-.023
Ce	.670	-.129	-.079	.063	-.176		.119
Cr	.032	-.060	.011	.905			.032
Ga	.172	.831	.057	-.095	-.059	.219	-.023
Distance	.269	.027	-.017	-.369	.363		.012

* Total iron as Fe_2O_3
Distance - distance from massive sulphides or most intense alteration

Table C-3: Varimax-rotated factors extracted from Data Group 3 - Data Group 2 excluding sulphide-rich samples

Factor	1	2	3	4	5	6	7
Variance	20.7%	18.3%	14.3%	10.4%	13.0%	16.1%	7.3%
SiO_2	-.080	-.628	.152	-.301	-.144	-.470	-.267
TiO_2	.451	-.072	.034	.145	.076	.369	.031
Al_2O_3	.154	.014	.106		.107	.766	-.093
Fe_2O_3*		.040	-.074	-.025	-.099	.142	.816
MnO	.031	.309	-.380	.511	.038	.358	.106
MgO	-.047	.668	-.356	-.044	.194	.357	-.130
CaO	.013	.028	.031	.891	-.045	-.254	
Na_2O	.083	-.398	-.108	.141	-.303	.107	-.211
K_2O		-.099	.940		.066	.032	.030
P_2O_5	.737	.178	-.043	.025	.103	-.068	-.207
LOI	.012	.595		-.021	.184	-.033	.243
Pb	-.048	.293	.463	-.163	-.273	-.360	
Rb	.036	-.066	.906	-.068	.091	.038	.097
Sr	-.133	-.222	.149	.693	.020	.040	-.111
Y	.611	-.016	-.165	.040	-.142	.064	-.111
Zr	.725	.019	-.055	-.053	-.035		-.033
Nb	.734	.186	.223	.037	.144	-.107	.389
Zn	.158	.822	.014	-.037	-.167		-.149
Cu			-.016	.429	.011	-.417	.266
Ni	.103		-.014	.091	.910	.101	-.067
Ba	-.209	.035	.738	.205	-.105	.029	-.292
V	-.120	.107	-.063	-.121	.067	.861	.186
Ce	.573	-.027	-.111	-.190	.161	.045	.177
Cr	.129			-.011	.908	.068	
Ga	.351	.290	.107	-.111	-.138	.603	.148
Distance	.060	-.162	-.060	.309	-.406	.066	.076

* Total iron as Fe_2O_3
Distance - distance from massive sulphides or most intense alteration

Table C-4: Varimax-rotated factors extracted from Data Group 4 - samples from the Skidder Prospect chlorite, calcite, epidote ± hematite alteration zone

Factor	1	2	3	4	5	6	7
Variance	20.3%	21.8%	21.5%	12.7%	10.0%	7.3%	6.4%
SiO_2	-.114	-.727	-.206	-.302	-.245	-.106	.172
TiO_2	.865	.065	.040	.027	-.161	-.062	-.068
Al_2O_3	-.131	.256	-.010	-.109	.783	-.166	-.142
Fe_2O_3*	.213	-.243	.040	.027	.025	-.035	-.703
MnO	.021	.083	.017	.922	-.167	-.081	
MgO	-.232	.433	.116	.700	-.080	.069	-.010
CaO	.210	.414	.398	-.332	-.602	-.136	-.099
Na_2O		-.387	-.659	-.280	.257	.020	.161
K_2O		-.095	.870	-.017	.033	.102	.027
P_2O_5	.239	-.022	-.160	-.239	.315	-.482	.253
LOI	-.025	.606	-.165	.174	.398	.315	.238
Pb	.036	-.041				.910	.010
Rb	.018	-.171	.834	-.043	.133	.192	.121
Sr	-.037	.218	.795	-.052	-.099	-.101	-.137
Y	.782	-.236	-.029		-.275		-.058
Zr	.861	-.014		.010	-.088	-.076	.044
Nb	.783	.186	.088	-.042	.134	.197	.082
Zn	.110	-.273	-.029	.827	.301	.128	.013
Cu	.271	-.059	.504		-.073	-.141	.598
Ni	.201	.791	.049	.012	-.091	-.114	.116
Ba	-.054	-.217	.783	.058	-.113	-.091	.161
V	.295	-.526	-.063	.431		.015	-.088
Ce	.437	.214	-.221	.030	.442	-.014	-.033
Cr	.131	.875	-.065	-.079	-.105	-.027	-.057
Ga	.429	-.136	-.067	.274	.138	-.357	
Distance	.348	-.699	.196	.124	-.325	.068	-.035

* Total iron as Fe_2O_3
Distance - distance from massive sulphides or most intense alteration

Table C-5: Varimax-rotated factors extracted from Data Group 5 - samples from the Skidder Prospect chlorite, calcite, quartz, epidote alteration zone

Factor	1	2	3	4	5
Variance	29.3%	23.3%	19.9%	19.0%	8.6%
SiO_2	-.520	-.582	-.112	-.088	.056
TiO_2	-.144	.362	.012	.564	-.241
Al_2O_3	.115	.716		.102	-.051
Fe_2O_3*	-.041	.872	.146	.026	.082
MnO	.148	.542	.384	-.195	.480
MgO	.594	.424		.056	-.248
CaO	.718	-.148	.123	-.198	-.053
Na_2O	-.789	-.127	-.022	.018	.031
K_2O	-.039	.028	.839	-.066	-.020
P_2O_5				.751	
LOI	.689	.375	-.447	-.073	.189
Pb	-.035	-.043	-.207	-.091	.733
Rb	.169		.683	-.111	-.018
Sr	.508	.019	.118	-.359	-.044
Y	-.235	.126	-.154	.630	.038
Zr		-.079	-.199	.745	.095
Nb	.251	.044	-.238	.640	-.233
Zn	.079	.838	.068	.156	.161
Cu	.511	-.142	-.117	-.513	-.168
Ni	.911	-.186		.056	.031
Ba	.075	-.042	.835	.028	-.017
V	-.291	.703	-.088	-.304	
Ce	.267	-.180	-.711	.188	.215
Cr	.896	-.195	.038	.080	
Ga	-.050	.505	.041	.292	-.249
Distance	-.284	-.154	.411	.299	.418

* Total iron as Fe_2O_3
Distance - distance from massive sulphides or most intense alteration

Table C-6: Varimax-rotated factors extracted from Data Group 6 - samples from the Skidder Prospect chlorite, quartz, calcite alteration zone

Factor	1	2	3	4	5	6
Variance	20.7%	21.2%	14.2%	17.0%	16.5%	10.5%
SiO_2	-.429	-.239	-.572	-.120	.242	.088
TiO_2	.519	.413	.047	.260	.170	
Al_2O_3	.126	.806	.081	-.127	-.266	.164
Fe_2O_3*	.717	-.181	.218	-.101	-.144	-.266
MnO	-.048	-.161	.650	-.229	.094	.441
MgO	.455	-.583	-.140	.512	-.338	.049
CaO	-.257		.880	-.198	.194	
Na_2O	-.155	.207	-.228	-.598		-.270
K_2O	-.117	.949	.054	-.055	.011	
P_2O_5	-.030	-.041	.012	.150	.712	.109
LOI	.032	.082	.669	.209	-.042	-.014
Pb		.717	-.179	.158		-.207
Rb	-.072	.950	.081	-.058		-.042
Sr	-.310	.070	.380	.021	.129	-.251
Y	.195	.080	-.095	-.091	.405	.151
Zr	.417	.275	-.026		.297	.084
Nb	.181	.343	.218	.317	.453	.328
Zn	.608	-.089	-.166	-.015	-.241	.146
Cu	-.577	.231	-.011	.030	-.134	.282
Ni	-.277	.066		.669	.150	.010
Ba	.090	.478	-.130	.020	.088	-.691
V	.287	.402	.024	-.020	.646	.070
Ce	-.178	.182	-.052	.200	.184	.732
Cr	-.177	.145	-.160	.685	.081	-.018
Ga	.264	.480	.236	-.220	-.163	.215
Distance	.015	-.050	.196	-.302	.402	-.163

* Total iron as Fe_2O_3
Distance - distance from massive sulphides or most intense alteration

Table C-7: Varimax-rotated factors extracted from Data Group 7 - samples from the Skidder Prospect chlorite, quartz, pyrite alteration zone

Factor	1	2	3	4	5	6	7	8
Variance	19.3%	20.9%	10.5%	13.6%	10.7%	10.3%	5.6%	9.1%
SiO_2	-.243	-.884	.041	-.038		.246	.204	-.156
TiO_2	.249	-.419	-.123	.271	.108	.296	-.164	.039
Al_2O_3	.899		-.026	.114	-.037	.042	-.123	.037
Fe_2O_3*	.252	.365	.036	.059	.131	-.782	-.197	.158
MnO	.119	.396	-.238	-.118	.174	.178	-.200	-.548
MgO	.243	.867	-.139	.037	-.049	.149	.161	-.128
CaO	-.762	.042	.042	-.145		.400	-.112	.084
Na_2O	.061	-.753	-.036	.075	-.203	.293	-.225	.299
K_2O	.047	-.113	.931		-.046	.083	.041	-.086
P_2O_5	.074	.081	-.076	.792	.304	.103	.078	.027
LOI	-.239	.749	.020	-.057	-.013	-.312	-.177	.066
Pb	-.617	.365	.058	-.108	-.249	-.015	.129	
Rb	.050	.026	.816	-.059		-.202		.084
Sr	-.480	-.310	.133	.025	-.053	.553	-.196	.420
Y	.322	.083	.014	.612	.424	.164	.217	.199
Zr	.178	-.098	-.041	.806	.176	-.072	-.106	.108
Nb	-.104	.095	.073	.748	-.141	-.518	-.192	-.188
Zn	-.089	.709	-.040	.171	-.077	.013	-.051	-.147
Cu	-.082	-.046	-.028			.073	.817	.113
Ni	-.011	-.060	-.033	.123	.948		-.057	.011
Ba	-.165	-.030	.653		-.044	.472	-.100	.264
V	.890	.061	.109	.091	-.027	.039	.027	-.163
Ce	.192	.107	.069	.547	-.242	-.155	.228	-.617
Cr	-.028			.241	.924	-.078	.035	-.048
Ga	.729	.565	.031	.020	-.076	-.373	-.133	-.076
Distance	-.066		.074	.094	-.018		.151	.796

* Total iron as Fe_2O_3
Distance - distance from massive sulphides or most intense alteration

Table C-8: Varimax-rotated factors extracted from Data Group 8 - samples from the Skidder Prospect quartz, chlorite, pyrite alteration zone

Factor	1	2	3	4	5	6
Variance	28.1%	20.9%	15.9%	12.8%	10.0%	12.4%
SiO_2	-.243	-.126	-.561	-.354	.302	-.378
TiO_2	.875	.226	.058	-.127	.013	.092
Al_2O_3	.748	.458	-.070	-.140	.182	.121
Fe_2O_3*	-.178	-.212	-.016	.498	-.558	.252
MnO	-.029	-.049	.807	-.241		.245
MgO	-.194	.070	.408	-.020		.773
CaO		-.017	.956	-.089	.015	-.130
Na_2O		.743	-.013	-.068	.169	-.111
K_2O	.801	-.274	-.127	.010	.320	-.162
P_2O_5	.605	.626	-.033	-.075	-.142	.213
LOI	-.103	.318	.225	.457	-.422	.229
Pb	.043	-.021	-.167	.792		-.233
Rb	.793	-.306	-.123	.040	.243	-.163
Sr	-.033	.640	.504	-.016	.106	-.093
Y	.368	.714	-.011	-.180	-.215	-.106
Zr	.482	.447	-.120	-.332	-.144	-.173
Nb	.794	-.066	.184	.054	-.446	-.259
Zn		-.011	-.070	.822		-.064
Cu	-.217	-.179	.804	.044	.048	-.121
Ni	.195	-.137	-.175	-.234	.247	.703
Ba	.258	.078	.020	.176	.735	.157
V	.665	-.012	.044	-.020	.129	.307
Ce	.605	.068	-.178	-.366	-.489	-.161
Cr	.130	-.201	-.215	-.183	.112	.709
Ga	.819	.335	-.207	.132	-.078	.126
Distance	-.095	.852	-.286	.202	-.024	.096

* Total iron as Fe_2O_3
Distance - distance from massive sulphides or most intense alteration

Table C-9: Varimax-rotated factors extracted from Data Group 9 - samples of Skidder Prospect semimassive and massive sulphides

Factor	1	2	3	4	5	6	7
Variance	30.6%	13.7%	17.4%	11.9%	11.8%	9.1%	5.6%
SiO_2	-.375	.077	-.808	-.029	-.194	-.118	.161
TiO_2	.624	.024	.120	-.050	-.102	-.101	.130
Al_2O_3	.777	.067		.016	-.049	-.023	-.029
Fe_2O_3*	-.128		.753	-.374	-.036	-.087	-.016
MnO	.687	-.193	.127	.084	.564		-.124
MgO	.876	-.131	.076	.074	.051	.060	-.091
CaO	-.099	-.030	-.011	-.012	.832	-.034	-.067
Na_2O	-.026	.888	-.030	.023	.137	.032	
K_2O	-.250	.714	-.112	-.140	-.177	-.196	-.013
P_2O_5		.194		-.118	-.155	-.120	.890
LOI	-.014	.019	.828	-.123	-.092	-.015	-.075
Pb	-.346	-.020	-.068	-.118		.679	.066
Rb	-.321	.578	.209	-.037	-.282	-.399	-.056
Sr	-.093			-.012	.842		-.012
Y	.251	-.090	-.249	.728		-.161	.019
Zr	.829	.042	.125	.013	.014	-.083	-.104
Nb	.202	-.169	.702	-.029	-.156	.311	.233
Zn	-.277	-.079	-.061	.676	-.031	.163	-.041
Cu	-.045	-.030	.064	.107	-.030	.684	-.064
Ni	.380	.028	-.517	-.168	-.092	.465	-.218
Ba	.082	.834	-.156	-.022	.094	.217	-.102
V	.843	.019	.069			.040	
Ce	.669	-.283	-.037	-.046	-.016	-.046	.260
Cr	.553		-.351	-.276	-.133	.258	.019
Ga	-.136	-.119	-.036	.817	-.035	-.038	-.139
Distance	-.140	-.303	-.024	-.564	-.609	-.024	-.480

* Total iron as Fe_2O_3

Distance - distance from massive sulphides or most intense alteration

APPENDIX D

RARE-EARTH ELEMENT ANALYTICAL PROCEDURES

Rare earth elements were determined at Memorial University of Newfoundland using the thin film/XRF method of Fryer (1977). This method involves repeated digestion of the sample by HF, HCl and $HClO_4$. Passage of the solution, in 3.1 N HCl, through an ion exchange resin separates the rare-earth elements, Y and Ba from the others. Barium is precipitated as $BaSO_4$ by addition of sulphuric acid. The REE-bearing HCl solution is concentrated by evaporation and then taken up on an ion exchange paper disc. The dried disc is analyzed by X-ray fluorescence techniques.

Rare-earth element concentrations for internal Memorial University of Newfoundland granite standard MUN-1 determined during this study are presented in Table D-1.

Table D-1: Rare-earth element concentrations for Memorial University of Newfoundland internal standard MUN-1 according to results of an analysis conducted during this study

	ppm	chondrite normalized
La	22.8	72.4
Ce	47.0	57.8
Nd	20.4	34.2
Sm	3.9	20.3
Eu	0.1	1.4
Gd	3.4	13.1
Dy	2.8	8.6
Er	1.6	7.5

Chondrite-normalizing values used are those of Taylor and Gorton, 1977